



ISBN: 978-81-942561-2-0

PROCEEDINGS



International Conference on

Impact of Changing Energy Mix in the Power Sector

Organised by

The Institution of Engineers (India)
West Bengal State Centre

under the aegis of Electrical Engineering Division, IEI

In association with







With Best Compliments from:



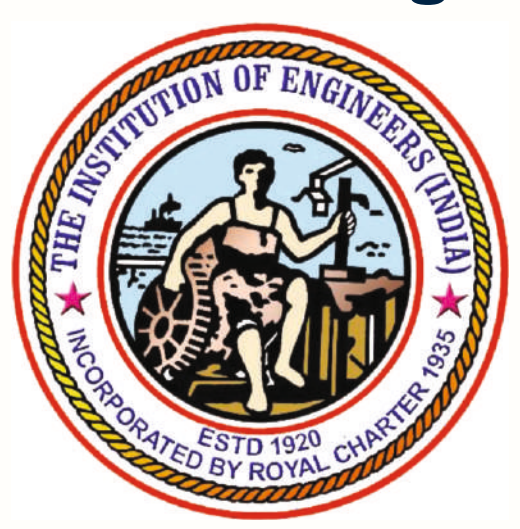
With Best Compliments from: Systems and services to monitor and control the use of energy SECURE WWW.SECUREMETERS.COM

International Conference On Impact of Changing Energy Mix in the Power Sector

ICIEMPS-2019

ISBN: 978-81-942561-2-0

Proceedings



Organised by

The Institution of Engineers (India)

Under the aegis of Electrical Engineering Division West Bengal State Centre

Hotel: LaLit Great Eastern 23rd & 24th November 2019

(ESTABLISHED 1920, INCORPORATED BY ROYAL CHARTER 1935)

Mest Bengal State Centre 8, GOKHALE ROAD, KOLKATA - 700020

Er. Sandip Kumar Deb, FIE
Chairman
Er. Kalipada Das, MIE
Honorary Secretary



Telephone: +91-33-2223 8914
Fax: +91-33-2223 3140
E-mail: wbsc@ieindia.org
iei.wbsc@gmail.com
Website: www.ieiwbsc.in

"100 Years of Relentless Journey Towards Engineering Advancement for Nation-building"

Editorial

Stability in energy supply sustains the growth in agriculture and industry, leading to rise in per capita income. This, added with constant improvement in transport systems, educational opportunities, health care delivery and other social services, transforms to sustainable development. For optimum utilization, the energy sources should be diversified, because no single resource in a country can sustainably meet the energy demands providing all the energy requirements for sustainable development in the wake of steady increase in population, urbanization and industrialization. Integrating energy sources is a viable way to address the energy problems in any country, which include irregular power supply and rising costs / scarcity of conventional or traditional energy sources. Utilization of the country's abundant renewable energy resources combined with efficient use of fossil fuels facilitated by technological innovations can improve the environmental and economic conditions. Moreover, efficient management of energy resources is imperative for economic growth, environmental protection and energy systems sustainability.

To meet its energy needs, each country uses the types of energy available to it in differing proportions. This is what we call energy mix. It varies significantly from one country to another. The term energy mix should also not be confused with the power generation mix. It refers to the combination of the various primary energy sources used to meet energy needs in a given geographic region. It includes fossil fuels, nuclear energy, non-renewable waste and various sources of renewable energy. These primary energy sources are used, for example, for generating power, for providing fuel for transportation and heating and for cooling residential and industrial buildings. For each region or country, the composition of the energy mix depends on the availability of usable resources domestically or the possibility of importing them, the extent and type of energy needs to be met and the Policy choices determined by historical, economical, social, demographical, environmental and geopolitical factors.

The concept of energy mix is becoming a potential force in shaping the social and industrial revolution in the recent future. The span of the impact is wide, affecting not only how the people live, learn and interact, but also the way the economic and industrial growth and a sustainable development of a country take place.

To deliberate upon the recent development in the area of energy mix and its impact and to exchange ideas on the related issues, The Institution of Engineers (India) has organized this International Conference 'Impact of Changing Energy Mix in Power Sector', to provide a suitable platform for the researchers from all over India and from abroad to present their original research work.

(ESTABLISHED 1920, INCORPORATED BY ROYAL CHARTER 1935)

Mest Bengal State Centre 8, GOKHALE ROAD, KOLKATA - 700020

Er. Sandip Kumar Deb, FIE
Chairman
Er. Kalipada Das, MIE
Honorary Secretary



Website : www.ieiwbsc.in

"100 Years of Relentless Journey Towards Engineering Adavancement for Nation-building"

The scientific and technological fraternity working in the field of energy mix and related issues responded to our call for participation, and contributed a good number of research papers. Papers accepted and included in this volume are reviewed thoroughly. It may be mentioned here that the final manuscript submitted by the authors following the recommendation received from the reviewers, have been published in full without editing. Regarding the results and comments presented in the papers, the responsibility lies with the respective authors.

Hope, the proceedings will be helpful to the future researchers and practicing engineers to carry out their work in the related field.

On behalf of the organizing committee and technical committee in particular, we extend our sincere thanks to the reviewers of the papers for their tremendous effort to maintain the schedule and standard of publication. Thanks are also due to all the authors who have painstakingly prepared their manuscript adhering to the format prescribed. Finally, we will be failing our duties, if we do not express our thanks to all those who have contributed in some way or other in the process through which this proceedings took its final shape.

Arabinda Das

Avalinda Das

[Technical Committee] [ICIEMPS-2019]

Subrata Paul

[Technical Committee] [ICIEMPS-2019]

Ashok Kumar Maitra

[Technical Committee] [ICIEMPS-2019]

Kolkata November 22, 2019



(ESTABLISHED 1920, INCORPORATED BY ROYAL CHARTER 1935)

Headquaters: 8, Gokhale Road, Kolkata - 700 020, India Website: http://www.ieindia.org

A Century of Service to the Nation

Dr T M Gunaraja, FIE President

MESSAGE



I am glad to know that West Bengal State Centre of The Institution of Engineers (India) is organising the International Conference on "Impact of Changing Energy Mix in Power Sector" on 23-24 November 2019 at Kolkata under the aegis of Electrical Engineering Division Board of the Institution.

I thank the organiser for choosing such a contemporary theme for the Conference. In the near future, India is set to be at the centre stage of the world's energy map. It is likely to contribute more than any other country to the projected rise in overall global energy demand. Still, Coal is the preferred fuel in the total supply mix. But to reduce greenhouse gas emission, India has set a target of substantial amount of Installed Capacity from Renewable Energy Sources by 2022. I am sure that the experts will highlight the issues related to the changes that the country is going to witness as it gradually shifts from fossil-based fuels to clean and sustainable renewable sources of energy. The recommendations out of the deliberations at the Conference will benefit the policy makers, implementing agencies and all concerned stake-holders.

I wish a grand success of the Conference and laud the efforts of West Bengal State Centre.

(Dr T M Gunaraja)



(ESTABLISHED 1920, INCORPORATED BY ROYAL CHARTER 1935)

Hest Hengal State Centre

8, GOKHALE ROAD, KOLKATA - 700020



A Century of Service to the Nation

Er. Sandip Kumar Deb, FIE
Chairman
Er. Kalipada Das, MIE
Honorary Secretary

Telephone: +91-33-2223 8914
E-mail: wbsc@ieindia.org
Website: www.ieiwbsc.in



Message

It is a matter of immense pleasure and great delightment that the Electrical Engineering Division, West Bengal State Centre, The Institution of Engineers (India) is hosting the two days International Conference on "Impact of Changing Energy Mix in the Power Sector" during November 23-24, 2019 at the LaLit Great Eastern Hotel, Kolkata. The Conference is being organized as a part of the Centenary of IEI under the aegis of its Electrical Engineering Division Board (ELDB) in collaboration with University of Johannesburg, South Africa and Techno India University along with knowledge partnership of World Federation of Engineering Organisation (WFEO).

Impact of Changing Energy Mix in the Power Sector - being established as new class of power sector reform are believed to be the answer to the quest of power sector with superior properties, the topic of the conference is very relevant and as on March 2019, the total Installed capacity for power generation in India is 350GW, out of which thermal capacity accounts for 64%, RES & others is 36%. The energy mix is projected to undergo radical changes with increased focus on RE (especially solar and wind) considering the operational and environmental issues related to coal power plants. The projected installed capacity by the end of 2026-27 is 619 GW, out of which RE will account for 44% of the total capacity. In future, India is set to be at the centre stage of the world's energy map. It is set to contribute more than any other country to the projected rise in overall global energy demand, around one-quarter of the total. We are really fortunate that this International Conference will be graced by the renowned experts in the field of power sector and will provide an open platform to the electrical engineering fraternity from across India and abroad and we are confident that through their participation and contribution, this conference should achieve its goal of exchange and enhancement of knowledge in this exciting field of modern science and technology.

We also express our sincere thanks and gratitude to all those who have extended their support both technically and financially to make this conference a grand success.

Sandip Kumar Deb

Telephone : 40106299, +91-33-2223 8311/14/15/16 Facsimile : +91-33-2223 8345 Web : http://www.ieindia.org

(ESTABLISHED 1920, INCORPORATED BY ROYAL CHARTER 1935)

Mest Bengal State Centre 8, GOKHALE ROAD, KOLKATA - 700020

Er. Sandip Kumar Deb, FIE
Chairman
Er. Kalipada Das, MIE
Honorary Secretary



"100 Years of Relentless Journey Towards Engineering Adavancement for Nation-building"



Chairman
Electrical Engineering Division
The Institution of Engineers (India), WBSC

Message

It is a matter of pride and honour to host the International Conference on the theme "Impact of Changing Energy Mix in the Power Sector" being organized by the West Bengal State Centre of the Institution of Engineers (India) during November 23rd to 24th at Kolkata.

The power sector in India is at an interesting crossroad. On one hand there are climate change concerns associated with conventional sources of energy while on the other there are challenges of integrating renewables sources with the grid and storage concerns. This changing energy mix is therefore throwing up new challenges for the power sector professionals, scientists, policy makers and consumers. The shift towards renewable energy will also require the development of new and efficient technologies, trained manpower in emerging jobs and government policies that ensure sustainable and economic operations.

Therefore, the International Conference on this very important theme will serve as a powerful platform to discuss the ways and means of addressing these present and future challenges. I am sure that the congregation of insightful minds will result in the formulation of a roadmap that will serve as an important contribution to this sector.

I am confident that together we will contribute to the successful conduct of this important scientific event in the infinite pursuit of knowledge.

Dr.P.K. Mukhopadhyay



8, Gokhale Road, Kolkata - 700 020

R R TANWAR, FIE
BE(E), C ENG (I), PGDMM, PGDPOM, PGADBM, MBA



Chairman, Electrical Engg. Division Board (ELDB).

Member Committee for Advancement of Technology & Engineering (CATE)

Member Board of Governors-Safety & Quality Forum(BOG-SQF)

Member All India Technician Committee (AITC)

FMR - Chief Project Manager, NALCO Smelter, NIDC (GOIU).

FMR - Chief Engineer (Elect.), NIDC (GOUI)

FMR - General Manager (Elect.), THDC India Ltd. (GOUI)

CEO & MD NGR RISING ENERGY

Message

It gives me immense pleasure to note that The Institution of Engineers (India), West Bengal State Centre is organizing Two Days International Conference on "Impact of Changing Energy Mix in the Power Sector" during 23rd & 24th November 2019 under the aegis of Electrical Engineering Division Board of Institution of Engineers (India) at Kolkata. The International Conference is very relevant for the purpose to highlight the issues related to the changes that the country is going to witness as it gradually shifts from fossil based fuels to clean & sustainable renewable sources of energy. Coal is the preferred fuels in the total supply mix; this is because of its costs competitiveness in comparison to other clean energy sources like Hydro Power etc. There is a scope for balancing this preference for Coal through appropriate policy intervention in other green and clean technologies.

As per latest report of Central Electricity Authority as on March 2019 the total Installed capacity for power generation in India is 350 GW, out of which thermal capacity accounts for 64%, RES & others is 36%. The energy mix is projected to undergo radical changes with increased focus on RE (especially solar and wind) considering the operational and environmental issues related to coal power plants. The projected installed capacity by the end of 2026-27 is 619 GW, out of which RE will account for 44% of the total capacity. With projected change in dynamics of energy mix, there is urgent need to develop storage technologies like Hydro Power & Pumped storage projects besides batteries to integrate 175 GW of renewable energy capacity by 2022. I feel a scientific study needs to be conducted to determine right kind of energy mix for stable operation of Indian Power Grid going forward.

I am sure that eminent speakers and the participants would deliberate on the issues during Two Days International Conference and come out with cost effective viable solutions and international best practices for the policy makers and others stakeholders.

I wish the event a great success and convey my best wishes to the participants & organisers.

R R TANWAR





15 October 2019

Many years ago, in June 1987, I attended 6th IEEE Pulsed Power conference, my first international conference in the USA. I was very excited but also appreciated the privilege to be part of a conference and meet people from across the world, all with a keen interest and much more knowledge than myself, in the field of power. As a young engineer the fact that researchers from all over the world share their work freely made a big impression on me. Fortunately for all of us who are eager to learn, this is still true today. By attending conferences we are able to freely share ideas and build networks. Ultimately, this is used for the improvement and wellbeing of humanity. I am therefore happy and privileged to be part of the *Impact of a Changing Energy Mix in the Power Sector Conference*.

Electrical supply companies are faced with many challenges today, for example: blackouts, distortion, unbalance in the network and high electricity cost. To ensure improved energy security and economic development and to increase electrical supply in rural areas, renewable energy technologies and the rollout thereof are on the increase worldwide, including India.

I welcome all attendees to this conference on the very important topic of the *Impact of a Changing Energy Mix in the Power Sector*. A reliable energy supply with a changing energy mix is very important for the wellbeing of a country. I am looking forward to an excellent conference which will also contribute to the advancement of our own research.

Yours faithfully,

Prof. Jan Harm C Pretorius, Pr Eng

Head of School: Postgraduate School of Engineering Management Professor: Faculty of Engineering and the Built Environment

University of Johannesburg Email: jhcpretorius@uj.ac.za

(ESTABLISHED 1920, INCORPORATED BY ROYAL CHARTER 1935)

Mest Bengal State Centre 8, GOKHALE ROAD, KOLKATA - 700020

Er. Sandip Kumar Deb, FIE
Chairman
Er. Kalipada Das, MIE
Honorary Secretary



Telephone: +91-33-2223 8914
Fax : +91-33-2223 3140
E-mail : wbsc@ieindia.org

: wbsc@ieindia.org iei.wbsc@gmail.com

Website : www.ieiwbsc.in

"100 Years of Relentless Journey Towards Engineering Adavancement for Nation-building"

Dr. Raju BasakOrganizing Secretary
ICIEMPS - 2019
Electrical Engineering Division
WBSC, IEI



Message

It is my proud privilege to announce that we, the Electrical Engineering Division, The Institution of Engineers (India), West Bengal State Centre has decided to organized this International Conference on "Impact of Changing Energy Mix in the Power Sector" on 23rd and 24th November 2019 at Hotel Lalit Great Eastern, Kolkata.

It is always endeavor of Electrical Engineering Division of West Bengal State Centre, IEI to update our members and interested technocrats about the ongoing developments in Electrical Engineering for its application in the Industry and establishments.

This program is also such an effort to apprise the interested community for shifting from fossil based fuels to clean & sustainable renewable sources of energy.

Hope the participant will enjoy the Technical sessions as well as technical lectures of this International Conference.

All your questions/comments and valuable suggestions during the discussion will be much appreciated. I thank you once again for your glorious presence in this Conference.

Dr. Raju Basak

Telephone: +91-33-2223 8311/14/15/16/34 Facsimile: +91-33-2223 8345

COMMITTEE

INTERNATIONAL ADVISORY COMMITTEE

Chairman : Prof. (Dr.) Samiran Choudhuri, FIE, Past President, IEI

Co-Chairman : Dr. T. M. Gunaraja, FIE, President IEI

Members : Prof. (Dr.) Jan Harm Christiaan Pretorius

Professor, University of Johannesburg Prof. (Dr.) Jens Bo Holm-Nielsen Professor, Aalborg University, Denmark

Mr Arvind Kumar Mishra

MD, Mangdechhu Hydroelectric Project Authority, Bhutan

Dr. Ratan Das, Founder, Ica Power, USA

Prof. (Dr.) Arnesh Telukdarie, University of Johannesburg

Dr. Surajit Bag

Sr. Research Associate, University of Johannesburg

NATIONAL ADVISORY COMMITTEE

Chairman : Dr. T.M. Gunaraja, FIE, President, IEI

Co-Chairman : Prof.(Dr.) Sivaji Chakravorti, FIE, Director, NIT Calicut

Members : Mr. Balraj Joshi, Chairman & Managing Director, NHPC Ltd.

Mr. V. K. Singh, Chairman & Managing Director, NEEPCO

Mr. Rajeev Sharma

Chairman & Managing Director, Power Finance Corporation Ltd.

Mr. D. V. Singh

Chairman & Managing Director, THDC India Limited Mr. Yatish Kumar, CMD, Braithwaite & Co. Ltd.

Prof. (Dr.) Gautam Sengupta

FIE, Vice Chancellor, Techno India University

Mr. Ranjan Chakravarti

Vice President, Tractable Engineering Pvt. Ltd. **Mrs. Debarati Basu,** Head, Eastern Region,

Power Research & Development Consultant Pvt. Ltd.

Prof. (Dr.) Parimal Acharjee, NIT Durgapur **Prof. (Dr.) Subrata Banerjee,** NIT Durgapur

Prof. (Dr.) N K Roy, NIT Durgapur Prof. (Dr.) Surajit Chattopadhyay

Ghani Khan Choudhury Institute of Engineering and Technology

Mr. R R Tanwar, FIE, Chairman, ELDB, IEI Mr. P Rajamani, FIE, Member, ELDB, IEI

Prof. Himansu Bikas Goswami, FIE, Member, ELDB, IEI **Mr. Mahendra Ratanlal Kothari,** FIE, Member, ELDB, IEI

Mr. R K Sharma, FIE, Member, ELDB, IEI

Prof. (Dr) Sudhir Kumar Calla, FIE, Member, ELDB, IEI

Mr. Rup Lal Mahajan, FIE, Member, ELDB, IEI Mr. M Marbaniang, FIE, Member, ELDB, IEI Prof. (Dr.) K K Rout, FIE, Member, ELDB, IEI

Mr. N S Singh, FIE, Member, ELDB, IEI

Mr. N K P Sinha, FIE, Member, ELDB, IEI Mr. N M Rao Nadella, FIE, Member, ELDB, IEI Mr. K K G Nair, FIE, Member, ELDB, IEI Mr. P R Natarajan, FIE, Member, ELDB, IEI

Mr. Donray Awungshi Shishak, FIE, Member, ELDB, IEI

Mr. S Dharmalingam, FIE, Member, ELDB, IEI Er. R Ramdoss, FIE, Chairman, TNSC, IEI Dr. R Kumar, FIE, Council Member, TNSC, IEI

Dr. Sunil Luthra, Asst. Professor

State Institute of Engineering & Technology, Haryana

STEERING COMMITTEE

Chairman : Dr. Prabir Kumar Mukhopadhyay, FIE, Chairman,

Electrical Division, WBSC, IEI and Member Secretary, Damodar

Valley Corporation, Govt. of India

Convener : Mr. Kalipada Das, MIE, Hony Secretary, WBSC, IEI and

Adjunct Faculty, Maulana Abul Kalam Azad University of

technology, Govt of West Bengal

Members : Mr. Sandip Kumar Deb, FIE, Chairman, WBSC, IEI and

Council Member, IEI

Mr. S. C. Rudra, FIE, Council Member, IEI Prof. K C Ghanta, FIE, NIT Durgapur,

Chairman, Durgapur Local Centre and Council Member, IEI

Mr. Kashmir Lal Mallick, FIE, Immediate Past Chairman, WBSC, IEI

Prof. (Dr.) Indranath Sinha, Joint Hony Secretary, WBSC, IEI and

Professor, IIEST, Shibpur

ORGANIZING COMMITTEE

Chairman : **Mr. Sandip Kumar Deb,** FIE, Chairman, WBSC, IEI

Working Chairman : Dr. Prabir Kumar Mukhopadhyay, FIE, Chairman,

Electrical Engineering Division, WBSC, IEI

Co-Chairman : Mr. R R Tanwar, FIE, Chairman, ELDB, IEI

Organizing Secretary : Dr. Raju Basak, MIE, Jt. Honorary Secretary, WBSC, IEI

Members : Prof. (Dr.) Swapan Kumar Ghosh, FIE

Mr. Aparesh Kanti Ghosal, MIE, Joint Convener

Mr. Gopal Chandra Dutta, FIE

Mr. Saroj Sarkar, FIE Mr. Prasanta Saha, MIE Mr. Anirban Dutta, Convener,

Mechanical Engineering Division, WBSC, IEI

TECHNICAL COMMITTEE

Chairman : Prof. (Dr.) Ashoke Kumar Maitra, IIEST, Shibpur

Co-Chairman : Prof. (Dr.) Subrata Pal, Jadavpur University

Members : Prof. Amar Nath Sanyal

Prof. (Dr.) Arabinda Das Prof. (Dr.) Gautam Sarkar Prof. (Dr.) Pradip Kumar Sadhu

PUBLICATION COMMITTEE

Chairman : Professor (Dr.) Nil Ratan Bandyopadhyay, FIE, Chairman,

MMDB, IEI and Professor, IIEST Shibpur

Co-Chairman : Dr. Subimal Roy Barman

Members : Dr. Debabrata Roy

Mr. Biswajit Basu Mr. Rakesh Das

FINANCE COMMITTEE

Chairman : Prof. Himansu Bikas Goswami, FIE,

Council Member and Member, ELDB, IEI

Co-Chairman : Mr. Smarajit Das (Convener)
Members : Mr. Subhomoy Dasgupta

Mr. Joy Chakraborty Mr. Prodip Golder

Mr. Gopal Chandra Gorai Mr. Debmoy Chakraborty

LOGISTIC COMMITTEE

Chairman : Mr. Sujit Kr. Banerji, FIE, Council Member, IEI

Co-Chairman : Mr. Prabir Choudhury

Members : Mr. Debasis Bandyopadhyay

Mr. Gadadhar Pan

REGISTRATION COMMITTEE

Chairman : Mr. Aparesh Kanti Ghosal Co-Chairman : Dr. Nabamita Banerjee Roy

Members : Mr. Manas Sanyal

Mr. Rakesh Das



PREFACE

The Institution of Engineers (India) [IEI] is a statutory body devoted to promote and advance the engineering science and technology, established in 1920 and incorporated by Royal Charter in 1935. It is the largest multi-disciplinary professional body of engineers encompassing 15 (fifteen) engineering disciplines with a membership of more than 0.8 Million, and serving the nation for more than 9 decades. The IEI has its headquarters located in Kolkata and it function through more than hundred Centers and several Overseas Chapters, Foras and Organ.

The IEI focuses on advancement of the Engineering and Technology and related areas. The IEI also conducts and sponsors technical meetings, conferences, symposia, and exhibitions all over India, publishes technical journals and provides continuing education as well as career advancement opportunities to its members.

Electrical Engineering Division Board of West Bengal State Centre, IEI is organizing this Conference with an objective to highlight the issues related to the changes that the country is going to witness as it gradually shifts from fossil based fuel to clean and sustainable renewable sources of energy.

We have received technical 126 papers on the related field from industries and academic institutions, from which only 56 papers have been selected after rigorous single blind review process. We express our thanks to the reviewers for giving their valuable time from their busy schedule.

We extend our sincere thanks to the National and International Advisory Committee members for guiding and inspiring us by providing their valuable advice.

We would also like to present our gratitude towards Authors, Sponsor, Technical Committee members, Keynote Speaker and organizing Committee members.

Dr. Subimal Roy Barman Mr. Aparesh Ghoshal Prof. (Dr.) Arabinda Das Dr. Raju Basak

An Overview of Renewable Energy Pricing Mechanisms

By MD SADIQUR RAHMAN BORUAH,

Abstract:

In this paper the existing mechanisms used for pricing of Renewable Energies practiced all over the world have been explained. The most commonly used Levelised Cost of Energy (LCOE) has been described with a little elaboration. Renewable Energy projects are incentivized to encourage investments in the sector to propel growth to meet the commitments to reduce the Greenhouse Gas (GHG) emissions by many governments in the world. Some methods utilized through policy interventions for incentives have been discussed.

Keywords: LCOE, LACE, FIT, RPO, REC

Introduction:

The method widely used for pricing or the determination of tariff for a generating plant is the Cost based where the tariff is determined by balancing the cost incurred by the plant with the future estimated revenues. In a regulated market the price is determined with a set of regulatory guidelines and policies framed for the purpose. The method so used provides security to the investments of the generating plants by guaranteeing a minimum return so as to recover the investment also at the same time protect the end consumers by fixing a reasonable price to pay for the service.

Renewable energy (RE) generations were earlier costly because of high capital cost and for the unpredictability and variability of generations. However in recent times the capital costs for most of the RE technologies have declined and also cost effective Smart Grid and Energy Storage technologies have emerged which could address

the issues of grid integration of REs (primarily Solar PV and Wind) effectively. As a result the price of REs particularly Solar PV has drastically declined.

Determination of price of RE generations:

Broadly the Mechanisms are used for determination of prices of RE generations-

(1) Cost based tariffs[1]

The levelized cost of generation/energy (LCOE / LCOG) is an economic assessment of the average total cost to build and operate a power-generating asset over its lifetime divided by the total energy output of the asset over that lifetime. The LCOG can also be regarded as the average minimum price at which electricity must be sold in order to break-even over the lifetime of the project.

LCOE= Sum of costs over life time

Sum of electrical energy produced in life time

$$= \frac{\sum_{t=1}^{n} \frac{I_t + M_t + F_t}{(1+r)^t}}{\sum_{t=1}^{n} \frac{E_t}{(1+r)^t}}$$

International Conference On "Impact of Changing Energy Mix in the Power Sector" (ICIEMPS-2019) The Institution of Engineers (India), WBSC $23^{\rm rd}~\&~24^{\rm th}$ Nov. 2019

Where,

It : Investment expenditures in the year t

M. . Operations and Maintenance expenditures in

the vear t

Ft : Fuel expenditures in the year t, if any

Et : Electrical energy generated in the year t

r : Discount rate

Expected lifetime of the system or the power

station

Salient features of cost based tariffs-

- Based on a project developer's operating and capital costs along with an assured return on capital
- Cost components typically comprise of Operation & Maintenance expenses (including any escalation), Loan repayment and Fuel Cost (if any)
- Technology specific tariffs based or performance and costs
- The cost based approach is heavily dependent on cost and performance parameters as input data

The LCOE of renewable energy technologies varies by technology, country and project, based on the renewable energy resource, capital and operating costs, and the efficiency/performance of the technology.

This method of calculating the cost of renewable energy technologies is based on discounting financial flows (annual mainly) to a common basis, taking into consideration the time value of money. Given the capital-intensive nature of most renewable power generation technologies and the fact that fuelcosts are low, or often zero, the weighted average cost of capital (WACC) used to evaluate the project is used as the discount rate – has a critical impact on the LCOE. There are many potential trade-offs to be considered when

developing an LCOE modeling approach. The various assumptions have to be based on real world data else it may lead to inaccurate result.

One drawback of LCOE is that it ignores time effects associated while matching generation to demand. This happens at two levels:

- Dispatchability, the ability of a generating system to come online, go offline, or ramp up or down, quickly as demand swings.
- The extent to which the availability profile matches or conflicts with the market demand profile.

Capital intensive technologies such as wind and solar are economically disadvantaged unless generating at maximum availability since the LCOE is nearly all sunk-cost capital investment. As such they may incur extra costs to have storage or backup generation in case it is so needed. At the same time, intermittent sources can be competitive if they are available to produce when demand and prices are highest, such as solar during summertime mid-day peaks seen in hot countries where air conditioning is a major consumer. Despite these time limitations, leveling costs like for energy storage is often a necessary prerequisite for making comparisons on an equal footing before demand profiles are considered, and the levelized-cost metric is widely used for comparing technologies at the margin.

Some important assumptions standardized for calculating LCOE:[2],[3]

As was said earlier, for estimation of an accurate of value of LCOE the assumption of various input data should be real world based. Based on the prevailing conditions, the assumptions can be standardized in different countries and regions. Below, some assumptions that have been in use in different countries is shown –

(a) Economic life of different RE Technologies:

Technology	Economic Life (Years)
Wind Power	25
Solar PV	25
CSP	25
Hydropower	30
Biomass for Power	20
Geothermal	25

(b) Capacity Utilisation Factor:

This is an important factor used to estimate the projected annual energy output(E_t in the year t) of the candidate project. This factor depends on the efficiency of the technology utilized to convert the resources in to useful energy(electrical), availability of the resources in the area and also on the load shape and the existing resource mix in an area where additional capacity is needed. Proper assessment of the load demand and the technology efficiency needs to be carried out to accurately estimate the output.

(c) Discount Rate estimation:

The discount rate is assumed as the Weighted Average Cost of Capital (WACC) of the project/technology. This is calculated as below-

WACC = (%of the Equity Capital in the Project Cost) x (Post Tax Return on Equity in %)

+

(%of the Debt Capital in the Project Cost) x (% Interest rate on Debt after deducting Tax benefit on interest, if any)

(d) O & M Cost:

Solar PV:

Country	Value Per Year
USA	10-19 USD/kW
India	10-11 USD/kW
**OECD market	20-25% of the value of LCOE

** OECD stands for Organisation for Economic Cooperation and Development, a front body consisting of 36 countries.

Onshore Wind:

Country	Value Per Year
USA	10-19 USD/kW
India	10-11 USD/kW
**OECD market	20-25% of the
OECD Market	value of LCOE

Concentrated Solar Power (CSP):

Type (all countries)	Value Per Year
Parabolic Trough Collector (PTC)	0.0203 USD/kWh
Solar Tower (ST)	0.03-0.04 USD/kWh

Onshore Wind:

	Variable	Fixed cost
Country	cost Per	Per Year
	Year	
OECD	0.01-0.04	52-79
countries	USD/kWh	USD/kW
India		12-15
IIIuia		USD/kW

Offshore Wind:

	Variable	Fixed cost
Country	cost Per	Per Year
	Year	
OECD	0.02-0.05	52-79
countries	USD/kWh	USD/kW
India		35-40
India		USD/kW

Small Hydropower:

Country	Cost per year
OECD	2% to 3% of the
countries	Project Cost
India	3% to 4% of the
IIIuia	Project Cost

Bioenergy:

Average for OECD countries:

	Fixed cost	Variable
Technology	(% of Project	cost
	Cost) Per	(USD/MWh)
	Year	Per Year
Stoker/Bfb/Cfb	3.2	4.25-5.25
Boilers	5.2	4.25-5.25
Gasifier	3-6	4.25
Anaerobic	2.1-3.2	4.68
Digester	2.1-3.2	4.00
Landfill Gas	11-20	

Average for India (Bioenergy):

	Fixed cost (% of	
Technology	Project Cost) Per	
	Year in USD	
Stoker/Bfb/Cfb	3.2	
Boilers	3.2	
Gasifier	8-9	
Anaerobic	4-5	
Digester	4-5	

Geothermal:

O & M cost for Geothermal is assumed at USD 11/KW per year based on average in different countries/locations

Important issues inLCOE pricing of RE:

Apart from other costs like operating cost, cost of capital, depreciation just like other conventional generation, the following points are to be taken into account in pricing.

(i) Renewable Energy generations are unpredictable in nature. The generation of a plant depends on the weather conditions. Unlike conventional fossil fuel based power plant where the production is almost within the human control, the same is not true in case of RE plant. Long term average generation predictions are made based on historical measured data of the resources (Solar Irradiation in case of Solar plant and Wind velocity in case of Wind plant) of that particular area. Thus it is not possible to fix a generic performance or capacity utilization of RE assets for a particular technology. This is very much depended on the location of the plant.

Hence, this aspect of energy generation of a RE plant is to be taken into account while working out of the price.

(ii) Because of the variability and of RE unpredictability generations, manv countries have made it obligatory to incorporate energy storage system of grid scale along with the plant in order to mitigate the impact on the grid. In such cases the cost of the storage systems which are of considerable costs also need to be taken into account.

(2) Avoided cost based tariffs

It is a measure of what it would cost the grid to generate the electricity that is otherwise displaced by a new generation project, as well as its levelized cost. Avoided cost, which provides anestimated measure for the annual economic value of a new project under consideration, may be summed over its financial life and converted to a stream of equal annual payments. The avoided cost is divided by average annual output of the project to develop the "levelized" avoided cost of electricity (LACE) for the project.

LACE=
$$\sum_{t=1}^{n} \frac{A_{t}}{(1+r)^{t}} = \sum_{t=1}^{n} \frac{E_{t}}{(1+r)^{t}}$$

International Conference On "Impact of Changing Energy Mix in the Power Sector" (ICIEMPS-2019) The Institution of Engineers (India), WBSC $23^{\rm rd}~\&~24^{\rm th}$ Nov. 2019

Where,

At : Avoided Cost in the year t

r : Discount rate

n : Expected lifetime of system or power

station

The US Energy Information Administration has recommended that levelized costs of non-dispatchable sources such as wind or solar may be better compared to the avoided energy cost rather than to the LCOE of dispatchable sources such as fossil fuels or geothermal. This is because introduction of fluctuating power sources may or may not avoid capital and maintenance costs of backup dispatchable sources. Levelized Avoided Cost of Energy (LACE) is the avoided costs from other sources divided by the annual yearly output of the non-dispatchable source. However, the avoided cost is much harder to calculate accurately.

Salient features of avoided cost based tariffs-

- Incremental cost to the electric utility that the utility would either generate itself or purchase elsewhere if it did not purchase from a (renewable energy) supplier
- Prices being set equal to marginal cost results in market equilibrium at a certain level and pattern of electricity supply that leads to the most efficient allocation of scarce resources
- A detailed performance data of all conventional power plants, in terms of plant availability and energy generation is required

(3) Marginal cost based pricing[4]

Marginal cost of generation or energy is the additional cost incurred in producing one unit of

energy (kWh). Marginal costs include every cost incurred to bring that one more unit to the market. If producing one more kWh requires building a new power plant, that plant is included in the marginal cost. This is marginal cost at its most basic level. It seems straightforward, but there are many different circumstances that play a role in the determination of this price that create complexity.

Marginal energy prices represent a theoretically valuable and challenging refinement to the usual life-cycle cost analysis conducted for assessment of a proposed project. Marginal prices, from a consumer perspective, are those prices consumers pay (or save) for their last unit of energy used (or saved). For utilities, marginal electricity costs are the costs experienced by utilities for the last unit(kWh) of electricity produced. A utility's marginal cost can be higher or lower than its average price, depending on the relationships between capacity. generation. transmission, and distribution costs.

Power markets with diverse energy mix operating on marginal cost based price discovery use the price set by marginal cost of the last producer needed to cover all load, usually that is a fossil fuel power plant. In such a situation addition of renewable generations would impact the price levels as the renewable plants mostly built with government supports would have low marginal cost.

Incentives and subsidies:

Many countries want to become energy independent and minimize their carbon footprints as part of their obligations to minimize greenhouse gas (GHG) emissions. Renewable energies (REs) are the alternatives to replace emissive fossil fuel based power generation. The standard costing mechanisms as mentioned above do not cover the external environmental and social benefits a renewable project brings. As such the renewable generators are remunerated

through some policy driven mechanism for this "Generic" for the particular technology, extra benefit. Some of the prominent incentives preferential tariff system the tariff has been fixer are -

(i) Feed-In Tariff (FIT): [5]

The structure of a feed-in tariff is relatively simple. In order to increase investment in technologies that have not advanced enough to become costefficient, in a FIT system, governments pay private firms a premium over market price for electricity generated renewably. The tariff generally has three provisions: the energy producer is guaranteed continued access to the grid, the purchase agreement exists over a long period of time (10-25 years) at stable prices, and the payment levels cover both the costs of generating the renewable electricity and a small premium to ensure profitability. Because investors are almost guaranteed to make a profit under this FITs have historically caused an system, explosion in renewable investment that has led to more advanced, efficient energy technologies in the long term. Ideally, investments achieve "grid parity" at some point, meaning they become costcompetitive compared to other methods of electricity generation, and will be able to function with no additional government spending into the future.

Although the success of feed-in tariffs has varied slightly based on location, geography, resources, and the sophistication of various grids, FIT implementation has been largely successful. Feed-in tariff policies are now in place in 87 different jurisdictions, and Germany became the first country to achieve grid parity by using FITs when its PV technology became cost competitive with other sources of electricity in 2014.

(ii) Preferential Tariff:

The basic difference in preferential tariff from FIT is that while FIT is fixed for all the plants built across the same technology or in one word it is

"Generic" for the particular technology, in preferential tariff system the tariff has been fixed using the same methodology of LCOE applied for other non-RE technologies but with higher values of return on equity, shorter loan tenure, accelerated depreciation, energy generation as assessed for the particular area and appropriate normative rate of interest on debt. In some technologies like small hydro power projects, the actual project cost is also considered instead of a normative project cost in determining the tariff. Thus the preferential tariff so calculated yields a higher value comparing to that of a non-RE technology.

(iii) Renewable Purchase Obligation (RPO) and Renewable Energy Certificate (REC): [6]

Renewable Purchase Obligation (RPO) refers to the obligation imposed by law on some entities to either buy a specified portion of their energy requirements from electricity generated byrenewable sources, or buy, in lieu of that, 'renewable energy certificates (RECs)' from the market. The 'obligated entities' are mostly electricity distribution companies and large consumers of power. RECs are issued to companies that produce renewable energies, who opt not to sell it at a preferable tariff to the distribution companies. These RECs represent proof of renewable electricity delivered to the grid and the environmental effect of that renewable electricity to reduce the average grid emissions near the project that produced the RECs.

RECs are marketable commodity; the renewable generators who are issued RECs can sell those certificates to entities who are obligated to reduce emission by sourcing a stipulated portion of their energy requirements from renewables. A retail REC purchase provides no physical delivery of electricity to customers. The customer

purchasesits physical power from a separate lower the cost in a market dominated by fossil fuel entity than the one selling them the RECs.

Recent Trend in pricing RE:[7]

Tesla has recently started renting out their Solar panels to prosumers(consumers who also produce). The price is based on the installed capacity(kW or MW) not on the volume of energy (kWh) produced. This may lead to a paradigm shift of charging for RE consumers. This will be a very simple mechanism and will do away with the References: need of energy metering and related overhead.

Conclusion:

Out of all these pricing mechanisms the cost based LCOE (levelised cost of energy) is the most commonly used mechanism all over the world. Because it is simpler, convenient and results a more reasonable price if the assumptions made for various inputs are based on real world data. However this mechanism has some limitations. Key inputs to calculate LCOE include capital costs, fuel costs, fixed and variable operations and maintenance (O&M) costs, financing costs, and an assumed utilization rate for each plant type. As with any projection, there is uncertainty about all of these factors and their values can vary regionally and across time as technologies evolve. In order to make a better assessment of a new project as far as its value to be added to the grid is concerned, the Levelised Avoided Cost of Energy (LACE) mechanism can be used. The LACE value may then be compared with the LCOE value for the new project to provide an indication of whether or not the project's value exceeds its cost. If multiple technologies are available to meet load, comparisons of each project's LACE to its LCOE may be used to determine which project provides the best net economic value.

Pricing at marginal cost for electricity is not suitable for a renewable project as it would tend to

based plants. So, marginal cost based pricing is not generally recommended to assess a renewable project supported with incentives and subsidies.

There is likelihood that RE pricing may shift to capacity based instead of present generated based. This pricing system will not need metering arrangement and will reduce operational cost.

- https://en.wikipedia.org/wiki/Cost_of_electr icity by source
- 2. Renewable Power Generation Cost in 2018 by IRENA
- 3. CERC (Central Electricity Regulatory Commission, India) RE Tariff Order 2019-20
- 4. https://fresh-energy.org/how-marginalcost-pricing-impacts-rates/
- 5. http://large.stanford.edu/courses/2016/ph2 40/barry2/
- 6. https://www.epa.gov/greenpower/greenpower-pricing
- 7. https://www.extremetech.com/extreme/296 847-tesla-begins-renting-solar-panels-foras-little-as-50-per-month
- 8. Levelized Cost and Levelized Avoided Cost of New Generation Resources in the Annual Energy Outlook 2015 :: US Energy Information Administration

Installation of Roof Top 50 KWp Solar Photovoltaic Power Plant-Grid Connected

Tuhin Das (EEE, AM, CE) Assistant Manager-Tech (Elect) NTSC-Howrah

Introduction:

In support of Renewable and Green Energy and as per Guideline of MNRE, Govt. Of India installation of Roof Top Solar Power Plant is going on all over the India.

Renewable energy sources will the future of the primary energy resources all over the world. China is the biggest investor in the field of Solar Energy Mix in Power Generation in the world.

For the development of a country there must be sufficient energy sources of its own. Developing new energy sources within a nation is the key for the development of the particular nation. At present the majority of electric energy is coming from oil, coal, nuclear which are going to finish in a very short time. To sustain economic growth and to overcome the energy deficit situation we must have to utilize our immense potential in solar energy in all areas specially in power sector. India is the only country which have a Ministry dedicated to New and Renewable Energy that is MNRE but still more efforts to be made in various stages to accelerate the development in the field of Green Energy Mix In Power Generation. It is expected that by 2050 there will be 2/3 of our Energy in power sector from sustainable energy sources.

ENERGY SECURITY - ECONOMIC SECURITY - NATIONAL SECURITY

Fortunately, India lies in sunny regions of the world. Most parts of India receive 4.7 kWhof solarradiation per square meter per day with 300-325 sunny days in a year. India has abundant solarresources, as it receives about 3000 hours of sunshine every year, equivalent to over 5,000 trillionkWh. India can easily utilize the solar energy. Today The Government encouraging generationof electricity from various renewable energy sources such as wind, solar, small hydro, biomass bygiving various fiscal & financial incentives. This the state governments apart, are procuringelectricity from renewable energy projects at preferential tariff. So far 29,536 MW of renewablepower capacity have been installed in the country, which includes 19,933 MW from wind, 2079MW from solar, 3746 MW from small hydro and 3776 MW from bio energy. The Ministry of New andRenewable Energy is providing various renewable energy systems fordecentralized generation of electricity. So far, 10,752 villages have been electrified using variousrenewable energy systems. About 2.55 lakh solar street lights, 9.93 lakh solar home lighteningsystems, 9.39 lakh solar lanterns and 138 MW of decentralized solar power plants have beeninstalled.

Socio-Economic Justification:

Now a days there is growing trend in installation of Roof Top Grid Connected

Solar Power Plant world wide. In grid connected system the solar power can be utilized to its full potential. All the requirements are being fulfilled by the site condition of NTSC-Howrah.

The project will add the power in utility grid thus indirectly will reduce the import of power from other source.

Non-renewable energy sources like fossil fuel, oil, nuclear energy, Natural Gas, etc are remains in limited quantity and are going to finish in a very short time. Whereas the abundant sun light is available with us for the next 5 billion years as per scientist.

We use very less renewable energy for production of electricity in India. Coal has the major contribution in India for the Generation of Electricity through thermal power plant. But Coal generate pollution and will be finished soon at present R/P ratio.

In connection with the energy mix power generation solar power plants which is pollution free at generation level, considered as green energy, and abundant availability of solar energy plays an important role to produce and export electricity power to the grid. This will reduce pollution.

Installation of 50 KWpRoof Top Grids Connected Solar Power Plant:

The Solar Power Plant is of 50 KWp capacity connected directly to the Grid. The solar panels mounted in the roof can generate DC Electric Power which can't be directly fed to the utility grid which is a AC System. The Grid Connected Inverter (GCI) invert the DC Power output from the solar array into grid compliant Conventional 3 Phase AC Power and fed into the utility grid system with proper protection and control.

AC Power from inverters will be fed to LV Panel.

The system automatically starts whenever it receive solar energy and starts to export power to the grid , provided there is sufficient solar energy and the grid voltage , frequency within the range. If the grid goes out of range the inverter will be immediately disconnected and reconnected automatically at a predetermine time after the grid comes back within the range.

Monitoring system provided with the system is mainly used to monitor the performance of the Inverters, Energy Yield, Temperature, Irradiance Level etc. It provides an extremely flexible interface to facilitate PC-based inverter monitoring via analog modem, GSM, Ethernet or Internet Connection.

Bi-directional meter is installed to calculate import and export of power from Grid.

For protection earthing to be provided for each module. There must be minimum 5 earthing pits. Two earthing pits for DC Panels, Two earthing for AC Side, and two earthing for LA. There must be earthing for Inverter also.

Impact of the Solar Energy in Power Sector:

Cost of Electricity:

It has been observed that the cost of the solar energy have been reduced by 80% than 2010.

The latest cost is approximate Rs.2.41/Unit. Reduce Carbon Emission:

By reducing the electricity generated by thermal power plant use coal as a fuel the carbon emission is also reduced which leads to clean and green energy and will reduce global warming. Pollution will also be reduced.

Profitable Investment:

The investment in solar power plant is a profitable investment because it can give return within 5-6 years. Most of the solar panels are having warranty of 25 years. In case of a project the maintenance is free for 5 years. By reducing the electricity bill it becomes free after 5-6 years.

Suitable for Indian climate Rooftop solar panels utilize sunlight to convert it into electricity. India is situated at an ideal geographical location and receives ample tropical sunlight. There are almost 300 sunny days with clear skies each year in India. Thus, rooftop solar panels are ideal to be used here.

Multiple applications of solar power

Along with the generation of electricity, solar power can meet several other purposes. It can be used to heat water and supply hot water or air to a building. It can also be used to run electric generators.

Efficiency of Roof Top Solar Power Plant:

Performance Ratio: The performance ratio is a measure of the quality of a PV plant that is independent of location and it therefore it is also called as Quality Factor. If the PR value is 100% than it is assumed that the plant is operating at maximum efficiency. However, some losses are there which are always unavoidable, as a result practically the maximum efficiency we get i.e 80%.

Formula for manual calculation of the performance ratio:

PR =(Actual reading of plant output in kWh p.a.) /(Calculated, nominal plant output in kWh p.a.)

Factor Influence The Efficiency of Roof Top Solar Power Plant:

Environmental factors:

- i) Temperature of the PV module
- ii) Solar irradiation and power dissipation
- iii) The measuring gage (e.g. Sunny SensorBox) is in the shade or soiled
- iv) PV module in the shade or soiled

Other factors:

- i) Recording period
- ii) Conduction losses
- iii) Efficiency factor of the PV modules
- iv) Efficiency factor of the inverter
- v) Differences in solar cell technologies of the measuring gage and of the PV modules.
- vi) Orientation of the measurement gage (e.g. Sunny Sensor Box).

Reduce Of Electricity Bill:

At present the Electrical Energy Consumption of NTSC-Howrah is 7500 Kwh / month.

Solar power plat will produce 3.6 Kwh/KWp/Day (Considering 4 pear hours of high intensity of sun light in a Day)

Then total Kwh per month from solar plant will be – 5400 Kwh/month.

Solar Plant will reduce the energy charges by – Rs.7.20 X Kwh 5400 = Rs.38880/-

Location-NTSC (Howrah), Balitikuri-711113

Soft Computing for Integration and location of Wind Power Generation in a Distributed System

Dr. J.Vijaya Kumar
Department of Electrical Engineering
ANITS(A)
Visakhapatnam,India
jvkeee@gmail.com

T. Mahesh Department of Electrical Engineering NIT Warangal Warangal, India Adarsh. C. Anand Dept. of EEE, ANITS(A) Visakhapatnam,India

Abstract—Wind generation is one of the leading renewable energy sources and has much potential to improve the distribution system performance by reducing Transmission and Distribution losses and improve the voltage stability of the system. The paper here describes, modeling and simulation of wind power generation, with AC/DC-DC/AC conversion are done by using PSCAD software. The optimal location of the DG is determined based on voltage index and loss reduction index using Fuzzy IF-THEN rules on an IEEE-33 bus distribution system. The Simulation process is carried out with and without DG penetration at the optimal location. From the simulations results it is observed that there will be reduction in losses and there is improvement in voltage profile with DG penetration at optimal location.

Keywords— Distributed generation, distributed system, optimal location, fuzzy, PSACD Introduction

I.Introduction

A small-scale generation situated at or near the load centers is known as "Distributed Generation". It is also been known as on-site generation, embedded generation, distributed decentralized generation, energydispersed generation etc..,With high availability uncertainties wind power is well known intermittent power source in distributed generation. Wind energy plays an important role in future energy generation in most of the areas of the world due to its high reliability and the level in sophistication of wind turbine technology and the reduction in cost. Generally, most of the wind turbines are connected to distribution grids not to the main grids still now. And because of this reason, these generators which provide power through wind affect the current flow and also power flows in the distribution system to which the connections are made, and voltages at the nodes are mainly related to power flows and are changed accordingly. When injecting wind power into a distribution grid, voltage quality is changed [1].

Induction machines are sometimes used as generators, in wind power stations, but with the new permanent magnet generators development, the AC-DC-AC conversion improvement and the advantages for other solutions are possible. The use of permanent magnet generator is a recent solution with a conversion stage and variable speed [2]. There are many uncertainties in various power system problems. Because of this it becomes very difficult to stick to mathematical formulae alone. To overcome this, theory

of fuzzy set has applied for many problems of the power systems. Fuzzy sets theory (FST) provides a solution for the lack and uncertainty in the data given. Huristic rules are used for fuzzy expert system to determine the placement suitability index at each node in the distribution system. Rules are defined to determine the suitability of a node for DG unit placement [3]-[7]. Load Flow is a power system analysis approach that determines the steady state system operating conditions. For the analysis of power systems it is very important toolfor the operation as well as planning stages. In some applications, especially in automation distribution and optimization require repetitive load flow analysis. As the power distribution networks become more and more complex, there is a higher demand for efficient and reliable system operation. The distributed network is a radial network and the current measurement are based on the protection [8].

In this paper wind power generation and AC/DC – DC/AC conversion was modeled for IEEE-33 bus radial distribution system using PSCAD software and optimal placement of DG is determined by calculating loss reduction index and voltage index by running load flow analysis and these inputs are given to the fuzzy inference system in order to obtain the location of DG at optimal locality.

II. DG ON DISTRIBUTION SYSTEM

A. Wind power Generation

Distributed Generation (DG) is assumed to play a vital role in the electric power generation system of the future. Photovoltaic, wind turbines, fuel cells and internal combustion engine-generators are included in DG technologies [9]-[11]. The paper is a consideration of a permanent Magnet Synchronous Generator to which a wind turbine is attached with 100 pairs of poles. The connection is given to AC/DC-DC/AC converter and a step up transformer from the grid. This method helps in the removal of the gear box in the system. The wind source component simulates every condition of the wind i.e. Mean wind speed, sinus form of Periodic gust, NoiseRamp, and Damper for all the conditions that are preceding. Thefollowingthree wind characteristics are important for a wind turbine:

The mean wind speed: The rated characteristics of the turbine and the generator are determined according to the mean speed of the wind. Based on the speed of the wind

economic studies are also developed. The mean speed of the wind is nearly equals to 13 m/s, in general.

The cut-in speed of wind: mechanical brakes are released, at speeds higher than the cut-in speed, in order to turn the turbine. Generally, the cut-in speed of the wind nearly equals to 4 m/s.

The cut-out speed of wind: the turbine rotation is stopped when the speeds are higher than the cut-out speed,to avoid damage to the blades of the turbine.

Generally, the cut-out speed of the wind nearly equals to 25 m/s. The speed of the wind is regulated throughout a day in dynamic simulations. The speed of windshould vary from the cut-in to the cut-out speed of the wind in order to analyzethe reaction of the wind turbine for all the conditions of wind flow. The paper here describes, a beginning below the cut-in speed of the wind and a termination above the cut-out speed of the wind are neglected. The range of speed of the wind is limited to 4m/s and 25m/s. Theoretical study of wind turbine as follows:

Through the rotor blades, the kinetic energy of the air is:

$$E_c = \frac{1}{2} m W_s^2 \tag{1}$$

The power from a wind turbine is given by:

$$P_{th} = \frac{1}{2} \rho SW_s^3 \qquad (2)$$

Where ρ = density of the air given by 1.22 kg/m³

S = surface of the rotor (m²)

 W_s = speed of the wind (m/s)

Practically, because of the wind speed the power obtained is less which is not 0 behind the hub. The efficiency obtained is analyzed by the coefficient of Betz (by Bernoulli's equations), also called as the Coefficient of power (C_p) and is given by

$$C_{P} = \frac{P_{real}}{P_{th}}$$

$$C_{p} = \frac{1}{2}(1-a)^{2}(1+a)$$
 (4)

Where,a= speed of the wind behind the rotor / speed of the wind in front of the rotor.

The parameters of permanent magnet generator shown in Table I

TABLE I. PARAMETRS OF PERMANENT MAGNET GENERATOR

pole pairs number	100
speed at 50Hz	$2\pi f/100 = 3.1416 \text{ rad/sec}$
power	S _n =100 MVA
voltage	0.69 kV
X _d	0.4 p.u
current	$I_n = S_n/(3V_n) = 1450 \text{ A}$

Power Coefficient (C_p) computations at rated conditions are as follows: Hub Speed when there is no gear box = rated speed of the permanent magnet Synchronous Generator.

The mean wind speed at the nominal speed: 13 m/s.

$$\gamma$$
 = Wind Speed*2.237/Hub Speed (5)

$$= 13*2.237/3.1416 = 9.25$$

Then the value of

 $C_p (\gamma = 9.25, \beta = 0) = 0.4$ as depicted in Fig.1.

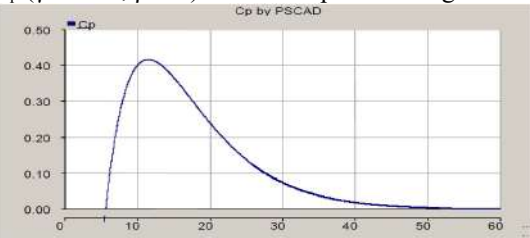


Fig. 1. Power Coefficient (Cp) with $\gamma = 9.25$, $\beta = 0$.

Generally, the turbine rating is 20% greater than the generator because of the friction in the cycle of machanics.

Rated power of the Turbine calculations are as follows:

Rated Power of the Turbine: $S_{nturb}=1.2 * 3 = 3.6 \text{ MVA}$

Computation of the radius of rotor(R) and Area(S):

In PSCAD the formula given to the power:

$$P = 0.5 \rho S W_s^3 C_p$$
 (6)

with $C_p = 0.4$, $W_s = 13$ m/s, $\rho = 1.22$ kg/m³, R = 46.2 m S = 6716 m²

Theoretical study of wind turbine governor:

$$C_p = 0.5(\gamma - 0.022\beta 2 - 5.6) e - 0.17\gamma$$
 (7)

The β regulation enables the C_pregulation and therefore enables the control of the output power of the turbine depends on the conditions of the wind.Permanent magnet synchronous generator with a classical synchronous model with constant excitation voltage is 1 p.u.

Transient time for large instauration is ' T_{do} ', and the field leakage increases to 10 s. A small unsaturated sub transient time is given by ' T_{do} ', large damper resistance of 0.0001s effect and field current is nearly too permanent value.

Wind speed = rated value = 13 m/s β is forced to be 0 in order to have the maximum power and the wind turbine delivers 3.6 MW:

$$P = 3VI\cos\Phi \tag{8}$$

 $= 3V_2R/Z_2$

$$= 3V_2R / (R_2 + X_{d2})$$

With $X_d=0.4$ pu = 0.4* $V_n/I_n=0.4*$ 690/1450=0.19 Ω The generator rated load is given by: R=0.257 Ω .

The wind speed source is a variable, a converter AC/DC-DC/AC should be developed for the connection to the output of the synchronous generator of the grid.

The power conversion stages and parameters are described as follows:

It comprises of a Rectifier, DC bus, and 6-pulse bridge thyristor inverter. The present model demonstrates a single wind turbine and the firing angle of the thyristor are not controlled functions of the voltage level at the grid connection point but to keep the DC bus voltage to its threshhold level +/- 10%. This involves the modeling of HVDC control systems. AC/DC -DC/AC Conversion and 3-phase rectifier are modeled in PSCAD.

Design of over voltage protection:

The DC voltage is given by

$$V_{DCbus} = (3*V_n*\sqrt{6}) / \pi = (3*690*\sqrt{6}) / \pi = 1600 \text{ V}$$

The generator output voltage is proportional to the speed. The generator speed is not controlled and so there is necessity for the DC bus protection from over-voltages with secure margin of 10%, and voltage = 1.1*1600 = 1760 V.

For the bus security, rectifier should be blocked, if possible in case of over-voltages. The Single Input Level Comparator should do this. In "Master Library/CSMF" programming this type of component is found.

Design of DC bus:

CapacitanceStorage: The storedenergy in the DC bus must be tolerated to the voltage sags up to 1 second.

The stored energy must be $W = P_n*1s=3MJ$.

$$E = \frac{1}{2} * C * (V_{DCbus})^{2}$$

$$V_{DCbus} = 1600 V$$

$$C = 2*W / (V_{DCbus})^{2} = 2*3*1e^{6} / 1600^{2} = 2.3 F$$

Resistor: when the capacitor is discharged, it should be short circuited. In order to limit the current peak, a resistor has to be added to the rated value when there is low charge for the capacitor.

$$\begin{split} V_{DCbus} &= V_{res} + V_{cap} \approx V_{res} \text{ at low charge} \\ R &= V_{DCbus} \, / \, I_n = 1600 \, / \, 1450 = 1.1 \, \, \Omega \end{split}$$

Breaker: first order system and time constant of the load is given by $T_r = 3 * \tau (\tau = RC)$

$$T_r = 3*RC = 3*1.1*2.3 = 7.5 s$$

The resistor should be shunted after 7.5 seconds in order to control the Joule losses.

To shunt the resistorasingle-phase breaker will be used.

The DC bus and operation of the breaker are modeled in PSCAD.

6-Pulse Thyristor inverter: The paper here describes, the modeled inverter with thyristorsis a current inverter (monodirectional in current, bi-directional in voltage). In order to model a current source an inductor is added at the input of the inverter.

Design of Inductor: The energy in the DC bus must be enough to bear a voltage sag of 1 second W= 3000000 J.

The energy stored in a self-inductor is $W = \frac{1}{2} * L * I_{dc}^2$

$$I_{dc} = P_{dc}/V_{dv} = 3*1e^6/1600 = 1875 A$$

$$L = 2*E / I_{dc}^2 = 2*3000000 / 1875^2 = 1.7 H$$

Inverter:To obtain a thyristor current inverter, the 6 pulse bridge component is used to serve the purpose. Theexhibition of high changes in overtime of current is done by CSIs and due to this reason capacitors are generally employed on the AC side, while inductors are generally employed on the DC side. The power circuit is reduced in size and weight, due to the absence of freewheeling diodes and this is more reliable than VSIs. The inverter also provides two other functions, i.e. limitation in case when DC bus voltage is collapseddue fault on the distribution system, voltage control on DC bus and limitation in voltage collapse.

In case of fault condition, the bus must be protected from short-circuit on the distribution network; otherwise, there will be collapse in the voltage. The secure margin is about 10% for the overvoltage limitation. Limitation for the low voltage =0.9*1600=1440~V

The rectifier is stopped in the low-voltage case for the security of the bus. The analysis is done by the Single input level comparator component. The single input level comparator is connected to the inverter in order to obtain the following scheme.

Regulation of the voltage:One single wind turbine is to be modeled at this point of time. The voltage control is done on the DC bus and at the connection point because of the weak impact of the turbine. The fluctuation of the voltage in the DC busvaries between 0.95 p.u. and 1.05p.u:

$$V_{dv}$$
-5% $< V_{Dcbus} < V_{dv}$ +5%

$$1520 \text{ V} < V_{Dcbus} < 1680 \text{ V}$$

With the available components in the PSCAD Master library (under HVDC, FACTS & Power Electronics) the control for the HVDC line is done. To maintain the DC voltage limit, generally two voltage values "Applying Limit" (V_{on}) and "Removing Limit" (V_{off}) are preferred along with the current of minimum value, knownas "Current Limit", then the following conditions are taken into account:

if VD >Removing Limit :Current Order CO = Current Input CI

if VD <Applying Limit : Current Order CO= Current Limit Then, to provide a hysteresis type characteristic between the V_{on} and V_{off} a second option exists.

For the rated power the input current will the current itself: $I_{dc} = P_{dc}/V_{DCbus} = 3000000/1600 = 1880 \ A = 1.88 \ KA$

To produce an alpha in this model from a convectional proportional-integral controller, acting between current order (CO) coming from "Voltage Dependent Current Limits" and measured current (CD) on the DC bus is the error. The overall PSCAD simulation diagram by combining all the components is depicted in Fig.2.

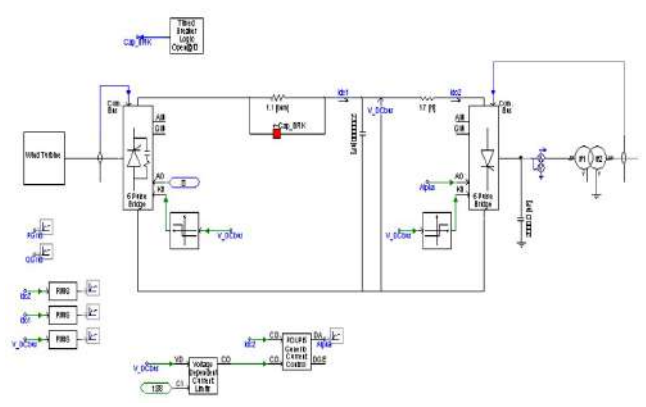


Fig. 2. Complete model of wind power generation.

III. DG OPTIMAL PLACEMENT

Distributed generation optimal placement is very important because of thetechnical and economical aspects. The placement of distributed generation devices in power systems for reinforcement of the grid, for reduction of power losses and on-peak costs operating, improvement of voltage profiles and load factors, and improvement in the system integrity, reliability and efficiency and the power loss of the system is to be minimized. The voltage and the line flows at each bus should be in the acceptable limits.

The load-flow of distribution system is radial in nature and has very high R/X ratio and so it is different from the transmission lines. The load flow convergence is very important. The main aim in the load flow analysis is to reduce the preparation of the data. The method proposed above efficientlycomputes branch power flow and storage of nodes is not necessary at each branch. The voltage is calculated at each node by using a simple algebraic equation. A 33-node distributed network was with the following parameters. They are constant power (CP), constant current (CC), constant impedance (CZ), composite and exponential load modeling. The three-phase radial distributed networks are to be balanced and represented by single line diagrams and capacitances that are charging are to be neglected at the distributed voltage level and this only an assumption. The optimal placement for given capacity (70% of load), obtained as bus 10 for 33-bus distribution system using proposed method and in this methodeach encircle forms a single cluster [12].

A. Clusters Formation

The basic rules to be followed for cluster formation are as follows:

Step 1: In the cluster there should be no further bifurcation.

Step 2: Except first clusterall the clusters will start from a branch and not from the node.

Step3: one parent node and one terminal node are present in a cluster.

By using the structures in the Matlab the clusters are formed which gives the special definition to the cluster. Now the cluster can be used as a user defined data type.At

each bus of distributed network active and reactive load values to be taken in chronological order. For better computational ability these cluster sets are copied into an array of structures with dynamic memory location. The structure element is designed to allocate the entire data i.e. the data required for the calculation of voltage and current profiles of cluster constituents.

B. Load flow methodolgy

Currents are determined after the clusters are formed in the backward direction i.e. from the last cluster the evaluation start. The current through each branch is determined when each cluster is passed to the backward sweep function. The last cluster i.e., here 7th cluster when it is passed through the backward sweep it checks the terminal node of the cluster whether it is end node or not, the current flowing out of the node is zero and the current at each and every node is calculated by using equation only if it is the end node (10).

$$I_{N}^{*}(i,k) = (P_{L}(i,k) + jQ_{L}(i,k))$$

$$V_{N}(i,K)$$
(10)

Where

i = cluster number; k = node number

The equation of the branch current is determined by following analysis

$$I_B(i,k-1) = I_N(i,k) + I_B(i,k)$$
 (11)

The current through the cluster terminal is determined when the terminal is not at the end point is by the following equation

$$I_B(i,k-1) = I_N(i,k) + I_B(i+1,x) + I_B(i+2,y)$$
 (12)

Where x, y are the branches of the cluster that connects the terminal node.

While calculating the branch currents, the proposed software checks the node numbers with the nodes stored in the array. The voltages at the nodes are given by the expression (13) if the node is not the start node of the cluster.

$$V_N(i, k) = V_N(i, k-1) + I_B(i, k-1) * Z(i, k-1)$$
 (13)

The voltage is given by equation if the node is the end node is as follows(14)

$$V_N(i, k) = V_N(i-1, k-1) + I_B(i, k-1)*Z(i,k-1)$$

For the system, the power losses is given by the equation as follows

$$L_P(i, k) = I_B^2(i, k) *R(i, k)$$
 (15)

The voltages at each and every node after computing are given by the convergence of the solution that is to be checked. The method proposed in this paper describes, the solution converges if the voltage magnitude maximum difference (ΔV max) after successive iterations is nearly equal to 0.00001.

C. DG optimization methodology

The DG location is chosen as onewith the best voltage profile that gives minimum losses. By injecting the

available DG value, the best voltage profile can be obtained in the given network at all the nodes and then the voltage index can be calculated and choose the minimum voltage index point for the DG placement.

The voltage index is defined as follows

$$V_{index} = \sqrt{\frac{\sum ((V_{SS} / V_{base}) - V_i)^2}{N}}$$
 (16)

Where, V_{index} is voltage index

V_{ss} is substation voltage

V_{base} is voltage base value

Vi is per unit voltage at ith bus

N is total buses

The loss reduction is given by the expression

Loss reduction $\Delta LP = LP_{(without DG)} - LP_{(with DG)}$ (17)

Where LP is power loss

D. Fuzzy control methodology

For obtaining the best voltage profile and minimum losses in the system it is important to choose an optimal point which cannot be done randomly because it is difficult to get always the common point for both minimum voltage index and maximum loss reduction index. Hence, this can be done by using the fuzzy logic control.

In fuzzy inference system (FIS) the loss reduction index (LRI) is taken as the input variable 1 and the voltage index (VI) is taken as theinput variable 2 and the output variable will be the DG suitability index (DGSI). Few membership functions are designed for both input and the output variables using trapezoidal type. The membership functions of input variable LRI is described by the linguistic terms very low, low, low-medium, medium, high-medium, high, very high, input variable VI is described by the linguistic terms low, low-medium, medium, high-medium, high and the output variable DGSI is described by the linguistic terms very low, low, lowmedium, medium, high-medium, high, very high. The inference involves heuristic rules for determining the output decisions. As there are 2 input variables (LRI, VI) and (7, 5) fuzzified variables respectively; FIS has a set of 35 rules.

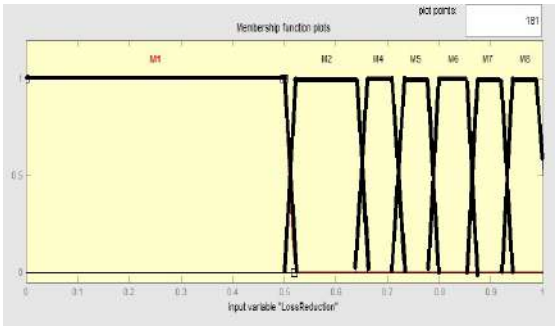


Fig. 3. Loss reduction index membership function

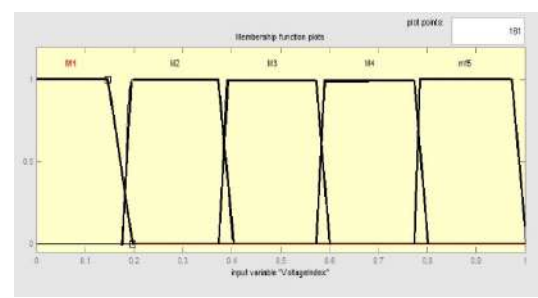


Fig. 4. voltage index membership function.

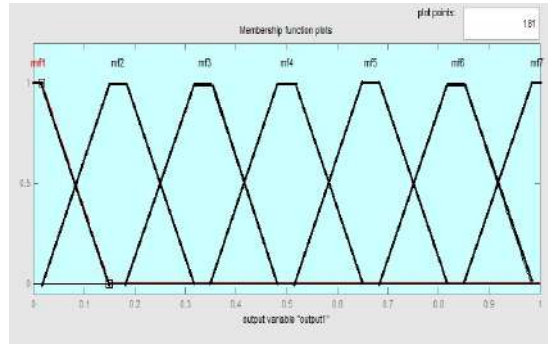


Fig. 5. DG sutability index membership function.

For the loss reduction index should be maximum and the voltage index should be minimum, the available capacity of DG is to be placed into the system in optimal place. The two objectives that are to be considered while designing heuristic rules in fuzzy inference system (FIS). The fuzzy rules pattern is developed in the following form:

If there is high (H) loss reduction index (LRI) and low (L) voltage index (VI) then there is very high (VH) DG suitability index (DGSI). The membership functions for loss reduction, voltage index and DG suitability index are shown in Fig. 3, 4 and 5 respectively.

IV. SIMULATION AND RESULTS

Wind Power generation of Capacity 3 MVA is modeled and simulated for rated load and Simulation results for Active Power , Reactive Power ,Mechanical torque, Angular velocity are plotted in Fig. 6 and 7 respectively.

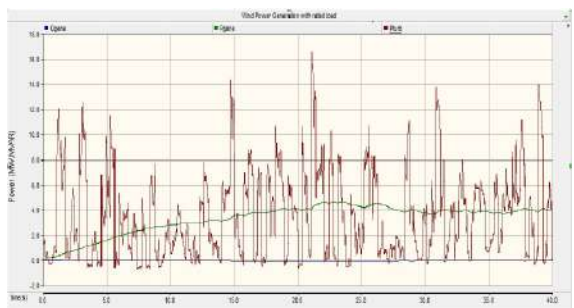


Fig. 6. active and reactive power wind power generation with rated load.

From the Fig. 6 it is observed that reactive power generated in this case is zero since the load is purely resistive. The synchronous generator active power is

steady; wind turbine active power is fluctuating due to variable turbine speed.

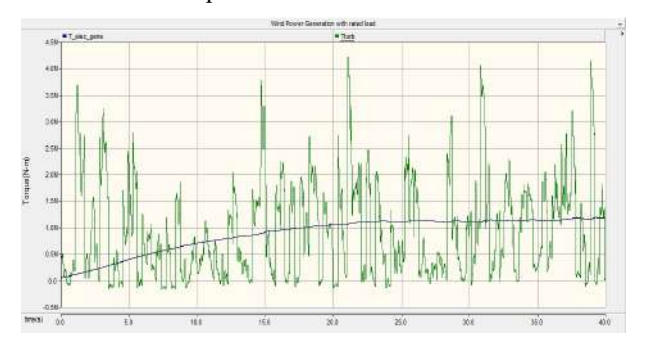


Fig. 7. electrical torque and mechanical torque of wind power generation with rated load.

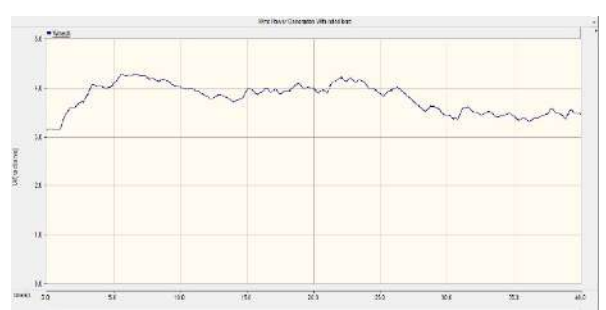


Fig. 8. angular vekocityof wind power generation with rated load.

From the Fig. 7 it is observed that synchronous generator torque is steady and turbine torque is fluctuating. From the Fig. 8 it is observed that the current of DC bus on rectifier side (Idc₁) is fluctuating due to harmonics, but current of DC bus on inverter side (Idc₂) is steady due to inductor. And we can also observe that the grid voltage ($V_{\rm grid}$) is lower than DCbus voltage ($V_{\rm dc}$).

A. Impact of DG penetration into 33-bus distribution network

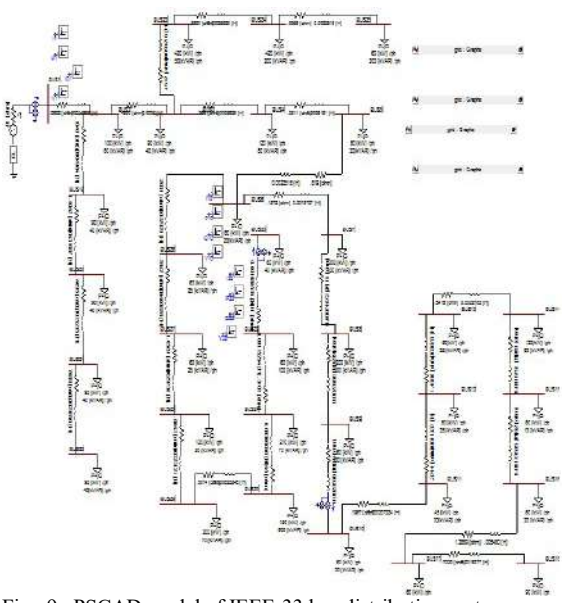


Fig. 9. PSCAD model of IEEE-33 bus distribution system.

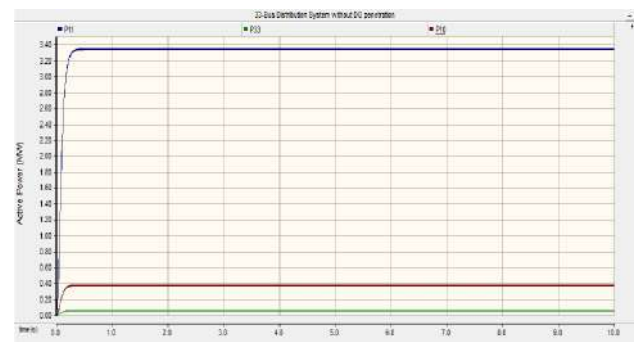


Fig. 10. active power at buses 1, 10, 33 of IEEE 33 bus distributed system without $\,\mathrm{DG}$ penetration.

Fig. 9 shows the PSCAD model of IEEE-33 bus distributed system. From the Fig. 10 and 11 it is observed that active Power losses are to be reduced with power of the wind penetration at optimal location. From the Fig. 12 and 13 it is observed that voltage profile can be improved with wind power penetration at optimal location.

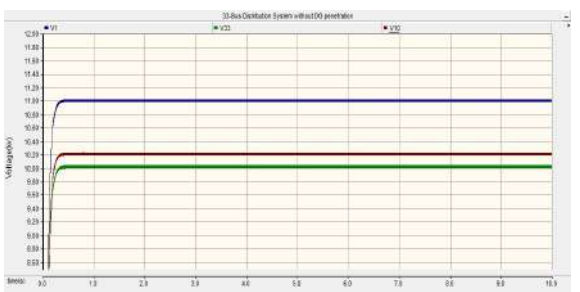


Fig. 11. voltage magnitude at buses 1, 10, 33 of IEEE 33 bus distributed system without $\,$ DG penetration.



Fig. 12. active power at buses $1,\,10,\,33$ of IEEE 33 bus distributed system without DG penetration at bus 10.

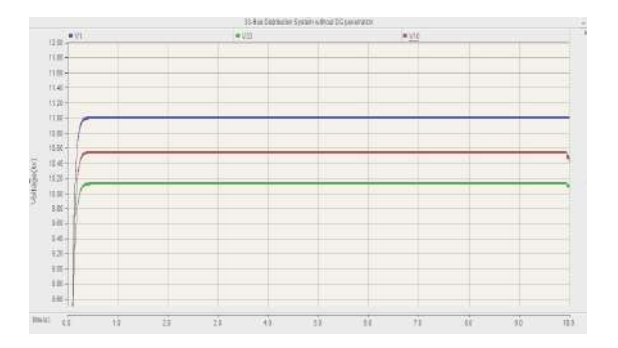


Fig. 13. voltage magnitude at buses 1, 10, 33 of IEEE 33 bus distributed system with DG penetration at bus 10.

V.DISCUSSION AND CONCLUSIONS

The paper here describes, modeling and simulation of wind power generation, AC/DC-DC/AC conversion is presented. The optimal location of DG on 33-bus distributed system is calculated for the given size. The simulation results of 33-bus distributed system without DG penetration and with the DG penetration at optimal location are plotted, with these simulations it is observed that there will be reduced losses and improvement in voltage profile with DG penetration at optimal location.

REFERENCES

- [1] Fazeli Meghdad, Asher M. Greg, Klumpner Christian, and YaoLiangzhong, "Novel Integration of DFIG-Based Wind Generators Within Micro-grids", IEEE Transactions on Energy Conversion, vol.26, no. 3, pp 840-850, September 2011
- [2] Working Group on Distributed Generation Integration, "Summary of distributed resources impact on power delivery systems," IEEE Trans. Power Del., vol. 23, no. 3, pp. 1636–1644, July 2008.
- [3] R. S. Al Abri, Ehab F. El-Saadany, and Yasser M. Atwa, "Optimal Placement and Sizing Method to Improve the Voltage Stability Margin in a Distribution System Using Distributed Generation", IEEE Trans. Power Systems., vol. 28, no. 1, pp. 326–334, Feb. 2013.
- [4] Dheeraj K. Khatod, Vinay Pant, and Jaydev Sharma, "Evolutionary Programming Based Optimal Placement of Renewable Distributed Generators", IEEE Trans. Power Systems., vol. 28, no. 2, pp. 683– 695, May 2013.
- [5] Pierluigi Siano, and Geev Mokryani,," Assessing Wind Turbines Placement in a Distribution Market Environment by Using Particle Swarm Optimization", IEEE Trans. Power Systems., vol. 28, no.4, pp. 3852–3864, Nov. 2013.
- [6] Zhipeng Liu, Fushuan Wen, and Gerard Ledwich," Optimal Siting and Sizing of Distributed Generators in Distribution Systems Considering Uncertainties", IEEE Trans. Power Delivery., vol. 26, no.4, pp. 2541–2551, Oct. 2011.
- [7] Benjamin Kroposki, Pankaj K. Sen, and Keith Malmedal," Optimum Sizing and Placement of Distributed and Renewable Energy Sources in Electric Power Distribution Systems", IEEE Transactions on Industry Applications, vol. 49, no. 6, pp.2741-2752, Nov. 2013
- [8] Libao Shi, Chen Wang, Liangzhong Yao, Yixin Ni, and Masoud Bazargan," Optimal Power Flow Solution Incorporating Wind Power", IEEE System Journal, vol. 6, no. 2, pp. 233-241, June 2012
- [9] J. P. Lopes, N. Hatziargyriou, J. Mutale, P. Djapic, and N. Jenkins, "Integrating distributed generation into electric power systems: A review of drivers, challenges and opportunities," Elect. Power Syst. Res. vol.77, No. 9, pp. 1189–1203, 2007
- [10] J. Driesen and R. Belmans, "Distributed generation: Challenges and possible solutions," presented at the IEEE Power Eng. Soc. Gen. Meeting Montreal, QC, Canada, Oct. 2006.
- [11] Torbjorn Thiringer, "Grid friendly connection of constant speed wind turbines using external resistors," IEEE Transactions on energy conversion Vol 17, No.4; Dec. 2002.
- [12] T Murali Krishna, Dr.N.V.Ramana and Dr.S.Kamakshaiah,"Power Flow Algorithm for Radial Distribution System with Voltage Sensitive Loads" Annual IEEE India Conference (INDICON), Dec. 2012.

Cost-optimal design of a 3-phase distribution transformer using Cauchy's steepest decent method

*RajuBasak¹, Arabinda Das², Amarnath Sanyal³, Ajay Kumar Sen sarma⁴

¹Associate Professor, Electrical Engineering Department, Techno India University,

E-mail: basak.raju@yahoo.com

² Professor, Electrical Engineering Department, Jadavpur University,

E-mail: adas ee ju@yahoo.com

³Formerly Faculty Member, Electrical Engineering Department, Jadavpur University.

E-mail: ansanyal@yahoo.co.in

⁴Indusree, Designer & Manufacturer of Transformer, 13, Gaurangamandir road, Kolkata-700086

E-mail: asensarma@yahoo.com

Abstract:

Transformer has a major role in power system. It either steps up the operating voltage or steps it down according to need. Its cost is a sizable proportion of the total cost of the system. Therefore the designer always aims at optimization of its cost. There are various techniques for cost-optimization. The computer run-time for optimization depends on the method chosen and also the initial values chosen for the design variables and its number. This paper illustrates the Cauchy's steepest decent method using gradient search technique. A case-study has been made following this method and results given at the end.

Keywords:

Transformer design, Optimization, Market price, Quality of materials, Single variable and multivariable optimization, Cauchy's steepest decent.

1. Introduction

Design of transformer and its optimization is a complex task. Computer-aided design of transformers started long back in 1956, 1958 and 1959 [1, 2, 3]. Before the age of computer, design was made using calculators with reference to standard text-books [4, 5, 6] In 1967, Anderson advanced the concept of optimal design of electrical machines using digital computers [7]. The same thing was presented in a much better way in a book composed by by M. Ramammorty in 1987 [8]. From the last decade of 20th century, various attempts have been taken by authors to make use of optimality theory, not only for cost-optimization but also for optimization of efficiency subject to given constraints. The data-books for design also came to regular use [9]. Research scholars felt interested in this area and made their thesis works [10, 11]

Optimal design involves many variables and constraints. Designers have to choose thekey variables, identify the constraints, then frame an objective function for optimization in presence of given constraints. A large no. of optimization techniques are given in books of mathematics and programming [12].

Computationally the simplest method is the method of exhaustive search. In this method, the chosen design variables are varied in steps between the boundaries. The design variables giving minimum possible cost is chosen by using nested loops. The method gives exact solution, but the no of steps is too high, and hence the computer run-time. Other conventional optimization techniques like Hooke's and Jeeve's method, Powell's method, Method of random search, Gradient search techniques etc. are more time-economic. Some soft computing techniques like simulated annealing, genetic algorithm, ant colony optimization, particleswarm optimization etc. are also finding wide application in optimization [13, 14].

Out of all the conventional techniques, the gradient search technique following steepest decent method of Cauchy is most time-economic. The Newton's method employing 2nd derivative is still more time-economic, but the further gain in time is not much.

2. Classical vs. soft-computing optimization technique

Classical or conventional optimization technique is the old and accurate process for some of the mathematical expressions. This method is applicable almost in all the field of optimization in mathematics. Specific optimization problems can be solved by these conventional optimization techniques with proper programming through computers. Gradient search, Golden search, Hooks and Jeeves method, Random

searchtechnique etc. are popular methods of classical optimization. They may be single variable or multivariable optimization. The exhaustive search technique remains as the last choice. On the other hand, there are soft-computing based optimization techniques which are much used now-a-days. It has not been used as there is no ambiguity in the search space.

3. The Gradient Search

The gradient is denoted by ∇ , when applied to a function f, it gives its directional derivatives. The direction along new axis can be found by a new function g(h) where current location is the origin of the new coordinate axis. The slope is calculated with the derivative of the new function g(h) at this point. In gradientsearch method the direction of the vector is taken from the derivative, or has the steepest ascent. If the target was to decrease the value of the objective function, then it is termed as the steepest descent method.

The gradient ∇f is the vector along the direction of the slope at that point. For a 2-dimensional function, the gradient is calculated as $\nabla f = \frac{\partial f}{\partial x}\mathbf{i} + \frac{\partial f}{\partial y}\mathbf{j}$

For a multidimensional problem. It is given as:

$$\nabla f = \frac{\partial f}{\partial x_1} \mathbf{a}_1 + \frac{\partial f}{\partial x_2} \mathbf{a}_2 + \dots + \frac{\partial f}{\partial x_n} \mathbf{a}_n \text{, where } x_1 - x_n$$

are n no. of design variables and $a_1 - a_n$ are corresponding unit vectors.

4. The key variables

The key variables in a transformer design are many. Some of them are continuous, some are discrete, some are logical or of choice type. Continuous variables are current density in the conductor, flux-density in the core, emf constant, window height/width ratio. No. of turns or no. of cooling tubes is a discrete (integer) variable. Choice between conductor material (copper or aluminium) is a logical variable; whether oil-cooled or air-cooled or bitumen filled, the choice of core material etc. may be considered as discrete. Out of them, only the continuous variables are involved in

Cauchy's gradient search. The progamme has to be severally run for different choices (e.g. between copper and aluminium) and the cost functions are to be compared to get the global minima.

If the above-mentioned continuous variables are chosen, the task is to find out the point of minimum altitude in a 4-dimensional hyper-surface of a 5-dimensioal space. The orthogonal projection of a 5-D space is given in fig. 1.

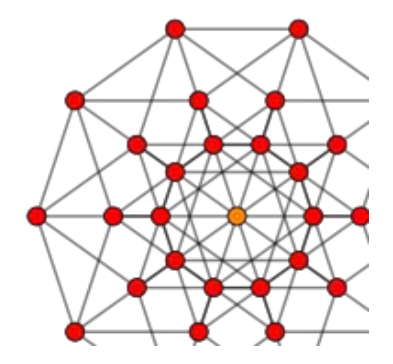


Fig. 1. The orthogonal projection of a 5-D space

5. The objective function

The production cost of the transformer can be found out in steps following the methods used in text-books. The cost function may be the manufacturing cost included labour charges, direct and indirect costs. Its minimality is of interest only for the dull-headed manufacturer. It does not guarantee a long trouble-free life for the transformer. The cost function should take into consideration the running costs (which indirectly accounts for the temperature rise) also.

In this paper a 500 KVA oil-filled distribution transformer has been taken for case-study. For assessment of the manufacturing cost the recent market-prices have been considered. For the running cost, recent tariff rate has been considered. The distribution transformer (urban area) has been considered to run on an average for 12 hours a day at full load, 6 hours at ¾ th.load and 6 hours at half load. The cost function has been considered to be the manufacturing cost plus cost equivalent of 7 years' accumulated losses.

6. The algorithm

The following steps are involved in gradient search technique.

Step 1: Read machine ratings, specific cost of materials chosen

Framing the objective function and computing the gradients

Step 2: Choose key variables and Initialize them;

 $K \leftarrow 0.45$; $R_{vv} (= H_{vv}/W_{vv}) \leftarrow 3.0$; $B_{vv} \leftarrow 1.5$ Tesla; $\delta \leftarrow 2.8$ A/mm²

Input user-specified data for design variables: no. of core steps, $N_{\rm sr}$ etc.;

Step lengths: $\lambda_{k}, \lambda_{rw}, \lambda_{bm}, \lambda_{s}$, Choose copper as conductor material, CRS as core material. Input associated data. Take for minimum cost C_{\min} - a large number).

Step 3: Go to transformer design sub-routine: Find the objective function C and evaluate the performance variables: If there be any constraint violation go to step 2

Step 4: If $C < C_{\min}$ then $C_{\min} \leftarrow C$: $C_{\min} \leftarrow C$

Step 5: $K \leftarrow 1.01K$; Go to transformer design sub-routine: Find cost CK

Step 6: $K \leftarrow K/1.01$

Step 7: $\partial C / \partial K \leftarrow (CK - C) / (0.01K)$

Step 8: $R_w \leftarrow 1.01 R_w$; Go to transformer design sub-routine: Find cost CR

Step 9: Set $R_w \leftarrow R_w / 1.01$

Step 10: $\partial C/\partial R_w \leftarrow (CR-C)/(0.01R_w)$

Step $11: B_m \leftarrow 1.01 B_m$; Go to transformer design sub-routine: Find cost CB_m

Step 12: Set $B_m \leftarrow B_m / 1.01$

Step 13: $\partial C / \partial B_m \leftarrow (CB_m - C) / (0.01B_m)$

Step 14: $\delta \leftarrow 1.01\delta$; Go to transformer design sub-routine: Find cost $C\delta$

Step 15: Set $\delta \leftarrow \delta/1.01$

Step 16: $\partial C / \partial \delta \leftarrow (C\delta - C) / (0.01\delta)$

Step 17: c(count) = c

New initial values for the design variables

Step 18: $K \leftarrow K - (\partial C / \partial K) \lambda_k$

Step 19: $R_w \leftarrow R_w - (\partial C / \partial R_w) \lambda_{rw}$

Step 20: $B_m \leftarrow B_m - (\partial C / \partial B_m) \lambda_{bm}$

Step 21: $\delta \leftarrow \delta - (\partial C / \partial \delta) \lambda_{\delta}$

Step 22: If c(count + 1) < c(count), goto step 5

Step 22: Go to transformer design subroutine with the current values of $K, R_w, B_m \& \delta$.

Find dimensions, cost, and performance variables.

Step 23: Print out results

Step 24: Stop

Step 25: End

Constraints: efficiency \geq 97%; voltage regulation \leq 5%; no load current \leq 1.0%

7. Case Study

The case study has been made for a 500 kVA oil-filled distribution transformer. The print out of the programme (converted to word-file) is given below:

Cost Optimal Design Of A 3-Phase Transformer by Cauchy's steepest decent.

Flux-density, $B_m = 1.4381$ Tesla; Current density, Cd= 2.8459 A/mm²,

The design details of the optimal machine are given below:

KVA-rating of the machine= 500; Nominal power factor= 0.8

Rated line voltage in L.T.= 433 V ;Rated line voltage in H.T.= 11000 V ; Nominal frequency= 50 Hz

Primary Connection: DELTA; Secondary Connection: STAR

Conductor material: Refined COPPER

No. of taps= 5; % turns between taps= 2.5

No of nominal turns of the primary= 1005

No of addl. turns of the primary for tapping= 50

Total no of turns of the primary= 1055

No of nominal turns of the secondary= 23

Current in Primary/ Secondary, A: 15.151, 666.69

Chosen current density = 2.8459 A/mm²

Cross section of primary/ Secondary,mm²: 5.32398 ; 234.262

Net area of core iron = 0.03427 mm²; 0.23 mm lamination is to be used.; Stacking factor= 0.97

Gross area of core iron = 3.532979E-02 mm²

5-stepped core has been used for greater economy of iron.

Diameter of the core circle= 0.22628 m

Length of the core sides in mm: 214 190 158 120 68

Area of the window, mm²= 8.778548E-02 Window height/width, m: 0.57842, 0.15177

Distance between core centers= 0.36560 m Width/height of yoke,m: 0.21383, 0.16522

Total length of core= 0.96994m; Total height of core= 0.90886 m

Iron loss = 1707.5 W; % Iron loss= 03415

Mean length of turn of Primary/ Secondary,m: 0.80624 , 1.0446

Resistance of Primary/ Secondary, ohm: 3.1973; 2.13973E-03

Copper loss = 5055.2 W; % Copper loss = 1.0110; Total % loss at full load = 1.352532

Efficiency at full load &0.8p.f= 0.98337

Maximum efficiency occurs at 58.118% load.

The magnetizing current = 0.63051%; the core loss current = 0.3415 %; The no load current = 0.71705 %

The % leakage reactance= 3.1933

The % voltage regulation at rated power &p.f= 2.7248 The tank length, width, height,m: 0.506 * 1.222 * 1.059 The no. of tubes (50 mm dia.) required= 137 The weight, Kg/ cost of tank: 407.48; Rs. 48898 /- The volume, liter; cost of oil: 0.65405; Rs. 58865 /- Volume of iron =1259461 m³; Weight of iron, Kg= 988.68; Cost of iron = Rs. 197735 /-

Volume of copper= 3.036927E-02 m³; Weight of copper,Kg= 270.29; Cost of copper = Rs. 162172 /-Direct cost allowing 25 % labour charge= Rs. 584588 /-Selling cost allowing 35 % overhead = Rs. 789193 /-Annual cost of lost energy at Rs. 5 /BOT, Rs. 189371 /-(on the basis of average 12 hrs. at full load, 6hrs. at 75% load, 6hrs at 50 % load.

Cost function (cost of production+ 7 years of energy loss) = Rs.2114791/-

8. Conclusion

Transformers are essential parts of a power distribution system. Their cost is a sizeable proportion of the total investment. Therefore transformers are to be designed cost-optimally. However minimum cost from the point of view of the manufacturer is no good. Increasing the flux-density in the iron core and current density in the conductor always reduce the manufacturing cost but with a consequent increase in iron loss and ohmic losses. Operation at relatively high temperature reduces the operating life, increases the chances of bursting and associated risk hazards and increase the running cost. Therefore the objective function for minimality should be judiciously chosen with a look to the interest of the manufacturer and the user. In this paper, the objective function has been chosen as sum of the manufacturing cost and capitalized running cost for the expected life span of the transformer. Cauchy's gradient search technique has been used for quickly achieving the minima. The program has been run for different choices of conductors and core iron and the global minima has been obtained for copper as conductor and 0.23 mm CRS stampings. The key variables have been judiciously chosen and step length for gradient search has been fixed properly to reduce the no. of iterations.

Reference:

- [1] S.B. Williams, P.A. Abetti, E.F. Mangnusson, "Application of digital comp uters to transformer design", AIEE trans., Vol-75, pt-III, pp. 728-35, 1956.
- [2] W.A. Sharpley, J.B. Oldfield, "The digital computer applied to the design of large power transformers", Proc. IEE, Vol-105, pt- A, pp. 112-25, 1958.
- [3] S.B. Williams, P.A. Abetti, H.J. Mason, "Complete design of power transformer with a large size digital

- transformer", AIEE trans., Vol-77, pt-III, pp. 1282-91, 1959.
- [4] M.G. Say, "Performance and design of a.c. machines", ELBS.
- [5] A.K. Sawhney, "A course in electrical machine design", DhanpatRai and Sons, 2003.
- [6] Dymkov, "Transformer design", MIR publications.[7] O.W. Anderson, "Optimum design of electrical machines",
- IEEE Trans. (PAS), Vol- 86, pp. 707-11, 1967.
- [8] M. Ramamoorty, "Computer-aided design of electrical equipment", Affiliated East-West Press Pvt. Ltd., 1987, ISBN: 81-85095-57-4
- [9] A. Shanmugasundaram, G. Gangadharan, R. palani, "Electrical machine design data book", Wiley Eastern Ltd. ISBN 0 85226 813
- [10] Xingxing Zhang, Stranded core transformer loss analysis, ME thesis, The Graduate School, University of Kentucky, 2008
- [11] Md., Y. Abu Sada, Design of transformer, ME thesis, King Fahd University of Petroleum and Minerals, Dhahran, Soudi Arabia.
- [12] N.S. Kambo, "Mathematical programming techniques", Revised edition,1991,1984, Affiliated East-West Press Pvt. Ltd. New Delhi – 110 001, ISBN 81-85336-47-4.
- [13] K. Deb, "Optimization for engineering design", PHI, 2010. ISBN 978-81-203-0943
- [14] S.S. Rao, "Engineering optimization- theory and practice", New Age Int.; ISBN 978-81-224-2723-3

The Institution of Engineers (India), WBSC

23rd & 24th Nov. 2019

Future Energy Mix Plan for Sustainable Power Market

SubhenduPodder, Amar NathBhadra

Abstract: The planet we inhibit is constantly put under severe threats for over industrialization, emissions from boilers of thermal power sector, construction sector activities and deforestation. The above situation has got aggravated due to the wanton use of the natural resources. In order to do our bit for mitigating the environmental impacts, we propose to leverage the cutting edge technologies and augment the uses of the Renewable Power. Government of India is committed to create an ecosystem that will lead to the path of the sustainable development goals through the INDC commitment that has been made to the Paris Agreement in December 2015.In that context, the proper Energy mix from the Energy Basket will be able to save our natural resources significantly while ensuring the stability of the power system under Business-As-Usual (BAU) mode. The thermal power plants are the major contributor of the GHG emissions but its inevitable presence / contribution in the energy-mix can only be ensured through the use of most advanced technology Boilers, like CFBC, ASCT Carbon SCT, Capture and Sequestration with a view to stabilize the average global surface temperature stay within two degree Celsius before the turn of this century. The above philosophy is more relevant under the visionary directions of "MODI 2.0 Government" which aims at making India a USD 5 trillion dollar economy within 5 to 6 years which corresponds to the GDP growth at around 8.5 percent annually. This paper is aimed at discussing the possible scenarios of power system stabilization in the wake of infusion of 175 GW of Renewable Energy within the basket of an energy-mix comprising of coal, gas, hydro, pumpstorage, Battery Storage and many more.

Keywords: Energy-Mix, BAU, INDC, Renewable Energy, Flexibisation, Power Market.

A Comprehensive literature review report on basic issues of power system restoration planning

Maitrayee Chakrabarty
Deptt. of Electrical & Electronics
Engineering, National Institute of
Technology, Nagaland, Dimapur797103, India.

email: moitry29@gmail.com

Dipu Sarkar

Deptt. of Electrical & Electronics Engineering, National Institute of Technology, Nagaland, Dimapur-797103, India. email: dipusarkar5@rediffmail.com Raju basak
Department of Electrical
Engineering, Techno India
University, Kolkata, India.
email:basak.raju@yahoo.com

Abstract - Modern power industries throughout the globe experience blackout problem in varying degrees due to several operational and maintenance issues. A review of past and existing literature highlighting the different causes leading to blackout is explored in this paper. In this paper, the Power System Service Restoration (PSSR) is investigated in more detail with regards to its limits, its operational constraints and the issues present in the existing PSSR schemes along with the different methodologies developed by earlier researchers working in this domain.

Keywords- Power system service restoration, Blackout problem, Power outage, Black-start, Micro-grid, Network-reconfiguration, Load restoration

INTRODUCTION

Past record of power industries has experienced enormous number of blackout problem. Several causes may be associated with this such as lighting effect hit to transmission lines and insulator etc.; transmission line and transformer overloading, line to ground fault, transient faults and transmission pole unavailability due to natural calamities etc. Power outage issues are possible to resolve and supply power to the isolated area within few minutes to few hours. Lack of generation insufficiency or inadequacy, transmission inadequacy; maloperation of synchronizing units, communication units or delay operation of protective device, remote operation, and irregular security monitoring like SCADA control etc. may reason behind of a catastrophic blackout. Some of blackout incident are address below:

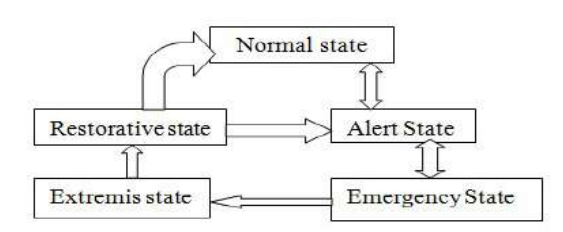
South Korean power grid [1] has been experienced a black out due to 1000MW capacity power plant unable to supply power through transmission lines. Due to this problem overall loads of the country suffered 3 to 10 days to completely cure these. 370million people on 22states of India had suffer the blackout problem due to northern power grid collapsed; due to shut down of 35.67GW power plant of Indian power grid [2] on 30th and 31st July2012. One massive blackout occurred at New York and New England on 14th August2003, 50million people were affected as three-units transmission circuit (each unit capacity was 345kv) was not working and disconnected total 61,800MW load which lasted for two week [3-4]. In [4] has been addressed several causes of blackout which held on 23rd September2003 in Southern Sweden, Eastern Denmark, and 28th September2003 in the Italian power grid. 8.46million people

were affected by harsh blackout on 29th July1999 at Taiwan due to 326transmission tower collapsed and another blackout occurred at 21st September1999 at Taiwan; details reason was addressed in [5].

Reliability is important factors to element the risks of blackout condition in transmission and distribution system. Reliability analysis has two wings, [6] which are

- i Adequacy gives information about generation capability limit to generation power normal and pick-load demand or available transmission line capacity (ATC) to supply power generation end to consumer end.
- ii Security monitoring parts gives the information how a system available runs at normal condition to tolerate different types of disturbances likes fault condition.

During normal operating condition all equipment likes generator, transformer, bus bar; protective devices etc. are working properly to maintain the equality constraint and inequality constraint. Due to some inconvenience, sometimes system may loss synchronisms and some equipment may not work properly. Symmetric and asymmetric fault, loading problem etc. use to occur in networks. There are some stages which are very much related to PSSR which as shown in Fig.1 i.e. 'Normal-state', 'Alert-state', 'Emergency-state', 'Extremisstate' and 'Restorative-state.



T Fig. 1 Power system operation Stage cur in power system. System goes to the normal running state to alert-state or pre-outage state or insecure stage. If it has been removed in small time duration system return to the normal-stage otherwise inequality constants has been violated it will reach to the emergency-stage or outage-state which is also called (N-1) security-state. As early as possible power outage should be removing from the system, it returns back to normal-state otherwise it might go to the in extremis-state. At that time may

be multiple failure i.e. massive blackouts are occurred at large area. Restorative-state [7] is used for sorting-out the blackout. Due to shortcoming may not be resolved; it may cause of blackout which has highly affected to the hospital, research canter, banking sector, communication, transportation industry etc. Blackout means the darkest-period on power industry. To remove this type of shortcoming PSSR is only solutions. Different issues are associated to execute the PSSR planning (PSSRP). Expert PSSR strategies should be efficiently suggested a plan and taken care to resolve in various way depending upon the severity of different types of blackout issues.

A. Outline of PSSR Issues

PSSRP [8] is difficult task for implementation, lot of problem associated with it. Initial stage of PSSR has been prepared a perfect plane to restore loads at blackout condition and next stage has been executed and implemented the PSSRP and trains the system. Some of the problems are discus here and Fig.2 shows the overall stages of PSSR.

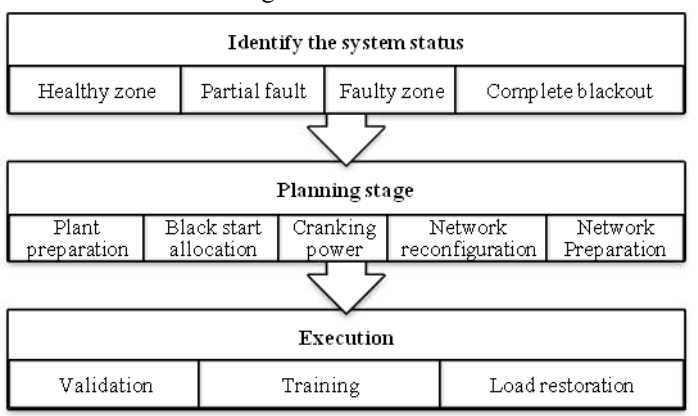


Fig. 2 Overview PSSR Stage

PSSRP has been handling the several aspects after partial or complete blackout; some major points are illustrated in this section. Types of fault identification [9] are important task for PSSRP to distinguish the fault severity. Next concerns are isolate or separated the faulty-zone to healthy-zone and take necessary action for restore as soon as possible. In this section address several publications on previous researchers to associate with PSSR issues [9-11] which helps to understand all the issues

ISSUES RELATED WITH PSSRP STAGE					
Sl no	Categories	Paper no			
1	Restoration issues	[9]			
2	Restoration planning	[8,28,29,35,49,50,52],			
3	Asymmetric issues	[10]			
4	Dynamic issues	[11]			
5	Bibliographic survey	[12,13]			

TABLE I

After identify the fault categories a proper planning should be required to hell the related problem [1,9,12-13]. Some solution has been given below:

Prepare plant for implement PSSRP:

- Black-start allocation to supply power to load at the emergency condition
- · Crank power distribution
- Cold load pickup

Prepare network preparation for PSSRP.

- · Reenergise the feeder lines, buses
- · Reenergise the protective devices such as circuit breaker, relay etc
- · Optimum switch operation
- · Network reconfiguration

Protection and Execution PSSRP:

- Load restoration
- · Load generation balance
- · Voltage stability
- Losses minimization
- Power control (active and reactive)
- Frequency control

A.1. Prepare plants for restoration:

If blackout happens due to generation insufficiency i.e. PSSRP requires some emergency-backup device like Black-Start-Unit (BSU) which helps to supply the emergency-power. Main concern of the distribution network is re-energizing the systems after power outage- known as Cold-Load-Pickup. There are two major issues using these methods Re-energize loads and Pickup of more connected load. Loads are classified into two parts:

Cyclic-loads (those are connected in normal operating condition including air-conditioners, refrigerators, etc) and

Non-cyclic-loads (lighting are turned off intermittently).

BSU has capability to stabilize system and provide the pickup power demands; manage active-power and reactive-power supply between BSUs and loads. BSU helps to supply emergency cranking-power to ensure restoration in a grid after catastrophic blackout and to restart different parts like prime mover of hydropower plant, boiler turbine of thermal power plant; and including other auxiliary parts like combustion-turbine, boiler-feed-pump of steam unit etc. need to be warm-up for properly supply power. In [35] was suggested some power plants with minimum start-up time like hydroelectric units, thermal, renewable (wind, solar) power plant and small diesel generator and large generator may be used to provide small and large power demand.

A.2. Prepare network for PSSR

Due to fault such as local, global or cascading failures have been affected some area in power network but reaming network has not affected. In [8] network-reconfiguration (NR) has been efficiently isolated faulty part from healthy parts and short-out blackout issues to operate tie switches and sectionalizing switches; otherwise healthy section also affected. Optimum switch allocation has assisted PSSRP to reconnect network. Proper switching's operation are helped to operate proper transformer which are helped to reduced the overvoltage operation in the transmission line as well as transient voltage of overall system; Phase angle difference should desire to hold

steady state and dynamic voltage level in connection of tie line closing.

A.3. Prepare protection and execution

PSSRP must design to manage frequency as well as overvoltage level, steady-state and transient stability. Generation and load balancing is vital factor at PSSRP otherwise it may reason of another massive blackout. This matching is not maintain properly sadden increment of load may effect on system frequency deviation as well as system stability. It is impossible to supply cranking power to all darkest-part at a time at fault condition. Black-start allocation helps to supply power and subdivide overall-area in different island as per load priority. Load restoration is last stage when all the load restarts for selfhealing of network and all area will get power and all generators will work synchronize with the bus-bar. In this time many other parameters [9, 14] have to be considering like balancing reactive power to connect static switched capacitor, switch reactors, pickup the load with lagging power factor and adjusting transformer tap setting, energizing Extra-High-Voltage(EXV) transmission section to provide constant impedance and transmission line loss. Sometimes high amount of current flow may damage the system and may cause of switching transient voltage i.e. energize large area to concern about system specification limit. Several symmetry issues and asymmetry issues [10] impact involve with PSSR.

Standard training or monitoring session in regular basics reduces the chances of catastrophic blackout and take some preventive emergency step to prevent failure. SCADA [13-14] and GPS system detects the fault, PMU device to identify the system status and make the system observable or not. These types of intelligent analysing system tools has been given data are assist to prevent real time collapse detection. Analysing tool [15-16] have support to make decision and study some analysis like fault (short circuit etc), load flow, rotor angle stability, voltage stability, dynamic stability, transient voltage, electromagnetic transient; intelligent coordination control reactive power flow, power generation and load demand balancing. At the time of NR, resynchronization and load restoration are used intellectual decision to minimize the loss and optimal path selection purpose. As an example: PSCAD/EMTDC tool [1] was used for re-energizing Power Restoration Line (PRL) in South Korea and supply power after blackout through BSU. Table II shows some tool based software which helps in PSSRP and operates system at post outage conditions.

TABLE II
TYPES OF TOOL USING PSSR PLANNING STAGE

1 FPES OF TOOL USING F35K PLANNING STAGE					
Sl no	Tools	Paper no			
1	PSCAD/EMTDC	[1]			
2	System restoration Navigator tool	[35]			
3	LINPACK	[45]			

B. PSSR problem formulation

Formulation of PSSRP lot of criteria and constraint factors are involved which need to be considering for efficiently fulfilment of process. Optimization scheme has been implement for better PSSR output. Minimizing and maximize optimization technique paying more attention on different objective function in different categories which have mention in Table III.

TABLE III

DIFFERENT OF	JECTIVE FU	JNCTION USED FOR PSSR PLAN	NING
Maximize Objective		Minimize Objective	
To restored power	[24,25,	To reduce time	[17,25,
in an isolated area	34]	duration 33	,34,36]
To increase	[30,34,	To reduce procurement cost	[17]
transfer capability	55]	of PSSR process	
		To reduces losses of	[25]
		the resultant network	
		Minimize the amount	[27]
		of	
		weighted outage load	
		To operate less	[27]
		number of switches	
		To minimize the cost	[42]
		function	

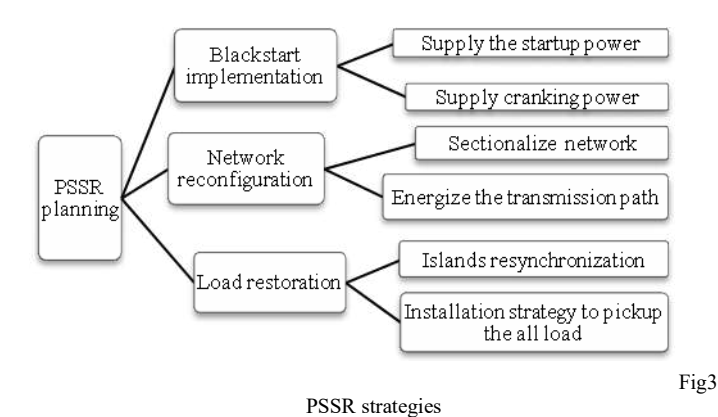
Table IV shows different criteria like limits and constrains of corresponding systems which has involve for implement the objective function which are mention below:

TABLE IV
LIMITS AND CONSTRAINTS USING PSSR

Divilio	THIS CONSTIGHT	o conto i boit	
Limits	Paper no	Constraints I	Paper no
Voltage limits	18,27,30,43,51	Time 22,3	4,36,37,5
			4
Power limit	27,30,34, 42	Frequency	46,51,54
Current limits	30,43	Priority of loads	25
Power balance between	24,25,42	Generation	22,34,
generation and load		excitation	36,37
Line capacity	42	Voltage	18,34
Switching connection	55	Clustering coeffici	ent 43
Distributed generation	27	Load constraints	18
_		Transient voltage d	lip 51

C. PSSR strategies for normal power grid:

PSSRP should require proper strategies which are recommended by previous researcher to clear sever outage problem. A sequential PSSR strategy is shown in Fig.3. Initially BSU implementations with special sequential operational procedures have taken to restore voltage in a grid.



C.1. Black-start implementation strategy:

BSU helps to supply start-up power or cranking power through transmission line to Non-Black-Start-Unit (NBSU); critical load, auxiliary transformer and steam turbine units etc. BSU resource allocation procurement have based on Black-Start-Ancillary-

Service. Optimal black-start resource procurements in right placed or proper location is essential factors which help to accelerate the PSSR and supply power to unserved loads with minimum time, minimum cost [17]. Black-start-Decision-Supporting-System (BSS) has able to restore isolated loads. In [18] recommended BSS at Taiwan power system and interface with Graphical-User-Interface (GUI) to reenergize transmissions line and reconnected isolated loads immediately.

C.1.1 BSU testing

Different testing approach recommends and examines the capacity of BSU as well as improves efficiency of PSSR. Testing method depends upon different criteria considering maximize restore loads; minimize production cost and time duration. For solving blackout condition, Independent-System-Operator (ISO) takes some decision to operate BSU for transmitted power in a network. In [19] some annual testing criteria was suggested based on Electric Reliability Council of Texas (ERCOT) rule for improving reliability, minimize procurement cost for black-start implementation in an optimal way. In [20] was discussed different types of scheme to check the black-start capacity at Swedish power station for energizing of major transmission lines, synchronizing of additional power stations, system loading; voltage, control, governor and frequency control synchronized with the help of PMU.

In [21] was recommended a field testing method in Shandong power grid based on Plan-Do-Check-Action (PDCA) cycle shows in Fig.4.

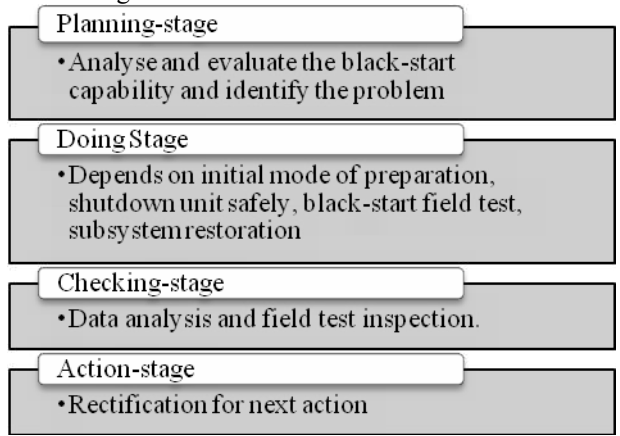


Fig4 PDCA Cycle

C.1.2. Start-up Strategy:

A proper strategy is very essential to contribute cranking power through the available BSUs to NBSUs. Some research work pay attentions on start-up time, ramping rate and the auxiliary parts of NBSUs to operate at emergency condition. In [22] discussed a formulation on startup sequence by Mixed-Integer-Linear-Programming (MILP). To make the start-up sequence decision for BSU and NBSU are very important for PSSR.

To execute proper PSSRP, network-reconfiguration is help to deliver unserved loads demands in secure way. Islanding operation of a network taken the concern of load-generation balancing issues and serves the critical loads. For implementing the Black-start Process, NR has been required to determine the path of a network and eliminate the chance of blackout. These reconfiguration processes [23] are divided in two-parts:

- (i) Series energizing
- (ii) Parallel energizing.

C.2.1 BSU implementation based NR strategy:

Sometimes BSUs are incapable to restore all effected loads in a network i.e. may need other provision to utilize BSUs. In this circumstance entire network partition in different island [24-27] based on BSU capacity to restore the isolated loads. In [24] NR based restoration technique was suggested on two-layer unit restarting framework (i) optimization modelling of NR, (ii)solving methodology of the multi-objective optimization. In [25-26] was addressed an emergency restoration process restored the highest or critical priority loads using Floyd-Warshall Shortest-path algorithm and Discrete Particle Swarm Optimization respectively. In [27] has been recommended an islanding technique based on distributed generation by using loop breaking methods for solving load shedding problem due to fault. In [28] PSSRP study was recommended for serving power at metropolitan areas. Depending upon the severity of fault NR has been classified in two parts

Utilize tie switches and available resources to reconfigure the system to collect power from unaffected areas without violating system constraints.

Utilize black-start resources when available resources are inadequate to reconnect power so altering the system configuration based on the black-start capability

C.2.2. System Partitioning Schemes and Parallel restoration:

System partitioning [29] helps to accelarate PSSRP. Fig.5 shows sequential prattitioning schemes for PSSR

C.2. Network reconfiguration:

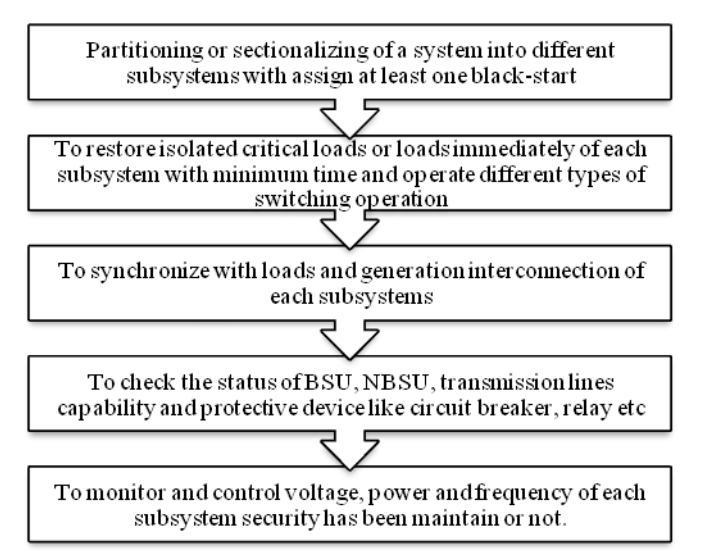


Fig.5 System Partitioning or parallel restoration Schemes

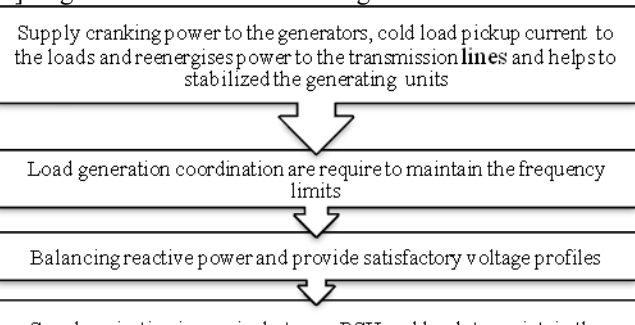
In [30-34] sectionalizing strategies was proposed by Ordered-Binary-Decision-Diagram (OBDD), Phasor-Measurement-Unit (PMU), Graph-theory, Genetic-algorithms, and Non-dominated sorting genetic algorithm (NSGA-II) respectively. In[35] was recommended some generic restoration milestones strategy for speedup restoration process and calculate restoration time with System-Restoration-Navigator (SRN) tool for proper used of BSU and provided some general suggestion to run the restoration process securely. In [36-37] focused on optimum transmission-line for supply start-up power by Mixed-Integer-Quadratically-Constrained-Program (MIQCP) and Firefly-algorithm. Knowledge-based system status information helps to build up a tool (ILOG CPLEX) which has guided an operator to take decision.

C.2.3. Cascading Blackout

Suddenly power demands may increase the cause of cascading blackout or power failure or power-shade in wide-area. Several cascading blackout incident have mention in [38-41]. Several cause may involved with this types of fault like limited of generated power, limited resources for power transfer, overloaded transmission line, voltage collapse, hidden relay failures, dynamic instability, inter-area oscillations etc. In [42-44] recommended restoration strategy to solve cascading problem due generation scarcity based on Linear Programming, Complex-Network-Theory (CNT) and division algorithm respectively. In [45], several Benchmarking techniques were addressed by IEEE working team to identify, forecast, alleviation and restoration of cascading failures and used to measure performance of system using different software tool (like LINPACK etc.) for business authentication. In [46] was considering the different characteristics like frequency responses and the loss of cascading failures tested on IEEE-RTS96 system. In [47] focused on cascading disturbance and evaluate risk and performance indexes, monitor security, performance of circuit breaker protection. In [48] was paying attention on vulnerability evaluation for identifying critical line and segments in the grid and also discover the early emergency and warning stage in power system.

C.3. Load restoration

Load restoration is last stage of PSSRP and main objective is to restore all loads and resolve all generators issues and is resynchronized overall island network again. During restoration phase update the critical load one by one as per priority. Next concern is to distribute power to reaming systems based upon available resources. The main concern of load restoration [49-52] stages are mention below in Fig.6.



Synchronization is require between BSU and loads to maintain the overvoltage limit and transient voltage dip operation and maintained the voltage constraint, frequency constraint, transient voltage dip constraint, clod load pickup characteristic, voltage stability etc. at post outage condition.

Fig6 Load restoration Schemes

In [51] was suggested a mathematical model using modified Bisection algorithm for maximum restore loads and maintained the voltage constraint, frequency constraint, transient voltage dip constraint, clod load pickup characteristic, voltage stability etc. at post outage condition. In [53] was focused on load restoration for finding critical path visualization by using Critical-Path-Method (CPM) and Program-Evaluation and Review-Technique (PERT) based upon graph theory approach. In [54] general steam turbine model has been designed in Power System Simulator for Engineering (PSS/E) for study the system frequency response for cold load pickup (SFRCLP) condition. In [55] has been used ant colony optimization algorithm to solve the cold load pickup problem with minimum restoration times. In [56-57] has been invented a algorithm based upon Intuitionistic fuzzy Choquet integral operator and intuitionistic fuzzy sets as well as intuitionistic fuzzy distance respectively to operate BSU and restored loads

D. PSSR planning strategies using micro-grid

Traditional power grid suffering from limited reliability, transmission line losses, security problems, emitted lot of environment pollutant gas. Microgrid gives better solution and provides more flexible, reliable, secure, efficient, quality service to consumer using minimum resources and better satisfaction at customer economic point of view. Initial microgrid established concern about generation unit, protection device, communication system, and storage device is required to store power to supply when resources are not available. In case of Distributed Generation based microgrid fuel cost is another consideration. Microgrid is design to monitor overall network and identify the reason behind a catastrophic blackout and take some preventive

emergency step to prevent. Microgrid has availed to mitigates, resilient to any kind of physical and cyber security attacks and self-healing capacity to respond any kind of fault, communication techniques monitor competitive markets, system planning, minimize operation and maintenance cost. SCADA and GPS system detects faults and gives data to prevent real-time collapse detection and intelligent coordination are required to control reactive power flow, power generation and load demand balancing by using microgrid implementation [57-58].

Fig.7 shows different activity during restoration stages such as utilized BSUs, NR for islanding operation; resynchronization and load-restoration used intellectual decision to minimize losses.

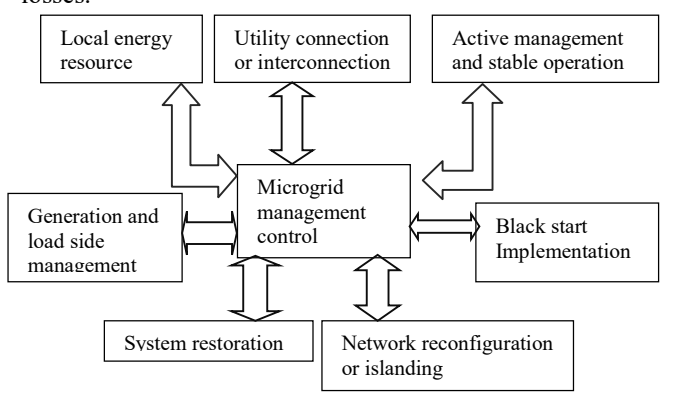


Fig7 PSSR strategies with using microgrid

was expressed unscheduled island NR technique based on Lagrangian and dynamic programming technique for PSSRP with the help of renewable microgrid power.

E. Overall planning strategies

A survey outcome of reviewed publications overall PSSRP strategies has been classified in different parts. Several planning strategies have been recommended by the previous researchers which are summarized in this section is listed in Table V.

TABLE V
DIFFERENT CATEGORIES FOR PSSR PLANNING STAGE

Sl no	Categories	Paper no
1	Black start	1,35,37,56,57
2	Black start unit plus Islanding	24,2526,30,31,32,33,36
3	Sectionalisation	30,31,32,34,59
4	Load restoration	24,32,34,36,51,53,54,55
. 5	Micro-grid	57,58,59

been recommended by previous researcher to operate post outage condition to return back to normal condition. Table VI shows different methodology.

TABLE VI DIFFERENT METHODOLOGY USED FOR PSSR PLANNING

SI no	Used Methodologies	Paper no
i.	Fuzzy logic control	56,57
ii.	Expert system	50
iii.	Heuristic search	18
iv.	Knowledge based	36
v.	Genetic algorithm	27,33,34
vi.	Ant colony search algorithm	55
vii.	Optimization	24,34
viii.	Graph theory application and ordered binary decision	n 25,30,32,
	diagram	

This review paper has highlighted the various problems, software package tool, objective function and constraints related to PSSRP and conjointly categorised in numerous components that embody typical power restoration and microgrid power restoration theme. Overall comprehensive review helps a new researcher to grasp the thought of PSSR. The information of the paper helps to identify blackout and also helps to take some preventive steps to regulate post disturbances conditions.

References

- [1] S.S.Lee, "Hydro and gas turbine blackout restoration strategies in the South Korean power system," In 2014 IEEE PES General Meeting | Conference & Exposition, pp.1-6. IEEE, 2014.
- [2] Y.Xue, X.Shijie, "Generalized congestion of power systems: insights from the massive blackouts in India," *Journal of Modern Power Systems and Clean Energy*, vol. 1, no. 2, 91-100, 2013.
- [3] EH.Allen, RB.Stuart, TE.Wiedman. "No light in August: power system restoration following the 2003 North American blackout," IEEE Power and Energy Magazine,vol.12,no.1,pp.24-33,December2013.
- [4] G.Andersson, P.Donalek, R.Farmer, et al. "Causes of the 2003 major grid blackouts in North America and Europe, and recommended means to improve system dynamic performance" *IEEE transactions on Power Systems*, vol 20,no(4),pp.1922-1928,pp.2005.
- [5] C.H.Lee, S.C.Hsieh. "Lessons learned from the power outages on 29 July and 21 September 1999 in Taiwan," *IEE Proceedings-Generation, Transmission and Distribution*, vol. 149,no.5,pp. 543-549, September 2002.
- [6]. P.Kundur,Power system stability and control. McGraw-Hill, New York,2001
- [7] T.D. Sudhakar, K.N. Srinivas, European transaction on electrical power 2010, Wiley Online Library, Restoration of power network –a bibliographic survey.
- [8] M.M.Adibi,L.H.Fink, "Power system restoration planning," IEEE Transactions on Power Systems,vol. 9,no.1, pp.22-28,1994.
- [9] M.M. Adibi, R.J. Kafka, "Power system restoration issues," IEEE Comput. Appl. in Pow.vol.4, no.2, pp.19-24, April 1991.
- [10] M.M Adibi, D. P. Milanicz, T. L. Volkmann, 1999,IEEE transactions on power system vol no 14,(1085-1091): Asymmetry issues in power restoration.
- [11] M.M.Adibi, N.Martins, "Power system restoration dynamics issues," In 2008 IEEE power and energy society general meeting-conversion and delivery of electrical energy in the 21st Century,pp. 1-8, IEEE, July2008.
- [12]D.Lindenmeyer,H.W.Dommel,M.M.Adibi, "Power system restoration—a bibliographical survey," International journal of electrical power & energy systems, vol.23,no.3, pp.219-227,2001.
- [13] L.I.U.Yutian, F.A.N.Rui, V.Terzija, "Power system restoration: a literature review from 2006 to 2016," *Journal of Modern Power Systems and Clean Energy*, vol.4,no.3, pp.332-341,2016.
- [14] M.M.Adibi, L.H.Fink, "Overcoming restoration challenges associated with major power system disturbances-Restoration from cascading failures," *IEEE power and energy magazine*, vol.4,no.5, pp.68-77,2016.
- [15] J.J.Ancona, "A framework for power system restoration following a major power failure," *IEEE Transactions on power systems*, vol. *10, no.* 3, pp. 1480-1485, 1995.
- [16] F.F.Wu, A.Monticelli, "Analytical tools for power system restoration-conceptual design," *IEEE Transactions on Power Systems*, vol. *3,no.* 1, pp.10-26,1988.
- [17] Q.Feng, W. Jianhui, C.Chen Jianzhong Tong: "Optimal Black Start Resource Allocation," IET Generation, Transmission & Distribution, pp.0885-8950,2015.
- [18] G.Meysam, M.Jamal,G.Naji, "Service Restoration In distribution network using combination of two heuristic methods considering load shedding," State Grid Electric Power Research Institue, Springer, July, 20015.
- [19] S.Nitish,M.Kenneth,D.John, S.Santoso, "The Annual Black Start Service Selection Analysis of ERCOT Grid," IEEE Transaction on Power System, vol24 No4, pp.1867-1874, September 2009.
- [20] H. Fendin, T.Hansen, M Hemmingsson (2011) IEEE Trondheim power Tech: Black Start test of the Swedish power system.
- [21] W.Hongtao, L.Yutian, 2010, International Conference on Electrical and Control Engineering: Research on the black start field test of Shandong power grid based on PDCA cycle.
- [22] S.Wei, C.C.Liu, L. Zhang, "Optimal Generation Start up Strategy for bulk power system restoration," *IEEE Transactions on Power Systems*, vol. 26, no. 3, pp. 1357-1366, December 2011.

- [23] Z.H.O.U.Yunhai, M.I.N.Yong, "Optimal algorithm for system reconstruction," In Proceedings. International Conference on Power System Technology, vol.1, pp. 201-203, IEEE, October 2002.
- [24] X. Gu, H. Zhong, "Optimisation of network reconfiguration based on a two-layer unit-restarting framework for power system restoration," *IET generation, transmission & distribution*,vol.6,no.7, pp.693-700, January, 2012.
- [25] D.Sarkar,M.Chakrabarty, A.De, S.Goswami, "Emergency Restoration Based on Priority of Load Importance Using Floyd–Warshall Shortest Path Algorithm," In Computational Advancement in Communication Circuits and Systems, pp. 59-72, Springer, Singapore, 2020.
- [26] Y. Liu, X.Gu, "Skeleton-network reconfiguration based on topological characteristics of scale-free networks and discrete particle swarm optimization," *IEEE Transactions on Power Systems*, vol.22,no.3, pp.1267-1274,July2007.
- [27] X.Huang,Y.Yang,G.A.Taylor, "Service restoration of distribution systems under distributed generation scenarios," *CSEE Journal of Power and Energy Systems*, vol.2,no.3, pp.43-50,2016.
- [28] JW.Feltes, et al, "Some considerations in the development of restoration plans for electric utilities serving large metropolitan areas," IEEE Transactions on Power Systems, vol. 21, no. 2:pp. 909-15, May 2006.
- [29] MM.Adibi, et al, "Power system restoration-a task force report," *IEEE Transactions on Power Systems*, vol.2, no.2, pp.271-277,1987.
- [30] C.Wang,V.Vittal,K.Sun, "OBDD-based sectionalizing strategies for parallel power system restoration," IEEE Transactions on Power Systems; vol.26,no.3,pp.1426-33,September2010.
- [31] SAN.Sarmadi, "A sectionalizing method in power system restoration based on WAMS," *IEEE Transactions on Smart Grid*, vol.2,no.1, pp.190-197.March, 2011.
- [32] J.Quiros-Tortos, M. Panteli, W.Peter, T.Vladimir, "Sectionalising methodology for parallel system restoration based on graph theory," *IET Generation, Transmission & Distribution*, vol. 9, no. 11, pp. 1216-1225, March 2015.
- [33] L.Haiping, G.Xueping, Z.Dongwen, "Optimization of system partitioning schemes for power system black-start restoration based on genetic algorithms." In 2010 Asia-Pacific Power and Energy Engineering Conference, pp. 1-4. IEEE, 2010. [34] W.Hongtao, H.Chengming, L.Yutian, "Pareto optimization of power system reconstruction using NSGA-II algorithm." In 2010 Asia-Pacific Power and Energy Engineering Conference, pp. 1-5. IEEE, 2010.
- [35] W.Sun, C.C. Liu, S.Liu, "Black start capability assessment in power system restoration," In 2011 IEEE Power and Energy Society General Meeting (pp. 1-7). IEEE,July2011.
- [36] W.Sun, C.C.Liu, R.F.Chu. "Optimal generator start-up strategy for power system restoration." 2009 15th International Conference on Intelligent System Applications to Power Systems. IEEE, 2009.
- [37] E.l.Zonkoly, A.Mohamed, "Renewable energy sources for complete optimal power system black-start restoration," *IET Generation, Transmission & Distribution* vol.9,no.6,pp.531-539,Octember2014.
- [38] B.A.Carreras, V.E.Lynch, I.Dobson, D.E.Newman, "Complex dynamics of blackouts in power transmission systems," *Chaos: An Interdisciplinary Journal of Nonlinear Science*, vol. 14, no. 3, pp. 643-652, September 2004.
- [39] R.Kinney, P.Crucitti, R.Albert, V.Latora, "Modeling cascading failures in the North American power grid," *The European Physical Journal B-Condensed Matter and Complex Systems*, vol.46,no.1,pp.101-107,July2005. [40] P.Crucitti, V.Latora, M.Marchiori, A topological analysis of the Italian electric power grid. *Physica A: Statistical mechanics and its applications*, 338(1-2), pp.92-97July2004.
- [41] I.Dobson, B.A.Carreras, V.E.Lynch, D.E.Newman, Complex systems analysis of series of blackouts: Cascading failure, critical points, and self-organization. *Chaos: An Interdisciplinary Journal of Nonlinear Science*, vol.17no.2, p.026103,Jun2007.
- [42] B.A.Carreras, V.E.Lynch, I.Dobson, D.E.Newman, "Critical points and transitions in an electric power transmission model for cascading failure blackouts," Chaos: An interdisciplinary journal of nonlinear science, vol. 12, no. 4, pp. 985-94, December 2002.
- [43] S.Yushu T. Xisheng,"Cascading failure analysis of power flow on wind power based on complex network theory," *Journal of modern power systems and clean energy* vol.2, no. 4,pp.411-421, December,2014,.
- [44] Z. Z. Lin, F. S. Wen, C.Y. Chung, K.P. Wong, H. Zhou, "Division algorithm and interconnection strategy of restoration subsystems based on complex network theory," *IET generation, transmission & distribution, vol.* 5,no.6 pp.674-683, June 2011

- [45] Baldick, Ross, et al. "Initial review of methods for cascading failure analysis in electric power transmission systems IEEE PES CAMS task force on understanding, prediction, mitigation and restoration of cascading failures." 2008 IEEE Power and Energy Society General Meeting-Conversion and Delivery of Electrical Energy in the 21st Century. IEEE, 2008.
- [46] Y. Jun, Z. Xiaoxin, Y.Xiao, "Model of cascading failures in power systems," *International Conference on Power System Technology*. IEEE,Octamber2006.
- [47] I.P. Siqueira "Risk Sharing of Cascading Disturbances Among Power System Players," In 2006 International Conference on Probabilistic Methods Applied to Power Systems, pp. 1-6. IEEE, 2006.
- [48] W.Xu,Z. Jianhua,W. Linwei,Z.Xingyang, "Power system key lines identification based on cascading failure and vulnerability evaluation," In 2012 China International Conference on Electricity Distribution, pp. 1-4, IEEE.September 2012.
- [49] M.M.Adibi, "From Generic Restoration Actions to Specific Restoration Strategies," (2000).
- [50] M.M.Adibi, L.R.J.Kafka, D.P.Milanicz, "Expert system requirements for power system restoration," *IEEE Transactions on Power Systems*, vol. 9no. 3, pp.1592-1600, Augest 1994.
- [51] H.Qu.Y.Liu,: "Maximizing restorable load amount for specific substation during system restoration," *International Journal of Electrical Power & Energy Systems* vol.43,no.1,pp.1213-1220,December2012.
- [52] L.H.Fink, K.L.Liou, C.C.Liu, "From generic restoration actions to specific restoration strategies," *IEEE Transactions on power systems*, vol. 10, no. 2, pp. 745-752, May 1995.
- [53] A.A.Mota, L.T.M.Mota, A. Morelato, "Visualization of power system restoration plans using CPM/PERT graphs." *IEEE Transactions on Power Systems*, vol. 22,no.3,pp.1322-1329,July2007.
- [54] M.D.Rodriguez, et al,"Fast assessment of frequency response of cold load pickup in power system restoration," *IEEE Transactions on Power Systems* vol.31,no.4,pp.3249-3256,Octember2015.
- [55] W. J. Liu, Z. Z. Lin, F.S Wen, G Ledwich, "Intuitionistic fuzzy Choquet integral operator-based approach for black-start decision-making." *IET generation, transmission & distribution* vol.6,no.5,pp.378-386,May2012.
- [56]. W. J. Liu, Z. Z. Lin, F.S Wen, G Ledwich, "Analysis and optimisation of the preferences of decision-makers in black-start group decision-making," *IET Generation, Transmission & Distribution*,vol.7,no.1, pp.14-23January/013
- [57] F.O. Resende, N.J. Gil, J.A.P. Lopes, "Service restoration on distribution systems using Multi-Microgrids", *European Tran. on Elec. Power*, vol.21, pp. 1327-1342, 2011
- [58] C. Moreira, F. Resende, and J. Lopes, "Using low voltage microgrids for service restoration," *IEEE Trans. Power Syst.*, vol. 22, no. 1, pp. 395–403, Feb. 2007.
- [59] B.Zhao, X.Dong, J.Bornemann, "Service restoration for a renewable-powered microgrid in unscheduled island mode," *IEEE Transactions on Smart Grid*, vol.6, no.3, pp.1128-1136, December 2014.

Priority base load restoration technique for distribution network based on graph theory

Maitrayee Chakrabarty

Deptt. of Electrical & Electronics Engineering, National Institute of Technology, Nagaland, Dimapur-797103, India.

email: moitry29@gmail.com

Dipu Sarkar

Deptt. of Electrical & Electronics Engineering, National Institute of Technology, Nagaland, Dimapur-797103, India. email: dipusarkar5@rediffmail.com Raju basak

Department of Electrical Engineering, Techno India University, Kolkata, India. email:basak.raju@yahoo.com

Abstract - A new technique has been proposed to restore critical loads or highest priority loads in distribution system after a blackout or any kind of power outage condition by modifying the topological configuration to energies the transmission line with help of optimum switch allocation and maintaining electrical and operational limitations. This paper shows an optimum islanding allocation technique using a graph-theoretic approach with Black-Start-Unit (BSU) that makes best use of restored load and diminishes the overall active and reactive power losses. Priority depended K-means clustering algorithm is employed to execute the restoration plans. Main aim is to minimize the overall system power loss as well as restore maximum load as per black-start capability. Distribution Load flow is carried out to make sure that the suggested system network persuades is maintaining all operational limits. Simulation consequences are found on a modified IEEE14node system and exhibit the efficacy of suggested methodology with voltage stability indicator (Lindex).

Keywords- Power system restoration process, Islanding, Blackstart-unit, Distributed generator, Voltage response

INTRODUCTION

Power system restoration process (PSRP) has divided into three parts [1] like power generation use some alternate sources like BSU, network reconfiguration to reenergizes transmission line and load restorations. BSU can accelerate the restoration process to supply emergency power into the critical loads as well as other loads of a network. In the second stage is network reconfiguration which is an island or partitioning the network-based upon the capacity of each BSU. The capacity of BSUs should match with restored loads in every island of the network. Optimal transmission path has to reenergize for distributed highest priority loads demands.

Wang et al [2] have been presented a sectionalizing strategy for PSRP by using ordered binary decision diagram. Yang et al [3] have been worked on parallel restoration such as local distributed-generations and switching operation by using Heuristic-Moment-Matching (HMM) method. Afrikhte et al [4] have proposed PSRP for island network by using Genetic

algorithm which has efficiently given the solution at restoration condition.

Jairo et al [5] have been addressed a parallel PSRP using graph theory logic based on the cut-set matrix to sectionalize the network to solve the post blackout condition. Edström et al [6] have been presented solutions for PSRP by spectral clustering graph theory technique to restore the disconnected power. Sun et al [7] have been used graph theory based on constrained Boolean linear and quadratic programming problem to island network and restore the system.

In [8] a service restoration based technique has proposed by Floyd-Warshall Shortest-path algorithm for delivering power at blackout condition to restore highest or critical priority loads. One of the drawback of this algorithm is to check the each all pairs in a corresponding graph and find out each possible solution for the restoration i.e. this method is taking more time to give the solution.

In this proposed technique can find out the highest priority critical loads in networks and energies the optimal transmission line for reduced power losses by using the minimum switch at restoration as well as maintain the voltage stability for each island. The major concern for implementing BSU is proper coordination in between the source and consumer demands otherwise it may cause another blackout condition. Sudden increment of the load may affect the system stability. Some assumptions are taken into consideration like sufficient knowledge to make a feasible network for reconfigure coordination of load and generation, switch allocation status sequence, the capacity of BSU resources. A constraints based cluster method is proposed along with stability calculation.

A. Reconfiguration strategies

Reconfiguration criteria to choose optimal path are clearly explained in detail using the K-Means clustering algorithm to restore every critical load in a network. The main aim is to categorize the consumer nodes into different clusters by K-Means clustering algorithm are used to partition n node network in K-optimum cluster depends on the black-start capacity with minimum loss. Distance-based clustering is focus on multi constrains to evaluate the nearest mean

position node from the available black-start location. Distance-based clustering function: Give dimensional data input as i=(', ',...... i) and), the following common distance j=(, ,..... measures are applicable such as Euclidean distance:

$$d(i,j) = \sqrt{\left|\left(X_{i1} - X_{j1}\right)\right|^2 + \left|\left(X_{i2} - X_{j2}\right)\right|^2 + \dots + \left|\left(X_{in} - X_{jn}\right)\right|^2}$$

Hear each consumer nodes are presented only one cluster at a time. It deals to find out neighbour node to make the inter-cluster data points as close as to DG units. Next assign nodes into a cluster that is equal to the sum of squared distance between the load nodes and the source node (consider as a cluster's centroid). Cluster centroid is deal with the arithmetic mean distance of all the available nodes that fit into a cluster. The way k-means algorithm works are as follows: Initialize the specific number of clusters K. Next shuffle the available adjacency matrix and selecting the nearest nodes to reconfigure the network and Keep updating until optimal cluster set are forms.

В. *Voltage stability indicator (L-index)*

Kessel et al [9] determine a online voltage stability checking with the help of L-index and range of the L-Index are varies between 0 to 1 where 0 indicate the no load condition and 1 indicates the voltage collapse stage. If P and Q is the real and reactive power injection in a system; P_L and Q_L is the total real and reactive power requirement in same system; P_{Loss} and Q_{Loss} is the real and reactive power loss in same system; V is the voltage; r and x is the equivalent transmission line resistance and reactance respectively. So real and reactive power supply can be expressed as

$$P = \frac{r(p^2 + q^2)}{r^2} + P_L$$
 (i)

$$P = \frac{r(P^2 + Q^2)}{V^2} + P_L$$
 (i)
 $Q = \frac{x(P^2 + Q^2)}{V^2} + Q_L$ (ii)

Common part of equation (i) and (ii) is $\frac{(p^2+q^2)}{r^2}$ which can be eliminate in terms of

$$(P - P_L) = r(Q - Q_L) \tag{iii}$$

Rearranging equation (i),(ii) and (iii) overall system P and Q are expressed as

$$\begin{array}{l} P = \\ \frac{2x^2P_L - 2rxQ_L + r}{2(r^2 + x^2)} - \\ \frac{\left[(2x^2P_L - 2rxQ_L + r^2) - 4(r^2 + x^2)(x^2P_L^2 + r^2Q_L^2 - 2rxP_LQ_L + rP_L) \right]^{0.5}}{2(r^2 + x^2)} \end{array}$$
 (iv

$$\begin{array}{l} Q = \\ \frac{2r^2Q_L - 2rxP_L + x}{2(r^2 + x^2)} - \\ \frac{\left[\left(2x^2P_L - 2rxQ_L + r^2\right) - 4(r^2 + x^2)(x^2P_L^2 + r^2Q_L^2 - 2rxP_LQ_L + rP_L\right)\right]^{0.5}}{2(r^2 + x^2)} \end{array} \quad (v$$

For find out the real roots from P and Q solve quadratic equation (iv) and (v) and expressed as $(b^2 - 4ac) > 0$. Thus $4[(xP_L - rQ_L)^2 + xQ_L + rP_L] < 1$ (vi) Where L-index<1

Where L-index<1
$$r = \frac{(\sum P_{loss})}{(P_L + \sum P_{loss})^2 + (Q_L + \sum Q_{loss})^2}$$

$$x = \frac{(\sum Q_{loss})}{(P_L + \sum P_{loss})^2 + (Q_L + \sum Q_{loss})^2}$$

Sarkar et al. [10] has been proven that L-index is helpful and an efficient method to check the system stability.

C. Mathematical problem formulation with constrains:

The intention is to connect the nearest load to the BSU and deliver power to the neighbor loads for reduce losses and maintain system stability. K-means Clustering Algorithm has recommended for PSRP to satisfy following criteria like maximizing the total amount of load restored depending upon available DGs capacity; minimize the total number of switch in operation for energies the feeder lines; minimizing the power loss during restoration phase, while satisfying number of constraint and boundary condition expressed which are mention below:

(a) To maintained Power balance constraint:

$$P_{di} = \sum_{i}^{M} P_{G_i} - \sum_{j}^{N} P_{L_j}$$
 (1)

$$\mathbf{Q_d} = \sum_{i}^{\mathbf{M}} \mathbf{Q_{G_i}} - \sum_{i}^{\mathbf{M}} \mathbf{Q_{L_i}}$$
 (2)

Where, PG and QG are active and reactive power of BSU for ith cluster. P_{L_i} and Q_{L_i} are active and reactive power requirement for jth load. Total number of important load is levelling by N in every subsystem. M is total number of BSU. Each DG units are acted like as a cluster head at islanding operation. Pa and Qd represent active and reactive power imbalance in a subsystem.

(b) To maintained Line capacity constraint:

During restoration, the transmission line current should not go above the maximum tolerable current capacity limit.

Where, $I_{\text{Lin.efl}}$ is the line current, and $I_{\text{Cap:all}}$ is the line capacity.

All BSU supplies power to the essential nodes through power lines having specific impedance value comprising of resistance, reactance and consider some specific weight of the transmission line. Consequently, a significant amount of active and reactive power loss, as well as voltage drop occurs along the line. The power loss and voltage drop be able to be minimized by routing blackstart power through the optimum path. The target is to find out the mean distances between the BSU and vital consumption nodes in each subsystem. The flowchart has

been shown in Fig.2.

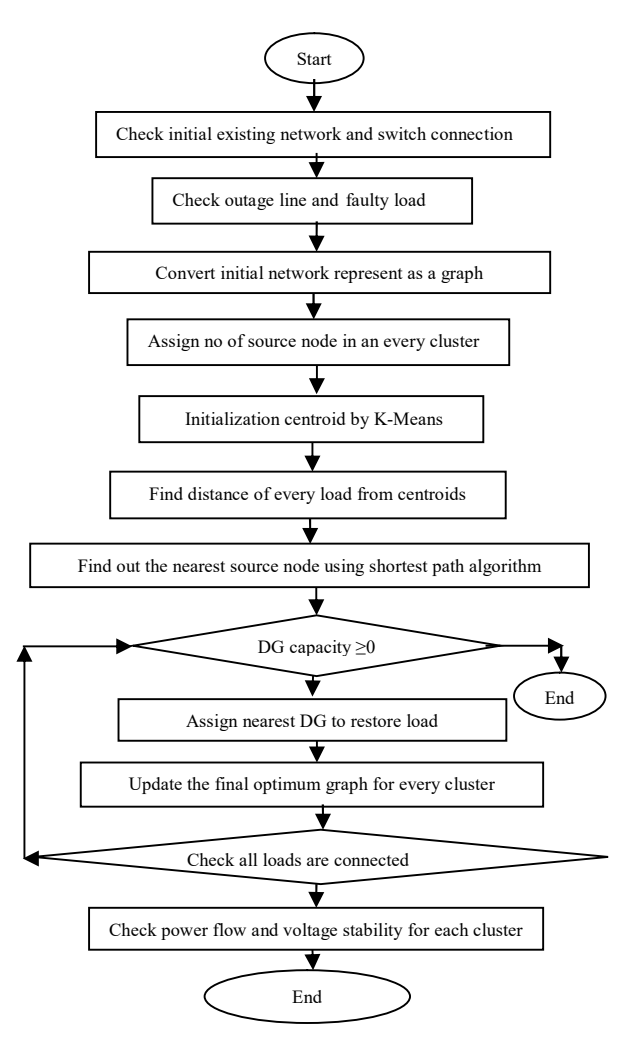


Fig.2. PSRP flowchart using K-means clustering algorithm

Step1. Convert initial network into a graph from depending upon the available BSU.

Step2. Set fixed amount of cluster head as per the DGs availability. Each cluster follows this flowing criteria for find out the Euclidean distance as

$$\sqrt{|S_{mw_i} - D_{mw_j}|^2} \ge 0 \qquad \text{and} \qquad$$

 $\sqrt{|S_{mvar_i} - D_{mvar_j}|^2} \ge 0$, where S_{mvar_i} and S_{mvar_i} is the active and reactive power capacity of i^{th} BSUs respectively. D_{mvar_j} and D_{mvar_j} is the active and reactive power demand of i^{th} loads respectively.

Step3. Assign nearest load to the cluster head depends on BSUs by using Dijkstra's based shortest path algorithm and check for all loads.

Step4. Update final graph for every cluster.

Step5. Calculate power flow and voltage stability calculation for every cluster.

B. Result and discussion:

To show the usefulness of PSRP performance, some studies are simulated and examined on modified IEEE 14 bus [11] system for validate the proposed method. During PSRP all the constrains likes total buses should be taken into consideration, only one transmission path should be present in between two buses and maximum transmission line power flow capacity should maintained. The optimal switching connection statuses are indicated by 1 and 0. Here, 1 indicates that two buses are connected by a transmission line and status 0 indicates corresponding transmission line is open. Initial case, a complete power blackout assumes in IEEE 14 bus network and also considers every transmission path is not affected. Total 20 switches were present in operation before blackout. Due to generation insufficiency power outage occur in a network. In that scenario to restore loads; some emergency backup device is required. IEEE 14 bus system has three black start units which are connected at bus 2, 5 and 9 and leveled by BSU₁, BSU₂ and BSU₃ with active and reactive power capacity are 15MW, 20MW and 20MW and 20MVar, 15MVar, 15MVar respectively. Overall network has been shown in Fig.2.

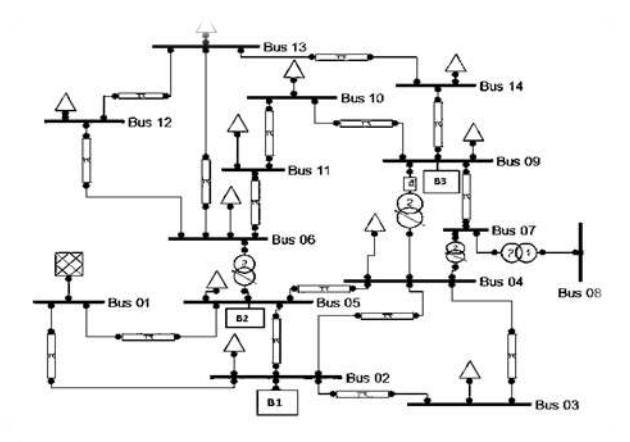


Figure 2. Modified IEEE14Bus system with three black start units

Table 1 shows the each load data along with priority value. Highest priority load value is level by 2 and lowest priority load value is leveled by 1.

Table1.Load data for modified IEEE 14 bus system

Bus	Active	Reactive	Priority
No.	Power[MW]	Power[Mvar]	value
2	2.17	12.7	1
3	9.42	19	2
4	4.78	-3.9	2
5	7.6	1.6	1
6	1.12	7.5	2
9	2.95	16.6	1
10	9	5.8	2
11	3.5	1.8	1
12	6.1	1.6	2
13	1.35	5.8	1
14	1.49	5	1

Table 2 shows the line data of the modified IEEE 14 bus

system with corresponding leveling off all available switches connection details.

Table2. Line data for modified IEEE14bus system

From Bus	To	Active	Reactive	Switch
	Bus	Power(p.u)	Power(p.u)	
1	2	0.01938	0.01838	S1
1	5	0.05403	0.04953	S2
2	3	0.04699	0.04461	S3
2	4	0.05811	0.05069	S4
2	5	0.05695	0.05469	S5
3	4	0.06701	0.06523	S6
4	5	0.01335	0.00921	S7
4	7	0.22412	0.20912	S8
4	9	0.57896	0.55618	S9
5	6	0.28236	0.25202	S10
6	11	0.09498	0.09235	S11
6	12	0.12291	0.10234	S12
6	13	0.06615	0.04613	S13
7	8	0.19658	0.17615	S14
7	9	0.14569	0.11001	S15
9	10	0.03181	0.0245	S16
9	14	0.12711	0.10038	S17
10	11	0.08205	0.05207	S18
12	13	0.22092	0.19988	S19
13	14	0.17093	0.12802	S20

Table 3 shows the cost-matrix of modified IEEE14Bus system. The values of cost matrix represents by C_{ij} , which refer to the impedance of line between, i and j bus. If any system has n bus so the overall size of the matrix will be $n \times n$. Each nonzero values of cost matrix represent the impedance of the connected transmission line of the corresponding two or nodes. Otherwise zero values signify no transmission line is available. The proposed algorithm will give the best possible sub-cluster after maintain all the operational constraints which have been mentioned in mathematical formulation section. Corresponding costmatrix is found out the least transmission path between any black start unit and the critical loads.

To validate the cluster output perform simulations study in PSAT [12] and MATLAB software to check the voltage response of the each load in a corresponding cluster and check the overall voltage stability after connecting black start unit. After implement the proposed algorithm overall surplus power capacity of black start units in every cluster has been mention in table 4 along with cluster details.

Table4.Surplus power capacity in different black start units and cluster details

Bus	BSU			Cluster
No		MW Capacity	MVar Capacity	
2	BSU_1	5.58	1	2, 3
5	BSU_2	6.65	4	4, 5, 6, 12, 13
9	BSU_3	6.01	2.4	7,8,9, 10, 11, 14

The K-means clustering technique has been successfully implemented on IEEE 14 Bus network and cluster representation has been shown in Figure 3

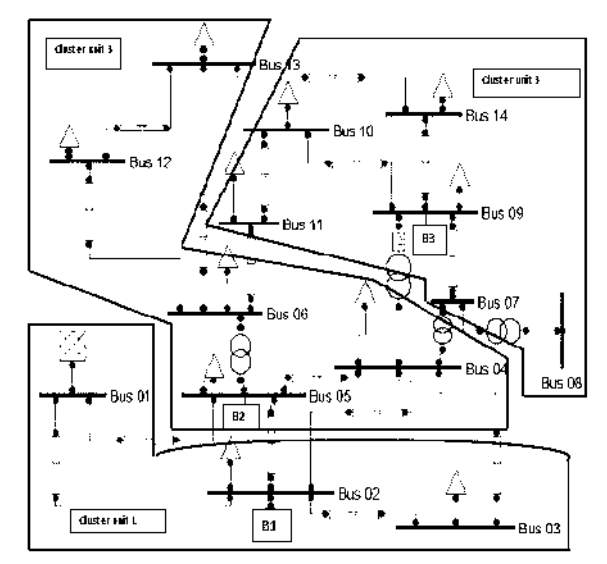


Figure 3. Cluster representation for Modified IEEE 14Bus system

Table3. Adjacency Matrix for 14 bus test system

Node	Nodel	Node2	Node3	Node 4	Node 5	Node 6	Node 7	Node 8	Node 9	Node10	Nodel 1	Node12	Node13	Node14
1	0	0.0622	0	0	0.2294	0	0	0	0	0	0	0	0	0
2	0.0622	0	0.2034	0.1856	0.1829	0	0	0	0	0	0	0	0	0
3	0	0.2034	0	0.1836	0	0	0	0	0	0	0	0	0	0
4	0	0.1856	0.1836	0	0.04417	0	0.20912	0	0.5562	0	0	0	0	0
5	0.2294	0.1829	0	0.04417	0	0.25202	0	0	0	0	0	0	0	0
6	0	0	0	0	0.25202	0	0	0	0	0	0.2204	0.2838	0.1461	0
7	0	0	0	0.20912	0	0	0	0.17615	0.11001	0	0	0	0	0
8	0	0	0	0	0	0	0.17615	0	0	0	0	0	0	0
9	0	0	0	0.5562	0	0	0.11001	0	0	0.09028	0	0	0	0.2987
10	0	0	0	0	0	0	0	0	0.09028	0	0.2088	0	0	0
11	0	0	0	0	0	0.2204	0	0	0	0.2088	0	0	0	0
12	0	0	0	0	0	0.2838	0	0	0	0	0	0	0.2979	0
13	0	0	0	0	0	0.1461	0	0	0	0	0	0.2979	0	0.3877
14	0	0	0	0	0	0	0	0	0.2987	0	0	0	0.3877	0

In first cluster: Black start unit1 connected at bus2 and supply power at bus2 and 3. BSU1 deliver power to the critical load which is connected at bus 3 and after that supply power to at bus2. Figure 4 shows the representation

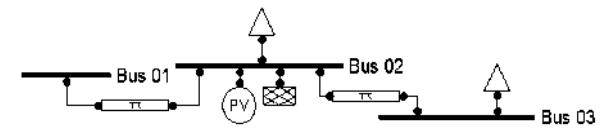


Figure 4. Cluster 1 representation

Surplus power capacity of BSU1 is 5.58 MW, 1MVar. Table5 has been mention the voltage and angle response in each bus and overall L-index stability value of this corresponding cluster1.

Table5. Voltage, angle at different buses and overall L-index for cluster1

Bus no	Voltage (p.u.)	Angle(rad)	L-index
Bus 01	1	0	
Bus 02	1	-0.10472	0.5787
Bus 03	1.01	-039404	

L-index value is 0.5787 in cluster1 which indicate the small sub-system is stable stage after connect BSU1. Table6 has been mentioned the transmission line power flow, power loss report and corresponding connected and operated switch status at different lines after reconfiguration. S1 and S3 switches are connected and status are 1.

Table6.Power flow and switch status for different lines at cluster1

From	To	P_{Flow}	QFlow	P_{Loss}	Q Loss	Switch in
Bus	Bus	(p.u.)	(p.u.)	(p.u.)	(p.u.)	operation
01	2	1.6228	-0.46533	0.05477	0.11442	S1
03	2	-1.3188	0.55375	0.0954	0.3577	S3

In second cluster: Black start unit2 connected at bus 5 and supply power to the critical loads which is connected at bus 4,6 and 12 and after that supply power to least priority loads which are connected at bus 5 and 13. Figure 5 shows the representation for cluster2.

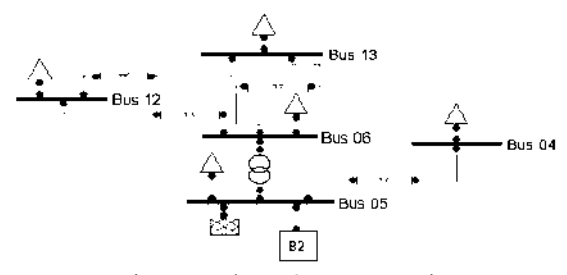


Figure 5. Cluster 2 representation

Surplus power capacity of BSU2 is 6.65MW, 4MVar. Table 7 has been mention the voltage and angle response in each bus and overall L-index stability value of this corresponding cluster2. L-index value is 0.5200 which indicate the small sub-system is stable after connect BSU2.

Table 7 Voltage, angle at different buses and overall L-index for cluster2

Bus no	Voltage(p.u)	Angle(rad)	L-index
04	0.98845	-0.2984	
05	1	-0.27056	0.5200
06	1.07	-0.1425	0.5200
12	1.0087	-0.09021	
1.2	1	0	

Table 8 has mention the power flow and power loss report and corresponding connected switch status at different lines after clustering and utilize capacity of black start unit2.

Table8. Power flow and switch status details for different lines at cluster2

From	To	P _{Flow}	Q _{Flow}	P _{Loss}	Q _{Loss}	Switch
Bus	Bus	(p.u.)	(p.u.)	(p.u.)	(p.u.)	
6	12	-0.7688	0.29897	0.01023	0.02129	S12
12	13	-0.1725	0.25528	0.02061	0.01865	S19
6	13	0.66167	0.99421	0.08241	0.16228	S13
5	4	0.67535	0.06275	0.00615	0.00675	S7
5	6	-0.5818	0.04991	0	0.07463	S10

In third cluster: Black start unit3 connected at bus9 and deliver power to the critical load which is connected at bus10 and after that supply power to the lowest priority load which are connected at bus 9,11 and 14. Figure 6 shows the representation for cluster3.

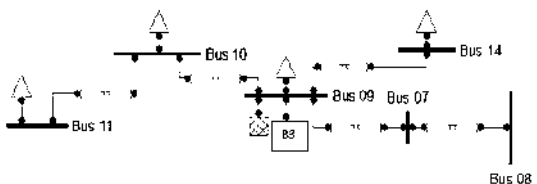


Figure 6. Cluster 3 representation

Surplus power capacity of BSU3 is 6.01MW, 2.4MVar. Table 9 has been mention the voltage and angle response in each bus and overall L-index value of this corresponding cluster3. L-index value is 0.0.4049 which indicate the small sub-system is stable after connect BSU3.

Table9. Voltage, angle at different buses and overall L-index for cluster3

Bus no	Voltage (p.u.)	Angle(rad)	L-index
07	1.0346	-0.1752	
08	1.09	-0.1752	
09	1	-0.1752	0.4 049
10	0.98738	-0.12809	
11	1	0	
14	0.95097	-0.22517	

Table 10 has mention the power flow and power loss report and corresponding connected switch status at different lines after clustering.

Table 10. Power flow and switch status for different lines at cluster 3

From Bus	To Bus	P _{Flow} (p.u.)	Q _{Flow} (p.u.)	P _{Loss} (p.u.)	Q Loss (p.u.)	Switch
11	10	0.5943	-0.1461	0.03073	0.07194	S18
9	10	-0.428	0.32356	0.00917	0.02435	S16
9	14	0.2154	0.08447	0.0068	0.01447	S17
7	9	0	0.32539	0	0.01088	S15
8	7	0	0.3481	0	0.01742	S14

For islanding operations: To isolate every cluster depending on the BSUs capacity. This proposed method are able to find out optimum Island operation to disconnect the switches \$2,\$4,\$5,\$6,\$8,\$9,\$11 and \$20 to make separate three separate islands with maintain the constrains. This novel algorithm is efficiently check each constrains of optimization problem after satisfy in all aspect DGs are connected to the corresponding loads and operate island operations for separate cluster. To distinguish the steady state response of different cluster a load flow investigation has been performed which are recorded for each cluster. For islanding operation condition all disconnect switch status will be zero. So this novel algorithm efficiently gives the solutions to restore the load as per available resources.

CONCLUSION

This technique has been revealed the best optimal result to search the optimal islanding configuration for the restoration scheme to restore load as per BSU availability and try to minimize system losses and also distributed steady state stable output response after connecting BSU resources as well as voltage stability performance in each islands. The case studies indicate that the suggested methodology can help a power system operator promptly determining the appropriate clustering for emergency blackout condition. The proposed algorithm productively is examined on a modified IEEE 14 bus system. The case study recommended methodology to determining the appropriate solution at emergency blackout condition when normal supply is unavailable or normal supplies out of order as well as complete blackout conditions or partial load shedding stages.

Reference

- J. J. Ancona, "A framework for power system restoration following a major power failure," *IEEE Transactions on power* systems, vol.10,no.3, pp. 1480-1485, Augest 1995.
- C.Wang, V.Vittal, K.Sun, "OBDD-based sectionalizing strategies for parallel power system restoration," IEEE Transactions on Power Systems, vol.26,no.3,pp.1426-1433,September 2010.
- Yang Q, Jiang L, Ehsan A, et al. Robust Power Supply Restoration for Self-Healing Active Distribution Networks Considering the Availability of Distributed Generation. Energies 11,no.1,p. 210,January,2018.
- 4. H.Afrakhteh, M. R. Haghifam. "Optimal islands determination in power system restoration.," pp.463-476, (2009).
- J.Quirós-Tortós, M.Panteli, P.Wall, V.Terzija, "Sectionalising methodology for parallel system restoration based on graph theory," *IET Generation, Transmission & Distribution*, vol.9,no.11, pp.1216-1225,March 2015.
- F. Edström, S.Lennart, "On spectral graph theory in power system restoration," In 2011 2nd IEEE PES International Conference and Exhibition on Innovative Smart Grid Technologies, 1-8. IEEE, 2011.
- L. Sun, C.Zhang, Z. Lin, F.Wen,Y. Xue, M.A.Salam, S.P. Ang, "Network partitioning strategy for parallel power system restoration,". *IET Generation, Transmission & Distribution*, 10(8), pp.1883-1892,May2016
- D.Sarkar, A.De, C.K.Chanda, S.Goswami, "Kruskal's Maximal Spanning Tree Algorithm for Optimizing Distribution Network Topology to Improve Voltage Stability," Electric Power Components and Systems,vol.43,no.17,pp. 1921-1930,Octember2015.
- P. Kessel, H. Glavitsch, "Estimating the voltage stability of a power system," IEEE Transactions on power delivery, vol.1,no.3,pp.346-

354, July 1986.

- D.Sarkar, P. Konwar, A. De, S. Goswami, "A graph theory application for fast and efficient search of optimal radialized distribution network topology," Journal of King Saud University-Engineering Sciences, 2019.
- H.Saadat, Power System Analysis, McGraw Hill Series in Electrical and Computer EngineeringMcgraw-Hill College, pp. 224-229,1999.
- 12. F.Milano, Power System Analysis Toolbox Documentation, Canada: University of Waterloo. 2006; PSAT version 2.0. 0.

Experimental Investigations on Comparison of Different Topologies of Three Phase Self Excited Induction Generator

B Murali Krishna. V^{1*}, V Sandeep², SS Murthy³

^{1,2}Department of Electrical Engineering, Central University of Karnataka, Gulbarga-585367 ³IIT Delhi (Rtd) Life Fellow- IE (I)

{Corresponding author's email: vsandeep@cuk.ac.in}

Abstract - This paper presents experimental investigations on self-excited induction generator (SEIG) for renewable energy based standalone applications. Many researchers get confused with doubts while experimenting on three phase generators since there are two possible connections, star (Y) and delta selecting (Δ) , induction generator, in capacitor(Cexc) and load bank. In this paper, this aspect is addressed to provide guidance to make simple and perfect practical combination for working on three phase SEIG with minimum reactive power compensation to meet the objective of maintaining constant voltage and frequency at end users. The experimental results draw a conclusion that the following combinations (i) Δ SEIG- Δ Cexc- Δ Load and (ii) Δ SEIG- Y Cexc- A Load providesgood voltage profile from no-load to full load. The combination (i) works well within voltage limits and does not require any additional reactive power up to 60% of the rated load and later need minimum VAR support compared to combination (ii).

Keywords - Renewable energy sources (RES), self-excited induction generator (SEIG), voltage regulation, reactive power (VAR) compensation.

Introduction

To meet peak demand of energy and improve reliability in energy supply, the emerging economies are focusing on power generation using renewable energy sources (RES) in recent times, which maximizes the utilization of locally available energy resources like wind, hydro, solar, biomass, tidal, geo-thermal etc. [1], [2]. Many advantages with RES based electric power generation systems as compared to conventional coal, oil and gas-based systems, are: eco-friendly, non-polluting, highly reliable, simple and safe operation, and easy installation. The distributed generation directly involves consumers and local utilities [3], [4].

RES based systems, except solar energy, the remaining major sources like, wind, hydro, and bio-mass are electric generator based in which the generator generates electric power by utilization of RES as a major input. Nowadays, distributed generation and isolated (off-grid) mode of operating systems are gaining popularity using RES. The f merits are: minimizing of transmission & distribution (T&D) losses, installation cost and maintenance. For small-scale applications, like domestic loads, offices, and micro

industries, the distributed generation systems are more attractive and promising than grid-connected systems [2]

As per the literature, induction generators (IGs) are becoming more suitable for small-scale generation. than conventional synchronous generators. The advantageous of IGs are rugged construction, brushless arrangement, low cost, simplicity of operation, less maintenance, quick dynamic response [9], self-fault detection capability, ability to generate power at varying input speeds and absence of synchronisation. But the IGs are not suitable for wide speed range of operations and variable load conditions and one more draw-back is that it is not self-fault tolerant [5]-[8],[18]-[21].

To operate IG as a self-started generator in a standalone mode, a suitable capacitor has to be connected across its stator terminals and rotor speed should be maintained at super-synchronous speed; this phenomenon in IG is called capacitor excitation phenomena and such a featured IG is called self-excited induction generator. In SEIG, the terminal voltage and frequency are not constant. At varying voltage and frequency, the air-gap flux varies and tends to operate at wider range of magnetic flux density in the saturated region and magnetizing reactance X_m assumes different values dependent on capacitor, speed and load[7], [8]. So, a much care should be needed to choose the minimum capacitance value in such a way to make the IG as a SEIG. Single-phase operation is also possible with the three-phase induction generator and is reported in literature [17]. This paper concerns experimental investigations on SEIG performance with different start/delta connections of windings, capacitors and loads.

CONFIGURATIONS AND STEADY-STATE ANALYSIS OF SEIG

A basic experimental diagram of RES based SEIG is given in Fig 1.a) and the simplified per-phase electrical equivalent circuit is presented in Fig 1.b), which is used for the steady-state analysis [11]. Fig.1b will useful for finding key parameters for SEIG operation.

A. Configurations of the Experimental Study with SEIG In this work, the following combinations are studied experimentally

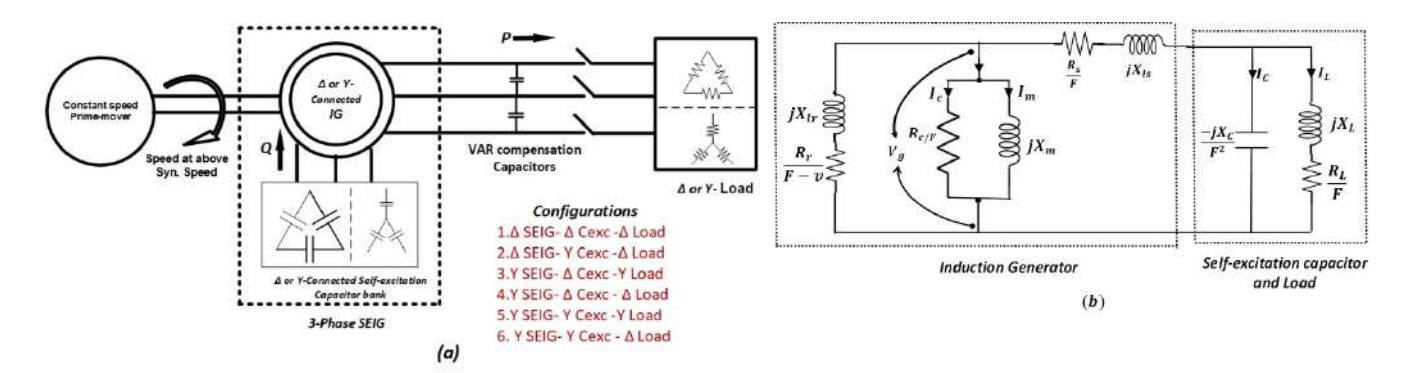


Fig. 1 a). Schematic diagram of isolated load system with SEIG. b). Per-phase equivalent circuit of SEIG

- Delta configured SEIG- Delta configured selfexcitation capacitors- Delta configured load (Δ SEIG-Δ Cexc -Δ Load)
- ii. Delta configured SEIG- Star configured selfexcitation capacitors- Delta configured load (Δ SEIG-Y Cexc -Δ Load)
- iii. Star configured SEIG- Delta configured self-excitation capacitors- Star configured load (Y SEIG- Δ Cexc -Y Load)
- iv. Star configured SEIG- Delta configured self-excitation capacitors- Delta configured load (Y SEIG- Δ Cexc - Δ Load)
- v. Star configured SEIG- Star configured self-excitation capacitors- Star configured load (Y SEIG- Y Cexc -Y Load)
- vi. Star configured SEIG- Star configured self-excitation capacitors- Delta configured load (Y SEIG- Y Cexc Δ Load)

B. Steady-State Analysis of SEIG

Steady-state analysis is an important aspect for both design and operation[9]-[16]. For steady-state analysis, a capacitor-excited induction machine with a balanced RLload equivalent circuitisshown in Fig. 2(a) & (b). All the values of equivalent circuit quantities are referred to stator side and reactance values are referred to the base frequency [11], [13], [14]. For the present analysis core loss component is taken in to account and rest of the assumptions in literature are: a) induced voltage's m.m.f harmonics and time harmonics b) all other parameters are considered as constant expect variation of magnetizing reactance with the saturation level of the core. All the notations of the presented paper are given in the Table.1 Appendix. For finding the unknown variables like, X_m and F from the IG of Fig. 1 (b), the Kirchhoff's voltage law (K.V.L) is applied and numerical solution for the unknown variables. The simplified loop equation for SEIG of Fig 1(b) is given by (1) and simplified value of $\mathbb{Z}_{\mathbf{z}}$ is given by (2.a) and (2.b).

$$\begin{split} Z_{S} &= \left\{ \left(\frac{R_{r}}{F-v} + jX_{lr} \right) / / \left(\frac{jX_{m}.R_{c}/F}{jX_{m}+R_{c}/F} \right) \right\} + \left\{ \frac{R_{S}}{F} + jX_{ls} \right\} + \\ &\left\{ \left(\frac{R_{L}}{F} + jX_{L} \right) / / (-jX_{C}/F^{2}) \right\} \\ &(2. \text{ a}) \end{split}$$

$$Z_{S} &= \left\{ \frac{jR_{c}X_{m}(R_{r}+jX_{lr}(E-v))}{[R_{r}+jX_{lr}(F-v)][R_{c}+jFX_{m}+jR_{c}X_{m}(F-v)]} \right\} + \left\{ \frac{R_{S}}{F} + jX_{ls} \right\} + \\ &\left\{ \frac{(R_{L}+jFX_{L})(-jX_{C})}{R_{L}F^{2}+j(X_{L}F^{2}-X_{C}F)} \right\} \end{aligned}$$

$$(2. \text{ b})$$

Under steady state condition, per phase stator current $(I_{\mathbf{z}})$ is not equal to zero [10]-[19] in (1), hence the per phase stator impendence $(\mathbb{Z}_{\mathbf{z}})$ must be equal to zero. Under this condition, both the real and imaginary parts of $\mathbb{Z}_{\mathbf{z}}$ is independently equal to zero. The solution of (1) either in terms of impedance (Nodal Impedance Method) or admittance (Admittance Method) different techniques were proposed in the literature.

$$\begin{aligned} &(X_m,F) = K_1 X_m F^5 + K_2 X_m F^4 + (K_2 X_m + K_4) F^2 + \\ &(K_5 X_m + K_6) F^2 + (K_7 X_m + K_8) F + K_9 X_m + K_{10} = 0 \\ &(3) \end{aligned}$$

$$g(X_m,F) = (K_{11} X_m + K_{12}) F^4 + (K_{12} X_m + K_{14}) F^3 + \\ &(K_{15} X_m + K_{16}) F^2 + (K_{17} X_m + K_{18}) F + K_{19} = 0$$

The (3) and (4) can be solved numerically for any given values of load impedance, speed, terminal capacitor, and the machine parameters. Value of air gap voltage (V_g) can be determined from the derived values of V_m and V_m . If the same analysis is required for V_m load, then the V_m value is equal to zero in equation values of V_m and V_m and V_m with V_m can be used for the calculation of V_m value. The calculation of V_m and V_m is calculated from the synchronous impedance test. The values

of R_2 and X_{12} can get from the nameplate details provided by the manufacturer of the generators. Once the values of X_{12} , F and Y_2 are determined theoretically the remaining electrical responses can be easily find out from the equivalent circuit, from simplified expressions given by (15)-(21).

Power Factor (PF) =
$$\frac{P}{VJ}$$
 (5)

$$\varphi = \cos^{-1}(PF)(6)$$

$$P_{core} = (P - (I^2.R_5)) \qquad (7)$$

$$I_{vector} = I(\cos\varphi - i\sin\varphi) \tag{8}$$

$$V_{\sigma} = abs \left[V - \left[I_{vsctor} (R_s + jX_{ls}) \right] \right]$$
 (9)

$$R_{\mathcal{C}} = \frac{v_{\mathcal{G}}^2}{P_{corr}} \tag{10}$$

$$I_{cc} = \frac{P_{xorg}}{V_{cc}}$$

$$I_{mc} = \sqrt{I^{2} - I_{cc}^{2}}$$

$$X_{mc} = \frac{I_{cc}}{I_{cc}}$$

$$(11)$$

$$(12)$$

$$(13)$$

$$X_{pn} = \frac{v_g}{t_-} \tag{14}$$

$$I_{\delta} = \frac{v_g / F}{v_g / F + j x_{1s} + \left[\frac{(R_1 + j X_1 F)(-j X_c)}{R_L F^2 + j (X_L F^2 - X_c F)}\right]}$$
(15)

$$I_r = \frac{-V_g/F}{\frac{E_r}{E_r + jX_{br}}}$$
(16)

$$I_{L} = \frac{-jZ_{c}I_{z}}{Z_{L}E + j(Z_{L}E^{2} - Z_{c})}$$
(17)

$$V_t = (R_L + jX_L F)I_L \tag{18}$$

Totalinput power
$$P$$
 input $=\frac{-|\mathbf{x}|_{F_{\nu}}|^{2}R_{\nu}}{F_{-\nu}}$ (19)

Total output power
$$P$$
 output = $3|I_L|^2R_r$ (20)
Total Losses $W_{TL} = 3\left(|I_r|^2R_r + |I_{\mathcal{S}}|^2R_{\mathcal{S}} + \frac{|v_{\mathcal{S}}|^2}{R_{\mathcal{S}}}\right)$ (21)

Finally, with help of curve fitting toolbox provided by MATLAB (cftool), using exponential equation approach mathematical model $f(x) = a * e^{b*x} + c * e^{d*x}$, relationship between Vg and Xm can be obtained for induction machine by using (22).

$$V_g(Xm) = -0.0005543 * e^{0.2128 \cdot Xm} + 249.4 e^{0.0007197 \cdot Xm}$$

In this work, the best practice method to validate among the configurations of star (Y) and delta (Δ) of SEIG withY and Δ excitation capacitors to generate the rated output voltage and frequency for isolated load applications is followed. In all configurations, the speed of the rotor should remain above the synchronous speed and which is further maintained at the same speed. The selection of excitation capacitance values for the respective configurations are given by the following (23)-(26). The calculated capacitance value for the (23) is $10.75\mu F$.

For **Y** SEIG

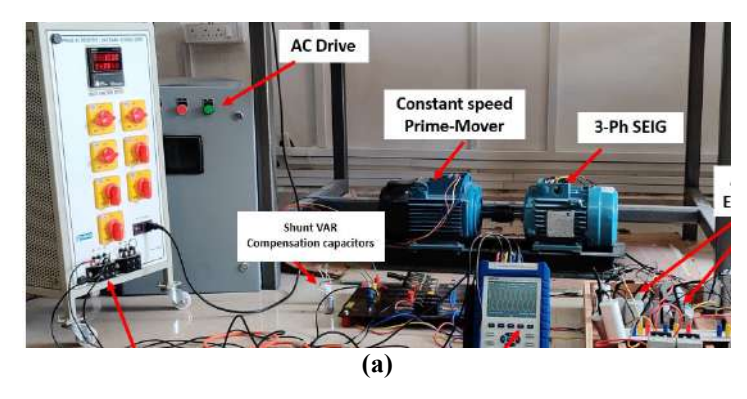
$$V SEIG [Cex] \Delta ph = \frac{q_g}{2 \times V_{ph}^2 \times 2 \times \pi \times f_{base}}$$
 (23)

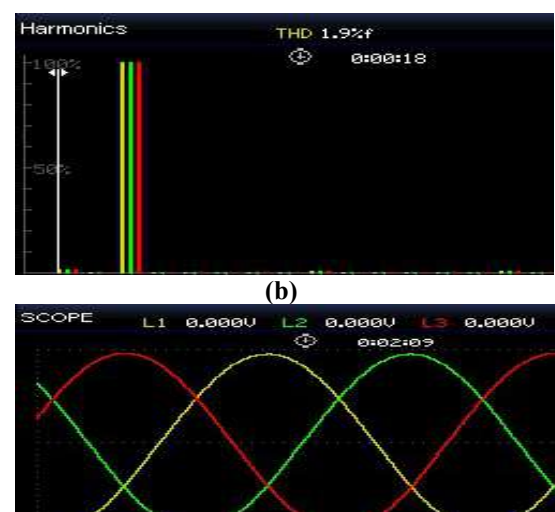
$$Y SEIG [Cex]_{yh} = 3 \times Y SEIG [Cex]_{\Delta ph}$$
 (24)

For Δ SEIG

$$\Delta \text{ SEIG[Cex]}_\Delta \text{ph} = 3 \times \frac{Q_g}{3 \times V_{ph}^2 \times 2 \times \pi \times f_{base}}$$
 (25)

$$\Delta SEIG[Cex]_Yph = 3 \times \Delta SEIG [Cex]_\Delta ph \qquad (26)$$





(c)

Fig. 2. a) Experimental set-up work diagram of SEIG b) Voltage wave of Δ SEIG- Δ Cexc- Δ Load configured condition at full load. c) THD value of Δ SEIG- Δ Cexc- Δ Load configured condition at full load

where
$$Q_g = \frac{\sin Q_g}{\sin Q_m} \times Q_m$$
 and $Q_m = \frac{\rho_m}{q_m} \times \tan(\cos^{-1}\varphi_m)$

EXPERIMENTAL VALIDATION OF SEIG

The verification on the SEIG is carried out to investigate voltagevariation from no-load to full-load condition and also a simple shunt reactive power compensation method was adapted for improving voltage regulation and compared among the configurations. The experimental setup and the obtained results are shown from Fig. 3 to Fig.5.In the presented work, 1.1kW, 415 V, 50 Hz, 6 –pole three phase induction machine is considered. The generated voltage is 240 for all combined configurations of delta and the same is 415 in case of all combined configurations of star SEIG. The allowable voltage regulation value considered was ±5% and frequency variation is ±1% for all the cases.

The noticeable two observations from Fig.3 is that without any VAR compensation, the system can be utilized up to 58% of its rated load with the Δ SEIG- Δ Cexc- Δ Load combination and is only 40% of its rated load in case of Δ SEIG- Y Cexc- Δ Load combination. With 42.25 VAR per phase compensation, the system can be utilized for 100% instead of 58% of its load with the Δ SEIG- Δ Cexc- Δ Load combination and with 63.63 VAR per phase shuntmanner compensation, the system can be utilized for 100% instead of 40% of its load with the Δ SEIG- Y Cexc- Δ Load.

From Fig.4, without any VAR compensation, the system generated voltage is about to zero value when the load is 100% in case of both Y SEIG- Δ Cexc- Δ Load and Y SEIG- Δ Cexc- Y Load combinations. These two are utilized up to 25% of rated load without VAR

compensation. For Y SEIG- Δ Cexc- Δ Load, with 135.25 VAR per phase shunt- manner compensation from 25-59% of the rated load, the system will be in the acceptable operating voltage range and the after the load range the voltage will drop to 320 Volts. In case of Y SEIG- Y Cexc- Δ Load, with 54.15 VAR per phase shunt- manner compensation from 25-59% of the rated load, the system will be in the acceptable operating voltage range and the after the load range the voltage will drop 320 Volts.

TABLE. I. NOTATIONS

R_a , R_r , R_z	: stator, rotor and core-loss resistances respectively			
C, C	: excitation, series and shunt capacitors respectively			
Cat				
$X_{\underline{1}}, X_{\underline{1}}$: per phase stator and rotor leakage reactance			
	respectively			
X	: magnetizing reactance			
X _a	: per phase capacitive reactance of the terminal capacitor			
R_x	: load resistance per phase			
F, v	: p.u. frequency and speed respectively			
I, I,	: per phase stator and rotor currents			
I_2	: load current per phase			
V ₂ , V ₃	: terminal and air-gap voltage respectively			
P _{im} P _{ous}	: input and output power respectively			

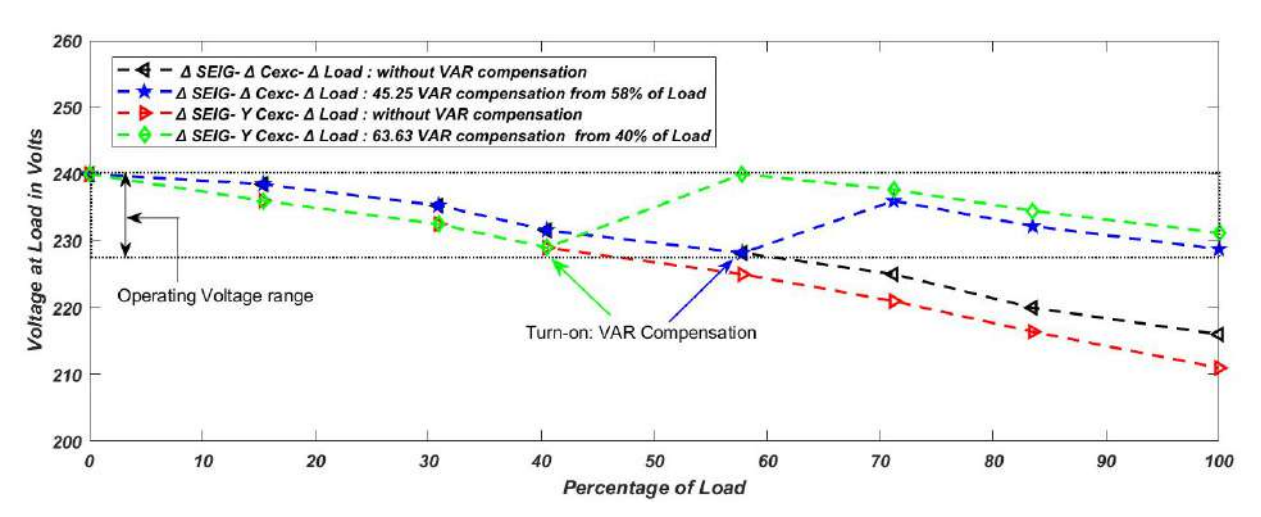


Fig.3. Performance of Δ SEIG- Δ and Y Cexc - Δ Load: with and without VAR compensation

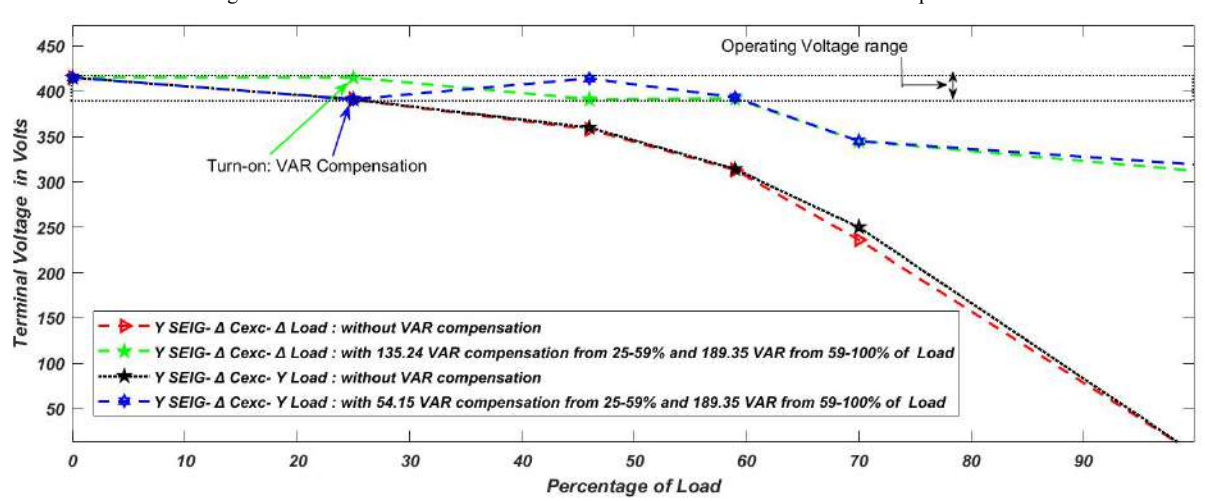


Fig.4. Performance of Y SEIG- Δ Cexc -Δ and Y Load: with and without VAR compensation

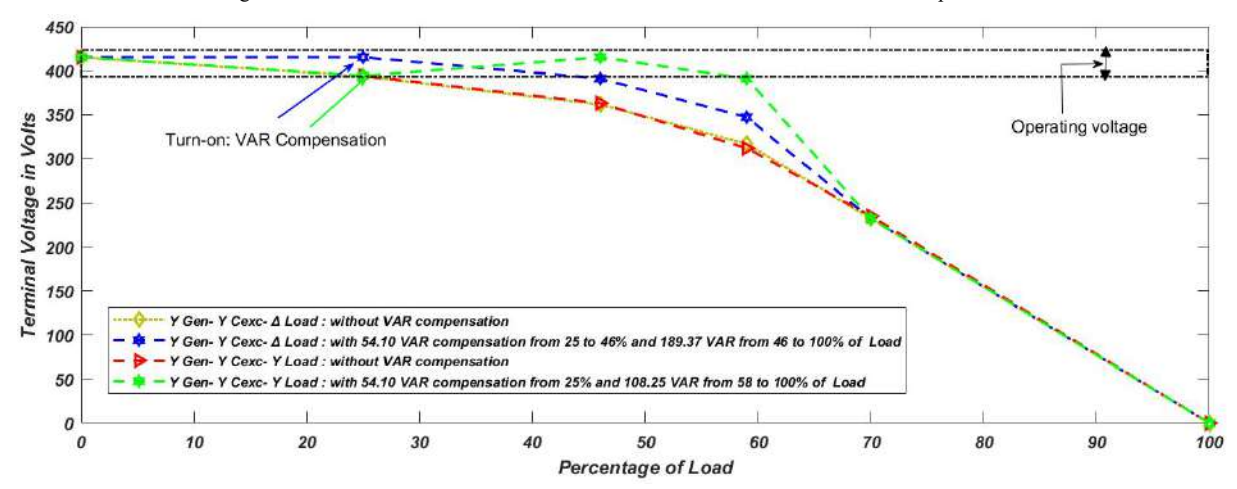


Fig.5. Performance of Y SEIG-Y Cexc-Δ and Y Load: with and without VAR compensation

TABLE III. COEFFICIENTS

Coefficients (3) and its value	Coefficient of (4) and its value
$C_{2} = X_{2}X_{2r}X_{2r}$	$D_{1} = -X_{2}(X_{2s}(R_{r} + R_{c}) + X_{2s}(R_{s} + R_{c})) - R_{2}X_{2s}X_{2s}$
$C_2 = -a_1 v$	$D_{a} = -R_{a}X_{a}X_{b}X_{b}$
$C_{1} = -X_{L}(X_{c} + X_{b} + R_{\tau}(R_{s} + R_{c})R_{s}R_{s}) - R_{L}(X_{b}(R_{\tau} + R_{c}) + X_{b}(R_{s} + R_{c$	$+ S D_{z} = v(X_{L}(X_{L}(R_{s} + R_{s}) + X_{L}R_{s}) + R_{L}X_{L}X_{L}X_{L})$
$C_{+} = -R_{c}(X_{L}(R_{c}X_{L} + R_{c}X_{L}) + R_{L}X_{L}X_{L}) + R_{L}X_{L}X_{L})$	$D_a = vX_bX_bX_bX_bR_c$
$C_5 = v\left(R_L(R_2X_b + R_c(X_b + X_b))\right) + X_L(X_cX_b + R_cR_p) + X_cX_bX_b$	$D_{\rm g} = R_{\rm g} (X_{\rm e} X_{\rm b} + R_{\rm g} (R_{\rm r} + R_{\rm g}) + R_{\rm g} R_{\rm r}) + X_{\rm g} (X_{\rm f} (R_{\rm r} + R_{\rm g}) + R_{\rm g} (X_{\rm b} + X_{\rm b}) +$
$C_{\rm g} = R_{\rm g} X_{\rm lr} v (R_{\rm g} X_{\rm lr} + R_{\rm lr} X_{\rm lr})$	$D_{0} = R_{\mathbf{x}}(X_{\mathbf{x}}X_{\mathbf{b}}(X_{\mathbf{b}} + X_{\mathbf{b}}) + R_{\mathbf{b}}(R_{\mathbf{y}}X_{\mathbf{b}} + R_{\mathbf{x}}X_{\mathbf{b}}) + R_{\mathbf{x}}R_{\mathbf{y}}X_{\mathbf{b}})$
$C_{\tau} = X_{\sigma} \left(R_{\sigma} (R_{\sigma} + R_{\tau} + R_{\perp}) + R_{\tau} (R_{\sigma} + R_{\perp}) \right)$	$D_{\tau} = -v \left(X_{c} \left(X_{b} (R_{s} + R_{c} + R_{L}) + R_{c} (X_{L} + X_{bs}) \right) + R_{s} R_{c} R_{L} \right)$
$C_{z} = R_{c} \left(X_{c} \left(R_{r} \left(X_{ls} + X_{l} \right) + X_{l}, \left(R_{s} + R_{L} \right) \right) R_{s} R_{r} R_{L} \right)$	$D_{\mathbf{E}} = -wR_{\mathbf{c}}X_{\mathbf{L}}\left(R_{\mathbf{c}}R_{\mathbf{L}} + X_{\mathbf{c}}(X_{\mathbf{L}} + X_{\mathbf{L}})\right)$
$C_v = -R_v X_v \psi(R_v + R_L)$	$D_{\alpha} = -R_{\alpha}R_{\alpha}X_{\alpha}(R_{\alpha} + R_{\alpha})$
$C_{10} = -R_a X_a v X_b$	

TABLE III. Voltage Regulation

% of	Δ SEIG- Δ	Cexc-	Δ SEIG-	Y Cexc-	Y SEIG-	Δ Cexc-	Y SEIG	- Δ Cexc-	Y SEIG-	Y Cexc-	Y SEIG-Y	Cexc-
Load	Δ Loa	ıd	ΔL	oad	ΔL	oad	YI	Load	ΔL	oad	Y Loa	ad
					Reac	tive power (VAR) Comp	pensation				
	Without	With	Without	With	Without	With	Without	With	Without	With	Without	With
0	0	0	0	0	0	0	0	0	0	0	0	0
25	1.66	1.66	3.20	0	5.00	5.00	5.00	5.00	4.81	4.81	4.81	4.61
45	3.75	3.75	4.58	3.20	13.25	0.48	13.05	0.24	12.77	0.24	11.17	0.24
58	4.95	4.95	6.25	0	23.33	4.90	22.95	4.57	22.04	4.81	21.04	14.45
80	6.25	2.5	8.75	1.66	66.26	16.86	64.16	16.86	61.16	20.48	59.16	26.50
100	8.33	4.95	12.08	4.16	100.00	18.07	100.00	17.58	100.00	26.50	100.00	24.05

Conclusion

The experimental performance investigation on the SEIG for isolated load applications are presented in this paper. From the results presented, it is observed that among the verified configurations, the delta connected SEIG – delta connected excitation - delta connected load confirmation shows the best performance almost up to 60% of the related load rating of the SEIG even without any additional VAR compensation. With a small reactive compensation value of 42.25 VAR, the remaining load can be operated smoothly without compromising the frequency value. In case of star configured SEIG, only 25% of rated load operation was observed for both star and delta excitation and load configurations. Even withadditional VAR compensation, the star connected generator operates only

up to 60% of rated load. Therefore, it is concluded from the experimental results that Δ SEIG- Δ Cexc- Δ Load is the best combination for standalone power generation applications.

REFERENCES

- [1] Puneet K. Goel, Bhim Singh, S. S. Murthy, and Navin Kishore, "Isolated Wind–Hydro Hybrid System Using Cage Generators and Battery Storage", IEEE Transactions on Industrial Electronics, vol. 58, no. 4, pp. 1141-1153, April 2011.
- [2] S.S. Murthy, B.P. Singh C. Nagamani and K.V.V. Satyanarayana, "Studies on the use of conventional Induction Motors as Self-Excited Induction Generators", IEEE Transactions on Energy Conversion, Vol. 3, No. 4, pp. 842-848, 1988.
- [3] Sreenivas S. Murthy, "Renewable energy generators and control", chapter. 12, Electric Renewable Energy Systems, pp. 238-289, 2016 Elsevier.

- [4] G. K Singh, "Self-Excited Induction Generator for Renewable Applications", Encyclopedia of Sustainable Technologies, Volume 4, pp. 239-256, 2017 Elsevier Inc.
- [5] R.C. Bansal, T. S. Bhatti, and D. P. Kothari, "Bibliography on the Application of Induction Generators in Nonconventional Energy Systems", IEEE Transactions on Energy Conversion, vol. 18, no. 3, pp. 433-439, September 2003.
- [6] R.C. Bansal, "Three-Phase Self-Excited Induction Generators: An Overview", IEEE Transactions on Energy Conversion, vol. 20, no. 2, pp. 292-299, June 2005.
- [7] B. Singh, "Induction generator -a prospective," Electric Machines and Power Systems, vol. 23, pp. 163-177, 1995.
- [8] Paul C. Krause, Analysis of Electric Machinery, McGraw-Hill, New York, 1987.
- [9] S.S. Murthy, O.P. Malik, and A.K. Tandon, "Analysis of self-excited Induction Generators", IEE Proc, Vol. 129, Pt. C, No. 6, pp. 260-265, 1982.
- [10] A.K. Tandon, S.S. Murthy and G. K Berg, "Steady State Analysis of Capacitor Self-Excited Induction Generators", IEEE Transactions on Power Apparatus and Systems, Vol. PAS-103, No. 3, PP.612-618, 1984.
- [11] N.H. Malik and S.E. Hague, "Steady-State Analysis and Performance of an Isolated Induction Generator", IEEE Transactions on Energy Conversion, Vol. EC-1, No. 3, pp. 134-140, September 1986.
- [12] T.F. Chan, "Steady-State Analysis of Self-Excited Induction Generators", IEEE Transactions on Energy Conversion, Vol. 9. No. 2, pp. 288-296, June 1994.
- [13] T.F.Chan, "Steady-State Analysis of Self-Excited Induction Generators using an Iterative Method", IEEE Transactions on Energy Conversion, Vol. 10, No. 3, pp. 502-507, September 1995.
- [14] S. Rajakaruna and R. Bonert, "A Technique for the Steady-State Analysis of Self-Excited Induction Generator with Variable Speed", IEEE Trans. an Energy Conversion, Vol. 8, No. 4, December, 1993, pp.757-761.
- [15] S. P Singh, M.P. Jain and Bhim Singh, "A New Technique for Analysis of Self-Excited Induction Generator", Electric Machine and Power Systems, vol.23, no.6, pp.647-656, 1995.
- [16] L. Shridhar, Bhim Singh, C. S. Jha, B. P. Singh, and S.S Murthy, "Selection of Capacitors for the self-regulated short shunt self-excited induction generator", IEEE Transactions on Energy Conversion, Vol. 10, No. 1, pp. 10-17, 1995.
- [17] Sandeep Vuddanti, S.S. Murthy, S.S. Murthy and Bhim Singh, "An Optimum Solution for Field Deployment of Single-phase Power Generation using 3-Phase Self Excited Induction Generator", 978-1-4673-8888-7/16/\$31.00©2016 IEEE.
- [18] E.D. Basset and E. M. Potter, "Capacitive Excitation for Induction Generator" AIEE Trans. on Electrical Engineering, vol. 54, pp. 540-545, May 1935.
- [19] N.H. Malik and A.A. Mazi, "Capacitance Requirements for Isolated Self -Excited Induction Generators", IEEE Transactions on Energy Conversion, vol. EC-2, no. 1, pp. 62-69, March 1987.
- [20] T.F. Chan, "Capacitance requirements of Self-Excited Induction Generators", IEEE Transactions on Energy Conversion, Vol. 8, No. 2, pp. 304-311, June 1993.
- [21] J.-M. Chappalaz, J. Dos Ghalli, P. Eichenberger, G. Fisher, "Mannual on Induction Motors used as Generators", MHPG Series Harnessing Water Power on Small Scale, Volume 10.

Comparative Analysis of Droop and Virtual Oscillator Control for Parallel Inverters in Standalone Microgrid

Gurugubelli Vikash, Arnab Ghosh and Subhobrata Rudra Department of Electrical Engineering, NIT-Rourkela Rourkela City, Odisha, 769008, India

vikas0225@gmail.com

Abstract - In recent times the Renewable energy sources (RES) have been potential alternatives for the conventional generation systems connected in the grid. The power electronic inverters are the principal media of interface for connecting the renewable energy sources to the utility grid system. The prime focus of this paper is on inverter coordination methods with the objective of maintaining system stability. The work is primarily focused on the comparative analysis of droop and Virtual Oscillator Control (VOC) techniques for the parallel operated inverters in a standalone Microgrid (MG). In droop control, the feedback signals such as voltage and current are measured to calculate the averaged real and reactive powers, such that the transient response of this controller is not significant. And the VOC works on the instantaneous feedback signals. The steady-state performance of the system with the aforementioned controllers is almost similar, but the dynamic performance of the system differs remarkably. The simulation results substantiate that VOC gives a better dynamic performance compared to droop control.

Keywords – Droop control, VOC, Parallel Inverters, Standalone Microgrid.

INTRODUCTION

Microgrids are a natural extension of the distributed and renewable energy setting. A microgrid is a decentralized electrical power system composed of generation, storage, and loads that can operate independent of the bulk power system. As envisioned, the future infrastructure could be composed of a large number of interconnected microgrids which each contain energy resources and storage. Microgrids are poised to become a valuable technology in the distributed generation domain and are expected to provide several system level advantages including: increased renewable integration, reduced transmission and distribution losses, and reliable power supply to loads in mission-critical applications [1, 2].

Droop control and Virtual Oscillator Control (VOC) are the two different control strategies to achieve synchronization, and power-sharing between the parallel connected inverters in a standalone MG. The reactive power has its direct influence on the inverter output voltage, and the active power has its direct influence on the frequency. Therefore, the inverter output voltage and frequency response depend on the average active and reactive power output

respectively, which are to be controlled using a controller like the droop controller [3-5]. Since the active and reactive powers are phasor quantities, the dynamic performance of the droop controller is observed to be insignificant.

The VOC is a decentralized control strategy for standalone MGs where inverters are regulated to resemble the dynamics of the nonlinear oscillators [6-9]. The VOC regulates the amplitude and frequency of the inverter output voltage. Consequently, the inverters output voltages are synchronized. This technique ensures proportional load sharing according to their power ratings without any communication between the inverters. The VOC is principally a current based control working on the current demonstrates feedback signals. This paper aforementioned control methodologies in the context of standalone MG system as shown in Fig. 1. The simulation results of the system give a comparison of the control strategies. The steady-state performance of the system with the aforementioned controllers is almost similar, but there is a remarkable difference observed in the dynamic performance of the system. The simulation results substantiate the arguments that VOC gives a better dynamic performance compared to droop control.

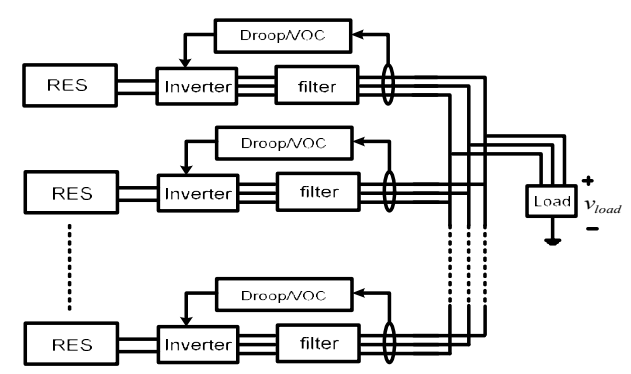


Fig. 1: Two different control strategies in the context of standalone MG.

This paper is organized into five sections. The first section being the introduction, the second section introduces the droop control theory and droop control implementation for a single inverter unit. The third section introduces the VOC implementation. The fourth section includes simulations results and its validation. In the fifth section concluding remarks are made on the two control strategies considered.

DROOP CONTROL

A. Droop control theory

In microgrid, the system reliability and stability is achieved only by the voltage regulation when more micro sources are interconnected. This voltage regulation damps the reactive power oscillations and thus the voltage. In a complex power system, when multiple DGs are attached to the microgrid, the power sharing among them is made properly with the help of droop control. Droop control also enables smoother transitions of the MG to connect and disconnect to the complex power system. The role of droop control in power sharing is to control the real power on the basis of frequency droop control and the reactive power on the basis of voltage control [10].

Control over the voltage and frequency can be achieved by regulating the real and reactive power of the system. This forms a conventional droop control equation. In a transmission line, the real and reactive powers are derived as:

$$P = \frac{E_1 E_2}{X} \sin \delta \tag{1}$$

$$Q = \frac{E_1^2}{X} - \frac{E_1 E_2}{X} \cos \delta \tag{2}$$

In the above mentioned equation (3.1) and (3.2), Resistance (R) is neglected for an overhead transmission lines as it is much lower than inductance (L). Also the power angle δ is lesser, Therefore, it can be assumed that $\sin \delta = \delta$ and $\cos \delta = 1$.

$$\delta = \frac{XP}{E_1 E_2} \tag{3}$$

$$E - E_0 \cong \frac{XQ}{E_1} \tag{4}$$

From the equation (3.3) and (3.4), it is evident that the power angle δ can be controlled by regulating real power (P). Also the voltage (E_1) can be controlled through reactive power (Q). Dynamically, the frequency control leads to regulate the power angle and this in turn controls the real power flow. Finally, the frequency and voltage amplitude of the microgrid are controlled by adjusting the real and reactive power autonomously. As a result, the frequency and voltage droop regulation can be determined as:

$$f = f_0 + mP \tag{5}$$

$$E = E_0 + nQ \tag{6}$$

$$m = \frac{\Delta \omega}{P_0} \tag{7}$$

$$n = \frac{\Delta E}{Q_0} \tag{8}$$

Where f, E are the frequency and voltage at a new operating point; P, Q are the active and reactive power at the new operating point; f_0 , E_0 are the base frequency and voltage; P_0 , Q_0 are the temporary set points for the real and reactive power; m, n are the Droop constants; $\Delta \omega$, ΔE are the maximum change in frequency and voltage amplitude respectively.

B. Droop control implementation

Droop control implemented in a single inverter unit as shown in figure. The PQ calculation is the first stage for the controller to compute average active power (P) and reactive power (Q) using the output current and bus voltage. The slope of the frequency droop is "m" and the slope of the voltage droop is "n". Finally, the droop rules fetch the frequency and voltage amplitude signals. These signals are useful to construct the control signal- $E\sin(\omega t)$.

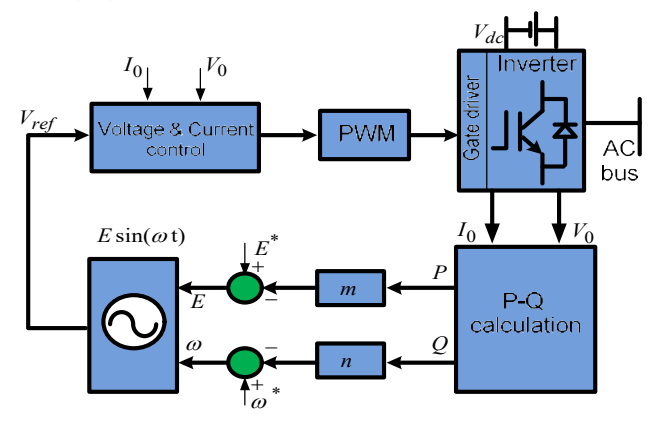


Fig. 2: Three-phase voltage source inverter with Droop control.

From Fig. 1, one can understand the droop control implementation. The actual real and reactive powers of the load side are calculated using the respective load voltages and currents. The temporary real and reactive powers are known already. Using equation (5) and (6) the reference signal is obtained. This reference signal is given as the input to the current and voltage controllers, the output of which will be used to generate switching pulses to the inverter using a PWM technique.

VIRTUAL OSCILLATOR CONTROL

A. Nonlinear dead-zone oscillator

The electrical schematic of the nonlinear dead-zone oscillator is as illustrated in Fig. 3. The construction of the dead-zone oscillator is inspired by the construction of familiar van der pol oscillator. The linear subsystem of the oscillator is a passive RLC circuit with impedance Z_{osc} [5].

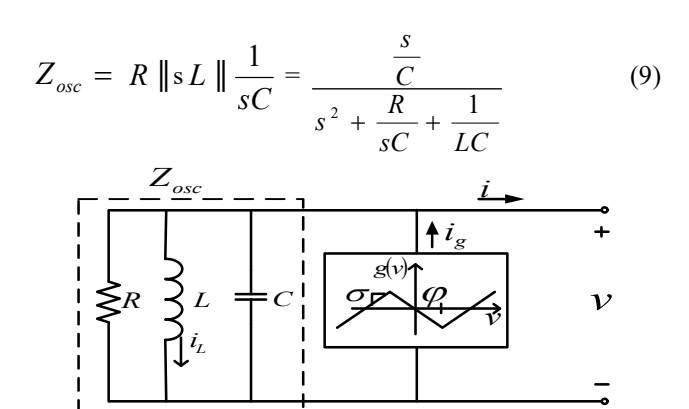


Fig. 3: Electrical schematic of the dead-zone oscillator.

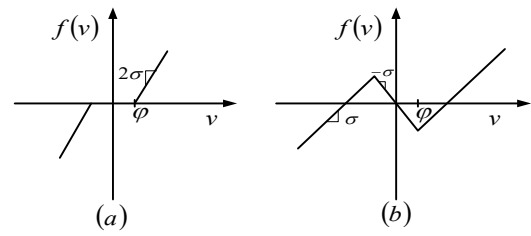


Fig. 4: Dead-zone function f(v) in (a) and the nonlinear voltage dependent current source g(v) in (b) are illustrated for dead-zone oscillator.

The voltage dependent current source is a static nonlinear function g(v) and defined as

$$g(v) = f(v) - \sigma v \tag{10}$$

Where f(v) is a dead-zone function with slope 2 σ

$$f(v) = 0, |v| \le \varphi$$

$$2\sigma(v - \varphi), v < -\varphi$$

$$2\sigma(v + \varphi), v < -\varphi$$
(11)

The functions f(v) and g(v) are as shown in Figs. 4.12(a) and (b), respectively.

The dynamics of the oscillator inductor current, i_L , and the capacitor voltage, v, are given by

$$\frac{dv}{dt} = \frac{1}{C} \left[(\sigma - \frac{1}{R})v - f(v) - i_L - i \right]$$

$$\frac{di_L}{dt} = \frac{v}{I}$$
(12)

Applying lienard's theorem to the system (12), unique and stable limit cycle can be obtained, if $\sigma > \frac{1}{R}$. From Fig. 4.11(b), the nonlinear subsystem acts as a power source for vg(v) < 0, and as a resistor (with resistance of $1/\sigma$) for vg(v) > 0. Due to the nonlinear subsystem, the amplitude of large oscillations is damped and the amplitude of small oscillations is increased [6].

B. VOC implementation

To control a three-phase inverter is done such that it emulates the dynamics of the nonlinear dead-zone oscillator. The dynamics of the oscillator can be programmed on the digital controller of the inverter. Because the nonlinear oscillator cannot be implemented physically, it is described as "virtual". A representative implementation of the control on a three-phase H-bridge inverter is given in Fig. 5. The oscillator voltage and scaled inductor current are orthogonal to each other. The two orthogonal signals are converted into three-phase signals by using inverse α - β transformation.

The real and imaginary components of g(t) are denoted by $g_{\alpha}(t)$ and $g_{\beta}(t)$, respectively. The relationship between the orthogonal signals in $\alpha\beta$ frame and the three-phase signals is captured by the following

$$\begin{bmatrix} g_{\alpha} \\ g_{\beta} \end{bmatrix} = \frac{2}{3} \begin{bmatrix} B \end{bmatrix} \begin{bmatrix} g_{\alpha} \\ g_{b} \\ g_{\alpha} \end{bmatrix}, \qquad \begin{bmatrix} g_{\alpha} \\ g_{b} \\ g_{\alpha} \end{bmatrix} = \begin{bmatrix} B \end{bmatrix}^{T} \begin{bmatrix} g_{\alpha} \\ g_{\beta} \end{bmatrix}$$

Where

$$\begin{bmatrix} B \end{bmatrix} = \begin{bmatrix} 1 & -\frac{1}{2} & -\frac{1}{2} \\ 0 & \frac{\sqrt{3}}{2} & -\frac{\sqrt{3}}{2} \end{bmatrix}$$

Digital Control

Virtual Oscillator $i_{a}K_{i}$ i_{abc} $i_$

Fig. 5: Three-phase voltage source inverter with virtual oscillator.

SIMULATION RESULTS

Simulation results of the considered system are provided in this section. Two inverters are connected in parallel for which droop and VOC control strategies are applied. Two cases are considered, the first case being application of the droop control to the system of inverters and the second case being application of VOC.

A. Case I:

In this case, droop control is applied to the system of parallel inverters as shown in Fig. 1. In this case two inverters are considered for testing the droop control performance. Initially the load is 1kW which suddenly increases to 1.5kW. The corresponding frequency changes

with load change are as shown in Fig. 6. The current sharing between the two inverters is as shown in Fig. 7. The THD is obtained to be 1.82 % as shown in Fig. 8.

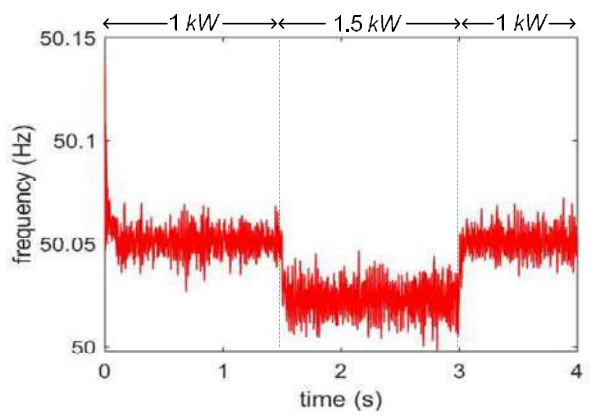
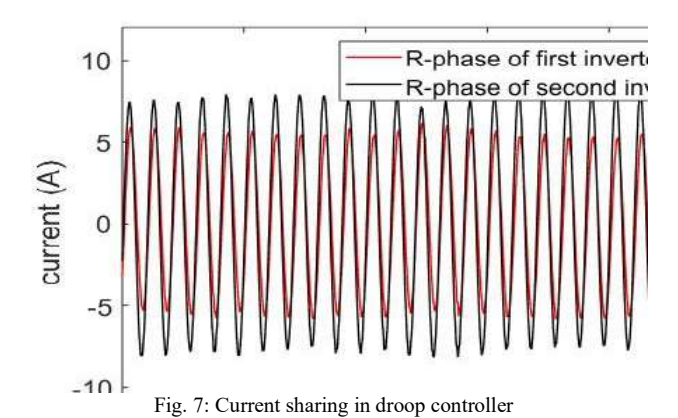


Fig. 6: Frequency response in droop controller



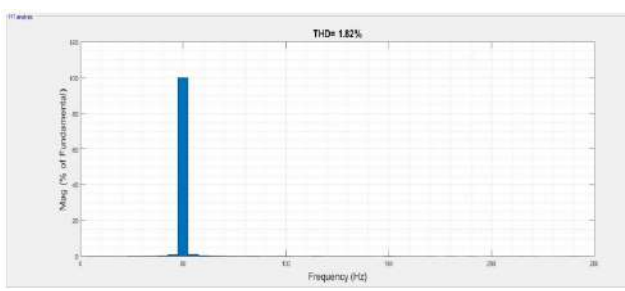


Fig. 8: FFT analysis in droop controller

A. Case II:

In this case, VOC is applied to the system of parallel inverters as shown in Fig 1. In this case two inverters are considered for testing VOC performance. Initially the load is *1kW* which suddenly increases to *1.5kW*. The corresponding frequency changes with load change are as shown in Fig. 9. The current sharing between the two inverters is as shown in Fig. 10. The THD is obtained to be 0.30 % as shown in Fig. 11.

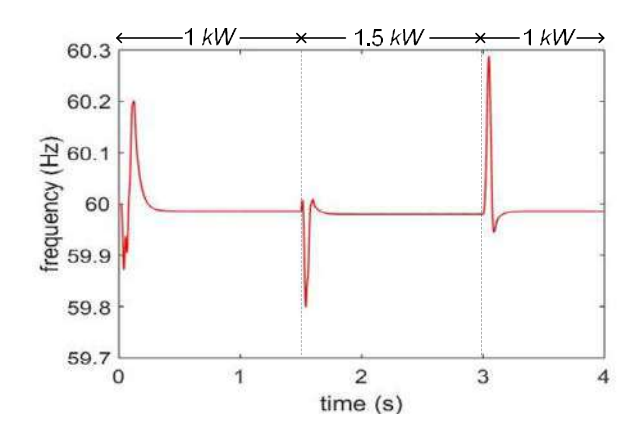


Fig. 9: Frequency response in VOC

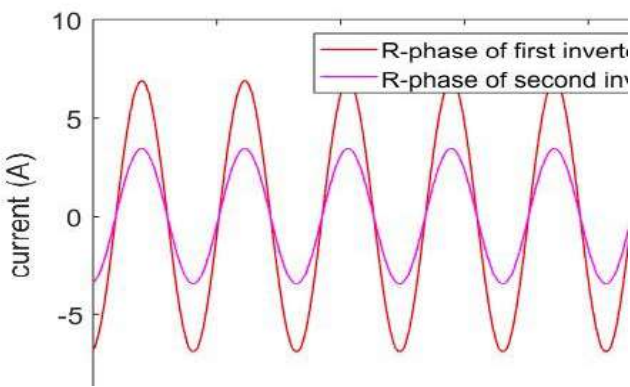


Fig. 10: Current sharing in VOC

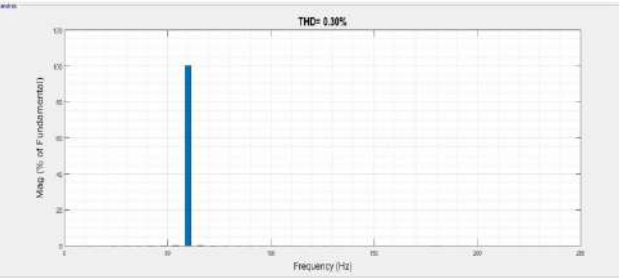


Fig. 11: FFT analysis in VOC

CONCLUSION

The droop and VOC are implemented in the system of parallel inverters, in which two three-phase inverters are present. The two controllers synchronize the output voltage of the each inverter and share the load proportional to their power ratings. Compared to droop, in VOC the current sharing is more effective. The resulting microgrid does not require communication between the inverters. In VOC, the synchronization condition is independent of the load parameters and number of inverters present. The simulation results substantiate that VOC gives a better dynamic performance compared to droop control.

REFERENCES

- S.K. Panda, and A. Ghosh. "A Low Ripple Load Regulation Scheme for Grid Connected Microgrid Systems." In 2018 IEEE 8th Power India International Conference (PIICON), pp. 1-6. IEEE, 2018.
- [2] S.K. Panda, and A. Ghosh. "Design of a Model Predictive Controller for Grid Connected Microgrids" in International Journal of Power Electronics (IJPElec), 2019.
- [3] Rocabert, J., Luna, A., Blaabjerg, F. and Rodriguez, P. "Control of power converters in AC microgrids," IEEE transactions on power electronics, 27(11), pp.4734-4749, 2012.
- [4] Zhong, Q.C. "Robust droop controller for accurate proportional load sharing among inverters operated in parallel," IEEE Transactions on Industrial Electronics, 60(4), pp.1281-1290, 2011.
- [5] Hou, X., Sun, Y., Han, H., Liu, Z., Yuan, W. and Su, M. "A fully decentralized control of grid-connected cascaded inverters," IEEE Transactions on Sustainable Energy, 10(1), pp.315-317, 2018.
- [6] Johnson, B.B., Dhople, S.V., Cale, J.L., Hamadeh, A.O. and Krein, P.T. "Oscillator-based inverter control for islanded three-phase microgrids," IEEE Journal of Photovoltaics, 4(1), pp.387-395, 2013
- [7] Raisz, D., Thai, T.T. and Monti, A. "Power Control of Virtual Oscillator Controlled Inverters in Grid-connected Mode," IEEE Transactions on Power Electronics, 34(6), pp.5916-5926, 2018.
- [8] McKone, R.P., Wolfs, P.J. and Palmer, E. "Direct Design Approach for Virtual Oscillator Control Synchronisation Condition & Parameter Selection using Describing Functions," In 2018 Australasian Universities Power Engineering Conference (AUPEC) (pp. 1-6). IEEE, 2018, November.
- [9] Opila, D.F., Kintzley, K., Shabshab, S. and Phillips, S. "Virtual oscillator control of equivalent voltage-sourced and currentcontrolled power converters," Energies, 12(2), p.298, 2019.
- [10] C. Natesan, S. Ajithan, S. Mani, and P. Kandhasamy, "Applicability of droop regulation technique in microgrid - A survey," Eng. J., vol. 18, no. 3, pp. 23–35, 2014.



Estimating Inertia Support at Identified Sensitive Nodes to Mitigate the Effect of Reduced Inertia Due to Increased Penetration of Renewable Energy Generation in a Power System

Jayashri . V. Satre, Department of Electrical Engg. Trinity College of Engg & Research Pune Dr. S. R. Deshmukh
Department of Electrical Engg.
PVG's College of Engg &Technology
Pune

Dr. D. J. Doke, Electrical Power System & Educational Consultant Ex-Council Member of IEI)

Abstract - The power system witnessed the continuously increasing penetration of Renewable Generation for last two decades. Renewable Energy (RE) Generation is inertia-less as against the conventional large inertia generators. Thus RE penetration reduces system inertia and makes it node dependent and time variant. The reduced inertia introduces high rate of change of frequency (RoCoF). It may result in mal-operation of frequency dependent protection. To avoid such situation it is necessary to analyse the system network and obtain inertia-profile, Perturbation Sustainability Level (PSL) of nodes and total system as a whole, considering prescribed limit of RoCoF. The inertia support required at sensitive nodes is then calculated and remedial action is recommended.

Keywords -Node-dependent, Inertia-profile, RoCoF, Perturbation Sustainability Level, Inertia support.

I Introduction

The percentage penetration of non conventional Renewable Energy (RE) sources in the generation mix has been continuously increasing, for last two decades. Wind and Solar PV are the major non conventional renewable sources available easily and on large scale, hence used as alternative to conventional sources. These RE generators replace conventional generators having large inertia with non inertial generation. RE generators are located at distribution level and are distributed throughout the network. Thus available generation and load at each node are different at each time and hence, inertia is "node dependent" and "time-variant." [2],[5]

Increased percentage of these RE generation in the grid creates problem of reduced rotational inertia and random fluctuations in the available power at any instant. The reduced inertia introduces very high rate of change of frequency (RoCoF) along with frequency overshoot or frequency dip (nadir) [3]. It may result in mal-operation of

frequency dependant protection and hence initiate tripping of generators or shedding of loads, which further initiates chain reaction, perhaps resulting in blackout, before primary control system gets activated.

In the paper, the effect of reduced inertia due to RE penetration is discussed with the help of 8-bus test system. The inertia-profile, Perturbation Sustainability level-(PSL) profile, aggregated system inertia and PSL are calculated to obtain the required inertia support at sensitive nodes to limit RoCoF to specified limit. Methods to provide support are also discussed.

II Node Dependent, Time-Variant Inertia

The inertia of system provides online buffer energy storage in the system in the form of kinetic energy of rotating masses. The switching of load or generator results in instantaneous mismatch between load and generation (ΔP). Inertia takes care of this mismatch by changing its kinetic energy during first few seconds before primary control (governor) takes over. The kinetic energy ($\frac{J\omega^2}{2}$) in rotating masses (inertia), adjusts itself to either absorb extra generation or supply extra load. For about 10 seconds the system dynamics is inertia-driven before primary control (Governor) takes over.

In a large power system, renewable sources inject power in the grid at different nodes. Every node comprises of either generators or loads or both and transmission lines with bidirectional power flow. Generators may be conventional generators or Renewable Energy (RE) generators or both and loads are static or rotating. RE generators are distributed throughout the network. Thus RE unit commitment, available generation and load at every node of the network are different at any time and hence inertia is node-dependent and time-variant [9].



III Effect of Inertia on the System Dynamics

For first few seconds after perturbation, the inertia of system decides the dynamics of the system, to maintain balance between generation and load.

To understand system response to perturbation, let us consider a system having inertia J and angular velocity ω. The stored kinetic energy in the rotating masses (inertia) is

$$KE = \frac{1}{2} J \omega^2$$
 (1)

In case of perturbation, there is mismatch between generation and load, which tends to change the frequency. In initial period, inertia opposes the change by changing its kinetic energy. Neglecting losses in the system, the rate of change in kinetic energy at any instant is equal to mismatch at that instant. If ΔP is mismatch, it is given by [4]

$$\Delta P = P_G - P_L = \frac{d \left(\frac{1}{2} J \omega^2\right)}{dt} = J\omega \frac{d\omega}{dt}$$
 (2)

Where.

 P_{G} - Generated power, P_{L} -load demand including losses & ΔP - Power imbalance.

The inertia constant H in the normalized form is defined as, the ratio of kinetic energy to rating of the system. If S is power rating of the system in MVA, inertia constant (H) of the system is defined as,

 $H = \frac{\text{Kinetic energy at an instant in inertia at frequency } \omega}{}$

i.e.
$$H = \frac{\frac{1}{2}J\omega^2}{S}$$
 (3)

From (4) and (2) we get

$$\frac{d\omega}{dt} = \frac{\omega \, \Delta P}{2HS} \label{eq:deltaP}$$
 Substituting $\omega = 2\pi f,$

$$\frac{\mathrm{df}}{\mathrm{dt}} = \frac{\mathrm{f}\,\Delta\mathrm{P}}{2\mathrm{HS}}\tag{6}$$

Where $\frac{df}{dt}$ - Rate of Change of Frequency (RoCoF) in Hertz per second, f- System frequency in Hertz.

Thus rate of change of frequency (RoCoF) is inversely proportional to the inertia of the system. If the system inertia is large there will be large kinetic energy stored in the rotating masses. This is available to support the additional requirement for the first few seconds, in case of sudden increase in demand, till the control system takes over. Similarly in case of sudden loss of load, the system inertia acts as a fictitious load and stores extra generation in the form of increased kinetic energy for first few seconds, till the control system takes over.

Power system can be approximated by a second order Swing equation [7].

$$J\omega \frac{d\omega}{dt} + D\Delta\omega = \Delta P = (P_{in} - P_{out})$$
 (7)

Where, $\Delta \omega = \omega - \omega_0$, ω_0 is Nominal Frequency,

D - Damping factor

P_{in} – Mechanical input power

 P_{out} – Electrical power output of the generator

A typical power system using above swing equation was simulated using MATLAB. The system was subjected to step change of load by 20%. The response of the system is shown in figure 1.

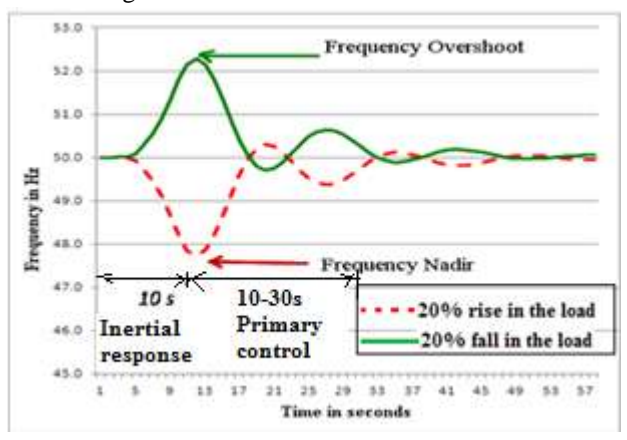


Fig.1. System Frequency after a Step-Change of Load

In case of sudden drop in load, the frequency will increase, resulting in overshoot and in case of increase in load, the frequency will reduce, resulting in drop in frequency. Figure 1 shows this effect. In both cases RoCoF and overshoot or dip increases with decrease in inertia.

Increase in percentage penetration of renewable generation in the grid, reduces inertia of the system. It introduces high rate of change of frequency, frequency overshoot or frequency nadir for first few seconds.

In this paper only high rate of change of frequency is considered. The maximum (RoCoF) occurs immediately after perturbation. At this instant system is node-inertia controlled. The support from links or other nodes is available only after some laps of time since power flow in lines depends upon the difference in phase angle between two ends of the line.

As such, link power may be assumed constant; this enables us to treat each node in isolated mode to assess its inertia similar to free body diagram approach in kinetics. When isolated, a node can be represented by inputs from



generator and links and outputs to loads and links. Input will be always equal to output.

As pointed out in section –II each node has different inertia and hence with the same perturbation, RoCoF of each node will be different. To get the total view of the network it is necessary to obtain inertia-profile, perturbation sustainability level-profile and total system aggregated inertia and perturbation sustainability level.

Total system inertia and system perturbation sustainability level can be calculated considering permissible rate of change of frequency. It is presumed that, this perturbation applied to system at any node, will limit RoCoF of all nodes to assumed limit. However in reality each node behaves as an independent node and decides RoCoF as per its own inertia, which is different for each node. Evaluation of inertia-profile, perturbation sustainability level at each node along with knowledge of RoCoF helps in deciding inertia support required at each node.

As such support inertia-profile of the network can be calculated and remedial action can be suggested accordingly. A test case is reported in next section.

IV Inertia-Profile, Perturbation Sustainability-Profile of Test System

A typical test system of 8 buses is considered for demonstrating the concept of getting inertia-profile, Perturbation sustainability level-profile and finally to calculate inertia support needed at each node.

The system is shown in figure 2. The system has nine generators and total capacity of 600MVA and load of 590 MVA. A load flow study is carried out and line flows are calculated and shown in figure.

To demonstrate the effect of RE generation, two different cases are investigated. In first case all generators are assumed conventional generators with inertia constants as per their type. In second case four out of nine generators are replaced by Solar/Wind generators.

In both cases, inertia-profile, perturbation sustainability level of nodes, aggregated system inertia, aggregated perturbation sustainability level of the system, RoCoF and inertia support-profile are calculated.

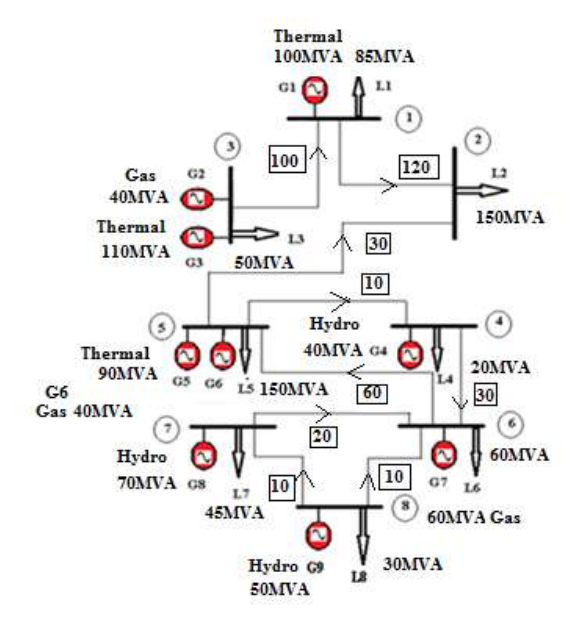


Figure 2 Eight Bus Test System

Case 1: Conventional Power System

All generators are considered as conventional generators. Table I gives test System data [1].

Table I Eight Bus Test System Data

Node	Connections	Type of generator	MVA rating	Inertia H (s) on own rating
1	G1	Thermal	100	7.5
1	L1		85	0
2	L2		150	0
	L3		50	0
3	G2	Gas	40	4
	G3	Thermal	110	7.5
4	G4	Hydro	40	5
4	L4		20	0
	G5	Thermal	90	7.5
5	G6	Gas	40	4
	L5		150	0
6	G7	Gas	60	4
U	L6		60	0
7	G8	Hydro	70	5
,	L7		45	0
8	G9	Hydro	50	5
O	L8		30	0



a) Inertia Profile of the system:

To get inertia at each node, load flow study is conducted and power flow is obtained at the instant of study. Each node is isolated and its effective inertia is calculated.

For example, node 5 is shown in figure 3 below. It consists of two generators, one load and three links as shown in figure.

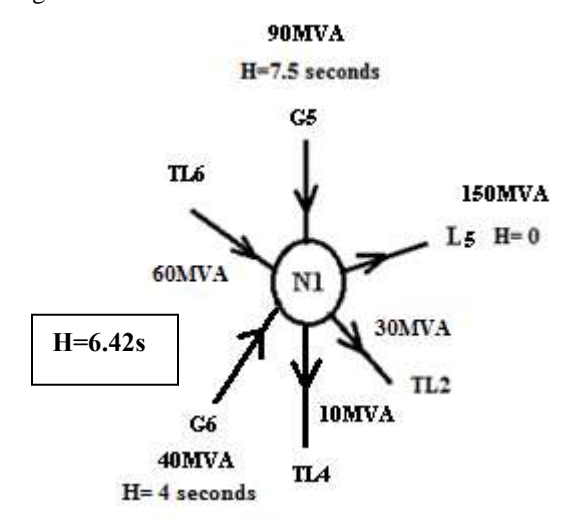


Figure 3 Isolated Node Diagram of Node 5.

In case of perturbation at the node, power from transmission link is assumed to be constant and no inertia support is provided from other nodes. Generation-Load imbalance is taken care by inertia of the node for first few seconds. The node inertia is calculated by using following equation [8].

Inertia of node (H) =
$$\frac{\sum_{i=1}^{m} H_i * S_i}{\sum_{i=1}^{m} S_i}$$
 (8)

Where H_i –Inertia of ith link, S_i –MVA of ith link, m- Number of links.

Magnitude of effective node-inertia for node 5 works out to be 6.42 second. Similarly inertia is calculated for all nodes and given in table II

Table II Magnitude of Effective Node-Inertia

Node	Node MVA	Node-Inertia (sec)
1	100	7.5
2	0	0
3	150	6.57
4	40	5
5	130	6.42
6	60	4
7	70	5
8	50	5

Inertia of node 2 is zero as it is only load bus.

b) Perturbation Sustainability Level (PSL) of nodes:

Perturbation sustainability level is defined as the ability of node to sustain perturbation, with RoCoF not to exceed the specified limit. To evaluate Perturbation Sustainability level, rate of change of frequency is assumed to be 0.2Hz/sec as per directives from CERC for Indian system [1]. At each node Perturbation Sustainability level is calculated using equation (6) rearranged as

$$\Delta P = \frac{H*2*S*\frac{df}{dt}}{f} \tag{9}$$

Table III shows perturbation sustainability levels.

Table III Perturbation Sustainability Level at Nodes

Node	Node	Perturbation
	inertia(s)	Sustainability Level
		of nodes ΔP (MW)
1	7.50	6.00
2	0	0
3	6.57	7.88
4	5.00	1.6
5	6.42	6.68
6	4.00	1.92
7	5.00	2.8
8	5.00	2

Node 3 is strongest node due to connection of large capacity thermal and Gas generators. Node 4 is the most sensitive node due to connection of small capacity hydro generator.

c) System Aggregated Inertia:

To understand the overall system performance, aggregated system inertia is calculated which is **6.02 seconds** using equation (8).

d) Perturbation Sustainability Level (PSL) of the System.

Every node has different Perturbation Sustainability Level the system also exhibits it's aggregated PSL as **28.88MW** using equation (9).

It indicates the magnitude of perturbation that the system can sustain limiting RoCoF to 0.2Hz/sec. However the nodes behave independently and hence in certain nodes RoCoF may be more than 0.2Hz/sec unless support inertia is provided to such nodes. The total perturbation sustainability level, if distributed uniformly in eight buses,



its magnitude will be **3.61MW** per bus. It is represented along with PSL of each node in figure 4.

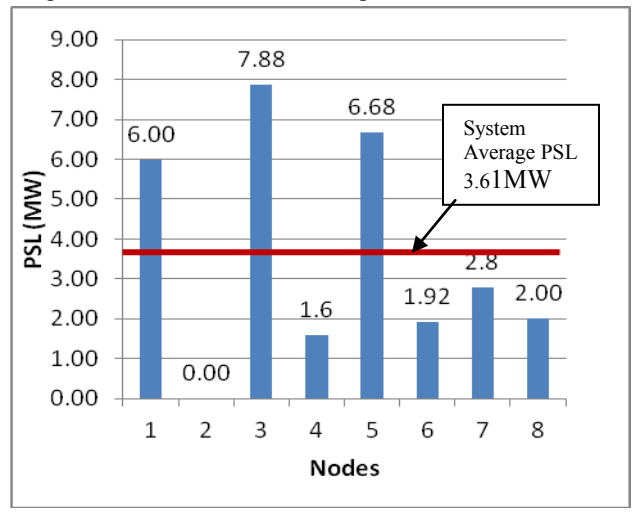


Figure 4. PSL of Nodes and System

PSL of node 4 is lowest hence it is treated as a sensitive node. To sustain system average perturbation of 3.61MW nodes 4, 6,7 and 8 needs inertia support.

e) Inertia Support-Profile:

Assuming the occurrence of perturbation of 3.61MW, the requirement of inertia at each node to sustain the perturbation is calculated and presented in table IV.

Table IV Effect of Perturbation of **3.61MW** at Each Node

Node	Node inertia (s)	RoCoF (Hz/s)	Inertia required to Sustain perturbation (s)	Inertia Support (s)
1	7.50	0.12	4.51	-2.99
2	0.00			
3	6.57	0.09	3.01	-3.56
4	5.00	0.45	11.28	6.28
5	6.42	0.11	3.47	-2.95
6	4.00	0.38	7.52	3.52
7	5.00	0.26	6.45	1.45
8	5.00	0.36	9.03	4.03

Positive sign indicates external inertia support required at the node to sustain PSL.

Negative sign indicates surplus inertia available to support other nodes.

As already observed in previous section, node 4 being sensitive in nature, experiences highest RoCoF of 0.45Hz/s. Hence to control RoCoF to required magnitude, inertia support of 6.28seconds is required.

Excess inertia of node 1,3 and 5 can be utilized to give support to weak nodes if required along with additional

inertia support measures. Figure 5 shows inertia-support profile.

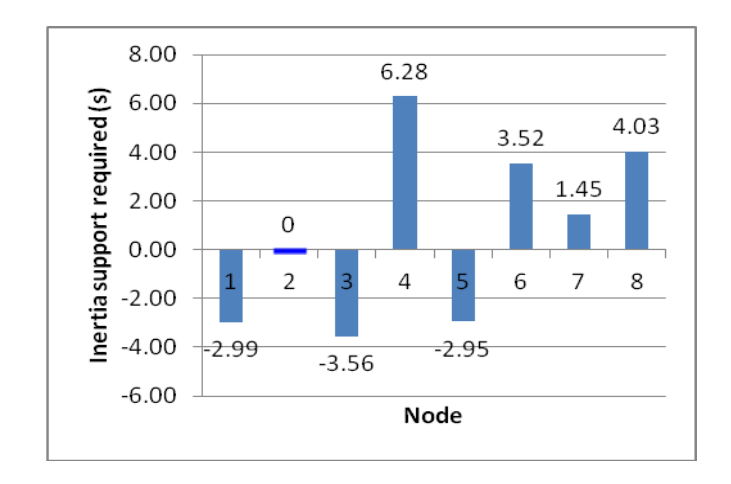


Figure 5 Inertia Support-Profile

Case 2: Conventional + RE generation Power System

In this case, out of nine generators, four conventional generators are replaced by RE generators of same capacity. Generator G2 at bus 3 is replaced by Solar PV of same capacity.

Generator G4 at bus 4 is replaced by Wind generator.

Generator G6 at bus 5 is replaced by wind and Generator G9 at bus 8 is replaced by Solar PV generator.

All these RE generators are assumed to have no inertia. Thus capacity of the system and connected load remains same.

a) Inertia profile of the system:

Inertia of each node is calculated by using same procedure as used is case 1. Inertia profile of the system is as shown in figure 6.

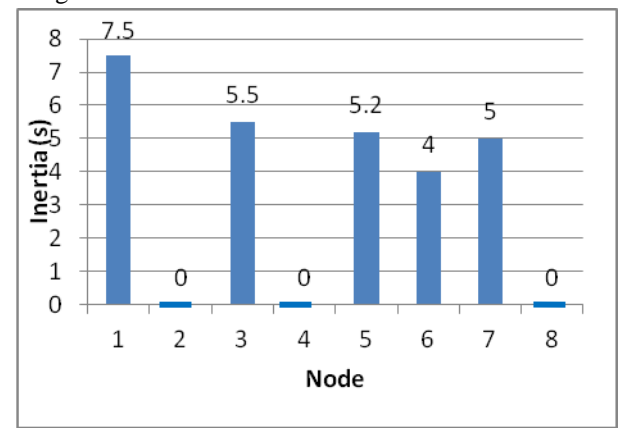


Fig. 6 Inertia Profile of the Test System with RE

Node 2,4and 8 have zero inertia due to presence of RE generators.



b) Perturbation Sustainability Level (PSL) of each node:

To evaluate Perturbation Sustainability level at each node, 1. similar procedure is followed and presented in Table VIII

Table VIII Perturbation Sustainability Level at node

Node	Node inertia(s)	Perturbation Sustainability Level ΔP (MW)
1	7.5	6.00
2	0	
3	5.5	6.60
4	0	
5	5.2	5.41
6	4	1.92
7	5	2.80
8	0	

Node 2, 4 and 8 are not able to sustain any perturbation as inertia is zero. Node 3 is strongest node can sustain 6.6 MW perturbation.

c) System Aggregated Inertia:

Aggregated system inertia works out to be 4.74 seconds.

d) Perturbation Sustainability Level of the System (PSL)

System aggregated PSL works out to be **22.73MW** with around 28% RE penetration.

e) Inertia Requirement-Profile to Sustain System Perturbation at each Node:

With the perturbation of **2.84MW** (Total system PSL distributed uniformly in 8 buses), the requirement of inertia at each node to limit RoCoF to 0.2Hz/s is calculated and presented in table IX.

Table IX Effect of Perturbation of 2.84MW at Each Node

Node	Node inertia on 100MVA base (s)	RoCoF (Hz/s)	Inertia required to Sustain perturbation (s)	Inertia Support (s)
1	7.5	0.095	3.55	-3.95
2	0			
3	5.5	0.086	2.37	-3.13
4	0			
5	5.2	0.105	2.73	-2.47
6	4	0.296	5.92	1.92
7	5	0.203	5.07	0.07
8	0	0.000		

Comparing two cases it is observed that,

- With increased penetration of RE, the inertia of the node to which RE is connected is reduced. In present case aggregated system inertia changes from 6.02seconds to 4.74 seconds.
- The Perturbation sustainability level of system is also reduced from 28.88 MW to 22.73 MW in presence of RE.
- 3. Node 4 has become more sensitive due to replacement of conventional generator with RE.
- 4. The nodes 2, 4, 6, 7 and 8 needs inertia support as shown in table IX

V Possible Ways to Provide Support Inertia

Providing inertia support means providing arrangement to transfer energy immediately online to cope up with change in load or generation for short time, till primary controller takes over.

This demand for

- i) Source of energy
- ii) Arrangement to transfer it automatically sensing perturbation.

This can be done by:

- Connecting replaced conventional generator as synchronous motor [8].
- ii) Add a diesel generator
- iii) Using Solar PV with battery for providing virtual inertia. i.e. on-line power transfer arrangement to increase/decrease power flow from battery in case of perturbation [6].
- iv) The profile will help in Indian scenario in planning installation Solar PV generating stations with battery backup to provide virtual inertia at sensitive nodes.

VI Conclusion

The increased penetration of RE generation decreases system inertia introducing high rate of change of frequency, frequency overshoot or dip (nadir) in case of perturbation.

To avoid mal-operation of frequency dependent protection, it is necessary to know inertia-profile, perturbation sustainability level-profile, identify sensitive nodes and provide inertia support by adding inertia using synchronous motor or Solar PV with battery and provision for virtual inertia. This will help India in planning future Solar PV projects, limiting node RoCoF to 0.2 Hz/s as directed by CERC.



References

- [1] CERC India "Report of Expert Group to review and suggest measures for bringing power system operation closer to National Reference Frequency (V-I)"November 2017, CERC India
- [2] Theodor S. Borsche, Tao Liu, David J. Hill, "Effects of Rotational Inertia on Power System Damping and Frequency Transients" 2015 IEEE 54th Annual Conference on Decision and Control (CDC) December 15-18, 2015. Osaka, Japan.
- [3] Ujjwol Tamrakar, Dipesh Shrestha, Manisha Maharjan, Bishnu P. Bhattarai, Timothy M. Hansen and Reinaldo Tonkoski ,"Virtual Inertia: Current Trends and Future Directions" Article in Applied Sciences 7(7):654 · June 2017
- [4] Pieter Tielens, Dirk Van Hertem, "Grid Inertia and Frequency Control in Power Systems with High Penetration of Renewables" Published in 2012.
- [5] Andreas Ulbig, Theodor S. Borsche and Göran Andersson, "Impact of Low Rotational Inertia on Power System Stability and Operation" 22 Dec 2014
- [6] Mohammad Dreidy, H. Mokhlis, Saad Mekhilef, "Inertia response and frequency control techniques for renewable energy sources: A review", Renewable and Sustainable Energy Reviews 69 (2017) 144–155
- [7] P. Kundur, "Power system stability and control," McGraw-Hill Inc., New York, 1994
- [8] Nahid-Al Masood1, Ruifeng Yan, Tapan Kumar Saha, Simon Bartlett, "Post-retirement utilization of synchronous generators to enhance security performances in a wind dominated power system" IET Generation, Transmission & Distribution Journal Publication Year: 2016, Page(s): 3314 – 3321
- [9] Ti Xu, Wonhyeok Jang ,Thomas J. Overbye, "Investigation of Inertia's Locational Impacts on Primary Frequency Response using Large-scale Synthetic Network Models" IEEE Power and Energy Conference at Illinois, Champaign, IL, February 2017

Self-Excited Induction Generator Employing an Intelligent Electronic Load Controller for Small Hydropower Applications

S.Karmakar and S.N Mahato

Department of Electrical Engineering

National Institute of Technology

Durgapur-713209,India

shukla.k1317@gmail.com, snmrec@yahoo.co.in

Abstract— Theperformance of a three-phase Self- Excited Induction Generator (SEIG) employing an intelligent Electronic Load Controller (ELC) is evaluated in this paper.A SEIG lags the inherent property of voltage and frequency regulation with varying loaddemands, thereby load controllers are used for the purpose. Levenberg-Marquardt and Scaled Conjugate Gradient are two algorithmic variants of Artificial Neural Network (ANN) which have been used here as load controllers. A comparison of the controlling ability of the two techniques is also featured. Simulation is done in MATLAB and it is found that the results are well acceptable.

Keywords - Self- Excited Induction Generator; Electronic load controller; Levenberg-Marquardt; Scaled Conjugate Gradient.

I.INTRODUCTION

The ever increasing electricitydemands and the limited reserve of fossil fuels have made it necessary to harnesselectrical energy from renewable resources such as solar, wind, biomass and hydro energy. Hydro energy is more reliable compared to other non-conventional resources. Micro and pico hydro systems provide constant input power due to the constant head and discharge [1]. The generated output power is also required to be constant. Self-ExcitedInduction Generators withsuitable control techniques arefound to be the appropriate choice for such applications [2-5]. Some of the advantages of SEIGs arehigh mechanical strength and ruggedness of the induction machine,

reduced short-circuitrisks, brushless, low initial and maintenance costs. These advantages of SEIGs have made it superior compared to the conventional synchronous generators.

For maintaining a constant voltage and therefore constant power at the generator terminals at varying load demands, Electronic Load Controllers are used. The ELC considered in this analysis consist of a diode rectifier and a chopper in series with a dump load. The analysis and implementation of ELC using a Proportional Integral (PI) controller andan intelligent controller using Artificial Neural Network have been done.

ANN follows the human neural network working mechanism for problem-solving. As reported in the literature [6-7], the Back propagation algorithm of ANN has been successfully implemented in controllers. This work focuses on evaluating the control action of two variations of the Back propagation algorithm. The algorithms are used to control the switching pattern of the chopper. These are namely the Levenberg-Marquardt (LM) and the Scaled Conjugate Gradient (SCG) algorithms.

II. SYSTEM DESCRIPTION

A schematic diagram of the SEIG-ELC system is shown in Figure 1 for feeding three-phase loads.

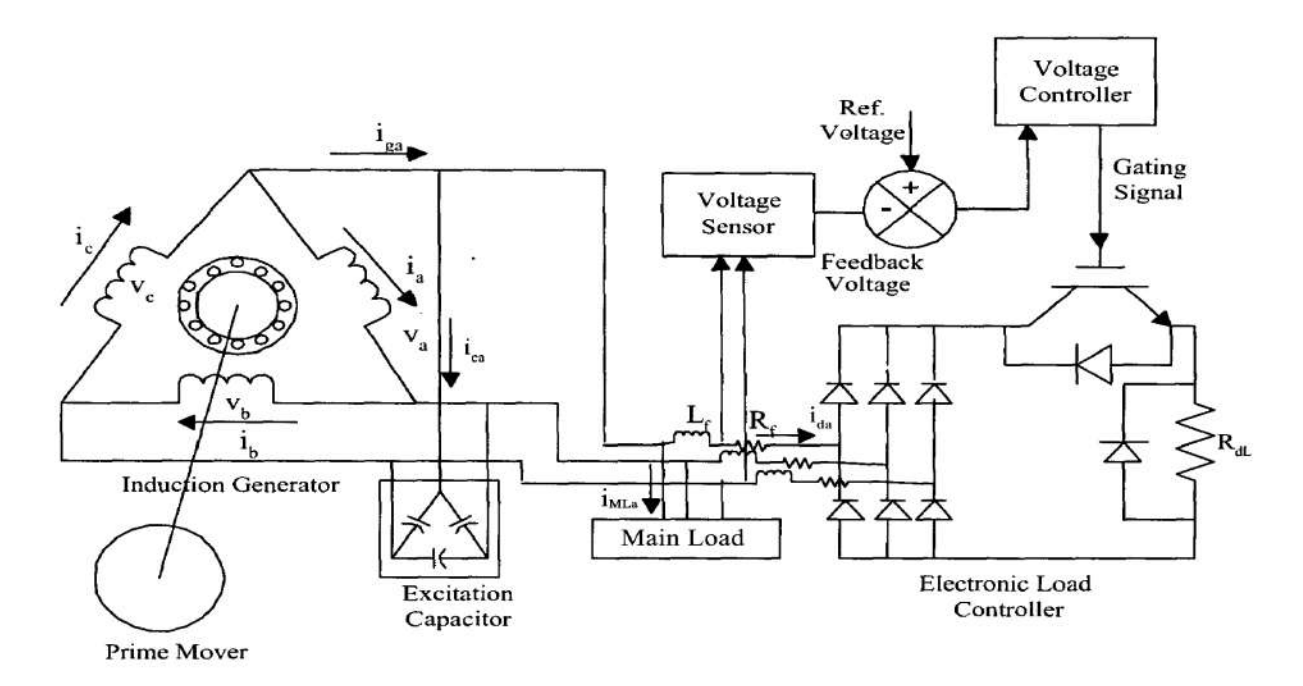


Figure 1. Schematic diagram of three-phase SEIG - ELC system

The system consists of a three-phase delta-connected induction generator excited by an external capacitor bank. The ac from SEIG is converted to dc by the three-phase rectifier circuit of ELC. The chopper switch is turned on by an appropriate gate driver circuit. The chopper used is an insulated-gate bipolar transistor (IGBT). The IGBT is switched on when the main load across the SEIG terminals is less than its rated value and switched off whenthe main load is at its rated value. The dump loadcomprises of resistors used as heating elements and connected in parallel with the main load such that the total generated power at the SEIG terminal is maintained constant.

$$P_G = P_M + P_D(1)$$

Where P_G is generated power of the generator, P_M is the main load power and P_D is the dump load power.

III. DESIGN OF INTELLIGENT ELC

The 3-phase rectifier circuit and chopper switch will have the same voltage rating and that depends on the Root Mean Square (RMS) value of ac input voltage and the average value of output dc voltage. The dc voltage is calculated as [8] and [9]

$$V_{dc} = (3\sqrt{2} V_{LL})/\prod = (1.35)V_{LL} = 1.35 \times 230 = 310.6V (2)$$

The RMS value of the SEIG line voltage is denoted by V $_{\rm LL}$. Accounting a 10% of over-voltage of the rated value during transient conditions, the peak voltage is calculated as

$$V_{ac(peak)} = \sqrt{2} \times (230 + 10\% \times 230) = 357.8V$$

The 3-phase rectifier and chopper switch will have a current rating determined by the active component of input ac and is calculated as

$$I_{ac}=P/(\sqrt{3}\times V_{LL}) = 2200/(\sqrt{3}\times 230) = 5.52A$$
 (3)

The power rating of SEIG is denoted by P.

Taking into account a distortion factor of 0.955 and crest factor of 2.0 for the three-phase uncontrolled rectifier, the peak value of input ac to the ELC is calculated as

$$I_{ac(peak)} = (I_{ac}/0.955) \times 2 = 11.56A$$
 (4)

From these calculations, it is found that the ratings of voltage and current of the rectifier circuit and IGBT should be at least 400V and 11A respectively.

The resistance of the dump load (R_{dL}) is calculated as

$$R_{dL} = (V_{dc})^2 / P = 43.85\Omega$$
 (5)

Artificial neural networks (ANNs) can learn the relationship between the inputs and the outputs of a system[10-14]. The input and output data to the ANN controller are the error (that is the difference between the actual generator voltage and a reference voltage) and the rate of change in error. The controller is trained using these data for optimization. After training, the output is compared with a saw-tooth carrier wave to generategate pulses using Pulse Width Modulation (PWM)technique for the IGBT to function.

Figure 2 shows the block diagram of ANN. The proposed controller is simulated in MATLAB by the following two algorithms:

A.Levenberg-Marquardt (LM) algorithm: The Levenberg-Marquardt Algorithm is used to provide a

solution in minimizing a complex nonlinear function. The performance function is the mean of the square of a nonlinear relationship.

B. Scaled Conjugate Gradient (SCG) Algorithm:Inthe Scaled Conjugate Gradient algorithm, a search is performed in the direction along which the performance function decreases rapidly while minimizing the error.

As shown in Figure 3 and Figure 4, it is observed that the performance function is different for both the cases. As the gradient decreases and reaches close to zero, the performance function is minimized. This implies that the output becomesclose to the target and the network is perfectly trained.

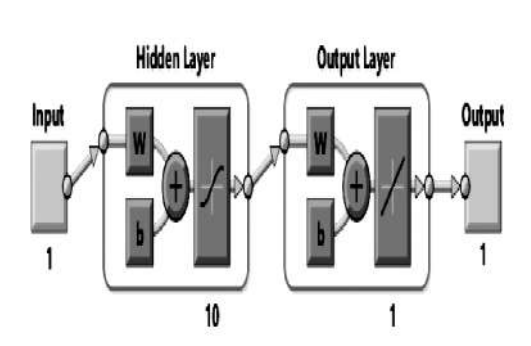


Figure 2. Block diagram of ANN

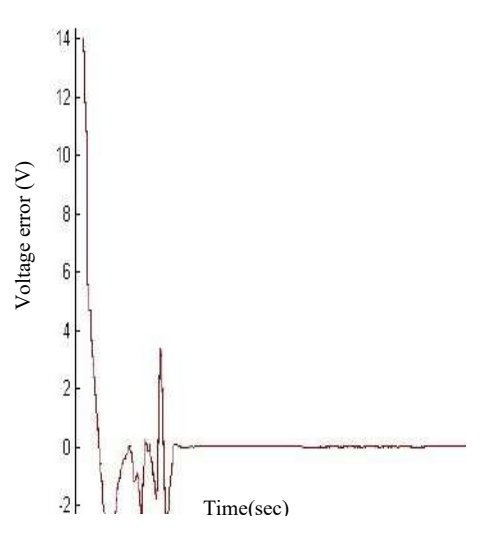


Figure 3. Error minimization by SCG Algorithm

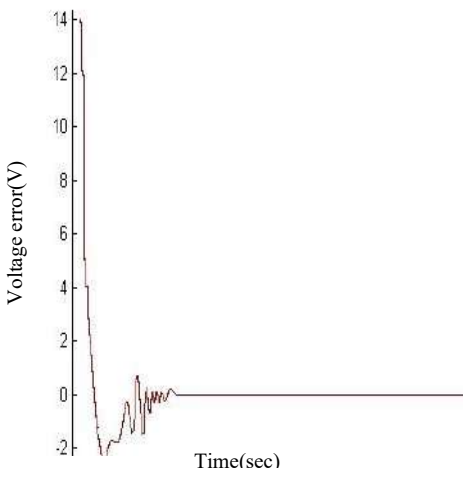
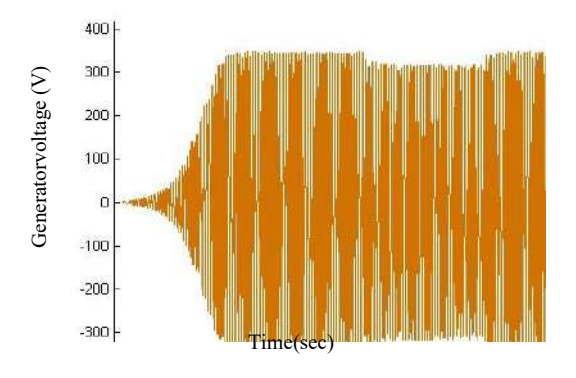


Figure 4. Error minimization by LM Algorithm

IV. RESULTS AND DISCUSSIONS

A 3-phase, 230 V, 7.8A, 2.2 kW deltaconnected SEIG has been modeled in MATLAB Simulink environment. Load perturbation is given at 2 seconds (sec) and 3 sec. To achieve the rated voltage at the rated speed, a capacitor bank of $50.6\mu F$ per phase is connected across the generator terminals. The results of Generator phase voltage(V_a,V_b, V_c) and current(i_a,i_b,i_c)of SEIG without ELC is shown in Figure 5.Figure6 shows the Generator phase voltageand current of SEIG with ELC using a conventional PI controller.



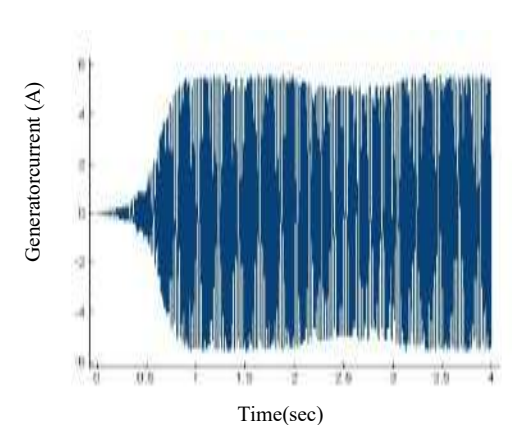
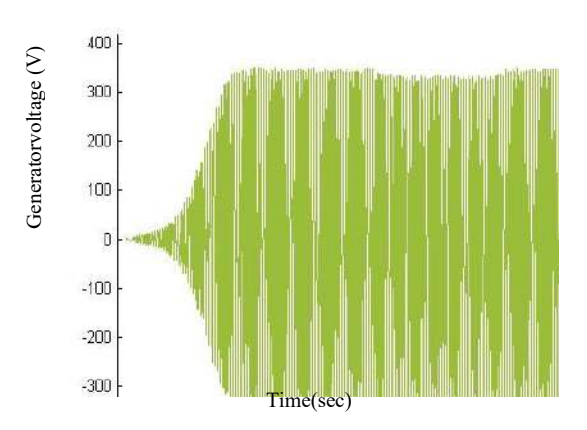
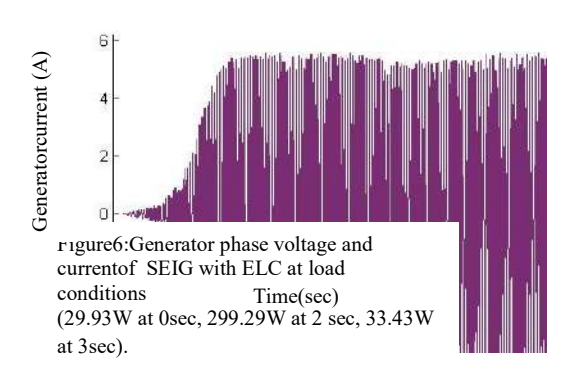


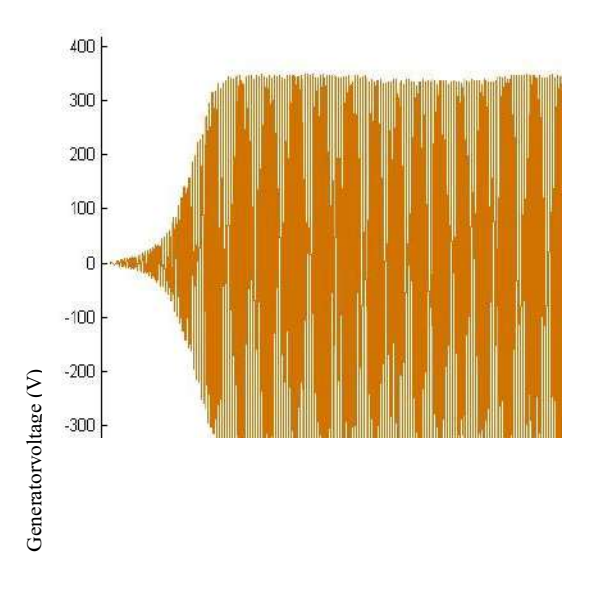
Figure5:Generator phase voltage and currentof SEIG without ELC at load conditions (29.93W at 0sec, 299.29W at 2 sec, 33.43W at 3sec).





From Figure 5 it is observed that generatorvoltage decreases on increasing the load at 2sec and increases on decreasing the load at 3sec. Whereas Figure 6 shows that voltage and current are regulated to remain constant compared to those Page 4 of 7

The phase voltage and current of Self-Excited Induction Generator controlled by an ANN-based ELC using the Scaled Conjugate Gradient and Levenberg Marquardtalgorithms is shown in Figure 7 and Figure 8 respectively.



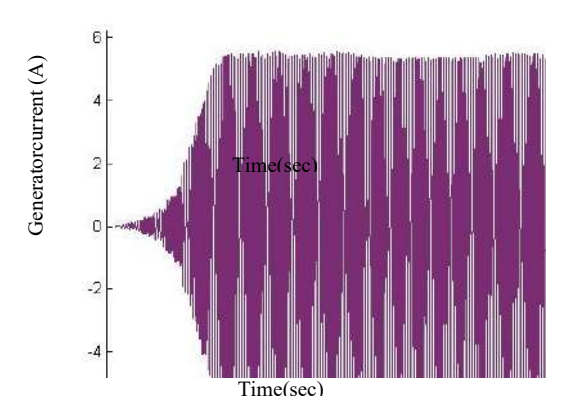
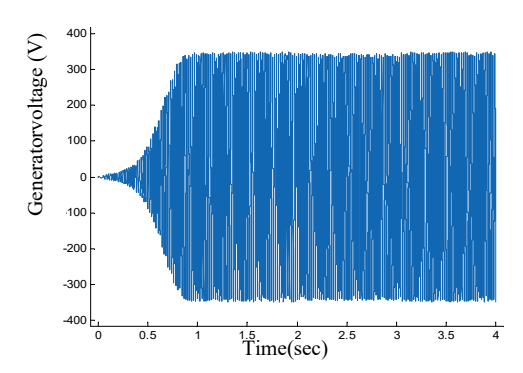
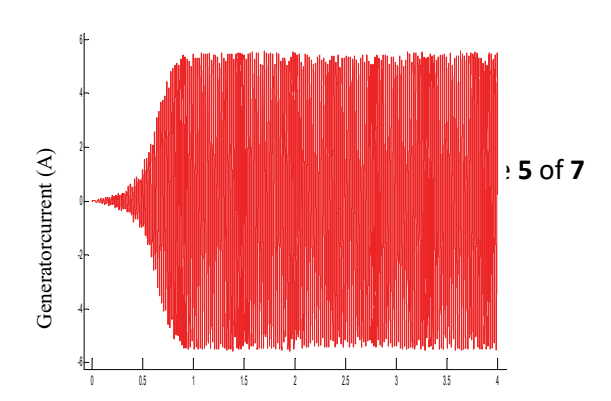


Figure7:Generator phase voltage and currentof SEIG with SCG algorithm at load conditions (29.93W at 0sec, 299.29W at 2 sec, 33.43Wat 3sec).





Time(sec)

Sl No.	Parameters	Scaled Conjugate Gradient	LevenbergMarquardt algorithm
		algorithm	
1	Time	1 sec	7sec
2	Eporhure8:G	enefator phase v	ol229eiterations
	currentof	SELEranibal M	lgorithm at load
3	Mean conditions (29.93W a Square 33.43Wat Error	0.136 t 0sec, 299.29W 3sec).	0.0213 at 2 sec,
4	Regression		0.999
	value	0.994	
	after		
	training		

Figure 7 shows that the generated voltage is better-controlled by the SCG algorithm-based control scheme. The waveformsof Figure 8 shows best-controlling efficiency with the LM algorithm compared to the other two controllers under varying load conditions.

A comparison of the performance of LM and SCG algorithms working as controllers is represented in Table 1.

Table 1: Performances of both the algorithms.

Time(sec)

Based on the training results of ANN, it is observed that both the algorithms are comparable in terms of speed and accuracy. However, better error minimization

is obtained by the Levenberg-Marquardt algorithm. On the other hand, the Scaled Conjugate Gradient algorithm excelled in terms of speed as found on a simple Multi-LayerPerceptron structure with two hidden layers.

V. CONCLUSION

An analysis of the 3-phase SEIG with load controller using the three control techniques namely PI controller, Levenberg-Marquardt and the Scaled Conjugate Gradient algorithms of artificial neural network controller has been done. Simulated results reveal that the ANN controllers are more capable of maintaining constant voltage and power at varying loads compared to the conventional controllers. Thereby these controllers can be used satisfactorily for small hydropower applications.

APPENDIX

The parameters of the machine are:2.2 kW, 3-phase, 4-pole, 50 Hz, 230 V, 7.8 A, delta connected, $X_{ls}{=}0.00446~k\Omega,~X_{lr}{=}~0.00446~k\Omega,~R_s=0.00384k~\Omega,~R_r=0.00288~k\Omega,~C=50.6~\mu F.$

The relation between the magnetizing inductance (L_m) and the magnetizing current (I_m) is expressed as:

 $L_{\rm m} = 0.31 / {\rm for } I_{\rm m} \le 0.75$ = 0.3502 -0.0349 $I_{\rm m}$ - 0.0017 $I_{\rm m}$ 2for 0.75 $< I_{\rm m} \le$

4.25 = 0.17667 for $I_m > 4.25$

REFERENCES

- [1]N. P. ASmith, "Induction generators for stand-alone micro-hydro systems," IEEE International Conf. On PowerElectronics Drivesand Energy Systems, New Delhi, January 1996, pp. 669-673.
- [2] S. S. Murthy, O. P. Malik, and A. K. Tandon, "Analysis of Self-excited Induction Generators," in Proc. IEEE, vol. 129, part C, no. 6, pp. 260-265, 1982.
- [3] A. K. Tandon, S. S. Murthy, and G. J. Berg, "Steady-state analysis of capacitor self-excited induction generators," IEEE Trans. PowerApparatus and Systems, vol. PAS 103, pp. 612-618, Mar. 1984. [4] J. L. Bhattacharya and J. L. Woodward, "Excitation balancing of a self-excited induction generator for maximum power output," in Proc. IEEE, vol. 135, pt. C, no. 2, pp. 88-97, 1988.
- [5] S.S. Murthy, B. Singh, S. Gupta, and B.M. Gulati, "General steady-state analysis of three-phase self-excited induction generator feeding three-phase unbalanced load/single-phase load for standalone applications," in Proc. IEEE, vol. 150, no. 1, pp. 49-55, 2003.
- [6] Jung-Wook Park, Venayagamoorthy, G.K., & Harley, R.G., (2005) "MLP/RBF neural-networks based online global model identification of synchronous generator", IEEE Trans. Industrial Electronics, Vol. 52, No. 6, pp1685-1695.
- [7] Venayagamoorthy, G.K., & Kalyani, R.P., (2005) "Two separate continually online-trained neuro controllers for a unified power flow

- controller", IEEE Trans. Industry Applications, Vol. 41, No. 4, pp 906-916.
- [8] N. Mohan, T. M. Undeland, and P. Robbins, Power Electronics: Converters, Applications, and Design, 2nd ed. New York: Wiley, 1995.
- [9] M. H. Rashid, Power Electronics, Circuits, Devices, and Applications, 2nd ed. New Delhi, India: Prentice-Hall of India Private Limited, 1996.
- [10]Halpin, S.M. & Burch, R.F.,(1997) "Applicability of neural networks to industrial and commercial power systems: a tutorial overview", IEEE Trans. Industry Applications, Vol. 33, No. 5, pp1355-1361.
- [11]Liu, Y., Cukic, B., & Gururajan, S. (2007). Validating neural network-based online adaptive systems: A case
- study. Software Quality Journal, 15(3), 309-326. http://dx.doi.org/10.1007/s11219-007-9017-4
- [12]MATLAB: Accelerating the pace of engineering and science. (2012). About MATLAB. Retrieved September 21, 2012, from http://www.mathworks.com
- [13]Sabahi, K. (2011, August). Application of ANN technique for DC- motor control by using FEL Approaches (pp.131-134). Paper presented at 5th International Conference on Genetic and Evolutionary Computing(ICGEC), IEEE.
- [14]Hagan, M.T., H.B. Demuth, and M.H. Beale, Neural Network Design, Boston, MA: PWS Publishing, 1996.

Liquid Solar Array

Soumik Roy¹, Satarupa Mukherjee² and Manisankar Chakraborty³

¹Exec. Engineer (M), ²Exec. Engineer (C&I), ³Supt. Engineer (M), Damodar Valley Corporation, Ministry of Power, GoI soumik.roy@dvc.gov.in, satarupa.mukherjee@dvc.gov.in, manisankar.chakraborty@dvc.gov.in

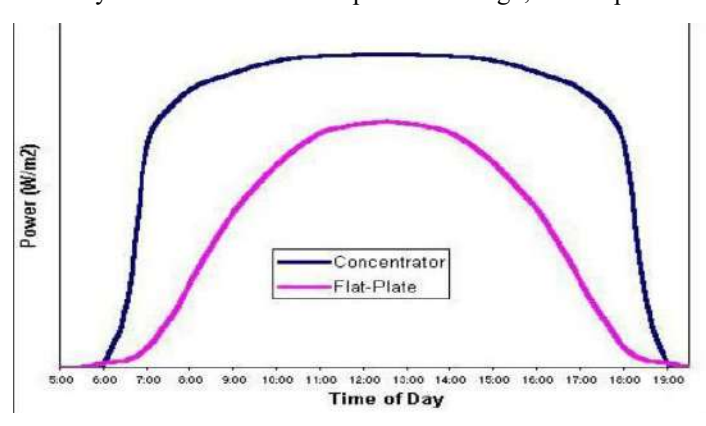
INTRODUCTION:

A solar array refers to a group of photovoltaic (PV) solar panels or cells that converts sunlight to electricity, arranged and linked in such a way as to operate as a single unit. The term can also refer to a similar set of reflecting mirrors used for directing and focusing sunlight onto such a group of photovoltaic units (PV concentrators). A solar array can range from a group of panels on the roof of a family home to an array covering several acres, containing hundreds or thousands of individual panels. A typical solar panel is made up of several photovoltaic cells linked together and bound, or contained, within a single unit. A typical solar array is composed of solar panels of one type, but this does not necessarily have to be the case. Photovoltaic cells are the basis for most solar arrays. These devices convert sunlight into electric current, and can generate substantial amounts of electricity. India has ratified the Paris agreement on 02.10.2016 which requires member countries to make binding commitments to curb CO₂ emissions to keep global average temperatures from rising too much. India aims at producing 40% of its total installed electricity capacity by 2030 from non-fossil fuels. Large scale power generation from renewable sources requires vast areas of LAND. Liquid solar array comes as a rescue in this situation.

A. Advantage of PV Concentrators:

The main potential advantage of PV concentrators over flat plate semiconductor PV systems derives from the fact that it reduces costs by trading large areas of high grade semiconductor-underglass (silicon) for similar areas of cheaper materials, such as acrylic plastic in the form of a thin Fresnel lens or a thin glass mirror, needing only a small area of PV cells. The light is concentrated to the extent that the area of silicon typically required is reduced by 50 to 100 fold (low concentration photovoltaic, LCPV) or by 300 to 1000 fold for a given output (high concentration photo-voltaic, HCPV). LCPVs record efficiencies of 30-33% while HCPVs record around 38-40% under commercial production. It is evident that PV concentrators have a greater efficiency than normal flat panelsPV cell, which is around 15-17%. The main reason behind this higher efficiency is the fact that the capacity utilisation of sun rays by using PV concentrators is much higher, throughout the day and year. Silicon cells in concentrator systems are quoted as low as ₹14 per watt; however, difficulties arise from the lens or mirror structure that focuses light onto these economical cells with a very high accuracy as the structure needs to be substantial. Added to this is the cost of the tracker that, along with the structure, needs to withstand winds of at least 150 km/hr in many locations. Thus it may be seen that the structure must withstand pressure of 120 kg/m² if exposed to winds of 150

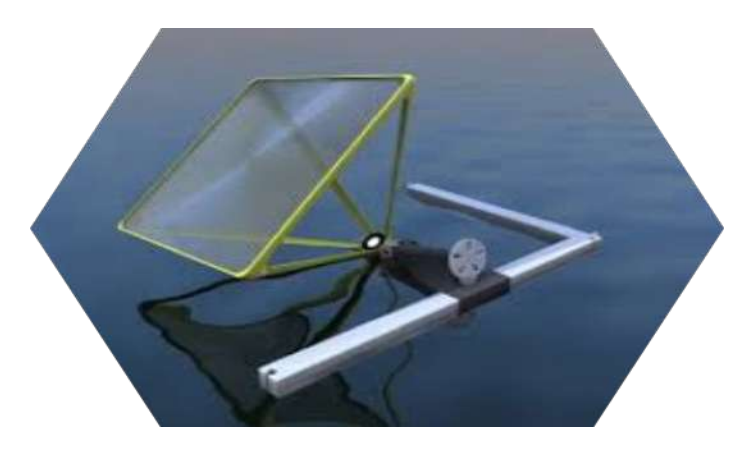
km/hr. If exposed to wind forces of only 60 km/hr, the peak forces per square metre acting on the structure are reduced to 20 kg/m². Thus, if the effective pressure could be reduced, there would be requirement for lesser substantial structure and tracking mechanism. Around one sixth of the strength/mass should be adequate without compromising performance. The concept of employing the lowest costing transparent elastomers as pottant, by permitting UV sensitivity, requires in turn the need for an outer cover material that is both UV screening and naturally weatherable. For a superstrate design, this is provided



by glass, which is also the module for structural panel.

B. Liquid Solar Array:

1) The Idea: By arranging the PV concentrators in an array that is placed on water rather than on land, a simple solution has been realised that gives efficient cooling of the PV cells and allows a lighter structure to be used, resulting in major cost savings. A buoyant raft comprising moulded plastic members supports a tracking mechanism and light weight lens as shown in figure depicted below. The lens system can be rotated into the water at any time when wind-speed exceeds some threshold value, or as per the weather predictions and thereby obviate the need for the large area components to withstand high winds. An array of such rafts and submersible collectors can be termed a liquid solar array(LSA).



With such a design the lens and its supports can be very light – as little as 3 or 4 kg for a square metre of Fresnel lens with its frame (versus 20 kg/m² for a standard concentrator). So the mass of the moving components is greatly reduced. Hence the tracking motor drive is also reduced in size and power. Another significant advantage of this approach is that the system is likely to survive coastal cyclonic conditions that are expensive to manage with existing solar collectors and wind farms, leading to lower insurance costs for the LSA.

PV cell electrical output is extremely sensitive to shading. When even a small portion of a cell, module, or array is under the shade, while the remainder is in sunlight, the output falls dramatically due to internal 'short-circuiting' (the electrons reversing course through the shaded portion of the p -n junction). If the current drawn from the series of string of cells is not greater than the current that can be produced by the shaded cell, the current (and so power) developed by the string is limited.

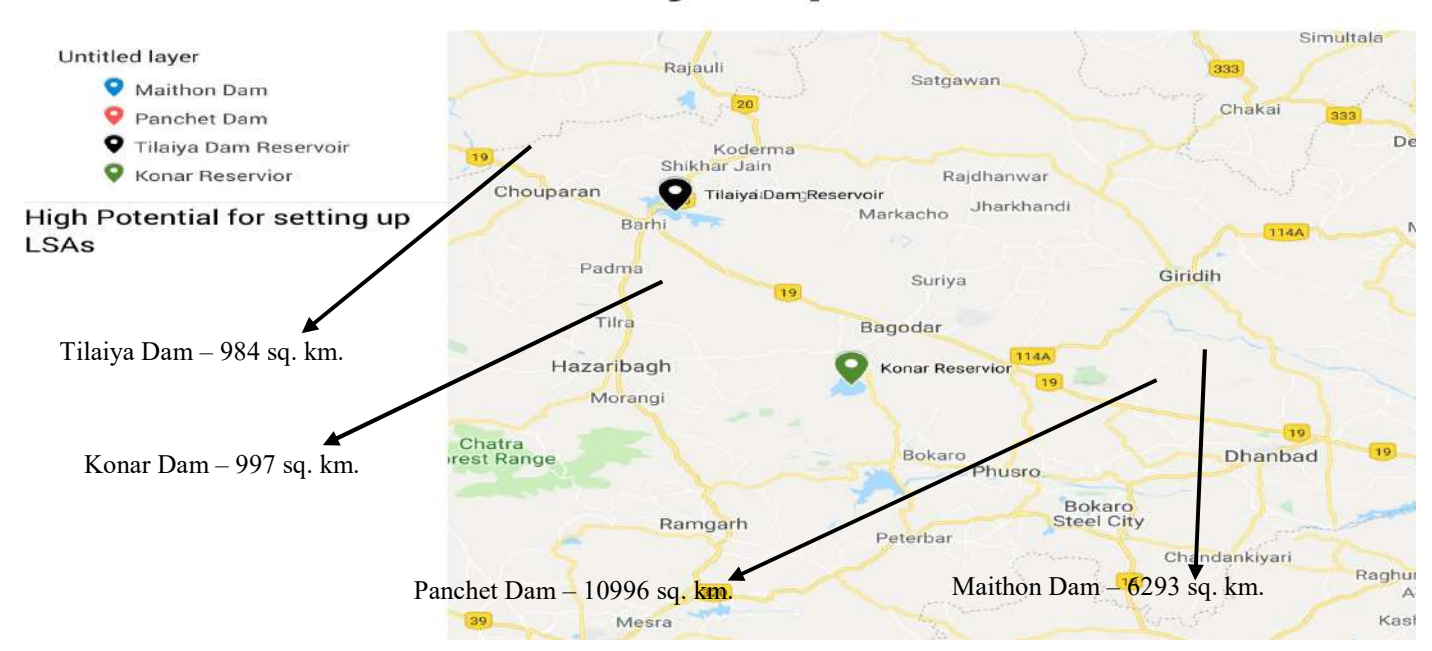
2) Applications: Most coastal areas and inland reservoirs within 35 degrees of the equator can be suitable for application of LSA. The basic requirement is a protected area of water between one and ten metres deep (with some flexibility). About 25 square metres of water area is required for each kilowatt of electrical output if using silicon concentrator cells of 19% efficiency (at 40 degrees C). Where suitable bodies of water are already available, and the sunlight availability is over 2000 hours per year, the

LSA system can offer an extremely competitive source of raw electric power. Lesser hours of sunlight give higher power costs but in many situations this may be acceptable. Likewise, in some good solar situations, custom built ponds may be economically feasible. In each case the water itself is not consumed or changed at all, so multiple usage of the water is possible (drinking, aquaculture). Given that the basic one square metre module of this system will generate about 120 W, quite small systems should still have good economics. Bigger is generally better. If contributing to a national power grid, the LSA component would be most effective if broken into hundreds of systems each of about 10-100 MW, as this would be least affected by local cloud.

C. LSA in DVC

1) The plan:LSA units can be setup on the huge catchment area under the dams of Damodar Valley Corporation i.e. Maithon, Panchet, Konar & Tilaiya. As basic one sq. m. module can produce up to 120 Wp, 25 sq. m. of water area can lead to a peak power generation of 3 kW. However, considering average production of power, it is absolutely safe to assume that at least 25 sq. m. is required to generate 1kWp of electrical power through LSA. 100 MW requires 2.5 sq.km. (1.6 km X 1.6 km) of water area. Since the dams have a huge catchment area, there is enormous potential for LSAs lying untapped till now. Even if the LSAs are set up at the central portions of the reservoirs (away from the banks), which will help in doing away with the adjustment in tracking mechanism due to shading of the panels by nearby trees or construction, the potential is still huge. However, a close study of outlay of the panels all over the reservoirs need to be done as the water area of dams are not in the form of symmetric design such that a simple deduction of area along the periphery for LSA set-up will yield the perfect result. Rather the reservoirs are often in curved form or in trail shape in certain peripheral areas, where the set-up has to be less broad than that at the middle of the reservoirs. Hence, as a pilot project, only a mere 25 sq. m. of water area is being considered for the present paper. This much of area isamply available anywhere on the reservoirs irrespective of its shape&size, without any shading from the banks.

Dams of Damodar Valley Corporation



In order to assure well-founded decisions in designing profitable solar power plants, the sun irradiation needs be measured at the planned site. Photovoltaic concentrator applications require specific measurements to get relevant irradiation information, so that the solar panel mirrors receive sun rays at zero incidence angle always. The sun's radiation on the earth surface combines Direct Normal Irradiation (DNI) and Diffuse Horizontal Irradiation (DHI). Both are linked in the formula for Global Horizontal Irradiation (GHI):

Normally, on a sunny day the insolation is 100% GHI with 20% DHI and 80% DNI \cdot cos (θ).

The output of the system can be efficiently increased by the dual-axis solar tracking mechanism. By the use of this mechanism we can rotate the module according to the movement of the sun so that the sun rays fall exactly perpendicular (DNI) to the module throughout the day (1st axis for daily rotation), for the entire year (2nd axis for seasonal rotation).

GHI = DHI + DNI \cdot cos (θ), (Where θ is the solar zenith angle)

Table – I <u>Irradiance and Solar Angle data for LSA on Maithon Dam (23.8503° N, 86.7778° E)</u>

Month	GHI (kWh/m²)	DHI (kWh/m²)	Altitude Angle	Zenith Angle	DNI (kWh/m²)
Jan	129	47	44.92	45.08	116.12777
Feb	137	53	53.31	36.69	104.753837
Mar	179	68	64.15	25.85	123.341746
Apr	190	79	75.52	14.48	114.641592
May	198	95	83.15	6.85	103.74052
Jun	164	100	86.16	3.84	64.144006
Jul	140	89	86.48	3.52	51.096397
Aug	145	83	79.6	10.4	63.0355819
Sep	133	78	68.32	21.68	59.1867792
Oct	140	62	56.57	33.43	93.4624773
Nov	129	50	46.82	43.18	108.336785
Dec	125	43	42.58	47.42	121.190806
Total	1809	847	(12 noon)	(12 noon)	1123.0583

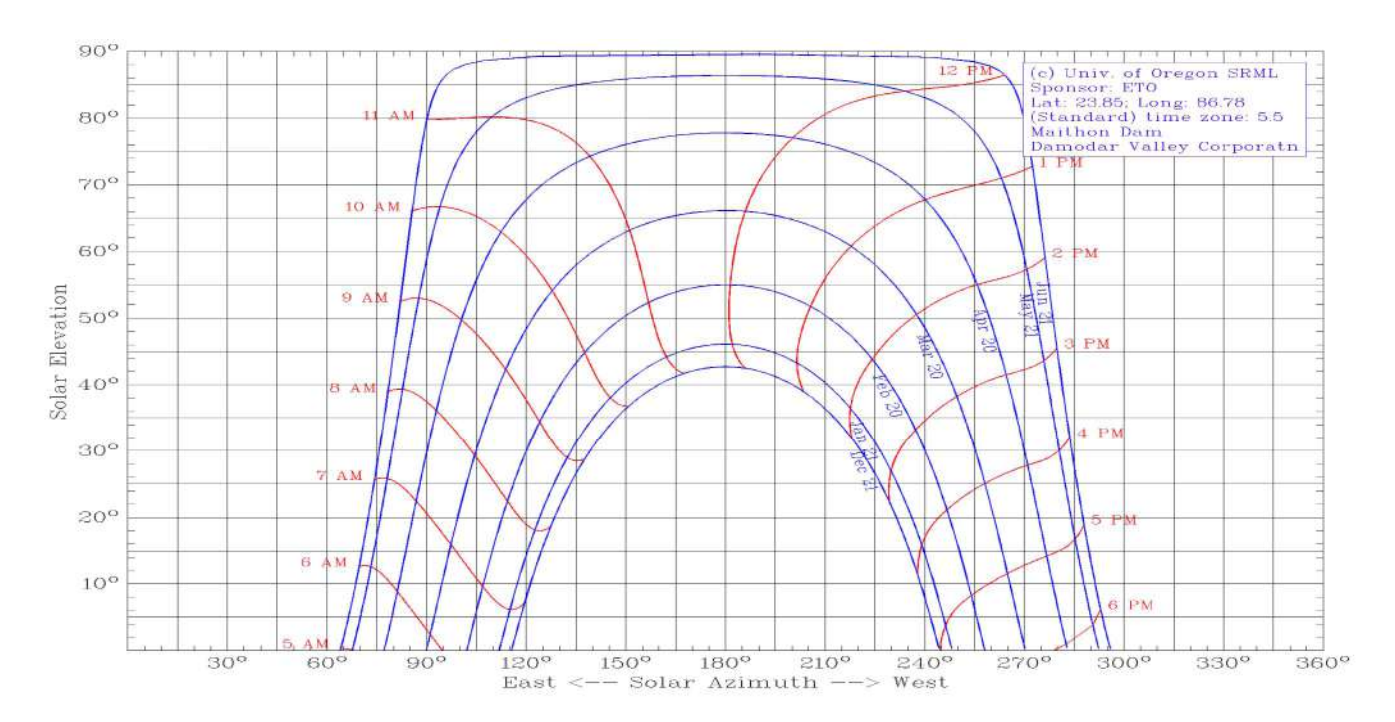


Fig. 1- Sun Path Chart at DVC's Maithon Dam, Dhanbad, Jharkhand, India

Power Generation (yearly): Irradiation (DNI)*Area*Efficiency = 1123*25*33%=9265kWh/yr

Table – II

Irradiance and Solar Angle data for LSA on Panchet Dam (23.6781° N, 86.7469° E)

Month	GHI (kWh/m²)	DHI (kWh/m²)	Altitude Angle	Zenith Angle	DNI (kWh/m²)
Jan	127	51	45.09	44.91	107.311798
Feb	136	53	53.49	36.51	103.265551
Mar	177	71	64.32	25.68	117.617251
Apr	190	77	75.69	14.31	116.618364
May	198	94	83.28	6.72	104.719437
Jun	162	98	86.21	3.79	64.1402735
Jul	139	91	86.61	3.39	48.0841394
Aug	<u>143</u>	86	79.77	10.23	57.920781
Sep	130	82	68.49	21.51	51.5932874
Oct	138	69	56.74	33.26	82.5170871
Nov	127	49	47	43	106.651542
Dec	123	46	42.75	47.25	113.43535
Total	1790	867	(12 noon)	(12 noon)	1073.87486

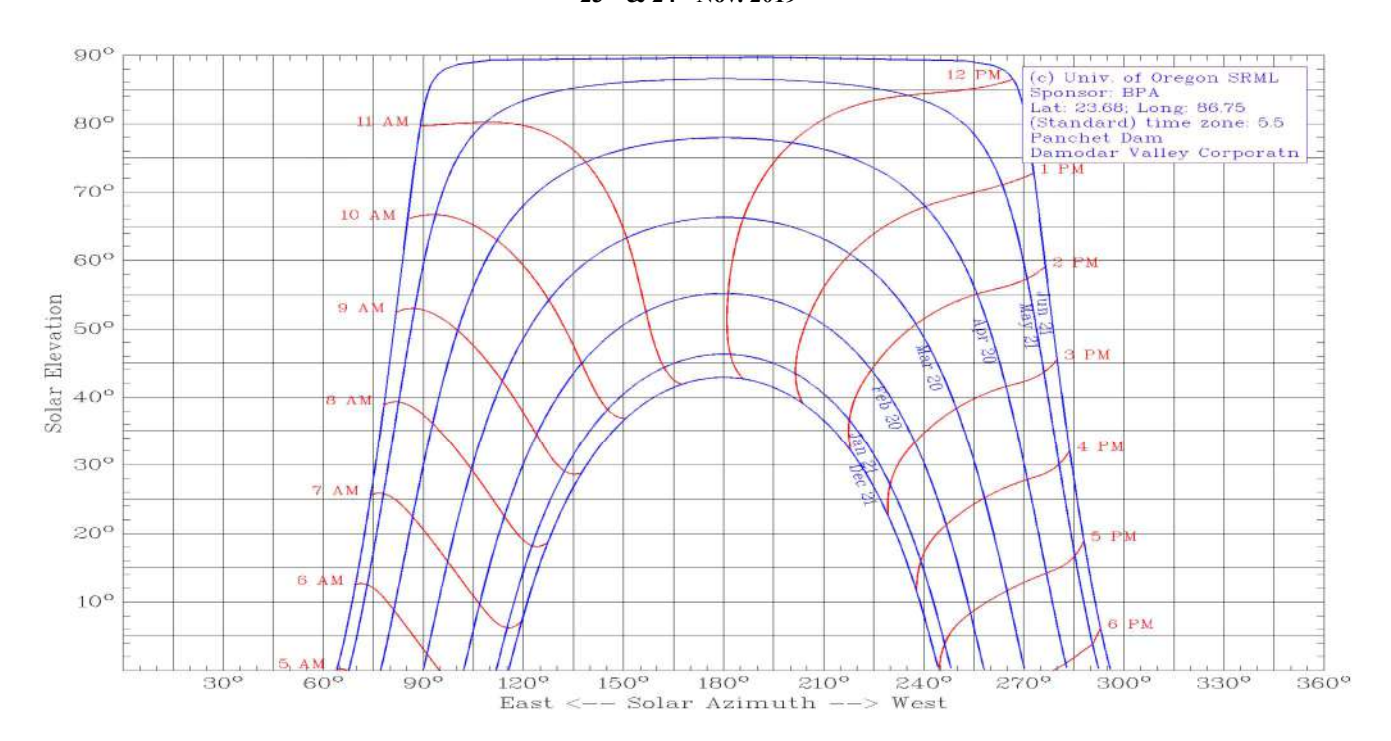


Fig. 2 - Sun Path Chart at DVC's Panchet Dam, Dhanbad, Jharkhand & Purulia, West Bengal, India

Power Generation (yearly): Irradiation (DNI)*Area*Efficiency = 1073.9*25*33%=8860kWh/yr

Table – III <u>LSA on Tilaiva Dam (24.3243° N, 85.5216° E)</u>

Month	GHI (kWh/m²)	DHI (kWh/m²)	Altitude Angle	Zenith Angle	DNI (kWh/m²)
Jan	128	41	44.48	45.52	124.168597
Feb	142	43	52.84	37.16	124.22332
Mar	190	59	63.74	26.26	146.075661
Apr	196	74	75.34	14.66	126.105403
May	208	88	83.53	6.47	120.76918
Jun	167	99	87.17	2.83	68.0830325
Jul	144	92	86.79	3.21	52.0817159
Aug	152	86	79.41	10.59	67.1436279
Sep	144	73	68.12	21.88	76.5113914
Oct	139	66	56.36	33.64	87.6840331
Nov	134	41	46.56	43.44	128.082446
Dec	129	36	42.23	47.77	138.37054
Total	1873	798	(12 noon)	(12 noon)	1259.29895

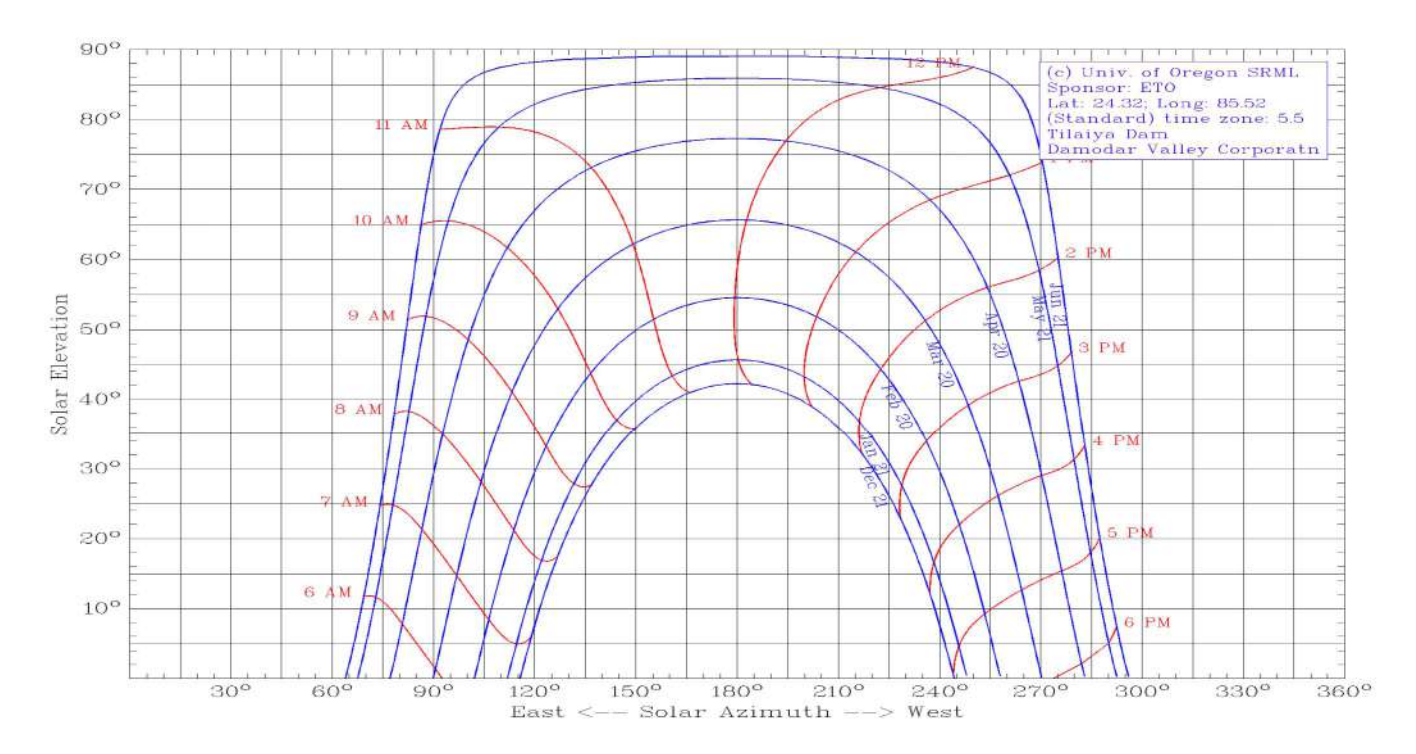


Fig. 3 - Sun Path Chart at DVC's Tilaiya Dam, Kodarma, Jharkhand, India

Power Generation (yearly): Irradiation (DNI)*Area*Efficiency = 1259.3*25*33%=10389kWh/yr

Table – IV LSA on Konar Dam (23.9292° N, 85.7619° E)

Month	GHI (kWh/m²)	DHI (kWh/m²)	Altitude Angle	Zenith Angle	DNI (kWh/m²)
Jan	136	41	44.87	45.13	134.65616
Feb	145	39	53.24	36.76	132.309908
Mar	190	54	64.13	25.87	151.146989
Apr	195	68	75.68	14.32	131.072494
May	207	85	83.71	6.29	122.738877
Jun	171	91	87.07	2.93	80.1047185
Jul	139	95	87.02	2.98	44.0595799
Aug	146	81	79.75	10.25	66.0541786
Sep	139	75	68.46	21.54	68.8052577
Oct	144	65	56.7	33.3	94.5193877
Nov	136	44	46.92	43.08	125.958251
Dec	132	34	42.6	47.4	144.782803
Total	1880	772	(12 noon)	(12 noon)	1296.2086

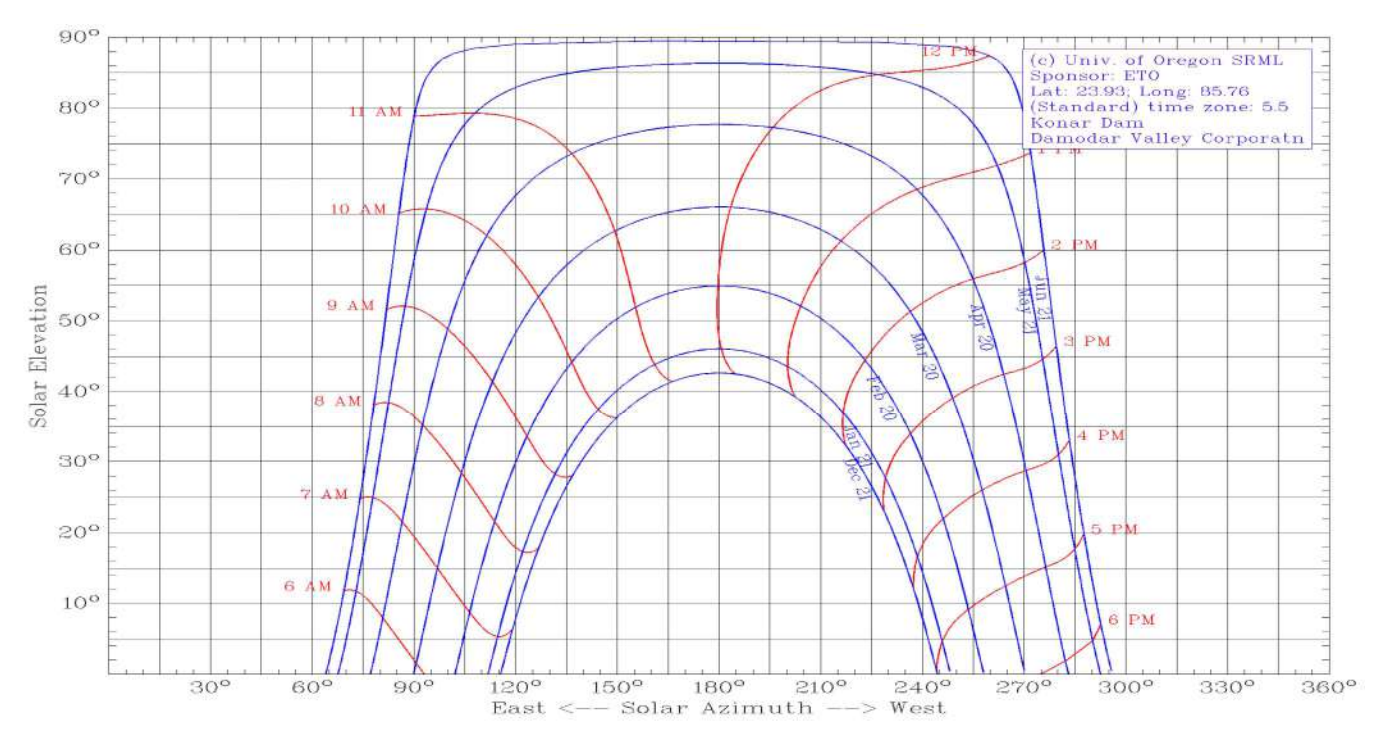


Fig. 4 - Sun Path Chart at DVC's Konar Dam, Hazaribagh, Jharkhand, India

Power Generation (yearly): Irradiation (DNI)*Area*Efficiency = 1296.2*25*33%=10697kWh/yr

2) Tracking Mechanism: The overall solar tracking system consists of a mechanism that enables the PV panels to follow or track the sun. The mechanical structure consists of one servo motor that drives the mechanism, LDR sensors for measuring light intensity, and a programmable microcontroller responsible for giving electric signals to the motors in accordance to the sun angle in order to achieve solar tracking (keeping the PV panel perpendicular to the sunlight). Tracking will be in accordance with the sun path chart of the corresponding locations of LSA set-up as depicted above (Fig. 1 to 4). The feedback control system operation isbased on servo mechanism principles and the controller is responsible for the solar tracker motion.

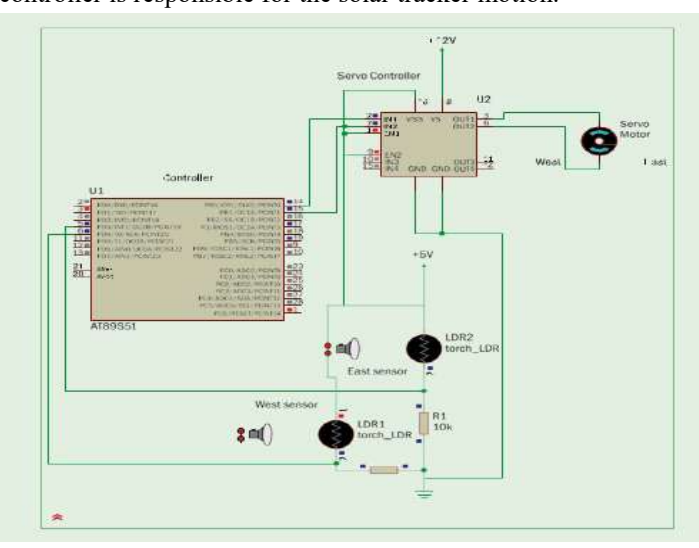


Fig. 5 – Mechanical Structure of the mechanism

Control system has two components. First one works with active components which controls the system automation. The second one is to prepare circuit using passive components for charge controller, voltage regulation, and connections of all components. The active components required are as follows:

Light-dependent resistor (LDR): It is the light-depending resisters that can detect lightning intensity in which they have been stored. The cell resistance falls with increasing light intensity. The sensitivity of a photo detector is the relationship between the light falling on the device and the resulting output signal. In the case of a photocell, one is dealing with the relationship between the incident light and the corresponding resistance of the cell.

Microcontroller: The microcontroller is the brain of the tracker, and it controls the tracking system. It receives input from the sensors, specifying the position of the sun and in response, it sends signal to the motors that are connected to the solar panel to move to the panel to the position of the sun in which optimum solar rays could be received. The microcontroller is made up of software and hardware components. The software component is basically the computer programme that decode the input signals and sends out appropriate signal in response to the inputs to control the tracking system. It is connected to the sensors and motors. The hardware executes the command. It requires 5 V DC.

Servo motor: Servomotors are handy, provide a high level of accuracy, are simple to wire up, and relatively simple to control. They are position controlled rather than rotation controlled. A good application for servomotors is a sun tracking system for solar panels. The system requires a fairly high positional accuracy, therefore, servomotors are ideal for the job. The motor used here requires 4.8 V and an operating speed of 0.18 sec/60° at no load.

Battery: The tracker needs a power source to keep it running due to the irregularity of the power received from the solar panel. A 6 V and 4.5 Amp rechargeable battery is used; the battery as it is connected to the tracking system is also connected to the output of the solar panel to keep it charging.

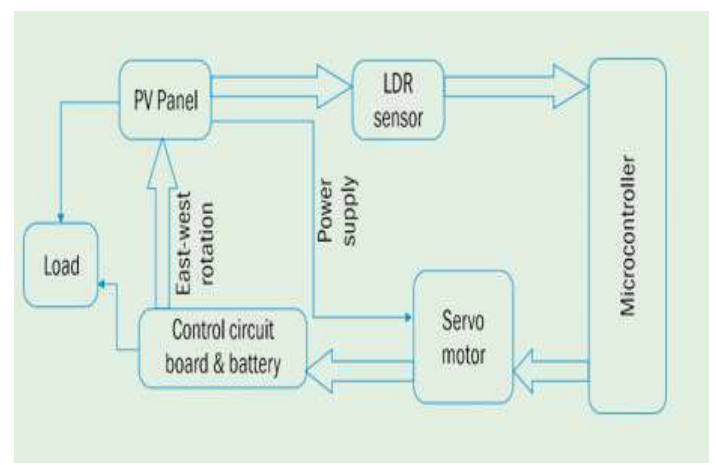


Fig. 6 – Schematic showing working of controlling equipment 3) Financials: The cost per panel of LSA is as

follows:

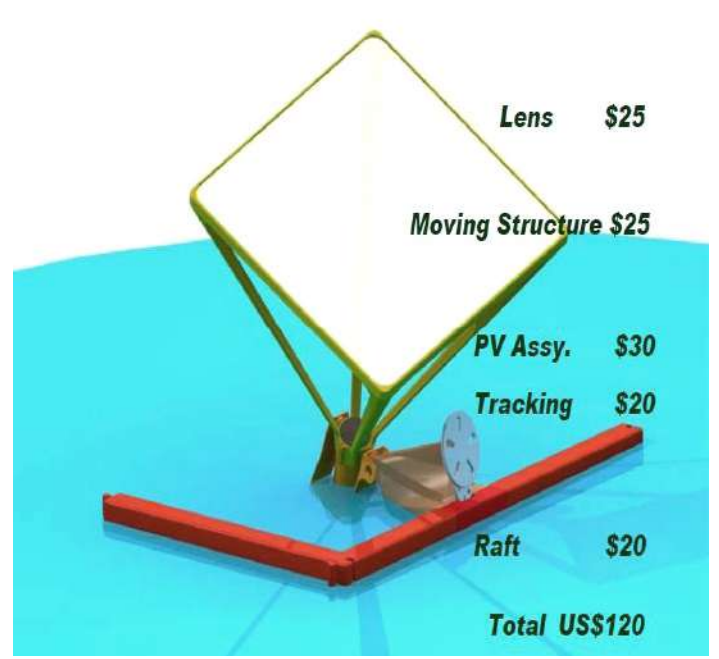


Fig. 7 – Cost break-up of 1m*1m size fully workable panel

Table – V

	Cost of LSA Installation on 25 sq. m. area (25 panels of 1 sq. m. area each) = 25X\$120X70 =Rs. 2.1 Lakh/-														
	Revenue			O&M C	ost (Rs.	in Lakh)					Cash Flo	ow (Rs. in	ı Lakh)		
Place of Installation	Generation (Rs. in Lakh)	Yr. 1	Yr. 2	Yr. 3	Yr. 4	Yr. 5	Yr. 6	Yr.7	Yr. 1	Yr. 2	Yr. 3	Yr. 4	Yr. 5	Yr. 6	Yr. 7
Maithon	0.39	0.05	0.053	0.056	0.059	0.062	0.066	0.070	-1.760	-1.423	-1.089	-0.758	-0.430	-0.106	0.214
Panchet	0.37	0.047	0.050	0.053	0.056	0.059	0.062	0.066	-1.777	-1.457	-1.139	-0.825	-0.513	-0.206	0.099
Tilaiya	0.44	0.055	0.058	0.061	0.065	0.069	0.073	0.077	-1.715	-1.333	-0.955	-0.580	-0.208	0.159	0.522
Konar	0.45	0.057	0.060	0.064	0.067	0.071	0.075	0.080	-1.707	-1.317	-0.931	-0.548	-0.170	0.205	0.576
Assun	nptions: \$1=R	s. 70/-, T	ariff@R	s. 4.20/-,	О&М с	ost = Rs.	8 lakhs/	1 MW (1	MW≈1.5 N	/IU consi	dering Cl	UF=17.19	6 for Eas	tern India)

CONCLUSION

The main advantage of PV concentrators over conventional flat plate PV cells is the capacity of former to utilise the sun rays to a much greater extent. Also, when mounted on water, the PV concentrators have added advantage of greater cooling effect available from the water body as well as the benefit of using lighter and less rigid structure, being on water and having protective feature of drowning the panel at times of cyclonic conditions, compared to ground mounted ones. So, PV concentrators, along with water mounted set-up, i.e. LSAs result

in two fold gains. In the instant paper, the payback period, even after considering very conservation O&M cost and competitive tariff, is around 64 to 76 months at maximum. However, from the data gathered and the outcomes so achieved, it is pertinent to mention that in the regions where LSA set-up is considered in the instant paper, the electrical output capacity (largely based on DNI) is higher during the winters compared to the summers, even though the GHI value is maximum during the summers. It can be attributed to the fact that the regions considered in the instant paper are having high moisture content in the atmosphere

during the summers, which results in a comparatively higher DHI and hence DNI decreases. However, during winters when the area is dry and even though GHI is much lower than in summers, the DHI is significantly low, making DNI the bulk contributor to the GHI. High vapour content during summers robs the LSAs of incoming DNI. Large clouds and incessant rains during monsoons, which is a season mostly perceptible in the Indian subcontinent, results in the lowest output. During monsoon, not only GHI is low (sometimes minimum) but the bulk of the heat is in the form of DHI, which is not of much use to LSAs. So it can be concluded that the drier the area throughout the year, the greater is the capacity of output through LSAs.

ACKNOWLEDGMENT:

The team is indebted to SPE section, DVC for providing data related to DVC Solar program from time to time.

REFERENCES:

[1]. ShubhamGavhane and Saurabh Shingare, "Liquid Solar Array", *IJARIIE-ISSN(O)-2395-4396*, Vol-2 Issue-5 2016.

- [2]. Hyun-Jin Lee, Shin-Young Kim and Chang-Yeol Yun, "Comparison of Solar Radiation Models to Estimate Direct Normal Irradiance for Korea", *energies-MDPI*, 30th April, 2017.
- [3]. Rohit Agarwal, "Concept of Mechanical Solar Tracking System", *IOSR Journal of Mechanical and Civil Engineering (IOSR-JMCE)*, e-ISSN: 2278-1684, p-ISSN:2320-334XPP 24-27.[4]. Khyati Vyas, "Automatic Solar Tracking System: Developm-
- -ent and Simulation", *IOSR Journal of Electrical and Electronics Engineering (IOSR-JEEE)*, June, 2017.
- [5]. Detailed Project Report by Solar Energy Corporation of India Limited to DVC for "Floating Solar Project on DVC Dams".
- [6]. Sponsored Technical Report by MaikeWiesenfarth, Dr. Simon P. Philipps&Dr. Andreas W. Bettof Fraunhofer Institute For Solar Energy Systems and Kelsey Horowitz&Dr. Sarah Kurtz of National Renewable Energy Laboratory, "Current Status of Concentrator Photovoltaic (CPV) Technology", April, 2017, online ordering:

http://www.ntis.gov/help/ordermethods.asp

XXX---XXX

Assessing the potentiality of agricultural residues in extending operational period of bagasse-based co-generation plants in India

Parashuram R. Madar¹ and Suresh T. Dundur^{2,*}

¹Research Scholar, ²Professor, Department of Industrial & Production Engineering Basaveshwar Engineering College, Bagalkot -587103, Karnataka, India, *Corresponding Author Email-Id: sureshdundur@gmail.com

Abstract: Under the signs of extinction of conventional fossil fuels in near future, more emphasis lies now on exploitation of renewable energy sources. The energy production in India from the biomass for the financial year 2017-18 is merely 2.06 percentage of total potential derived from all the renewable sources out of which 0.46 percentage is from cogeneration which is far below their installed capacity. This may be attributed to the fact that cogeneration is pertaining to the utilization of only the bagasse for power production. However, the supply of bagasse is adequate only during crushing season but its non availability for rest of the period leaves those plants inoperative. This void created in the supply of fuel for cogeneration in plants can be filled up through alternative agricultural residues and by managing properly, continued production of power can be ensured. The residues from the nine prime crops are considered for the investigation based on their available energy potential. The power potential of these residues, determined theoretically on the basis ultimate and proximate analyses figures out approximately one million MW of power year on year.

Key words: Agricultural residue, Biomass Energy, Cogeneration, Power Potential

1. INTRODUCTION

Under the signs of extinction of conventional fossil fuels in near future, more emphasis lies now on exploitation of renewable energy sources. The acclaimed reliable sources of renewable energy include solar, wind, biomass and hydro. The estimated energy potential in India from the biomass for the financial year 2017-18 is merely 2.06 percentage of total potential derived from all the renewable sources [1]. In contrast to it, agriculture is a major occupation in India since ages and is capable of producing more and more to meet the ever increasing demand due to swelling population. It also produces large quantity of agricultural residues that are usually considered as waste and the formers burn it in the fields to reduce the cost of cleaning. It is worthwhile estimating the potential of this huge biomass produced in the form of agricultural residue for boosting the productivity in co-generation plants. Though found in abundance, agricultural residues except bagasse were never been considered as the persuasive sources of energy for power generation. Major agricultural residues that are produced in large quantities every year other than bagasse include sugarcane trash, arecanut shell, coconut shell/coir, groundnut shell, cotton stalk, rice/wheat husk, corn cob etc. Proper utilization biomass results in the production of electricity at cheaper rate and benefits the environment by reducing the greenhouse gases (GHGs) in atmosphere due to their lower emissions as compared to conventional fossil fuels [2-3].

India being a major consumer of electricity in South-Asia contributing to 85% of its total production, is still facing sever power crisis due to its own production falling short by 30% of its demand. In filling this gap cogeneration of electricity using biomass is very attractive due to its low capital investment, short gestation period, reduced fuel consumption and associated environmental pollution and increased fuel diversity [ESCAP, 2000] [4]. It is estimated that the sugarcane production in India is expected to touch 38 million tons during kharif season of 2018-19 [5-6]. Never the less the power produced from cogeneration is just amounts to 0.46 percent of the total power produced from the renewable energy sources. The figure indicates that the potentiality of cogeneration in India has not been exploited to its fullest extent. This may be attributed to the fact that cogeneration is pertaining to the utilization of only the bagasse for power production. However, the supply of bagasse is adequate only during crushing season but its non availability for rest of the period leaves those plants inoperative. This void created in the supply of fuel for cogeneration in plants can be filled up through alternative agricultural residues and by managing properly, continued production of power can be ensured.

2. POTENTIALITY OF AGRO-BASED BIOMASS RESOURCES

About 58 % of population in India is depending on agriculture for their income and contribute to 18 % of

the gross domestic production. As a result of vast area of agriculture, a huge quantity of agricultural residue is produced every year. Traditionally, part of this agro-waste is utilized by the rural masses to fulfill their domestic energy requirements and remaining is burnt in the fields [5]. Utilizing the agricultural residues, cow dung, wood etc for domestic heating results in houses filled up with smoke and become sources of respiratory related health hazards. Nearly 100 million (42 %) of the total 240 million households were dependant on such unclean fuel. Under Pradhan Manthri Ujwala Yojana, a government run program, more than 70 million families have been provided with free LPG connection in order to safe guards their health. On the other hand the Indian Council of Agricultural Research (ICAR) has estimated the burning of 23 million tons of rice residue by the formers in Punjab, Haryana, Utter Pradesh and National Capital Territory (NCT) of Dehli within a span of 10-20 days while preparing their fields for sowing wheat. Burning paddy crop residue like this has become one of the major causes of the pollution. Central government evoked a scheme on "Promotion of Agricultural Mechanization for In-Situ Management of Crop Residue in the state of Punjab, Haryana, Utter Pradesh and NCT of Dehli" to address this problem which has resulted into paddy crop residue burning reduced by 41 % within two years.

Table 1: List of potential agricultural residues with gross produced per annum.

Crop	Type of residue	Crop to residue ratio	Growing area ('000 hectare)	Production ('000 tons)	Estimated quantity (Million tones/Year)
Sugarcane	Bagasse	0.33	4389	306720	101.2176
ougarcane	Trash	0.05	4309	300720	15.3360
Rice	Straw	1.50	42104	110150	165.2250
Mice	Husk	0.20	43194	110130	22,0300
Coconut	Shell	0.90	2096	12994	11.6950
Coconuc	Husk	3.08	2090	12994	400.2306
Groundnut	Shell	5.00	4013	9180	45.9000
Cioundia	Straw	2.60	4013	9100	23.8680
Maize	Stalk	2.50	9500	25000	62.5000
IVIAIZE	Cob	1.20	9300	23000	30.0000
Arecanut	Frond	3.00	466	730	2.1900
Arecanut	Husk	0.80	+00	/50	0.5840
Cotton	Stalk	3.80	10845	33090	125.7420
Wheat	Straw	1.50	30597	98380	147.5700

Potentiality of the biomass resources for the convenience of use in co-generation are characterized on basis of their energy content, ease of handling, chemical composition and the quality of ash it generates [7,15 and 19]. From the wide list of agricultural residues in India, the residues from the nine prime crops are considered for the investigation based on their available energy potential [7, 12]. The data regarding total production and gross residues produced per annum is presented in Table 1. The analyses is carried out utilizing the published data pertaining to crop demography, supply period, availability, ultimate and proximate analyses.

3. POWER POTENTIAL BASED ON ULTIMATE AND PROXIMATE ANALYSES

A theoretical estimation of energy from the utilization of these agricultural residues is carried out by many investigators in the past on the basis of ultimate analysis have determined the heat energy contributed by the basic constituent elements carbon, hydrogen and sulphur as 8084, 28922 and 2224 in Kcal/Kg respectively [6-7]. The power equivalent is determined taking into account the energy conversion and the boiler efficiencies as 30 % and 70% respectively and presented in table 2. These efficiencies were chosen based on unenthusiastic valves taken by the previous investigators [8-10], hence the actual power may be slightly higher than those represented in this paper.

Characterization utilizing the results of proximity analysis pertaining to volatile matter, ash content and moisture content in the agricultural residues is carried out which provides a prominent means of assessment for the usefulness of residues as fuels in cogeneration plants [11,15 and 22]. Ease of ignition of residue depends on the presence of volatile matter in it. The gases like hydrogen, methane, hydrocarbons, carbon monoxide, carbon dioxide and nitrogen constitute the volatile matter. All these gasses except carbon dioxide and nitrogen contribute to the combustion process; hence, the residues with higher volatile matter are favorable. In contrast to it, lower values of ash and moisture contents in residues is preferred to reduce pollution related problems. The table 3 depicts the results of proximate analysis carried out by various investigators [7-8, and 22] and power potential estimated on its basis.

Table 2: Theoretical estimation of power potential from ultimate analysis

	tity enr)	Ca	rbon	Hy	drogen	Sul	phar	g)	7	7	
Agriculture Residues	Estimated quantity (Million tones/Year	96	Heat Energy (Keal/lg)	96	Heat Energy (Keal/lg)	96	Heat Energy (Kenl/lg)	Total Energy/lg (Keal)	Energy potential (Keal)	Power Potential in MW	
Coconut husk	400.23	46.52	3760.68	5.50	1590.71	0.00	0.00	5.35E+03	2.14E+12	5.23E+05	
Paddy straw	165.23	35.97	2907.81	5.28	1527.08	0.00	0.00	4.43E+03	733E+11	1.79E+05	
Wheat Straw	147.57	40.21	3250.58	5.08	1469.24	0.11	2.45	4.72E+03	6.97E+11	1.70E+05	
Cotton stalk	125.74	39,47	3190.75	5.07	1466.35	0.02	0.44	4.66E+03	5.86E+11	1.43E+05	
Bagasse	101.22	44.80	3621.63	535	1547.33	0.38	8.45	5.18E+03	5.24E+11	1.28E+05	
Groundnut shell	45.90	45.72	3696.00	5.96	1723.75	0.00	0.00	5.42E+03	2.49E+11	6.07E+04	
Com cob	30.00	49.80	4025.83	5.87	1697.72	0.01	0.22	5.72E+03	1.72E+11	4.19E+04	
Rice husks	22.03	38.92	3146.29	5.10	1475.02	0.12	2.67	4.62E+03	1.02E+11	2.49E+04	
Cane trash	15.34	5121	4139.82	5.16	1492.38	137	30.47	5.66E+03	8.69E+10	2.12E+04	
Coconut shell	11.70	88.95	7190.72	0.76	219.81	0.00	0.00	7.41E+03	8.67E+10	2.12E+04	
Arecanut husk	2.19	63.18	5107.47	6.81	1969.59	0.63	14.01	7.09E+03	1.55E+10	3.79E+03	
										1.32E+06	

Table 3: Theoretical estimation of power potential from proximate analysis

Agriculture Residues	Estimated quantity (Million tones/Year)	Calorific Valve (Kcal/kg dry basis)	Energy potential (Kcals)	Power Potential in MW
Coconut husk	400.23	4152.732	1.66E+12	4.06E+05
Paddy straw	165.23	4131.240	6.83E+11	1.67E+05
Wheat Straw	147.57	3467.370	5.12E+11	1.25E+05
Cotton stalk	125.74	4370.000	5.49E+11	1.34E+05
Bagasse	101.22	3780.200	3.83E+11	9.34E+04
Groundnut shell	45,90	4584.960	2.10E+11	5.14E+04
Com cob	30.00	3741.990	1.12E+11	2.74E+04
Rice husks	22.03	4893.010	1.08E+11	2.63E+04
Cane trash	15.34	4632.720	7.11E+10	1.73E+04
Coconut shell	11.70	3111.560	3.64E+10	8.89E+03
Arecanut husk	2.19	4095.420	8.97E+09	2.19E+03
				1.06E+06

4. RESULTS AND DISCUSSION

Referring to figure 1, it may be observed that bagasse and cane trash are available from October to March. Paddy straw is one amongst the residues that is available during the off season of cane crushing i.e. April to December. Rice husk and Corn cob can provide energy security from June/July to September. On the other hand Groundnut residue is available during six months from April to June and October to December. It can be a potential energy source to fill the gap from April to June. Coconut trees yield biomass throughout the year and are also known as the energy trees as they produce variety of biomasses in large quantity. Harvesting period for cotton stalk and arecanut shell is wide and spread over eight months from September to April (Figure 1). However seasonal availability of them is more or less aligned with the availability of bagasse. Most of these residues are available in dry condition from fields hence, they have the advantage of ease of storage for the off season utilization [23, 26].

The opportunity to reap agricultural residues for power generation in India seems to be far above the ground as indicated by the present investigation. The estimated power potential (total 1.32X10⁶ MW) based on ultimate analysis is depicted in table 2 and estimated power potential (total 1.06X10⁶ MW) based on proximate analysis is depicted in table 3. The higher estimation of power potential utilizing ultimate analysis may be attributed to part of the carbon turns into CO which is not taken into consideration in the present analysis. Because

formation of CO leads to lower energy release of 2430 kcal per kg formation as compared to CO₂ formation which releases 8084 kcal/kg. Overall, approximately more than one million MW of power that can be produced year on year by the effective utilization of listed residues alone. Out of 11 residues presented in table 1, merely bagasse is effectively utilized by the existing co-generation plants. The rationale behind the consumption of bagasse in totality is based on certain benefits such as the residue is produced in the adjoining sugar plants hence no additional transportation cost is incurred, bagasse contains high volatile matter (90.15 %) which increases its ease of burning, no additional cost for raw material as most of the sugar mills own these plants, material handling within the premises is convenient, bagasse is received in the form of small chips which is in ready to use form etc [16-17]. Therefore, co-gen plants are designed specifically to go well with bagasse as a feed fuel. The burning mechanism changes drastically when feed fuels differ in their physical properties from the bagasse. Coal is not suitable for burning in co-generation boilers although it is having very high calorific value compared with biomasses. It takes more time to burn and turns into a lumpy mass in the burning chamber due to very high ash content. It also contain a very large amount of sulphur (approximately 4.7 wt %) as compared to agricultural residues (0 to 1.37 wt %) (table 2) which leads to environmental air degradation. The residues like paddy straw, cane trash or wheat straw when burnt in co-generation boilers, gets fluidized due to their very low relative density and the burning extends into the exhaust pipes, it increases fly-ash and severely affects boiler efficiency. In contrast to it, the residues like rice husk or cotton stalk produce large quantity of ash as compared to bagasse posing operational difficulties [1819-20]. The deviations of parameters of proximate analysis of other agriculture residues with respect to bagasse are shown in figure 2. The volatile matter in other residues is comparable with that of the bagasse and volatile matter contained in all agriculture residues fall in a range of approximately 30 % below level of volatile matter contained within bagasse. However, the deviation is less than 5 % in paddy straw and less than 15 % in coconut and groundnut shells.

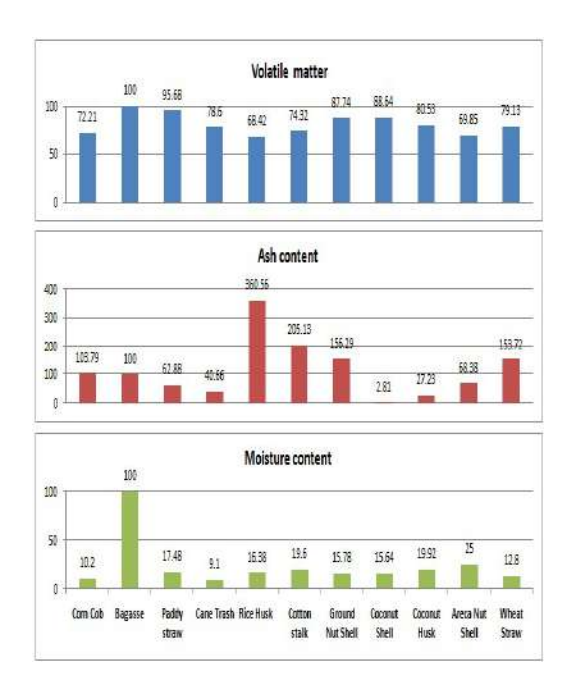
Figure 1: Seasonal availability of agricultural residues

esidue	Period of availability											
Agricultural residue	January	February	March	April	May	June	July	August	September	October	November	December
Com Cob							_	_				
Bagasse	_											
Paddy straw												_
Cane Trash	_		_	i i							_	_
Cotton stalk	_	-	-						_		-	_
Groundnut shell				_	_	H				_		_
Rice husks						_						
Wheat straw		_	_		_				_		_	_
Coconut husk				_			H	_			_	
Coconut shell			_		_			_				
Areca Nut Shell	_		_						_			_

The quantity of ash produced from rice husk, cotton stalk, groundnut shell and corn cob is more than the bagasse whereas it is less than that in paddy straw, cane trash, coconut shell/husk and arecanut shell. Coconut shell and husk produce the lowest level of ash i.e. just 3 % and 28 % in comparison with the ash produced by burning bagasse respectively. The moisture content in all other residues is much less as compared to bagasse. However, bagasse is an exceptional case where moisture content although is as high as 50 %, its combustion process is not affected due to presence of sucrose in it.

Generally, the agriculture residues are bulky and voluminous hence levy high cost on transportation. Alternative methods like pre-processing to form briquettes before transporting may prove to be viable [11, 20]. However, a detailed economic analysis needs to perform in order to choose the appropriate mixture of the available biomasses from the nearby places by individual plants.

Figure 2: Parameters of proximate analysis of agriculture residues as relative % of bagasse



5. CONCLUSIONS

Agricultural residues are produced in large quantities in India which can be the potential feed fuel for cogeneration boilers. Bagasse based cogeneration plants are faced with shortage of feed fuel to run their plants through all seasons. The commonly produced agriculture residues characterize well with bagasse, hence, can be considered for combustion in its place during off seasons of cane crushing. The residues considered in the present paper are chosen on the basis of their potential to produce higher and reliable power. The power potential of these residues determined theoretically on the basis of ultimate and proximate analyses figure out approximately one million MW of power year on year. Co-generation plants can be run throughout the year by properly choosing the agriculture residues. The agriculture residues are generally bulky and voluminous hence may require pre-processing like conversion into briquettes etc which may reduce the cost of their transportation. However, a deeper economic analysis is needed to establish such facts.

6. REFERENCES

- Report "Energy Statistics-2018 Central Statistics Office Ministry of Statistics and Programme Implementation Government of India New Delhi" 25th Issues.
- Sunil Pandey, Kanika Kalra, Pooja Singh, and Rajat Shukla, "Electricity Generation from Trash Eliminating the Unwanted, While

- Creating the Needed" *International Advanced Research Journal in Science, Engineering and Technology* (IARJSET), ISSN 2393-8021 Volume 2. May 2015.
- 3) Moonmoon Hiloidhari, Dhiman Das, and D.C.Baruah, "Bioenergy potential from crop residue biomass in India", *Renewable and Sustainable Energy Reviews* 32(2014)504–512.
- 4) Report, "Transforming the Energy Sector to Sustain Growth" OECD Green Growth Studies: Energy 2011.
- 5) Salman Zafar, "Sugarcane Trash as Biomass Resource" *Brazilian Journal of Microbiology*, (February 23, 2015).
- 6) Annual Report 2017-18, "Department of Agriculture, Cooperation & Farmers Welfare Ministry of Agriculture & Farmers Welfare Government of India Krishi Bhawan", New Delhi-110 001.
- 7) Rishi Kumar Dear, "Estimation of Power Generation Potential of Agricultural based Biomass Species" M.Tech Thesis in Department of Mechanical Engineering National Institute of Technology Rourkela.
- 8) Book: "Combustion Engineering and Fuel Technology". Publisher-Bureau of Energy Efficiency Publishing 1974.
- 9) Suleiman Jose Hassuani, and Manoel Regis Lima Verde Leal, "Biomass power generation Sugar cane bagasse and trash" PNUD -Programa das Nacoes Unidas para o Desenvolvimento and CTC - Centro de Technologies Canavieira (2005).
- 10) Mamta Awasthi, and Karishma Rani Deepika, "Energy through agricultural residues in rural India: potential, status and problems" International Journal of Emerging Technology and Advanced Engineering Volume 3, Special Issue 3: ISSN 2250-2459, (Feb 2013).
- 11) Deepak K.B, and N.A.Jnanesh, "Investigation of areca leaves as a biomass fuel by the method of briquetting" *IPASJ International Journal of Mechanical Engineering* (IIJME)-Volume 3, Issue 6, ISSN 2321-6441 (June 2015).
- 12) Koteswararao B., Yakkala M. K. Raghundh and Kalapala Prasad, "Alternative Fuel for Power Plant" *International Journal of Engineering Research and Applications* (IJERA) ISSN: 2248-9622 (10th January 2015).
- 13) Nagarajan Arumugam and Shanmugam Anandakumar, "Mini review on Corncob

- biomass: A potential resource for value-added metabolites" *European Journal of Experimental Biology* ISSN: 2248 –9215 (2016).
- 14) N. Radhakrishnan and V. Gnanamoorthi, "Pyrolysis of Groundnut shell biomass to produce bio-oil" *International conference on recent advancement in mechanical engineering & technology* ISSN: 0974-2115 (April 2015).
- 15) Vijay Krishna Moka, "Estimation of calorific value of biomass from its elementary components by regression analysis", M Tech Thesis, Department of Mechanical Engineering, National Institute of Technology, Rourkela (2012).
- 16) Mukesh Kumar Mishra, Nilay Khare and Alka Bani Agrawal, "Bagasse Cogeneration in India: Status, Barriers" *IOSR Journal of Mechanical and Civil Engineering* (IOSR-JMCE) e-ISSN: 2278-1684, Volume 11, Issue 1 (Jan 2014).
- 17) Suresh Chauhan, "Biomass resources assessment for power generation: A case study from Haryana state, India" *Biomass and Bioenergy* Volume 34 (17 March 2010).
- 18) B. M. Jenkins, L. L. Baxter, T. R. Miles Jr and T. R. Miles, "Combustion properties of biomass" *Fuel Processing Technology* Volume 54 (17-46) issue 1998.
- 19) Ayhan Demirbas, "Potential applications of renewable energy sources, biomass combustion problems in boiler power systems and combustion related environmental issues" *Progress in Energy and Combustion Science* Volume 31 issue 2 (2005).
- 20) Muhammad Arshad and Sibtain Ahmed, "Cogeneration Through Bagasse: A Renewable Strategy To Meet The Future Energy Needs" Renewable and Sustainable Energy Reviews Volume 54 Issue (2016).
- 21) Bhajan Dass and Pushpa Jha, "Biomass Characterization for Various Thermo-chemical Applications" *International Journal of Current Engineering and Scientific Research* (IJCESR) ISSN: 2393-8374, Volume-2, Issue (2015).
- 22) Harmandeep Singh, Pawan Kumar Sapra, and Balwinder Singh Sidhu, "Evaluation And Characterization Of Different Biomass Residues Through Proximate & Ultimate Analysis And Heating Value" *Asian Journal of Engineering And Applied Technology* ISSN 2249-068X Vol. 2 (2013).

- 23) Prabin Haloi, "Comparison of Locally Available Biomass Characteristics as A Gasification Feedstock" *International Journal of Current Engineering and Technology* E-ISSN 2277 4106 (August 2014).
- 24) Atul Kumar, Pallav Purohit, Santosh Rana and Tara Chandra Kandpal, "An Approach to the Estimation of the Value of Agricultural Residues Used As Bio Fuels" *Biomass and Bioenergy* Volume 22 (2002).
- 25) Bablu Das, "Estimation of Power Generation Potential of Non-Woody Biomass and Coal-Biomass Mixed Briquettes" Master of Technology Thesis in Department of Mechanical Engineering National Institute of Technology Rourkela [2011].
- 26) Arun K. Tripathi, P. V. R. Iyer, Tara Chandra Kandpal and K. K. Singh, "Assessment of Availability and Costs of Some Agricultural Residues Used as Feedstock's for Biomass Gasification and Briquetting In India" Elsevier Science and Energy Converse Management Vol. 39, No. 15 (1997).

Design of a solar cell based submersible pump for drinking water in remote area

Pousali Sarkar ^[1], Supriyo Set ^[1], Parijit Choudhury ^[1], Asoke Kumar Paul ^[2]

^[1] 3rd year B Tech student, Department of Electrical Engineering, Techno India University

^[2] Associate Professor, Department of Electrical Engineering, Techno India University

EM 4/1, Salt Lake, Sec-V, Kolkata 700091

Email: parijitchoudhury001@gmail.com

Abstract - This paper deals with the design and a prototype development of an inverter to feed AC power to an induction motor coupled with a submersible pump for drinking water purpose. The inverter is fed from a 12 V rechargeable battery, which is charged through solar cell. The basic intention of this research work is to run a pump in a remote area where there is no electric power supply or where there is problem in power distribution system and supply voltage is low. Drinking water submersible pumps are normally operated for a small interval (10 to 30 min). This energy can be supplied by a 12 V, 75 Amp-Hour Lead Acid type rechargeable batteries.

The solar panel is used to charge the battery for complete day time and with the fully charged battery, the pump is run through Variable Voltage Variable Frequency Drive for a short time of around 30 min.

An inverter has been designed to run a 1 hp induction motor coupled with a pump. The motor is started with low voltage with v/f control. Gradually the full voltage is applied and motor runs at rated speed. After an operation of a preset time, the motor is stopped.

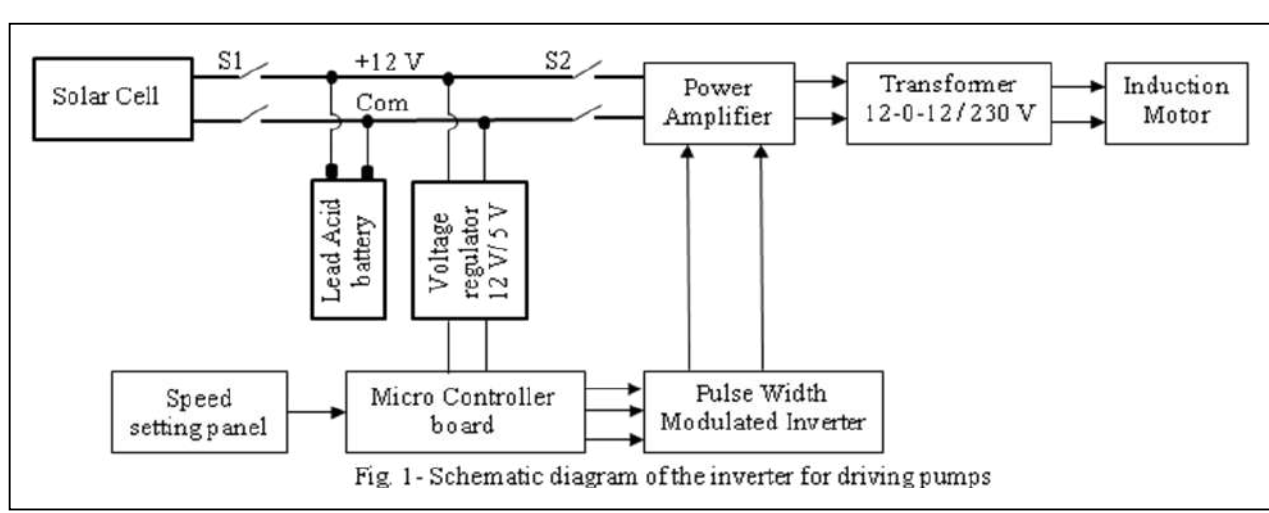
For running the pump more time, it is required to have multiple solar cells and multiple batteries.

Keywords—Pulse Width Modulation, Variable Voltage Variable Frequency drive, Submersible pump

I. INTRODUCTION

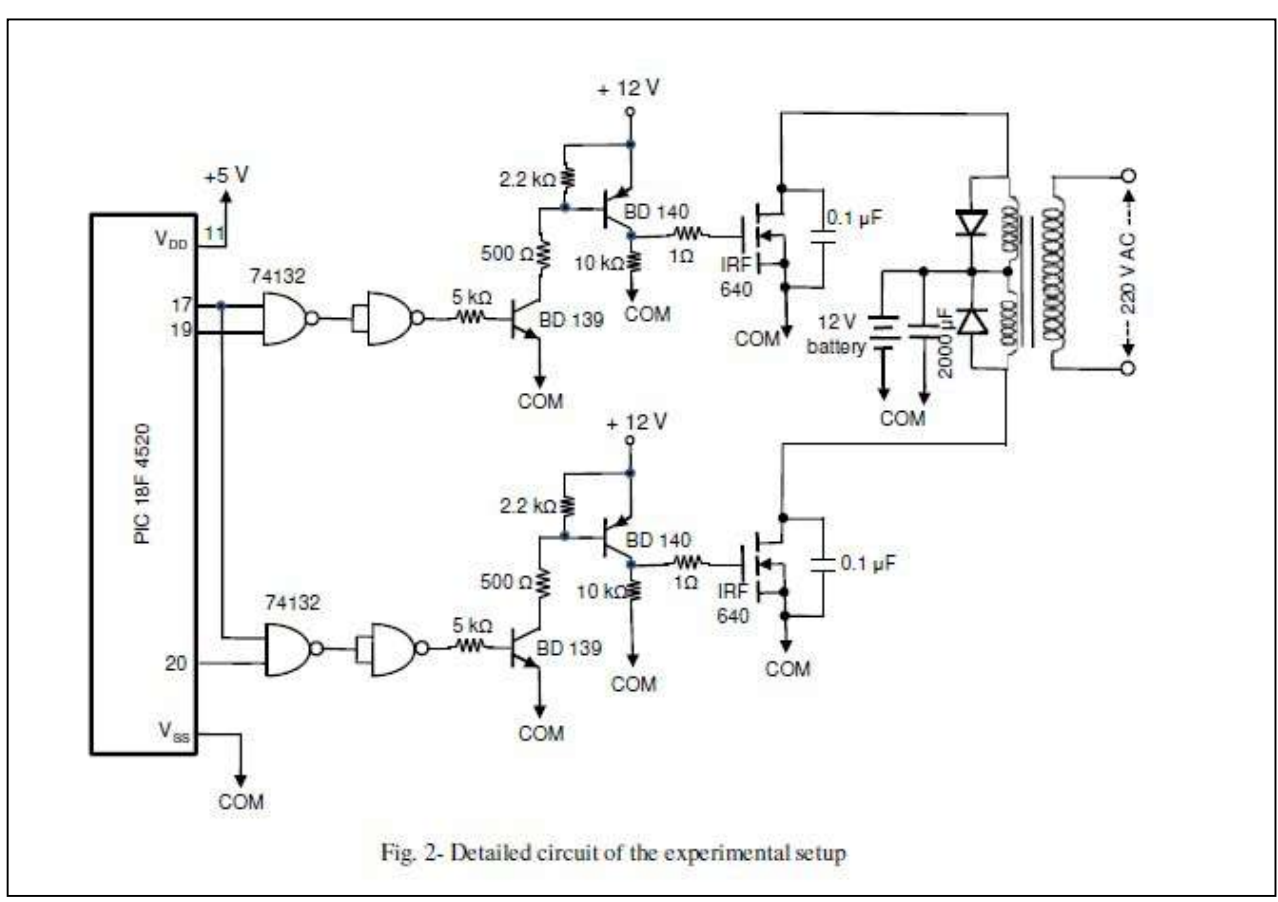
In remote area where there is non-availability

of electric power, it is often required to run a submersible pump to draw drinking water from deep tube well. A system has been designed and developed using solar cell based inverter to overcome this problem. A lead acid battery has been chosen to store the electrical energy which shall be used to drive the pump. The battery shall be charged by solar cell throughout the day. In the evening when the battery is fully charged, the batteryshall be connected with the inverter and pump shall be operated. The operating period of the pump shall depend on the charge stored on the Lead Acid type rechargeable battery. For efficient operation, the solar cell shall be kept on the roof top and battery with inverter can be kept near the pump. In this particular experiment, the rechargeable battery chosen is 12 V, 75 AH. With this battery, a 1 hp pump can be operated for 30 min efficiently. The submersible pump used for this experiment is 1 hp, 10 stage, 25 mm outlet size, suitable to draw water at flow rate of 24 – 90 liters per min, with 42 - 11 m head. The motor for this pump is a squirrel cage induction suitable for 180-240 V power supply, 50 Hz, single phase, capacitor start and capacitor run type motor. We have chosen lead acid battery as this type of battery can supply high surge current which is required for starting of the induction motor. Another advantage of lead acid battery is that it is easily available in remote places (A car battery or a motor cycle battery can also be used in emergency situation to run the pump). If it is required to run the pump for more time, we need to have multiple solar cells and multiple batteries.



As per BIS (Bureau of Indian Standards), IS 1172-1993, 200 liters of clean water is required per person per day for domestic consumption. Out of this amount, drinking water required is 10 liters per person per day (safe side limit). The pump as described above can supply an average of 50 liters per min. With 30 minutes of operation, the pump can supply 1500 liters of water and thus it shall be sufficient for 150 persons of that locality.

The solar panel used for this experiment is having an approximate dimension of 780 mm X 1580 mm. The power developed by the solar panel in normal sunlight is 220 W. The open circuit voltage for this solar panel is 52 V and short circuit current of 5 Amps. When the solar panel is under operation for charging the battery, the switch S1 shall be closed and switch S2 shall be open. A view of solar panel is shown in Fig.3.



II. DESIGN CONSIDERATION

The schematic diagram of the system is shown in Fig.1. The integrated system consists of solar panel, Lead Acid rechargeable battery, Micro controller board, Voltage regulator to supply 5 V from 12 V to the microcontroller board, Power amplifier, Centre tapped transformer and squirrel cage induction motor. The complete circuit is shown in Fig.2. The sub systems are as described below;

A. Solar panel:



building for experimental set up

B. Lead Acid battery:

The battery used in this experiment is 12 V, 75 AH. The Amp-Hour capacity of the battery is selected in such a way to run a 1 hp motor for around 30 min. A 1 hp capacity, capacitor start capacitor run squirrel cage induction motor

operated at 230 V, with power а factor of 0.7 shall draw 4.63 Α of current. With motor



Fig. 4- Rechargeable battery for the experimental set up

loading and considering other losses, we consider steady state motor current to be 6 amps. Thus, at 12 V level, current drawn from the battery shall be (6 *230/12) 115 Amps. Therefore battery can supply this current for (75/115)*60 min = 39.13 min. With safer side, we can thus operate the pump for 30 min. A view of lead acid battery is shown in Fig.4.

C. Speed setting panel:

A speed setting panel has been designed through which we can start the pump with low speed and gradually we can increase to full speed. Starting with a lower speed is an advantageous as initial inrush current drawn by the motor shall be less. Normally, starting current of an induction motor is 5 to 7 times than the full load current. High starting current of the motor shall give rise to voltage dip of the battery. In order to reduce the high starting current of the induction motor, we have adopted to start the motor at lower voltage and then gradually we can increase the voltage to rated voltage. during starting, the magnetizing component of the current flowing through the stator is proportional to the applied voltage and is independent of the load. These facilities are programmed in the microcontroller and depending on the situation, we can adopt a starting method.

III. PWM INVERTER FOR SINGLE PHASE INDUCTION MOTOR

The PWM inverter consists of four sub modules as explained under. The photograph of experimental set up is shown in Fig.5.

A. PIC Microcontroller:

The pulse width modulated inverter is designed around a PIC microcontroller 18F4520. PIC refers to Peripheral Interface Controller. The device has

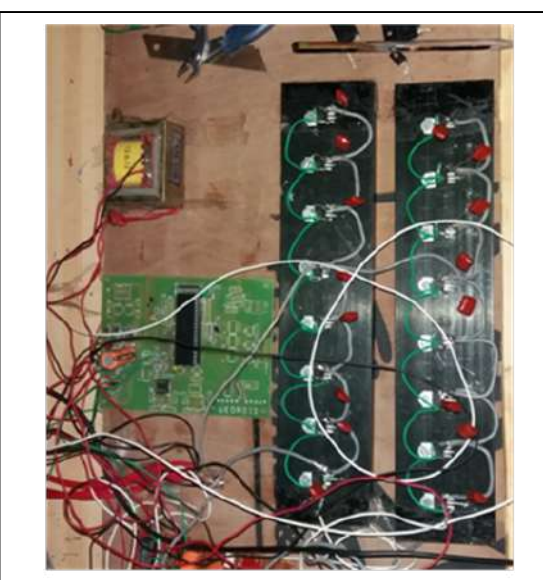


Fig. 5- Circuit assembly for the experimental set up

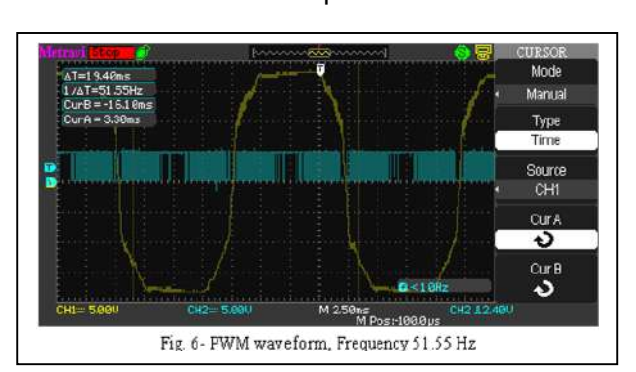
32 KB Program memory. The microcontroller is having an inbuilt PWM module which is used directly in this application. The purpose of selecting a PIC microcontroller is that it is readily available and its programming can be done in high level language. This is a 40 pin IC. It works on 4.2 to 5.5 V. The PIC microcontroller is programmed and the codes are stored in EEPROM. There are two programs which is stored in the EEPROM. We can run any one of the program depending on the pump application:

Program-1: In this program, initially 23 Hz, 106 V AC is generated and is supplied to the motor. With this setting the starting current of the motor is 3 A. The motor is allowed to run for 1 min. After 1 minute, the frequency is changed to 50 Hz and voltage generated is 230 V. With this voltage and frequency, the motor runs at full speed and required flow of water is obtained. The AC output at 50 Hz is shown is Fig. 6 and AC output at 23 Hz is shown in Fig 7

Program-2: In this program the V/f control is applied and the motor is started by soft starter principle. That is, initial frequency is 10 Hz and over a span of 2 min the frequency is increased to 50 Hz. In every frequency, voltage is generated in such a way that v/f is constant.

B. Voltage regulator:

This microcontroller operates on 5 V DC. This



5 V DC power is obtained from 12 V DC supply through a voltage regulator. The regulator is built up around the IC LM 7805. This is a 3 pin IC, where input is 7-35 volts and output is 4.8 to 5.2 volt. It can supply an output current of 1.5 A, which is most suitable for microcontroller operation. The IC is mounted on a heat sink for stable operation.

C. Transistor driver:

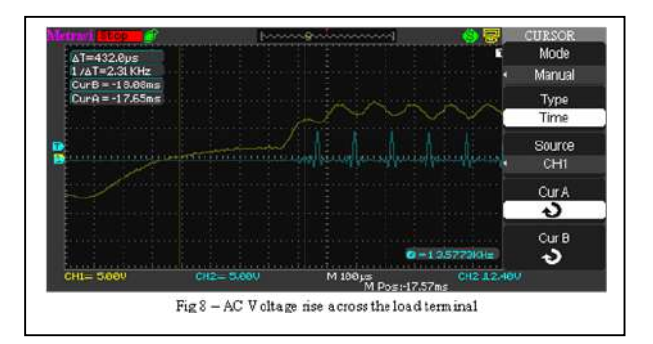
Two complementary low voltage transistor (BD 139 and BD 140) has been used as push-pull configuration to process the microcontroller output. BD139 is NPN type whereas BD140 is PNP type. This transistor output feds the base of power transistor. The collector current for BD 139 and 140 is 1.5 A. This transistor can handle a peak current of 3 A. The DC current gain of this transistor is around 100. This complementary pair transistor is chosen for this purpose. The base of the transistor is driven from NAND gate output through a 5 k Ω resistance.

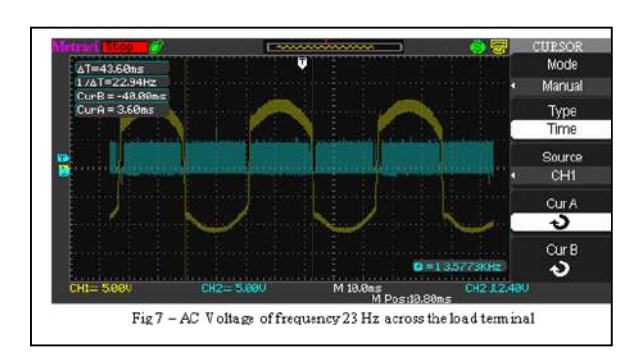
D. Power Amplifier:

Power amplifier is designed around power MOSFET, IRF640. This transistor can supply a continuous drain current of 18 A at 25°C. At 110°C, it drain current shall be 11 A. For design consideration, we consider a drain current of 15 A at 40°C. Since at 12 V level, we require 115 A of current, we have to connect 8 such MOSFET in parallel to supply 115 A of current. All the MOSFETs are mounted on a heat sink. The MOSFET assembly is shown in Fig 5. A capacitor of 0.1 μ F is connected between source and drain terminal of the MOSFET.

E. Transformer:

A center tapped transformer with primary of 12-0-12 V and secondary of 230 V has been used for increasing the voltage from 12 V AC to 230 V AC. The transformer VA rating should be 1380 VA. The designed value should be taken as 1500 VA. The primary winding shall carry a current of 115 A and accordingly the copper wire size and transformer size is calculated. One diode is connected across each primary winding of the transformer. This diode acts as freewheeling diode as transformer windings are switched ON and OFF at high frequency. A view of the transformer is shown in Fig.9.





IV. EXPERIMENTAL RESULT

Experiment has been conducted in three stages to establish the circuit. Initially to test the algorithm and circuits, a table fan was connected and variable frequency was applied in this fan speed was obtained. variable performing this stage a 1hp motor on no-load was connected and starting current was observed. In 3rd stage a submersible pump with 1 hp motor was connected. During running the waveform of the AC output has been observed and stored in oscilloscope as shown in Fig 6, Fig 7 and Fig.8. Fig 6, shows the AC outoput with a frequency of 51.55 Hz. Fig 7 shows the AC output with 23 hz frequency output. Fig. 8 shows the rise in AC voltage across the load. The basic Pulse Width Modulated output from microcontroller and final AC output across the motor terminal is shown in the waveform.

For running the pump motor with a variable speed drive, we have to take extra precaution on motor heating with harmonics. As seen in the oscilloscope, the AC output is not purely sinusoidal. Thus, it shall give some extra heating on the motor. Hence the compatibility of motor and drive is to be properly established by repeated experiments.

The induction motor connected with the submersible pump gives the following result as shown in Table-1.

Table-1: Test result with a submersible pump

- 1	SI. No	Applie d voltag e (Volts)	Freque ncy (Hz)	Starting current (A)	Steady state Current (A)
	1.	106	23	3.0	1.5

2.	172	37	5.0	2.3
3.	230	50	7.0	3.0

V. CONCLUSION

With the above experiment we can conclude that it is possible to run a submersible pump in places where there is no electric power distribution or places where voltage is very low, inadequate for runing a pump. This system is very useful for drinking water obtained from underground. As there is a trend to use renewable energy, we can use this system for irrigation purposes also. This pump shall be fed from a lead acid battery with an inverter. In this case the inverter is a variable frequency drive. The lead acid battery shall be charged using solar panel. This experiment has been conducted with the solar panel on the roof top. With the calculation given in this paper, it is possible to run a 1 hp pump for 30 min using a 75 Amp-hour battery. With this 1 hp pump and full 8 hours charging of the battery using solar panel, the system can supply drinking water for 150 persons per day.

The system can also be used to run a refrigeration system (domestic freeze) for storing emergency medicines (vaccines) in remote area. This has got a tremendous potential in our country to supply drinking water and storing medicines.

With higher capacity battery and solar cell the system can be used for lighting and fan load for hospitals and other domestic purposes.

With the above experiment we can conclude that it is possible to run a pump in places where there is no electric power distribution. This pump shall be fed from a lead acid battery with an inverter. The lead acid battery shall be charged using solar panel. With the calculation given in this paper, it is possible to run a 1 hp pump for 30 min using a 75 Amp-hour battery. With this 1 hp pump and full 8 hours charging of the battery using solar panel, the system can supply drinking water for 150 persons per day.



Fig 9 - A view of the transform erin the experim ental setup.

ACKNOWLEDGMENT

The authors wish to express their sincere thanks and gratitude to the collective of electrical engineering department of Techno India University for providing various facilities during experimental period.

REFERENCES

- [1] Tabish Nazir Mir and Abdul Hamid Bhat, "Comparative Analysis of Pulse Width Modulated Voltage Source Inverter Fed Induction Motor Drive and Matrix Converter Fed Induction Motor Drive" 1st IEEE international conference on Power Electronics, Intelligent control and energy systems, ICPEICES-2016
- [2] Abdul Shavan and R N Sharma, "Water Consumption Patterns in Domestic Households in Major cities", Economic and Political weekly, June 9, 2007.
- [3] Asoke Kumar Paul, I Banerjee, B K Santra and N Neogi, "Adjustable speed drives for rolling mill applications", Steel India, March 2008, Vol. 30, No. 2, pp 46-50, Published by Steel Authority of India Limited.
- [4] Subhojit Mukherjee, Arijit Ganguli, Asoke Kumar Paul and Ajay Kumar Datta, "Load flow analysis and reactive power compensation" 2018 International Conference on Computing, Power and Communication Technologies (GUCON) Galgotias University, Greater Noida, UP, India. Sep 28-29, 2018.
- [5] Sananda Biswas and Asoke Kumar Paul, "A Solar Cell based Inverter for Submersible Pumps", International Journal of Electronics, Electrical and Computational System, IJEECS, ISSN 2348-117X, Volume 7, Issue 1, January 2018.

Thermal behaviour on the heat sink area of LED for different Thermal Interface Materials

Debashis Raul¹, Kamalika Ghosh²

School of Illumination Science Engineering and Design^{1,2}
IEI Fellow (Life)²
(Jadavpur University)
(Kolkata 700032)

{debashis.raul@gmail.com, kamalikaghosh4@gmail.com}

Abstract-Light-Emitting Diode (LED) being solid state lighting device generates heat at the p-n junction, which causes damage not only to the life of the lamp but also to the performance of the same. So a well-designed thermal management system is essential for the longevity of the LED. Thermal Interface Material (TIM) is applied in between sink and source to reduce contact resistance at the junction of it.In this study, three new types of TIMs are used, namely Polyvinylidene (PVDF), Monomer Nfluoride Vinylpyrrolidone (NPV) and Graphene sheet with different thermal conductivities. Then photometric parameters i.e. luminous flux of the lamp was measured. The next step is to measure at the chip and sink area temperature by noncontact infra-red camera. The results demonstrate that the temperature of the LED lamp decreases sharply using the thermal interface material of Graphene sheet. So, it can be concluded that the heat dissipation from junction of the LED to sink or ambient, depends upon the thermal conductivity of the TIMs and other materials. This implies that Graphene sheet is a very good proposition for thermal design. This research showed that despite technological advancement, thermal management still remains an essential area for luminaire design.

Keywords - Graphene sheet; Heat sink; Light Emitting diode (LED); Thermal interface material (TIM)

A. INTRODUCTION

In today's world Light-Emitting Diodes (LED) based lighting systems is widely recognized as a revolutionary technology in lighting sector due to its superior lifetime, low energy consumption, high luminous efficacy, ecofriendly behaviour etc. LED generates light and some portion of the input power of the LED is converted into

heat.It is important to disperse the generated heat from LED junction to surrounding atmosphere and keep the LED light performances same as declared by the manufacturer [1]. So it is one of the challenges of designing LED modules to ensure proper thermal management system [2, 3]. Due to excess heat generation of the junction of a LED which is called 'Junction temperature', occurred optical degradation as a result of poor reliability of it. This junction temperature is estimated by different methods [4, 5, 6]. Chen Zhaohuiet. al. reviewed and compared the reliability test methods and failure analysis for different LED, whose collected from different manufacturers [7].LED's optical and phosphor degradation is also occurred by environmental effects, especially by relative humidity and temperature [8, 9, 10]. This environmental effects like temperature causes accelerated aging of the LEDs. This type of aging occurred not only the reduction of lifetime of it also decreased the power density, shift of optical spectrum, change of radiation pattern etc. [11,12,13].

Modelling and simulation of thermal distribution, heat transfer etc. are essential for any design of LED structure which make the design easier and enable optimization of many different parameters before fabrication of new structure [14,15]. Thermal Interface material is used in between LED substrate and heat sink to decrease contact thermal resistance of it [16, 17, 18, 19]. In this paper, three new types of Thermal Interface Materials (TIM) with different thermal conductivities are introduced and tried out. Higher thermal conductivity TIM material like Graphene sheet has been observed as good heat dissipation capability than other two TIM material like PVDF and NPV. Thus, Graphene proved as a very good material for thermal design.

B. Lamps and Thermal Interface Materials (TIM) selection

In this experiment five numbers each of same make of 5 W COB based cool white LED lamps are selected with same structure. Three different types of Thermal Interface Materials with different thermal conductivity are used at

the junction between substrate and heat sink interface of the LED modules. The details of LED modules and material specifications are given below in TABLE I and TABLE IIrespectively.

TABLE I

COB based Cool white LED details					
Parameters	values				
Power (W)	5 Watt				
Input Current (DC)	300 mA				
Input Voltage (DC)	18 Volt				
CCT (K)	6500 K				

TABLE II
Thermal Interface Materials specifications

Materials	Thermal Conductivity (W/mK)
Polyvinylidene fluoride (PVDF)	0.5
Monomer N-Vinylpyrrolidone (NPV)	1.1
Graphene Sheet	3500

C. Experimental Procedures

According to the selected COB based cool white LED with the power of 5W was selected. The overall dimension of the board of the heat sink is diameter of 70 mm and height of 20 mm and the material of the sink is aluminium. The chip becomes a heat source and the diameter of 2 mm and height of 0.1 mm. The thickness of PVDF and NPV materials are 60 and 80 μm respectively. The thickness of commercially available in-plane Graphene sheet is used in this work is 40 μm

In this method COB based cool white LEDs are placed in the center of an enclosure to measure the chip area and sink area temperature of it. For this measurement, an enclosure box constructed by plywood with a dimension of 350 mm \times 350 mm \times 350 mm was used and the temperature inside the box was set at 25°C - 27°C as specified by Joint Electron Device Engineering Council (JEDEC) [20]. Then each LED module is mounted at horizontally in the geometric centre of the box and two non-contact calibrated infrared (IR) camera (Fluke make Ti400) are fixed at half foot distance from the chip and end surface of the heat sink along the axis. The temperature measurements of chip area and end surface of the sink are recoded at initial condition of the lamps power-ON condition and carried forward it after every five minutes interval up to one hour. In this cases TIM materials of all the LEDs' are PVDF. The relative humidity was maintained at 45 % inside the box during the IR thermographymeasurements. Now the PVDF material has been removed and after that the NPV material, whose thermal conductivity is higher (1.1 W/mK) than PVDF (0.5 W/mK), is placed in between substrate and heat sink. Above experimental procedures have been repeated for each and every LED modules. After that in similar way the higher thermal conductivematerial, i.e., Graphene sheet whose thermal conductivity is 3500 W/mK, is placed into the same position. Then thermal parameters were measured accordingly. In this study all the LED lamps were driven at 300 mA current. The thermal sensitivity of the Ti 400 IRimager was ≤ 0.05 °C at 30 °C.

D. Results and discussion

The heat dissipation performance of cool white COB based LEDs with three different Thermal Interface Materials (TIMs) are evaluated. The chip as well as sink area temperature of the LED modules are measured and recorded in every five minutes interval up to one hour. The temperature variation as a function of time at the chip area of the LED modules when the TIM material are PVDF is shown in Fig. 1. The Figure is clearly depicted that the chip area temperature is higher than its sink area temperature. So the junction temperature of the LED chip could not dissipated towards the heat sink of the luminaire due to poor thermal conductivity (0.5 W/mK) of the PVDF material. The nonlinear temperature variation of the chip area of the LED was indicated that the generated heat very slowly dissipated from the chip area to sink area or ambient. Similarly, when NPV as TIM material was used then the chip area temperature was much more than sink area temperature but less when TIM as PVDF which is shown in Fig. 2 confirms that the thermal conductivity of the NPV material is higher than PVDF.

Now the LED module with Graphene sheet as TIM, the generated temperature at chip are is very much lower than other two modules. The temperature difference between chip and sink area issignificantly low. The temperature variation as a function of time is shown in Fig. 3. For this module, the heat dissipation from LED chip area to sink area is increased due to Graphene sheet used as a TIM materials whose thermal conductivity (3500 W/mK) is highest than other two TIMs.

The temperature at chip as well as sink areawas recoded at different burning time is summarized in TABLE III and IV and plotted in Fig. 4 and 5. It can be observed that the chip area temperature of NPV and Graphene module is about 16.8 °C and 40.9 °C lower than PVDF module respectively at initial condition (1 min). After 30 min of illumination or

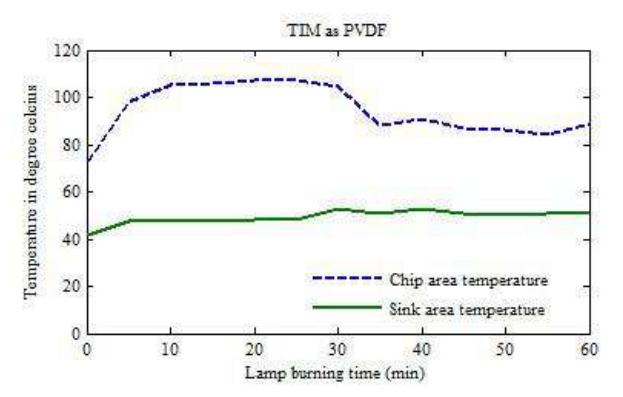


Fig. 1 Temperature of the Chip and Sink area as a function of time when TIM as PVDF

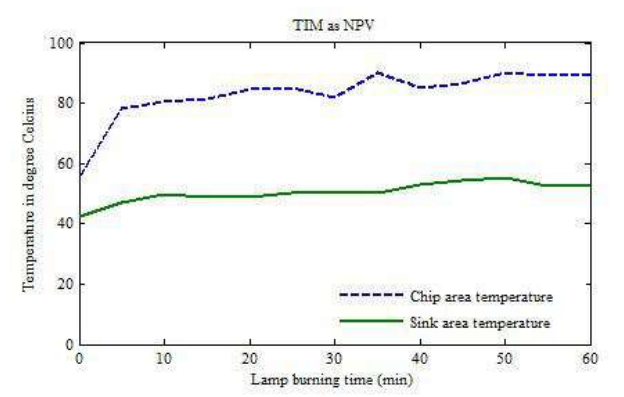


Fig. 2 Temperature of the Chip and Sink area as a function of time when TIM as NPV

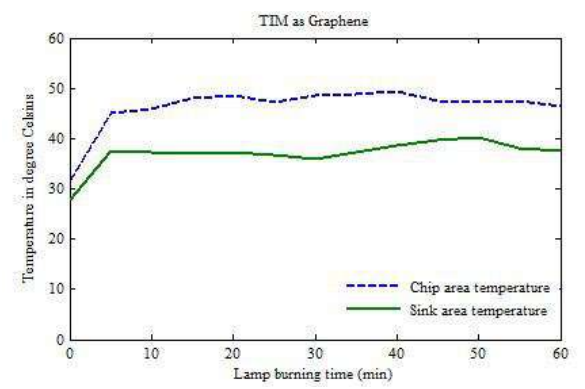


Fig. 3 Temperature of the Chip and Sink area as a function of time when TIM as Graphene

lamp burning time, the chip area temperature of Graphene module is about 57 °C and 22.4 °C lower than PVDF and NPV modules respectively. From TABLE IV, it can be seen that the heat sink area temperature of Graphene module is about 16.7 °C and 14.5 °C lower than PVDF and NPV module respectively after 30 min of lamp burning time or illumination.

Fig.4 shows the relationship between chip area temperature and lamp burning time. It can be seen that the chip area temperature for Graphene module is very low and the temperature increases about linearly with time (i.e. not rapidly varied like other two modules). But at heat sink area, the temperature for Graphene module is varied slightly like other two modules which is shown in Fig. 5. From TABLE V, it can be seen that the luminous flux of the LED lamp depends upon the heat dissipation rate from chip to ambient via heat sink. From this experiment, the

heat dissipation of Graphene module has been found highest. So, the luminous flux of Graphene module is more

than other two modules. From this experiment, it can be seen that Graphene sheet can lower the chip area temperature of the LED due to its higher thermal conductivity properties which dissipates heat from chip to heat sink quickly. So Graphene is a good candidate as TIM for LED heat dissipation and the application of Graphene as TIM is beneficial to increase the luminous flux of high power LED lamps

TABLE III
Temperature of LED Chip area at different burning time

7	Temperature of LED Chip area (°C)								
Time (min)	PVDF	NPV	Graphene						
1(Initial)	72.5	55.7	31.6						
5	97.9	78.3	45.2						
10	105.0	80.4	45.8						
15	105.7	81.5	47.9						
20	107.4	84.5	48.5						
25	107.4	85.1	47.3						
30	104.5	82.1	48.5						
35	88.3	90.0	48.9						
40	90.5	85.0	49.4						
45	86.8	86.5	47.5						
50	86.3	90.3	47.2						
55	84.1 89.2		47.4						
60	89.2	89.7	46.5						

TABLE IV
Temperature of LED Sink area at different burning time

Temperature of LED Sink area (°C)							
Time(min)	Graphene						
1(Initial)	41.5	42.3	27.8				
5	47.4	47.1	37.5				
10	47.5	49.9	37.3				
15	47.5	48.9	37.1				
20	48.3	48.9	37.3				
25	48.3	50.1	36.7				

30	52.5	50.3	35.8
35	50.7	50.2	37.3
40	52.9	52.8	38.6
45	51.1	54.3	39.6
50	50.3	55.4	40.3
55	51.1	52.5	38.1
60	51.3	52.9	37.5

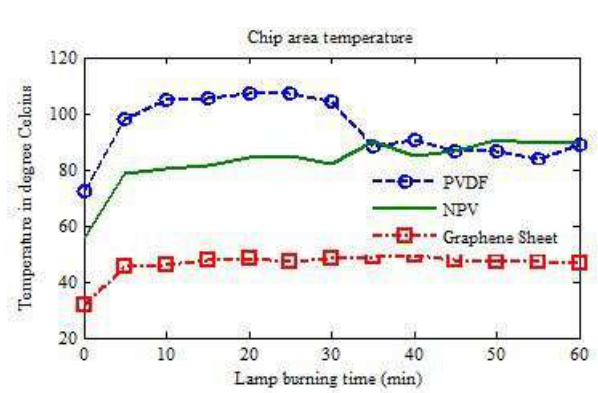


Fig. 4 Chip area temperature for different TIM

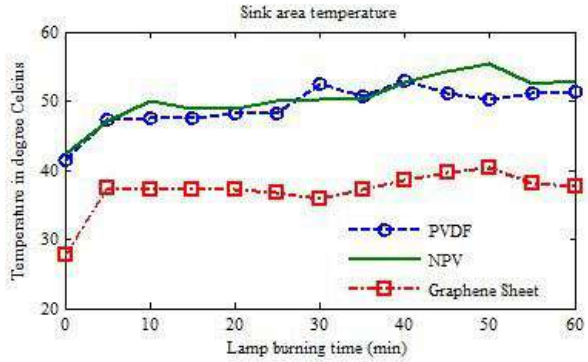


Fig. 5 Heat Sink area temperature for different TIM

TABLE V Luminous flux for different TIM

Thermal Interface Material (TIM)	Luminous flux (lm)
PVDF	494.7
NPV	510.0
Graphene	565.5

E. Conclusion

The LED lamp performance depends upon its heat dissipation from chip to heat sink, i.e. ambient. Heat dissipation depends upon the thermal conductivity of the TIM materials. In this study, PVDF, NPV and Graphene

sheet are introduced as Thermal Interface Materials (TIM) in LED modules and compared. The effect of Graphene sheet as TIM for heat dissipation of LED module at the junction of chip and end surface of sink area are measured and evaluated. The experimental data indicate that introduction of Graphene as TIM can reduce the chip area temperature of LED, which can increase the luminous flux and performance of LED lamps. As a result for good thermal dissipation from the LED chip to sink or ambient, which makes the longer life of it.

ACKNOWLEDGMENT

The authors wish to acknowledge the Government of West Bengal, India for providing the fellowship. Authors wish to acknowledge the support received from School of Illumination Sciences, Engineering & Design of Jadavpur University for facilitate with experimental set up to complete this work at the laboratory, therein.

REFERENCES

- [1] Anna Andonova, Namyong Kim, and Nikolay Vakrilov, "Estimation the Amount of Heat Generated by LEDs under Different Operating Conditions," ELEKTRONIKA IR ELEKTROTECHNIKA, ISSN 1392-1215, VOL. 22, NO. 2, pp. 49-53, 2016.
- [2] N. Badalan, P Svasta, "Analysis of LEDs Thermal Properties", IEEE 22nd International Symposium for Design and Technology in Electrinic Packaging,doi 10.1109/SIITME.2016.7777267, October, 2016.
- [3] Lan Kim, Jong Hwa Choi, Sun Ho Jang and Moo Whan Shin, "Thermal analysis of LED array system with heat pipe", ThermochimicaActa (ELSEVIER)doi:10.1016/j.tca.2006.11.031, PP. 21–25, 2007.
- [4] S. Chhajedet. al., "Junction temperature in light-emitting diodes assessed by different methods", doi: 10.1117/12.593696, 2005.
- [5] ANPadmasali and SG Kini, "A generalized approach for the estimation of junction temperature and its effect on light output", Lighting Research and Technology (SAGE), doi: 10.1177/1477153519846210, 2019.
- [6] Kamalika Ghosh and Debashis Raul, "Performance analysis of various types of high power Light Emitting Diodes", Light & Engineering (),ISSN 0236-2945, Volume 26, Number 1, pp. 91-98, 2018.
- [7] Chen Zhaohui, Zhang Qin, Wang Kai, Luo Xiaobing and Liu Sheng, "Reliability test and failure analysis of high power LED packages", Journal of Semiconductors, Vol. 32, No. 1, January 2011.
- [8] Preetpal Singh and Cher Ming Tan, "Degradation Physics of high power LEDs in outdoor Environment and the role of Phosphor in the degradation process", Nature: Scientific Reports, 6: 24052, 2016.
- [9] Debashis Raul and Kamalika Ghosh, "Performance of chip-on-board and surface-mounted high-power LED luminaires at different relative humidities and temperatures", Lighting Research and Technology (SAGE), doi:10.1177/1477153518819040, 2018.
- [10]Chunjing Hang et. al., "The effects of humidity and temperature aging test on flexible packaging LED module", IEEE14th International Conference on Electronic Packaging Technology, doi: 10.1109/ICEPT.2013.6756656, 2013.
- [11] Yu-Hsiang Yang, Yen-Fu Su and K-N Chiang, "Acceleration Factor Analysis of Aging Test on Gallium Nitride (GaN)-based High Power Light emitting Diode (LED)", 14th IEEE ITHERM Conference, ISBN 978-1-4799-5267-0, 2014.

- [12] Chun-Chin Tasiet. al., "Decay mechanisms of Radiation pattern and Optical Spectrum of High power LED modules in Aging Test", IEEE Journal of Selected Topics in Quantum Electronics, Vol. 15, No. 4, July 2009.
- [13] Fu- Kwun Wang and Tao-Peng Chu, "Lifetime Predictions of LED-based light bars by accelerated degradation test", Microelectronics Reliability (ELSIVIER) 52, pp. 1332–1336, 2012.
- [14] P Kulha, J Jakovenko and J Formanek, "FEMThermomechanical simulation of Low power LED lamp for energy efficient Light sources", International Conference on Renewable Energies and Power Quality (ICREPQ'12), Vol.1, No.10, pp. 1708-1711, April 2012.
- [15] Lisa Mitterhubetet. al., "Investigation of the temperature Dependent heat path of an LED module by thermal simulation and design of experiments", IEEE Therminic, ISBN 978-1-5090-5450-3, 2016.
- [19] Debashis Raul, "Analysis of Temperature at Substrate and Sink Area of 5 W COB-Type LEDs, with and Without Driver", Advances in Control, Signal Processing and Energy Systems (Springer), ISBN 978-981-32-9345-8, pp 135-145,doi: https://doi.org/10.1007/978-981-32-9346-5 11, 2019.

- [16] J Wu, M Zhuang, S Li, W Yang and J Zhang, "Study on the Application of Thermal Interface Materials for Integration of HP-LEDs", 2010 IEEE CPMT Symposium Japan, doi: 10.1109/CPMTSYMPJ.2010.5680285, 2010.
- [17] S Subramani and M Devarajan, "Influence of AIN Thin Film as Thermal Interface Material on Thermal and Optical Properties of High-Power LED", IEEE Transactions on Device and Materials Reliability, VOL. 14, NO. 1, MARCH 2014.
- [18] R Li, Q Liu, L Huang, L Yin and G Song, "properties of Thermal Interface Materials and its Impact on Thermal Dissipation and Reliability of LED Automotive Lighting", IEEE SSL China: IFWS, doi: 10.1109/IFWS.2018.8587314, 2018.
- [20] Integrated Circuits Thermal Test Method Environmental Conditions – JEDEC Solid State Technology Association – JESD51-2A, January 2008



Coordinated Power Management Scheme for PV based DC Micro-grid

P.Ramesh, M.Hari, P.Velrajkumar and V.Agalya

(Department of Electrical and Electronics Engineering) (CMR Institute of Technology, Bengaluru) (#132, AECS Layout, IT Park Road, Bengaluru 560037)

{Corresponding author's email: ramesh.p@cmrit.ac.in}

Abstract - Now a day's DC micro grids have more discussion in the power system research due to various advantages like more efficient, cheaper and less initial cost compared to the conventional AC micro-grids. The main issues in DC micro grid is to avoid power mismatch while injecting to utility grid, to have a cost effective utilisation of available grid power, to optimize the usage of renewable energy resource and storage energy and to have effective usage of system through power balancing and load shedding. This research is more focussed on the modelling of grid connected DC micro grid with PV array, battery energy storage system and converters with each segment connected to the DC bus. To establish a coordinated control between the converters, at the end is to implement an efficient power management scheme. The simulation results are shown by using MATLAB and Simulink software.

Keywords - DC-Micro Grid; Coordinated Power Management scheme; PV array.

INTRODUCTION

Recent innovations in small scale distributed power generation systems combined with technological advancements in power electronic systems. Environmental concerns and reduction of fossil fuel reserves gave rise to a growing increase in the penetration of distributed generators (DGs) that include renewable energy sources (RES), energy storage systems (ESS) and new types of loads like electric vehicles (EVs) and heat pumps in the modern power systems. However, these new components may pose many technical and operational challenges should they continue to be integrated in an uncoordinated way, as is the case today [1]-[4].

Micro grids in which the Distributed Generation units (DGs) and Battery energy storage systems (BESS) are connected to load using DC bus as coupling medium. DC MGs have been recognized as more attractive for numerous uses due to higher efficiency, more natural interface to many types of Renewable Energy Sources(RES) and BESS, better compliance with consumer electronics, also Electric Vehicle's [5]-[9].

In cost aspect DC micro grid are 11% cheaper than AC micro grid. DC micro grids are maintains good quality of power, control, unique and also higher efficiencies compared to the AC micro grids [9]-[13]. The overall energy efficiency may be further increased by replacing the conventional silicon based power converters with more efficient wide band gap (WBG) power converters which are being researched. The control and management of AC

and DC micro grids is a major area of research addressing some of the key challenges like the integration of renewable energy sources (RES), source optimization, and stability issues etc. Involvement of a large number of distributed energy sources demands significantly coordinated control based on a high bandwidth communication network to sustain uninterrupted operation under every working condition. control strategy based on a low bandwidth communication link for the management of a dc microgrid that permits execution of distinct operating states such as black-start or restoration of the microgrid, source, and power optimization during steady state operation and emergency conditions etc. [1], about DC microgrid structure have presented in [1]-[9].

Few grid control techniques presented in [6]. Various MPPT techniques have been presented in [6],[7],[9]-[10]. Conventional power management of PV system with hybrid in islanded mode is shown in [8],[10]. Few DC grid standards during power management have been given in [9]. In DC micro grids, coordinated control should be implemented in order to achieve an intelligent control system with extended objectives. Depends on the type of the communication available the DC microgrid can be coordinated in three different ways namely decentralized control, centralized control, distributed control.

There are different stabilization techniques available in the literature namely active damping (small- and large-signal strategies), linear feedback stabilization, adaptive stabilization and loop cancellation techniques. There are different operation modes related to dc microgrid namely storage operation mode, grid operation modes, PV operation modes and load operation modes.

POWER MANAGEMENT SCHEME WITH STATE OF CHARGE EQUALIZATION STRATEGIES

Electric loads in conventional distribution system can be regarded as a combination of power loads, current loads and impedance loads. For current and impedance loads, they normally do not induce stability degradation. However, power loads, also known as constant power loads (CPLs), refer to the loads which consume constant amount of power regardless of their input voltage. The CPLs degrade system stability due to their negative incremental impedance. The effect of CPL can be expressed as:



$$\left[\frac{\partial v_0}{\partial i_0}\right]_{(V_0, I_0)} = \left[\frac{\partial}{\partial i_0} \left(\frac{P_0}{i_0}\right)\right]_{(V_0, I_0)} = -\frac{P_0}{I_0^2} \tag{1}$$

where v_o and i_o are the instantaneous load voltage and current, respectively, and P_o , V_o and I_o are the steady-state load power, voltage and current at a given operating point. It is observed that the incremental impedance is negative, which degrades the system damping and may impose stability issues [3]. In DC MG, the most typical CPLs are the loads interfaced through tightly regulated power converters.

Fig. 1 shows the hierarchical control scheme in power management for both island mode and utility grid connected mode of dc microgrid.

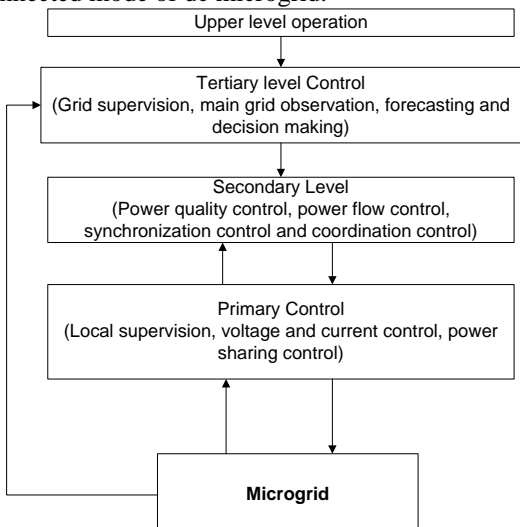


Fig.1 Hierarchical control scheme [10].

In charging process, the droop coefficient is set to be proportional to the nth order of SoC, while in discharging process, it is set to be inversely proportional to the nth order of SoC, as shown below:

During charging:
$$v_{dcx}^* = v_{dc}^* - m_0 SoC_x^n p_{ox}$$
 (2)

During discharging:
$$v_{dcx}^* = v_{dc}^* - \frac{m_0}{SoC_x^n} p_{ox}$$
 (3)

Where SoC_x is the SoC of ESS #x, n is the order of SoC, m_0 is the initial droop coefficient when SoC equals 100%, p_{oi} is the output power of converter #x. By using the above method, the SoC balancing and injected/output power equalization can be achieved automatically in both charging and discharging process.

SIMULATION RESULTS AND DISCUSSION

Simulation is done for the PV based dc micro grid and the various parameters that considered as shown in Table-I and the schematic block diagram of the circuit considered with 10kW of load which incorporates the power management scheme is shown in Fig. 2. In the simulation the input (i.e., solar irradiance) is considered as variable over a simulation period of time.

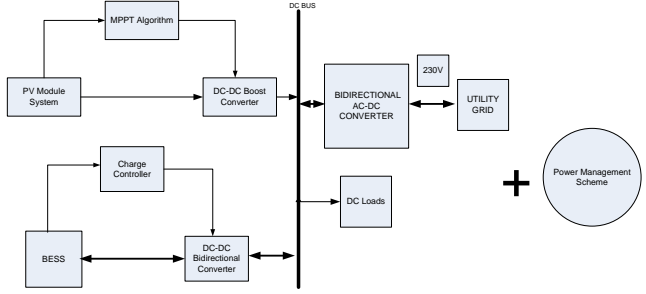


Fig. 2 DC microgrid with power management scheme.

 $\label{eq:table_interpolation} TABLE\ I$ (Parameters pertaining to the simulation)

K_d	0.8
SOC_{max}	0.8
SOC_{min}	0.2
Grid _{supply unit}	3000
Grid _{injectrion limit}	2000
PV_{peak}	25kW

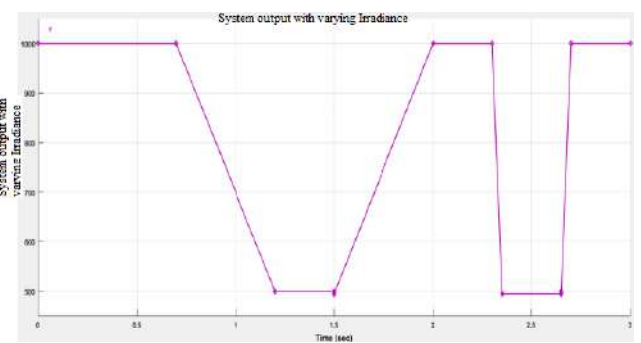


Fig. 3 System output with varying irradiation.

In the Fig.4, Fig.5 and Fig.6 shows the various simulation results like load voltage, load current, load power when the load is of 10kW (maximum).

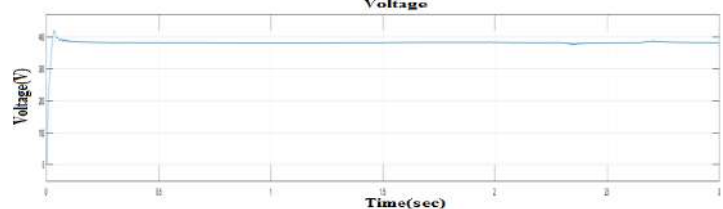


Fig. 4 Load voltage for 10kw load: (380V).

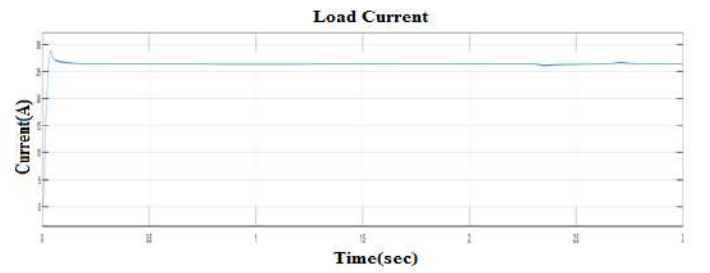


Fig. 5 Load current for 10kW load: (26A).



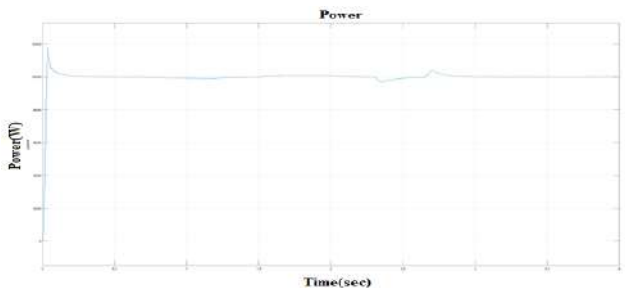


Fig. 6 Load power for 10kw load: (10kW).

In the Fig.7, shown the various simulation results with respect to battery (BESS) such as SOC (%), battery voltage is comparing with irradiance when the same load is of 10kW (maximum) is considered in Island mode. Slowly the SOC is increasing towards 100%, battery voltage has fluctuations and is due to reduction in irradiance.

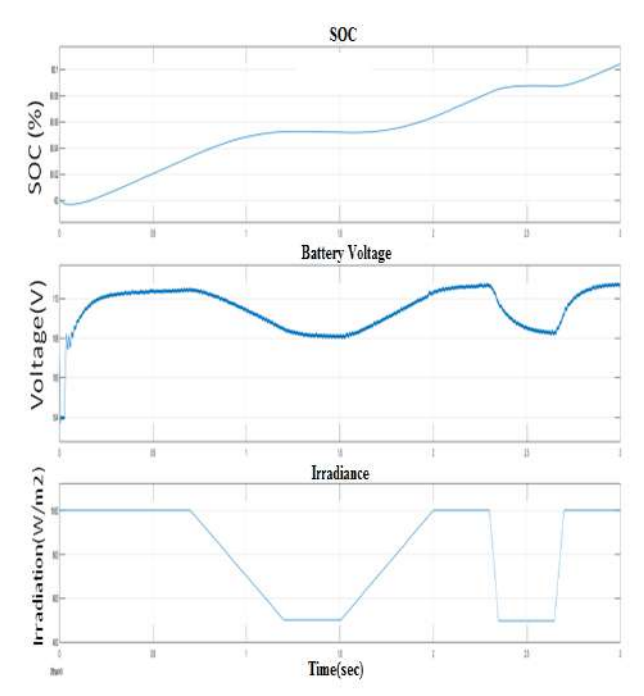


Fig. 7 SOC, battery voltage and irradiance vs time in Island mode.

In the Fig.8, shown the various simulation results with respect to the power management during the dc micro grid connection with main grid. And is shown battery current, grid current is comparing with irradiance when the same load is of 10kW (maximum) is considered in Grid connected mode. It is observed that the battery current is becoming maximum when the low irradiance occurred is due to the operation of BESS and the grid current is not affected due to reduction in irradiance.

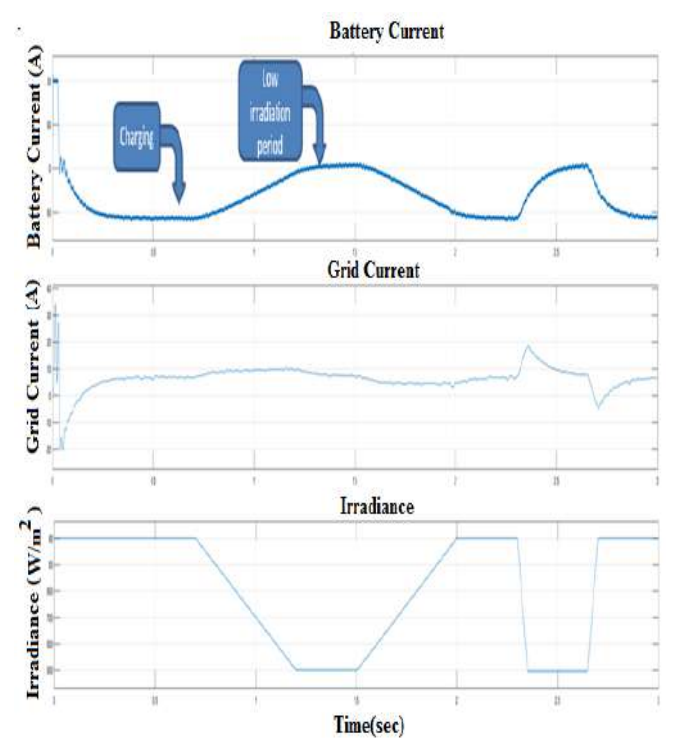


Fig. 8 Battery current, grid current and irradiance vs time in Grid connected mode.

A. Power management scheme with 5kW load
Table-II shows the various simulation data pertaining to the
5kW loading and comparison of various parameters with
and without power management scheme.

TABLE II
(POWER MANAGEMENT SCHEME WITH 5KW LOAD)

I	nputs			Without			With Power		
			M	anageme	nt	M	anageme	nt(Rec	eive)
			(Deliver)					
Irradia	PV	SO	MP	Stora	Gri	K	Stora	Gri	PV_{li}
nce	Pow	C	P	ge	d	L	ge	d	m
	er		Pow						
			er						
100	851	10	400	6093	13	0.	1700	25	400
			0		28	8		49	0
300	371	70	948	540	30	1	554	83	948
	5		2		66			1	2
800	124	10	121	7774	25	1	2938	20	121
	44		52		15			00	52
1000	163	90	145	0	17	1	0	20	700
	09		72		14			00	0

Fig. 9, Fig.10 shows the graphical representation of Table-II data withoutpower management. Fig. 11 shows the graphical representation of Table-II data with power management under 5kW loading condition.



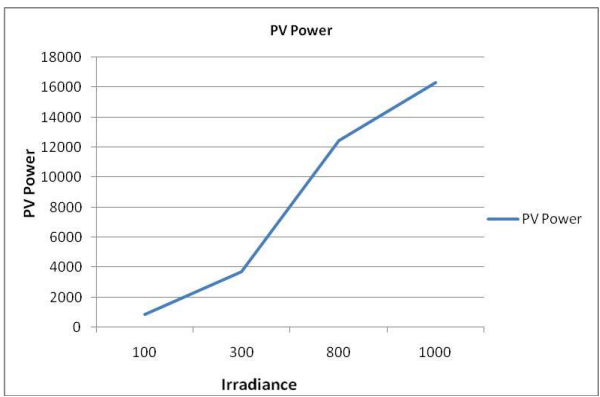


Fig. 9 PV power vs Irradiance at the load of 5kW.

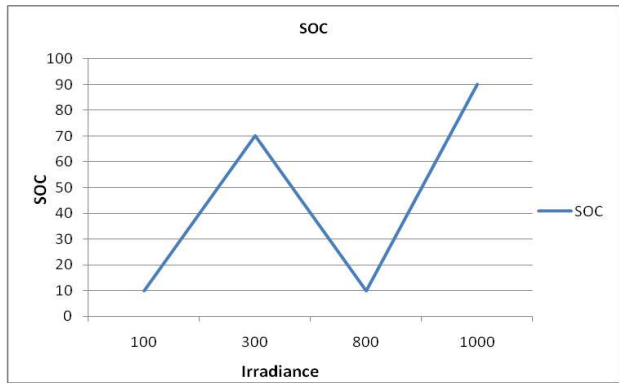


Fig. 10 SOC vs Irradiance at the load of 5kW.

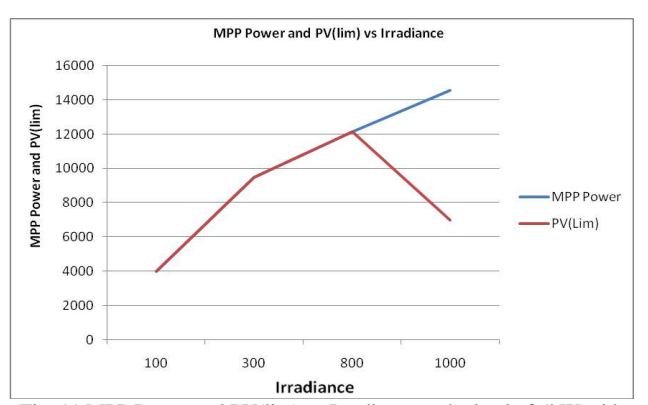


Fig. 11 MPP Power and PV(lim) vs Irradiance at the load of 5kW with Power management scheme.

It is observed from Table-II, Fig. 9, Fig. 10 and Fig. 11 that, as both irradiance and SOC is more, Battery power is not utilized and more power is injected to grid and also PV is limited instead of using entire MPPT power. When irradiance is decreased, Battery is made to deliver power and Supply from grid is reduced in system with power management. When SOC is less, system without power management is delivering power from grid and charging the battery with more power but in system with power management, power is not at all taken from grid and still demand is satisfied. When both irradiance and SOC is less, load is limited by load shedding and battery is also allowed to charge but not in case of previous system.

B. Power management scheme with 10kW load Table-III shows the various simulation data pertaining to the 10kW loading and comparison of various parameters with and without power management scheme.

TABLE III
(POWER MANAGEMENT SCHEME WITH 10KW LOAD)

T	nputs		Witho	nit		With Power			
	nputs		Management			Management(Receive)			eive)
			(Deliv	_				(
Irradia	PV	SO	MP	Stora	Gri	K	Stora	Gri	PV_{li}
nce	Pow	C	P	ge	d	L	ge	d	m
	er		Pow						
			er						
1000	163	60	149	2887	16	1	2513	20	149
	85		19		13			00	20
700	108	60	131	2555	28	1	600	15	131
	51		80		20			0	80
100	945	60	101	6630	34	1	7324	18	101
			80		15			31	80
0	0	60	0	7709	33	1	8080	20	0
					70			20	
100	943	20	475	6609	33	0.	7326	18	475
			0		84	4		31	0
100	855	0	400	0	17	0.	0	30	400
			0		87	4		00	0

Fig. 12, Fig.13 shows the graphical representation of Table-II data withoutpower management. Fig. 14 shows the graphical representation of Table-III data with power

management under 10kW loading condition.

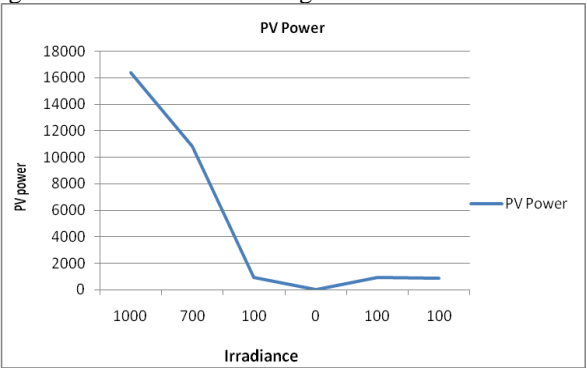


Fig. 12 PV Power vs Irradiance at the load of 10kW.

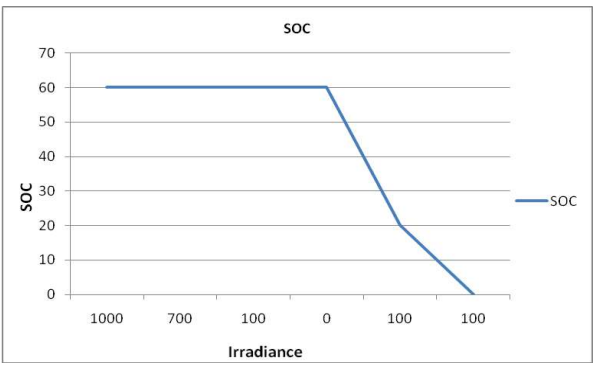


Fig. 13 SOC vs Irradiance at the load of 10kW.



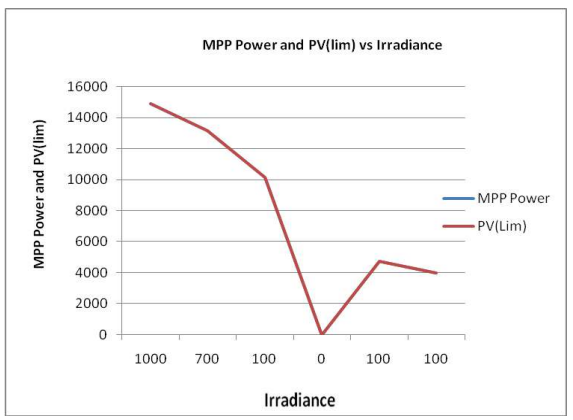


Fig. 14 MPP Power and PV(lim) vs Irradiance at the load of 10kW with Power management scheme.

It is observed from Table-III, Fig. 12, Fig.13 and Fig. 14 that that, the grid injection is more, less charging power to storage than system without power management. Power is injected to grid, less charging power to storage than system without power management. Despite less irradiance, less power is demanded from grid. Even under zero irradiance, power taken from grid is less than system without power management. When both SOC and irradiance is less, Load demand is constrained by load shedding which is not possible in system without power management. When battery storage is empty, Grid is made to supply its full limit and load demand is also limited where as system without power management fails to meet its demand.

C. Power management scheme with 15kW load

In the same manner, Table-IV shows the various simulation data pertaining to the 15kW loading and comparison of various parameters with and without power management scheme.

TABLE IV	
(POWER MANAGEMENT SCHEME WITH 15KW LOAD))

I	nputs			Without		With Power			
	1		M	Management			Management(Receive)		
			((Deliver)				,	
Irradia	PV	SO	MP	Stora	Gri	K	Stora	Gri	PV_{li}
nce	Pow	C	P	ge	d	L	ge	d	m
	er		Pow						
			er						
100	988	10	400	9691	64	0.	9007	30	400
			0		19	4		00	0
300	418	70	900	9197	32	1	8734	21	900
	3		0		94			83	0
300	418	10	900	9691	64	0.	9454	30	900
	3		0		19	6		00	0
900	141	20	121	646	29	0.	776	19	121
	30		70		35	8		4	72
1000	158	70	144	758	14	1	1025	14	144
	43		28		84			9	28

Fig. 15, Fig.16 shows the graphical representation of Table-II data withoutpower management. Fig. 17 shows the graphical representation of Table-IV data with power management under 15kW loading condition.

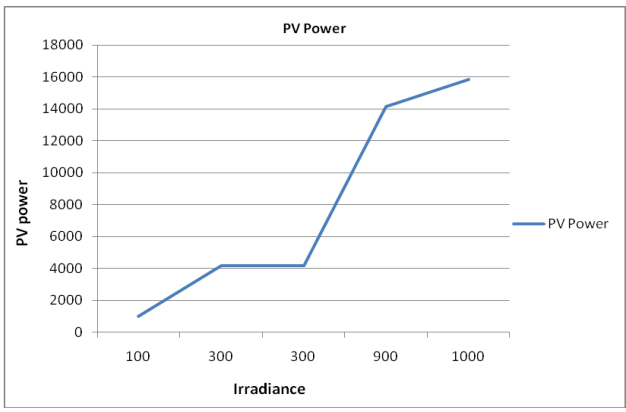
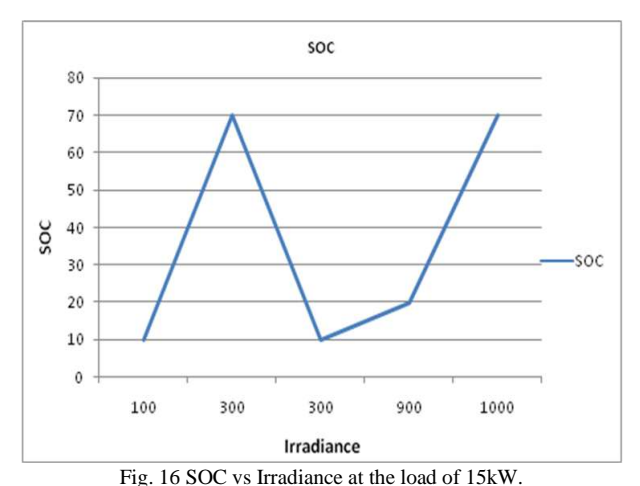


Fig. 15 PV power vs Irradiance at the load of 15kW.



MPP Power and PV(lim) vs Irradiance 16000 14000 Power and PV(lim) 12000 10000 MPP Power 8000 PV(Lim) 6000 MPP 4000 2000 100 300 900 1000

Fig. 17 MPP Power and PV(lim) vs Irradiance at the load of 15kW with Power management scheme.

It is observed from Table-IV, Fig. 15, Fig.16 and Fig. 17 that, when load is increased, still power is injected to grid under full irradiance and more SOC. When irradiance is decreased power is taken from both battery and grid but less than previous system. When SOC is less and irradiance is also reduced, load is constrained and power taken from grid is reduced than previous system. When both irradiance and SOC is reduced grid is made to supply its full limit and also load shedding is done. With same SOC when irradiance is increased load constrained is reduced than above case and still grid is made to supply its full limit to



meet the demand. On the contrary, previous system is taking more power from grid and battery is also forced to deliver more power under less SOC which may affect battery life time.

Inference from the results clearly shows that system with power management uses grid power in cost effective manner and demand from varying load is also satisfied optimally through power balancing and load shedding. Battery power is handled properly so that life time of battery does not get affected. Power management method also provides a chance to set grid supply and injection limits to avoid mismatch, and these can be collected from smart grids through implementation of intelligent layers.

CONCLUSION

DC microgrid with PV array, battery (BESS) and utility grid along with their respective converters and controllers is applied with power management scheme under three different loading conditions. Working of DC microgrid in both islanded and grid-connected modes are verified. Power management scheme is integrated with modelled DC microgrid, for optimum operation of the DC microgrid system. Performance of the DC microgrid with and without power management scheme is analyzed.

REFERENCES

- [1] R. Pradhan, M. Chirayath and S. Thale, "Coordinated control strategy for a DC microgrid with low bandwidth communication," 2016 IEEE International Conference on Power Electronics, Drives and Energy Systems (PEDES), Trivandrum, 2016, pp. 1-6.
- [2] Meng, L., Shafiee, Q., Trecate, G. F., Karimi, H., Fulwani, D., Lu, X., & Guerrero, J. M. (2017). Review on control of DC microgrids and multiple microgrid clusters. *IEEE Journal of Emerging and Selected Topics in Power Electronics*, 5(3), 928-948.
- [3] D. J. Becker and B. J. Sonnenberg, "DC microgrids in buildings and data centers," 2011 IEEE 33rd International Telecommunications Energy Conference (INTELEC), Amsterdam, 2011, pp. 1-7.
- [4] T. Dragicevic, X. Lu, J. C. Vasquez and J. M. Guerrero, "DC Microgrids—Part II: A Review of Power Architectures, Applications, and Standardization Issues," in *IEEE Transactions on Power Electronics*, vol. 31, no. 5, pp. 3528-3549, May 2016.
- [5] T. Ma, B. Serrano and O. Mohammed, "Distributed control of hybrid AC-DC microgrid with solar energy, energy storage and critical load," 2014 Clemson University Power Systems Conference, Clemson, SC, 2014, pp. 1-6.
- [6] Yilmaz, Unal, Ali Kircay, and Selim Borekci. "PV system fuzzy logic MPPT method and PI control as a charge controller." Renewable and Sustainable Energy Reviews, 81, pp: 994-1001, 2018.
- [7] Gautam, S., Raut, D. B., Neupane, P., Ghale, D. P., & Dhakal, R. (2016, November). Maximum power point tracker with solar prioritizer in photovoltaic application. In 2016 IEEE International Conference on Renewable Energy Research and Applications (ICRERA) (pp. 1051-1054). IEEE.
- [8] Justo, J. J., Mwasilu, F., Lee, J., & Jung, J. W. (2013). AC-microgrids versus DC-microgrids with distributed energy resources: A review. Renewable and sustainable energy reviews, 24, 387-405.
- [9] Mahmood, H., Michaelson, D., & Jiang, J. (2014). A power management strategy for PV/battery hybrid systems in islanded microgrids. *IEEE Journal of Emerging and Selected topics in Power* electronics, 2(4), 870-882.
- [10] Che, L., & Shahidehpour, M. (2014). DC microgrids: Economic operation and enhancement of resilience by hierarchical control. *IEEE Transactions on Smart Grid*, 5(5), 2517-2526.
- [11] Nithara, P.V., Hari, M., Sreelakshmi, C.S., Reshma, P.Eldho. (2019).
 V-f Controlled Autonomous Wind Energy Conversion System using

- Z2 Transformer connected STATCOM. *International Journal of Engineering and Advanced Technology*, 8(6), pp. 1492-1496.
- [12] Rodriguez-Diaz, E., Savaghebi, M., Vasquez, J. C., & Guerrero, J. M. (2015, September). An overview of low voltage DC distribution systems for residential applications. In 2015 IEEE 5th International Conference on Consumer Electronics-Berlin (ICCE-Berlin) (pp. 318-322). IEEE.
- [13] Planas, E., Andreu, J., Gárate, J. I., de Alegría, I. M., & Ibarra, E. (2015). AC and DC technology in microgrids: A review. *Renewable and Sustainable Energy Reviews*, 43, 726-749.
- [14] Rodriguez-Diaz, E., Vasquez, J. C., & Guerrero, J. M. (2015). Intelligent DC homes in future sustainable energy systems: When efficiency and intelligence work together. *IEEE Consumer Electronics Magazine*, 5(1), 74-80.
- [15] Elsayed, A. T., Mohamed, A. A., & Mohammed, O. A. (2015). DC microgrids and distribution systems: An overview. *Electric power* systems research, 119, 407-417.

Automated switch for operation of lights for energy saving

Swarnendu Bhattacharya^[1]and Asoke Kumar Paul^[2]

[1]B.TECH, 4th Year Student, Department of Electrical Engineering,
[2] Associate Professor, Department of Electrical Engineering,
Techno India University,
EM 4/1, SALT LAKE, SECTOR V,KOLKATA 700091
E mail: info.swarnendubhattacharya@gmail.com

Abstract - An automatic lighting system has been designed and developed for domestic use and for street use. The basic intention of this development is to switch ON and Switch OFF a few designated lights based on external light intensity to save electrical energy and to enhance personal safety. The system developed was initially for automatically switching on and off and later on it was redesigned and added the manually ON and OFF functions, because when the user is out of station in that time if the circuit operates automatically, then there will be loss of power. To prevent that manually ON and OFF function has been added.

The circuit comprises of three functions; ON, OFF & Automation mode. If the circuit is at ON state then the light will glow (ON), when it is at OFF state the light will be (OFF).

When the circuit is in automated state then it will operate logically i.e. in the morning when sun rises the LDR sense light, then relay is triggered and stays in the same position until sunlight light disappears.

Keywords - LDR; DPDT switch; Relays; Power contactor.

I. INTRODUCTION

An automatic lighting system has been developed for domestic use and for street use. The basic intention of this development is to switch ON and Switch OFF a few designated lights based on external light intensity to save electrical energy and to enhance personal safety. In India Automation is progressing day by day. The system developed is primarily designed for automatically switching ON and OFF. Then it was redesigned and added the manually ON and OFF functions, because when the user is out of station in that time if the circuit operates automatically, then there will be loss of power.(waste of power with no use). To prevent that we have added manually ON and OFF function.

II. SYSTEM OPERATION

The basic circuit is shown in Fig.1. This circuit comprises of three functions; ON, OFF & Auto mode. If the circuit is at on state then the light will glow (ON), when it is at off state the light will be (OFF).

If the circuit is in automated state then it will operate logically; here the logic is - in the morning when sun rises the LDR sense light, then Relay is triggered and common terminal gets attracted to "NO" (normally open) and stays at the same position until the dark. At the evening when sun sets the LDR sense darkness, the relay coil gets Denergised and common terminal gets attracted to "NC" (normally closed) and stays in the same position until sunlight light reappears. The whole operation; that is switching between on, off & automated function is done through a single DPDT switch.

III. SYSTEM IMPLEMENTATION

The system has been implemented in single flat and also in a housing complex for switching ON and OFF the street lighting load. The circuit is shown in Fig.1. When light falls on the LDR, the relay will be OFF and the bulb will be OFF. With this scheme one can implement a single or a few bulb. When we have to operate a large number of bulbs in the street of a residential complex, we have to use power circuit as shown in Fig. 2. When we have to switch ON the light, we operate a small electronic relay. With the NC contact of the electronic relay, we drive a contactor whose coil operates at 230 V, AC. This contactor (Siemens 3TA 21) has five change over contact. We have used 4 NO contact of this contactor. By this 4 Nos of NO contact we are switching 3 phases (R. Y. and B) and neutral. Each phase can supply 5 A AC current and thus around 1 kW of load can be connected in each phase. One MCB of 6 A rating, single pole has been used in the circuit to switch off during any fault.

To improve the performance and for stable operation, the load power factor is to be high, so that the current passing through the breaker is fully utilized as active power.

A prototype system has been developed and tested for two months with lighting load. Further modifications are in progress. A photograph of the system is shown in Fig.3.

International Conference On "Impact of Changing Energy Mix in the Power Sector" (ICIEMPS-2019) The Institution of Engineers (India), WBSC 23rd & 24th Nov. 2019

If the circuit is in Automatic Mode then it may encounter momentary abrupt switching condition due to sudden Thunder-Lightning. During this time if the circuit is ON it may turn OFF momentarily due to very bright light of thunder-lightning sensed by the LDR. To avoid the situation a capacitor has been added parallel to the Relay junction which will produce a momentary delay in turning on the circuit and will bypass the momentary switching scenario which will make the circuit healthy and more reliable.

IV. FUTURE SCOPE OF WORK

Further modification is also being carried out to eliminate the transformer by solid state devices. This development shall reduce the cost further.

Presently we are working is on 2nd mode of operation. In mode-1, the light shall be on or off based on sunlight. This mode has been tested and it is fully functional.

In mode-2, the GPS based interlock shall be provided to eliminate spurious triggering. There is a microcontroller, which receives GPS signal. Based on the geographical location and current date, the sunrise and the sun set shall be calculated and the system shall be switched on as per the local sunrise and sunset time this mode-2 is under development.

Effort is being made to improve the power factor of the lights

V. CONCLUSION

The basic advantage of this circuit is low cost and high reliability. The circuit components like LDR,

Transformer, SPDT relay, Diodes, DPDT switch etc. are easily available.

Automatic Switch needs no manual operation of switching ON and OFF when it is on the Automatic Mode. The system itself detects whether there is need for light or not. When darkness rises to a certain value then automatically streetlight is switched ON and when there is other source of light, the street light gets OFF. The extent of darkness at which the street light to be switched on can also be tailored using the potentiometer provided in the circuit.

Moreover, the circuit is carefully designed to avoid common problems like relay chattering and inductive kick back in relay and spurious triggering in case of thunder strike.

ACKNOWLEDGMENT

The authors wish to express their gratitude to various housing complex for providing facilities to test the circuit for its reliability and to test the circuit for its protection against spurious switching.

REFERENCES

- [1] M. A. Wazed, N. Nafis, M. T. Islam and A. S. M. Sayem "DESIGN AND FABRICATION OF AUTOMATIC STREET LIGHT CONTROL SYSTEM", Engineering e-Transaction (ISSN 1823-6379) Vol. 5, No. 1, June 2010, pp 27-34.
- [2] Subhojit Mukherjee, Arijit Ganguli, Asoke Kumar Paul and Ajay Kumar Datta, "Load flow analysis and reactive power compensation" 2018 International Conference on Computing, Power and Communication Technologies (GUCON) Galgotias University, Greater Noida, UP, India. Sep 28-29, 2018.
- [3] www.studymafia.org, "Automatic street light".

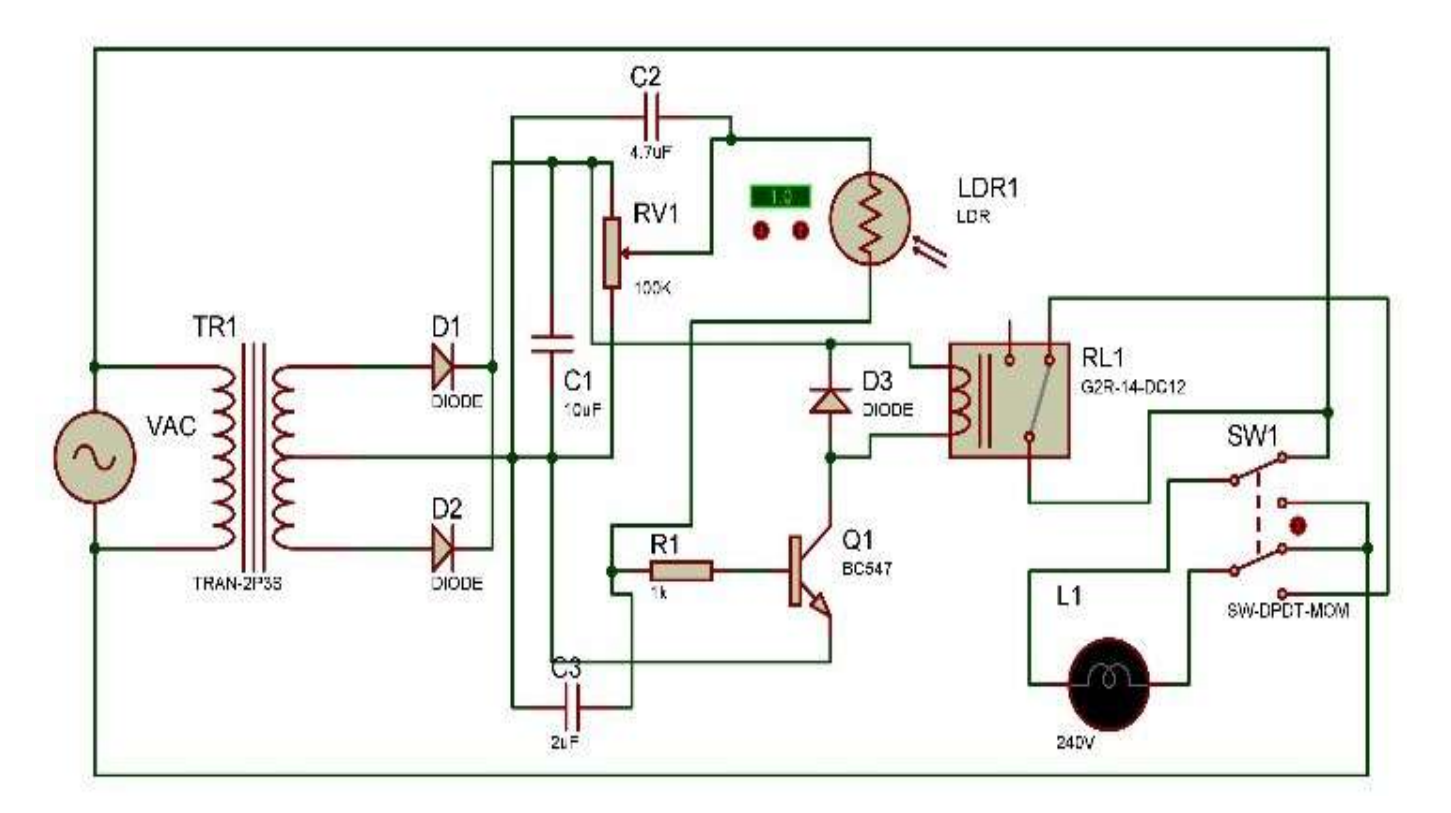
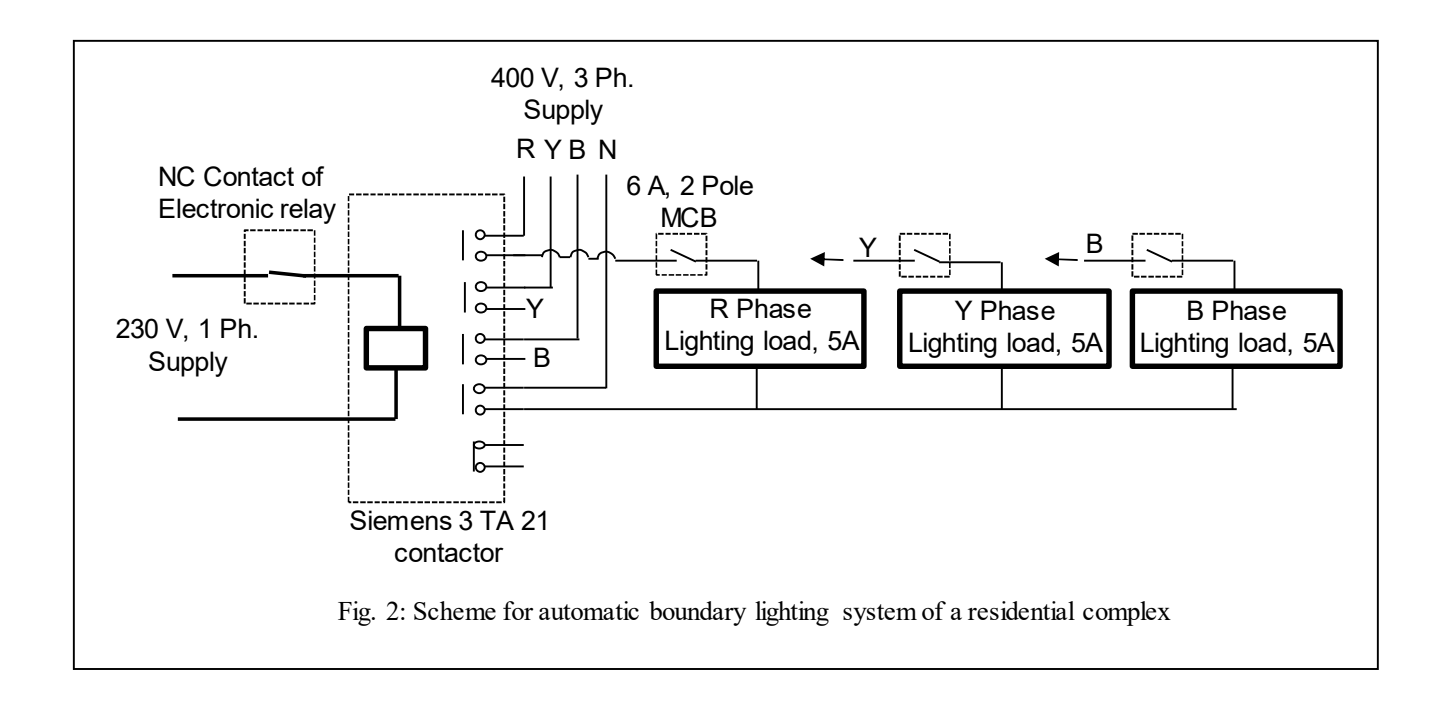


Fig.1: Circuit diagram of the automatic lighting system



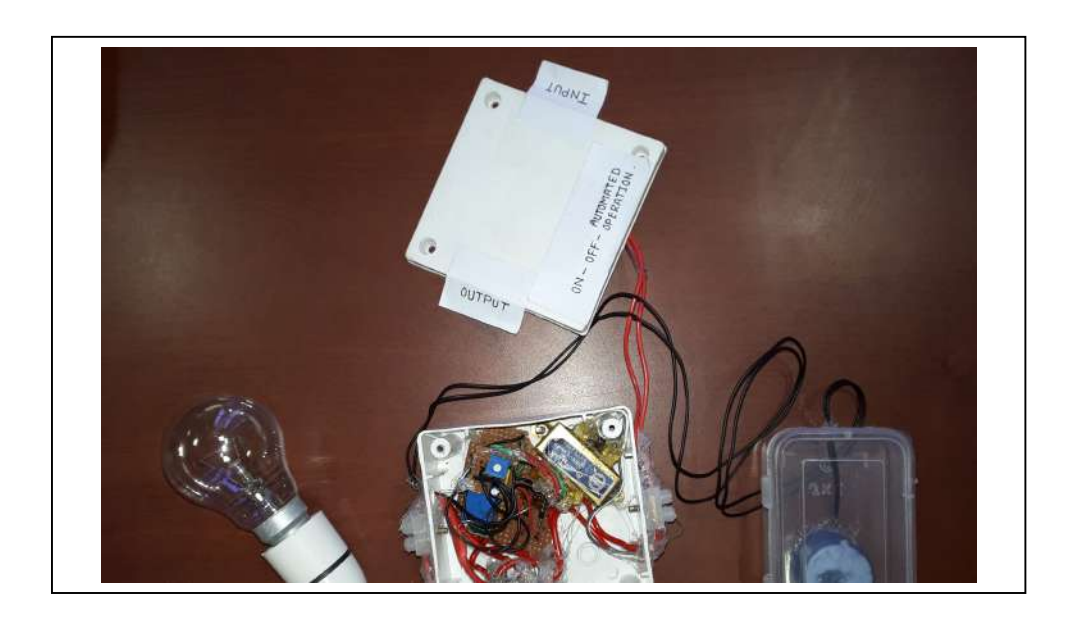


Fig. 3: Photograph of the implemented circuit

Random Grid Based Visual Secret Sharing (2, 2) & (3, 3)

Swapan Kumar Majumder

Department of Electronics and Communication Engineering and Electrical Engineering OmDayal Engineering College, Uluberia, Birshibpur, Howrah, PIN-711316, India swapan 112233@gmail.com

Abstract

This paper presents algorithms for Random Grid Based Visual Secret Sharing (2, 2) & (3, 3) scheme. The first algorithm represents Random Grid Based Visual Secret Sharing (2, 2) scheme. It uses random grid to produce two shares of a given secret. The secret image will be reconstructed by the Human Visual System (HVS) when both the shares overlaid stacked. just or cryptographic computation is required. The second algorithm also uses random grid to generate two shares of a given secret. But this (2, 2) threshold scheme has been devised to the give full clarity of the image by negligible computations reconstruction. The third algorithm presents for Random Grid Based Visual Secret This Sharing (3, 3) scheme. scheme generates three shares or shadow images. At the time of reconstruction of the secret image all three shares are used along with minor computations.

Keywords - Visual Secret Sharing (VSS), Random grid, Secret image, share, shadow image.

INTRODUCTION

Suppose, one desires to send an image electronically from one point to other. To do so, a network or a set of networks may be used. It may be the Internet or an entirely different network. Whatever it is, it may reach to unsafe hands as a network is essentially a porous one. An image can be anything- it can be a photograph or a scanned copy of some company's sensitive database or an image of

some critical information or so on and so forth. Question then arises how one can ensure safe transfer of an image through network. The answer could be the use of 'Visual Secret Sharing' technique. The very next question arises how this sharing technique ensures the safety. Definition and explanation of 'Visual Secret Sharing' will give the answer. Visual secret Sharing scheme (VSS) is a secured way that protects a secret image by dividing it into a number of components or shadow images. Under this technique, an image which is called 'a secret' here can be divided (broken) into 2 or more meaningless pieces which are called 'shares' and they can be sent over any chosen network.

Let us know the peculiarity of this technique. If someone finds the individual share on the way of its travel, it appears absurd and no can recognize it to be a piece of an image as it can be seen in my sample's output. The most stunning feature of this technique is that the original image will be reconstructed or the original image will reappear if the shares are just superimposed or overlaid one over another. No decryption is required at receiving end. But in some cases decryption may be done at the receiving end to enhance the clarity of the image.

One more question here arises how one can divide an image into two or more components. One way to break the secret image is to expand each pixel into two or more sub-pixels. The stacking of these sub-pixels will then reconstruct the original image. This was proposed by Moni Naor and Adi Shamir for the first time to the

world. With this Visual Cryptography (VC) or Visual Secret Sharing (VSS) took birth. And the world got a secured way to transfer images. Although it was unique of its kind, yet it was not It had pixel expansion pitfalls. problem. The share images were larger than the original secret image. Research work in this regard continued to exist. Another technique was developed by O. Kafri and E. Kareen (1987) to encrypt the secret using random grid that requires no pixel expansion. At this stage a brief review of literature is required to fathom the gamut and the current need of the Visual Secret Sharing.

Brief Review of Literature

1.Visual Cryptography: Moni Naor and Adi Shamir (1995)

Merits: (a) The scheme provides security of image by breaking it into shadow images. Here image is reconstructed by stacking the shadow images. (b) No cryptographic computation is required for decoding the image. Human Visual System (HVS) can decode the secret.

Demerits: (a) It suffers from the pixel expansion problem. The share images are larger than the original secret image. (b) The decoded image quality is not very good. (c) It needs code book design. (d) It needs more storage space.

2. Encryption of pictures and shapes by Random Grid:O. Kafri and E. Kareen (1987)

Merits: (a) The pixel expansion problem is eliminated. (b) Code book design is not needed. (c) No cryptographic computation is needed for decoding the image.HVS can decode the secret. (d) It provides the security of the image.

(e) The shadow image has the same size as that of the secret image.

Demerits: (a) The quality of the recovered image is not very good. (b) A white in the secret image may be interpreted as black with 0.5probability in the stacked image.

3. Image Encryption by Random Grid:S.J.Shyu (2,2) 2007

Merits: (a) S.J. Shyu extended Kafri and Kareen's RGVSS model with proposition of

three models using (2,2) threshold scheme. (b) It has all the advantages of Kafri and Kareen's model. In addition, it has the enhanced security. (c) building of (2,2) threshold scheme.

Demerits: (a) The reconstructed visual quality is not very good. (b) A white pixel in the secret image may be interpreted as black pixel with 0.5 probability in the stacked image.

4. Visual Secret Sharing by Random Grids Revisited (2,n): T.H.Chen,K.H.Tsao (2009)

Merits: (a) They extended S.J. Shyu's RGVSS model(2007) from (2,2) threshold scheme to (2,n) threshold scheme. (b) It renders the enhanced security of the images as compared to the previous model.

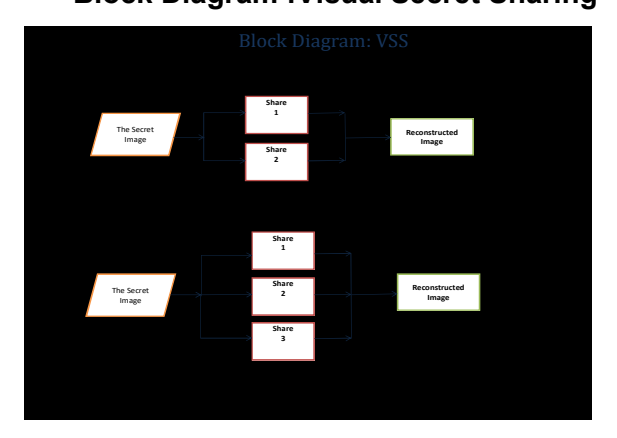
Demerits: (a) The quality of the reconstructed image is not very good. (b) A white pixel in the secret image may be interpreted as black pixel with 0.5 probability in the stacked image.

5. Image encryption by Multiple Random Grids Patten Recognition(n,n):S.J. Shyu (2009)

Merits: (a) He extended T.H. Chen and K.H. Tsao's RGVSS model (2009) from(2,n) threshold scheme to (n,n) threshold scheme. (b) This scheme enhanced security of the image as compared to the previous models.

Demerit: The quality of the reconstructed image is not very good.

Block Diagram: Visual Secret Sharing



Proposed Algorithms on Random Grid Based Visual Secret Sharing (RGVSS):

It has further been seen that the existing algorithms that produce shares are too complex. Not only they are complex, clarity of reconstructed image based on these complex algorithms is not also very good. Coupled with complexity and proportionate dissatisfied clarity of the reconstructed image, present situation demands availability of random grid based simplified or moderate complex algorithms which do not much compromise with the quality of the shares and the reconstructed image. The ease of implementing of algorithms and the volume of also important issues. The softwares are proposed algorithms have been designed in such a way that they are easily implemented. And algorithms also take care of the volume of softwares which can be kept low. Three different random grid based algorithms are given below:-

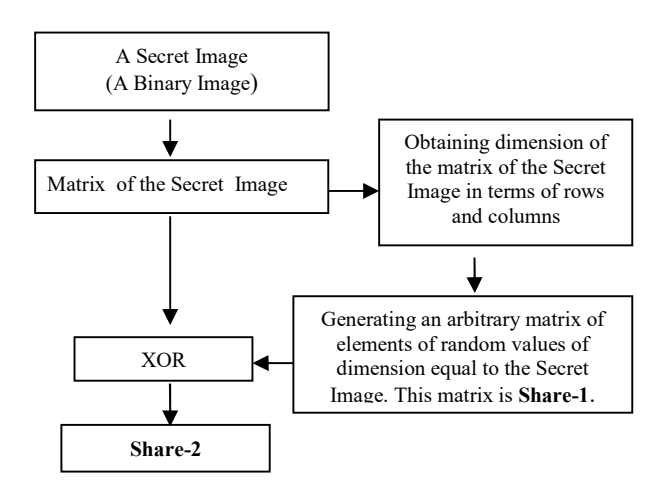
Algorithm-I Steps:

- A matrix equivalent to an image is obtained first.
- The image is then converted into a binary image (black and white). The binary image of a ball which will act as a secret image here is shown in Fig.1-1. This secret image needs to be communicated through networks.
- 3. A matrix equivalent to the secret image is obtained.
- 4. The dimension of the secret image in terms of rows and columns is obtained.
- 5. In this step, an **arbitrary matrix** of elements random values of dimension in terms of rows and columns equal to the Secret Image is generated. The image of the arbitrary matrix appears like noise and meaningless. This is nothing but the **Share1** (Fig. 1-1-1).
- 6. In this step, the matrix of the secret image that needs to be communicated through networks is XORed with the matrix of the share1. This process of XORing gives birth to **Share2** (Fig.1-1-2).
- The secret image will be reconstructed if the matrix of share2 is just ORed or

superimposed with the matrix share1. Fig.1-2 shows the reconstructed image.

(The stacked result of share1 and share2 will be either black or white with 0.5probability. Thus a white pixel can be misinterpreted as black with 0.5probability while shares are superimposed to reconstruct the secret image.)

GENERATION OF SHARES



RECONSTRUCTION OF THE SECRET IMAGE

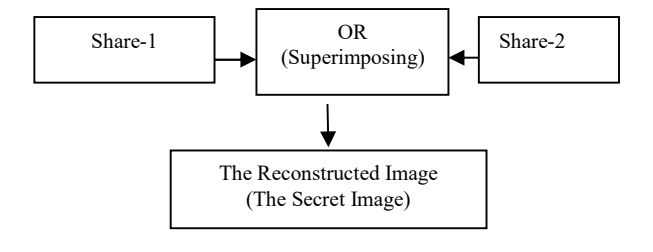


Fig. 1 Flow Chart of Algorithm-I

EXPERIMENTAL RESULT: ALGORITHM-I



Fig.1-1 Secret Image (Binary Image of a ball)

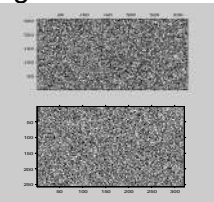


Fig.1-1-1 Share 1

Fig.1-1-2 Share 2

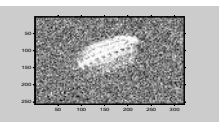


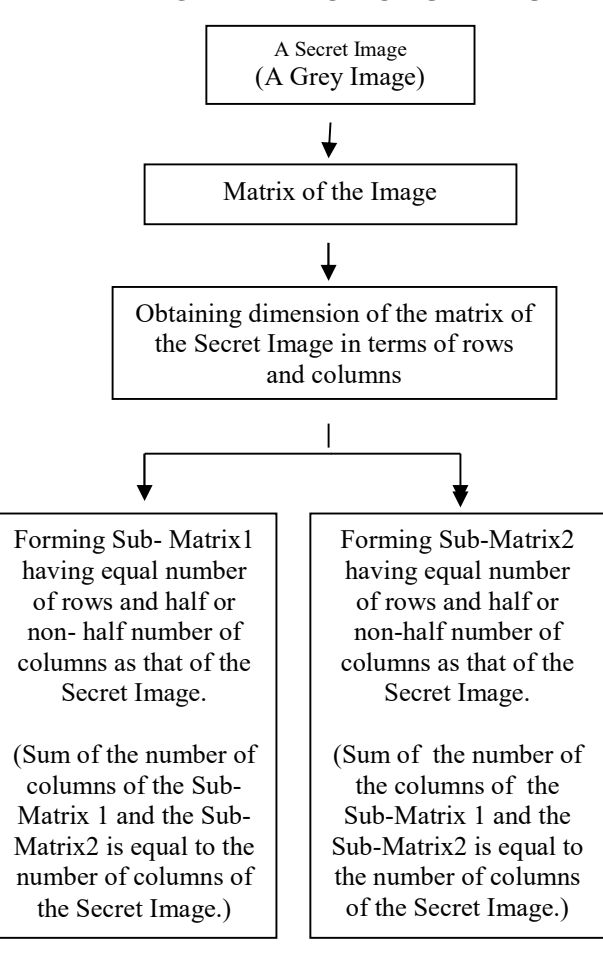
Fig.1-2 The Reconstructed Image

Algorithm-II Steps:

- 1. A matrix equivalent to a grey image is obtained first.
- 2. The dimension of the matrix in terms of rows and columns is then obtained.
- From the matrix, two sub-matrices say, an image sub-matrix1 and an image sub-matrix2 are obtained by dividing the columns into two keeping the rows intact.
- 4. A matrix of elements of random values of same dimension in terms of rows and columns as that of the image sub matrix1 and another matrix of elements of random values of same dimension in terms of rows and columns as that of the image sub matrix are generated.
- 5. The image sub-matrix1 and the matrix of elements of random values of same dimension as that of the image submatrix1 are added. This addition creates a altogether new matrix called **share1** (Fig.2-1-1) that has almost noise like appearance.
- 6. The image sub-matrix2 and the matrix of elements of random values of same dimension as that of the image sub-matrix2 are added. This addition creates a new matrix called **share2** (Fig.2-1-2) that has almost noise like appearance.

7. The reconstruction of the secret image is done in the following manner: Firstly, the matrix of elements of random values of same dimension as that of the image sub-matrix1 is subtracted from the matrix of share1. This gives the matrix of the image sub-matrix1. Secondly, the matrix of elements of random values of same dimension as that of the image sub-matrix2 is subtracted from the matrix of share2. This gives the matrix of the image sub matrix2. Thirdly, when the matrix of the image sub matrix1 and that of the image sub matrix2 are added, the original secret image is reconstructed.

GENERATION OF SHARES



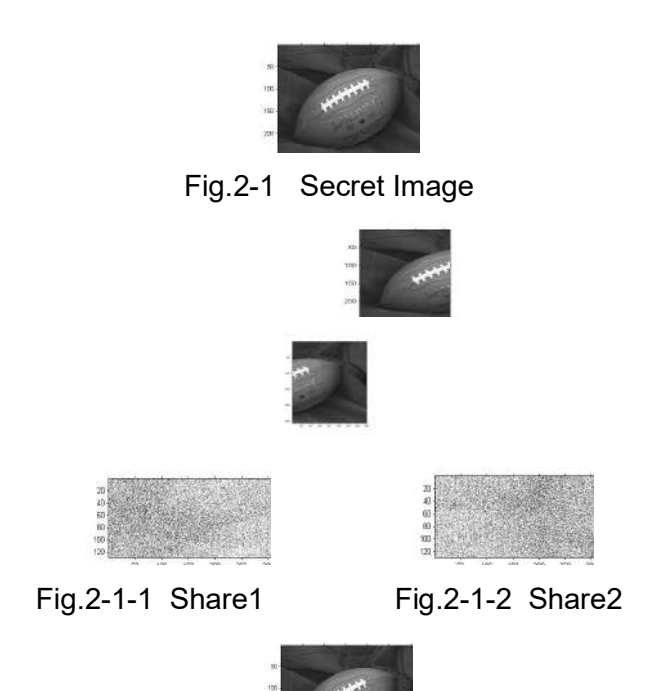
Obtaining dimension of the Sub-Matrix1 in terms rows and columns

Obtaining dimension of the Sub-Matrix2 in terms of rows and columns

Generating an Generating an Arbitrary Matrix1 Arbitrary Matrix2 of elements of of elements of random values of random values of same dimension as same dimension as that of Subthat of Sub-Matrix 1 Matrix2 Matrix Addition Matrix Addition Share1 Share2

Fig. 2 Flow Chart of Algorithm-II

EXPERIMENTAL RESULT: ALGORITHM-II



RECONSTRUCTION OF THE SECRET IMAGE

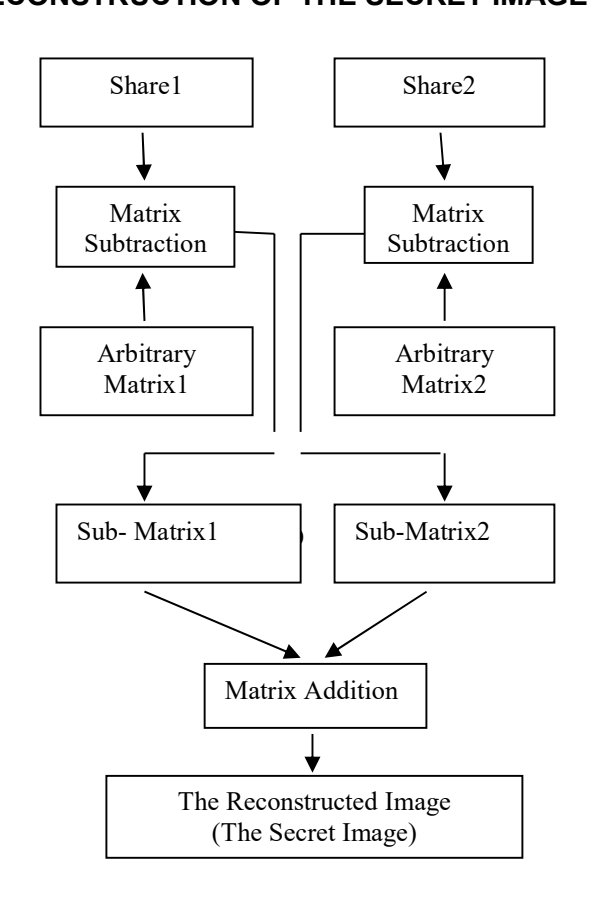


Fig.2-2 The Reconstructed Image

Algorithm-III

Steps:

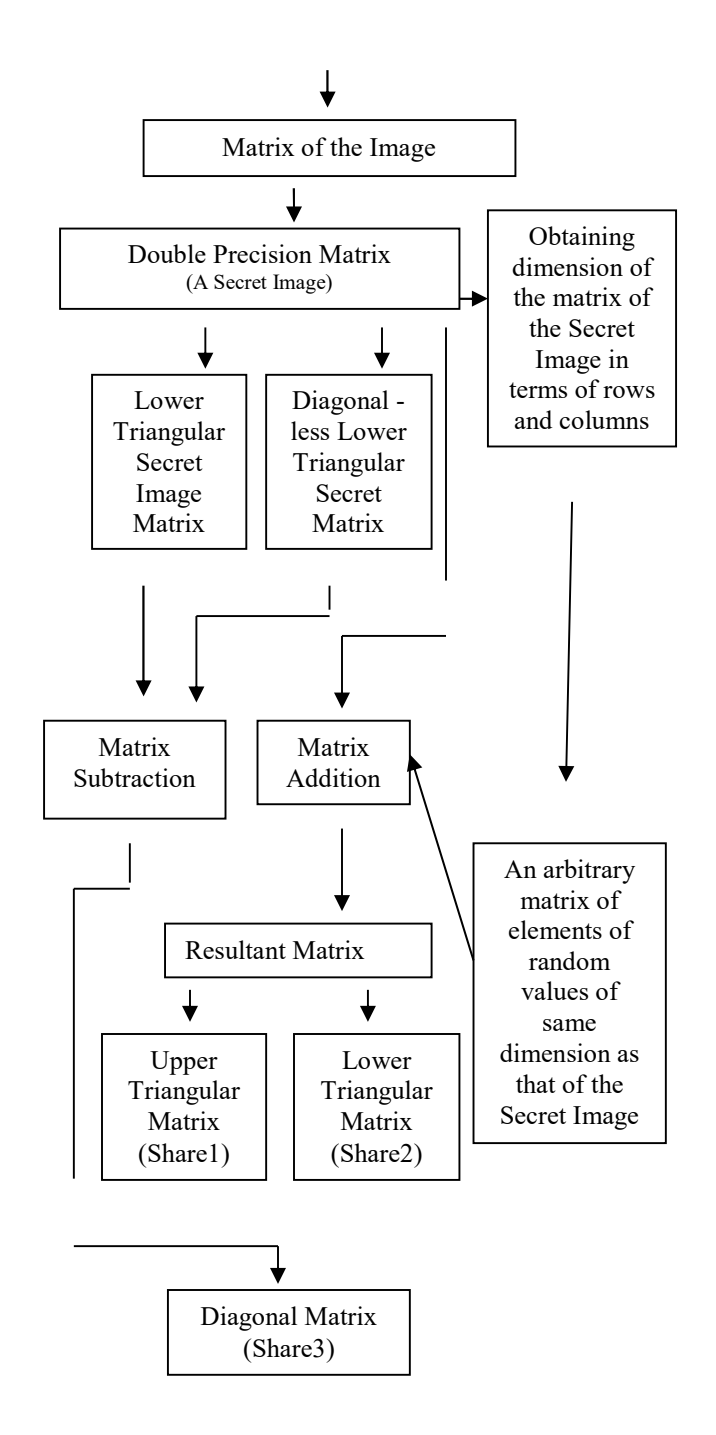
- A matrix equivalent to an image is obtained first. If it is a color image then it is converted to a grey image. And at the same time its dimension in terms of rows and columns is also obtained.
- The grey image matrix may then be converted to double precision matrix. The double precision scaled matrix is the secret image which is to be transported through networks by using shares or shadow images.
- An arbitrary matrix of elements of random values of same dimension in terms of rows and columns as that of the double precision matrix is generated.
- 4. The secret image matrix and the above arbitrary matrix of elements of random values are added. The resultant matrix obtained after addition as stated above is

International Conference On "Impact of Changing Energy Mix in the Power Sector"(ICIEMPS-2019) The Institution of Engineers (India), WBSC 23rd & 24th Nov. 2019

- considered to be the matrix of elements of random values.
- 5. The upper and lower triangular matrices are then obtained from the resultant matrix. These two triangular matrices form the two shares-share1 (Fig.3-1-1) and share2 (Fig.3-1-2).
- 6. Share3 is formed in the following manner: Firstly, a lower triangular secret image matrix is obtained from the secret image matrix. Secondly, another matrix is obtained from the secret image matrix by taking elements below the principal diagonal line only. This matrix henceforth will be called in this paper as a diagonalless lower triangular matrix. Thirdly, the diagonal-less lower triangular matrix is subtracted from the lower triangular secret image matrix of this step to generate a third matrix called share3 Fig.3-1-3.
- 7. For reconstruction of the secret image using shares, minor computations are needed. Firstly, an upper triangular matrix is obtained from the arbitrary matrix of elements of random values that was generated in the beginning of the algorithm. This upper triangular matrix is subtracted from the upper triangular matrix of share1 to give the upper triangular matrix of the secret image. Secondly, the lower triangular matrix is obtained from the arbitrary matrix of elements of random values. This lower triangular matrix is subtracted from the lower triangular matrix of share2 to give the lower triangular matrix of the secret image. Thirdly, the upper triangular matrix and the lower triangular matrix of the secret image are added. The secret image is reconstructed when the matrix of share 3 is subtracted from the matrix obtained after addition of the upper and lower triangular matrices of the secret image.

GENERATION OF SHARES

A colour Image



RECONSTRUCTION OF THE SECRET IMAGE

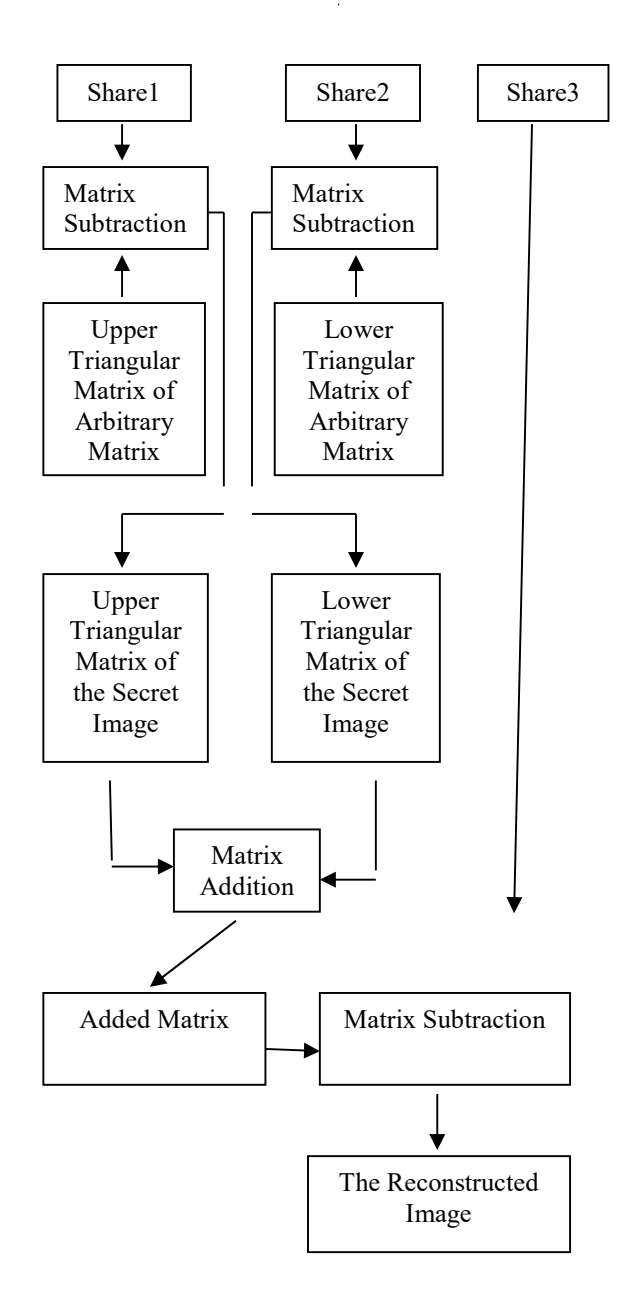


Fig. 2 Flow Chart of Algorithm-III

EXPERIMENTAL RESULT: ALGORITHM-III



Fig.3-1 Secret Image







Fig.3-1-1 Share 1 Fig.3-1-2 Share 2 Fig.3-1-3 Share 3



Fig.3-2 The Reconstructed Image

Applications Although applications of algorithms can be anything that user wants to use them. Generally VSS technique is used for transporting images from one point to other through networks. But algorithm-I can be used in non-network, non-electronic applications also. It is so because VSS also works in transparencies. We all know that school authoroty issues escort cards to guardians for collecting students from school. Taking a photo of a escort card is not a difficult task. The demerit of the old system is that anybody can make the same card by using the photo of the card and pick the child !!! Algorithm-I can here be used for making a

International Conference On "Impact of Changing Energy Mix in the Power Sector"(ICIEMPS-2019) The Institution of Engineers (India), WBSC 23rd & 24th Nov. 2019

the school authority and the other one will be with guardian. During collection of the ward, the guardian will hand over the share to the authority. If ward's face appear on overlaying the guardian's share with authority's share, the ward will be handed over to the guardian otherwise not. It is a more secured method than handing over the ward just based on old fashioned single escort card.

* Figures may not be in scale.

REFERENCES

- [1]Moni Naor and Adi Shamir_(1995) Visual Cryptography, in advances in cryptography, Eurocrypt 94. Lecture Notes, Computer Science 950:1–12
- [2] Kafri O, Keren E (1987) Encryption of pictures and shapes by random grids. Opt Lett 12(6):377–379
- [3] Encryption of pictures and shapes by Random Grid by S.J.Shyu (2, 2) 2007
- [4] Chen TH, Tsao KH (2009) Visual secret sharing by random grids revisited (2,n) Pattern Recogn 42:2203–2217
- [5] Shyu SJ (2009) Image encryption by multiple random grids (n, n). Pattern Recogn 42:1582–1596
- [6] Xiaotian W (2013) Wei Sun, Random gridbased visual secret sharing with abilities of OR and XOR decryptions. J Vis Communication Image R 24:48–62
- [7] Xiaotian W, Sun W (2013) Improving the visual quality of random grid-based visual secret sharing. Signal Process 93(5):977– 995
- [8] Tsung Lieh Lin et al., A novel visual secret sharing(VSS) scheme for multiple secrets without pixel expansion, Expert Systems with Applications, Vol. 37 PP.7858-7869, 2010
- [9] Yung-Fu Chen, Yung-Kuan Chan, Ching-Chun Huang, Meng-Hsiun, Tsai C, Yen-Ping Chu, 'A multiple-level visual secret sharing scheme without image size expansion', Information Sciences, Vol. 177,PP.4696-4710,2007

Methods adopted for detailed modeling in state spacefor stability analysis.

Milan Bose

AvikGhosh

Arabindo Das

Amar NathSanyal

Prof. & Head. EE, Techno India College of Technology Milanbasu43@gmail.com Asst. Prof, Ideal Inst. of Engg., Kalyani avik be@yahoo.com

Prof. Elect. Engg.

Jadavpur University

adas ee ju@yahoo.com

Formerlyfaculty member, Jadavpur University ansanyal@yahoo.co.in

Abstract: The earlier methods adopted for stability analysis of synchronous machines was approximations based and idealizing assumptions. As such, the accuracy of prediction was limited. The advent of fast-acting computers having large memory space opened up the avenue for accurate analysis by opening up the scope for handling detailed modeling. The earlier methods were based on equal area criterion or on swing equation or some of its modified form. But the methods applied now-a-days uses state space representation of the dynamic equations. The paper shows the steps to develop state space models (both with current and flux-linkage states) for transient stability analysis and the methods of linearizing the model about the operating point to assess dynamic stability. Two case-studies have been given at the end to illustrate the methods.

Key words: swing equation, transient stability, dynamic stability, state space, equivalencing, one machine on infinite bus

1. Introduction

Alternators seldom operate in isolated mode. They are run in parallel in a power station and the power stations are connected to form the grid. In a large grid system, the load supplied by an alternator is insignificant [1,2]. So they are individually considered as one machine on infinite bus, connected through a series impedance (fig. 1). If an alternator is modeled in detail, it is customary to use this representation as multimachine representation makes the dimension of the model very large and untractable.

The alternators may be of the cylindrical pole type (driven by steam turbine) or salient pole type (driven by water turbine). The alternators, and hence the parts of the power system, remains

synchronized to each other by rotating magnetic field produced by the multi-phase windings [3].

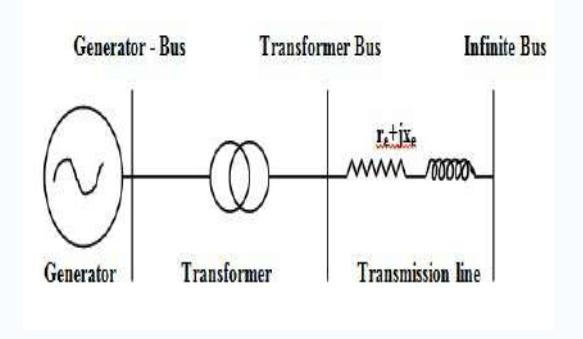


Fig. 1. One machine on infinite bus through series reactance

2. The reactance of alternators

In the classical analysis, a synchronous generator is represented by a source of e.m.f. behind an impedance (or simply a reactance as the effect of resistance is too small), summing up the effect of armature reaction with that of armature leakage. For cylindrical pole machines we use a single synchronous reactance X_{α} and for salient pole machines we use two synchronous reactance (X_d, X_g) for the polar or direct and the interpolar or quadrature axes [4]. Under transient conditions, the synchronous reactance undergoes changes due to constancy of flux-linkage before and occurrence of a sudden change (Doherty). This effect is accounted for by replacing synchronous reactance by transient reactance for slow transients and by subtransient reactance for fast transients. The effect of transient and subtransient saliency can also be accounted for. Improved analytical tools have now been improvised which give closer estimates of the transient phenomena [5]

3. Turbogenerator vs. hydrogenerator

A steam turbine driven generator has the following control loops [8]:

a. Boiler firing control

- b. Turbine governor control
- c. AVR and exciter control

The boiler firing control is absent in a water turbine driven generator. The AVR and exciter control has major role in shaping the transient. Modern fast-acting turbine-governor control has a minor role and the boiler-firing control has practically no role as the time-constants are too large. Turboalternators are invariably bipolar machines. To make the design economic, the airgap is made small and a lighter rotor is used. It reduces the short circuit ratio, increases the synchronous reactance and makes the inertia small. On the other hand, the rotor of a hydro-alternator is multi-polar and heavy. Hence the inertia is large, the SCR is also large and synchronous reactance relatively smaller. The saliency in a turboalternator is negligible, so it may be represented by a single synchronous reactance. But the airgap in a salient pole machine periodically varies from pole to interpole. Hence it has to be represented by two reatance, one for the polar axis (d-axis) and another for the interpolar axis (q-axis). As a small saliency is present even in cylindrical pole machine due to the presence of their big teeth

V_a		Cosθ	Sinθ	1/√2	V_d
V_b	= √(2/3)	Cos $(\theta - 2\pi/3)$	Sin(θ - $2\pi/3$)	1/√2	V_q
V_c		Cos $(\theta + 2\pi/3)$	Sin(θ + $2\pi/3$)	1/√2	V_o

inbetween poles, it is customary to use 2-axis representation for both types of alternators.

Block diagram and signal flow graph are good if initial conditions are zero i.e. the system is initially relaxed [13]. The response due to a forcing function can be easily obtained by these methods, but they cannot account for initial conditions and the influence of internal variables. The kind of control system used in alternators is best represented by state space models. In the following paragraphs we shall develop the state-space model of the generator-transformer connected to infinite bus.

5. Representation of the generator

A synchronous generator can be represented by the phase variable model [4,9,12] in which

 The distributed damper winding is represented by two concentrated coils- one along d-axis and another along q-axis.

- ii) The field winding is represented by a concentrated coil in the d-axis
- iii) The armature is represented by three coils for the three phases, having mutual space phase difference of 120°.

V_d		Co	`	$Cos(\theta + 2\pi)$	V_a
		sθ	2π / 3)	/ 3)	
V_q	= √(2/3	Sin	Sin(θ -	Sin(θ +	V_b
	V(2/3	θ	2π/3)	2π/3)	
V_o	,	1/√	1/√2	1/√2	V_c
		2			

In this model the inductances are time-varying and the describing equations are nonlinear, as the coupling angles of the rotating coils with the stationary coils continuously change. It is difficult to solve such non-linear equations. The computer run time & memory space requirement for such a model are large. Hence this model is seldom used.

To obviate this problem Park and Gorev introduced a transformation matrix which transforms phase quantities into axis quantities as shown below:

where, V_a, V_q etc. are transformed quantities $\&V_a, V_b$ etc. are phase quantities. A similar relation exists for the current variables. To get phase quantities from the axis quantities, the following inverse transformation is made:

2

The Park's transformation is orthogonal. It reduces a machine with time-varying inductances to one having fixed inductances in terms of axis variables. The resulting model is similar and can be solved much more easily. In this model the coils D, Q are pseudo-stationary i.e. fixed in space but having the property of inducing emf by the speed action of the rotor. The circuital representation of the actual and the transformed machine are given in fig. 2a and 2b.

The transformer is represented as a T-circuit. The shunt element in this T-representation absorbs very small current. So we generally neglect it and represent the transformer as aseries impedance. This impedance is clubbed together with that of the generator. The reactance and time constants are modified accordingly.

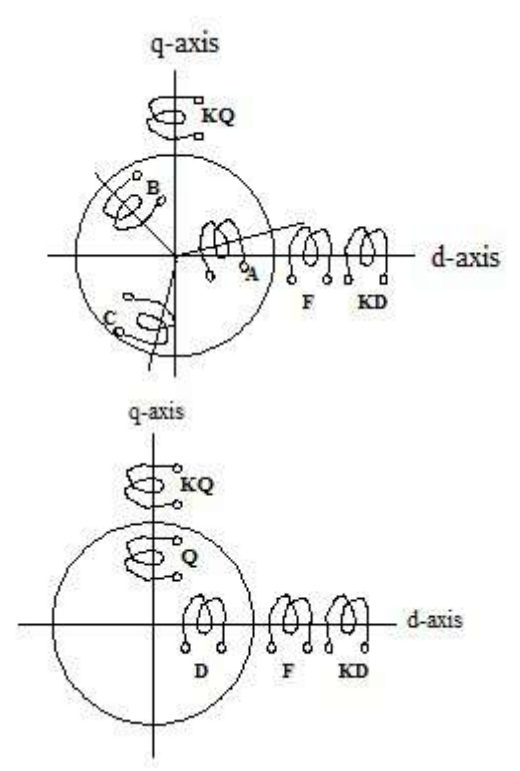


Fig 2aPhase variable model of alternator Fig 2b d-q axes transformed machine

6 Base quantities, p.u. values and transformed impedance matrix

In power system analysis it is customary to use p.u. parameters and variables in terms of appropriate base quantities. For analysis of a single machine its nominal voltage/current etc. are used as base quantities. For rotor quantities, we choose a base on the basis of equal mutual flux linkage [10].

The transformed impedance matrix is obtained from:

$$[Z'] = [C^T] [Z] [C]$$

where [C] is the transformation matrix and [C]^T is its transpose. By algebraic manipulation we get the transformed impedance matrix. It is a (4x4) matrix for a polyphase induction machine and a (5x5) for a polyphase synchronous machine with the damper winding represented by one coil per axis.

The transformed **Z**-matrix does not have any time-variant inductance and is much more tractable. It yields closed from solution for most of the machine-problems and forms the basis of the classical model of synchronous machine.

The following are the limitations of the genaralised machine model:

- a. It cannot be applied to double salient machines like inductor-alternator.
- b. It cannot be applied to machines having unbalanced winding like single phase alternator.
- Secondary effects like saturation, distribution of eddy currents in solid iron and commutation phenomena need separate considerations.

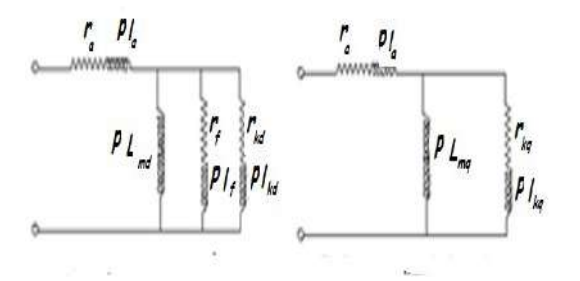


Fig. 3a d-axis equivalent circuit Fig. 3b q-axis equivalent circuit

7. Equivalent circuit of synchronous machine

The equivalent circuits for the transformed machine are given in fig 3a for the d-axis and 3b for the q-axis. The coil F is the field Coil, KD & KQ are the damper coils, D & Q are the pseudostationary equivalents of the 3-phase armature coils. Nomenclature of other parameters is given below [4]:

L_{md}= Magentising inductance of the D-axis

 L_{mq} = Magetising inductance of the Q-axis I_a = Leakage inductance of the armature

r_a = Resistance of the armature

I_f = Leakage inductance of the field

r_f = Resistance of the field

 I_{kd} = d-axis damper leakage inductance

 r_{kd} = d-axis damper resistance

 I_{kq} = q-axis damper leakage inductance

 r_{kq} = q-axis damper resistance

Under steady state asynchronous condition, as in the case of loss of excitation, ${\bf p}$ may be replaced by ${\bf i}\omega$.

8 Machine parameters from the manufacturer's

Power station managers are provided with manufacturer's data from which the equivalent circuit for the d & q axes can be found out by the following set of equations [10]. The parameters are

generally given in p.u. and time-constants in seconds.

$$X_{md} = X_d - x_a; X_{mq} = X_q - x_a$$

$$4$$

$$1/X_f = 1/(X_d' - x_a) - 1/X_{md}; X_f = x_f + X_{md}$$
5

$$1/X_{kd} = 1/(X_d - X_a) - 1/X_f - 1/X_{md}; X_{kd} = X_{kd} + X_{md}$$

$$\begin{split} 1/\left.X_{kq} &= 1/\left(\left.X_{q}^{"} - x_{a}\right) - 1/\left.x_{f} - 1/\left.X_{mq}; X_{kq} = x_{kq} + X_{mq} \right.\right.\right. \\ & 7 \\ r_{f} &= X_{f} / \left(\omega T_{do}^{'}\right); \quad T_{do}^{'} &= T_{d}^{'}\left(X_{d} / X_{d}^{'}\right) \\ & 8 \\ r_{kd} &= \left(x_{kd} + \frac{X_{md} x_{f}}{X_{md} + x_{f}}\right) / \left(\omega T_{do}^{"}\right) \\ T_{do}^{"} &= T_{d}^{"}\left(X_{d}^{'} / X_{d}^{"}\right) \\ T_{kq}^{"} &= X_{kq} / \left(\omega T_{qo}^{"}\right); T_{qo}^{"} &= T_{q}^{"}\left(X_{q}^{'} / X_{q}^{"}\right) \end{split}$$

These parameters are with reference to the classical model of Park, Concordia & Adkins. However, some of the data may not be available for existing machines e.g. the q-axis magnetization data or subtransientreactance. In that case appropriate values for the missing data should be assumed by referring to standard tables & text-books.

9 Extension of the classical model

The classical model can be extended to include [4,10]:

- a. *Mechanical parameters*: Inertial and damping effects through motional Z-matrix.
- b. Solid iron effects: By representing damper with more than one coils per axis. At least one more coil in q-axis may be used as proposed by Anderson and Fouad, giving rise to q-axis transient reactance and timeconstants.
- Saturation: by using saturated values of reactance corresponding to quiescent point on the O.C.C.
- d. *Harmonics*: Through the principle of superposition, as indicated by Kopylov.

10. Inclusion of effects hitherto neglected

Inertial and damping effects are accounted for computation of electromechanical transients. The inertia of the turboalternator is given as inertia constant H and the p.u. damping as D. The toque balance equation (known as swing equation) is given [11] as:

$$T_m - T_e = \frac{2H}{\omega} \frac{d^2 \delta}{dt^2} + \frac{D}{\omega} \frac{d\delta}{dt}$$

12

The effect of saturation is to reduce the value of X_{md} (also X_{mq} to a lesser degree) depending on the degree of saturation. The common practice is to use a saturated value of synchronous reactance (Kingslay's method) for conditions at or near CMR and an unsaturated value under small/capacitive load. If the O.C.C./S.C.C for the machines are available then the appropriate value for the reactance may be found out graphically or by computer program. For more detailed analysis of saturation, Frolick's method or exponential method may be applied using curve-fitting procedure.

The effect of induced eddy currents in the solid iron rotor is not accounted for in the classical model. The classical model holds good only for laminated rotor which are never used now-a-days. The various electromagnetic models which account for the induced eddy currents in the solid iron parts of the rotor & in the retaining rings are not suitable for dynamic performance analysis. It has been found that the solid iron rotor acts as a q-axis damper and it suffices to represent the effect by two damper circuit coils for the q-axis. This gives rise to concept of a q-axis transient reactance.

In addition, there is a mutual coupling between the field & the damper which may be represented by an additional parameter X_{fkd} . The parameter can be experimentally found out by the method of Takeda and Adkins. No information on this parameter is available from manufacturer's data. Effect of harmonics is not accounted for to avoid complexity.

11. Equivalencing and the concept of one machine on infinite bus

For disturbance at a particular location, a multimachine system may be reduced to a 2-machine system by circuital analysis [12]. If the rating of the faulty machine is significant with respect to the grid capacity, then the two-machine

representation is to be adopted. But if the rating of the generator is small compared to the system capacity, then it becomes advantageous to equivalence the 2-machine system into one machine connected to an infinite bus through a series impedance. The circuital representation of a one machine system is given in fig. 6

12. The reactance& time constants of synchronous machines

Neglecting the small effect of resistances in the equivalent circuit, the following expressions have been found out for the p.u. reactance and time constants of a synchronous machine [4,11]

From,
$$X_{a} = X_{1} + X_{md} \updownarrow X_{f}$$
; $\updownarrow \rightarrow in parallel$

15

we get: $\mathbf{x}_{\mathrm{f}} = \left(\mathbf{X}_{\mathrm{d}} - \mathbf{X}_{\mathrm{d}}^{'}\right) / \left\{\mathbf{X}_{\mathrm{md}}\left(\mathbf{X}_{\mathrm{d}}^{'} - \mathbf{x}_{1}\right)\right\}$

where, X_d = d-axis transient reactance and x_f = field leakage reactance.

From,
$$X_d'' = X_1 + X_{md} \updownarrow X_f \updownarrow X_{kd}$$

we get:

$$\mathbf{x}_{kd} = \mathbf{x}_{md} \mathbf{x}_{f.} (\mathbf{X}_{d}^{"} - \mathbf{x}_{1}) / [\mathbf{X}_{md} \mathbf{x}_{f} - \mathbf{X}_{f} (\mathbf{X}_{d}^{"} - \mathbf{x}_{1})]$$
18

where, $X_d^{"} = d$ -axis subtransient reactance and x_{kd} = d-axis damper leakage reactance.

From,
$$X_q^{"}=x_1+x_{mq} \mathop{\updownarrow} x_{kq}$$
 19
$$x_{kq}=\left(X_q-X_q^{"}\right)/\left\{X_{mq}\left(X_q^{"}-x_1\right)\right\}$$

where, $X_q^{"} = q$ -axis subtransient reactance and $x_{kq} = q$ -axis damper leakage reactance.

From,
$$T_{do}^{'}=X_{_{\rm f}}/(\omega_{_{\! 0}}r_{_{\! f}})$$
 21 we get:
$$r_{_{\! f}}=X_{_{\! f}}/(T_{do}^{'}\omega_{_{\! o}})$$
 22

where, T_{do} = d-axis O.C. transient time constant and r_f = field resistance.

The corresponding short circuit time-constant is given by:

$$T_{d}^{'} = T_{do}^{'} X_{d}^{'} / X_{d}$$

$$23$$
From
$$T_{do}^{"} = (x_{kd} + x_{f} | X_{md}) / (\omega_{o} r_{kd})$$

$$24$$

we get:
$$r_{\rm kd} = \left(x_{\rm kd} + x_{\rm f} X_{\rm md} / X_{\rm f}\right) / \left(\omega_o T_{do}^{"}\right)$$
 25

where, $T_{do}^{"}$ = d-axis subtransient time constant and r_{kd} = d-axis damper resistance.

The corresponding short circuit time-constant is given by:

$$\begin{aligned} \textbf{T}_{d}^{"} &= \textbf{T}_{do}^{"} \textbf{X}_{d}^{'} \ / \ \textbf{X}_{d}^{"} \\ & \textbf{26} \\ \textbf{From,} & \textbf{T}_{qo}^{"} &= \textbf{X}_{kq} / \left(\omega_{\text{o}} \textbf{r}_{kq} \right) \\ & \textbf{27} \\ \textbf{we get,} & \textbf{r}_{kq} &= \textbf{X}_{kq} / \left(\textbf{T}_{qo}^{"} \omega_{\text{o}} \right) \\ & \textbf{28} \end{aligned}$$

where, $T_{qo}^{"}$ = q-axis O.C. subtransient time constant and r_{kq} = q-axis damper resistance.

The corresponding S.C. time constant is given by:

$$T_{q}^{"} = T_{qo}^{"} X_{q}^{"} / X_{q}$$

The manufacturers' data of a synchronous machine gives the synchronous, transient and subtransientreactance and the time-constants. Other reactance of the equivalent circuit used in the state space model can be calculated by using the above formulae. The reactance and time constants are modified if the generator is conceived to operate on an infinite bus through a series impedance.

13. Transfer function vs. state space approachsuperiority of state space

The block diagram and transfer function approach [13] (or the signal flow graph) gives the input/output relationship of a system or the free response but it cannot take care of initial conditions prior to a disturbance. It is also incapable of dealing with non-linear functions. But the state space approach can deal with both linear and non-linear functions and can account for the initial conditions. It is also capable of dealing with inter-relation of variables within the system.

The transfer function approach also has some advantages. It provides more local information. It is important as it can give information about inputs which affect inter-area modes of oscillation and it can operate on measured system data without the need for any modelling.

Parameters and functions of a generator are interrelated in a complex way. To analyse such a system, it is essential to reduce the complexity of the mathematical expressions. From this point of

view, state space approach to system analysis is best-suited.

14 The classical model- a critical estimate

Electrical machines play the main role in a power system, of which synchronous generators are most important. Rotating electric machinery is characterized by time-varying inductances, which makes the differential equations of such machines non-linear. Before the invention of computers it was not possible to solve differential equations with time-varying coefficients. Therefore, the alternator was represented by a voltage source behind an appropriate reactance and the swing equations were solved by iterative methods. The concept of idealized system, of one machine on infinite bus and of two machine system were frequently used.

G.Kron advanced the concept of basic machine and R.H.Park [9] that of transformed machine in the early decades of the 19th. century. conceptualization revolutionized the field modeling. By a kind of tensorial reasoning G.Kron evolved the concept of basic machine and its associated equivalent circuit. R.H.Park proposed the d-g axes reference frame which enabled us to reduce the time-varying inductances to their nontime-variant form. Park's reference frame yielded a differential equations of with constant coefficients in terms of a set at transformed variables. These equations could be easily solved. The transient solution in terms of actual variables could be obtained by applying Park's transformation [9]

Later on, Charles Concordia and Bernard Adkins made outstanding contribution to the field of analytical studies on synchronous machine [4]. They developed the so called classical model of the synchronous machine in d-q reference frame. B. Adkins proposed the generalised machine theory. His approach to short-circuit and transient analysis of rotating electrical machines got universal acceptance. The classical model is based on simplifying assumptions & approximations, some of which are given below:

- i). Time & space harmonics are neglected.
- ii). Saturation & other non-linearities are neglected.
- iii). Distributed parameters are replaced by their lumped equivalents

In its most simplified form the amortisseur winding is represented by a single coil per axis. In

this reduced form, dimension of the machine impedance matrix is five and that of the motional impedance matrix is seven, which includes the effect of inertia and damping.

The classical model has been modified by many authors to include the secondary effects of saturation, partial linkage between damper and field winding, and distributed eddy currents in solid iron parts. It has the following drawbacks:

- i) It cannot solve the back-swing phenomenon.
- ii) It can deal with asymmetric loads but not with an asymmetric machine.
- iii) It fails to account for induced eddy currents in solid iron very accurately.

In spite of these drawbacks, the classical model is popularly used for its simplicity. Coherent group of generators, during a swing, are equivalenced into a single machine and the network is reduced to important load-nodes, before we apply the classical model. For convenience, all parameters and quantities are transformed to a standard 100-MVA or 500 MVA base.

15 State space equation

Reducing the governing differential equations of a system to their normal form [13], the following expressions are obtained:

$$X_1 = f_1(X_1, X_2, \dots, X_n, u_1, u_2, \dots, u_m, t)$$

 $X_2 = f_2(X_1, X_2, \dots, X_n, u_1, u_2, \dots, u_m, t)$

$$X_{n} = f_{n}(X_{1}, X_{2}, \dots, X_{n}, u_{1}, u_{2}, \dots, u_{m}, t)$$
30

or in a compact form:

$$X = f(X,u,t)$$

where, **X** = a vector of state variables, **u** = the system driving functions

f = a set of non-liner functions,

t = time

If the equations are linearized about the operating point, the equation reduces to the following form:

$$X = A.X + B.U$$

where, \mathbf{A} is a (n x n) matrix and B is a (n x m) matrix. The state variables describe the dynamic states of the system.

The above equations constitute a set of first order differential equations in the state space form.

The state variables are not unique- there are numerous possibilities for the choice of state variables. For representing electrical machines, generally we choose any one of the following:

i) A set based on the currents as state variables,

i.e.
$$X^T = \begin{bmatrix} i_d & i_q & i_F & i_{KD} & i_{KQ} \end{bmatrix}$$
 32,

 i_d , i_q : d & q axis components of the where, armature current; i_F: field current

ikd, ikg: d & q axis components of the damper current.

This method has the advantage of offering simple relations in terms of the voltages \mathbf{v} and the state

ii) A set based on flux linkages as state variables,

i.e.
$$X^{T} = (\lambda_d \ \lambda_f \ \lambda_{kd} \ \lambda_q \ \lambda_{kq})$$

33

 λ_d , λ_q : d & q axis armature flux-linkages; λ_f : field flux linkages;

 λ_{kd} , λ_{kq} : d & q axis damper flux-linkages. The set to be chosen depends upon the particular field of study.

16 Current state space model of the alternator:

The matrix model for a machine in terms of normalised quantities in Park's reference frame [10]

												is
V		ra			ω		ωLmc	1			i _d	given
d					Lq							as:
-			r _f							X	İf	
V	L	L	nd	L_{md}					1		: 1 _d	
f	d								Ц		u .	
Q	L	L _f		[kdd							$rac{1}{1}_{ m f}$	
V	m d	-	-	-	ra				T		İq	Using
q	L	ωLr	ω_{pr}	$\underline{\omega}_{kd}$					11		: 1 _{kd}	matrix
	m	L	L	L					Ш		kd	notati
	d	d	md	md					Ш			on :
0						l	rkq	L _{mq}		F	i I _k	[V]
					_	_	7	.	4]	L	*q	= -
			•			t	-mq	L_{kq}	ľ		i _{kq}	(R +
		-			!			<u> </u>		_		ω N) [i]

 \mathbf{R} = Resistance matrix; \mathbf{N} = Matrix for speed voltage inductances, **L** = Inductance matrix Therefore, we get:

$$[i] = -[L]^{-1}(\mathbf{R} + \omega \mathbf{N})[i] - [L]^{-1}[\mathbf{V}]$$
 p.u.

This equation is in the required state space from and is used for transient analysis. Additional

equations are to be added now to include the effects of inertia & damping.

17 Normalizing the swing equation

Normalising the swing equation the following expression is obtained [11]:

$$\frac{2H}{\omega_{R}}\frac{d^{2}\delta}{dt^{2}} = T_{m} - T_{e} = \tau \frac{d\omega}{dt}$$

36

The electrical torque is given as:

$$T_{_{e}}=\!\left(1/\,3\right)\!\left(i_{_{q}}\lambda_{_{d}}-i_{_{d}}\lambda_{_{q}}\right)$$
 , where

$$\lambda_{d} = X_{d}i_{d} + X_{md}\left(i_{f} + i_{kd}\right) ; \lambda_{q} = X_{q}i_{q} + X_{mq}i_{kq}$$
27

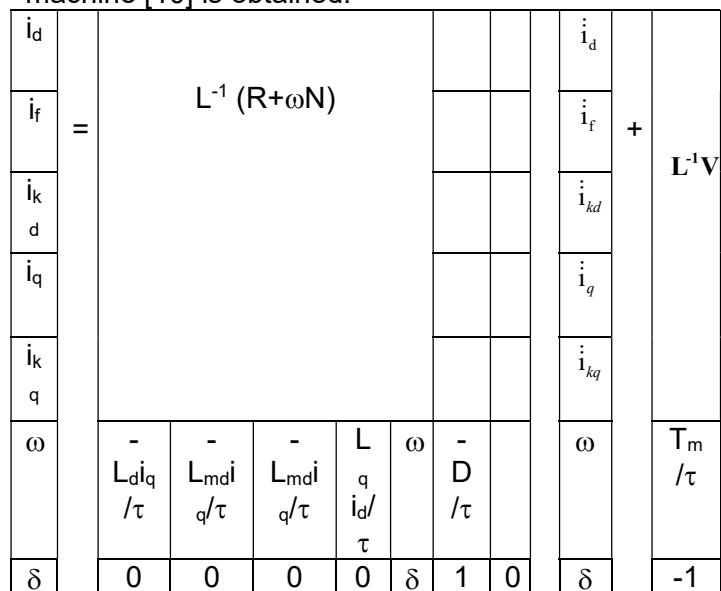
Including the damping coefficient **D**, for greater accuracy, the swing equation becomes:

$$T_a = T_m - T_e - T_D = T_m - T_e - \omega D$$

18 Inclusion of mechanical parameters in the current state space model

Including mechanical parameters, the following motional state space model for the synchronous

machine [10] is obtained:



where,
$$\tau = 3\tau_j$$

39

It is in the desired state space form: X = f(X,u,t). The inputs are [V] & T_m. It is known as the current state space from. This model has product nonlinearities. An alternative approach is to use flux linkages as state variables.

Flux linkage state space model of the alternator- the alternative approach

International Conference On "Impact of Changing Energy Mix in the Power Sector"(ICIEMPS-2019) The Institution of Engineers (India), WBSC 23rd & 24th Nov. 2019

An alternative approach [10] is to use the flux linkage state space model. In this model the state variables are: $\mathbf{X}^T = (\lambda_d \ \lambda_f \lambda_{kd} \lambda_q \ \lambda_{kq})$

40.

where, λ_{d} , λ_{q} = d-axis/q-axis armature flux-linkage

 λ_{kd} , λ_{kq} = d-axis/q-axis damper flux-linkage

 λ_f = field flux-linkage

A similar expression may be obtained by mathematical manipulation [10].

6.21 Linearization under small perturbation:

a) Current state space model:

If the state vector has an initial value of X_0 at time t_0 and the perturbation is X_{Δ} , then we get after linearization [10]:

$$X_{\Delta} = A(X_0)X_{\Delta} + B(X_0)U$$

42

The elements of the **A**-matrix depend on the initial value of the state vector X_0 , held fixed for a specific case study, and the infinite bus constraints. The dynamic behaviour of the system is dictated by the eigenvalues of the state matrix. The operating conditions define a hyper-plane in n-dimensional hyper-space of the state variables. By linearizing the non-linear current state space model, we get the following form:

$$V = -KX - MX$$

43

The state equation for the synchronous generator not including the load equation is given as:

$$X = -(M^{-1} K) X - M^{-1} V = AX + BU$$

This is the required state space form. The expressions for the elements of **M**-matrix and **K**-matrix for an alternator directly connected to infinite bus are given below:

M =

141—						
L _d	L _{md}	L _{md}	()	()
L _{md}	L _F	L _{md}				
L _{md}	L _{md}	L_D				
	0		Lq	L _{mq}	()
			L _{mq}	Lq		
	0		()	-T _j	0
					0	1

K=

R	0	0	$\omega_{o}L_{q}$	$\omega_{o}L_{mq}$	λ_{qo}	-Kq
0	r _F	0	0	0	0	0
0	0	r_{D}	0	0	0	0
- ω _o L _d	- ω _o L _{md}	- ω _o L _{md}	r	0	- λ _{do}	K _d
0	0	0	0	r _Q	0	0
(λ _{qo} -	-	-	(L _d .i _{do} -	L _{mq} .i _{do} /3	D	0
L _d .i _{qo})/3	L _{md} .i _{qo} /3	L _{md} .i _{qo} /3	λ _{do})/3			
0	0	0	0	0	-1	0

Where, infinite bus constants

$$K_d = -\sqrt{3}.V_{\infty}. \sin \delta_o$$

47(a)

$$K_q = \sqrt{3}.V_{\infty}. \cos \delta_0$$

47(b)

b) Flux-linkage state space model:

By similar treatment on the non-linear flux-linkage model, we get the following form by algebraic manipulation [10]

$$TX = CX + D$$

or $X = (T^{-1}C)X + T^{-1}D = AX + BU$
48

This is in the required state space form. The expressions for the elements of **A**-matrix and **B**-matrix may be obtained by algebraic manipulations as in the earlier caseand have been given in ref.

22 Case study 1

The methods suggested by Mazumdar, Ghosh, Sanyal etc. is being followed for computing the results (14,15,16]. A modern turbogenerator of rating 120 MW, 11 KV, 50 Hz is under consideration (Santaldihi TPS). The parameters, time constants and the variables pertaining to the machine at operating conditions are given below:

The d-axis synchronous reactance, $X_d = 1.7$ p.u. The q-axis synchronous reactance, $X_a = 1.64$

p.u.

The d-axis transient reactance, X_d = 0.244

The d-axis subtransient reactance, $X_d^{"} = 0.185$

The d-axis transient time constant, $T_a = 1.016 \text{ s}$

The d-axis subtransient time constant, $T_d^{"} = 0.0274$

s

The q-axis subtransient time constant, $T_q^{"} = 0.0102$

We make dynamic stability analysis of the alternator for a small perturbation neglecting the effects of exciter and governor control. The boundary conditions are mixed. The solution is being made by iterative procedure. Given:

The infinite bus voltage V_{inf} = 1.0 The generator power, P = 0.85 p.u.; The generator power factor = 0.85 (lag) The generator terminal voltage, V_g = 1.1723 Phase angle w.r.t infinite bus = 19.31°;

The axis components of currents and voltages (in p.u.):

Power angle = 34.43°

Elements of the state matrix using current state space representation for the given operating conditions are given below:

Λ.	7	7)	*1	ın	Λ	n	_
A		/			u		=

$A(7,7)^{\circ}$	1000 =					
-	0.44	14.1	-	-	-	1752
36.0	0	31	3489	2548	2445	.3
81			.0	.4	.9	
12.5	-	77.7	1210	884.	848.	-
16	4.99	22	.3	02	47	607.
	9					86
22.7	4.40	-	2200	1607	1542	-
57	2	96.8	.6	.3	.7	1105
		68				.2
3588	2648	2648	-	90.1	1776	2386
.8	.9	.9	36.0	07	.2	.6
			52			
-	-	-	35.2	-	-	-
3504	2586	2586	02	123.	1734	2330
.2	.4	.4		37	.3	.3
-	-	-	-	-	0.00	0.00
0.00	0.20	0.20	0.79	0.44	0	0
8	3	3	9	2		
0.00	0.00	0.00	0.00	0.00	1000	0.00
0	0	0	0	0	.0	0

Characteristic equation of the matrix has been found out by Fadeev-Leverrier method. The characteristic polynomial of the matrix is given below:

```
x^7 + 0.29737 x^6 + 1.0279 x^5 + 0.22621 x^4 +
1.384532e-02 x^3 + 2.331442e-04 x^2 + 1.026837e-05
x + 3.074246e-08 = 0
```

The real roots have been found out by Newton-Raphson method and the degenerate equation by algebraic division. The real roots are given below: R(1) = -3.1826e-03 ; R(2) = -0.12241 ; R(3) = -9.873e-02

The complex roots are being found out by Lin-Bairstow' method

Complex pair(1): $-5.7606e-04 \pm j \ 2.8296e-02$ Corresponding frequency of oscillation in Hz.= 1.698; damping ratio= 4.605

Complex pair(2): -3.5948e-02 ± j .99826 Corresponding frequency of oscillation in Hz.= 59.9 ; damping time const.= 7.379e-02

The system is stable as there is no positive real root or no root having positive real part.

Case-study 2

Now another estimate of dynamic stability is being made using flux-linkage state space model for a 210 MW alternator. Stability analysis has been made both by eigenvalue technique and by Routh's criterion. The parameters are given below:

The d-axis synchronous reactance, $X_d = 2.225$ p.u.

The q-axis synchronous reactance, X_q

2.11p.u.

The d-axis transient reactance, X_d = 0.305

The d-axis subtransient reactance, $X_d^{"} = 0.214$

The d-axis transient time constant, T_d = 1.0 s

The d-axis subtransient time constant, $T_d^{"} = 0.125 \text{ s}$

The q-axis subtransient time constant, $T_q^{"} = 0.06 \text{ s}$

The boundary conditions are given at generator terminals.

The generator rated power = 210 MW; The generator rated voltage = 15.75 KV

The generator power P = 0.85p.u.; The generator power factor (lag) = 0.85

The generator terminal voltage $V_g = 1.0$; The infinite bus voltage $V_{inf} = 0.9307$

Phase angle w.r.t inf. bus = -7.0030°; Power angle = 40.307°

The axis quantities for the voltages and the currents are given below:

 V_d = -0.6469 V_q = 0.7626 I_d = -0.9516 I_q = 0.3074 E= E_{fd} = 2.8804 I_{fd} = 2.4067 Infinite bus constant, K= 1.6121

Elements of State-Matrix A(7,7)*1000:

-	9.44	6.162	-	246.2	-	667.
16.4	12	8	878.	8	730.	16
28			42		18	
1.78	-	2.601	0.00	0.000	0.00	0.00
33	4.51	3	00	0	00	00
	54					
12.7	11.7	-	0.00	0.000	0.00	0.00
88	66	25.49	00	0	00	00
		17				
1138	-	-	1.17	-	762.	823.
.4	166.	263.8	17	3.707	04	34
	43	6		8		
0.00	0.00	0.000	59.0	-	0.00	0.00
00	00	0	78	63.66	00	00
				38		
0.59	0.25	-	-	0.495	0.00	0.00
88	00	0.396	0.74	6	00	00
		4	86			
0.00	0.00	0.000	0.00	0.000	1000	0.00
00	00	0	00	0	.0	00

The characteristic equation of the matrix is being found out by Fadeev-Leverrier method. The characteristic polynomialis given below:

 $x^7 + 0.10893x^6 + 1.0045 x^5 + 7.399E-02 x^4 + 2.3252E-03 x^3 + 6.1547E-05 x^2 + 8.4629E-07 x + 8.1277E-10 = 0$

Stability analysis is being made by Routh's criterion. The Routh's tabulation is given below:

1.0000000000000	1.0045360000000
0.0023251500000	0.0000008462933
0.1089272000000	0.0739918900000
0.0000615473300	0.0000000008128
0.3252573000000	0.0017601180000
0.0000008388317	
0.0734024400000	0.0000612664100
0.0000000008128	
0.0014886370000	0.0000008352302
0.0000200824800	0.0000000008128
0.0000007749825	

The system is stable as all elements in the first column are positive.

The real roots are being found out by Newton-Raphson method.

r(1)=-1.0354e-03 ; r(2)=-2.3262e-02 ; r(3)=-4.2517e-02

Complex roots are being found out by Lin-Bairstow' method

Complex pair(1): $-3.5313e-03 \pm j \ 2.7956e-02$ Corresponding frequency of oscillation in Hz.= 1.3978; damping ratio= 0.9014

Complex pair(2): -1.752522e-02 ± j 0.99966 Corresponding frequency of oscillation in Hz.= 49.98; damping time const.=0.1816

The system is stable as there is no positive real root or no root having positive real part.

23 Conclusion

Mathematical modeling of a system is essential to understand the behaviour of a system and topredict its performance. Modeling of the synchronous generator is the most difficult part in this exercise. The general approach is to use Park-Gorev transformation to reduce the machine into a no. of coupled coils along d-q axes. It makes the model simple and tractable. It also reduces the computer run-time and memory space requirement.

Under many kinds of disturbance, a no. of synchronous generators swing together similarly. Such a group of swinging machines is called a coherent group. To reduce the dimension of the resulting model, the coherent group can be represented by a single large machine with equivalenced parameters.

The block diagram and transfer function approach, once popular, has some major limitations. Such limitations are absent in the state space method. Hence, state variable model has been used. Two types of state variables are in common use viz. the current state variables and the flux linkage state variables. The state variable model must include the effects of mechanical parameters of inertia and damping, the effects of the turbine (and boiler, if any), ant preferably the secondary effects of saturation etc.

The electromechanical transient of a turbinegenerator is described by its swing equation. Usually, the parameters are in per unit system and the time constants are in second. In earlier days, the mechanical power input and the voltage behind transient reactance were assumed to be constant during swings. But now-a-days a more accurate description is obtained through state space approach.

The state space model for analysis of electromechanical transients is non-linear. For small

perturbation, the model is linearized about the quiescent point. The eigenvalues of the linearized state vector determine the stability conditions. This model has not included the effect of exciter control [17,18] which may be give more accurate result as the AVR-exciter dominantly control the power angle swing.

Reference:

- 1. J. Y. Fan., T. H. Crtrneyer, R. Mukundan, "Power system stability", IEEE Trans. on Power System, Vol. 5, No. 1, pp. 227-233, Feb. 1990.
- 2. W. Stagg and A. H. El-Abied, "Computer methods in power system analysis", McGraw-Hill Book Company, New York, 1968.
- P. Kundur, "Power system stability and control", McGraw Hill, 1994
- 4. B. Adkins and G. Harley, "Generalized theory of A.C. Machines", Book, Chapman & Hall.
- 5. K.R. Padiyar (IIT, Bangalore), "Power system dynamics", 2008, ISBN: 1 904798 012
- 6. F. Selwa, L. Djamel, "Transient stability analysis of synchronous generator in electrical network", International Journal of Scientific and Engineering Research, Vol. 5, Issue 8, August-2014, ISSN 2229-5518 IJSER © 2014
- 7. M. Pavella, P.G. Moorthy, "Transient stability of power systems: Theory and practice", Scitech, 1994
- 8. P. Kundur and P.L. Dandeno, "Implementation of advanced generator models into power system stability programs", IEEE Trans., Vol. PAS-102, July'83
- 9. R.H. Park, "Two reaction theory of synchronous machines", Pt. 1, AIEE Trans. Vol-48, 1929; Pt. 2, AIEE Trans. Vol-52, 1933.
- P.M. Anderson and A.A. Fouad, "Power system control and stability", IOWA State University Press, Galgotia Publications, 1977
- 11. V.A. Venikov, "Transient processes in electrical power sysrems", MIR publication, 1977
- 12. D.P. Kothari, I.J. Nadrath, "Power system engineering", 2nd. Ed, TMH
- 13. K. Ogata, "State space analysis of control systems", Book, Prentice-Hall, Englewood Cliffs, N J, 1967.
- 14. T.K. Majumdar, A.N. Sanyal, B. Majumdar, Dynamic stability analysis of remote hydel power station connected to infinite bus through long transmission line- Indian Journal of Power and River Valley Development, Vol-50, No- 384, March-April' 2000.

- 15 T.K. Majumdar, A.N. Sanyal, Reduced order model of a captive power plant for dynamic stability analysis, VidyutBharati, No. 4, Vol. 23, Jan.-Mar' 2001
- 16. A. Ghosh, A. Das, A.N. Sanyal, Transient Stability Assessment of an Alternator connected to Infinite Bus through a Series Impedance using State Space Model, J. Inst. Eng. India, Series. B, March'2019
- 17. F.P. Demello and C. Concordia, "Concepts of synchronous machine stability as affected by excitation control", IEEE Trans., Vol. PAS-88, April'69
- 18. C. C. Young, "Computer representation of excitation system", IEEE Transaction on Power Apparatus and Systems, Vol.-PAS-87, No.6, June 1968, p.-1460.

Opportunities for ergonomics design interventions associated with installation and maintenance of solar PV panels

Abhijit Sen¹, Akshay Mohankar² and Sougata Karmakar²

¹Damodar Valley Corporation, VIP Road, Kolkata-700054, West Bengal, India

²Department of Design, Indian Institute of Technology (IIT) Guwahati, Guwahati 781039, Assam, India

{Corresponding author's email: abhijit.sen@dvc.gov.in}

Abstract

The United Nations Framework Convention on Climate Change (UNFCC) aims to keep global warming below 1.5 °C and thus countries are gradually shifting towards Renewable Energy (RE). 7 lakh people are directly or indirectly engaged in this sector in India. New technologies, tools, work methods, materials and skill sets results in a mismatch between the worker and the job, exposing the workers to multiple hazards.

The current exploratory study aims to focus on the opportunities for ergonomic design interventions associated with the installation and maintenance of solar PV panels to ensure better Occupational Health & Safety (OHS) of workers.

Research papers were reviewed to explore the existing ergonomic interventions adopted for the proper OHS of the workforce and future scope from an ergonomic perspective.

It was revealed that the workforce is exposed to various hazards which include falls from heights, electrocution, unfavorable microclimate conditions, musculoskeletal disorders, exposure to toxic chemicals &nanomaterials and burns. No studies were found which considered the ergonomic

factors orwhich provided ergonomic design solutions to remove the hazards.

Future scope may include adopting an ergonomic approach in order to design out the hazards.

Keywords: climate change; renewable energy; risk factors; occupational health; safety;

1.Introduction

In 2018, the United Nations Secretary-General emphasized the need for adopting a goal to keep global warming below 1°Cin line with the Intergovernmental Panel on Climate Change (IPCC) Special Report [1], which recommends net zero emissions by 2050. This reportalso indicated that failing to meet this target would bring risks which is likely to harm the health, livelihoods, food security, water supply, human security and global economic growth.

1.1 Transition to Renewables

Climate change concerns have prompted countries to harvest renewable sources of energy from solar, wind, geothermal bio mass/gasetc. to reduce the carbon footprint. A major percentage of this renewable energy is slated to come from Solar PV installations of different kinds. The International Energy Agency (IEA)

estimates that roughly 6000 TWh of PV electricity will be generated from solar PV in 2050, which is roughly 16% of the total global electricity demand [2].

1.2 The Indian Scenario

As on August 2019, the renewable energy capacity of India is more than 80.6 GW, which is 22% of the total installed capacity [3]. India has committed to generate 40 per cent of electricity from non-fossil fuel-based energy resources by 2030[4]. Harvesting of energy from various renewable sources are opening new job opportunities in the RE sector which currently employs more than 7 lakh people directly or indirectly in India [5].

1.3 Impact on the Occupational Health & Safety of workers

The technology, tools, work methods, materials and required skill sets are new. This results in a mismatch between the worker and the job, potentially exposing the workers to multiple hazards. These hazards can lead to injuries/accidents which have both human and economic costs. Tveiten et al. (2011) identified ergonomics issues related to the installation and commissioning of offshore wind power as physiological effects due to heavy lifting, repeated movements and uncomfortable working positions; work at height; slippery surfaces and psychological effects due to poor working and living conditions [6].

The present paper focuses on the solar PV industry which forms the largest share of RE and include the manufacturing, transportation, installation, maintenance and decommissioning of solar PV systems. Installation and maintenance are performed by locally hired casual labourers in an unorganized/ informal fashion leading to compromising of occupational health and

increased risk of accidents. Therefore, the workplace health and safety of the workers engaged in this segment must be considered favourably.

2. Objective of the Review

To delimit the research scope and go into the deep, current exploratory study mainly focuses on the opportunities for ergonomic design interventions associated with the installation process of solar panels to ensure better Occupational Health & Safety (OHS) of the workers.

The aim of the current research is to explore the opportunities for ergonomic design interventions for OHS of workers engaged in the Solar Photovoltaic (PV) industry.

3. Review Methodology

A systematic literature search was conducted using the online databases of Google Scholar and Science Direct to shortlist papers using suitable search terminologies(Table 1) associated with different aspects of OSH issues in the Solar PV industry. The search was limited to articles in the English language published between the years 1980 to 2019. After completing the search in the online databases, all the papers were uploaded into a database manager and all duplicates were removed.

For a manuscript to be included among the shortlisted papers, the paper was required to have at least the keyword(s) or one of the keyword combinations in its title or abstract. The manuscripts were carefully studied to include only those papers fulfilling the criteria, that, the manuscripts must contain studies reporting the prevalence of OHS risks among Solar PV installers and maintenance workers, psychosocial and

environmental risk factors and ergonomic design interventions to address the risks if any.

Table 1: Search terms used in the review

Keywords	Keyword combinations
Solar PV	Solar Photovoltaics +
	psychosocial, environmental,
	occupationalhealth and
	safety factors& training,
	green jobs
Ergonomics	Ergonomic interventions +
-	Solar PV
Design	Design + Solar PV

The online search resulted in the shortlisting of 41papers. The full papers and abstracts were read, and divided into fivebroad headings naming solar PV installations, occupational risks/hazards for workers engaged in the Solar PV industry, psychosocial factors affecting such workers, availability of training modules and existence of ergonomic design interventions to address the risks. The future scope for each paper was also studied.

In addition to the review of existing research, preliminary field studies were carried out to explore the risks faced by the workers and photographs were obtained [Figures 2 (a) to (d)].

4. Literature Review Outcomes

4.1 Types of Solar PV installations& their functioning

The different types of solar PV installations can be classified into ground mounted, roof top, canal top, offshore and floating (Fig 1). Photovoltaic systems use

cells to convert solar radiation into electricity. The sunlight creates an electric field across the layers of a semiconducting material which produces an electric direct current. A power inverter transforms the direct current into alternating current. The conversion of radiation is based on a physical effect and cannot be switched off [7].

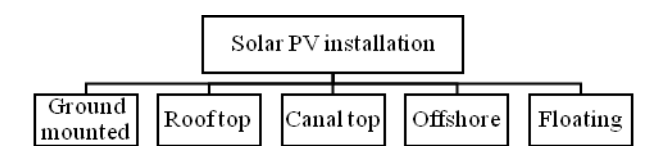


Figure 1: Classification of Solar installations [8]



Figure 2 (a) Workers engaged in installation of floating solar PV



Figure 2 (b) Workers exposed to ergonomic risks while carrying solar PV panels



Figure 2 (c)Work in confined spaces, awkward postures and lack of PPE are potential hazards



Figure 2 (d) Roof top installations exposes workers to risks of fall from heights and injuries from sharp edges of solar panels/frames

4.20SH risks associated with installation and maintenance of Solar PVs

Figures 2 (a) to (d) depict some of the postures and working conditions that workers engaged in solar PV are exposed to. Installation and maintenance of Solar PV involves several OSH related risk factors. There are potential occupational risks from arsenic and cadmium. Silicosis is a potential hazard in the photovoltaics industry which is entirely preventable [10].

Schulte et al. [11] reported that thin-film photovoltaics contain chemical agents such

as Silane which is pyrophoric affecting the respiratory tract & skin and hydrogen sulphidewhich is an acute irritant affecting the Central Nervous System. Falvo et al. [12] found that presence of Direct Current (DC) in the Solar PV system can lead to electrical faults and fire. He indicated that this risk can be ameliorated by installing multiple small inverters.

A study by Bakhiyi et al. [13]revealed that the risks associated with the PV industry are likely to occur at each step of the PV system life cycle. Installation & maintenance and dismantling of PV systems present safety risks from physical agents essentially associated with accidents and injuries. Some findings are summarized in Table 2.

Table 2: Main physical risks related to PV systems installation, major sources and some example of aggravating factors. Adapted from [13].

Major Physical risk for workers	Some major causes
Ergonomic risks	Awkward body postures, repetitive movements and confined spaces during PV panels installations (e.g. handling and carrying heavy loads& lack of PPE)
Fall from heights	 Working at heights, on slopes, from scaffolding; climbing ladders etc.
Falling objects	 Collapsing surfaces under workers' weight (PV panels, roof, structural components, etc.)
	 Unwieldy equipment (e.g. handles, harnesses)

International Conference On "Impact of Changing Energy Mix in the Power Sector"(ICIEMPS-2019) The Institution of Engineers (India), WBSC 23rd & 24th Nov. 2019

Electric	Direct current (DC)
Shock	arching
Electrical	Electrical work on AC
burns	and DC circuits (PV
	panel serial connection)
Thermal	 Excessive heat from PV
burns/Heat	panels/working in hot
Stress	and humid conditions

PV systems present electrical risks if the electrical system is compromised or the protective coverings on the components are damaged. The typical voltage, in the range of 600 volts, can cause electrical shocks (electrocution) or electrical, thermal and arc burns [14]. OSHA recommends the implementation of "Lockout/Tagout (LOTO)" which are specific procedures to safeguard workers from the unexpected energization or start-up of machinery and equipment. LOTO also prevents the release of hazardous energy [15].

[16] Another major cause of job hazard/fatalities is the use of crane during installation and maintenance. The source of risks includescrane boom and load line touching power lines.

4.3 Effects of Heat/Cold stress

Adverse weather conditions such as extreme temperatures present further risks such as cold or heat stress. Exposure to sun radiation may lead to sunburns, eye disorders and certain types of cancers. Rain or snow may result in slippery surfaces and lead to slips and falls. Workers mainly during the day in very hot weather. The hazards include dehydration, heat exhaustion, heat stroke, and death[17].

4.4Psychosocial risk factors

A study found that relative to non-green collar workers, green collar workers were

more likely to report job insecurity and worklife imbalance but less likely to experience workplace harassment [18].

4.5Training

The lack of skilled installers' workforce for the installation and maintenance may result in technical failures of the installed PV/BIPV systems [19]. Therefore, adequate training important for Solar critically installers. The PVTRIN (Training of PV installers) under the aegis of the European Union (EU) is a training and accreditation scheme for technicians/engineers engaged inthe installation and maintenance of small scale PV systems [20]. Shortage of skilled workers in the RE industry is likely to result in low-skilled workers being pushed into accepting poor working conditions and unstructured jobs [21].

5. Literature Review outcomes& Problem Statement

The review revealed that the workforce is exposed to various hazards which include falls electrocution. from heights. unfavourable microclimate conditions, musculoskeletal disorders, exposure to toxic chemicals & nanomaterials and burns. Hanson et al. [22] informs that materials used in the manufacture of solar panels are known to be harmful to health. Protecting the health of workers involved in their manufacture, maintenance and decommissioning can be supported by Ergonomics/Human Factors professionals through the design of appropriate PPE and safe systems of work. This knowledge can also be applied to protect workers involved in installation of solar panels in areas of high temperature and excessive sunlight.

No studies were found which considered the development of ergonomic design solutions

International Conference On "Impact of Changing Energy Mix in the Power Sector"(ICIEMPS-2019) The Institution of Engineers (India), WBSC 23rd & 24th Nov. 2019

for OSH of the workers engaged in the process of different types of solar PV panel installations and maintenance for ensuring a safe workplace.

The existing literature also did not reveal any OSH interventions to address the risks for the Indian worker population engaged in the solar PV value chain. The risks for workers engaged in solar installations may also vary from type of installation, climatic conditions, safety culture/policies, worker related issues, work methods, and location of projects. Hence, the importance of considering and developing context specific design interventions.

Table 3. Occupational risks of workers engaged in solar PV installation & maintenance and future scope based on the present review

	Existing/Sug	
Risks	gested Solutions	Future scope
Fall from heights	PPE	Matching PPE with workers and context + safety training
Falling objects	PPE	- Do -
Ergono mic hazards	Hazard prevention manual	Ergonomic Design interventions/co de + training
Psychos ocial	None	Job redesign/manag ement policies/better working conditions
Fire	Use of multiple inverters	PPE + installation of firefighting equipment
Electric Shocks	Safety manual	Design solutions such as visual cues and PtD

		principles
Chemical	None	Sustainable/environment friendly manufacturing
Lack of trained manpow er	Limited training resources	Comprehensive training modules for all types of solar PV such as floating solar/offshore etc.

6. Opportunities for Ergonomic Design Interventions & future scope

Behm [23] established a clear link between construction fatalities and the design for construction safety concept. He reviewed 224 fatality investigation reports which showed that 42% of fatalities were linked to the concept which states that the associated risk that contributed to the incident would have been reduced or eliminated had the design for construction safety concept been utilized.

[24] Some researchers have developed a safety protocol for workers engaged in solar installations(roof top) from the perspective of Prevention Through design (PtD). The limitation of the project is that it makes safety suggestions based on OSHA regulations and does not attempt to develop and test context specific design interventions from the ergonomic perspective. A solar construction safety manual [25] has been developed by the Oregon Solar Industries Association which contains guidelines to minimize workplace hazards. However, it is felt that designing out hazards completely can only be possible through PtD principles. Figure 4 indicates

some controls that employers/contractors can adopt to address the risks.

Hierarchy of Controls

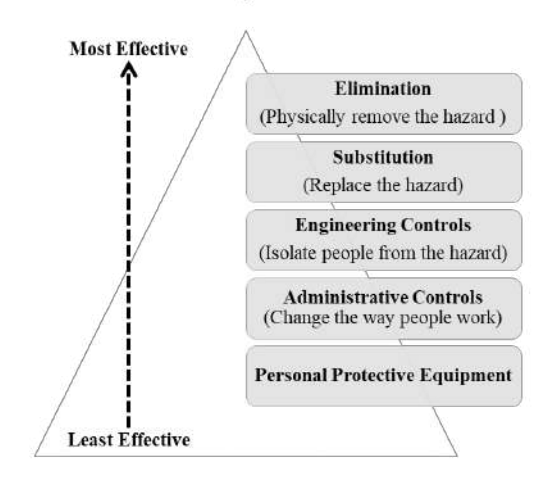


Figure 4: Hierarchy of controls. Adopted from [26]

Ergonomic design interventions w.r.t installation and maintenance of solar PV can consider a) Design of solar PV module and allied components from an ergonomics perspective b) context/population specific design of PPE to guard against falls, noise, heat, chemicals etc. and c) development of ergonomic design codes/checklist from the OSH perspective (Table 3).

In addition to the above, proper training and job redesign to address psychosocial factors related to workers should also be considered especially for utility scale solar installations with lengthy construction schedules.

7. Relevance to the Solar PV industry

The fast growing RE industry in India is bringing into its fold a host of untrained workers at various skill levels who are exposed to new and emerging risks. A safe and accident free environment can only be achieved if proper matching of the worker and the job is ensured. Context specific

ergonomic design interventions can play a critical role in reaching that objective. This review will be helpful to researchers, industrialdesigners, manufacturers, contractors, policy makers and health &safety professionals.

The proposition of the authors of the present paper is also in accordance with the Moray's seven problems of the future and role of ergonomics which includes designing efficient and safe energy industries [27].

Acknowledgment

The authors are grateful to the workers, their supervisors and authorities for providing access to the different kinds of Solar PV installations for conducting the present study.

References

[1] United Nations. UN Climate Change Annual Report (2018): published by the UNFCC (2019). ISBN 978-92-9219-184-9. Available

from:https://unfccc.int/sites/default/files/reso urce/UN-Climate-Change-Annual-Report-2018.pdf

[2] Pringle, A. M., Handler, R. M., & Pearce, J. M. (2017). Aquavoltaics: Synergies for dual use of water area for solar photovoltaic electricity generation and aquaculture. Renewable and Sustainable Energy Reviews, 80(December 2016), 572–584. Available from: https://doi.org/10.1016/j.rser.2017.05.191

[3] Ministry of Power, Government of India. Power Sector at a Glance, All India, 21st August, 2019.[Online] Available from: https://powermin.nic.in/en/content/powersector-glance-all-india [Accessed 10th Sep 2019].

International Conference On "Impact of Changing Energy Mix in the Power Sector"(ICIEMPS-2019) The Institution of Engineers (India), WBSC 23rd & 24th Nov. 2019

- [4] Press Trust of India (PTI), Energyworld.com. "India's renewable energy capacity crosses 80-GW mark, says R K Singh", 16th July 2019 [Online] Available from:
- https://energy.economictimes.indiatimes.co m/news/renewable/indias-renewableenergy-capacity-crosses-80gw-mark-says-r-
- energy-capacity-crosses-80gw-mark-says-r-k-singh/70244092 [Accessed 19th July 2019]
- [5]N. McCarthy, The State of Global Renewable Energy Employment, 23rd July 2019 [Online] Available from: https://www.forbes.com/sites/niallmccarthy/2019/07/23/the-state-of-global-renewable-energy-employment-infographic/#17bb6624e63ffAccessed 28th
- infographic/#17bb6624e63f[Accessed 28th July 2019]
- [6] Hanson, M. A. (2013). Green ergonomics: Challenges and opportunities. Ergonomics, 56(3), 399–408. Available from:
- https://doi.org/10.1080/00140139.2012.751 457
- [7] European Agency for Safety and Health. Hazard identification checklist: OSH risksassociated with small-scale solar energy applications(2013): Available from: https://osha.europa.eu/en/publications/e-fact-69-hazard-identification-checklist-osh-risks-associated-small-scale-solar-energy/view
- [8] Sahu, A., Yadav, N., & Sudhakar, K. Floating photovoltaic power plant: A review (2016). Renewable and Sustainable Energy Reviews, 66, 815–824. Available from: https://doi.org/10.1016/j.rser.2016.08.051
- [9] Kim, S. H., Yoon, S. J., & Choi, W. Design and construction of 1MW class floating PV generation structural system using FRP members (2017). Energies,

- 10(8). Available from: https://doi.org/10.3390/en10081142
- [10] Moskowitz, P. D., Hamilton, L. D., Morris, S. C., Novak, K. M., Briggs, T., Owens, T., &Ungers, L. Photovoltaic energy technologies: Examining public and occupational health risks (1981). Solar Cells, 5(1), 1–18. Available from: https://doi.org/10.1016/0379-6787(81)90010-7
- [11] Schulte, P. A., McKernan, L. T., Heidel, D. S., Okun, A. H., Dotson, G. S., Lentz, T. J., Branche, C. M. Occupational safety and health, green chemistry, and sustainability: A review of areas of convergence (2013). Environmental Health: A Global Access Science Source, 12(1), 1–9. Available from: https://doi.org/10.1186/1476-069X-12-31
- [12] Falvo, M. C., &Capparella, S. Safety issues in PV systems: Design choices for a secure fault detection and for preventing fire risk (2015). Case Studies in Fire Safety. Available from: https://doi.org/10.1016/j.csfs.2014.11.002
- [13] Bakhiyi, B., Labrèche, F., &Zayed, J. The photovoltaic industry on the path to a sustainable future Environmental and occupational health issues (2014). Environment International, 73, 224–234. Available from: https://doi.org/10.1016/j.envint.2014.07.023
- [14] International Finance Corporation (IFC), World Bank Group. Utility-Scale Solar Photovoltaic Power Plants; a Project Developer's Guide (June 2015). Available from:
- https://www.ifc.org/wps/wcm/connect/topics ext content/ifc external corporate site/su stainability-at-
- ifc/publications/publications utility-

International Conference On "Impact of Changing Energy Mix in the Power Sector"(ICIEMPS-2019) The Institution of Engineers (India), WBSC 23rd & 24th Nov. 2019

scale+solar+photovoltaic+power+plants[Acc
essed 2nd August 2019]

[15] Occupational Safety and Health Administration. Green Job Hazards: Solar Energy - Lockout/Tagout. [Online] Available from:

https://www.osha.gov/dep/greenjobs/solar I oto.html[Accessed 12thSeptember 2019]

- [16] Occupational Safety and Health Administration (OSHA). Green Job Hazards: Solar Energy Crane and Hoist Safety.
 [Online] Available from: https://www.osha.gov/dep/greenjobs/solar crane.html [Accessed 12th September 2019]
- [17] Occupational Safety and Health Administration (OSHA). Green Job Hazards: Solar Energy Heat/Cold Stress. [Online] Available from: https://www.osha.gov/dep/greenjobs/solar heat.html[Accessed 12th September 2019]
- [19] M. Mrohs, Training and Photovoltaic Rural Electrification (1998). Progress in Photovoltaics: Research and applications, Res. Appl. 6, 307-313. Available from: https://doi.org/10.1002/(SICI)1099-159X(1998090)6:5%3C307::AID-PIP240%3E3.0.CO;2-Y
- [20] Tsoutsos, T. D., Tournaki, S. K., Gkouskos, Z. K., Despotou, E., & Masson, G. Training and certification of PV installers

- in Europe (2013). Renewable Energy, 49(September), 222–226. Available from: https://doi.org/10.1016/j.renene.2012.01.02
- [21] European Agency for Safety and Health at Work. Foresight on new and emerging risks associated with new technologies by 2020 (2013): published by the European Union (EU). Available from: https://doi.org/10.2802/39554
- [22] Hanson, M. A. Green ergonomics: Challenges and opportunities (2013). Ergonomics, 56(3), 399–408. Available from :

https://doi.org/10.1080/00140139.2012.751 457

- [23] Behm, Michael. Linking construction fatalities to the design for construction safety concept (2005). Safety Science. 43. 589-611. Available from: https://www.researchgate.net/publication/22 2388127 Linking construction fatalities to the-design for construction safety concept
- [24] The Centre for Construction Research and Training. Applying Prevention through Design (PtD) to Solar Systems in Small Buildings (July 2017). Available from: https://www.cpwr.com/sites/default/files/publications/PtD-Solar-Solar-Systems-in-Small-Buildings.pdf [Accessed 16th August 2019]
- [25] Oregon Solar Industries Association. Solar Construction Safety. [Online] Available from: http://www.coshnetwork.org/sites/defa

ult/files/OSEIA Solar Safety 12-06.pdf[Accessed 24th September 2019]

06.pdf|Accessed 24th September 2019|

[26] Occupational Safety and Health Administration (OSHA). Recommended

International Conference On "Impact of Changing Energy Mix in the Power Sector"(ICIEMPS-2019) The Institution of Engineers (India), WBSC 23rd & 24th Nov. 2019

Practices for Safety and Health Programs in Construction. Occupational Safety and Health Administration (2016), 10(1), 1–40. https://www.osha.gov/shpguidelines/docs/8524 OSHA Construction Guidelines R4.pdf

[27] Thatcher, A., Waterson, P., Todd, A., & Moray, N. State of Science: ergonomics and global issues (2018). Ergonomics, 61(2), 197–213. Available from: https://doi.org/10.1080/00140139.2017.139 8845



Large Scale Penetration of Renewable Energy and Grid Integration - Issues and Challenges

D.V.Rajan¹, Goutam Mattagaj² and A.Indira³

¹ (Damodar Valley Corporation, West Bengal, India, ²Brighter Globe Solar Solution, Odisha, India & ³National Power Training Institute (ER), Durgapur, West Bengal, India)

{\begin{align*} \displaystyle{1.5cm} \displaystyle{2.5cm} \displaystyle{

Abstract - Grid integration is a key need for scaling Renewable Energy (RE) in India, not just to 175 GW (targeted for 2022) but far higher in the future. Integration isn't just a technical issue for grid management but impacts the holistic economics of RE. India has unilaterally announced ambitious plans in 2014 to quadruple RE to 175 GW by 2022 in Paris Accord on climate change. Against the target of 175GW RE especially for grid scale solar power of 100GW has been planned. This rapid growth in renewables will result into large scale penetration of RE into the Indian Grid becoming a challenging task for grid operations and have various implications not only on grid stability, security but also on the grid reliability. It also lead inference of finances of distribution companies (Discoms), consumer tariffs and incumbent power generating companies, especially traditional thermal power plants.

In the present scenario with the large penetration of RE which has wide variability and conventional thermal (coal) plants' ability to flexible operation of the output may differ measurably than what is assumed by 'Greening The grid' (GTG). The key challenge is that how much RE varies and how much coal plants can reduce output in response to RE are key factors affecting RE grid integration. This paper reviews the various issues and challenges of integrating renewable energy into power system grid. Also, the paper will discuss some difficulties that faced during RE integration such as Forecasting & Scheduling. Improved transmission capacity and system operation. In addition, the paper will briefly describe simulation study of feasibility of a roof top solar PV system. Finally, the key issues of RE integration has been discussed.

Keywords-grid; integration; global warming; renewable energy $\ensuremath{\mathbf{RE}}$

1.0 INTRODUCTION

Many countries have developed ambitious action plans and strategies to increase their share of renewable energy in the power system in order to reduce the greenhouse gas emissions, be independent of the use of fossil fuels and reduce the total energy costs. Operation of the power plants and their flexibility in the electricity supply is nowadays challenged by the increasing integration of renewable energy sources. Due to the intermittent nature of renewable sources, measures have to be undertaken to improve its flexibility. Also, gradual depletion of fossil fuel resources and emissions into the environment are poses a major concern worldwide. Each country uses the types of energy available to it, in differing proportions to meet its energy needs,. This is what we call the energy mix. The energy

mix of India has been dominated by thermal and hydro power. Power generation using fossil fuels result in emission of carbon dioxide which will ultimately affect the earth's atmosphere. According to a report by the International Energy Agency (IEA), .India emitted 2,29 9 million tonnes of carbon dioxide in 2018, a 4.8% rise from last year 2017. If we will see the trend of total emissions of the power sector for the FY 2012-13 to 2016-17 is as depicted below:

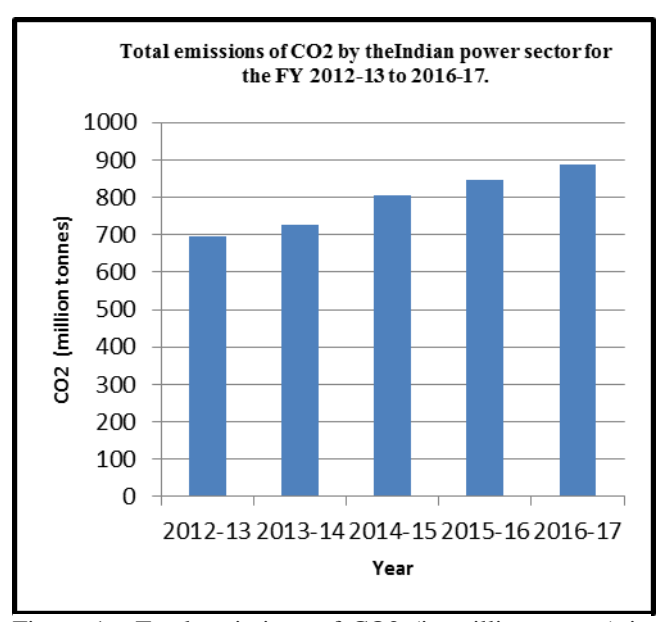


Figure 1: Total emissions of CO2 (in million tonnes) in India by the power sector for the FY 2012-13 to 2016-17.

Climate change and global warming leads us to find alternative resources of generation of electricity. Thus the Government of India has increased its focus on greening the grid, targets to install 175 GW of grid-connected RE by 2022 keeping in mind our commitments that 40% of India's power capacity would be based on non-fossil fuel sources under the Paris Agreement. This would place the Indian economy on a low-carbon trajectory in the years to come [1].

The Indian RE sector, of late, has been witnessing a major transformation. In the last decade (2007–2017) [3,4], the renewable energy sector has taken a quantum jump in terms of total installations and its positive impact is visible on the total energy mix of India which is depictured in the



table 1. India is now the fourth largest country in the world with around 71 GW of RE installations [5] after China (334 GW), the USA (161 GW), and Germany (106 GW).

Table 1
Installed Grid Interactive RE Capacity

Grid-Interactive Power	Cumulative Achievements
	(Installed capacity in MW)
Wind Power	34,402.12
Solar Power - Ground Mounted	21,892.42
Solar Power - Roof Top	1,222.65
Small Hydro Power	4,493.2
Biomass - Bagasse Cogeneration	8,700.8
Biomass (non-bagasse) Cogeneration/Captive Power	6,76.81
Waste to Power	138.3
Total	71,526.3

Out of 71 GW installed grid-interactive RE capacity (Table 1), wind energy plays a dominant role comprising 48.5% of total RE installations, followed by solar (32.5%), biomass (12.3%), small hydro (6.4%) and waste-to-energy (0.2%). In the last four years, solar energy has seen a record jump from 3.7 GW in 2014-15 to 23 GW by July 2018. However, such focus to scale up solar power may have overshadowed the development of other RE technologies such as wind, biomass and others.

As per the Bloomberg New Energy Finance's Climate scope 2018 report, India jumped three places to become the second —largest clean energy worldwide investment market. The first solar-wind hybrid auction was successfully conducted with the lowest tariff at Rs.2.67 per kWh being comparable to solar and wind power tariffs. With low power tariffs and a short gestation period as compared to fossil-fuel based plants, renewable have become the preferred choice for developers and investors alike, leading to the emergence of new entrepreneurs offering a range of services.

Hence, the country has achieved 80.47GW of installed renewable energy capacity (as on June 2019) in a short span of time, with the share of renewable in the total generation mix increasing from 7.06% in 2018-19 to 9.7% in 2019-20 for the April-May period.

At the same time, the limitations associated with the RE technologies, needs to be addressed in the power system. One of the options which can help in large scale integration of RE generation sources can be adoption of grid scale energy storage technologies which can complement RE generation sources. The cost of battery energy storage systems has been reducing at a fast pace with the technological advancement and the world is anticipating that it may help to absorb more RE into the power system in the future. To facilitate renewable energy into the grid, new transmission corridors would be required for

evacuating green energy from states such as Tamil Nadu, Gujarat, Rajasthan and J & K (Ladakh).

In this paper, we focus on the major knowledge gaps when it comes to planning for and adapting to the rapid expansion of renewable energy power in India. The structure of the paper is as follows: In section 2, we give present scenario and grid integration what the broad issues and challenges of RE integration are. In section 3, discussion of Future of the Indian Grid based on the draft report recently published by Central Electricity Authority (CEA) on India's optimal generation mix for 2030, followed by the flexible operation of the thermal plants an important effort in this direction in section 4. In section 5, we conducted detail simulation study of solar roof top PV design, Energy produced and energy cost, along with CO₂ emission balance. The last section concludes with a discussion on various issues of RE integration, challenges and analytic gaps that could be addressed in the future.

2.0 PRESENT SCENARIO:

The coal based generation capacity stood at 200.75GW in June 2019, accounting to 56.1% of the country's total installed capacity. During the current year (as of June 2019), the all-India PLF has been around 62.94%, slightly better than the 62.38% PLF recorded during the same period in the previous year.

With the growing influx of renewable energy, the demand for coal-based power has been declining. Moreover, coal-based plants are subjected to frequent ramp up and ramp down in order to balance renewable based power, thereby making them less efficient and resulting in higher maintenance requirements. Therefore, coal based plants are required for bringing in flexibility in operations and ensuring grid discipline.

Nearly 65GW of capacity was under execution as of April 2019 and is expected to be commissioned over the next two to three years. In the short term, the key focus areas for coal based plants will be the installation of emission control technologies and enhancing the flexibility of operations.

Objectives of Renewable energy integration is to

- Reduce carbon emissions and emissions of other air pollutants.
- increase the use of assets through integration of distributed systems and customer loads thus lower the costs of electricity
- Enhance reliability, security, and resiliency from micro grid applications in critical infrastructure protection.
- support reductions in oil use by enabling plug-in electric vehicle (PHEV) operations with the grid
- By declaration of all hydro projects as in the ambit of renewable energy. Their inclusion in the renewable energy sector will provide HEPs access to the subsidies and benefits available to renewable projects.



 Going forward, new areas of opportunity such as solar – wind, hybrids and energy storage will help in better utilization of resources and result in higher generation levels.

3.0 FUTURE OF THE INDIAN GRID

As per the report published by CEA, the overall grid capacity in the country will reach 831GW to meet a peak demand to 340GW. Solar and wind will constitute the largest share of about 53% (431GW) in the proposed capacity mix) while coal will constitute around 32% (266GW).

While there are many advantages of adding more renewable to the power system, there are some inherent challenges too. Both solar and wind can be intermittent and variable in nature. From a system operator's perspective, this intermittency coupled with frequent changes in power demand, can quickly make the system unstable. Moreover, operating thermal power plants at low plant load factor, and, at a technical minimum load, the cycling up / down to balance the variability of renewable energy generation may extract a heavy cost and reduce the economic life of plants. Hydro is a good option to ensure system stability, as it is not only technically well suited for managing system variability, but is also a clean source of electricity generation. However, hydro plants are constrained by site considerations, seasonality and a competing demand from irrigation. Hence, relying on hydro beyond a certain point to meet balancing requirements seems unrealistic.

4.0 FLEXIBLE OPERATION OF COAL BASED POWER PLANTS

As renewable in India continue on a strong growth trajectory to hit the GOI's target of 175GW by 2022, the key concerns are: a growing need to address the intermittency / grid instability issues that arise with an increasing proportion of VRE penetration into the grid, and the cost of balancing renewable, which, if not contained, would impact retail tariff in future.

With most of the coal plants currently operating at low PLFs, balancing renewable through flexible coal based generation will also be cheaper than other alternatives. However, as the largest contributor to India's total greenhouse gas emissions, coal based power generation, even if made flexible to balance renewable as mentioned above, will remain a key concern for the policymakers, who are addressing the challenge of climate change, unless it is made emission compliant.

The GOI has taken several initiatives to transition towards sustainable, clean coal-based generation by imposing mandatory emission norms to be achieved within a specified period, which will need capex on equipment like flue gas desulphurization (FGD) to make these plants emission compliant.

1. Making coal based generation plants flexible enough (with faster ramp rates) to balance renewable to continue the momentum on

- renewable energy capacity addition.
- 2. Transition to cleaner coal-based generation and
- 3. Remain tariff neutral while achieving both these much needed objectives.

We hope policymakers will find such a framework balanced, logical and fair, as being in the best interest of the environment and end consumers, and will accelerate the pace of emissions compliance and balancing support to upcoming renewable energy capacity.

5.0 HARNESSING MAXIMUM SOLAR ENERGY WITHIN MINIMUM SPACE ON BUILDING ROOF TOP SOLAR PV: A study on harnessing maximum solar energy within Minimum Space on roof of "Suruchi Bhawan" DSTPS canteen using solar PV has been conducted.

Project: DSTPS-DVC

Geographical Site: DSTPS-DVC Country India Situation: Latitude 23.6°N Longitude 87.2°E Legal Time UT+7 Altitude 190 m Albedo 0.20 Simulation parameters 0° Perez, Meteonorm Collector Plane Orientation Tilt 23° Azimuth Models used Transposition Hay Diffuse Free Horizon, Near Shadings No Shadings

PV Array Loss factor

Thermal Loss factor Uc (const) 29.0 W/m²
Wiring Ohmic Loss Global array res. 35 mOhm
Module Quality Loss Loss Fraction -0.4 %
Module Mismatch Losses Loss Fraction 1.0 % at MPP
Incidence effect, ASHRAE parameterization
IAM = 1 - bo (1/cos i - 1) bo Param. 0.05

Main system parameters

System type: Grid-Connected

PV Field Orientation: tilt 0° azimuth: 23°

PV modules Model: Poly 320 Wp 72 cells Pnom 320Wp PV Array: Nb. of modules 527 Pnom (total) 169 kWp Inverter Model TRIO-20_0-TL-OUTD-S1 20.00 kW ac Inverter pack: Nb. of units 8 Pnom (total) 160 kW ac Total area Module area 1012 m² Cell area 924 m²

User's needs: Unlimited load (grid)

Main simulation results

Produced Energy: 267.3 MWh/year Specific Production: 1585kWh/KWp/year

Performance Ratio **PR 84.1 %** Investment incl. taxes **INR 8770178**

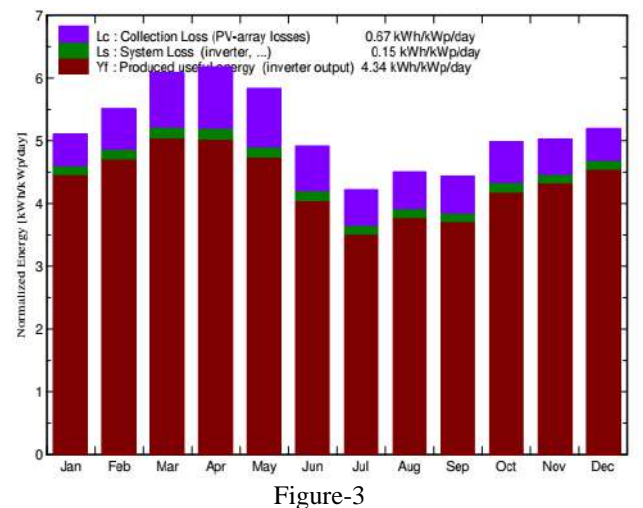
Specific 52.0 INR/Wp

Yearly cost Annuities (Loan 5%, 20Yrs):703742 INR/Yr.

Energy cost: 2.63 INR/kWh



Figure-2
Normalized Power Production/year
Normalized productions (per installed kWp): Nominal power 169 kWp



Performance Ratio: 84.1%

Performance Ratio PR

0.8

O.2

O.2

Jan Feb Mar Apr May Jun Jul Aug Sep Oct Nov Dec Table-2

Balances Main Result

	GlobHor	T Amb	Globino	GlobEff	EArray	E_Grid	EffArrR	EffSysR
	kWh/m²	°C	kWh/m²	kWh/m²	MWh	MWh	%	%
January	125.6	18.07	158.4	154.2	24.09	23.34	15.04	14.56
February	132.3	21.98	154.4	150.4	22.97	22.24	14.70	14.24
March	175.5	26.85	188.8	183.7	27.28	26.42	14.28	13.83
April	187.0	30.42	185.4	180.0	26.31	25.45	14.03	13.57
May	194.8	31.44	180.9	174.9	25.66	24.81	14.02	13.55
June	161.3	29.68	147.5	142.2	21.28	20.51	14.26	13.75
July	139.8	28.52	130.8	126.1	19.11	18.37	14.44	13.88
August	145.5	28.12	139.7	134.8	20.51	19.76	14.51	13.98
September	130.9	27.40	133.1	128.8	19.49	18.78	14.47	13.95
October	139.1	26.22	154.6	150.3	22.66	21.89	14.49	13.99
November	124.5	22.01	150.9	146.7	22.60	21.91	14.81	14.36
December	122.7	18.35	161.1	157.0	24.53	23.79	15.05	14.59
Year	1778.9	25.77	1885.6	1829.0	276.49	267.27	14.49	14.01

Logends: GlobHor Horizontal global irradiation EArray Effective energy at the output of the array
T Amb Ambient T Emperature E_Grid Energy injected into grid Energy injected into grid Efficiency injected into grid Ef

Grid-Connected System: CO₂ Balance Produced Emissions Total: 321.73 tCO₂ Replaced Emissions Total: 7504.8 tCO₂ Grid Lifecycle Emissions: 936 gCO₂/kWh

Source: IEA List Country: India

CO₂ Emission Balance Total: **6190.0 tCO₂**

6.0 RENEWABLE INTEGRATION: KEY ISSUES

Major issues and focus areas for mitigation of the challenges faced in Indian context are discussed below.

6.1 Flexible operation of coal-based power plants -

While Coal is expected to provide majority of the flexibility, Hydro and Gas are also expected to play a pivotal role. Because of their temporal fluctuations and geographical dispersion of wind and solar generation, the power system is affected with the penetration of RE. This variability affects the power systems with the increasing penetrations of RE sources. It is also important to allow flexibility in operation of the existing conventional generating plants as well as widen the scope of gas, hydro and pump storage plants which could be utilized for meeting the fluctuations in load profile as well as maintain system stability.

6.2 Hydro Power Plant - Quick start up and stop time of hydro plants make them suitable to handle the fluctuation due to solar & wind generation. More flexing of hydo generation is expected during integration of large scale renewable generation for both Peak & Off peak demand. Also pumped hydro storage plays a pivotal role to meet peak load demand of the system and utilize excess available power during off peak hours, thus flattening the load demand curve. The development of pumped hydro storage scheme is a precursor to integrate renewable generation. To meet up for the additional requirement, flexible generators such as reservoir hydropower plants, gas based generating plants which could respond and adjust to the demand-supply fluctuations in a short time frame would be required. Storage as well as automated demand side management are flexible energy services which may help in shifting the generation or load.

6.3 Forecasting and Scheduling

With large penetration of renewable energy mainly solar and wind into the grid, forecasting becomes an essential requirement for grid stability. Suitable regulatory framework for Forecasting, Scheduling and Imbalance Settlement for RE generators at both inter-state and intrastate level needs to be in place. Improved forecasting of RE is also essential to enable System Operators to manage grid operations.

6.4 Improving Transmission capacity and System Operations – The Renewable potential is concentrated in a few states and therefore it is important to have expanded transmission capacity for accommodating higher RE generation at few locations and its evacuation to load centres. Considering the small gestation period of the RE projects it is important to plan and execute the transmission projects for speedier implementation. Adequate planning and coordination between the various agencies (generation, transmission, system operator, etc.) would be required for overcoming the transmission constraints and derive value for the consumers.



7. CONCLUSION

The integration of 175 GW of renewable capacity will result in 36% share of RE in the total installed capacity. For system stability, Hydro power plants are especially suitable for quick supply of flexible power. It has been seen that Pumped storage units are used exclusively for peaking or balancing of system on the direction of system operator.

Since Gas power plants have better start / stop capability they need to contribute to flexible generation as much as possible. Among the units of different sizes such as 200 MW, 500/600 MW or 660/800 MW, those units which are efficient and have low ECR should be given preference over others in terms of generation schedule.

Traditionally most of the coal-fired units are designed to operate as base load plants. Hence, several measures need to be undertaken to make the plants capable of low load operation.

ACKNOWLEDGEMENT

The authors would like to thank to the authorities of National Power Training Institute, Durgapur, India, Brighter Globe Solar Solution (Solar EPC org, India) and special thanks to Damodar Valley Corporation for providing us with necessary information, required data and time to time suggestions.

REFERENCES

- [1] MNRE, 2017. Working Paper on International Solar Alliance (ISA).
- [2] CEA, July 2018. Executive Summary on Power Sector. Central Electricity Authority, Ministry of Power, Govt. of India.
- [3] REN21, 2018. Renewables 2018 Global Status Report. Paris: REN21 Secretariat.
- [4] Boyle, Godfrey. Renewable Electricity and the Grid: The Challenge of Variability. London: Earthscan, 2007.
- [5] Irena. "ETSAP." Renewable Energy Integration in Power Grids (n.d.): 1-36. International Renewable Energy Agency. Apr. 2015.
- [6] Rooftop Solar Photovoltaic System Design and Assessment for the Academic Campus Using PVsyst Software. Sujoy Barua and R. Arun Prasath Centre for Green Energy Technology, Pondicherry University.

Power distribution line infrastructure consensus for Extra Low Voltage DC Microgrid: A comprehensive study

Sushri Mukherjee¹, Sumana Chattaraj¹, Md. Irfan Khan¹, Dharmbir Prasad² and Harish Agarwal¹

¹Supreme & Co. Pvt. Ltd., Kolkata-700020, WB, India ²Asansol Engineering College, Asansol-713305, WB, India {Corresponding author's email: sushri.engg@supreme.in}

Abstract - Traditional power generation and consumption are undergoing major transformation. One of the tendencies is to integrate microgrids into the distribution network with high penetration of renewable energy resources. The leaps in the field of solar energy have boosted the source of renewable energy and have been also proven as the best source as a portable energy. These solar panels are scalable to generate power from watts to MW capacity and hence most versatile for remote population. Rural electrification involves high initial capital investments per capita due to its stumpy energy demand and scattered population density. These factors effect in a higher cost of electricity than that for urban consumers. DC microgrids are networks composed of DC sources, loads and interconnecting lines. Related to DC distribution system, the concept of DC microgrids is also witnessing a significant research contribution in the recent times. In this paper, a case study of a village with 30 households is provided to elaborate microgird generation and distribution system incorporating prepaid metering system. The model is found to be apt in meeting basic electricity needs of the livelihoods. The proposed operation and maintenance is also superficial and can be managed easily by the support team.

Keywords - DC microgrid, ELV, Distribution line, Economical, Hardware accessories.

Introduction

The proliferation of renewable energy sources and storage devices that are intrinsically stimulating interest in the design and operation of DC microgrids, which have the additional desirable feature of preventing the use of inefficient power conversions at different stages [1]. Given the rapid development of modern power electronic technologies, DC microgrids and distribution systems have become more attractive than their aging conventional AC counterparts [2-3]. Off grid microgrid systems are independent of conventional grid and their standards, but microgrid project developers follow specifications, keeping in mind the future compatibility with the grid. Distribution lines can be categorized into two voltage ratings LV (<= 1.1 kV) and MV (1.1 kV to 33 kV) [4]. Thus, Extra Low Voltage DC (ELVDC) can be used for microgrid power distribution network since it removing the need for synchronization and frequency adjustment as well as appropriateness in supporting DC loads [5]. Along with this feature, the DC network for power distribution is considered to be optimal and safe to transfer at low voltage level compared to that of AC network [6-8]. The electrical network at low voltage has limited power distribution capacity and is viable for electrification for the region which is without electricity due to remote geographical positioning and economical backwardness [9]. Since, most of the portable devices and appliances are DC with some of them battery backed up [10]. Transmitting end-to-end DC at extra low voltage emerging to be a viable solution for small distance since it is safe and can be harnessed on the existing infrastructure and doesn't need huge infrastructure investment where the distribution cost supersede the generation cost [11-14].

PAPER ORGANIZATION

The Case Study: Conesus Overview of the DC microgrid is introduced in Section A. The Design Perspective of ELVDC microgrid system is introduced in Section B. Description of System Architecture is carried out in Section C. The Power Distribution Network is described in Section D. Conclusions are drawn in Section E.

(A) Case Study - Conesus Overview: The proposed extra low voltage DC microgrid system, comprising available renewable energy sources in an off-grid rural community, based on a commissioned field study carried out in a rural, off-grid Unnao village in Uttar Pradesh, which has solar resource available (as presented in Table 1).

Table 1 Basic information of the project

Capacity	800-1200 Wp solar power plant
Type	48 V DC distribution network
Application	Household, Shop
Project Description	800-1200 Wp solar powered plant with battery backup 200-400 Ah to meet the demand of un-electrified hamlet consisting of 20-30 households.
	Average power consumption of 20-30 Wp per house hold.
	Reduces AT&C loss
	HDI improved
Benefits	It improved the basic livelihood of the extreme rural area where transportation mobility is not possible.
	This also enhanced the people livelihood by providing them opportunity to work at night time.
	Small scale power distribution made easy.

The distribution grid for ELVDC is mostly at geographically remote location where the transportation of bulky hardware's also not feasible and needs head loading. The paper elaborates mechanism and sizing of overall system for small villages or hamlets consisting of 20-50

households. The portable hardware used to lay the distribution network used the existing infrastructure of the villages and supporting the cables with wall fixtures. Sectional poles of different heights are used to use for the particular application and the design with work load capacity is being elaborated. Downsizing of the cables and use of messenger cable to increase the span and various latching mechanisms are being considered. Utilization of the roofs and walls of cemented housed with corner support bracket and extension angle to raise height of the conductor for road crossing and various fittings for anchoring the hardware on the wall and roof.

(B) Design Perspective of ELVDC Microgrid System: The paper presents economical way to lay distribution network for ELVDC network. The control mechanism to distribute power efficiently has been explained as per the consumption pattern of the consumer. ELVDC network is used for the reason as it needs to be safe enough to control and transmit in terms of health hazard and fatality can happen for voltage higher than 48 V DC. Since the arcing and sparks are higher in DC; thus, 48 V is considered to be optimal level for safe switching of power. Microgrid model developed has been optimized to reduce the conversion losses which could be higher if we consider for AC grid as the generation are through solar panels and storage medium is battery both of which are DC in nature. The advance in electronic equipment which are DC power sourced have also boosted more efficient appliances which are powered with DC source such as LED lights, DC fans, mobile charging, LED TV and many more. The ELVDC microgrids specially can be adopted for the region which are just not only power deficit but also far away from the reach of grids due to several factor as explained above. These grids can be on the difficult terrain and for nonperennial civilization which needs low investment infrastructure. Since, the goal is to cater the households of 20-50 numbers with basic facilities as lights, fan, mobile charging with approximate loading of 20-30 W. As per the load of appliances, per house hold average power consumptions per day is 0.150 kWh for a basic household with peak power demand at 30 W (as presented in Table 2).

Table 2 Load size for basic house hold appliances

Table 2 Load size for basic flouse floid appliances							
Appliances	Rated Power (W)	Quantity	Total Power (W)	Usage Hours	Watt Hours		
Light	5	2	10	4	40		
Fan	15	1	15	6	90		
Mobile charging	5	1	5	4	20		
Maximum Co	nsumption	of HH (W)	30		150		
No of House l	Holds				30		
Total consum	4500						
Storage & Los	500						
Power Estima	5600						
Power Plant C	800						
Production Ho	7						

*HH: House Hold

The balance of the power estimated shall be for regulated supply and demand which may vary. The target to cater the people with such a low consumption pattern is possible with the DC grid where the generation, storage and consumption are at DC voltage. This has eliminated the conversion losses and also prevented the non-technical losses because of the power transmission voltage at 48 V DC unavailable for tap and readily available to use directly.

(C) System Architecture: The power is generated by the solar panels is 800-1200 Wp and is stored by the battery at 48 V DC. The battery charging mechanism and the load distribution is controlled by the controlling unit which also keeps track of the power generated and consumed. The power is then supplied to the households through from the distribution board to the distribution line is as shown in Fig. 1. The power is distributed to the household with the application of special hardware designed for optimum mechanical loads on the hardware and conductor. The consumers have controller cum energy meter which supply the required power to the appliances at the regulated voltage and tracks the energy consumption.

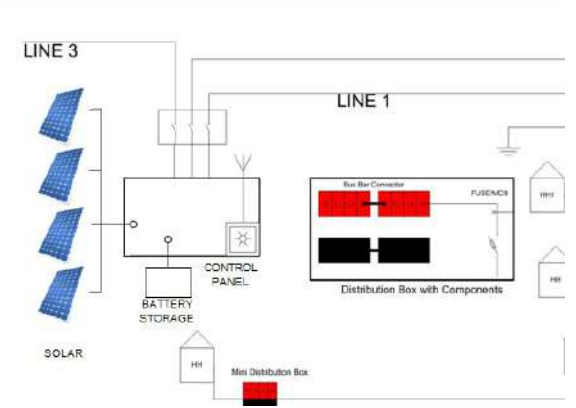


Fig. 1 Basic layout of ELVDC microgrid

(D) Power Distribution Network: Most of the conventional distribution systems operate radially, where the power flows unidirectional from large power plants to the customers. In such systems, since the magnitude of short circuit currents is proportional to the fault location, the protection is done by overcurrent based protective devices. Also, the time-graded coordination between them enables upstream devices to operate as backup for downstream ones.

However, overhead distribution line is considered to be cheaper than underground and the wires are stringed over poles and hardware. Since, capacity of the distribution system is quite low, unarmoured Aluminium cables of 4-6 m² can be used to distribute the power depending on the load per branch. These wires size can be further lowered

for the sub branches where it needs to serve 2-3 households and for the service connection from the distribution box. The size of the unarmoured cable is not sufficient to carry the load for the span of more than 15 m. The stringing of the cables needs support by the messenger wire to increase the span up to 30 m. It would be not economical if the poles are used to string the cable and hardware. The optimization aspects of significant components are illustrated as under:

(i). Triangular Wall bracket: This assembly arrangement is used for cable mounting in distribution lines. It is used to avoid complication of pole and its hardware accessories mounting due to right of way issue and cost constraint. This triangular bracket is mounted on the walls with help of anchor bolts and can use for carry the load of cable as depicted in Fig. 2 and Fig. 3.

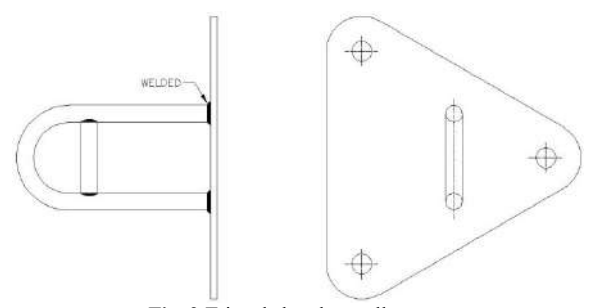


Fig. 2 Triangle bracket wall mount

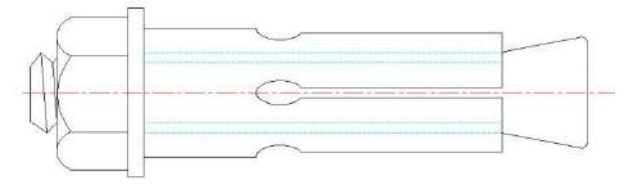


Fig. 3 Expanding anchor bolt

These are used for lateral hanging of cables along with the arrangement designed to isolates the cables from touching the walls preventing wear and tear of the cables and can be easily used for 10-40 m span length depending on the wall mechanical capacity and cables weight. These are designed to carry tension as well as suspension fitting assembly. Fitting items are changed for suspension and tension type. GI wire carries the load of the electrical cables. These types for bracket are suitable for flat concrete walls to support.

(ii). Suspension assembly arrangement: This suspension assembly is used in between tension bracket to support the cable in between to carry and distribute the load evenly. Unlike conventional tension and suspension assemblies which are in the ratio of 1:5 or 1:6; these can be used 1:1. Since the distribution line length are not so long and also hardly any cost difference between both. A helical wire is required to grip the messenger (GI) wire with direct

mounting from a wall bracket. The whole arrangement is shown in the Fig. 4 below.

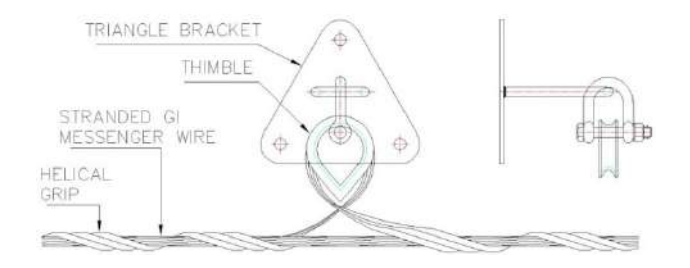


Fig. 4 Suspension assembly arrangement

D-shackle is fitted with the thimble, which supports the helical grip used to grip the GI wire. Dropout lines for distribution box (DB) can also be drawn from the line as it will take the load of the cable and dropout lines can also be drawn from the suspension points with proper support and required grip to the cable along with messenger wire.

(iii). Tension assembly arrangement with wall bracket: This assembly is mainly used at the terminating points or at the places, where tension is required to carry the cable and maintain the sag. The thimble is attached to the wall bracket by means of nut and bolt to support the messenger wire. The applicable tension of 10 kN is sufficient to grip and string the messenger wire. This arrangement is given in the Fig. 5.

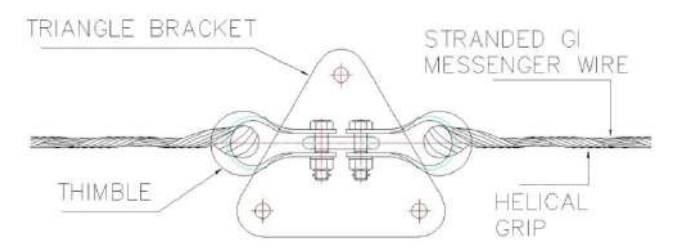


Fig. 5 Tension assembly arrangement

(iv). Corner Bracket: These brackets are used at the corner of the houses or buildings to bend the distribution line at 90°. It is also used instead of poles to mount a wire at that point. This process curtails the cost of a pole and simultaneously supports the wire mounting providing required load bearing capacity. The Fig. 6 alongside shows a corner bracket. This bracket support tension assembly and is used for 90° bend of line. This bracket is fitted on the wall with the help of anchor bolt. It can also be used for dead end fittings in case of termination of the line.

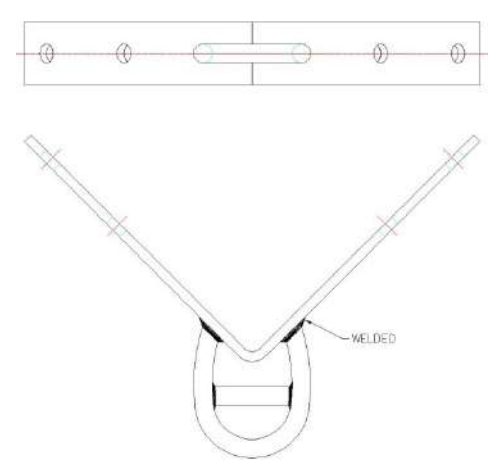


Fig. 6 Corner wall bracket

(v). Cable lashing rod: The cable lashing rod is used to bind GI messenger wire which act as a strength member and electrical cable together. Lashing rod can bind multiple cables with thinner gauge together. Lashing rod covers wider section of the cable hence distributing the load on the cable and GI wire; hence it can be used easily over a span of 5-10 m lashing rod are made of neoprene dip Al-Aloy to provide corrosion resistance and its arrangement is shown in Fig. 7 and Fig. 8 lashing clips are suitable for the cables with bigger cross section. In lashing clips, all steel clamps securely attaches two lashing wires or a ground wire on strand and two grooved plates fit on opposite sides of the strand. Helical shape lashing rods accommodate different cable sizes.

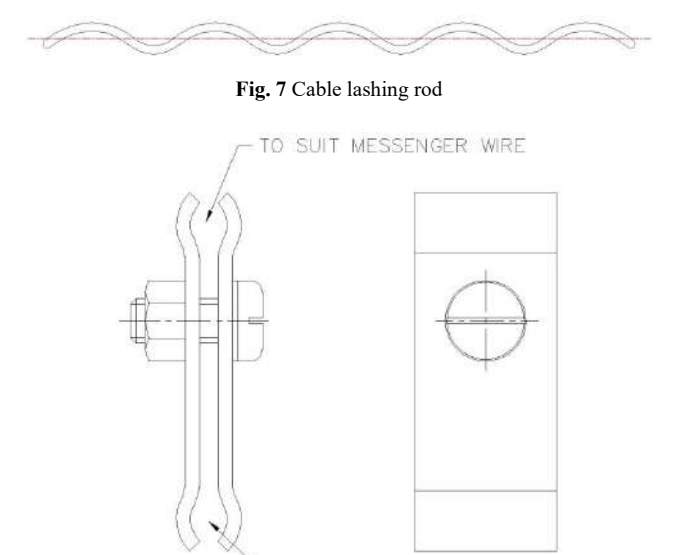


Fig. 8 Cable lashing clip

TO SUIT CONDUCTOR

(vi). Raised Arm wall bracket: Raised arm wall bracket is a simple design and arrangement made from angle, eye bolt and stringing accessories to carry the cable along with the

walls and then raise to a height of 2-3 m in order cross the road change the orientation and transfer cable on other side of the road. It can be used where the roads are narrow and mounting of poles is extremely difficult.

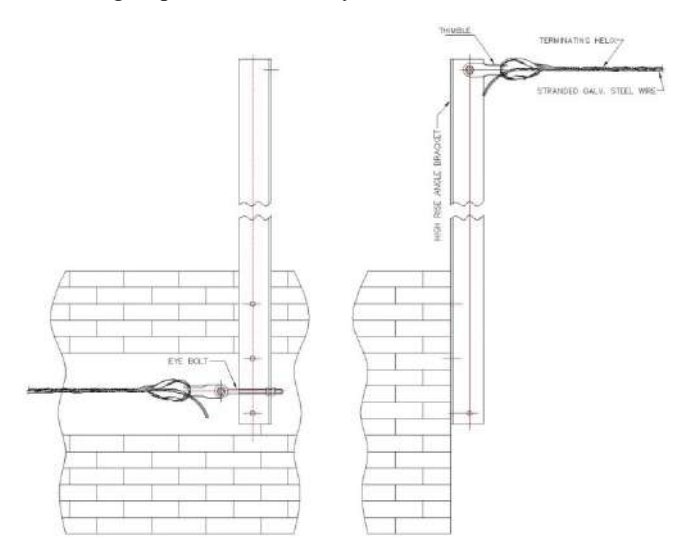


Fig. 9 Road cross wall bracket

It also overcomes the RoW issues generally happen in case of poles for narrow road. It is also a cheaper solution to pole for micro grid. The wall used to anchor the raised arm wall bracket should have sufficient strength to take the load because of the cantilever load on the wall due to height of the raised arm. These can be fitted with the anchor bolts to the walls where there is no roof protruding out as shown in Fig. 9.

(vii). Sectional pole and its assembly: Microgrid deployment is feasible, where the reach of conventional grid is either very difficult or extremely expensive. To overcome site transportation issues no of poles can be reduced, still they are important part of overhead lines. Where there is no other medium to support the conductor for stringing. Options as available are:

- PSC Poles Handling and transportation expensive as well as difficult for interior region when requirements are low since not cost effective.
- Steel Pole Strong but Expensive, transportation and handling inconvenient.

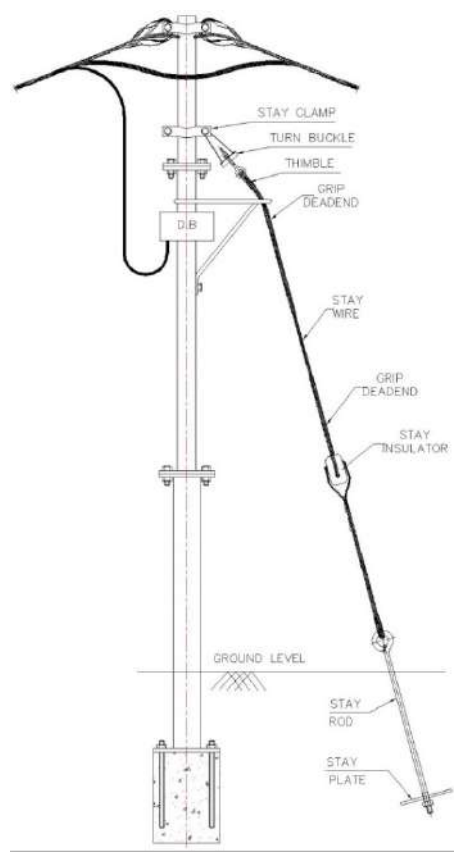


Fig. 10 Pole mounting arrangement

Sectional GI poles overcome those issues for length of 6-10 m, where it can be divided into 2-3 section as per requirements. These poles can be easily fabricated from tubular pipes of different diameter welded with flange to fix two different sections together with nut & bolts. Base of steel poles can be fixed with the concrete mixture as well can be rooted deeply gripped with the help of TMT bars or anchor bolts the holes on the base plate of the poles. Poles accessories can be mounted easily on the poles to string the distribution line cables, and stays can be fixed on it as portrayed in Fig. 10.

(viii). Distribution box: Distribution boxes (DBs) are majorly required for microgrid since the households are densely spread near the distribution lines and the power requirement is quite high as results higher current rating cables are required. These boxes generally accommodate bus bars and allow service connection to bunch of houses as depicted in Fig. 10. It helps to isolate the grid with group of users which also eases the maintenance. Ferruling makes it very effective to debug fault. DB also makes it very convenient for new service connection. It is accommodated with resettable fuses / CB for protection of connected equipment from fault at either ends. It can be designed as per grids requirement but at-least need IP-52. Design should be such it can be mounted on poles as well as on walls.

(ix). Wall clamps & service lines: These are brought to households with the help of anchor wall plug which can draw more than one service connection for households nearby. Service lines can travels on the distribution line path and can be drawn perpendicularly where the Households are on the distribution line path but away from the DB. Since the messenger wire can withstand the load of more than require load of the distribution cables.

CONCLUSION

Microgrid is also an example of infrastructure leapfrog for sparsely populated regions where grid penetration requires huge infrastructure cost. In many areas, these are found to be superior over grid expansion. Hence, in today's scenario, where there are so many types of generation sources available for power and utilization of DC systems can avoid conversion losses, offering high reliability. redundancy and optimize the cost. The challenge was to have robust distribution system which can be deployed for the region where the conventional distribution line hardware is expensive compared to the overall microgrid components cost. The distribution line equipment used for power distribution are generally bulky, which increases the component and transportation cost. This optimization initiative encourages renewable generation investors to focus on profitable grid tied power systems tailored for large utility scale and smaller peri-urban implementations. It addresses the challenges faced in selection & installation of hardware accessories required in microgrid. The system provides very high degree of reliability in terms of safety to line-men and consumers and freedom from outages. The overall architecture of ELVDC microgrid is low generation and low consumption, which can replace conventional hardware and use the hardware which are sufficient enough to carry the electrical and mechanical load required by the system design.

ACKNOWLEDGMENT

This Extra Low Voltage DC power distribution line project was executed for Boond Solar at Unnao district in Uttar Pradesh, India.

REFERENCES

- [1]. C. De Persis, E.R. Weitenberg and F. Dörfler, "A power consensus algorithm for DC microgrids." *Automatica*, vol. 89, pp. 364-375, 2018.
- [2]. J. Wang, N. Xie, W. Wu, D. Han, C. Wang and B. Zhu, "Resilience enhancement strategy using microgrids in distribution network. *Global Energy Interconnection*," vol. 1, no. 5, pp. 537-543, 2018
- [3]. Abdali, K. Mazlumi, and R. Noroozian, "High-speed fault detection and location in DC microgrids systems using Multi-Criterion System and neural network," *Applied Soft Computing*, vol. 79, pp. 341-353, 2019.

- [4]. Babaiahgari, M.H. Ullah and J.D. Park, "Coordinated control and dynamic optimization in DC microgrid systems," *International Journal of Electrical Power & Energy Systems*, vol. 113, pp. 832-841, 2019.
- [5]. F. Dastgeer, H.E. Gelani, H.M. Anees, Z.J. Paracha and A. Kalam, "Analyses of efficiency/energy-savings of DC power distribution systems/microgrids: Past, present and future," *International Journal* of Electrical Power & Energy Systems, vol. 104, pp. 89-100, 2019.
- [6]. Hossain, M.A., Pota, H.R., Haruni, A.M.O. and Hossain, M.J., 2017. DC-link voltage regulation of inverters to enhance microgrid stability during network contingencies. *Electric Power Systems Research*, vol. 147, pp. 233-244.
- [7]. J. Hu, Y. Shan, Y. Xu and J.M. Guerrero, "A coordinated control of hybrid ac/dc microgrids with PV-wind-battery under variable generation and load conditions," *International Journal of Electrical Power & Energy Systems*, vol. 104, pp. 583-592, 2019.
- [8]. Hussain, V.H. Bui and H.M. Kim, "Microgrids as a resilience resource and strategies used by microgrids for enhancing resilience," *Applied energy*, vol. 240, pp. 56-72, 2019.
- [9]. J. Kitson, J. S. Williamson, P.W. Harper, C.A. McMahon, G. Rosenberg, M.J. Tierney, K. Bell, and B. Gautam, "Modelling of an expandable, reconfigurable, renewable DC microgrid for off-grid communities," *Energy*, vol. 160, pp. 142-153, 2018.
- [10]. H. Lotfi, and A. Khodaei, "AC versus DC microgrid planning," *IEEE Transactions on Smart Grid*, vol. 8, no. 1, pp. 296-304, 2015.
- [11]. S. Mirsaeidi, X. Dong and D.M. Said, "Towards hybrid AC/DC microgrids: Critical analysis and classification of protection strategies," *Renewable and Sustainable Energy Reviews*, vol. 90, pp. 97-103, 2018.
- [12]. M. Pourbehzadi, T. Niknam, J. Aghaei, G. Mokryani, M. Shafie-khah and J.P. Catalao, "Optimal operation of hybrid AC/DC microgrids under uncertainty of renewable energy resources: A comprehensive review," *International Journal of Electrical Power & Energy Systems*, vol. 109, pp. 139-159, 2019.
- [13] Sabir, and M.S. Javaid, "Minimizing neutral currents in distribution microgrids using smart loads," *International Journal of Electrical Power & Energy Systems*, vol. 113, pp. 436-448, 2019.
- [14]. M.U. Shahid, M.M. Khan, K. Hashmi, R. Boudina, A. Khan, J. Yuning and H. Tang, "Renewable energy source (RES) based islanded DC microgrid with enhanced resilient control," *International Journal of Electrical Power & Energy Systems*, vol. 113, pp. 461-471, 2019.

Techno-Economic Analysis of Grid Connected Integrated Energy System for most Polluted City on Earth: A Case Study in Gurugram, India

Samrat Chakraborty and Rajen Pudur

Department of Electrical Engineering

National Institute of Technology Arunachal Pradesh

Yupia – 791112, Arunachal Pradesh

{Corresponding author's email: samrat.phd@nitap.ac.in}

Abstract - The power generation scenario of India is still largely dependent on conventional ways like coal fed thermal power plants. Whereas, some states of India has amazing achievement of generating power renewable resources. Recent report reveals that India tops in having some of the polluted cities on Earth due to pollution from conventional power stations and use of conventional fuel driven vehicles. Gurugram comes first in the list. Thus a major shift is required from using conventional sourced power to non-conventional renewable sourced power. In this paper optimization case study of the grid connected solar/wind/biomass integrated system has been done using HOMER Pro® software. A specific area of the city of Gurugram has been chosen as a model. The optimization result indicates that the setting up of hybrid system in the proposed area is economical. The levelized cost of energy is only \$ 0.0161 /kWh or Rs. 1.14/kWh and the net present cost in total is \$ 621,391.20 which is roughly Rs. 4.41×10⁷. The result also suggests that the CO₂ emission level of the proposed model is very less as compared to the emission scenario of Gurugram.

Keywords - Integrated Energy System; Renewable Energy; Grid Connected; Optimization; HOMER Pro^{\otimes} .

INTRODUCTION

India is one of the countries with largest population on the planet. Within last few decades, there is an extraordinary shift in Indian

economy especially in the field of power generation, its transmission, distribution and obviously the consumption of power, which is still booming. On, the other hand it is very hard to believe that India has the most polluted city on the Earth! Recent studies reveal that Gurugram, a city in India is the most polluted city having a score of 135.8 range of annual mean PM2.5 (μ g/m²) which is very much high with respect to the prescribed limitations of World Health Organization (WHO) [1].

Gurugram belongs to the Indian state of Haryana. 82.84% of power is generated from Thermal Power Plants and the rest is from Renewable Resources [2]. The conventional way of power generation is one of the main reasons for pollution. Gurugram, although a Smart City and which generates some power from Renewable Sources (RS) like solar power, but due to improper institutional plan the demand is not totally fulfilled by RS. Eventually most of the power demand is fulfilled by thermal power plants. There are many reports available on the internet which states the reasons behind the pollution. The reasons can be classified mainly of two categories. The first is the man made pollution and the other is the industry and vehicle made. The industries especially the thermal power station running from coal feed emits huge amount of toxic gases. Moreover, as Gurugram being one of the tech-city in India, the population is too high and the use of diesel or petrol fed vehicles are huge in number which adds to the pollution [2]. Table 1 indicates the pollutants emitted in Gurugram, Haryana due to thermal power station and other heavy industries.

TABLE I
(POLLUTANTS EMITTED IN GURUGRAM [1])

SI. No.	Pollutants							
	Pollutant Compound	Emission (mil. tones/year)						
1	CO ₂	600						
2	СО	9700						
3	Particulate Matter	23000						
4	SO ₂	850						
5	NO	11100						

From the above it is very much clear that the existing thermal power plants have to be stopped in order to reduce the enormous amount of pollutants emitted from them. This has only one solution. The use of renewable energy must be encouraged and small hybrid system must be built in every locality of the city.

Many researches have been conducted, selecting different places of India where renewable energy can be harnessed so that hybrid energy system can be built in those places. In [3] grid integrated solar-battery system has been designed for a village of Uttar Pradesh in the district of Ghaziabad. Results found in the research suggests that the cost for levelized energy (LCOE) in case of grid connected battery storage system is less than the cost for levelized energy (LCOE) in case of grid connected solar photovoltaic system. The computed value of LCOE is Rs. 11.23/kWh and total net present cost (TNPC) is Rs. 1.99×10⁷ with fraction of

renewable is 31.06. The designed system is found to be very cost-effective with low emission. In [4] an integrated solar, hydro, battery and diesel system has been designed for three villages of Himachal Pradesh in the district of Chamba. The carbon emission of the system is found to be very low and the fraction of renewable in the total system is found be around 98%. The computed value of LCOE is Rs. 5.37/kWh and total net present cost (TNPC) is Rs. 26288078 million. It is found in the result that system of solar, diesel and battery combination will work with lowest energy cost and net present cost in total. In [5] an integrated solar-biomass has been designed for an inn on Neil Island of Andaman & Nicobar Island, India. Here, four cases have been considered. In first case: load is directly connected to grid with diesel generator in the backup. In the second case: on-grid solar, battery and diesel generator based integrated system is taken. In the third solar, biomass, battery and diesel case: generator based integrated system is taken which is not connected to the grid. Finally in the fourth case all the setup is just like the last case except an extra thermal load is taken which is connected to a boiler for smoothing running of loads like AC, geezer, heater etc. The system in total is called CCHP i.e. combine coolingheating-power. The result shows that the fourth case is the best one and a savings of Rs. 44096561.00 can be save up-to twenty years. Moreover the carbon emission of 365000 kg can be saved per year. In [6] solar and diesel generator integrated grid connected system has been designed in an institute of education in India. The result suggests that the system can easily served the education institution and thereby reducing the use of

conventional power. The computed value of LCOE is Rs. 11.36/kWh and total net present cost (TNPC) is Rs. 228118633.70 which is found least in the 8th iteration. In [7] solar and tidal based integrated system has been designed in the coast of Cochin, India. Optimization of the system shows that solar, tidal, diesel and battery integrated system is the best system and is very feasible. The

emission level of carbon is also very less in the order of gram/kWh. The computed value of LCOE is Rs. 26.91/kWh and total net present cost (TNPC) is Rs. 2502843788.66. and Renewable Energy, Government of India [10].

SYSTEM RESOURCES

The grid supported integrated renewable based system has been designed in HOMER environment. The case study has been done in Block A, Sector 35, Gurugram City, India. HOMER software needs some



Fig. 1 Location of Case Study

Figure 1 shows the area of study. From the above figure it is seen that the case study has been done in Block A, Sector 45, Gurugram City, Haryana, India which is demarcated by red coloured boundary. The block contains 26 households as per the Census data of Government of India [8]. In this paper, a grid supported Solar-Wind-Biomass hybrid system with battery backup has been designed for the specified area in order to lessen the emission of huge pollutants from traditional power plants. The load data of the specified area has been taken by calculating an average demand of each household. The solar irradiance data and the wind speed data has been taken from NASA Prediction of Worldwide Energy Resources [9]. The biomass data of the specified region has been taken from Biomass Portal, Ministry of New

data for input in order to find the result of optimization [11] which is obtained from NASA surface meteorology and solar energy database for the area of study. The integrated system consists of three main sources of power: solar, wind and biomass. There is a battery backup provided for an emergency situation. A grid is connected in this hybrid system to sell extra power as well as to purchase power during requirement.

A. Load Profile

In this paper, it is calculated that the average consumption of energy in the specified areas is 978.12 kWh/day. Figure 2 portrays every day's mean profile for load demand, in which the maximum demand has been found between the intervals of 08:00 hours to 21:00 hours [12]. Figure 3 portrays the monthly mean load where the maximum demand for the load is 82.81 kW [12]. The main reason for selecting this location is that it has a good possibility of renewable power generation and also the area is facing huge pollution from thermal power plants.

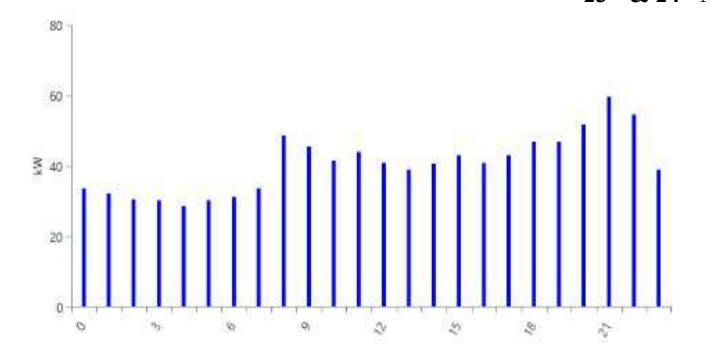


Fig. 2 Daily Profile for Load (Average) [12]

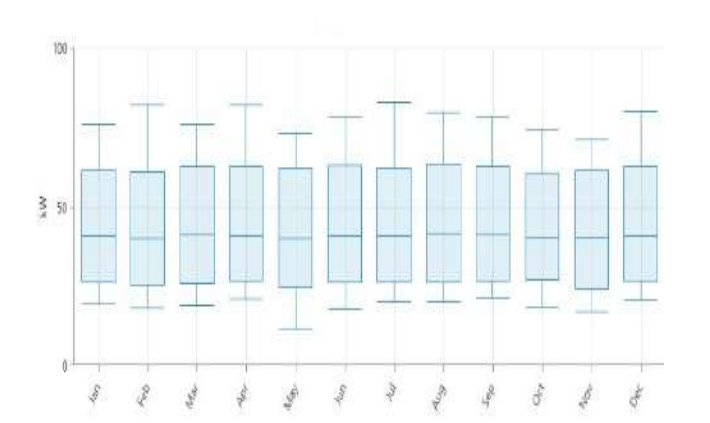


Fig. 3 Monthly Profile for Load (Average) [12]

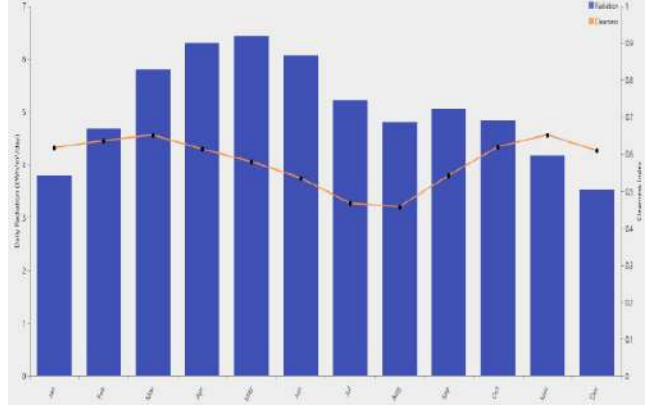


Fig. 4 Solar Radiation and Clearness Index (Monthly Average) [12]

C. Biomass Resource

Biomass resource is available in huge quantity in Block A, Sector 45, Gurugram, Haryana. The state of Haryana is agricultural based state so here cow dung, vegetative waste, and plant waste are available all round the year. So, the biomass resource has been taken constant. The yearly average biomass resource is 106.25 t/day. The carbon content is only 5% and the gasification ratio (kg/kg) is 0.70.

B. Solar Radiation and Wind Speed

The latitude and longitude of Block A, Sector 45, Gurugram in Haryana are 28°26.9' N, 77°3.9' E which is found by using HOMER software. The average yearly solar radiation of the area is 5.06 kWh/m²/day. Figure 4 portrays the mean data in favour of solar irradiance in the Block A, Sector 45, Gurugram for monthly basis. The data for the speed of wind flow is taken at 50 meters over the earth's surface. Figure 5 indicates the wind data for the area whose wind speed data varies from 3.52 m/s to 5.47 m/s. The mean yearly speed of the wind is 4.22 m/s with the month of April having the maximum speed of the wind.

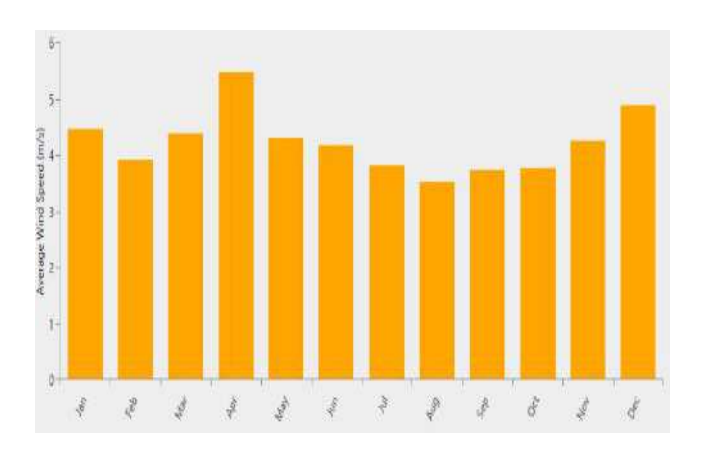


Fig. 5 Wind Speed (Monthly Average) [12]

ECONOMIC EVALUATION BY HOMER

HOMER software was developed by Dr. Peter Lilienthal in National Renewable Energy Laboratory (NERL) in the USA. Later in 2009, the software was commercialized by Dr. Lilienthal [12]. This software is meant for modelling, optimization, and study of any hybrid energy plant which uses renewable sources of energy. The design of models and analysis of both island and grid-connected hybrid energy system is done using HOMER [13]. Depending upon the input parameters like a profile of the load, solar radiance and speed of the wind, which is used in this chapter all possible configurations are simulated. The results are displayed according to the most economical manner in which the loads are satisfied [13]. Results are also displayed in HOMER in Graphs and Table format [14]. HOMER uses the following economic steps for performing the cost analysis.

A. Net Present Cost

NPC comprises of setting up charge and operating charge for the model all over its life span, analysed by the subsequent formula [15]:

Here, TAC indicates the total annualized cost in terms of \$, CRF indicates the capital recovery factor, *i* indicates the rate of interest in terms of % and *Rpr_j* indicates the project lifetime in terms of a year.

B. Total Annualized Cost

The total annualized cost comprises of the addition of the cost of all equipment used in power system which is comprised of capital cost, operation cost, maintenance cost, replacement and fuel cost calculated annually [15].

C. Capital Recovery Factor

The Capital Recovery Factor also is known as CRF calculates the series of cash flow annually in ratio with respect to the present value [15].

$$CRF = \frac{i \times (1+i)^n}{(1+i)^{n-1}}$$

Here, *n* indicates the years and *i* indicate the rate for real interest annually.

D. Annual Real Rate

The Annual Real Interest Rate represents the nominal interest rate as a function [15].

$$i = \frac{i' - F}{1 + F}$$

Here, *i* indicate the real interest rate, *i* indicate nominal interest rate and F indicate annual inflation rate.

E. Cost of Energy

The Cost of Energy also known as COE represents the average cost/kWh of the system producing electrical energy which is useful in practice. The calculative formula for COE is as follows [15]:

$$\mathtt{COE} = \tfrac{\mathtt{TAC}}{\mathtt{L}_{\mathtt{prim},\mathtt{AC}} + \mathtt{L}_{\mathtt{prim},\mathtt{DC}}}$$

Here, $L_{prim,AC}$ indicate primary AC load and $L_{prim,DC}$ indicate the primary DC load.

SIMULATION MODEL

B. Wind Turbine

The system has been designed by taking various components from the software. For simulating the model we have taken three renewable resources. These are solar, wind and biomass. In real sense the resources are chosen depending on the availability in specified area of research. The simulation model also contains battery, converter, residential load and grid connection. Figure 6 shows the designed simulation model. The model works on the proposed controller. The lifespan of the project is 25 years.

The full name of the wind-based turbine employed in this chapter is BWC Excel-R contrived by Bergey Windpower. The labeled capability for one windmill is 8.1 kW with a capitalized expenditure of \$29,000 and functional and repair expenditure 25,000 \$/year. The number of wind turbine used here is 40. The total installed capacity is 405 KW. The life of each turbine is 20 years and the height of the hub of each turbine is 10 m.

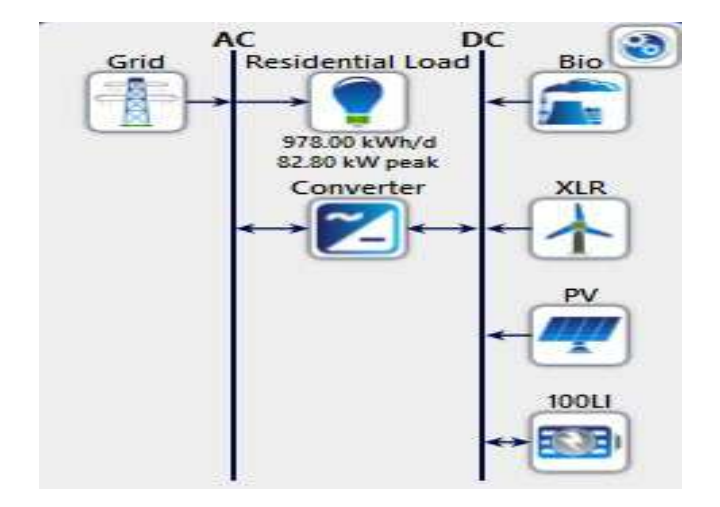


Fig. 6 Simulation Model in HOMER Environment

A. PV Panel

The full name of the array of PV which has been utilized for this chapter is Generic Flat Plate PV, is synthesized by Generic. The labeled capability of this array of PV is 1500 kW with temperature for operation is about 47°C. The capitalized expenditure is 430 \$/kW with operation & preservation expenditure is 10 \$/year. The life span of the array of PV is 25 years an effectiveness of 13%. These unequivocally modeled with maximum power point tracker with the labeled capability of 2000 kW. The capitalized expenditure of maximum power point tracker is 100 \$/kW with functional and repair expenditure is 5 \$/year. The substitution expenditure of maximum power point tracker is 100 \$/kW. The life span of the tracker is 15 years having effectiveness of 95%.

C. Biomass Generator

The name of the biomass generator used is Generic 120 kW Biomass Genset manufactured by Generic. The rated capacity is 120 kW with lifetime 15,000 hours. The initial capital cost is \$40,000 and functional and repair expenditure (per op. hour) cost is \$ 2 with a replacement cost of \$40,000.

D. Power Converter

The name of the power converter is System Converter manufactured by Generic. The life span of the converter is 20 years having effectiveness of 95%. The capitalized expenditure is 720 \$/kW with functional and repair expenditure 0 \$/year. The repairing expenditure of the converter is 460 \$/kW. The total capacity is 1800 kW.

E. Battery

The full name of the battery is Generic 100 kWh Li-lon manufactured by Generic. The capacity of one battery is 100 kWh with a voltage of 600 V. The life span for the battery is 15 years and the effectiveness of 90%. Its capitalized expenditure is \$ 70,000 with functional and repair expenditure 10 \$/year. The initial state of charge of the battery is 80% and the minimum state of charge is 20%. The nominal capacity is 100 kWh or 167 Ah. Maximum discharge current of the battery is 500 A.

F. Grid

Grid is considered to be an infinite source of power. Power can be either purchased or sold to grid. The power price of grid is taken as 0.20 \$/kWh and the net excess price of grid is taken as 0.15 \$/kWh.

OPTIMIZATION RESULTS

Table 2 shows that on the basis of the given system architecture, the optimization is done. In this simulation a total of six components have been considered.

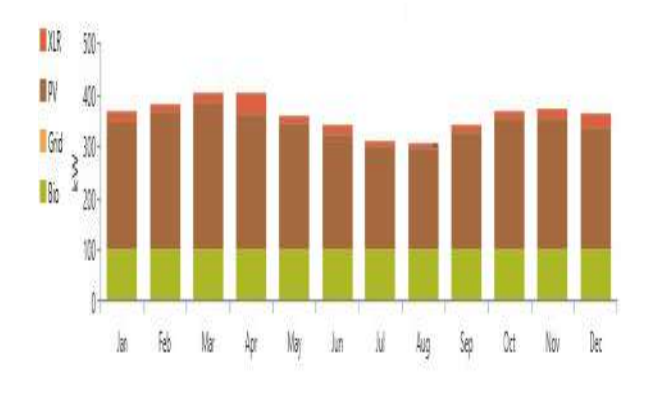


Fig. 7 Electrical Power Generation from Renewable Resources (Monthly)

TABLE II (SYSTEM ARCHITECTURE)

Component	Architecture					
-	Name	Size	Unit			
Biomass	Generic 120 KW Biomass Genset	120	KW			
PV	PV	1500	KW			
Storage	Generic 100 kWh Li-Ion	1	strings			
Wind Turbine	BWC Excel-R	40	ea.			
System Converter	Converter	1800	KW			
Grid	Grid	Infinite	W			

Optimization result shows that the NPC obtained for the grid connected solar-wind-biomass system with battery backup is only \$ 621,391.20 which is very cheap and economical. Further the levelized COE shows to be \$ 0.0161/kWh which equivalents to Rs. 1.14/kWh only. This implies that for generating 978.12kWh/day, only Rs. 1115.06/kWh has to be expended. This is the most economic way. Figure 7 shows the total electrical power generation per month from renewable resources.

The above figure indicates that maximum power is generated in the month of April. It is also seen that Biomass power is constant in every month and is nearly equal to 100 KW. The interesting thing is that the area has good potential of wind, for that reason in each and every month wind power generation is highest. Table 3 shows the NPC of the integrated energy system and table 4 shows the annual expenditure of the total system.

TABLE III (NET PRESENT COST)

Name	Types of Cost						
	Ca pita I	Ope ratin g	Repl acem ent	Salva ge	Reso urce	Tot al	
BWC Excel-R	\$1. 45 M	\$25 8,55 0	\$398, 509	- \$224, 585	\$0.00	\$1. 88 M	
Generic 100 kWh Li-Ion	\$7 00, 00	\$12, 928	\$29,6 99	- \$5,59 0	\$0.00	\$10 7,0 37	

	0					
Generic 120 KW Biomass Genset	\$3 40, 00 0	\$22, 649 0	\$290, 187	- \$3,83 3	\$529, 624	\$1. 08 M
Generic Flat Plate PV	\$6 45, 00 0	\$19 3,91 3	\$0.00	\$0.00	\$0.00	\$83 8,9 13
Grid	\$0. 00	- \$5.1 0M	\$0.00	\$0.00	\$0.00	- \$5. 10 M
Conver ter	\$1. 30 M	\$0.0 0	\$263, 972	- \$148, 765	\$0.00	\$1. 41 M
PV Dedicat ed Conver ter	\$2 00, 00 0	\$12 9,27 5	\$84,8 55	- \$15,9 71	\$0.00	\$39 8,1 59
System	\$3. 70 M	- \$4.2 8M	\$1.07 M	- \$398, 744	\$529, 624	\$62 1,3 91

It is interesting to know that no energy has been purchased from grid. In return huge energy has been injected to grid. Table 5 shows the energy sold to grid and purchased from grid in kWh. The highest energy sold to grid is in the month of March. Table 6 and 7 shows the production and consumption summary in kWh/year. It is seen from the table that only 12% of the power generated is being consumed by the load and the rest is injected to grid after charging the battery. Figure 8 shows the emission data from the whole system after optimization.

TABLE IV
(ANNUALIZED COST)

	'	,AININO/	TLIZLD	0031)		
Name			Types	of Cost		
·	Ca pita I	Ope ratin g	Repl acem ent	Salva ge	Reso urce	Tot al
BWC Excel-R	\$1 12, 16 4	\$20, 000	\$30,8 26	- \$17,3 73	\$0.00	\$14 5,6 18
Generic 100 kWh Li-Ion	\$5, 41 5	\$1,0 00	\$2,29 7	- \$432. 39	\$0.00	\$8, 280
Generic 120 KW Biomass Genset	\$3, 09 4	\$17, 520	\$22,4 47	- \$296. 49	\$40,9 69	\$83 ,73 4
Generic Flat Plate PV	\$4 9,8 94	\$15, 000	\$0.00	\$0.00	\$0.00	\$64 ,89 4
Grid	\$0. 00	\$39 2,42 0	\$0.00	\$0.00	\$0.00	\$39 4,4 20
Converter	\$1 00, 25 1	\$0.0 0	\$20,4 19	- \$11,5 08	\$0.00	\$10 9,1 63
PV Dedicat ed Conver ter	\$1 5,4 71	\$10, 000	\$6,56 4	\$1,23 5	\$0.00	\$30 ,79 9
<u> </u>	-				0 (10	

International Conference On "Impact of Changing Energy Mix in the Power Sector" (ICIEMPS-2019)

	- \$3:	3	- \$30,8			_	eric Flat te PV	2,118,039	67.4
	\$2 0,9 86, 0 25 9		45	\$40,9 69	\$48 ,06 7	kW B	eric 120 iomass enset	876,000	27.9
							Excel-	149,598	4.76
		TABLE \	/				Grid Shases	0	0
ENERGY S		GRID ANI GRID IN KV		HASED I	FROM	T	otal	3,143,637	100
Month		Pa	rameter	S					
	Er	nergy Sold (kWh)		Energy Purchas (kWh)	ed			TABLE VII	
JAN		230498		0			•	ONSUMPTION SUM	,
FEB		217181		0		Comp	oonents _	Deta	ails
MAR		252193		0				Consumption (kWh/yr)	Percentage
APR		245393		0			Primary oad	356,970	12.0
MAY		224480		0	_		Primary	0	0
JUN		201956		0			oad	U	U
JUL		189417		0		Grid	Sales	2,629,465	88.0
AUG		185042		0		T	otal	2,986,435	100
SEP		204170		0					
OCT		229326		0				TABLE VIII	
NOV		225237		0		(EN	/ISSION S	SCENARIO AFTER	OPTIMIZATION)
DEC		224571		0		SI. No.		Pollutants	
						140.	Pollu	tant Compound	Emission (kg/year)
		TABLE V	′ I			1	CO ₂		4473
	(PRODI	JCTION SI		Y)		2	СО		438
Component			Details	- /	_	3	Particula	te Matter	18
F 23.00.00		roduction		_		4	SO ₂		260
		kWh/yr)		Percenta	age	5	NO		350

NO

350

23rd & 24th Nov. 2019

CONCLUSION

From the optimization results it can be concluded that the setting up of hybrid power plants in Block A, Sector 35 of Gurugram City is economical. It is understood from the result data that the place has enormous potential of renewable energy. It is to be noted that a bulk amount of power is being generated from the renewable resources and is being injected or sold to grid. This indicates that the other locality can also consume power based on renewable resources without consuming from grid. The emission level has fall down from million tone / year to kg/year. The most interesting result is that the cost of energy production is only Rs. 1.14 / kWh and the net present cost is Rs. 4.41×10⁷.

REFERENCES

- [1] "2018 WORLD AIR QUALITY REPORT Region & City PM2.5 Ranking," Accessed 14 April 2019. https://www.airvisual.com/world-most-polluted-cities/world-air-quality-report-2018-en.pdf
- [2] "24*7 POWER FOR ALL A JOINT INITIATIVE OF GOVERNMENT OF INDIA AND GOVERNMENT OF HARYANA," Accessed 14 April 2019. https://powermin.nic.in/sites/default/files/uploads/j

oint initiative of govt of india and haryana.pdf

- [3] J. Kumar, B.V. Suryakiran, A. Verma and T.S. Bhatti, "Analysis of techno-economic viability with demand response strategy of a grid-connected microgrid model for enhanced rural electrification in Uttar Pradesh state, India," *Energy*, vol. 178, pp. 176-185, July 2019.
- [4] S. Kumar, T. Kaur, M.K. Arora and S. Upadhyay, "Resources estimation and sizing optimization of PV/micro hydro-based hybrid energy system in rural area of Western Himalayan Himachal Pradesh in India," *Energy Sources, Part A:* Recovery, Utilization, and Environmental Effects, vol. 41, no. 22, pp. 1-13, February 2019.
- [5] M. Wegener, A. Isalgue, A. Malmquist and A. Martin, "3E-Analysis of a Bio-Solar CCHP System for the Andaman Islands, India—A Case Study," *Energies*, vol. 12, no. 6, pp. 1113, March 2019.
- [6] T.S. Kishore and S.M. Kumar, "Techno-economic Analysis of Different Combinations of an Existing Educational Institute-Based PV-Diesel-Grid Hybrid System in India," Soft Computing in Data

- Analytics, Advances in Intelligent Systems and Computing, vol. 758, pp. 343-350, August 2018.
- [7] V. Khare, "Prediction, investigation, and assessment of novel tidal—solar hybrid renewable energy system in India by different techniques," *International Journal of Sustainable Energy*, vol. 38, no. 5, pp. 447-468, October 2018.
- [8] "SERIES-07 PART XII-A DISTRICT CENSUS HANDBOOK GURGAON," Accessed 15 April 2019. http://censusindia.gov.in/2011census/dchb/DCHB
 - A/06/0618_PART_A_DCHB_GURGAON.pdf
- [9] "NASA Prediction of Worldwide Energy Resources", Accessed 15 April 2019. https://power.larc.nasa.gov
- [10] "Biomass Resource Potential in Haryana", Accessed 15 April 2019. https://biomasspower.gov.in/haryana.php
- [11] W.D. Kellogg, M.H. Nehrir, V. Gerez and G.V. Venkataramanan, "Generation unit sizing and cost analysis for stand-alone wind, photovoltaic and hybrid wind/pv systems," *IEEE Trans. on Energy Conversion*, vol. 13, no. 1, pp. 70-75, March 1998.
- [12] "HOMER Energy", Accessed 14 August 2019. https://www.homerenergy.com/
- [13] H. Rezzouk and A. Mellit, "Feasibility study and sensitivity analysis of a stand-alone photovoltaic–diesel–battery hybrid energy system in the north of Algeria," *Renewable and Sustainable Energy Reviews*, vol. 43, pp. 1134-1150. March 2015.
- [14] T. Lambert, P. Gilman and P. Lilienthal, "Micropower system modeling with HOMER," Integration of alternative sources of energy, vol. 1, no. 1, pp. 379-385, 2006.
- [15] M. Nurunnabi and N.K. Roy, "Grid connected hybrid power system design using HOMER," International Conference on Advances in Electrical Engineering (ICAEE), IEEE, pp. 18-21, July 2016.

[16]

The Institution of Engineers (India), WBSC

23rd & 24th Nov. 2019

ERROR BUDGET ANALYSIS OF RESISTANCE TYPE LEVEL PROBE FOR FAST REACTORS

M.Shanmugasundaram*¹, B.K.Choudhary² and D.Thirugnanamurthy³

¹Fast reactor Technology Group

²Metallurgy and Materials Group

³Electronics Instrumentation Group

Indira Gandhi Centre for Atomic Research, Kalpakkam- 603 102

Level sensors are needed for monitoring the sodium level in the various capacities of the reactor systems and to ensure that the coolant level is always kept at the top of the core. Resistance type works on the principle of a step change in its resistance on contact with liquid sodium. It consists of a stainless steel tube inside which copper rod is kept insulated along its length by ceramic beads. The lower end of the copper rod is brazed internally to the stainless steel tube bottom, establishing electrical continuity between the tube and the rod at the bottom end. The arrangement is mounted on the vessel in which the sodium level is to be detected. Under healthy condition fixed, voltage of about 75mV is dropped across he sensor whose resistance constitutes the resistances of copper rod and stainless steel tube in series. During sodium level approaches the bottom of the sensor the liquid sodium thereby shorting the stainless steel tube. As the resistance of copper rod is much lower than that of the stainless steel tube there is a step decrease in the sensor output (ie. From 75 to about 10mV). The step change is detected by the

electronics and is used for level monitoring. Environmental conditions like external stress, temperature, humidity and radiation are applied to each electronics component. External electrical inputs that affect the component quality and causes drift. Error budget analysis for the INSOT facility resistance type level electronics circuit carried out. and evaluated. Errors added in the resistance type level measurement electronics system are identified.

Keywords: Error budget analysis, Sodium, Level, Safety, High Temperature, INSOT, sodium

loop

Rooftop Solar PV: A shining business Proposition: Lessons of West Bengal

Shreya Karmakar · Joy Chakraborty

Electrical Engineering, Member of the Institution of Engineers (India), (IIT, Dhanbad)

(Ashrampara, Basirhat, Pin: 743411)

{Email: shreya03karmakar@gmail.com / joychakro@rediffmail.com}

AbstractFor the first time in the history, in 1881, at Godalming, a picture post card looking small town near London has got electricity driven lights. As technology advances in generation, transmission, distribution sectors, electricity reaches across the globe. From hilltop to desert, island to forest village, electricity penetrates everywhere as a very important medium of providing livelihood requirements like irrigation for agriculture, pumping system for drinking water, computer for education and utility, life care system through diagnostic and life support equipments, entertainment through television - talkies etc. But, like many developing and under developed nations, India could not extend its grid quality electricity infrastructure at every corner of this country. Since 2005, for Indian Power Sector, the most important target was ensuring access to electricity for all households of this country through different flagship programmes like Rajiv Gandhi Garmin Vaidutikaran Yojana (RGGVY), Deendayal Upadhyaya Gram Jyoti Yojana etc. The Govt. of India says that mission is accomplished in 2018. The grid has made connectivity to all households, commercial and industrial establishments of this country excepting a few remote locations where solar power is provided. Now onwards, the IndianPower Sector target has become to provide affordable and quality power supply for 24 *7 for all consumers.

The above is the one side of the story. On the other hand, India has made commitments before the International Community for time bound reduction of fossil fuel based Green House Gases (GHG) emissions to its 1995 level by 2022. To meet up this target, the Govt. of India has framed two programmes: 175 GW capacity addition to the Indian

Grid by 2022 from Renewables, out of which Solar PV contribution is targeted as 100 GW (Rooftop: 40 GW + Ground Mounted: 60 GW). This is further extended to 275 GW by 2027 and 500 GW (with250 GW of Solar PV) by 2030. Another programme is electric vehicles- charging stations to reduce petrol-diesel dependency in the transport system.

This is targeted at a point of time; Indian economy is witnessing its ever lowest growth rate with 5% GDP.India has now 357 Gig watt (GW) Installed capacity of Electricity with 184 GW Peak Demand. During 2018-'19, Indian Power Sector has witnessed 4.2% growth. 41% of new power capacity addition in the first half of 2019 comes from Solar Energy [3.2] GW]. The cumulative installed Solar capacity in India reaches at 31.5GW (by July, 2019). Out of this, rooftop contributes to 3816 MW. The Solar electricity generation has crossed 12 Billion Units in the 2nd Quarter of 2019 (Q2). Inspite of that, the Solar installation in Indiain Q2 2019 has witnessed 14 % Quarter over Quarter (QoQ) and 9% Year-over-Year (YoY) decline. The rooftop installation has declined by 30% YoY, as compared to Q2 2018.

In recent discussions in the United Nation Climate Conference (September,2019) Swedish GirlGreta Thunberg has accused developed countries like U.S, E.U etc for not doing enough for climate mitigation. It is also highlighted that Indian Governments, both at Centre and at States, are not really serious in climate mitigation and adaptation exercises. In its current edition, the Nature magazine shows that in India per capita only 28 trees exist in the backdrop of China: 130 per capita, Sri Lanka: 118 per capita etc. The Environmental Performance Index as presented

at the World Economic Forum,2018 shows that India stands at 177 among 180 countries.

In this background, authors of thepresent article have analyzed 126 cases of Solar PV Installation (capacity of the plant varies from 37 Watt to2.6MW) in Net Metering and self-consumption mode in West Bengal, as it takes place during 2009-19. The potential and trend in respect of future promotion of Rooftop Solar PV programmer in terms of more tolerance to changing technology, business and employment generation is studied through feedback collection on real life installation experiences.

Rooftop PV programme in West Bengal: Initiated at remotest areas, shifted towards urban fringes

Rooftop PV programme has existence in West Bengal since early nineties when people has installed a 37 Wp Solar PV Home System [Solar Photovoltaic Home lighting System: SPV HLS] with 4-6 hours of battery backup. With these SPV HLS, those people of un-electrified or semi electrified areas use CF Lamps, Portable TVs, Table Fan etc for a limited (4 to 6 hours daily) duration. These systems were used in plenty in Sundarban Islands, Hilly areas, Forest Villages, Char areas, Urban Slums. The Census of India, 2011 counts that 2, 34,000 no of families in West Bengal use solar energy for their daily use.

During 2010 to 2015, almost all remote areas in West Bengal including Sagar Island, Gosaba Island, Jogeshganj have got grid quality electricity. Capital Subsidy for yearly average 10,000 no of Solar Home System has been discontinued since 2010. The Govt. of India has introduced loan plus subsidy linked schemes for SPV HLS. But that didn't continue for long. Slowly, Solar Home System has lost its primary role to provide electricity at thousands of households in West Bengal. The Grid has taken that place. This is because, Solar System is a limited source, provides service for a limited duration and that is for limited appliances only. The Grid is an infinite source and can be utilized in customized form for 24×7 duration across the year for all available electrical and electronic appliances.

From 2016 and onwards, in West Bengal Rooftop Solar PV activities have been shifted from remote rural areas to urban fringes. At urban slums, Solar Home Systems are still active. [TheCensus, 2011 shows almost 11 % of population in Kolkata does not have electricity, as they reside in unauthorised settlements like slums.]Thousands of such systems function daily which are not so far covered through any organized programme or major initiative. Parallel to this, medium and large industries have started installing 100KW+ PV Power plant at their roofs, shades etc. According to Bridge to India Report, 2018 and July, 2019; 125 MW+ Rooftop Grid Connected (without battery) Solar PV Installation has been taken place, so far in West Bengal. Out of this, 75 MW + installation have been taken place without government support incentives. or Unlike, Gujarat, Rajasthan, (all India trend also) in West Bengal, Rooftop Solar PV penetration is higher than Ground Mounted Solar PV.

Changing pattern of Rooftop PV business in Bengal: Impact on Stake Holders

Climate Compulsion: Homelighting programme has started when climate compulsion was not there. It was to avail minimum amount of electricity to operate mainly lighting system and allied products. The climatecompulsion is now already in existence. One hand there is a target on other hand looming economy is there. In such a state of affairs, cutting the cost of electricity consumption appears as main driving force behind Rooftop Solar PV installation.

Employment: Employment is the most important concern cutting the borders across the globe, now. It is estimated by the NitiAyog that 9.39 lac job per year for skilled and semi-skilled workers will be there through the Phase –II of National Solar Mission. In a densely populated and agriculture dependent state like West Bengal, small and medium enterprises always play an important role in economy and in employment generation. This aspect is also linked with promotion of Rooftop Solar PV in West Bengal in specific and for the country in general.

Awareness among users: Rural consumers were accustomed with solar power, as they have the experience in using such system for more than 20 years. Urban consumer wants to reduce its electricity bill. But, the common idea among consumers, as it is observed, is that Net Metering is the only way to reduce electricity bill. Prevailing Govt regulation, Net Meter/ Gross Meter/Self Consumption/Anti Grid Export Controller: there are so many options, but guidelines regarding specific applicability for the respective consumer are absent. An industrial consumer under TOD tariff want grid connectivity through net metering which is a loss financial proposition to them, rather they may opt for selfconsumption, which means it is a grid connected, but not grid interactive system. Without appropriate awareness, consumers will not find much interest in Rooftop PV installation.

Mindset of DISCOM: It is a popular belief among professionals of Discom that more PV injection (through roof top system) to the grid corresponds to loss of revenue of Discom. But the reality is that, in case of commercial and industrial consumers [contributes 98% of the Net-metered roof top PV installation in West Bengal], only a part of their electricity bill is reduced through such Solar system. Since such systems are in operation in a part of the day time only, the peak demand, as it is in the evening and morning (main business time for provider/Discom) electricity service remain unaffected as Solar PV is not functional at that time. On the other hand, Discom avails quality solar power at their grid (the surplus which is pushed to the grid by the consumer) at no investment cost. This Solar Power is used by the DISCOM to mitigate their RPO obligation at no investment cost of the Discom. The tail end voltage is also improved at no investment cost of the Discom. So, an appropriate mechanism is need of the hour to initiate a sustained exercise to change the mindset of DISCOM people. Without the active support of the DISCOM, Rooftop PV can't be flourished properly.

Phase II of National Solar Mission: Needs Change of WBERC Regulation in West Bengal: In West Bengal, so far, Net Meter is not allowed to domestic [individual household owners] consumers. In the

Phase –II of the National Solar Mission, the Govt. of India has introduced Performance based incentive for Distribution Companies [DISCOMs] where upfront capital subsidy in the tune of 20% to 40 % is proposed for domestic consumers against rooftop PV installation. To implement such scheme, the West Bengal Electricity Regulatory Commission [WBERC] has to change its regulation, based on application of DISCOMs to allow individual household owner to avail Net Meter.

Gross Meter: At present, in the Net Metering system, adjustment of electricity bill is done at the same rate of procurement of electricity by consumers. Say, if a consumer procures electricity @ Rs.9.50 per kWh from the DISCOM, adjustment of electricity bill against surplus push to the grid from Solar Power is made at the same rate of Rs. 9.50per kWh. While preparing draft implementation policy, DISCOM is cultivating the option of Gross Meter where the adjustment rate may be much less than the procurement rate of the consumer. Say, if a consumer procures electricity @ Rs.9.50 per kWh from the DISCOM, adjustment of electricity bill against entire [not surplus] push to the grid from Solar Power may be made at the rate of Rs. 4.50per kWh in gross metering arrangement. Naturally, it may not be a lucrative proposition to consumers.

Alternative to proposed Gross Metering arrangement:

DISCOM as RESCO: It is found out through data analysis that 30 to 35 % consumers of DISCOMs has connected load of 1KW to 3 KW. These consumers may be offered PV Net Metering system with provision of 100% adjustment of electricity bill. The study shows these consumers are prone to payment defaulter. So, if Rooftop Solar Home System can be made available to them with 40 % of upfront capital subsidy [as offered by the Govt. of India] and for balance the DISCOM can act as Renewable Energy Service Company [RESCO] . They may bear the cost of balance 60 % of system cost and the same can be recovered from monthly electricity bill of such consumers.

System with Anti-Grid Export Controller: For consumers with connected load of 3 to 05 KW, Rooftop PV system with Anti Grid Export Controller can be provided where capital subsidy @ 20 % [as offered by the Govt. of India] will be available and no surplus push to the DISCOM grid will take place.

System with Net Meter with lower adjustment cap: For all consumers above 05 KW PV installations, Net Meter may be continued. It may also be extended to domestic consumers. Time of the Day [TOD] meter replacement may also be allowed with lower upper cap for adjustment of electricity bill, say upto 70 % of electricity consumption in a billing cycle. Through such practices, interest of both consumers and DISCOM can be protected.

Ease of doing business:

At the time of looming economy, some 150+companies are in operation in Rooftop Solar PV business in West Bengal. Roughly, some 5000+people in West Bengal earn their bread and butter from this business. The areas of intervention, as observed in respect of ease of doing business are as following:

Help the transition: There exist some 30 + companies which have started business in nineties with PV system with battery backup. It is observed that these companies cannot cope up with the transition from battery system to grid connected rooftop PV. A brief orientation and counseling through sustained interaction can make these companies capable of handling grid connected PV projects.

Capacity building: As the technology of Solar PV is witnessing rapid day to changes, different able institutions, initially at-least four corners of this state can be upgraded as Technical Backup units which can conduct regular orientation courses to upgrade the skill and knowledge base of practicing professionals in this field.

Developing standard operating practices:As of now, there is no guideline available in respect of preparation of design and bill of materials. It is now anybody's job. The MNRE, Govt of India has a set of

guidelines; the Skill Development Council has released Standard Protocol of Checking. Consolidating these documents, filtering ambiguities and framing a standard set of practices in designing and execution is the need of the day.

Linkage with Chamber of Commerce: Study on recent installations clearly indicates that roof sheds of factories and warehouses are potential area for rooftop PV installation. Existing Solar companies are not in regular touch with Chamber of Commences. This linkage is very much needed to tap the unutilized potential of roof space, as owned by different industry and commercial houses that are under cover of different Chamber of Commences.

Linkage with RESCO and DISCOM: Financing PV projects, both at residential and commercial establishments is one of the most important aspects for its promotion. Renewable Energy Service Companies can be promoted and linked with Solar Enterprises to meet up the gap in between the aspiration and ability of consumers for PV installation. Linkage with DISCOMs will make the clearances easier and can provide a clear certainty for clearances towards time bound grid connectivity.

Single Window Clearance: In the present scenario, a consumer has to submit three documents to the Discom to avail net meter: project completion report, technical clearance from Nodal Agency, agreement in between consumer and Discom. In such system, problem is that as the consumer is not aware about technical and tariff proposition, he/she comes to know about all the difficulties/problems after completion of the project. Then it is very difficult for them to make any rectification. As Solar PV grid tied system is functioning in either grid interactive or grid non-interactive mode, technical clearance in respect of PV installation from Nodal Agency/Discom (as per direction of the Regulatory Commission) and electrical safety clearance from electrical inspector are necessary. In such a position, it is felt that, a single window clearance portal /app based system is the need of the day to guide the consumer before doing the project and to make the process of availing of Net Meter, if it is required, hassle free.

Conclusion: The Rooftop Solar PV installation in West Bengal, as taken so far is not so bad and at the same time not very good also. While we are at the end of 2019, a lot still needs to be done to make things better in this sector. In Pan India perspective, for the first time, decarbonized electricity appears feasible in the near future. It is not an abstract vision now. In West Bengal, already 50 MW + rooftop PV installation has been taken place without any Government support. Here, right strategy, policies and programmes in terms of ease of doing business, more tolerance to changing technology, capacity building and easy financing with time bound clearances can help the state to promote the Rooftop PV as a Sunrise industry which can crate immense employment and can lead and cater the entire east and north east India from West Bengal.

References:

- [1] The Times of India, Kolkata Edition, 14.09.19
- [2] The Telegraph: Kolkata Edition, 16.09.19
- [3] The Executive Summary, prepared by Prayas Energy Group, Pune on Rooftop PV Sector, December, 2018
- [4] Phase-II, National Solar Mission: MNRE, Govt of India
- [5] Rooftop PV: Bridge to India Report, July, 2019
- [6] Presentation of WBSEDCL on Phase-II, National Solar Mission at the Indian Chamber of Commerce, August, 2019
- [7]EiSamai, Kolkata Edition: 12.09.19
- [8] Role of DISCOMs as an aggregator for Rooftop in India: A.J.Bhattacharya, August, 2019
- [9] Millennium Post, Kolkata Edition, 09.09.19
- [10] MERCOM report: August, 2019
- [11] PhD Thesis: Viability of different Renewable Energy Resources in West Bengal: R. Chakraborty, 2019, Rabindra Bharati University

Different topologies transformerless inverter for application Of PV to grid tie system

Tejaswini Bhaskar Dhole

Abstract:

In recent power generation solar energy has become popular due to its abundant availability of energy compared to conventional energy sources. The grid connected photovoltaic system is increasing due to its higher efficiency output .When transformer is connected between Grid and the PV system, galvanic isolation is provided to control the leakage current. When transformers are connected, the system becomes bulky and the maintenance cost also increases. To overcome this problem, PV grid connected transformer less inverters are constructed. Transformerless inverter is developed to provide high efficiency and low leakage current. Transformer less inverter are capturing a market because of its advantages just like higher efficiency, lower cost, less complexity and smaller volume compared to their counterparts with transformer galvanic isolation.

Unfortunately, there are some safety issues because a galvanic connection between the grid and the PV array exists in the transformerless systems. A common-mode leakage current flows through the parasitic capacitor between the PV array and the ground once a variable common-mode voltage is generated in transformerless grid-connected inverters. The common-mode leakage current increases the system losses, reduces the grid-connected current quality, induces the severe conducted and radiated electromagnetic interference, and causes personal safety problems.

Keywords: Transformerless inverter, photovoltaic generation system, common mode leakage current, Simulink model, Topology.

Determination of Fault Location in a Long Transmission Line based on Feature Extraction, Regression and Artificial Neural Network

Dr. Nabamita Banerjee Roy, Associate Professor and HOD, Life Member of IE(I)

Department of Electrical Engineering (Narula Institute of Technology) (81, Nilgunj Road, Agarpara, Kolkata-700109)

{Email: roynab@gmail.com}

Abstract - Fault is an inevitable phenomenon in every power system network. Identification of fault and its location is a challenging task. As the dimension of network increases, finding the location of a fault becomes more complicated. An extensive research work has been conducted in this domain. Expert systems based on soft computing techniques and Artificial Neural Network (ANN) have shown promising results. This paper has proposed a method of finding the location of a fault in a long transmission line. Short Circuit Faults involving single/multiple phases to ground have been simulated at different locations on the transmission line. The method is based on feature selection by S-Transform (ST). ST is a popular signal processing tool which gives information about both the time and magnitude of frequency component of any transient signal. In this paper, two features have been selected from the voltage/current signal at a single terminal of a long transmission line using ST. The profile of the features for different fault locations has been obtained and it is observed that the pattern is not suitable for training by ANN. Polynomial Regression has been applied on both the features to obtain a regular pattern of the profile and the resulting features after regression have been trained by Back Propagation Neural Network (BPNN) to obtain the fault location. All the simulations and programming have been done in MATLAB. Satisfactory results have been obtained as the magnitudes of fault locations have been obtained within ±5% accuracy.

Keywords - Artificial Neural Network (ANN); Back Propagation; Neural Network (BPNN); Fault location; Feature extraction; Polynomial Regression; S-Transform (ST)

INTRODUCTION

Advancement of power electronics and solid state devices has made possible EHV and UHV ac transmission of power over long distances. Researches and experiments are being conducted for realization of these vast transmission networks. Designing of relaying and protection system of these complicated networks requires additional skill with respect to speed, cost and accuracy. Implementation of Digital and smart relaying system is justified as the results are promising. Identification of a type of fault and obtaining its location is quite challenging in a long transmission line. An extensive research work has been addressed in this domain as available in [2-3].

Signal Processing methods using Wavelet Transform (WT) have shown outstanding performances in classification of faults of transmission lines and obtaining their location.

A method based on Discrete Wavelet Transform (DWT) has been proposed in [4] for classification of faults in transmission systems. In this paper, percentage of energy levels were calculated for identifying the nature of fault. A protection scheme for a three-terminal transmission system has been presented in [5]. In this paper, DWT has been used to calculate several features like signal energy, maximum value of detail component, from current of each phase to detect the type of fault and its location. Another way of fault classification has been proposed in [6] by using a technique of wavelet based current signature analysis. An approach based on DWT has been suggested in [7] for fault classification of a transmission line using phase currents of its two terminals. On the other hand, current signals of only end of an overhead line have been used in [8] for obtaining features by DWT in order to detect a nature of fault. A simulation model of MATLAB has been considered in [9] to generate different types of fault- data. In this paper, MATLAB wavelet toolbox has been used to detect and to classify the type of faults.

Artificial neural network (ANN) has an excellent capacity of learning from a known system of data by using any kind of training algorithm. Once successfully trained, it can be put to powerful use in understanding "untrained" or "unknown" case of the problem. back-propagation (BP) neural system design has been implemented in [10] for identification. In this paper, different regions of a power system network have been segregated and a corresponding neural system is designed to identify the nature of fault in that region.

A comparative study of fault analysis of double circuit transmission line has been presented in [11] involving three different feed forward neural networks, namely, Correlation Feed Forward Network (CFBPN), Radial Basis Function (RBF) network and Back PropagationNetwork(BPN).

An ANN based relay system has been proposed in [12] for fault identification in an EHV overhead system. A technique of fault identification has been presented in [13] based on ANN. In this paper, current and voltage of each phase have been used as the input parameters for training by an ANN to identify the nature of fault as the output. Another technique has been proposed in [14] for fault classification based on BP neural network architecture in

which rms values of voltage and current have been used as inputs for fault classification. A MATLAB Simulink model has been developed in [15] for the study of different fault conditions in transmission lines and the output of the Simulink model has been used to train the ANN for fault identification.

Application of fuzzy logic has helped in many cases to build a convenient relationship amongst input and output variables without the need of any numerical model. Recognition of both symmetrical asymmetrical faults has been done in [16] for both single and double-circuit transmission lines using the method of fuzzy logic. A scheme based on fuzzy logic has been developed to detect the line to ground fault in case of 400 kV, 300 km transmission line model. Different kinds of short circuit faults have been diagnosed using two fuzzy rule systems in [17]. A new strategy has been developed in [18] for investigation of faults in overhead lines based on fuzzy system.

Combination of more than one technique involving WT, ANN and fuzzy logic has evolved into stronger techniques as Hybridization overcomes the drawbacks in one approach during its application, with the strengths of the other by appropriately integrating them. These techniques are classified into 4 types as given below:

- Neuro-fuzzy technique.
- Wavelet and ANN technique
- Wavelet and fuzzy-logic technique
- Wavelet and neuro-fuzzy technique

These techniques havecontributed in producing a huge quantity of research work. Adaptive neuro fuzzy inference system (ANFIS) has been implemented in [19] for fault identification in long transmission lines in which input data have been obtained from the fundamental components of the current and voltage. A method based on WT and ANFIS has been developed in [20] for obtaining fault location in a series compensated transmission system. In this method, line currents of both ends of transmission system have been considered for obtaining features by WT and the corresponding features are used as input parameters by ANFIS for calculating the fault location. A fuzzy logic based system using DWT has been developed in [21] for identification of ten different types of faults in an unbalanced power distribution system. The proposed method in this work has been tested in an IEEE 13 bus system. A fault classification scheme based on WT and ANN has been implemented in [22] for identification of double line faults in a six phase transmission line. In this paper, standard deviation of approximated coefficients of instantaneous voltages and currents has been calculated and used as the input parameter of ANN. A fault classification scheme has been developed in [23] for an EHV transmission line.

S-Transform is another method of signal processing. It gives a Time-Frequency Representation of any signal. Unlike WT, selection of mother wavelet is not needed in

case of ST. ST give the information of magnitude of a frequency component and its phase angle at any point of time. Abundant research work has been done by implementing ST in analysis of seismic conditions of earth, transient conditions of power system and power quality, [24-26].

In the present paper, a hybrid method of finding fault location in an EHV transmission system has been suggested. This method is based on ST and ANN. Section 1 describes the simulation of the system and the different kinds of faults. A brief overview of Discrete S-Transform, the method of feature extraction and Polynomial Regression have been discussed in Section2. The method of obtaining fault location by BPNN has been described in Section 3. The conclusion has been provided in Section 4, followed by Acknowledgement and References.

SIMULATION OF LONG DISTANCE TRANSMISSION LINE AND FAULTS

The Fig. 1 shows a single line diagram of an EHV long transmission line, [27]. Fig. 1 shows the simulation model in which a three-phase, 50 Hz, 735kV power system is transmitting power from a powerplant consisting of six 350 MVA generators to an equivalent network through a 600 km transmission line. The transmission line is split in two 300 km lines connected between buses B1, B2, and B3. The system has been simulated in MATLAB Simulink in which sampling times of all the signals have been taken to be 0.0003125µs and the time period of simulation has been taken up to 0.16 secs. The sampling frequency is 3.2 kHz.

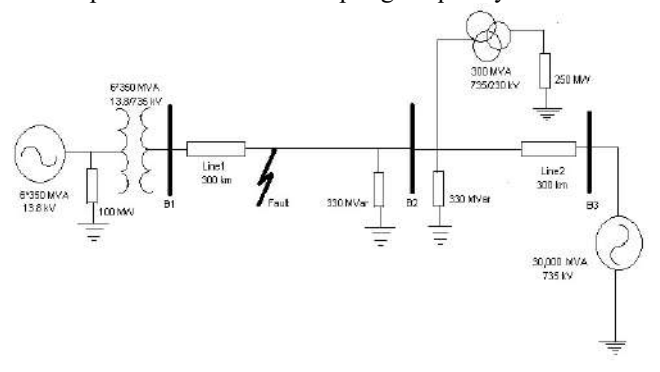


Fig.1: Single-Line Diagram of three phase EHV transmission system

Short circuit faults have been simulated in the following way at different locations on the transmission line:

AG: Phase A shorted to ground BG: Phase B shorted to ground CG: Phase C shorted to ground

AB: Phases AB shorted BC: Phases BC shorted CA: Phases CA shorted

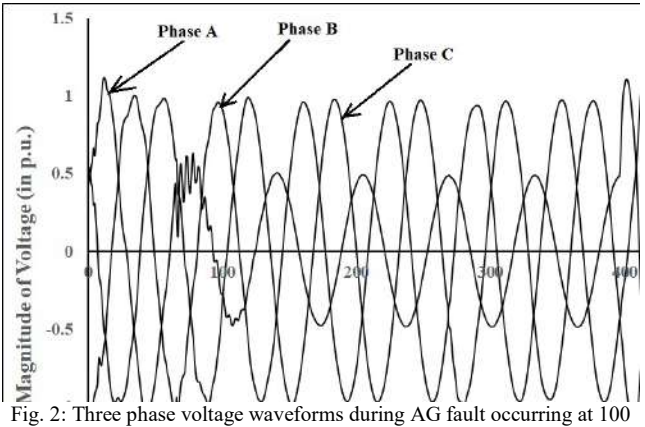
ABG: Phases AB shorted to ground BCG: Phases BC shorted to ground

CAG: Phases CA shorted to ground

ABC: Phases ABC shorted

The fault locations have been selected in steps of 10 km from the bus B1 of the network shown in Fig. 1. Classification of faults has been already done for this system in [27]. For the purpose of obtaining fault location, the fault resistances(R_F) considered are 0, 5, 15 and 20 ohm. The fault inception angle is taken to be 0° .

Fig. 2 shows the three phase voltage waveforms during a AG fault occurring at 100km on the transmission line at B1 with $R_F = 0$ ohm.



km from B1, with $R_F = 0$ ohm

FEATURE EXTRACTION USING DST

A. Brief Overview of DST

S-Transform is a modified version of Continous Wavelet Transform (CWT). The basic definition of CWT is given by equation (1).

$$W(\mathbf{d},\tau) = \int_{-\infty}^{+\infty} f(t) \frac{1}{\sqrt{|d|}} \psi\left(\frac{t-\tau}{d}\right) dt \qquad \dots \dots \dots (1)$$

In equation 1, τ represents Translation, i.e., the location of the window and drepresents Scale, i.e., the frequency parameter.

The S-Transform is an effectively efficient tool for time frequency representation (TFR) of a time series. ST is a hybrid of the STFT and WT and it produces a frequency dependent resolution with simultaneously localizing the real and imaginary spectra. Due to its easy interpretation, multiresolution analysis and the ability of maintaining the meaningful local phase information, the ST has established successes in many areas including power quality, geophysics and biomedicine [24-26].

An electrical signal h(t) can be expressed in discrete form as h(kT), $k = 0, 1, \dots, N-1$ and T is the sampling time

The discrete Fourier transform of h(kT) is obtained as,

$$H\left[\frac{n}{NT}\right] = \frac{1}{N} \sum_{k=1}^{N-1} h(kT) e^{\frac{-i2\pi k}{N}} \tag{2}$$

Where $n = 0, 1, \dots, N-1$.

The ST of a discrete time series is obtained by letting

$$f \to n/NT$$
 and $\tau \to jT$ as

$$S\left[jT, \frac{n}{NT}\right] = \sum_{m=0}^{N-1} H\left[\frac{m+n}{NT}\right] G(m, n) e^{i2\pi mj/N}$$
 (3)

and
$$G(m,n) = e^{-2\pi^2 m^2/n^2}$$
, $n \neq 0$ where j, m = 0,1,2,.....N-1 and n = 1,2,....N-1 (4)

A complex matrix (S-matrix) is generated from equation (3) in which the rows are the frequencies, whereas the columns are the corresponding times. The amplitude of the ST spectrum is obtained from the absolute values of the complex matrix. Each column, thus, represents the local spectrum at one point in time. The matrix preserves the amplitude information of the frequency content of the signal at different resolutions.

B. Feature Extraction

Once the type of fault is identified, the simulated data of the voltage signal corresponding to the faulty phase at Bus B1 have been considered for feature extraction. In case of faults involving more than one phase, voltage signal of any one of the phases has been considered.DST has been performed on the simulated data. As the total number of samples of the voltage signal are 512, the number of rows and columns of the S-matrix are 256 and 512 respectively. The rows and columns of the S-matrix have been investigated thoroughly. The elements of each column are plotted with respect to the row numbers of the S-matrix. It is observed that the elements corresponding to column no. 456 have two prominent peaks as shown in Fig. 3. The magnitudes of the two peaks have been noted and termed as peak1 and peak 2 respectively. This process has been followed for every fault location and a profile has been plotted for all the values of peak 1 and peak 2, as shown in Fig. 4.

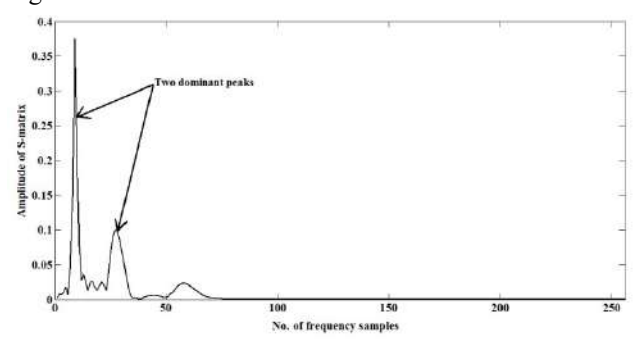


Fig.3: Profile of the magnitudes of elements of S-matrix corresponding to column no. 456 with respect to the no. of frequency samples in case of an AG fault occurring at 100 km from B1, with $R_F = 0$ ohm

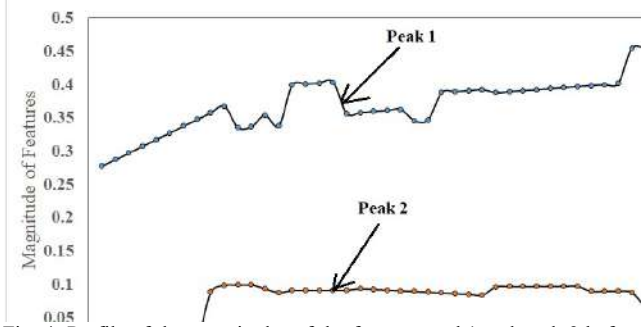


Fig. 4: Profile of the magnitudes of the features peak 1 and peak 2 before regression in case of an AG fault occurring at 100 km from B1, with $R_F = 0$ ohm

The profile of both the features, peak 1 and peak 2, is unsuitable for training in a neural network due to its irregular pattern. The nature of irregularity also differs with the change in the type of fault. Subsequently, the results that would be obtained after training would be highly unpredictable. Hence, polynomial regression is applied in these features as described in section C.

C. Polynomial Regression

Polynomial models are a special case in Linear Regression Models. Polynomial models have the advantages of being simple, familiar in their properties, and reasonably flexible for following data trends. They are also robust with respect to changes in the location and scale of the data. Choosing a polynomial model is often a trade-off between a simple description of overall data trends and the accuracy of predictions made from the model.

In the present work, polynomial regression is applied on the features peak1 and peak2 by programming in MATLAB. The profiles of the features after regression have been shown in Fig. 5 respectively.

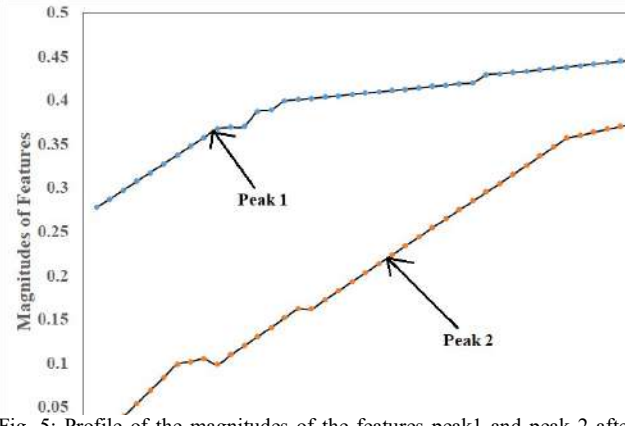


Fig. 5: Profile of the magnitudes of the features peak 1 and peak 2 after regression in case of an AG fault occurring at 100 km from B1, with $R_F = 0$ ohm

DETERMINATION OF FAULT LOCATION BY BPNN

A. Brief Overview of BPNN

Artificial Neural Network (ANN) provides an efficient and intelligent technique of data classification and function approximation. There are different types of architectures of neural network available. Selection of a particular type depends on the nature of the problem. BPNN has produced promising results in analysis of power system faults, [28-29]. In this paper, the fault location has been obtained using BPNN. BPNN consists of different kinds of training algorithms, like, Levenberg-Marquardt (LM), Resilient Backpropagation (RP), Variable Learning Backpropagation (GDX), etc. It is very difficult to determine which training algorithm will be suitable for a given problem with respect to speed and accuracy. The compatibility of any algorithm would depend on many factors, such as, the nature of the problem, the number of data points in the training set, the number of weights and biases in the network, the error goal, and whether the network is being used for pattern recognition or function approximation. In this paper, LM algorithm has been chosen for obtaining fault location as it has produced convincing results in published literatures, [28-29].

B. Application of BPNN in obtaining Fault Location

The two features after regression corresponding to 20 fault locations have been chosen to be the elements of the input vector. The rest of the data have been used for testing purpose. As an illustration, Table I shows the magnitudes of a few fault locations obtained after training. Fig. 6 shows a comprehensive plot of the actual fault locations and the ones obtained after training. The maximum percentage error is 4.43% which is below 5% and hence, it is acceptable.

TABLE I (COMPARISON BETWEEN ACTUAL FAULT LOCATIONS AND THE ONES OBTAINED FROM BPNN)

	OBIA	INED FROM DI	ININ)	
Type of Fault	Fault Resistance (ohm)	Actual Fault Location (km)	Fault Location obtained from BPNN	% Error
AG	0	20	19.89	0.55
BG	0	40	38.97	2.58
CG	0	60	61.45	-2.42
AB	0	80	79.57	0.54
BC	0	100	104.43	-4.43
CA	0	120	118.67	1.11
ABG	0	150	150.03	-0.02
BCG	0	180	179.92	0.04
CAG	0	200	203.45	-1.72
ABC	0	220	220.45	-0.20
AG	5	250	248.78	0.49
BG	5	270	271.35	-0.50
CG	5	300	303.32	-1.11
AB	15	320	318.34	0.52
ABG	15	350	352.67	-0.76
BC	15	370	371.56	-0.42
BCG	15	400	400.15	-0.04
CAG	20	430	428.56	0.33
CA	20	450	449.67	0.07

ABC	20	460	456.78	0.70
ABC	20	480	480.78	-0.16

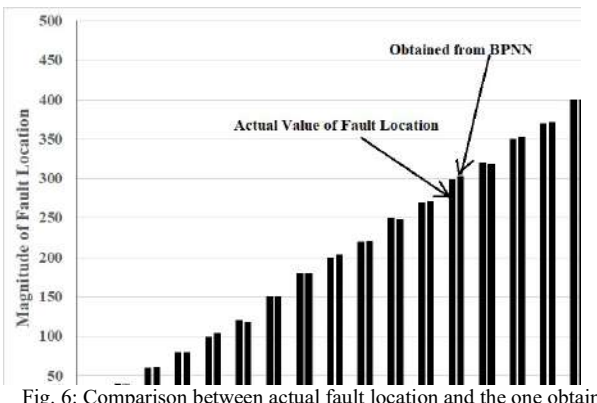


Fig. 6: Comparison between actual fault location and the one obtained from BPNN

CONCLUSION

A method of obtaining fault location in a long transmission line has been proposed in this paper. This method is based on signal processing, feature extraction and ANN. DST offers a convenient way of extracting feature from any transient signal. In this paper, different fault conditions have been simulated so that maximum number of transient conditions can be studied and the fault locations can be predicted accordingly. Only the voltage signal of the faulty phase has been used for feature extraction resulting in reduction of consumption of memory and time of computation. The technique of polynomial regression has helped in enhancing the performance of training by BPNN by producing a regularised pattern of the input features. The use of LM training algorithm in BPNN has been justified as the fault locations have been obtained with a maximum error of 4.43%, which is reasonably acceptable.

ACKNOWLEDGMENT

The author is thankful to the authorities of Narula Institute of Technology for the continuous encouragement and motivation in conducting research activities.

REFERENCES

- Ch.DurgaPrasada, N.Srinivasua, Fault Detection in Transmission Lines using Instantaneous Power with ED based Fault Index, SMART GRID Technologies, August 6-8, 2015, Procedia Technology 21 (2015) 132 – 138.
- [2] Avagaddi Prasad, J. Belwin Edward, K. Ravi, 2018, A review on fault classification methodologies in power transmissionsystems: Part—I, Journal of Electrical Systems and Information Technology 5 (2018) 48–60, https://doi.org/10.1016/j.jesit.2017.01.004.
- [3] Avagaddi Prasad, J. Belwin Edward, K. Ravi, 2018, A review on fault classification methodologies in power transmissionsystems: Part—I, Journal of Electrical Systems and Information Technology 5 (2018) 8–61-67, https://doi.org/10.1016/j.jesit.2016.10.003.
- [4] Ashok, V., Bangarraju, K.G.V.S., Murthy, V.V.N., 2013, Identification and classification of transmission line faults using wavelet analysis,. ITSITrans. Electr. Electron. Eng. 1 (1), 117–122.
- [5] Dileep Kumar, A., RaghunathSagar, S., 2014, Discrimination of faults and their location identification on a high voltage transmission lines

- usingthe discrete wavelet transform, Int. J. Educ. Appl. Res. 4 (January–June (1)), 107–111.
- [6] Jose, Prince, Bindu, V.R., 2014, Wavelet-based transmission line fault analysis, Int. J. Eng. Innov. Technol. 3 (February (8)), 55–60.
- [7] Lakshmana Nayak, B., 2014, Classification of transmission line faults using wavelet transformer, Int. J. Eng. Sci. Res. Technol. (February), 568–574.
- [8] Ali Rana, Shahzad, Ahmad, Aziz, NoorullahQuadri, Mohammad, 2014, Faults detection and classification on long transmission line using wavelet analysis, Int. J. Res. Eng. Adv. Technol. 2 (June–July (3)), 1–6.
- [9] Prasad, Avagaddi, Belwin Edward, J., 2016, Application of wavelet technique for fault classification in transmission systems, Procedia Comput.Sci. 92, 78–83.
- [10] Tayeb, EisaBashier M., Aziz AlRhim, Orner A.I., 2011, Transmission line faults detection, classification and location using artificial neural network, IEEE Conf. Publ., 1–5.
- [11] Tayeb, ÉisaBashier M., 2013, Faults detection in power systems using artificial neural network, Am. J. Eng. Res. 2 (6), 69–75.
- [12]Saha, Suman Kumar, Das, Priyanath, Chakrabothy, Ajoy Kr, 2012, An ANN based relay design for identification faults of 400kv high voltage ACtransmission line, Int. J. Comput. Appl. 46 (May (20)), 8– 13
- [13] Hessine, Moez Ben, Jouini, Houda, 2014, Fault detection and classification approaches in transmission lines using artificial neural networks, IEEE Conf. Publ., 515–519.
- [14]Kumar K, Sanjay, Swamy R, Shivakumara, Venkatesh, V.,2014, Artificial neural network based method for location and classification of faults on a transmission lines, Int. J. Sci. Res. Publ. 4 (June (6)), 1– 6
- [15]Kesharwani, Smriti, Singh, Dharmendra Kumar, 2014, Simulation of fault detection for protection of transmission line using neural network, Int. J.Sci. Eng. Technol. Res. 3 (May (5)), 1367–1371.
- [16] Cecati, Carlo, Razi, Kaveh, 2012, Fuzzy-logic-based high accurate fault classification of single and double- circuit power transmission lines, IEEEConf. Publ., 883–889.
- [17] Shashi, R., Neelam, L., Nidhi, C., Richa, N., Ramesh, P., 2012, Fuzzy-logic-based fault classification for transmission line protection, Int. J. Res. Eng. Appl. Sci. 2 (February (2)), 281–291.
- [18]Samantaray, S.R., 2013, A systematic fuzzy rule based approach for fault classification in transmission lines, Appl. Soft Comput. 13 (2), 928–938, Elsevier.
- [19]Kamel, T.S., Moustafa Hassan, M.A., El-Morshedy, A., 2009, Advanced distance protection scheme for long transmission lines in electric powersystems using multiple classified ANFIS networks, IEEE Conf. Publ., 1–5.
- [20]Tag Eldin, El Sayed Mohamed, 2010a, Fault location for a series compensated transmission line based on wavelet transform and an adaptiveneuro-fuzzy inference system, IEEE Conf. Publ., 229–236.
- [21] logicMajid Jamil, Rajveer Singh, Sanjeev Kumar Sharma,2015, Fault identification in electrical power distribution system using combined discrete wavelet transform and fuzzy logic, Journal of Electrical Systems and Information Technology 2 (2015) 257–267, http://dx.doi.org/10.1016/j.jesit.2015.03.015.
- [22] Kumar, Ravi, Koley, Ebha, Yadav, Anamika, Thoke, A.S., 2014, Fault classification of phase to phase fault in six phase transmission line using haar wavelet and ANN, IEEE Conf. Publ. (February), 5–8.
- [23] Raikwar, V.T., Kankale, R.S., Jadhav, S.S., 2014, EHV transmission line fault classification, In: Proceedings of 10th IRF International Conference, June, pp. 78–82.
- [24]F. Zhao and R. Yang, Localization of the Complex Spectrum: S-Transform, IEEE Trans. On Signal Processing, vol. 44, No. 4, pp. 998-1001, April 1996.
- [25] Stockwell, RG (1999), S-Transform Analysis of Gravity Wave Activity from a Small Scale Network of Airglow Imagers, PhD thesis, University of Western Ontario, London, Ontario, Canada.
- [26] S. Mishra, C. N. Bhende, and B. K. Panigrahi, Detection and Classification of Power Quality Disturbances Using S-Transform and Probabilistic Neural Network, IEEE Trans. On Power Delivery, Vol. 23, No. 1, pp. 280-287, Jan 2008.

- [27] Nabamita Roy, Kesab Bhattacharya, Identification and Classification of Fault in an EHV transmission line using S-Transform and Neural Network, International Journal of Electrical, Electronics and Computer Engineering, Special Issue Vol. 2(2): 80-87(2013), ISSN No. (Online): 2277-2626.
- [28] Nabamita Roy & Kesab Bhattacharya (2015) Detection, Classification, and Estimation of Fault Location on an Overhead Transmission Line Using S-transform and Neural Network, Electric Power Components and Systems, 43:4, 461-472, DOI: 10.1080/15325008.2014.986776.
- [29] Nabamita Roy, Kesab Bhattacharya, Signal Analysis based Fault Classification and Estimation of Fault Location of an Unbalanced Network using S-Transform and Neural Network, Transactions on Electrical and Electronic Engineering (IEEJ), Vol. 11, No. 4, July 2016, pp. 401-409, published online in Wiley Online Library (wileyolinelibrary.com), DOI: 10.1002/tee.22256.

DISCRETE DESIGN OPTIMIZATION OF 3-PHASE INDUCTION MOTORS USING STANDARD LAMINATIONS

Pritish Kumar Ghosh *, Pradip Kumar Sadhu *, Amarnath Sanyal +

Department of (Electrical Engineering) (IIT (ISM) Dhanbad*) (Dhanbad-700141)

Department of (Electrical Engineering)

(Jadavpur University*)

(Kolkata-700032)

{Corresponding author's email: pritish_ghosh80@rediffmail.com}

Abstract - 3-phase squirrel-cage type induction motors are very widely used as industrial drives. They have outpaced their predecessor the d.c. motors for various advantages they have. Slip-ring or phasewound types are used as adjustable-speed drives. Cage-type motors are also being used as adjustable-speed drives after the advent of power-electronic devices. The single-phase motors are also widely used for running small machineries and domestic appliances. The total expenses for these motors constitute the largest fraction of the total investment at the consumer end. Therefore, they must be designed costoptimally. At the same time they must conform to the standards specified by the customer or the statutory regulations imposed by the authorities. If the design is made according to guidelines given in the text-books, we may expect to reach only a feasible solution but not the cost-optimal solution. For job work, it is economic to use stampings standard as this practice eliminates the cost of dies which is quite high. The paper presents an iterative procedure to get the cost-optimal solution subject to usual design constraints, using standard stampings available in the market. A case study has been made on its basis.

Keywords - Boost converter, Gridconnected, Photovoltaic (PV), PWM inverter, Transient current limiter (TCL), Stability analysis, Total harmonic distortion (THD).

Symbols and abbreviations:

G	Rating, Kv	.,
(7	naunu. Kv	v

ac Amp.conductor/m

 B_{av} Average flux-density in the air-gap, Tesla

 K_n, K_k Pitch/breadth factor of stator winding

V_s / V_n Stator line/phase voltage, V

 I_{s}/I_{n} Stator line/phase current, A

 $\delta_{\rm s}/\delta_{\rm r}$ Stator/rotor current density, A/mm²

 K_{\circ}, K_{\circ} Stacking factor, copper space factor

 D,D_{\circ} Stator bore/outer diameter

 D_a, D_i Stator outer/Rotor inner diameter

 D_r, D_i Rotor outer/inner diameter

 L, L_r Length of stator/rotor

 T_s, a_s No of stator turns/phase; C.S. of stator conductor

l_g Length of air-gap

 a_b, l_b Cross-section/ length of rotor bar

 $I_{\scriptscriptstyle \mu}, I_{\scriptscriptstyle \mathrm{w}}, I_{\scriptscriptstyle 0}$ Magnetizing/ core and friction loss/

no load current

starting torque. The phase-wound or slip-ring types are used for such drives though they are more expensive and they suffer from problems arising out of rotating contacts.

INTRODUCTION

For job production of transformers or induction motors standard laminations are normally used. The practice is economically better. If laminations are freely designed, then the die-set required for fabricating the laminations is quite costly. If the order is for a few machines, purchasing die-sets for laminations is not economically viable. The usual practice is to use standard stampings for the same. Standard stampings of various sizes are available in the Indian market. Once upon a time Shankey wing of M/S Guest, Keen and Williams dominated the market of stampings. Now several other companies like M/S Debidayal etc. makes mass production of stampings.

Designs conforming to standard stampings and standard frames cannot be made by following the test-book procedure. Specially constructed programmes are required for their design.

CONSTRUCTIONAL FEATURES OF INDUCTION MOTOR

Induction motors are broadly classified as squirrel-cage type and phase-wound or slipring type. The squirrel-cage types are more robust and rugged, cheaper and maintenance-free. So they are more in common use. However they were not suitable for variable speed drive (until the advent of power electronic control). They run at a lagging power factor thus drawing substantive amount of VAR from the system causing excessive voltage drop. They are also not suitable for loads requiring high

A. Cage-type motors

Stator construction: The main parts of the stator are the stator core and the stator core-coil structure windings. The assembled in the frame. The frame sizes are standardized. The stator core is made by assembling stampings of Si-steel (Lohys or special Lohys) having one or two coats of varnish. Different grades of materials are available in the market. Semiclosed slots, either parallel-sided or rectangular, are commonly used. Depending on the size of the motor, a no. of radial and axial ducts is provided while cores are assembled, for adequate cooling and if necessary a cooling fan is also added. The slots are lined with insulating paper and coils made of insulated conductors are placed in slots to form the windings. The individual phase windings are similar to each other- they are internally separate but externally connected in star or delta according to the designer's choice. Copper conductors of appropriate cross section are used. Aluminium conductors are used for transmission lines but are not suitable for rotating machines as they take more space which offsets the over-all economy.

Rotor construction:

The rotor core is also made of laminations of the same material, with coats of varnish to limit the eddy current. However, solid cores are also used for large machines to get a mechanically stronger rotor. As the rotor frequency is much smaller than the line frequency, the rotor iron loss is negligible. The no. of slots should not equal to that of

stator- also a no. of unfavorable combinations of stator and rotor slots are to be avoided so that vibration, noise, cogging and crawling may not occur.

The cage type rotor is made by placing bars of copper or aluminum in the slots and brazing them to two end-rings. Presently die-cast rotors are used which mechanically stronger, aluminum are being the commonly used material. The cage type rotor is short-circuited in itself. Hence no resistance can be inserted in the rotor circuit of a cage type motor to limit the starting current and increase the starting torque. Larger starting torque may be realized by using deep and narrow slots or by using double squirrel cage construction.

The rotor core & winding structure is keyed on to an M.S. shaft of required diameter which is placed on ball/roller bearings in end-plates bolted to the stator frame on its two sides. The diameter is determined by the consideration of torsional and bending stresses. The enclosure is to be chosen according to the environment and the mounting according to the specific use.

B.Phase-wound motors

The phase-wound or slip-ring type motors are used for adjustable speed drives. Their stator construction is similar to that of squirrel-cage motor. But the rotor construction is different- it houses a polyphase winding wound for same no. of poles (but may be of different no. of phases) as for the stator. The windings connected in star and the terminals brought Variable slip-rings. rheostats connected to the windings through slip-rings and brushes. Their function is to limit the starting current and to increase the starting torque. They may also be used for rheostatic speed control. However slip-power recovery schemes employing power-electronic devices are better options as they do not waste power in the rheostats and hence they are power-economic. They can be used also in the VAR-compensating mode by injecting emfs with q-axis components.

THE DESIGN PROCEDURE

Four different approaches are made for designing an engineering equipment viz. analytic, synthetic, optimal and standard. The analytic procedure is very common and easiest. It starts from identifying the design variables and assigning appropriate values to them. These values are obtained either from the experience of the designer or from design data books. Then data entry is made for the equipment to be designed. The program runs through multiple steps for calculating the dimensions of the machine and for computing the performance variables. There is no feedback from the output or the results into the input section. So one must be content with whatever results he get or he may take another chance changing the values of the design variables.

The shortcomings in the analytic approach can be partially offset by following the synthetic method in which specifications and constraints are given. The program is designed to give multiple feedback from the output in respect of the constraints and to bring forth necessary changes in the variables to conform to the specifications.

A.Design variables

There are many variables in a 3-phase induction motor. Some of them continuous variables, some of them are decision variables and some of them are integer variables. The variables that have large influence on the cost-function are called key variables. In an induction motors, the continuous variables are: i) length/polepitch ratio, ii) average flux-density in the gap, iii) flux-density in the stator/rotor core iv) teeth flux-density in stator/rotor v) ampconductor/m of periphery, vi) slot depth/slot width, etc. The decision variables are: i) single laver or double laver winding in the stator, ii) configuration of slot, iii) conductor material for rotor, iv) type of bearing iv) laminated or solid rotor etc. The integer variables are: i) no of stator/rotor slots, ii) no of slots/pole/phase (generally integral slot winding is used in induction motor, iii) no. of conductors/slot (even integer for double layer winding) iv) no of ducts etc.

At first, the key variables are identified. Then they are initialized. Their values are changed gradually to get the best possible or optimal design. Many of these variables do not come into picture in case of standard design e.g. the no of stator/rotor slots, slots/pole/phase, slot depth/slot width etc. as these are defined by the standard lamination to be used.

B.Design constraints

The optimization has to be sought in presence of a no of inequality and other constraints viz.

 a) Full voltage starting torque/full load torque must more than a pre-defined value e.g. 1.75.

- b) Maximum torque/full load torque must more than a pre-defined value e.g. 2.25.
- c) The efficiency must be more than a predefined value e.g. 85%
 - d) The power factor must be more than a pre-defined value e.g. 0.8 lagging
 - e) The no. of stator slots/ rotor slots must be integers
 - f) No. of slots/pole/phase must be an integer

ALGORITHM

The algorithm for optimal design with standard laminations is given below:

- 1. Read data on design variables $(B_{w}, ac, L/\tau)$, specific cost etc.
- 2. Read data files on SWG no of wires, thickness of insulation etc.
- 3. Read specifications of the motor.
- 4. Check the validity of the specifications. For invalid specifications go to step 2
- 5. Find the output coefficient. Find input power/apparent power from assumed values of efficiency & power factor.
- 6. Find the approximate friction & windage loss by using data file on the same.
- 7. Find no. of poles, synchronous. speed and the D²L-product.
- 8. Find shaft diameter from mechanical considerations.
- 9. Choose length/pole pitch ratio as 0.8 and find the stator bore diameter.
- 10. Open the data file for standard laminations available in the market and keep the data in an array. Compare the calculated diameter with the diameters of standard laminations and choose the frame size of nearest available diameter.
- 11. Read the details of the lamination. Check the feasibility of accommodating the shaft. If the inner diameter of the lamination is less

- than the shaft diameter then goto step 33.
- 12. Find the length of stator from D²L product, net length of iron, number of ducts, pole pitch, flux per pole.
- 13. Find pitch factor by short pitching the coil to about 5/6th. of the pole pitch. Find the breadth factor and the winding factor.
- 14. Find number of turns/phase.
- 15. Find stator current, no. of conductors in parallel and the cross-section of the conductor.
- 16. Open the data file for SWG number and choose the appropriate conductor available in the market.
- 17. Find the depth of insulation and outer diameter of the conductor.
- 18. Choose parallel-sided teeth and semi-closed slots.
- 19. Find depth of stator core and width of teeth for specified flux density of core and the teeth.
- 20. Find the slot dimensions to accommodate the conductors.
- 21. Find mean length of turn of stator and its resistance per phase.
- 22. Calculate iron loss in teeth & core of the stator by opening data file on special LOHYS.
- 23. Find the air gap, rotor diameter and length.
- 24. Choose Aluminium as rotor conductor material. Find dimensions of the rotor bars and the end rings and dimensions of the rotor slots.
- 25. Find Carter's coefficients from the data file and the total AT of stator, rotor & air-gap.
- 26. Find the magnetisation current & the no load current.
- Find the slot leakage, overhang and zigzag presences & the leakage reactance.
- 28. Find the rotor resistance & the short circuit impedance.
- 29. Make performance evaluation at full load slip, efficiency, power factor and temperature rise.
- 30. Find critical speed and maximum torque.

- 31. Find starting current and starting torque, taking increase in rotor resistance due to skin effect into considerations.
- 32. Calculate the weight of iron, copper and aluminium and find the total cost inclusive of labour & overhead cost.
- 33. Keep all calculated values in array.
- 34. Decrease the diameter by one step &goto step 11
- 35. Examine the calculated values of the array and choose the lamination for cost-optimality.
- 36. Print the values corresponding to optimal design.
- 37. Stop
- 38. End

In this work, the cost function includes the running cost of the motors in addition to its capital cost to preserve the interest of the customer.

CASE STUDY

A programme has been developed to design the motor using standard stampings, changing design variables like L/τ ratio etc. and compute the cost function. This function is a weighted combination of the cost of production and the running cost so as to cover the interest of both the manufacturer and the customer. The design has been made following the algorithm given in the earlier paragraphs.

A. The specifications

Type of motor: 3-phase Squirrel Cage

Induction motor

Type of starter: Star-Delta (Yd)

Frame Material: Normalised Grey C.I., with

holes for axial flow.

Stator winding connection: DELTA; Type of

stator winding: Double layer

23rd & 24th Nov. 2019

Slot insulation: Bonded Polyester; Stator/ Rotor core material: Super-varnished

Special Lohys

Class of insulation: B: Temperature rise as

per grade

Type of enclosure: SPDP with fan-cooling Stator conductor material: Synthetic

resin-enameled copper

Rotor material: Die-cast Aluminium; Roller bearings on both ends: Rotor to be

dynamically balanced

B. The ratings

KW/HP output: 30 / 40.2; Line voltage = 415 V; variation: -15% to +6% Frequency = 50 Hz.; variation: ± 4%; R.P.M.= 1450; Duty: Continuous

C.Chosen design variables and assumptions

Amp.-conductor/m = 35000; Average flux-density = 0.45 Tesla
Length/pole-pitch ratio varying from: 0.8 to 2
Stator current density: = 6 A/mm²;
Rotor current density = 4.575 A/mm²
Stator teeth/ core density in Tesla: = 1.2; 1.25; Rotor core density = 0.6627
Tesla

Copper space factor = 0.6; Assumed efficiency /power factor: 0.9 / 0.9

D. The specific costs

Cost of iron = Rs. 120/ kg; Cost of copper (nomex-coated) = Rs 720/ Kg; Cost of aluminum = Rs. 180/Kg

E. The findings

The programme finds out the following possibilities:

Frame	Stato	Stato	Roto	Stato	Roto
no.	r	r	r	r no.	r no.
	outer	inner	inner	of	of
	diam,	diam,	diam	slots	slots
	mm.	mm.	,		
			mm.		
144M	260.	177.	44.4	36	40
	4	8	5		
102M	304.	190.	50.8	36	40
	8	5			
146M	304.	215.	50.8	36	40
	8	9			
104M	366.	228.	50.8	36	59
	6	6			
103A	355.	254.	50.8	48	59
М	6	0			

Out of these, frame no. 104M of Shankey division of GKW gives the cost-optimal solution. So the design has been made on the basis of this stamping.

*F.*The solution of the design problem

Main dimensions:

No. of poles = 4; Synchronous speed = 25 R.P.S

Approx. KW/KVA input: 33.333 ;

37.037

Output coefficient =164.59; D²L-product

 $= 0.00900 \text{ m}^3$

We choose standard stampings from table, but slots are freely designed. The frame designation chosen by iterative procedure: 104M

Stator design

Stator bore diameter = 228.6 mm;

Stator length = 170 mm; Length/polepitch ratio = 0.947; No. of ducts = 1:Width of ducts = 10 mm

Net length of iron = 147 mm; Pole pitch = 179.5 mm; Flux/pole = 0.3740 Waber; No. of stator slots/ no. of rotor slots: 36 / 59; Stator slot angle.= 20°

No. of stator/rotor slots/pole/phase: = 3 / 4.917; Stator/rotor slot pitch in mm: 19.9 12.1; Pitch factor of stator = 0.9848; Breadth factor of stator = 0.9598; Winding of stator = 0.9452; No factor conductors/slot = 24; Total no. of conductors = 864; No of turns/phase = 144; No of parallel conductors in stator = 2; SWG No. of stator conductors = 15; Area of stator conductor = 2.627 mm^2 ; Diameter of stator conductor = 1.8288 mm: Diameter of stator conductor with insulation 2.059 mm; Total copper area/slot = 126.08 mm²; Parallal teeth & trapezoidal slots are used. ;Width of teeth = 8.5 mm; Lip / Wedge in mm: 1 / 3; Width of slot over wedge = 12.1 mm; Width of slot at bottom = 16.0 mm; Depth of slot = 26.0 mm; Actual copper space factor = 0.407 : Depth of stator core = 37.0 mm : Outer diameter of stator = 356 mm; Clearance with frame = 4 mm.

Rotor design:

Airgap length = 0.6 mm; Rotor length = 160.0 mm

Rotor bar current = 370.6 A ;Rotor bar area = 81 mm2 ; Rotor bar width = 4.5 mm ; Rotor bar length = 160.5 mm ;Rotor bar depth = 18 mm ;Slip-ring width = 21 mm; Depth of rotor core = 70.4 mm ; Inner diameter of rotor = 50.8 mm = Shaft diameter ; Flux-density at 1/3 rd. tooth height of rotor = 0.999 Tesla ; Width of rotor teeth at 1/3 rd. tooth height = 6.3 mm ; Minimum width of rotor teeth = 5.7 mm; Rotor bars are skewed by one slot pitch. Ring depth is equal to bar depth.

No load current calculation:

Carter's coefficient: for stator slot = 0.637; for duct= 0.763; for rotor slot= 0.253; Gap contraction factor: for stator slot = 1.190; for rotor slot = 1.021; for duct = 1.047; Equivalent gap contraction factor = 1.272; Amp.turn required: for airgap = 372; for

stator teeth = 92; for rotor teeth = 9; for stator core = 31

for rotor core = 4; Total Amp.turn required = 508

Magnetizing current = 6.37 A = 21.9 %Losses: Friction & windage = 522 W; Stator teeth = 130.5 W; Stator core = 229.4 W; Stator iron = 359.8 W; % iron Loss = 1.1; Rotational loss current = 0.71 A 2.43 %

No load current = 6.41 A 22.04 %; Losses at full load:; Rotor ohmic loss = 867.6 W 2.64 %; Stator ohmic loss = 1088.3 W 3.31 %; No load loss = 881.83 W 2.69 %; Total loss = 2837.7 W 8.6 %; Parameter estimation:

Stator resistance = 0.508 Ω 3.643 %; Rotorresistance referred to stator = 0.405 Ω 2.904% ; Eddy loss ratio = 5.724Leakage reactance: due to slotting = 1.15 Ω ; due to overhang = 0.40 Ω ; due to zigzag = 0.92 Ω Total leakage reactance = 2.47 Ω 17.74 %Magnetising reactance = 65.13 Ω 466.84 %

Iron loss resistance = 585.91 Ω 4200 %; Equivalent impedance referred to stator = 2.638 Ω 18.91 %

Full load condition:Full load torque = 202.12 N-m; Full load stator current/phase = 29.09 A; Full load line current = 50.39 A; Full load power factor = 0.9309

Full load power input =32838 W; Full load efficiency = 0.9136; Full load slip =0.0273; Full load speed = 1459 rpm; Starting current = 110.5 A; Starting torque at full voltage = 540.31 N-m; Starting torque at reduced voltage (Y-D starter) = 180.1 N-m; Starting current/full load current for full voltage starting = 3.796; Starting torque/full load torque for full voltage starting = 2.673; Starting torque/full load torque at reduced voltage (Y-D starter) = 0.891; Critical slip = 0.16037; Maximum torque = 541.96 N-m; Maximum torque /full load torque = 2.681; temperature rise:Copper loss in embedded portion of stator winding = 419.1 W; Total loss in embedded portion of stator winding = 778.9 W; Temperature rise of stator = 28.68 oC; Cost analysis:Weight of iron = 90.65 Kg ; Cost of iron = Rs.10877/-Weight of copper = 17.83 Kg; Cost of copper = Rs.12841/-

Weight of aluminium = 2.87 Kg; Cost of aluminium = Rs. 517/-Material cost including 20% auxilliaries = Rs. 29083/-Manufacturing cost inclusive of labour & establishment = Rs. 40716/-The average running cost for a life span of 10 years = Rs. The cost function = Rs. The cost functions for all other feasible solutions have been found to be more.

CONCLUSION

Optimization is the process of finding out the best possible solution out of many feasible solutions. The feasible solutions of a design problem are found out by varying the design variables within their normal bounds. The solution giving minimum cost may be found out either by exhaustive search in the parameter-space or by techniques like gradient search, method of random walk etc. The advanced mathematical techniques need not be used for finding out the optimal solution using standard laminations, as the no. of solutions is few. Therefore the method of exhaustive search is acceptable in this case. The only thing of interest is to check the compatibility of the design with the chosen standard core and whether the specifications have been fulfilled.

If we aim at getting only the minimum cost of production, that will be good for the manufacture. It will keep down the cost of the machine and increase the sale. However, the machines will be less efficient, will have higher ohmic and no-load losses and will give rise to more environmental pollution indirectly. Therefore, the best practice is to frame an objective function accounting for the capital cost and the running cost.

In this work, a computer programme has been developed for the design of 3-phase squirrel-cage induction motor. Provisions have been made for switching over to standard lamination available in the market after finding out the bore diameter. It has been repeated for a no. of times changing the (length:pole pitch) ratio within its normal bounds. Also changes have been made in the value of average flux-density and amp. Conductor/m. The best possible solution has been chosen from the set of

solutions obtained by this process. The case-study has been made on a 30 KW, 415 V, squirrel-cage induction motor.

REFERENCES

- [1] O.W. Anderson, "Optimum design of electrical machines", IEEE Trans. (PAS), Vol-86, pp. 707-11, 1967.
- [2] M. Ramamoorty, "Computer-aided design of electrical equipment", Affiliated East-West Press Pvt. Ltd., 1987, ISBN: 81-85095-57-4
- [3] M.G. Say, "Performance and design of a.c. machines", ELBS.
- [4] A.K. Sawhney, "A course in electrical machine design", Dhanpat Rai and Sons, 2003
- [5] K. Deb, "Optimization for engineering design", PHI, 2010. ISBN 978-81-203-0943-2
- [6] S.S. Rao, "Engineering optimizationtheory and practice", New Age Int.; ISBN 978-81-224-2723-3
- [7] N.S. Kambo, "Mathematical programming techniques", Revised edition,1991,1984, Affiliated East-West Press Pvt. Ltd. New Delhi 110 001, ISBN 81-85336-47-4.
- [8] A. Shanmugasundaram, G. Gangadharan, R. Palani, "Electrical machine design data book", Wiley Eastern Ltd. ISBN 0 85226 813 0
- [9] S.F. Lindsay & T.H. Barton, "Parameter identification for squirrel cage induction machines", IEEE Trans. Power

Apparatus System, 1973, pp. 1287-1291

- [10] G. Erajskar, M. Bhattacharyya & S.N. Mahendra, "Computer-aided design of three phase squirrel cage induction motor- technical design, hybrid process and optimization", J.I.E (India), E.E. Div., India, 1974, pp. 2-50
- [11] H.B. Ertan, C. Aykanat, "A new approach to optimized design of induction motor", Dept. of Elect. Engg., Middle East Technical university, Ankara, Turkey.
- [12] F. Kentli, "A survey of design optimization studies of induction motor

- during the last decade", Dept. of Elect. Education, Marmara University, Goztepe, Istambul, Turkey.
- [13] R.N. Hasanah, "Energy saving through design optimization of induction motor", Journal EECCIS, Vol. 3, No. 1, June, 2009.
- [14] C. Thanga Raj, S. P. Srivastava, and P. Agarwal, "Energy-efficient control of three-phase induction motor a review", International Journal of Computer and Electrical Engineering, Vol. 1, No. 1, April, 2009.
- [15] R. Kannan, R. Bhuvaneswari, and S. Subramanian, "Optimal design of three-phase induction motor using Particle warm Optimization", Iranian Journal of Electrical and Computer Engineering, Vol. 6, No. 2, 2007.
- [16] S. S. Sivaraju& N. Devarajan, "Novel design of three phase induction motor enhancing efficiency, maximizing power factor and minimizing losses", European Journal of Scientific Research, ISSN 1450-216X, Vol. 58, No.3, (2011), pp.423-432

DISCRETE DESIGN OPTIMIZATION OF 3-PHASE INDUCTION MOTORS USING STANDARD LAMINATIONS

Pritish Kumar Ghosh *, Pradip Kumar Sadhu *, Amarnath Sanyal +

Department of (Electrical Engineering) (IIT (ISM) Dhanbad*) (Dhanbad-700141)

Department of (Electrical Engineering)

(Jadavpur University*)

(Kolkata-700032)

{Corresponding author's email: pritish_ghosh80@rediffmail.com}

Abstract - 3-phase squirrel-cage type induction motors are very widely used as industrial drives. They have outpaced their predecessor the d.c. motors for various advantages they have. Slip-ring or phasewound types are used as adjustable-speed drives. Cage-type motors are also being used as adjustable-speed drives after the advent of power-electronic devices. The single-phase motors are also widely used for running small machineries and domestic appliances. The total expenses for these motors constitute the largest fraction of the total investment at the consumer end. Therefore, they must be designed costoptimally. At the same time they must conform to the standards specified by the customer or the statutory regulations imposed by the authorities. If the design is made according to guidelines given in the text-books, we may expect to reach only a feasible solution but not the cost-optimal solution. For job work, it is economic to use stampings standard as this practice eliminates the cost of dies which is quite high. The paper presents an iterative procedure to get the cost-optimal solution subject to usual design constraints, using standard stampings available in the market. A case study has been made on its basis.

Keywords - Boost converter, Gridconnected, Photovoltaic (PV), PWM inverter, Transient current limiter (TCL), Stability analysis, Total harmonic distortion (THD).

Symbols and abbreviations:

G Rating, Kw

ac Amp.conductor/m

 B_{av} Average flux-density in the air-gap, Tesla

 K_n, K_h Pitch/breadth factor of stator winding

V_s / V_n Stator line/phase voltage, V

 I_{s}/I_{n} Stator line/phase current, A

 $\delta_{\rm s}/\delta_{\rm r}$ Stator/rotor current density, A/mm²

 K_{\circ}, K_{\circ} Stacking factor, copper space factor

 D,D_{\circ} Stator bore/outer diameter

 D_a, D_i Stator outer/Rotor inner diameter

 D_r, D_i Rotor outer/inner diameter

 L, L_r Length of stator/rotor

 T_s, a_s No of stator turns/phase; C.S. of stator conductor

l_e Length of air-gap

 a_b, l_b Cross-section/ length of rotor bar

 $I_{\scriptscriptstyle \mu}, I_{\scriptscriptstyle \mathrm{w}}, I_{\scriptscriptstyle 0}$ Magnetizing/ core and friction loss/

no load current

starting torque. The phase-wound or slip-ring types are used for such drives though they are more expensive and they suffer from problems arising out of rotating contacts.

INTRODUCTION

For job production of transformers or induction motors standard laminations are normally used. The practice is economically better. If laminations are freely designed, then the die-set required for fabricating the laminations is quite costly. If the order is for a few machines, purchasing die-sets for laminations is not economically viable. The usual practice is to use standard stampings for the same. Standard stampings of various sizes are available in the Indian market. Once upon a time Shankey wing of M/S Guest, Keen and Williams dominated the market of stampings. Now several other companies like M/S Debidayal etc. makes mass production of stampings.

Designs conforming to standard stampings and standard frames cannot be made by following the test-book procedure. Specially constructed programmes are required for their design.

CONSTRUCTIONAL FEATURES OF INDUCTION MOTOR

Induction motors are broadly classified as squirrel-cage type and phase-wound or slipring type. The squirrel-cage types are more robust and rugged, cheaper and maintenance-free. So they are more in common use. However they were not suitable for variable speed drive (until the advent of power electronic control). They run at a lagging power factor thus drawing substantive amount of VAR from the system causing excessive voltage drop. They are also not suitable for loads requiring high

A. Cage-type motors

Stator construction: The main parts of the stator are the stator core and the stator core-coil structure windings. The assembled in the frame. The frame sizes are standardized. The stator core is made by assembling stampings of Si-steel (Lohys or special Lohys) having one or two coats of varnish. Different grades of materials are available in the market. Semiclosed slots, either parallel-sided or rectangular, are commonly used. Depending on the size of the motor, a no. of radial and axial ducts is provided while cores are assembled, for adequate cooling and if necessary a cooling fan is also added. The slots are lined with insulating paper and coils made of insulated conductors are placed in slots to form the windings. The individual phase windings are similar to each other- they are internally separate but externally connected in star or delta according to the designer's choice. Copper conductors of appropriate cross section are used. Aluminium conductors are used for transmission lines but are not suitable for rotating machines as they take more space which offsets the over-all economy.

Rotor construction:

The rotor core is also made of laminations of the same material, with coats of varnish to limit the eddy current. However, solid cores are also used for large machines to get a mechanically stronger rotor. As the rotor frequency is much smaller than the line frequency, the rotor iron loss is negligible. The no. of slots should not equal to that of

stator- also a no. of unfavorable combinations of stator and rotor slots are to be avoided so that vibration, noise, cogging and crawling may not occur.

The cage type rotor is made by placing bars of copper or aluminum in the slots and brazing them to two end-rings. Presently die-cast rotors are used which mechanically stronger, aluminum are being the commonly used material. The cage type rotor is short-circuited in itself. Hence no resistance can be inserted in the rotor circuit of a cage type motor to limit the starting current and increase the starting torque. Larger starting torque may be realized by using deep and narrow slots or by using double squirrel cage construction.

The rotor core & winding structure is keyed on to an M.S. shaft of required diameter which is placed on ball/roller bearings in end-plates bolted to the stator frame on its two sides. The diameter is determined by the consideration of torsional and bending stresses. The enclosure is to be chosen according to the environment and the mounting according to the specific use.

B.Phase-wound motors

The phase-wound or slip-ring type motors are used for adjustable speed drives. Their stator construction is similar to that of squirrel-cage motor. But the rotor construction is different- it houses a polyphase winding wound for same no. of poles (but may be of different no. of phases) as for the stator. The windings connected in star and the terminals brought Variable slip-rings. rheostats connected to the windings through slip-rings and brushes. Their function is to limit the starting current and to increase the starting torque. They may also be used for rheostatic speed control. However slip-power recovery schemes employing power-electronic devices are better options as they do not waste power in the rheostats and hence they are power-economic. They can be used also in the VAR-compensating mode by injecting emfs with q-axis components.

THE DESIGN PROCEDURE

Four different approaches are made for designing an engineering equipment viz. analytic, synthetic, optimal and standard. The analytic procedure is very common and easiest. It starts from identifying the design variables and assigning appropriate values to them. These values are obtained either from the experience of the designer or from design data books. Then data entry is made for the equipment to be designed. The program runs through multiple steps for calculating the dimensions of the machine and for computing the performance variables. There is no feedback from the output or the results into the input section. So one must be content with whatever results he get or he may take another chance changing the values of the design variables.

The shortcomings in the analytic approach can be partially offset by following the synthetic method in which specifications and constraints are given. The program is designed to give multiple feedback from the output in respect of the constraints and to bring forth necessary changes in the variables to conform to the specifications.

A.Design variables

There are many variables in a 3-phase induction motor. Some of them continuous variables, some of them are decision variables and some of them are integer variables. The variables that have large influence on the cost-function are called key variables. In an induction motors, the continuous variables are: i) length/polepitch ratio, ii) average flux-density in the gap, iii) flux-density in the stator/rotor core iv) teeth flux-density in stator/rotor v) ampconductor/m of periphery, vi) slot depth/slot width, etc. The decision variables are: i) single laver or double laver winding in the stator, ii) configuration of slot, iii) conductor material for rotor, iv) type of bearing iv) laminated or solid rotor etc. The integer variables are: i) no of stator/rotor slots, ii) no of slots/pole/phase (generally integral slot winding is used in induction motor, iii) no. of conductors/slot (even integer for double layer winding) iv) no of ducts etc.

At first, the key variables are identified. Then they are initialized. Their values are changed gradually to get the best possible or optimal design. Many of these variables do not come into picture in case of standard design e.g. the no of stator/rotor slots, slots/pole/phase, slot depth/slot width etc. as these are defined by the standard lamination to be used.

B.Design constraints

The optimization has to be sought in presence of a no of inequality and other constraints viz.

 a) Full voltage starting torque/full load torque must more than a pre-defined value e.g. 1.75.

- b) Maximum torque/full load torque must more than a pre-defined value e.g. 2.25.
- c) The efficiency must be more than a predefined value e.g. 85%
 - d) The power factor must be more than a pre-defined value e.g. 0.8 lagging
 - e) The no. of stator slots/ rotor slots must be integers
 - f) No. of slots/pole/phase must be an integer

ALGORITHM

The algorithm for optimal design with standard laminations is given below:

- 1. Read data on design variables $(B_{av}, ac, L/\tau)$, specific cost etc.
- 2. Read data files on SWG no of wires, thickness of insulation etc.
- 3. Read specifications of the motor.
- 4. Check the validity of the specifications. For invalid specifications go to step 2
- 5. Find the output coefficient. Find input power/apparent power from assumed values of efficiency & power factor.
- 6. Find the approximate friction & windage loss by using data file on the same.
- 7. Find no. of poles, synchronous. speed and the D²L-product.
- 8. Find shaft diameter from mechanical considerations.
- 9. Choose length/pole pitch ratio as 0.8 and find the stator bore diameter.
- 10. Open the data file for standard laminations available in the market and keep the data in an array. Compare the calculated diameter with the diameters of standard laminations and choose the frame size of nearest available diameter.
- 11. Read the details of the lamination. Check the feasibility of accommodating the shaft. If the inner diameter of the lamination is less

- than the shaft diameter then goto step 33.
- 12. Find the length of stator from D²L product, net length of iron, number of ducts, pole pitch, flux per pole.
- 13. Find pitch factor by short pitching the coil to about 5/6th. of the pole pitch. Find the breadth factor and the winding factor.
- 14. Find number of turns/phase.
- 15. Find stator current, no. of conductors in parallel and the cross-section of the conductor.
- 16. Open the data file for SWG number and choose the appropriate conductor available in the market.
- 17. Find the depth of insulation and outer diameter of the conductor.
- 18. Choose parallel-sided teeth and semi-closed slots.
- 19. Find depth of stator core and width of teeth for specified flux density of core and the teeth.
- 20. Find the slot dimensions to accommodate the conductors.
- 21. Find mean length of turn of stator and its resistance per phase.
- 22. Calculate iron loss in teeth & core of the stator by opening data file on special LOHYS.
- 23. Find the air gap, rotor diameter and length.
- 24. Choose Aluminium as rotor conductor material. Find dimensions of the rotor bars and the end rings and dimensions of the rotor slots.
- 25. Find Carter's coefficients from the data file and the total AT of stator, rotor & air-gap.
- 26. Find the magnetisation current & the no load current.
- Find the slot leakage, overhang and zigzag presences & the leakage reactance.
- 28. Find the rotor resistance & the short circuit impedance.
- 29. Make performance evaluation at full load slip, efficiency, power factor and temperature rise.
- 30. Find critical speed and maximum torque.

- 31. Find starting current and starting torque, taking increase in rotor resistance due to skin effect into considerations.
- 32. Calculate the weight of iron, copper and aluminium and find the total cost inclusive of labour & overhead cost.
- 33. Keep all calculated values in array.
- 34. Decrease the diameter by one step &goto step 11
- 35. Examine the calculated values of the array and choose the lamination for cost-optimality.
- 36. Print the values corresponding to optimal design.
- 37. Stop
- 38. End

In this work, the cost function includes the running cost of the motors in addition to its capital cost to preserve the interest of the customer.

CASE STUDY

A programme has been developed to design the motor using standard stampings, changing design variables like L/τ ratio etc. and compute the cost function. This function is a weighted combination of the cost of production and the running cost so as to cover the interest of both the manufacturer and the customer. The design has been made following the algorithm given in the earlier paragraphs.

A. The specifications

Type of motor: 3-phase Squirrel Cage

Induction motor

Type of starter: Star-Delta (Yd)

Frame Material: Normalised Grey C.I., with

holes for axial flow.

Stator winding connection: DELTA; Type of

stator winding: Double layer

23rd & 24th Nov. 2019

Slot insulation: Bonded Polyester; Stator/ Rotor core material: Super-varnished

Special Lohys

Class of insulation: B: Temperature rise as

per grade

Type of enclosure: SPDP with fan-cooling Stator conductor material: Synthetic

resin-enameled copper

Rotor material: Die-cast Aluminium; Roller bearings on both ends: Rotor to be

dynamically balanced

B. The ratings

KW/HP output: 30 / 40.2; Line voltage = 415 V; variation: -15% to +6% Frequency = 50 Hz.; variation: ± 4%; R.P.M.= 1450; Duty: Continuous

C.Chosen design variables and assumptions

Amp.-conductor/m = 35000; Average flux-density = 0.45 Tesla
Length/pole-pitch ratio varying from: 0.8 to 2
Stator current density: = 6 A/mm²;
Rotor current density = 4.575 A/mm²
Stator teeth/ core density in Tesla: = 1.2; 1.25; Rotor core density = 0.6627
Tesla

Copper space factor = 0.6; Assumed efficiency /power factor: 0.9 / 0.9

D. The specific costs

Cost of iron = Rs. 120/ kg; Cost of copper (nomex-coated) = Rs 720/ Kg; Cost of aluminum = Rs. 180/Kg

E. The findings

The programme finds out the following possibilities:

Frame	Stato	Stato	Roto	Stato	Roto
no.	r	r	r	r no.	r no.
	outer	inner	inner	of	of
	diam,	diam,	diam	slots	slots
	mm.	mm.	,		
			mm.		
144M	260.	177.	44.4	36	40
	4	8	5		
102M	304.	190.	50.8	36	40
	8	5			
146M	304.	215.	50.8	36	40
	8	9			
104M	366.	228.	50.8	36	59
	6	6			
103A	355.	254.	50.8	48	59
М	6	0			

Out of these, frame no. 104M of Shankey division of GKW gives the cost-optimal solution. So the design has been made on the basis of this stamping.

*F.*The solution of the design problem

Main dimensions:

No. of poles = 4; Synchronous speed = 25 R.P.S

Approx. KW/KVA input: 33.333 ;

37.037

Output coefficient =164.59; D²L-product

 $= 0.00900 \text{ m}^3$

We choose standard stampings from table, but slots are freely designed. The frame designation chosen by iterative procedure: 104M

Stator design

Stator bore diameter = 228.6 mm;

Stator length = 170 mm; Length/polepitch ratio = 0.947; No. of ducts = 1:Width of ducts = 10 mm

Net length of iron = 147 mm; Pole pitch = 179.5 mm; Flux/pole = 0.3740 Waber; No. of stator slots/ no. of rotor slots: 36 / 59; Stator slot angle.= 20°

No. of stator/rotor slots/pole/phase: = 3 / 4.917; Stator/rotor slot pitch in mm: 19.9 12.1; Pitch factor of stator = 0.9848; Breadth factor of stator = 0.9598; Winding of stator = 0.9452; No factor conductors/slot = 24; Total no. of conductors = 864; No of turns/phase = 144; No of parallel conductors in stator = 2; SWG No. of stator conductors = 15; Area of stator conductor = 2.627 mm^2 ; Diameter of stator conductor = 1.8288 mm: Diameter of stator conductor with insulation 2.059 mm; Total copper area/slot = 126.08 mm²; Parallal teeth & trapezoidal slots are used. ;Width of teeth = 8.5 mm; Lip / Wedge in mm: 1 / 3; Width of slot over wedge = 12.1 mm; Width of slot at bottom = 16.0 mm; Depth of slot = 26.0 mm; Actual copper space factor = 0.407 : Depth of stator core = 37.0 mm : Outer diameter of stator = 356 mm; Clearance with frame = 4 mm.

Rotor design:

Airgap length = 0.6 mm; Rotor length = 160.0 mm

Rotor bar current = 370.6 A ;Rotor bar area = 81 mm2 ; Rotor bar width = 4.5 mm ; Rotor bar length = 160.5 mm ;Rotor bar depth = 18 mm ;Slip-ring width = 21 mm; Depth of rotor core = 70.4 mm ; Inner diameter of rotor = 50.8 mm = Shaft diameter ; Flux-density at 1/3 rd. tooth height of rotor = 0.999 Tesla ; Width of rotor teeth at 1/3 rd. tooth height = 6.3 mm ; Minimum width of rotor teeth = 5.7 mm; Rotor bars are skewed by one slot pitch. Ring depth is equal to bar depth.

No load current calculation:

Carter's coefficient: for stator slot = 0.637; for duct= 0.763; for rotor slot= 0.253; Gap contraction factor: for stator slot = 1.190; for rotor slot = 1.021; for duct = 1.047; Equivalent gap contraction factor = 1.272; Amp.turn required: for airgap = 372; for

stator teeth = 92; for rotor teeth = 9; for stator core = 31

for rotor core = 4; Total Amp.turn required = 508

Magnetizing current = 6.37 A = 21.9 %Losses: Friction & windage = 522 W; Stator teeth = 130.5 W; Stator core = 229.4 W; Stator iron = 359.8 W; % iron Loss = 1.1; Rotational loss current = 0.71 A 2.43 %

No load current = 6.41 A 22.04 %; Losses at full load:; Rotor ohmic loss = 867.6 W 2.64 %; Stator ohmic loss = 1088.3 W 3.31 %; No load loss = 881.83 W 2.69 %; Total loss = 2837.7 W 8.6 %; Parameter estimation:

Stator resistance = 0.508 Ω 3.643 %; Rotorresistance referred to stator = 0.405 Ω 2.904% ; Eddy loss ratio = 5.724Leakage reactance: due to slotting = 1.15 Ω ; due to overhang = 0.40 Ω ; due to zigzag = 0.92 Ω Total leakage reactance = 2.47 Ω 17.74 %Magnetising reactance = 65.13 Ω 466.84 %

Iron loss resistance = 585.91 Ω 4200 %; Equivalent impedance referred to stator = 2.638 Ω 18.91 %

Full load condition:Full load torque = 202.12 N-m; Full load stator current/phase = 29.09 A; Full load line current = 50.39 A; Full load power factor = 0.9309

Full load power input =32838 W; Full load efficiency = 0.9136; Full load slip =0.0273; Full load speed = 1459 rpm; Starting current = 110.5 A; Starting torque at full voltage = 540.31 N-m; Starting torque at reduced voltage (Y-D starter) = 180.1 N-m; Starting current/full load current for full voltage starting = 3.796; Starting torque/full load torque for full voltage starting = 2.673; Starting torque/full load torque at reduced voltage (Y-D starter) = 0.891; Critical slip = 0.16037; Maximum torque = 541.96 N-m; Maximum torque /full load torque = 2.681; temperature rise:Copper loss in embedded portion of stator winding = 419.1 W; Total loss in embedded portion of stator winding = 778.9 W; Temperature rise of stator = 28.68 oC; Cost analysis:Weight of iron = 90.65 Kg ; Cost of iron = Rs.10877/-Weight of copper = 17.83 Kg; Cost of copper = Rs.12841/-

Weight of aluminium = 2.87 Kg; Cost of aluminium = Rs. 517/-Material cost including 20% auxilliaries = Rs. 29083/-Manufacturing cost inclusive of labour & establishment = Rs. 40716/-The average running cost for a life span of 10 years = Rs. The cost function = Rs. The cost functions for all other feasible solutions have been found to be more.

CONCLUSION

Optimization is the process of finding out the best possible solution out of many feasible solutions. The feasible solutions of a design problem are found out by varying the design variables within their normal bounds. The solution giving minimum cost may be found out either by exhaustive search in the parameter-space or by techniques like gradient search, method of random walk etc. The advanced mathematical techniques need not be used for finding out the optimal solution using standard laminations, as the no. of solutions is few. Therefore the method of exhaustive search is acceptable in this case. The only thing of interest is to check the compatibility of the design with the chosen standard core and whether the specifications have been fulfilled.

If we aim at getting only the minimum cost of production, that will be good for the manufacture. It will keep down the cost of the machine and increase the sale. However, the machines will be less efficient, will have higher ohmic and no-load losses and will give rise to more environmental pollution indirectly. Therefore, the best practice is to frame an objective function accounting for the capital cost and the running cost.

In this work, a computer programme has been developed for the design of 3-phase squirrel-cage induction motor. Provisions have been made for switching over to standard lamination available in the market after finding out the bore diameter. It has been repeated for a no. of times changing the (length:pole pitch) ratio within its normal bounds. Also changes have been made in the value of average flux-density and amp. Conductor/m. The best possible solution has been chosen from the set of

solutions obtained by this process. The case-study has been made on a 30 KW, 415 V, squirrel-cage induction motor.

REFERENCES

- [1] O.W. Anderson, "Optimum design of electrical machines", IEEE Trans. (PAS), Vol-86, pp. 707-11, 1967.
- [2] M. Ramamoorty, "Computer-aided design of electrical equipment", Affiliated East-West Press Pvt. Ltd., 1987, ISBN: 81-85095-57-4
- [3] M.G. Say, "Performance and design of a.c. machines", ELBS.
- [4] A.K. Sawhney, "A course in electrical machine design", Dhanpat Rai and Sons, 2003
- [5] K. Deb, "Optimization for engineering design", PHI, 2010. ISBN 978-81-203-0943-2
- [6] S.S. Rao, "Engineering optimizationtheory and practice", New Age Int.; ISBN 978-81-224-2723-3
- [7] N.S. Kambo, "Mathematical programming techniques", Revised edition,1991,1984, Affiliated East-West Press Pvt. Ltd. New Delhi 110 001, ISBN 81-85336-47-4.
- [8] A. Shanmugasundaram, G. Gangadharan, R. Palani, "Electrical machine design data book", Wiley Eastern Ltd. ISBN 0 85226 813 0
- [9] S.F. Lindsay & T.H. Barton, "Parameter identification for squirrel cage induction machines", IEEE Trans. Power

Apparatus System, 1973, pp. 1287-1291

- [10] G. Erajskar, M. Bhattacharyya & S.N. Mahendra, "Computer-aided design of three phase squirrel cage induction motor- technical design, hybrid process and optimization", J.I.E (India), E.E. Div., India, 1974, pp. 2-50
- [11] H.B. Ertan, C. Aykanat, "A new approach to optimized design of induction motor", Dept. of Elect. Engg., Middle East Technical university, Ankara, Turkey.
- [12] F. Kentli, "A survey of design optimization studies of induction motor

- during the last decade", Dept. of Elect. Education, Marmara University, Goztepe, Istambul, Turkey.
- [13] R.N. Hasanah, "Energy saving through design optimization of induction motor", Journal EECCIS, Vol. 3, No. 1, June, 2009.
- [14] C. Thanga Raj, S. P. Srivastava, and P. Agarwal, "Energy-efficient control of three-phase induction motor a review", International Journal of Computer and Electrical Engineering, Vol. 1, No. 1, April, 2009.
- [15] R. Kannan, R. Bhuvaneswari, and S. Subramanian, "Optimal design of three-phase induction motor using Particle warm Optimization", Iranian Journal of Electrical and Computer Engineering, Vol. 6, No. 2, 2007.
- [16] S. S. Sivaraju& N. Devarajan, "Novel design of three phase induction motor enhancing efficiency, maximizing power factor and minimizing losses", European Journal of Scientific Research, ISSN 1450-216X, Vol. 58, No.3, (2011), pp.423-432

A Scheme for Reduction in Harmonic and Establish the Stability of Hybrid System Connected in Grid

Ankur Ganguly+, Alok Kumar Shrivastav+, Pradip Kumar Sadhu*

Department of (Electrical Engineering) Department of (Electrical Engineering)

(Techno International Batanagar+) (IIT (ISM) Dhanbad*)

(Maheshtala, Kolkata-700141) (Dhanbad-700141)

{Corresponding author's email: alok5497@gmail.com}

Abstract - This paper focuses on the investigation of stability of voltage and total harmonic distortion at the point of common coupling (PCC) for network with PV system. Intermittent nature of sunlight and wind-based power injection scheme into the grid becomes a challenging task and it also affects the stability of the power system. The suggested scheme not only generates and step-up the dc voltage but also transforms the generated dc power into superior quality of ac power with the help of PWM inverter. Furthermore, to enhance the quality of power and stability of the overall PV system integrated with grid, a transient current limiter for limiting the transient has been incorporated in the system. The suggested model is tested on MATLAB / Simulink environment and the results show its superiority over other existing method.

Keywords - Boost converter, Grid-connected, Photovoltaic (PV), PWM inverter, Transient current limiter (TCL), Stability analysis, Total harmonic distortion (THD).

INTRODUCTION

Up till now, with the stopping petroleum product and over the top ascent in contamination, PV innovation is emerging as one of the promising sustainable power sources. By the end of 2019, global cumulative installed PV capacity reached about 512 giga watts (GW), of which about 180 GW (c. 35%) were utilityscale plants. Moreover, the cost of the system is supported by the government. It also affects the stability of the PV system. This brings the fast PV showcase development in the coming years [1-3]. Power produced from photovoltaic energy system is the key source of sustainable power which includes just about zero ozone depleting substance discharge and doesn't devour any non-renewable energy source [4–6]. For the most part, matrix associated sustainable power source assets have area requirements since they are interconnected to the system by means of long transmission lines far from burden focuses [7].

Proposed PV system associated with the grid is appeared in Fig. 1. The work on the PV systems support the three stage inverter associated to the network for smooth long run and expands for the most reliable system in electric power. With the progression and development of intensity gadgets, the power created from the converters, particularly the 3- stage inverter having dc-dc converters can be used and step-up to the grid. The primary phase of plan is utilized to help the output voltage of PV and the 2-stage modifies this DC control into excellent air power conditioning [8].

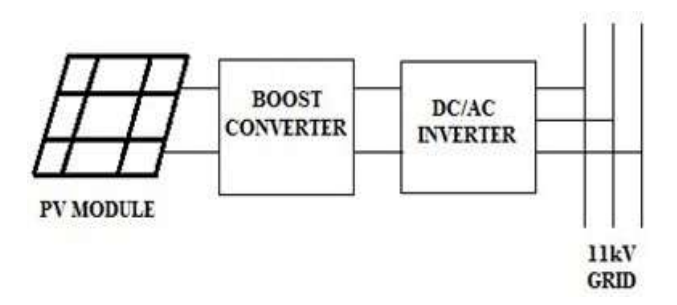


Fig 1. Schematic diagram of PV module connected with grid

This paper exhibits the investigation on stability and total harmonic distortion (THD) of voltage for the purpose of regular coupling of a system associated PV network [9, 10]. This paper presents one method, known as the harmonic current decrease control plot for network associated with PV systems. This harmonic current reduction scheme also controls the distortion of voltage that occurs at the junction point of the associated grid. Furthermore, it improves the power quality of the grid and reduces the THD [13].

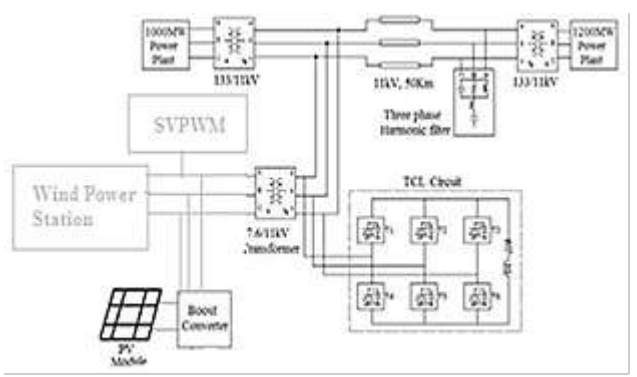


Fig. 2 - Proposed Model of Hybrid system

ILLUSTRATION OF THE SUGGESTED MODEL

Physical layout of the system model for 500 MW PV and 2000 MW Wind power plants individually, coordinated at line voltage of 11kV [14]. The schematic plan of the model is shows in Fig 2. As per the design of the model, novel procedure has been created utilizing MATLAB to improve the quality of power and certify the interconnected stability of hybrid system. The detailed modeling can be found in [15, 16]. The power-molding unit is designed by DC-DC chopper. The power-molding unit is most as often as possible a DC-DC chopper. It expresses that the step-up converter is the most appropriate tool for enhancing the power. This chopper is associated with the PV module and the DC-AC converter [17]. Simulink model of boost converter is appeared in Fig. 3.

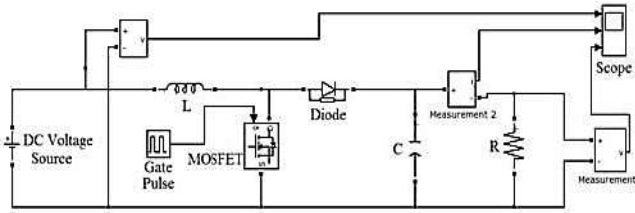


Fig. 3. Simulink model of boost converter

The chopper duty-cycle (α) is specified by eq. (1) and the reducing proportion (Y) is specified by the eq. (2) and (3), with the chopper switching on time as t1 and T1 as the exchanging time of the switch [18].

$$\alpha = -\frac{t_1}{T} \tag{1}$$

$$\frac{V_0}{V} = \frac{1}{1-\alpha} \tag{2}$$

Where, V_0 and V is the load and supply voltage of network respectively.

$$Y = \frac{\alpha}{1-\alpha} \tag{3}$$

A 3-stage PWM inverter alters DC power of the network into surprising AC power which is built up here [19]. The output of Simulink model of SVPWM is shown in Fig. 4.

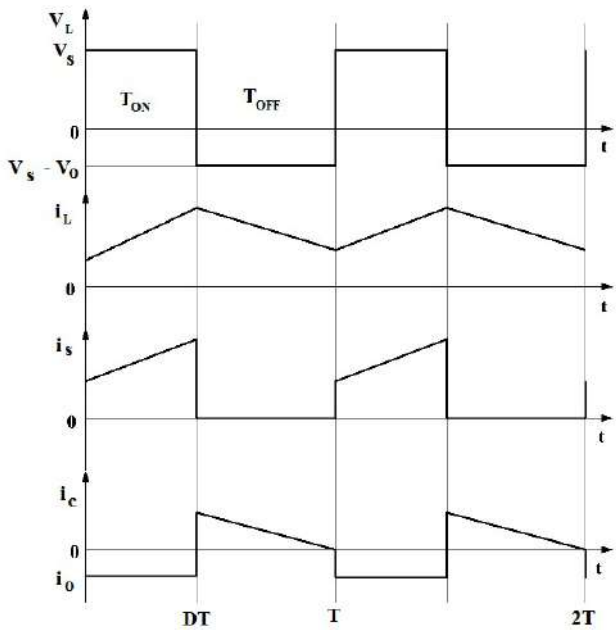


Fig 4. Boost converter switching waveform

The easiest method for delivering the space vector pulse width modulation (SVPWM) signal is by looking at a sinusoidal wave of having low power reference with a high frequency of triangular shape shown in the Fig. 5. A SVPWM inverter yields better waveforms at no genuine increment in expense.

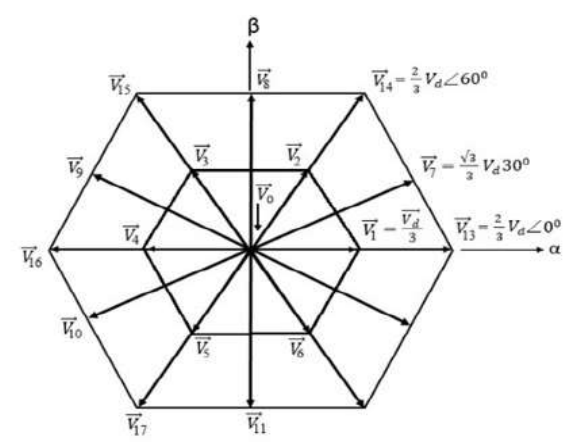


Fig 5. Three phase sinusoidal system with rotating equivalent space vector

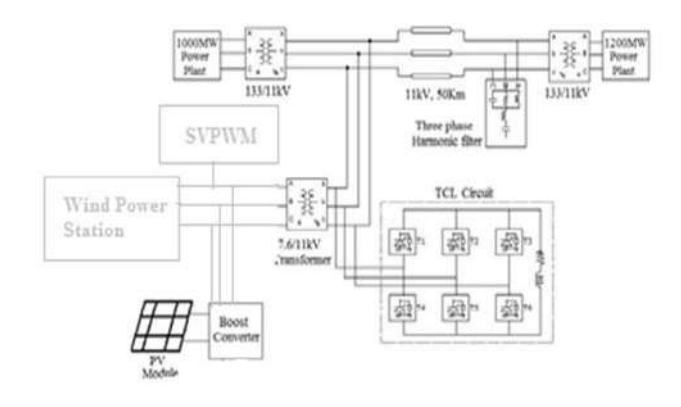
The ac voltage (rms) output will be;

$$V_{ac} = V_s \sqrt{\frac{p\delta}{\pi}} \rightarrow V_s \sqrt{\sum_{m=1}^{2p} \frac{\delta_m}{\pi}}$$
(4)

Where, p = no. of pulses and δ = width of pulse.

MODELING OF HYBRID POWER SYSTEMS

A sustainable power system is formed by incorporating the wind and PV sources of energy through the separately devoted step-up converters. The wind and PV energy sources are incorporated simultaneously at the junction point of DC-link



capacitor to construct a wind and PV energy system. In Fig.4 the switching waveform of the suggested scheme of energy sources designed for MPPT using Artificial Neural Network control is presented. Here, suggested MPPT control computation, the most extreme obtained from PV and Wind energy sources by implementing the algorithm. The wind and PV overall layout is presented in subsequent subsections:

A. Photovoltaic Energy System

The structure of Photovoltaic model for building sustainable power source network is exhibited here. Also, a diode base structure PV module is taken as appeared in Fig. 6(a) and its emblematic symbol is appeared in Fig. 6(b). The solar characteristic of current, voltage and power is shown in the Fig. 7 and the detail specifications are shown in Table 1.

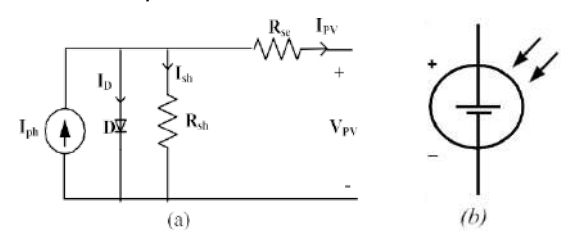


Fig 6.Solar module: (a) network connections and (b) emblematic representation.

The generalized mathematical form for developing voltage and current equations from the given PV panel are presented in (5) and (6) correspondingly [14], [16].

$$V_{pv} = \frac{\eta KT}{q} \ln(\frac{I_{PH}}{I_{PV}} + 1)$$
 (5)

$$I_{pv} = I_{ph} - I_{pvrsc} \left(e^{\frac{q(V_{pv} + I_{pv}R_s)}{\eta KT}} - 1 \right) - \frac{V_{pv} + I_{pv}R_{se}}{R_{sh}}$$
 (6)

The PV panel output power is computed based on the following (7) [17].

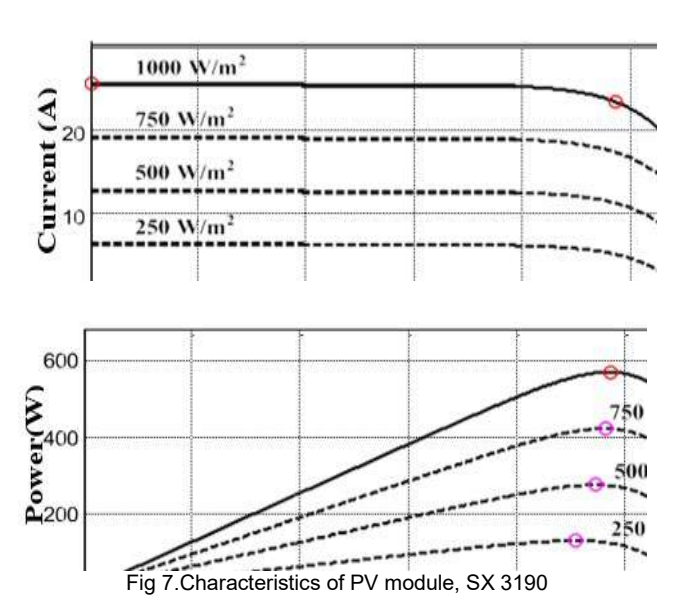
$$P_{PV} = A_{PVP} G_n \eta_{PVP} \tag{7}$$

The resistance connected in series and parallel across the diode is computed as shown:

$$R_{se} = 0.09 \frac{V_{oc}}{I_{sc}} \tag{8}$$

$$R_{sh} = 11 \frac{V_{oc}}{I_{sc}} \frac{G}{G_n} \tag{9}$$

where, V_{pv} is output voltage of PV panel, R_{sh} is parallel resistance diode, I_{ph} is Phase current of PV panel, V_{oc} is open circuit voltage and I_{sc} is short circuit current.



B. Wind Power System

The structure of wind power station consists of wind turbine and electric generator as specifications are presented in Table 1. The velocity of wind is taken as turbine input and thus generator generates the output. The mechanically developed total power created by turbine of wind is developed by (10) [18].

$$P_{\rm w} = 1/2 \, \rho A V_{\rm v}^3$$
 (10)

Where, P_w is the output power of wind, V_v is wind velocity, ρ is air density and A is sweep area of wind blade.

TABLE I
SPECIFICATIONS OF 500W WIND SYSTEM

Particulars	Values
Power	500 MW
Impedance	0.845Ω
Inductance	4.52 mH
Magnetizing Flux	0.34 wb
No. of Poles (DFIG)	2
Torque (Max)	1.12 Nm/A
Wind speed (Avg)	12 m/s

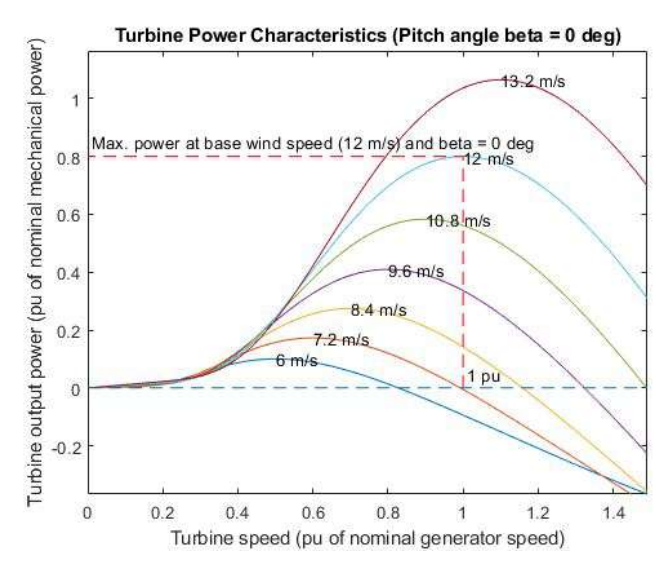


Fig 8. Power Characteristics of 500MW Wind turbine

The generation of power by wind turbine at variable speed of wind is shown in the Fig.8 and the mathematical computation for overall generated power is obtained from (11) [19].

$$P_{w}(W_{v}) = \begin{cases} P_{w} \frac{V_{v}^{2} - V_{d}^{2}}{V_{n}^{2} - V_{d}^{2}}; & V_{d} \leq V_{v} \leq V_{n} \\ P_{w}; & V_{n} \leq V_{v} \leq V_{c} \\ 0; & V_{v} \leq V_{d} and V_{v \geq V_{c}} \end{cases}$$
(11)

Where, P_w is wind output power, V_d is reduced wind speed, V_n is standard wind speed and V_v is velocity of wind.

TABLE II
PARAMETERS OF PV SYSTEM POWER CIRCUIT

	Parameters	Value
PV array	Number of cells	72
	Highest power	300 W
	OC voltage (Voc)	54.12 V
	SC current (Isc)	9.42 A
	Highest power volt.	45.76 V
	Highest power current	9.14A
Boost Chopper	Duty cycle	0.99
	Time period	2e-4
	L	0.2042 H
	С	3.0242e-05
		F
	R	38.5 kΩ
Inverter	Power electronic device	IGBT
	No. of bridge leg	3
	Snubber resistance ®	1e5 Ω
	Snubber capacitance ©	Infinity
TCL	No. of thyristors	6
	Resistance	0.005 Ω
	Forward voltage	0.5 V
	Snubber resistance	100 Ω

RESULT & DISCUSSION

As observed in the previous section, the voltageobtained from PV array is directly applied to the

system through PWM inverter. As the level of penetration of PV generation increases, it may even cause voltage stability issues. That is the reason TCL network is executed to decrease harmonics for the purpose of basic coupling of a matrix associated with photovoltaic system. The presentation and security examination of the procedure under security are completed utilizing the reproduced model that is figured, in light of the genuine procedure.

Fig.9 to 14, illustrates the effect of transient current limiter on the stability of voltage for grid integrated wind and PV system using Bode, root-locus and Nyquist tools.

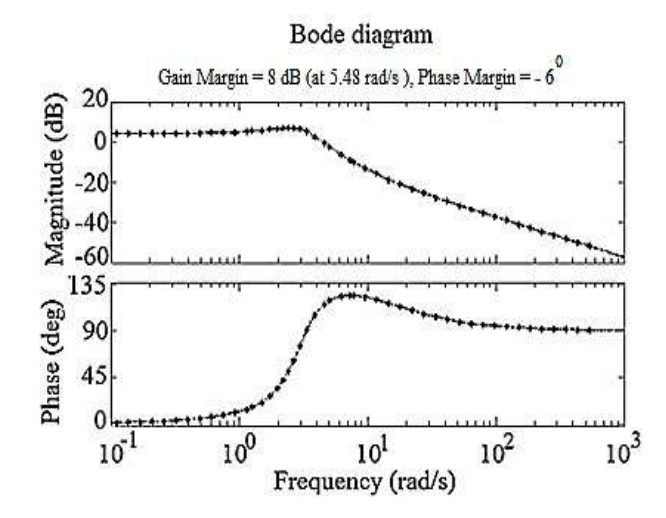


Fig 9.Bode plot of the proposed model without TCL

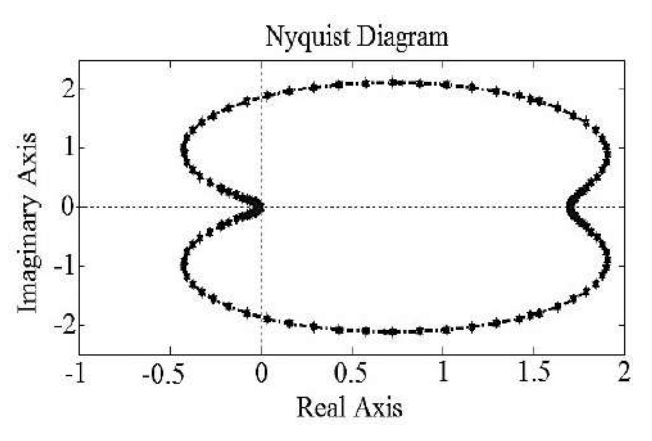


Fig 10. Nyquist plot of proposed model without TCL

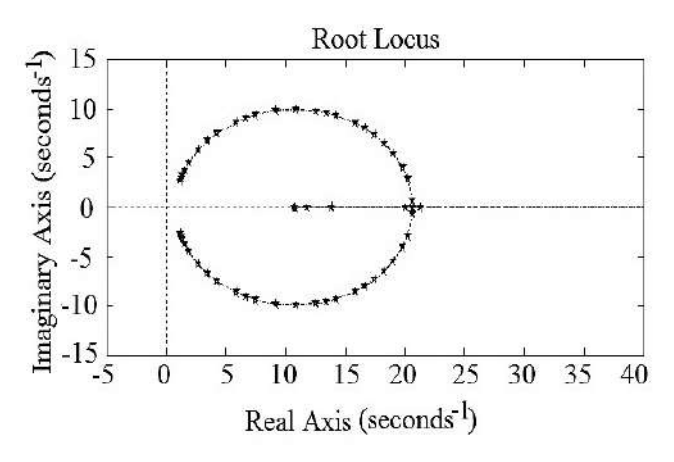


Fig 11. Root locus plot of proposed model without TCL

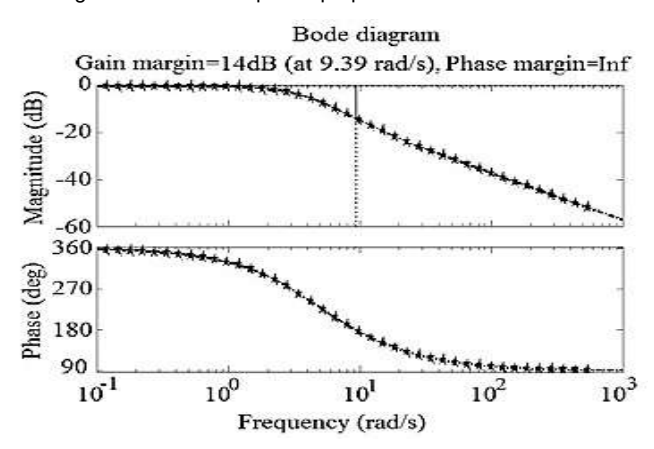


Fig 12. Bode plot of proposed model with TCL

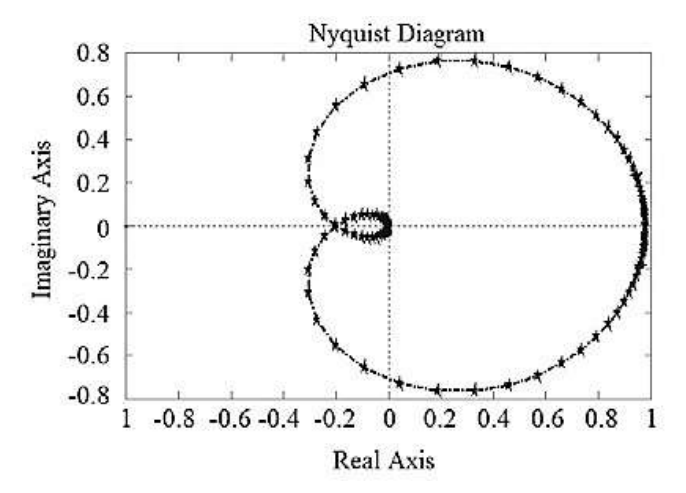


Fig 13. Nyquist plot of proposed model with TCL

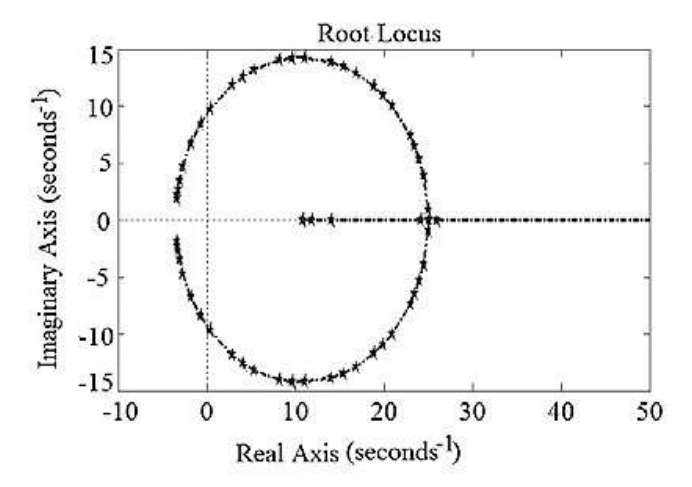


Fig 14. Root locus plot of proposed model with TCL

According to the stability model, such as: (a) Bode plot, any network be able to be stable if the system lies under positive gain and phase margin, otherwise unstable; (b) Nyquist plot depicts that, if gain plot unable to circle the fundamental area and also open circle structure have no any open - loop pole in splane placed at the right side then the structure will be under stable condition; (c) Root - locus explains that, a structure might be determined if the considersseparatelyfor root can turn dimensional, generally unstable; (b) Nyquist plot, if TGH shape does not circle the essential point noting of the DFT into a two dimensional one with the accompanying difference in factors has a place with the left sideopen for an adequately total estimation of open loop gain. This is clear from Figs.9 to 10, the interconnected network without transient current limiter neglects to follow the dependability criteria for example gain margin: 1.2 dB and phase angle: -304.3°, which make systemunstable.

Further, comparative study for the associated networks with TCL and double tuned harmonic filter is shown in the Figs. 11 to 12. The pre-factor is excluded, as it is usually done. It can convert mathematical computation of DFT from one to two dimensional as shown below;

$$e = e(k,1) = kN_1 + 1; 0 \le k \le N_2, 0 \le 1 \le N_1$$
 (12)

$$f = f(p,q) = pN_2 + q; 0 \le p \le N_1, 0 \le q \le N_2$$
 (13)

It follows for
$$X_j = X(a,b), \widehat{X}_k = \widehat{X}(c,d)$$
 and $W_N = e^{-2\pi i/N},$

$$\widehat{X}(c,d) = \sum_{a=0}^{N_2-1} \sum_{b=0}^{N_1-1} X(a,b) W_N^{(a+N_1+b)(cN_2+d)}$$
(14)

$$\widehat{X}(c,\widetilde{d}) = \sum_{b=0}^{N_1 - 1} W_N^{(cN_2 + d)} \underbrace{\sum_{a=0}^{N_1 - 1} X(a, b) W_{N_2}^{ad}}_{=\widetilde{X}(b, d)}$$
(15)

Since $W_N^{\text{acN}_1 \text{N}_2} = W_N^{\text{acN}} = 1$ and $W_N^{\text{adN}_1} = W_{N_2}^{\text{ad}}$. It can be taken as computing first discrete Fourier transform then computing $N_{2}(i.e; \tilde{x}(b,d))$ and values $N_{2}(i.e;\tilde{x}(b,d))$ with new data $\tilde{x}(b,d)$.The presence of harmonics in the system network can be measure by FFT with and without TCL is carried out simultaneously and consequences are presented in Fig. 15 and 16, respectively. It is observed that the distortions caused by harmonic are very significant. However, it is cleared from Fig. 15, that the execution of TCL and double tuned three phase harmonic filter has significantly reduced the distortion caused by harmonic. All even harmonics become more or less and the odd harmonics spectrum are considerably decaying a large amount.

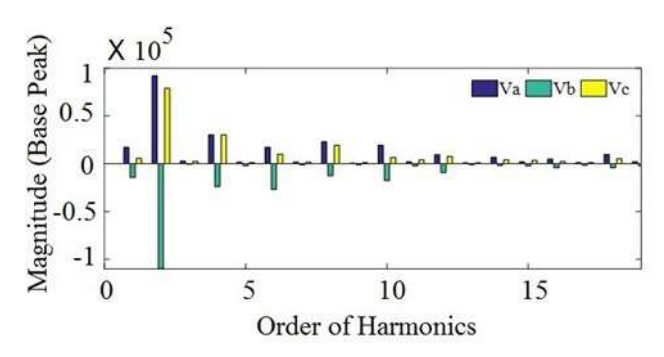


Fig 15. FFT observation (without TCL) of 3-φ voltages

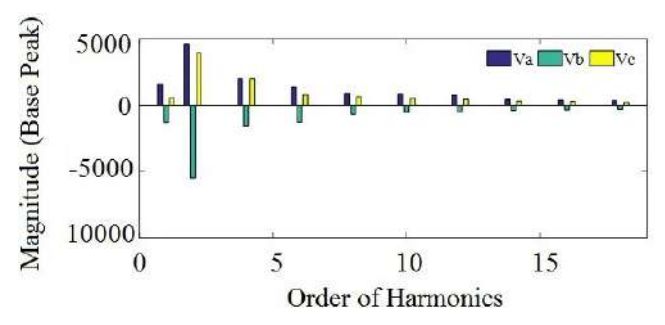


Fig 16. FFT observation (with TCL) of 3-φ voltages

Figures 17 to 19 demonstrate the effect of TCL and observeTHD for line and phase voltage correspondingly. The mathematical computation of THD is,

$$THD = \frac{\sqrt{\sum_{n=2,3}^{\alpha} V_{nrms}^2}}{V_{1,cms}}$$
 (16)

The level of THD and its associating line voltage distribution is appeared in figure 17 section (a) and (b) individually. Figure 15b demonstrates the estimation of most extreme THD is 7.32 % without TCL model. The comparable kind of activity has been done with TCL model and introduced in Fig. 18 (a) and (b), individually. It is appeared from the

assumption that, after execution of TCL model at the purpose of normal pairing of a matrix associated PV system, value of maximum THD is reduced to 4.33 %.

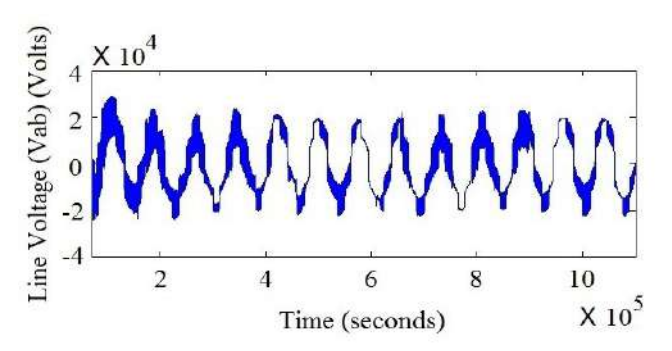


Fig 17a. Line voltage without TCL

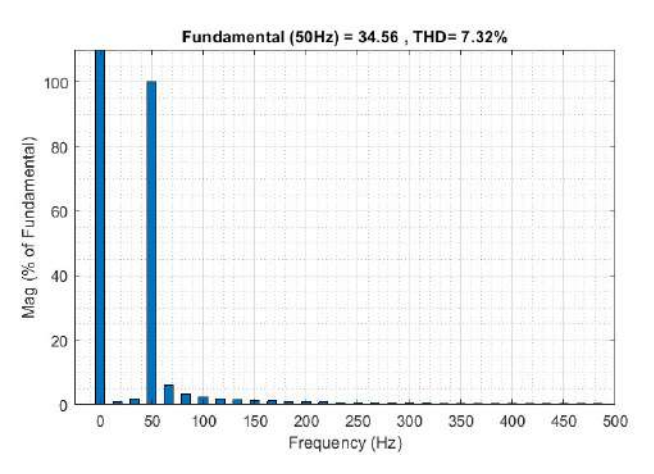


Fig 17b. Without TCL THD for line voltage =7.32 %

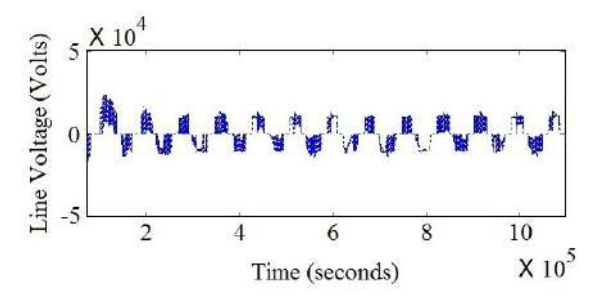


Fig 18a. Line voltage with TCL

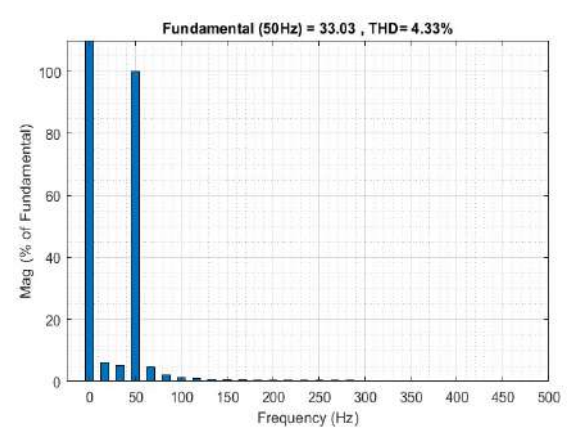


Fig 18b. With TCL THD for line voltage = 4.33 %

The total harmonic distortion of the hybrid energy system is shown in the Fig. 19 (a) and (b) correspondingly. In the same way, TCL is implanted and the results are appeared in Fig. 20 (a) and (b) correspondingly. TCL results in decrease of THD by 2.15%.

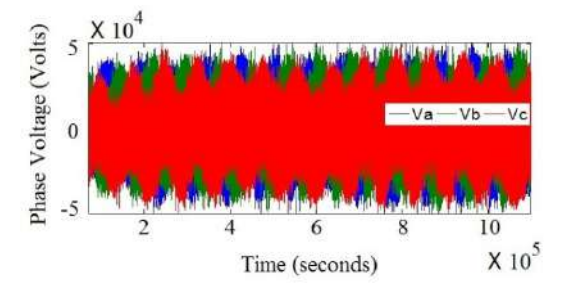


Fig 19a. Grid Phase-voltage without TCL

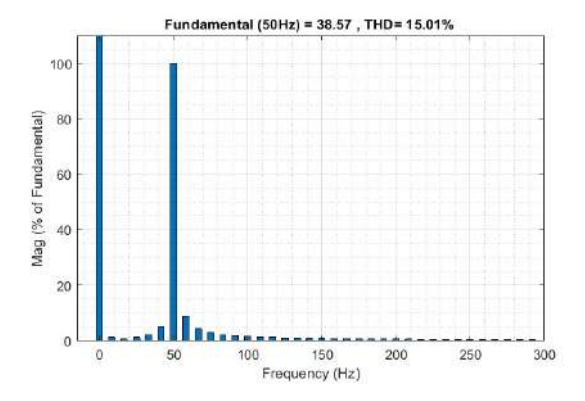


Fig 19b. Phase Voltage THD = 15% without TCL

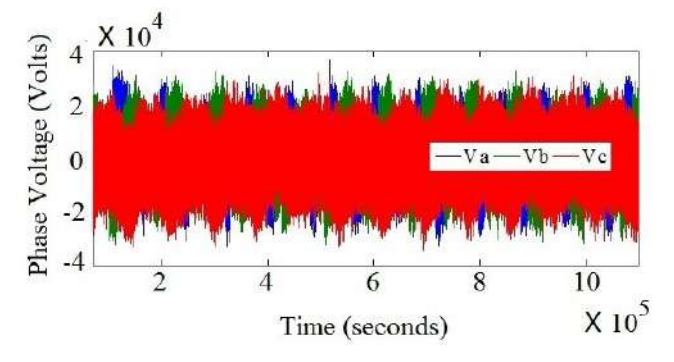


Fig 20a. Grid Phase-voltage with TCL

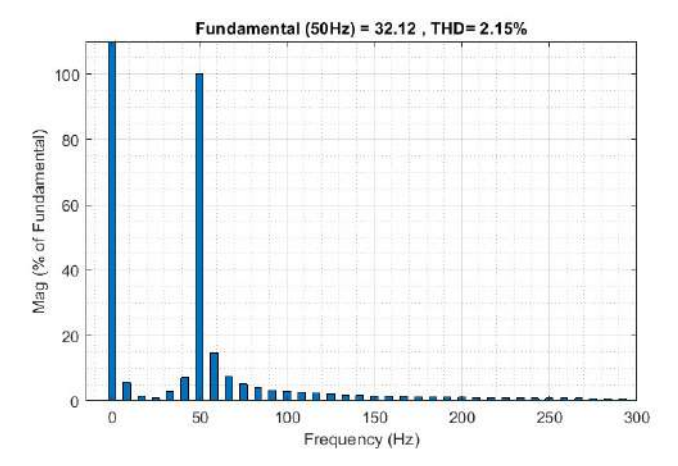


Fig 20b. Phase Voltage THD = 2.15 % with TCL

CONCLUSION

A transient current limiter controller is designed for hybrid wind and PV energy system. The mainpurpose of the limiter is to reduce distortion of harmonic as well as maintain the stability of the system. Moreover, several methods of harmonic reduction are explained in literature. The suggested TCL controller is designed for 500MW wind and 2000MW PV system integrated with step-up converter. The efficacy of the designed model is tested in both grid connected and standalone mode. The harmonicbehavior in terms of THD % is also measured. The study reveals that the power quality has significantly improved by reducing the harmonic distortion and at the same time the overall stability of the interconnected system is increased to a large extent in the presence of the TCL circuit in the grid-connected hybrid wind and PV energy system.

REFERENCES

- [1] G. Wu, X. Ruan, and Z. Ye, "Non-isolated high step-up DC-DCconverters adopting switched-capacitor cell," IEEE Trans. Ind. Electron., vol. 62, no. 1, pp. 383–393, Jan.2015.
- [2] T.-J. Liang, J.-H. Lee, S.-M. Chen, J.-F. Chen, and L.-S. Yang, "Novel isolated high-step-up DC-DC converter with voltage lift," IEEE Trans. Ind. Electron., vol. 60, no. 4, pp. 1483–1491, Apr.2013.
- [3] M. Sitbon, S. Schacham, T. Suntio, andA.Kuperman, "Improved adaptive input voltage control of a solar array interfacing current mode controlled boost power stage," Energy Convers. Manage. vol. 98, pp. 369–375, Jul. 2015.
- [4] M. E. Lotfy, T. Senjyu, M. A. Farahat, A. F. Abdel-Gawad, and A. Yona, "Enhancementofasmallpowersystemperformanceusingmultiobjective optimization," IEEE Access, vol. 5, pp. 6212–6224, 2017.
- [5] Cumulative Development of Various Renewable Energy System/Devices in Country, Accessed on Apr. 30, 2017. [Online]. Available: http://mnre.gov.in/mission-and-vision-2/achievements
- [6] N. T. Pathan, S. P. Adhau, P. G. Adhau, and M. Sable, "MPPT for grid connected hybrid wind driven PMSG-solar PV

- power generation system with single stage converter," J. Elect. Power Syst. Eng., vol. 3, no. 1, pp. 41–59, 2017.
- [7] S.LiandJ.Li, "Outputpredictor-based active disturbancerejectioncontrol for a wind energy conversion system with PMSG," IEEE Access, vol. 5, pp. 5205–5214, 2017.
- [8] H. Fathabadi, "Novel highly accurate universal maximum power point tracker for maximum power extraction from hybrid fuel cell/photovoltaic/wind power generation systems," Energy, vol. 116, pp. 402–416, Dec. 2016.
- [9] H. Fathabadi, "Novel fast and high accuracy maximum power point tracking method for hybrid photovoltaic/fuel cell energy conversion systems," Renew. Energy, vol. 106, pp. 232–242, Jun.2017.
- [10] H. Fathabadi, "Novel high-efficient unified maximum power point tracking controller for hybrid fuel cell/wind systems," Appl. Energy, vol. 183, pp. 1498–1510, Dec. 2016.
- [11] C. M.Hongand C. H.Chen, "Intelligent control of a grid-connected wind-photovoltaic hybrid power systems," Int. J. Elect. Power Energy Syst., vol. 55, pp. 554–561, Feb. 2014.
- [12] F. Baghdadi, K. Mohammedi, S. Diaf, and O. Behar, "Feasibility study and energy conversion analysis of standalone hybrid renewable energy system," Energy Convers. Manage. vol. 105, pp. 471–479, Nov.2015.
- [13] B. Bhandari, S. R. Poudel, K.-T. Lee, and S.-H. Ahn, "Mathematical modeling of hybrid renewable energy system: A review on small hydro-solarwindpowergeneration,"Int.J.Precis.Eng.Manuf.GreenTechnol. vol. 1, no. 2, pp. 157–173, 2014.
- [14] T. H. Kwan and X. Wu, "Maximum power point tracking using a variable antecedent fuzzy logic controller," Solar Energy, vol. 137, pp. 189–200, Nov. 2016.
- [15] E. Kabalci, "Design and analysis of a hybrid renewable energy plant with solar and wind power," Energy Convers. Manage. vol. 72, pp. 51–59, Aug. 2013.
- [16] S. S. Dihrab and K. Sopian, "Electricity generation of hybrid PV/wind systems in Iraq," Renew. Energy, vol. 35, no. 6, pp. 1303–1307, 2010.
- [17] A. Kirubakaran, S. Jain, and R. K. Nema, "The PEM fuel cell system with DC/DC boost converter: Design, modeling and simulation," Int. J. Recent Trends Eng., vol. 1, no. 3, pp. 157– 161, 2009.
- [18] F. Nejabatkhah, S. Danyali, S. H. Hosseini, M. Sabahi, and S. M. Niapour, "Modeling and control of a new three-input DC–DC boostconverter for hybrid PV/FC/battery power system," IEEE Trans. Power Electron., vol. 27, no. 5, pp. 2309–2324, May2012.
- [19] B. S. Revathi and M. Prabhakar, "Non-isolated high gain DC-DC converter topologies for PV applications—A comprehensive review," Renew. Sustain. Energy Rev., vol. 66, pp. 920–933, Dec.2016.

Modeling of inverter based grid connected distributed generators for transient stability using droop control schemes

Alok Kumar Shrivastav, Bhaskar Sengupta, Ankur Ganguly, Ratindra Nath Lahiri

Department of (Electrical Engineering)

(Techno International Batanagar⁺)

(Maheshtala, Kolkata-700141)

{Corresponding author's email: alok5497@gmail.com}

Abstract - The renewable energy use in wide scale is likely to resolve the crisis of energy across the world. However, inverters play the major role to integrate the renewable energy into the microgrids or distribution networks. The gain of using inverter interfaced distributed generators (IIDGs) affects the sustainable energy flexibly and effectively. Though, the broad network connection of IIDGs maintains transient stability to the local grid. The aim of this paper is to control transient stability of the grid with the use of droop control technique. The transient stability control mechanism is developed by merging the complete dynamic trace and condition of transient stability. The complete dynamic trace is designed by the curves of active and reactive power happens for the period of transient. The condition for transient stability is suggested by IIDGs and transient model operation characteristics. The control mechanism is capable to maintain the correlation between droop factors and transient stability. The judgment of transient stability is presented respectively. A sequence of simulations presents the effectiveness and correctness of the suggested mechanism of transient stability.

Keywords - Droop Control, Stability analysis, IIDGs, Total harmonic distortion (THD).

INTRODUCTION

The energy utilization and natural contamination of nonrenewable energy sources are expanding quickly everywhere throughout the world. The effective and secure use of sustainable power source turns into a basic answer for the energy emergency [1-4]. Inverter-interfaced dispersed generators (IIDGs) are considered as a productive answer for believer various types of assets into power [5-8]. They highlight high flexibility as far as control and application. The wide implantation of IIDGs incredibly improves the usage of sustainable power source, decreases the power misfortune and chops down contamination. In any case, with the enormous scale reconciliation of DGs, there are as yet various specialized difficulties in using IIDGs. One of the difficulties is the subtle and confounded transient strength [9, 10]. Most IIDGs are generally installed in dispersion systems or small scale lattices, which suffer various transient occasions, for example, flaws, moment change of burdens and switch of network structure [11–13]. The transient occasions ordinarily lead to a synchronization of IIDGs with the open power framework. The synchronization of IIDGs brings very negative affects towards power shoppers, control offices and the usage of sustainable power source [14, 15]. IIDGs need to be isolated from the public grids, in case the transient events further develop. A great deal of studies has been focusing on the transient stability of IIDGs. Simulation and mathematical models are two main approaches [32]. Simulations are used to investigate the factors that interact with transient stability. The factors can be categorized as transient events and operation parameters. Transient events include faults, induction machines starting and grid structure switch. Operationparameters include network parameters control types. Refs. [16–19] considered the fault type, fault clearance time, loads types and control types as variables in simulation experiments to scale their influence and sensitivity of the transient stability. Ref. [20] utilized center of inertia to expand the application of the simulation and managed to provide a general analysis in various applications. The models in these literatures can concisely describe the transient behaviors of IIDGs. However, simulations fail to provide the mechanism of the transient behaviors. Other literatures use mathematical models to study the transient stability. The commonly used methods are Nyquist criterion [21], eigen- value test [22] and Lyapunov methods [23]. Nyquist criterion and eigenvalue test are easy to give the stable boundary of the IIDGs. They are widely used for IIDGs in different grid structures [24. 25] as well as for multi-IIDG system [26]. However, the two conventional methods cannot reflect the nonlinear influence from the control strategy thus making the stable boundary less convincing. A Lyapunov method is capable of solving the nonlinear feature of the control strategy [27, 28]. However, these methods failed to present a thorough transient stabilitymechanism. A few studies attempted to explain and describe the transient stability of the IIDGs. Some of them use the conventional transient stability analysis methodology to obtain the transient features [29, 30]. Ref. [29] described the virtual angle synchronous instability of a single IIDG under droop control and virtual generator control strategies in consideration of current saturation. However, the model in the literature is only for voltage drop, which is not common in energy conversion and lacks the generality and applicability. Ref. [30] used small-signal modeling and dynamic analysis to profile the voltage changing. It is not suitable for large transient events. Ref. [31] developed the transfer function of the control system of the IIDGs that use virtual synchronous generators control. By linearizing the transfer function, the frequency characteristics and the effect of inertia were studied. The resonance was clearly explained in the frequency domain. The power angle curves are used to investigate the transient stability mechanism in a similar way of conventional transient stability analysis [34,35]. The theoretical influence from the droop control factors on the transient stability is learned. The transient stability judgment is developed. A simulation study is conducted to demonstrate the proposed transient mechanism and to verify the correctness of the judgment.

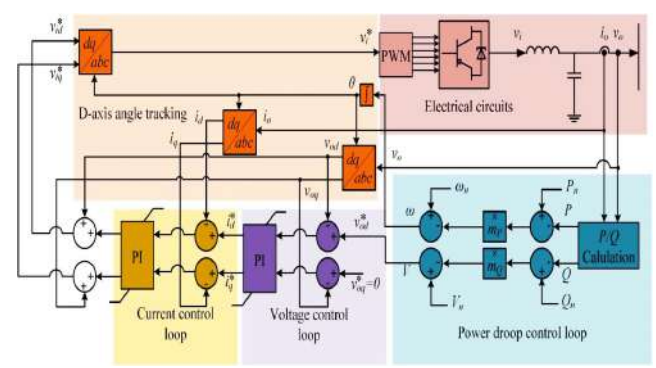


Fig. 1. IIIDGs system designed for three-stage control mechanism.

The fundamental commitments of this paper are three stages: (1) According to the activity highlights of the IIDG under droop control, the transient stability system is uncovered. This system clarifies and portrays the transient practices of the IIDGs during the transient occasions; (2) The influence of droop factors on transient steadiness are inferred and obviously explained. It enables matrix to level direct get familiar with the IIDG's transient strength affectability to the hang factors and modify the control parameters; (3) Procedures to pass judgment on the transient dependability of the IIDG is proposed dependent on the transient component. This paper is sorted out as follows. Segment 2 forms the activity model of the IIDG and builds up the power point curves. The transient stability condition and the accompanying transient component of the IIDG are determined in Section 3. Segment 4 first presents the investigation of the droop factors and afterward presents techniques of the transient stability judgment. A progression of recreations is led in Section 5 to confirm the accuracy and effectiveness of the proposed transient strength instrument and its judgment strategies. Area 6 makes the implication and future work.

TRANSIENT MODEL AND OPERATION FEATURES OF IIDG

IIDG is normally connected to distribution network or in microgrids. Its electrical characteristics depend on the control methods and connected network. It is required to build a concise and comprehensive yetappropriate simplified model for the analysis of the transient stability.

A. Control system of IIDG

When connecting to the public grid, IIDGs output the active and reactive power according to the setting values assigned from upper controllers. IIDGs are usually subjected to the three-loop control system to regulate the

output [33,36]. The control system is shown in Fig. 1. The first loop, which is called the droop power control loop, adjusts the active and reactive power outputs by generating the angular speed and voltage references [33]. The second control loop, which is called the voltage control loop, stabilizes the voltage of IIDGs. The third control loop, which is called the current control loop, follows the output currents and rapidly alters the output. When a transient event occurs, droop power control loop detects the significant outputs changes and changes the frequency and reference voltage references. Proportional plus integral controllers are implemented inside the voltage control loop and produces reference cur- rent signals I_d and I_q to the current control loop. Finally the current control loop generates the control signal to the pulse wavelength modulation modules to control the transistors. The control function of the three-loop control system is as follows:

$$\omega - \omega_n = m_p(p_n - p)$$

$$V - V_n = m_q(Q_n - Q)$$
(1)

B. Distribution networkmodeling

A common distribution network with numerous IIDGs appears in Fig. 2. IIDGs give their capacity to their nearby loads and the associated dispersion organizes. The highlights of the nearby loads and open grids affect the transient stability enormously. The power from IIDG flows through a link to the circulation organize. In the typical activity, the distribution grid gives frequency and voltage references to the IIDGs. The conveyance system can be adjusted to a solid source with consistent voltage and frequency. For a single IIDG, different IIDGs can be treated as a piece of the open grid, which is a lot more grounded power source than those IIDGs. Thusly the influence of different IIDGs can be ignored and the activity condition for an individual IIDG can be simplified, as is appeared in Fig.3.The simplified operation condition consists of IIDG, the voltage source, local loads and the connecting cable. The voltage source is the representative of the distribution network with constant voltage U and constant frequency f. The load PLOAD + jQLOAD stands for the local loads whose value adheres to the voltage:

$$P_{Load} = \left(\frac{V}{V_n}\right)^2 P_{nLoad}$$

$$Q_{Load} = \left(\frac{V}{V_n}\right)^2 Q_{nLoad}$$
(2)

The load is in quadratic relation with the voltage. The connecting cable impedance is $Z_1 \angle y$.

C. Mathematicform for Power Generation

According to the model in Section 2.2, the active power and reactive power of IIDG can be derived as:

$$P = \frac{V^2 \cos y - VU \cos(y + \delta)}{Z_I} + \left(\frac{V}{V_n}\right)^2 P_{nLoad}$$

$$Q = \frac{V^2 \sin y - VU \sin(y + \delta)}{Z_I} + \left(\frac{V}{V_n}\right)^2 Q_{nLoad} \tag{3}$$

Usually the nominal voltage of the IIDG is equal to the voltage of the distribution network. In droop control, the active power is controlled directly by revising angular frequency ω , which is in fact controlling thevoltage angle difference δ . δ and V can be treated as two independent variables. For a fixed voltage V, there is a corresponding power angle curve reflecting the connection between the active power P and δ , which is shown in Fig. 4(a). Analogously, the connection between reactive power Q and V can be obtained as is shown in Fig. 4(b). The active power and reactive power each consists a cluster of power curves.

D. Transient Stability Mechanism

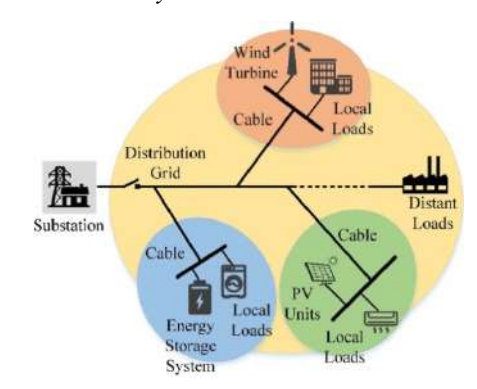


Fig. 2. Typical arrangement of distribution network

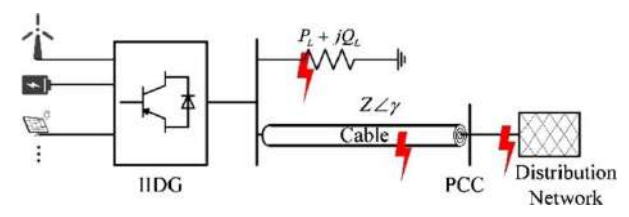


Fig.3.Single IIDG operation condition designed for distribution network.

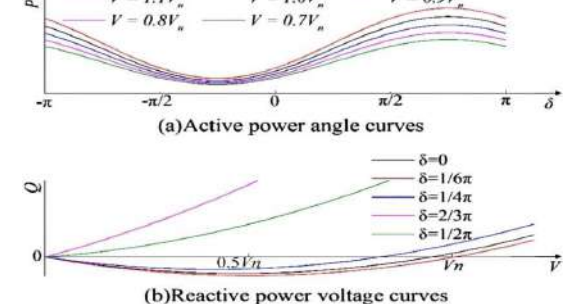


Fig. 4. Clusters of reactive and active power.

E. Transient Stability Condition

Under normal working condition, the IIDG works at the nominal point. When a transient event occurs, the working point of IIDG will deviate from the nominal point. The droop power control loop detects the deviation and controls the frequency and voltage of IIDG towards the opposite direction of the deviation. Fig. 5 shows an example of the active power angle curves in a short-circuit fault. In Fig. 5, before the fault, the IIDG works in the nominal point A where V equals to Vn and P equals to Pn. The active power angle curve that IIDG is currently operating along is $PVn(\delta)$. When fault occurs, the voltage immediately drops to Vf and causes the active power angle curve deviates to $PVf(\delta)$. It should be noticed that $PVf(\delta)$ is not included in the cluster of active power angle curves deducted by Eq. (3) since the structure of the network changes. The voltage angle difference does not change immediately, leading to the drop of active power to Pf (δn), which is less than Pn. The working point alters from A to B. According to the droop function (1), the adjustment of δ attributes to unequal shift of active power, which can be described as:

$$d\delta = (\omega_f - \omega)dt = mp(P_p - P_f)dt \tag{4}$$

Based on Eq. (4), δ increases due to droop controller, which further creates the shift of active power. The working point moves along PVf (δ). The moment the fault is cleared naturally or by protection devices,V and δ reach Vc and δ c and the active power angle curve immediately changes to PVc(δ). The variation of δ and P will be decided by the value of δ c. As is presented in Fig. 5, the active power angle curve is divided by the critical stability angle δ ct|vc which corresponds to the following equation:

$$P_{V_c}\left(\delta_{ct} \mid V_c\right) = P_n \tag{5}$$

If fault is cleared at C1 where δc is smaller than δct|vc, P will rise up to D1 and be larger than Pn. P will gradually restore to the nominal value and δ will begin to reverse under the droop control. When the operation point reserves to E1, the difference between the output power and nominal power equals zero. Therefore IIDG will stay in E1 and operate in a steady state. The dynamic trace reflecting the transient behavior of IIDG is A-B-C1-D1-E1. If fault is cleared at C2 where δc is larger than δct|vc, P will first rise up to D2 and start to decrease, causing the continuous accelerating increase of δ and decline of P. But it can be inferred that if δ increases to E2 where P is larger than Pn, P will analogously restores to the nominal value. The IIDG will stay in E2 and operate stably. The dynamic trace is A-B-C2-D2-E2. However, if the dynamic trace of the IIDG is always lower than the nominal power Pn, the IIDG will accelerate along the active power curves and never be stable. Therefore, the transient stability conditioncan be concluded as: $P(\delta)$ is the transient dynamic trace of a IIDG. The IIDG will be transient stable if there exists $\delta > \delta c$ such that $P(\delta) = Pn$.

DYNAMIC TRACES OF IIDGs

According to Eq. (3), the dynamic trace of active power of IIDG is in fact determined by both δ and V. When transient events occur, the active power P and reactive power Q both shift from nominal points. The power droop controller adjusts δ and V simultaneously resulting in a three-

dimensional movement of P. Therefore, P moves along a cluster of active power angle curves. A surface consisting of all possible active power angle curves can be delineated with δ and V being two independent variables. The surface, shown in Fig. 6, is uniquely determined, indicated by Eq. (3), by the connection cable impedance, nominal voltage and the rated active power of local loads. The surface remains identical when the transient event is cleared comparing to normal condition. But it is not the same during the transient events as those determinants might change.

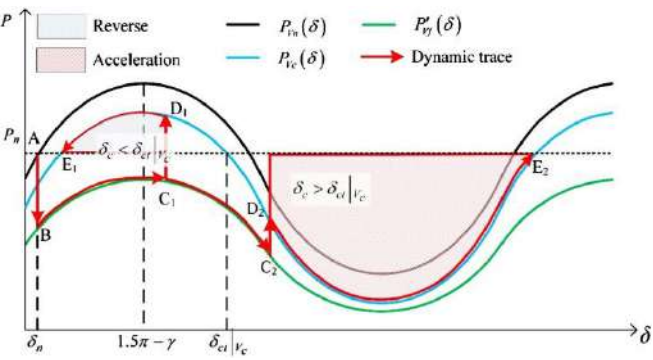
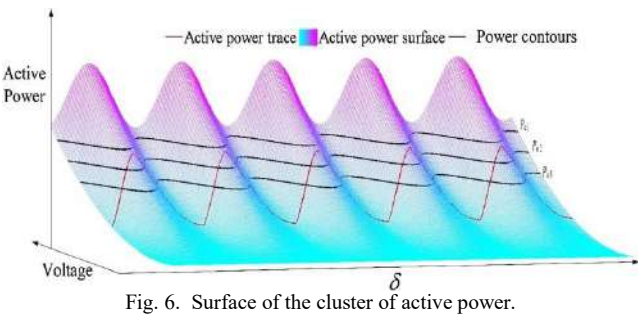


Fig. 5. Active power under short-circuit fault.



In Fig. 6, a red active power trace is highlighted among the active power surface. This periodic trace describes the possible dynamic characteristics of the IIDG in a transient event. The black curves re- present different setting values of the nominal active power output of IIDG. According to the transient stability condition, the IIDG will be stable only if its dynamic trace intersects the power contour of nominal power. If the power contour, such as Pn1, is higher than the periodic trace, IIDG will never reach the set point of outputs. The power droop controller will always detect the inequality between actual outputs and nominal outputs. The inequality will cause endless increase of δ and unceasing oscillation of V, which means the operation point, will move along the dynamic trace. Furthermore, the active power will always be oscillating. The IIDG is transient instable under this kind of endless oscillation.

A. Calculation for Dynamic Traces

From the inference in Section 3.2, the dynamic trace of the IIDG analysis of the dynamic trace can concisely computes the transient mention reduction is required to analyze the dynamic traces less part of Eq. (3) can be seen as a quadratic equation. Solve the quadratic. equation,

$$V(\delta) = \frac{\frac{U\sin(\gamma+\delta)}{Z_I} + \sqrt{4Q\left(\frac{Q_{nload}}{U^2} + \frac{\sin(\gamma)}{Z_I}\right) + \frac{U^2\sin(\gamma+\delta)^2}{Z_I^2}}}{2\left(\frac{Q_{nload}}{U^2} + \frac{\sin(\gamma)}{Z_I}\right)}$$
(6)

Where V is the larger one of the two roots of the quadratic function since V should be positive. Vn is assumed to be equal to U because the nominal voltage is approximate to the distribution network voltage. Eq.(6) reflects the direct relation between δ and V, which can reduce the dimension of the dynamic traces. However, in Eq. (6), Q is unknown. Analogously, the recovery of Q is oscillating like P. It is reasonable to assume that the trace of Q is composed of a process of rising and a process of oscillating as shown in Fig. 7. It is well known that IIDGs are generally set to maximally convert renewable energy in normal practice [37]. From economic concerns, the active power outputs assigned to IIDGs are relatively much higher than reactive power outputs [38]. So the fluctuation of O is negligible during the recovery after the transient events. Given the hypothesis that P_c and Q_c is lower than P_n and Q_n, respectively. Therefore, the recovery of Q can be linearized as two parts. The first part is the linearized rise of Q. The second part is Q being constant when Q rises up to its maximum value. Fig. 7 also shows the linearized trace of Q. The recovery process of Q can be equivalent as

$$Q(t) = \begin{cases} Q_c + \alpha(t - t_c) & t \sum [t_c, t_{\text{max}}] \\ Q_{\text{max}} & t \sum [t_{\text{max,}} + \infty] \end{cases}$$
(7)

According to Eq. (6), the maximum value of $V(\delta)$ and Q are positively correlated. According to Eq. (3), the maximum value of $P(\delta)$ and $V(\delta)$ are also positively correlated, which means the maximum values of $P(\delta)$ and O are positively correlated.

From Eq. (3), for a fixed V, Q_{max} is obtained when

$$\delta = -\gamma - \frac{\Pi}{2} + 2k\Pi \tag{8}$$

Infinite δ satisfy Eq. (10). Q starts to rise when the transient event is cleared with $\delta = \delta_c$. Then δ will increase until the first time $Q = Q_{max}$. Define the δ at t_{max} as δ_{con} which

$$\delta_{con} = \min \left\{ \delta \mid \delta = -\gamma - \frac{\Pi}{2} + 2k\Pi, \delta > \delta_{c,k} \Sigma N^{+} \right\} (9)$$

Then the linearized rising process of Q relate to δ changing from δ_c to δ_{con} . The process can be described by Eq. (10):

$$\delta_{con} = \delta_c + \int_{t_c}^{t_{\text{max}}} d\delta (10)$$

$$\delta_{con} = \delta_c + m_p \int_{t_c}^{t_{\text{max}}} (p_n - p) dt \quad (11)$$

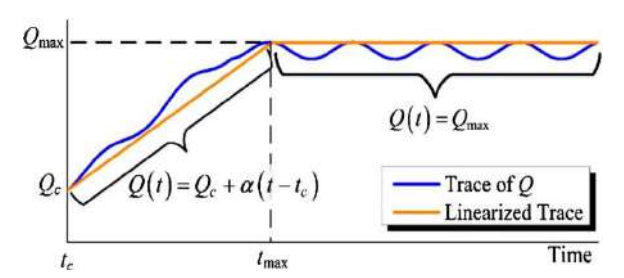


Fig. 7. Trace of Q during the recovery after the transient event

$$V(t+dt) = V_n + m_O(Q_n - Q(t))$$
(12)

Substitute Eq. (12) into Eq. (13) and we have:

$$Q(t+dt) - Q(t) = -Q(t) + \frac{Q_{nload} (m_Q (Q_n - Q_t) + U)^2}{U^2} + \frac{(m_Q (Q_n - Q_1) + U)((m_Q (Q_n - Q(t)) + U)\sin(\gamma + \delta)}{Z}$$
(13)

By integral of Eq. (13), the $\,Q_{\rm max}\,$ can be obtained:

$$Q_{\text{max}} = Q_c + \int_{t_c}^{t_{\text{max}}} [Q(t+dt) - Q(t)]dt$$

$$\alpha = \frac{Q_{\text{max}} - Q_c}{t_{\text{max}} - t_c}$$
 (15)

SIMULATION OF TRANSIENT STABILITY

So as to show the effectiveness of the proposed transient stability judgment, recreations are led to look at the genuine powerful follow and the processed unique follow. In this reenactment, m_P and m_O are recorded in Table 1 and Table 2. Fig. 18 demonstrates the correlation between the genuine unique follow and the processed CDT. It ought to be referenced that the figured powerful follow just reflects the dynamic procedure after the issue clearing in Fig. 18(a), (e) and (f), the IIDGs are transient instable. The processed CDTs demonstrate that $P(\delta)$ is interminably lower than Pn after the deficiency cleared. So the δ is continuously expanding and the dynamic power changes along the dynamic follow. The real powerful follows show comparative variety inclination. Despite the fact that there exist some deviation, the figured CDTs protect high congruity on the most elevated estimation of $P(\delta)$. In Fig. 18(a), (e) and (f), the IIDGs are transient stable. The figured CDTs are lower than the ostensible power, which means the IIDG is transient instable. It very well may be seen from the real unique follow that the IIDG balances out at the point where $P(\delta)$ equivalents to Pn. The figured area of the consistent point is nearly equivalent to the real enduring point, which shows high exactness of the methodology. In real unique follow, the real voltage point difference and the dynamic power progressively arrive at unfaltering state in a winding.

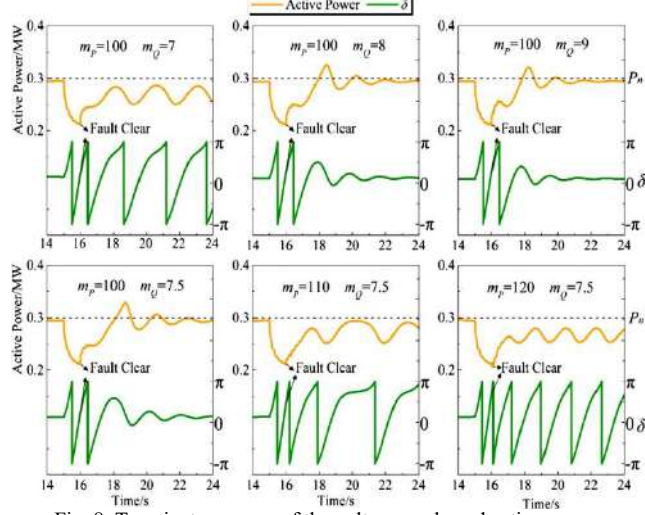


Fig. 8. Transient response of the voltage angle and active power.

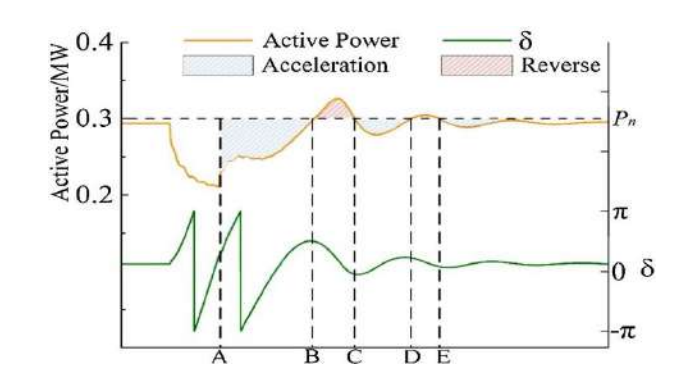


Fig. 9. Transient response of case B.

Table 1 t_{restore} (s) of stable cases with different m_P and m_O .

	m_Q				
	8	10	12	14	16
m _P 25	3.9668	2.8219	2.5748	1.8263	1.5929
50 75 100	5.0121 5.9579 9.7909	3.3739 3.9126 5.2910	2.9554 3.0708 4.4148	2.1747 2.4237 4.365	2.1349 2.3207 3.4204

Table 2 t_{period} (s) of instable cases with different m_P and m_Q .

	m_Q				
	2	4	6	8	
m _P 100 125 150 175 200	0.8208 0.6637 0.5575 0.4779 0.4115	1.2345 0.9491 0.7965 0.6704 0.5907	1.5663 1.2544 0.9956 0.8097 0.7433	- 2.0907 1.3407 1.0553 0.8827	

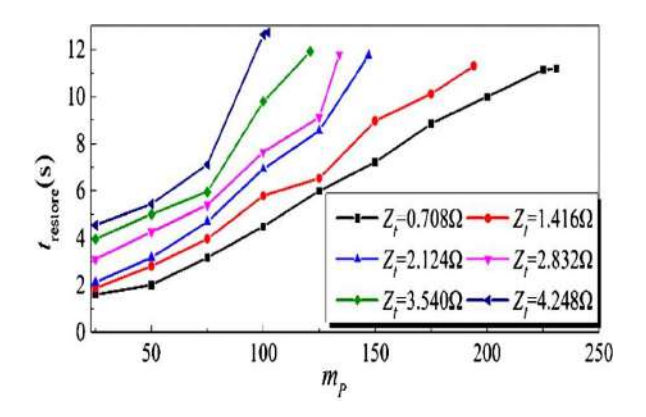


Fig. 10. The comparison among t_{restore} and m_P with variable impedance of cable (m_Q =8).

The reason for the spiral is possibly because of the time delay of the three-loop system. The simulation results show that the proposed transient stability judgment is effective and accurate. It suggests that the judgment can be used in formulating stabilization control with anticipatory transient events. It can also be utilized to find the stable operation zones for distribution networks or micro grids.

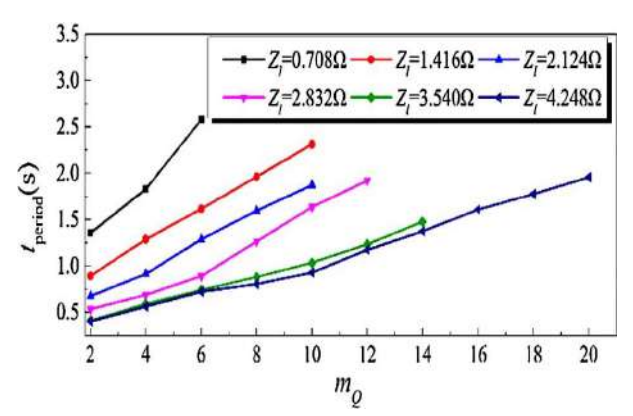


Fig. 11. The comparison among t_{period} and m_Q with variable impedance of cable ($m_P = 200$).

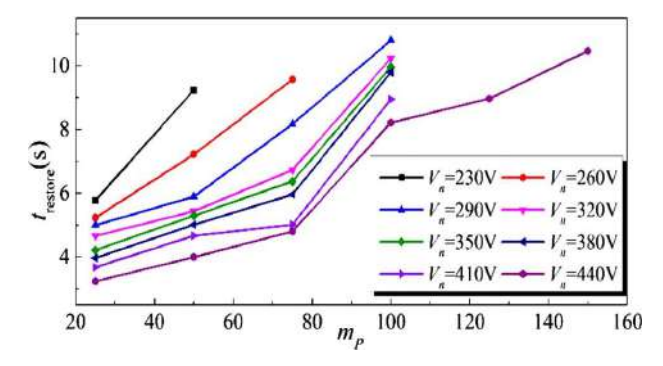


Fig. 12. The comparison among $t_{restore}$ and m_P at variable voltage levels ($m_Q = 8$).

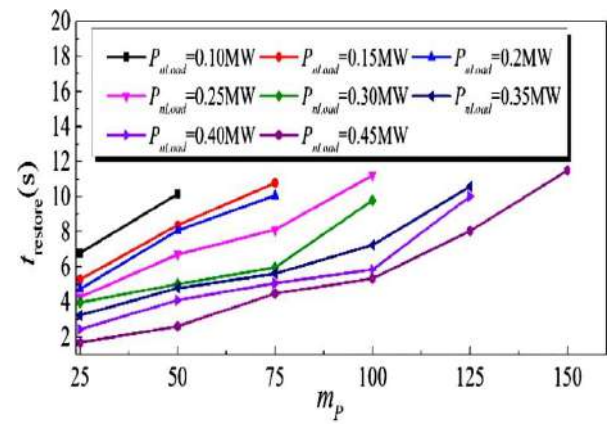


Fig. 13. The comparison among t_{period} and m_Q at variable voltage levels ($m_P = 200$).

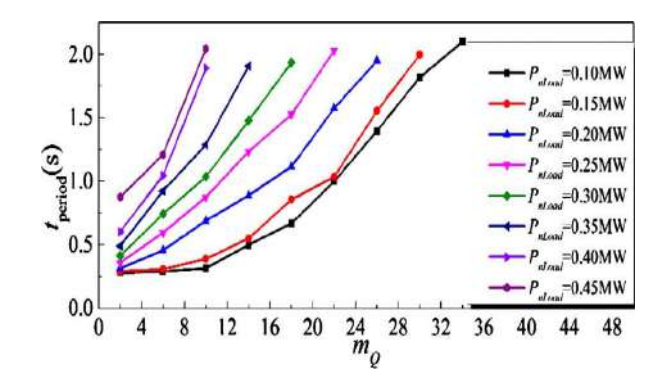


Fig. 14. The comparison among t_{restore} and m_P at variable local loads $(m_Q = 8)$.

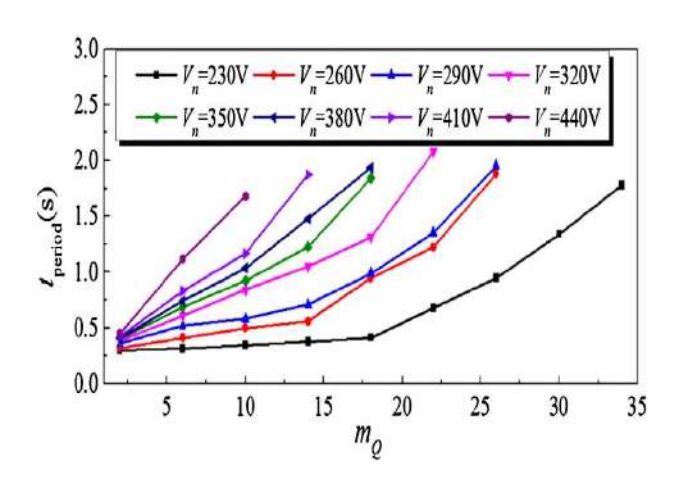


Fig. 15. The comparison among t_{period} and m_Q at variable local loads $(m_P = 200)$

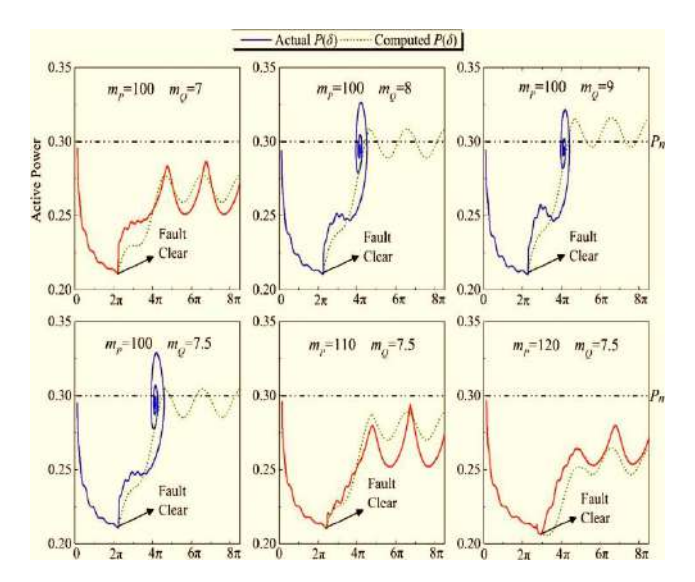


Fig. 16. Comparison among the actual dynamic trace and the computed dynamic trace according to the transient stability criteria.

CONCLUSION AND FUTURE WORK

This paper centers around transient security instrument of the power droop controller-based network associated inverter-interfaced conveyed generators (IIDGs). The transient soundness instrument is proposed and dissected by utilizing the complete powerful follow. It uncovers the influence factors on the transient security of IIDGs during transient occasions. The dynamic power droop factor is contrarily corresponded to the transient security though the responsive power droop factor is emphatically associated to the transient strength. The transient security judgment is intended to precisely recognize the dependability of an IIDG during transient occasions. It gives procedure to conveyance organize administrators to improve the administration and control of IIDGs. Also, it is fit for streamlining control parameters of IIDGs in like manner. The recreations are directed on PSCAD/EMTDC to show the rightness and effectiveness of the transient strength component. The relations between the transient solidness and droop elements are approved. Low link impedance, high voltage level and high neighbourhood burdens guarantee high transient soundness. The outcomes likewise demonstrate that the transient steadiness judgment is succinct and effective. The transient security issue is a basic issue in the sustainable power source age and dispersion. The exploration will step into the phase of researching the transient soundness instrument and rule of the miniaturized scale lattices and small scale network groups. The future work will be stretched out to improve and upgrade the integration of sustainable power source.

REFERENCES

- Arrillaga J, Liu YH, Watson NR. Flexible power transmission: The HVDC options. John Wiley & Sons Ltd; 2007.
- [2] Sood VK. HVDC and FACTS controllers applications of static converters in power systems. Kluwer; 2004.
- [3] Acha E, Agelidis VG, Lara OA, Miller TJE. Power electronic control in electrical systems. Butterworth: Newnes; 2002.
- [4] Padiyar KR. HVDC power transmission systems. 2nd ed. New Age International Publishers; 2012.
- [5] Kothari DP, Nagrath IJ. Modern power system analysis. 4th ed. New Delhi: Tata McGraw Hill; 2011.
- [6] Yazdani A, Iravani R. Voltage-sourced converters in power systems: modeling, control and applications. Wiley-IEEE Press; 2010. p. 171.
- [7] Flourentzou N, Agelidis GV, Demetriades GD. VSC-Based HVDC power transmission systems: an overview. IEEE Trans Power Electron 2009;24(3):592–602.
- [8] Asplund G. Application of HVDC light to power system enhancement. Proc IEEE PES winter meeting; 2000.
- [9] Blau J. Europe plans a north sea grid. IEEE spectrum; 2010. p. 12– 13.
- [10] Haileselassie MT, Uhlen K. Power system security in a meshed north sea HVDC grid.IEEE Proc, invited paper, vol. 101, No. 4, 2013. p. 978–90.
- [11] Lidula NWA, Rajapakse AD. A pattern-recognition approach for detecting power islands using transient signals—Part II: performance evaluation. IEEE Trans Power Deliv 2012;27(3):1071–80.
- [12] Boroojeni KG, Amini MH, Nejadpak A, et al. A theoretical bilevel control scheme for power networks with large-scale penetration of distributed renewable resources [C]//Electro Information Technology (EIT), 2016 IEEE International Conference on. IEEE, 2016: 0510-0515
- [13] Hashemi F, Mohammadi M, Kargarian A. Islanding detection method for microgrid based on extracted features from differential transient rate of change of frequency. IET GenerTransmDistrib 2016.
- [14] Basak P, Chowdhury S, nee Dey SH, et al. A literature review on integration of distributed energy resources in the perspective of control, protection and stability of microgrid. Renew Sustain Energy Rev 2012;16(8):5545–56.
- [15] Kaur A, Kaushal J, Basak P. A review on microgrid central controller. Renew Sustain Energy Rev 2016;55:338–45.
- [16] Liu S, Liu PX, Wang X. Stability analysis of grid-interfacing inverter control in distribution systems with multiple photovoltaicbased distributed generators. IEEE Trans Industr Electron 2016;63(12):7339–48.
- [17] Guo WM, Mu LH, Zhang X. Fault models of inverter-interfaced distributed gen- erators within a low-voltage microgrid. IEEE Trans Power Deliv 2017;32(1):453–61.
- [18] Alaboudy AHK, Zeineldin HH, Kirtley J. Microgrid stability characterization sub- sequent to fault-triggered islanding incidents. IEEE Trans Power Deliv 2012;27(2):658–69.
- [19] Alaboudy AHK, Zeineldin HH, Kirtley J. Simple control strategy for inverter-based distributed generator to enhance microgrid stability in the presence of induction motor loads. IET GenerTransmDistrib 2013;7(10):1155–62.
- [20] Alipoor J, Miura Y, Ise T. Stability assessment and optimization methods for microgrid with multiple VSG units. IEEE Trans Smart Grid 2016.
- [21] Khalik ASA, Massoud AM, Elserougi AA, Ahmed S. Optimum power transmission based droop control design for multi-terminal HVDC of offshore wind farms. IEEE Trans Power Sys 2013;28(3):3401–9.
- [22] Bellmunt OG, Liang J, Ekanayake J, Jenkins N. Methodology for droop control dynamic analysis of multi terminal VSC-HVDC grids for offshore wind farms. IEEE Trans Power Delivery 2011;26(4):2476–85.
- [23] Zhao X, Li K. Droop setting design for multi-terminal HVDC grids considering voltage deviation impacts. Electr Power Syst Res 2015;123:67–75.

- [24] Hertem JDV, Belmans R. VSC MTDC systems with a distributed DC voltage control-a power flow approach. IEEE Trondheim Power Tech 2011:1–6.
- [25] Wang W, Barnes M. Power flow algorithms for multi-terminal VSC-HVDC with droop control. IEEE Trans Power Syst 2014;29(4):1721–30.
- [26] Cao J, Du W, Wang HF. Minimization of transmission loss in meshed AC/DC grids with VSC-MTDC networks. IEEE Trans Power Syst 2013;28(3):3047–55.
- [27] Omagari Y, Funaki T. Numerical study of transient stability criteria for an inverter- based distributed generator[C]//Power Electronics for Distributed Generation Systems (PEDG). In: 2012 3rd IEEE International Symposium on. IEEE; 2012. p. 865–71.
- [28] Iyer SV, Belur MN, Chandorkar MC. A generalized computational method to determine stability of a multi-inverter microgrid. IEEE Trans Power Electron 2010;25(9):2420–32.
- [29] Zhang Y, Xie L. A transient stability assessment framework in power electronic- interfaced distribution systems. IEEE Trans Power Syst 2016;31(6):5106–14.
- [30] Zhang Y, Xie L. Online dynamic security assessment of microgrid interconnections in smart distribution systems. IEEE Trans Power Syst 2015;30(6):3246–54.
- [31] Xin H, Huang L, Zhang L, et al. Synchronous instability mechanism of Pf droop- controlled voltage source converter caused by current saturation. IEEE Trans Power Syst 2016;31(6):5206–7.
- [32] Chang CC, Gorinevsky D, Lall S. Dynamical and voltage profile stability of inverter- connected distributed power generation. IEEE Trans Smart Grid 2014;5(4):2093–105.
- [33] Hirase Y, Sugimoto K, Sakimoto K, et al. Analysis of resonance in microgrids and effects of system frequency stabilization using a virtual synchronous generator. IEEE J Emerging Selected Top Power Electron 2016;4(4):1287–98.
- [34] Tang X, Deng W, Qi Z. Investigation of the dynamic stability of microgrid. IEEE Trans Power Syst 2014;29(2):698–706.
- [35] Simpson-Porco JW, Dörfler F, Bullo F. Voltage stabilization in microgrids via quadratic droop control. IEEE Trans Autom Control 2017;62(3):1239–53.
- [36] Kundur P. Power system stability and control. New York: McGraw-hill; 1994.
- [37] Kimbark EW. Power system stability. John Wiley & Sons; 1995.
- [38] Rocabert J, Luna A, Blaabjerg F, et al. Control of power converters in AC microgrids. IEEE Trans Power Electron 2012;27(11):4734–49.
- [39] PapaioannouIoulia T. Mathematical and graphical approach for maximum power point modelling. Appl Energy 2012; 91:59–66.
- [40] Ding T, Li C, Yang Y, et al. A two-stage robust optimization for centralized-optimal dispatch of photovoltaic inverters in active distribution networks. IEEE Trans Sustain Energy 2017;8(2):744–54.

The Institution of Engineers (India), WBSC

23rd & 24th Nov. 2019

ERROR BUDGET ANALYSIS OF SODIUM WIRE TYPE AND PLUG TYPE LEAK DETECTORS FOR FAST REACTORS

M.Shanmugasundaram*¹, B.K.Choudhary² and D.Thirugnanamurthy³

¹Fast reactor Technology Group

²Metallurgy and Materials Group

³Electronics Instrumentation Group

Indira Gandhi Centre for Atomic Research, Kalpakkam- 603 102

Liquid sodium reacts readily with atmospheric air leading to sodium fire. Hence the piping and components are to be equipped with leak detection system to detect any leak in th incipient stage itself to limit the effects of fire. Various kinds of leak detractors have been developed for this purpose, namely wire type leak detector, spark plug type leak detector etc. Wire type leak detector comprise of a wire carrying small current which is wound on the sodium pipes and capacities with adequate ceramic bead insulation. In case of sodium leak sodium will short the wire with pipe/vessel body giving rise to a short circuit and this is sensed. In case wire type leak detector fails to detect the leak, sodium would come out of the insulation and drip into leak collection tray. These trays are provided with spark plug type leak detectors that work on the same principle as spark plug type level probe. It is used for detecting sodium leak in enclosed space like bellows sealed valves and thermowell. It is also used to detect sodium leak from the double wall pipelines and vessels of fast reactor system. It is usually mounted in a tray/pocket in to which the leaked sodium collects and causes electrical short between its insulated central conductor and the body. The absolute accuracy of the system electronics is affected by Common Mode Rejection

Ratio (CMRR), gains, offset voltage and offset current changes. Error budget analysis for the INSOT facility wire type and plug type leak detection electronics circuit were carried out. and evaluated. Errors added in the type and plug type leak detection electronics system are identified.

Keywords: Error budget analysis Sodium, Operation, level, Safety, High Temperature, sodium loop, INSOT

International Conference On "Impact of Changing Energy Mix in the Power Sector" (ICIEMPS-2019)

The Institution of Engineers (India), WBSC

23rd & 24th Nov. 2019

The Institution of Engineers (India), WBSC

23rd & 24th Nov. 2019

ERROR BUDGET ANALYSIS OF SODIUM IONISATION DETECTORS FOR FAST REACTORS

M.Shanmugasundaram*¹, B.K.Choudhary² and D.Thirugnanamurthy³

¹Fast reactor Technology Group

²Metallurgy and Materials Group

³Electronics Instrumentation Group *Indira Gandhi Centre for Atomic Research, Kalpakkam- 603 102*

Sodium ionisation detectors are used for area monitoring that on the principle of preferential ionisatin of aerosols of sodium and its compounds (oxides and hydrides) in carrier gases such as argon, nitrogen and air. It uses a heated platinum filament to ionise the sodium vapour or its aerosols in preference to the constituents of the carrier gas. These positively charged sodium ions are collected by a collector electrode to provide a measure of ion current which is an indication of sodium leak. Sampled air from the system area is admitted to the sensor and presence sodium ions in the order of nanogram / m³ level of sodium ion concentration can be detected by this sensor. The electronics system will drift in measurement due to change in operating temperature and will have an effect on characteristics of the circuit. Error budget analysis for the INSOT facility sodium ionisatin detection electronics circuit were carried out and evaluated. Errors added in the sodium ionisatin detection electronics system are identified.

Keywords: Error budget analysis Sodium, leak, Safety, High Temperature, sodium loop, INSOT

Reliability improvement of 400 kV transmission line using Quad Spacer Damper and Quad Rigid Spacer

Sumana Chattaraj¹, Sushri Mukherjee¹, Md. Irfan Khan¹, Dharmbir Prasad² and Harish Agarwal¹

¹Supreme & Co. Pvt. Ltd., Kolkata-700020, WB, India

²Asansol Engineering College, Asansol-713305, WB, India

{Corresponding author's email: sumana.engg@supreme.in}

Abstract - Overhead conductors are prone to wind-induced vibration which further affects reliability of transmission line infrastructures. Thus, conductor's failures may lead to major power outage. Considering severity of the issue, several analytical and experimental techniques have been evolved across the world in order to nullify the conductor's vibrations and its consequences. In this experimental work, the AAAC conductor has been used for power transmission and its damping, radio interference and corona discharge aspects were studied. These bundled conductors are susceptible to wind-induced vibrations in the recurrence scope of 10-60 Hz because of the vortex shedding. This paper presents Quad Spacer Damper and Quad Rigid Spacer for dissipation of vibration energy of 400 kV transmissions lines. This exclusively designed and in-house developed damper and spacer have successfully proven its effectiveness in reliability maintenance at High Voltage Laboratory, IISc Bangalore (India) and CPRI, Bangalore. It has been observed that the proposed damping and spacing hardware accessories would able to withstand the site specific requirements of mechanical and electrical stability. Finally, radio interference voltage (RIV) and visible corona discharge (VCD) tests along with clamp bolt torque test and clamp slip test were successfully performed to check viability of the product.

Keywords - High Voltage; Transmission; Quad; Spacer Damper; Rigid Spacer.

INTRODUCTION

The application of multi-conductor bundles in high voltage overhead transmission lines has been adopted for several decades. Conductor spacers rapidly become important pieces of hardware aimed at maintaining the geometry of the bundles to meet the requirements of electrical performance. Several solutions are now proposed as an adequate spacer system design. However, their role soon evolved as significant component of a complex electromechanical system subject to a range of environmental factors [1]. It led to the design of spacer damper and rigid spacer together with the problem of properly distributing them in a given span. Considerable knowledge has been acquired concerning the material requirements and selection criteria, including the use of clamping systems that provide a safe and reliable long term grip on the conductors, while maintaining installation ease [2].

- A. Proposed T&D Hardware Accessories: Typical conductor bundles comprise two, three, four, six or eight sub-conductors. In particular cases, bundles with twelve sub-conductors have also been used in India. Following this trends, the spacer and damper are applied for reliability improvement of overhead transmission system [3-6]. A quad rigid spacer or quad spacer damper typically consists of frame and conductor clamps that are connected to the central frame [7-8]. The proposed solution is briefly described as follows:
- (i). Spacer Damper: They are used for suppressing the sub-span oscillations in bundled conductors as these oscillations could cause damage to multiconductor bundle system. They could be used as a remedy against aeolian as well as wake induced oscillations. Even after experiencing severe loads due to short-circuit currents, ice and wind it must restore the bundle to normal posture.
- (ii). Rigid Spacer: A rigid spacer restricts the distances between the conductor clamps to the nominal values of the sub-conductor spacing. The clamps do not allow for any significant movement of the sub-conductors with regard to each other compared to the conductor diameter. They are no longer used on tensioned spans but on jumper loops and slack spans only.
- B. Constructional Features: A spacer damper consists of unbending focal casing made of aluminum alloy and relying upon the number sub-conductors of AAAC conductor and number of spacer damper & rigid spacer arms. Like for the case of quad spacer damper (as shown in Fig. 1(a)) and quad rigid spacer (as shown in Fig. 1(b)) there are four arms made up of aluminum alloy with rectangular configuration.

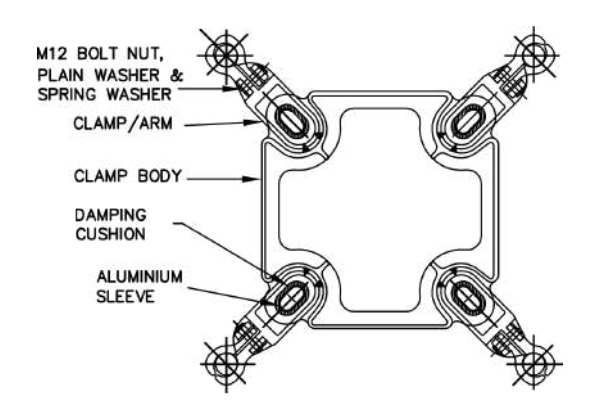


Fig. 1(a) Schematic of Quad Spacer Damper

The aluminum alloy made clamps are attached with the central rigid frame and its main function is to grip the conductor. The elastomers can be employed within the clamp arm assembly to grip the individual cables and to provide adequate dampening support. The spacer damper has elastomeric damping cushion (i.e., neoprene rubber bush) that are deployed within the junctions between the supporting frame and the clamp arms, which connect to the sub-conductors. Basically, these elastomeric elements absorb energy to dampen the motions in the bundle created by wind and various environmental conditions.

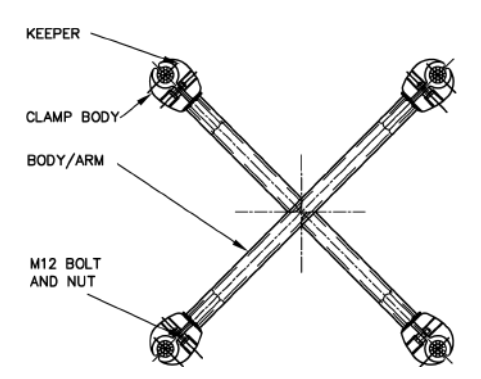


Fig. 1(b) Schematic of Quad Rigid Spacer

However, in rigid spacer - aluminium tube made arm and aluminium alloy made clamp body and keeper are used to maintain consistent spacing among conductors, thus keeping reliability of the system.

C. Paper Layout: In this paper, constructional feature of the proposed solution and positioning factors for reliability maintenance have been discussed under introductory section. Rest of the paper is organized as: Section-D presents mathematical formulation; Section-E highlights optimal location of spacers. However, Section-F describes validation of the proposed product and at the end conclusion of the present study is drawn.

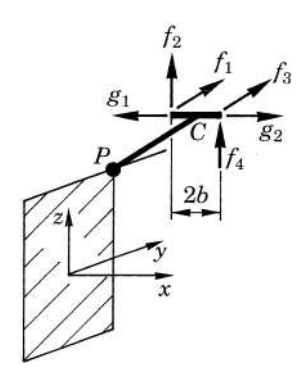


Fig. 2 A spacer damper with forces acting at clamp

D. Mathematical Formulation: In Fig. 2, only one of the four arms is shown attached to the central frame through a viscoelastic joint at the point P. The forces in the directions transverse to the conductor are denoted by f_i , i=1,2,3,4; while the forces in the axial direction of the conductor are g_s , s=1,2. There are total sixteen transverse force components $f_1, f_2,..., f_{16}$ and eight axial components $g_1, g_2,..., g_8$ acting on four arms of spacer damper and similar transverse and axial forces (except damping forces) will appear for rigid spacer too due to its four arms. The conductor displacements along the lines of action of $f_1, f_2,...$ will be denoted by $w_1(x,t), w_2(x,t),...$, respectively and can be given by the wave equation (1) [9-11],

$$\rho A_c \overset{\circ}{w}(x,t) = T_i w_i(x,t)^n, \quad i = 1,2,....,16$$
(1)

where, ρA_c being the conductor's mass per unit length and T_i represent its tension. Here, $T_1 = T_2 = T_3 = T_4$ indices were associated with the same conductor.

The individual conductors may, however, be subject to different tensions so that possibly $T_4 \neq T_5$, etc. The harmonic travelling waves in the conductors can be given by (2) [9-11],

$$w(x,t) = \text{Re}\left[\left(W_{i}^{+}e^{-jk_{i}x} + W_{i}^{-}e^{jk_{i}x}\right)e^{j\Omega t}\right] \qquad i = 1,2,....,16,$$
(2)

where, ω is the angular frequency, k_i is the wave number, and $\frac{\omega}{k_i} = \sqrt{\frac{T_i}{\rho A_c}}$ is the wave velocity in the

conductor.

The W_i^{\pm} are the complex amplitudes of the waves travelling in the conductors in the positive and negative x-axis directions, respectively. These

complex amplitudes will be split up into the complex amplitudes of the incident waves W_{ii} , i=1,2,....,16 travelling towards the spacer clamp in a given section of the conductor and the complex amplitudes W_{Li} , i=1,2,....,16 of the waves leaving the clamp.

However, true bundle motions can be considered as the result of a vectorial combination of a number of natural modes, the contribution of each depending on the spacer design and the frequency of oscillation. And it may be mathematically given by (3) [9-11],

$$f = \frac{n}{2l} \sqrt{\frac{T}{m}}$$

(3)

where n is the sub-span oscillation mode, that is generally 1 or 2 and l is the sub-span length.

E. Location of Spacers: The optimisation to suggest type and position of the spacers in a span is done with respect to problems of wind-excited vibrations: mainly instability phenomena (sub-span oscillations) and aeolian vibrations; other phenomena are ice galloping and wake-induced galloping (without ice). This optimisation should also consider short-circuit forces and bundle twisting due to ice loads. The maximum sub-span length depends on the wind speed and on the type of terrain typical of the site. It is also dependent on the oscillation amplitude allowed by the specifications issued for the specific site. In the sub-span mode, both sub-conductors in a windwardleeward pair usually participate in the motion, the leeward having the higher amplitude. Not all pairs in a bundle necessarily participate to the same degree. For example, in a four-conductor square bundle, the upper or lower pair may have greater amplitude than the other. However, due to the blow out angle, it may become unstable at extreme wind speeds, leading to very high amplitudes of oscillation. The bundle configuration has a major effect on the performance of the line [12-14]. All configurations of the bundles experience sub-conductor oscillation to a greater or a lesser degree. For example, the diamond quad bundle is stable at low wind speed as shown in Fig. 3. Following are the main factors affecting positioning of the spacer and damper:

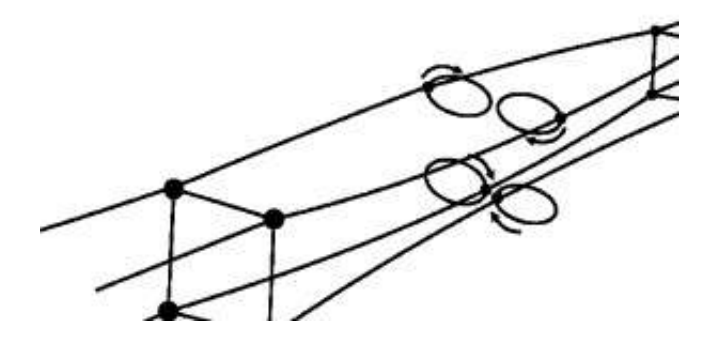


Fig. 3 Representation of Sub-span oscillation.

(i). Aeolian Vibrations: In this case, the parameter of interest is mainly number of spacers, whilst their location is not so important. The optimisation of the spacer location with respect to aeolian vibrations is not useful: it is much more important to optimise the spacer type and its characteristics (stiffness and damping of the elastic elements, geometry and inertia of the parts). It would be possible, from the aeolian point of view, to avoid spacers and to use dampers close to span ends; however, this solution obviously cannot maintain the bundle geometry along the span.

(ii). Instability Problems Sub-span Oscillation: Spacing is very important because sub-span oscillation is an instability phenomenon resulting from the coupling between two types of vibration mode of the bundle, one having a horizontal component of motion and another consist a vertical component. Some common modes of sub-span oscillation for quad bundles involve a combination of horizontal and vertical modes: these are less influenced by unequal sub-spans since both frequencies depend on sub-span length. The instability mechanism is complex as it depends, in general, on the horizontal and torsional modal frequencies which are structurally different and are made equal by the wind action, thus giving rise to typical flutter-type instability.

(iii). Other Instability Problems-Galloping with Ice: Spacer type, number and spacing do not have a great influence in controlling conductor galloping phenomenon. However, short sub-spans at the ends do increase the bundle torsional stiffness and as a result, achieve two goals: a partial contribution to detuning bundle torsional and vertical modes of vibration and a reduction in the risk of static, torsional collapse.

According to Hearnshaw (1974), a sub-span ratio is around 0.85-0.9 for the conductor's optimum stability solution. Regarding the end sub-spans, these are generally shorter than the others. A good value for the ratio between the lengths of an end sub-span and the adjacent one is between 0.55 and 0.65 [15]. Short end sub-spans (25-45 m) prevent sub-span oscillation

at span extremities which can damage the insulator hardware and increase the bundle torsional stiffness with two main advantages: a partial contribution to detuning bundle torsional and vertical modes of vibration, and a reduction in the risk of static, torsional collapse under ice loading and strong wind [16].

F. Validation Arrangement: Transmission project's site includes identifying and preventing wind induced conductor's motion damage. In this study, bundled conductors consisting of quad sub-conductors are adopted for transmission lines with rated voltages 400 kV. Rigid spacers keep the sub-conductors within a span and in jumper loops at designed spacing to avoid damage caused by clashing, twisting or entwining. Where motion control is a concern, rigid spacers are used in conjunction with Stockbridge dampers to give sufficient damping and spacing results. The design of the spacer is critical with respect to the dimensions of the inserting points and the hole location for the hardware. The relationship will change based on the conductor type. The spacer must pass a multitude of test sequences to assure reliability of performance, like as follows:

- Clamp torque and slip test longitudinal/torsional,
- Short circuit compression/tensile and
- Fatigue, corona, RIV and electrical resistance.

Vibration measurements on the overhead lines are commonly performed as a final acceptance test of the conductor damping system, at the end of the line construction, and, on lines in operation, for assessment of vibration intensity of the conductors. Measurements of aeolian vibration on operating lines have been made in different ways using a variety of instruments *viz.*, vibration detectors, transducers, optical vibration monitoring devices and specific vibration recorders (bending amplitude recorders).

Wake-induced oscillation encompasses several types of motion, observed in conductor bundles that are caused by the aerodynamic shielding of leeward-lying conductors by windward conductors. As per EPRI (2009), among several types of wake induced oscillations sub-span oscillations are the most dramatic and the most frequently reported and it is the motion that designers are confronted nowadays with greatest conflict between sources of information and modelling [17]. In fact, even through sub-span oscillation is a well known phenomenon in transmission lines, operators become more sensitive to the problem as sub-span oscillations have occurred in several lines. These oscillations were mainly stirred by the terrain configuration (desert) and the high probability of medium-high wind speeds [17].

Spacer dampers were used originally in order to maintain a constant distance between sub-conductors in the bundle, but they also play an important role from the mechanical point of view since they help to attenuate conductor vibration. The highest dynamic load usually occurs near the suspension or in the vicinity of the spacer clamp; therefore it is important to estimate the load acting on the spacer.

- Clamp Bolt Torque Test: The spacer damper was mounted on the specified size of conductor. A torque of 150% of the nominal value of toque (i.e., 60 Nm) was applied on each of the breakaway bolts.
- Clamp Slip Test-1: It was performed after successful performance of longitudinal and vertical vibration tests. A longitudinal pull of 450 kg parallel to the axis of the conductor was applied. No slip was observed at a pull of 450 kg and also during the hold period of one minute.
- Clamp Slip Test-2: After the successful completing of sub-span oscillation test, without disturbing or adjusting the torque on the clamp of the spacer damper connected to the conductor, a longitudinal pull of 450 kg parallel to the axis of the conductor was applied as per the standard. No slip was observed due to that and also during the holding period of one minute.

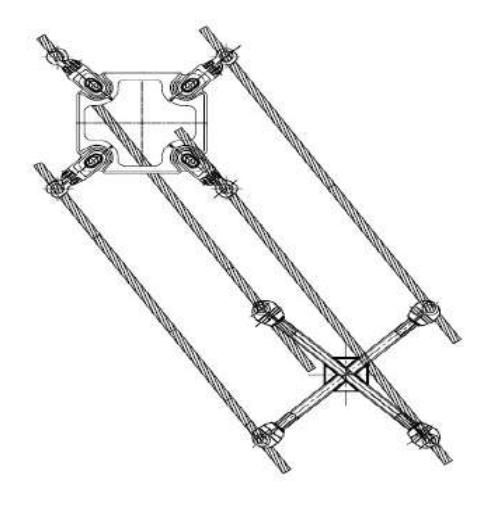


Fig. 2 Quad spacer damper and rigid spacer testing arrangement *Visible Corona Discharge Test:* The 400 kV conductor accessories loop consisting of Quad Spacer Damper and Quad Rigid Spacer was mounted at a height of 6.4 m above the ground. Care was exercised to ensure that no extraneous corona discharges occur from any other part of the test set up like connecting leads etc.

The visible discharge test was conducted (after sunset) in conditions of ambient light that can be described as almost pitch-dark. After adapting eyes to ambient darkness, the voltage was raised in small steps, from a low value at which there were no visible discharges, till the inception of visible discharges (called inception voltage). A pair of binoculars (optima zenith with 17X wide-angle, 8-17-40X zoom) was used to assist in this detection. The voltage was then lowered in small steps, till total disappearance of the discharges (called extinction voltage). The voltage was maintained at this level for a period of five minutes to observe whether any discharges reappear. This procedure was repeated four times and corresponding results are given below.

The test voltages applied to standard atmospheric conditions of 20°C, 760 mm of Hg and 11g of water per m³ of air, are as follows:

Discharge Inception voltage: 483 kV (rms)
Discharge Extinction voltage: 479 kV (rms)

Ambient temperature and pressure are as follows:

Dry-bulb temperature: 23.5°CWet-bulb temperature: 20.5°C

• Atmospheric pressure: 684.1 mm of Hq

However, voltage applied to test object is the product of low voltage reading and the scale factor of $3.27 \, \text{kV/V}$.

Radio Interference Voltage Test: The RIV measurement on the 400 kV conductor accessories loop consisting of Quad Spacer Damper and Quad Rigid Spacer was carried out in accordance with IEC 60437 (1997) and IS 8263 (1994), using a radio noise meter (SMV-11). The RIV is measured across a measuring resistance of 300 Ω , at a frequency of 1 MHz. However, the RIV meter is connected to a tap point of 50 Ω to match its cables characteristics impedence. Therefore, the experimental readings converted corresponding to resistance of 300 Ω . The power frequency voltages mentioned are actual values under the prevalent ambient conditions. After completing all preliminary measurements, the voltage is gradually raised in steps, to reach a value 15% above phase voltage and hold for at least five minutes, to allow RIV phenomenon to stabilization. Then, this voltage is reduced slowly in small steps, and RIV is recorded during the descending cycle. Three such cycles are repeated and RIV in dB (above 1 μV) at different voltages, during the third descending cycle is tabulated in Table 1. While finding solution, the ambient noise was measured as 12 dB, at 305 kV with test object removed. And, no correction should be applied to RIV values to compensate for ambient noise or for atmosphere conditions.

TABLE I RIV AT 1 MHZ ACROSS 300 ω

SI.	Power Frequency	Radio Interference \	√oltage
No.	Voltage, kV(rms)	dB (above 1μV)	μV
1	352	45.9	197
2	336	44.9	176
3	320	43.9	157
4	305	43.4	148
5	275	42.9	140
6	266	42.4	132
7	244	41.9	124
8	214	41.4	117
9	183	40.9	111
10	153	40.4	105
11	122	40.4	105
12	92	39.9	99

The voltage was raised in ambient darkness in small steps from a low value at which there were no discharges till the inception voltage which has been observed as 483 kV(rms) and the voltage was then lowered to the extinction voltage which was measured as 479 kV (rms). The RIV has been measured by increasing the voltage gradually in steps and then held for at least five minutes to allow RIV phenomenon to stabilize. RIV has been observed to be 45.9 dB and 197 μV at 352 kV (rms) power frequency voltage, 41.9 dB and 124 µV at 244 kV (rms) power frequency voltage and it has been noticed that at 92 kV (rms) the RIV is found to be 39.9 dB and 99 µV. Thus, the in-house developed dampers could able to withstand the site specific requirements as performed at the test station.

CONCLUSION

In this paper, spacer damper and rigid spacer are proposed and its control effect on the transmission line under the fluctuating wind load is validated. Whenever, a bundle is subjected to an asymmetrical static load, due to wind or ice, it rotates in an effort to restore static equilibrium between the applied loads and the forces generated by the rotations. When this occurs, the bundle remains twisted, even after the external forces have disappeared and its new position gives rise to both electrical and mechanical problems on the transmission line. The work described here involved the design and development of a damper and spacer for a quad conductor bundle. The proposed products are an important item of overhead line hardware and are extensively used to ensure that bundled conductors to provide reliable mechanical and electrical performance in service.

ACKNOWLEDGMENT

Author would like to thank Dr. Subba Reddy B., Senior Scientific Officer at IISc Banglore, High

Voltage Laboratory (Dept. of EE) and Mr. A. K. Pal, SGM at Supreme & Co. Pvt. Ltd. for their coordination in testing of the proposed spacer damper and rigid spacer.

REFERENCES

- [1] K. Anderson and P.Hagedorn, "On the energy dissipation in spacer dampers in bundled conductors of overhead transmission lines," *Journal of sound and vibration*, vol. 180, no. 4, pp. 539-556, 1995.
- [2] P.W.Davall, M.M. Gupta and P.R.Ukrainetz, "Mathematical analysis of transmission line vibration data," *Electric Power Systems Research*, vol. 1, no. 4, pp.269-282, 1978.
- [3] S.Sathikh, and R.T. Chari, "Acceptance curve-A practical means for EHV transmission line damper performance evaluation," *Electric Power Systems Research*, vol. 4, no. 1, pp. 67-78, 1981.
- [4] A.Jamaleddine, and J.Rousselet, "Generalized stiffnesses of spacer-dampers for two-conductor bundles," *Electric Power Systems Research*, vol. 10, no. 2, pp. 125-135, 1986.
- [5] L.E.Kollár, and M.Farzaneh, "Modeling the dynamic effects of ice shedding on spacer dampers," Cold Regions Science and Technology, vol. 57, no. 2-3, pp. 91-98, 2009.
- [6] F.Foti, and L.Martinelli, "A unified analytical model for the self-damping of stranded cables under aeolian vibrations," *Journal of Wind Engineering and Industrial Aerodynamics*, vol. 176, pp. 225-238, 2018.
- [7] R.Claren, G. Diana, F.Giordana, and E. Massa, "The vibrations of transmission line conductor bundles," IEEE Transactions on Power Apparatus and Systems, no. 4, pp.1796-1814, 1971.
- [8] D.Hearnshaw, "Spacer Damper Performance-A Function of In-Span Positioning," *IEEE Transactions on Power Apparatus* and Systems, no. 5, pp. 1298-1309, 1974.
- [9] L.E.Kollár, and M.Farzaneh, "Vibration of bundled conductors following ice shedding," *IEEE Transactions on Power Delivery*, vol. 23, no. 2, pp. 1097-1104, 2008.
- [10] C.G.Books, Modelling of Vibrations of Overhead Line Conductors, Springer, 2018.
- [11] G. ed.Diana, Modelling of Vibrations of Overhead Line Conductors: Assessment of the Technology, Springer, 2018.
- [12] M.D.Rowbottom, and J.G.Allnutt, "Mechanical dampers for the contiol of full span galloping oscillations," In *IEE Proceedings C (Generation, Transmission and Distribution)*, vol. 129, no. 3, pp. 123-135. IET Digital Library, 1982.
- [13] J.F.Adam, J. Bradbury, W.R.Charman, G. Orawski, and M.J.Vanner, "Overhead lines-some aspects of design and construction", In *IEE Proceedings C (Generation, Transmission and Distribution)*, vol. 131, no. 5, pp. 149-187, IET Digital Library, 1984.
- [14] S. Mukherjee, D. Prasad, Md. I. Khan, P.Barua and H.Agarwal, "Hexa Spacer Damper for Vibration Energy Decaying of 765 kV Transmission Line," 2nd International Conference on Innovations in Power and Advanced Computing Technologies, i-PACT-2019.
- [15] Diana, G. and Manenti, A., 2004. State of the art survey on spacers and spacer dampers: part 3-experience with current practice. In CIGRE Working Group 11 Task Force 5 of Study Committee B2 (pp. 1-8).
- [16] Phillips, A., 2008. Future Inspection of Overhead Transmission Lines. Electric Power Research Institute: Palo Alto, CA, USA.

[17] Belu, R. and Koracin, D., 2013. Statistical and spectral analysis of wind characteristics relevant to wind energy assessment using tower measurements in complex terrain. *Journal of Wind Energy*, 2013.

Pulmonary Nodule Segmentation using Adaptive Thresholding

Mainak Biswas¹, Debasis Maji², Souvik Maiti³, Gautam Sarkar⁴, Ashis Kumar Dhara⁵, Goutam Kumar Ghorai⁶, Sandip Sadhukhan⁷, Debprasad Sinha⁸

¹Department of Electrical Engineering, Techno International New Town, Kolkata-700156

² Department of Electrical Engineering, Haldia Institute of Technology, Haldia-721657

³Department of Electronics and Instrumentation Engineering, Bundelkhand University, Jhansi-284128

^{1,2,3,4,6,7,8}Department of Electrical Engineering, Jadavpur University, Kolkata-700032

⁵Department of Electrical Engineering, National Institute of Technology, Durgapur-713209

{Corresponding author's email: mainakbiswas041@gmail.com}

Abstract - Accurate segmentation is only measurable parameter for any computer-aided diagnosis system of lung nodules. All possible types of pulmonary nodules can be segmented using adaptive thresholding algorithm. The illumination as well as the intensity variation of the background of lung nodules are varying for the different angle of captured CT images. This method is novel by considering the stagnating the illumination variation. The presence of the external attachments is not checked like other benchmark processes, thus making it faster. This robust framework shows impressive results when implemented on Lung Image Database Consortium and Image Database Resource Initiative, a readily available database containing 891 pulmonary lung nodules within it. Performances in terms of Sensitivity, Specificity and Accuracy are reported as the experimental results. The empirical results achieved by using this proposed method for in terms of Sensitivity, Specificity and Accuracy are 0.58, 0.96 and 0.96 respectively.

Keywords- Lung cancer; pulmonary nodule; Adaptive thresholding; Lung Image Database Consortium and Image Database Resource Initiative (LIDC/IDRI).

INTRODUCTION

In the USA, one of the most leading causes of deaths from cancer is due to lung cancer [1], [2]. Pulmonary nodules are the potential manifestation of lung cancer. The only prevention is early detection of these nodules having varying shape. Internal texture of these nodules makes them in three major patterns such as solid, part-solid and then non-solid as shown in Figure 1. It is difficult to identify non-solid nodules as they have a lower density as compared to part solid nodules. Based on external attachment, the nodules are grouped into well circumscribed, juxta-vascular and juxta-pleural as shown in Figure 1. Proper segmentation and prevent boundary leakage problem is the most desirable parts to develop a CAD system. The primary challenge is not only the vascular or pleural attachments but also the variation in the internal texture of the nodules. The illumination as well as the intensity variation of the background of lung nodules vary when the CT images are captured from different angles. The novelty of the method suggested in this paper is in contrary to the other benchmarking processes currently being used, the presence of the external attachments is not checked, here the stagnation of the illumination variation is being checked. The major advantage that this novel segmentation framework enjoys is the stability in case of illumination variation. Furthermore, there is no grouping for solid, non-solid and part-solid nodules in any combination [16]. It also checks for the external attachments [3] exactly like the other reported works do, for which the proposed method gains an edge over the other works. This proposed segmentation results are compared with various aspects of some other renowned and benchmark techniques. The construction of the paper is as follows: "Previous Works on Pulmonary Nodules Segmentation" narrates the related and wellknown works. The entire segmentation structure is considered in "Database and Methods". The segmentation performance analysis based on metrics are illustrated in "Results Evaluation using Performance Metric"; then the result is accomplished in "Result and Discussion" and "Limitation" focuses on limitation. At last, the conclusion is stated in "Conclusion".

PREVIOUS WORK ON PULMONARY NODULE SEGMENTATION Kostis et al. [4] proposed a method to remove the external attachments, i.e., vascular and pleural attachment mainly by using the combination of a disk-type kernel and morphological operation. Selection of kernel size is very exquisite because some lobules are missed due to the decremented size. Reeves et al. [5] used a plane fitting process for removing the external attachments. But the result is reduced due to higher curvature in the region of the mediastinum. Kuhnigh et al. [3] used the convex hull technique as a removal process with an assumption that lung field is mostly curved. The result is good for nodule attached to the chest but bad for attachment with mediastinum. Moltz et al. [6] extended this work using ellipsoid fitting to enclose the nodule. The result is good for the removal of attachments using morphological

operation for both Kuhnigh *et al.* [3] and Moltz *et al.* [6]. Dehmeshki *et al.* implemented the fuzzy-based approach [7] to remove the attachments by using 3D region growing manner and a new seed point was defined. Though the reported result was (84%) accepted, no performance was taken care of based on quantitative. Using local shape analysis process, Diciotti *et al.* [8] segmented nodules from attachments keeping the exact shape of the nodule boundary. But segmentation result was reported only for small nodules, having a diameter less than 10 mm.

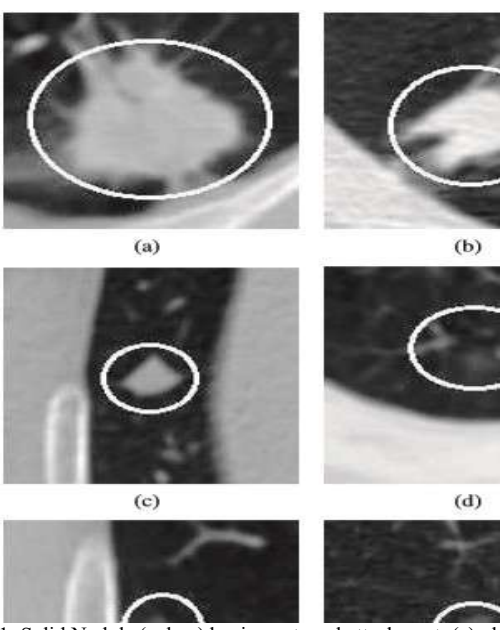


Fig. 1: Solid Nodule (a, b, c) having external attachment: (a) pleural attachment, (b) vascular attachment, (c) well-circumscribed, Non-Solid Nodule (d, e, f) having external attachment: (d) pleural attachment, (e) vascular attachment, (f) well-circumscribed.

Zhou et al. [9] used the eigenvalue analysis technique for a smaller number of non-solid nodules segmentation. But again, no such methods were enough to enhance results. Volumetric overlap was reported 0.68 while Tao et al. [10] used 20 non-solid nodules for segmentation using Probability map. Computational time focused work was reported by Lui et al. [11] for nodule segmentation by using a combination of modified fully convolutional network (FCN) and particle swarm optimization. Dhara et al. [12] ameliorated the result using a framework a framework where the nodules were encircled by ellipsoid fitting and the external attachments were removed by using Moltz et al. [6] and trimming from the end point of the vessel. The volumetric overlap was 0.46 for solid, partsolid and 0.32 in case of non-solid were reported. Mehdi et al. [13] used a small set of a dataset and focused on boundary leakage problem by using a contour-based approach. Kubota et al. [14] reported the volumetric overlap of 0.68 by analyzing the convexity models of the nodules to segment 105 cases.

DATABASE AND METHODS

A. Lung CT Image Database

To make the database more robust and challenging, few companies dealing with medical imaging and some academic centers worked in sync to establish a publicly available CT image database in Armato III *et al.* [15]. This novel proposed method is applied to that database, available in The Cancer Imaging Archive (TCIA), Lung Image Database Consortium and Image Database Resource Initiative (LIDC/IDRI) containing 928 lung nodule cases. Four radiologists levelled 891nodules out of 928 based on their unanimous decision and then combined their results to make it challenge enough.

TABLE I NODULE COUNT IN DATASET

Nodule Type	No. of Nodules
Solid, part-solid	849
Non-solid	42
Total	891

The result is collected in an XML file about the information about the boundary region. According to their marking, the texture index of nodules is classified into three types, i.e., solid, non-solid and part solid for texture index 4 or 5, 1 and 2 or 3 accordingly. Every 12-bit CT image slice of 512 X 512 are having 0.5 to 0.8 mm pixel size in HU. Table 1 shows the number of nodules in the database.

B. Segmentation Framework

Figure 2 depicts the flowchart for segmentation of the nodules. At first, the operator must select a point with a click of the mouse. The nodule is encircled by a cubic VOI having a size of 40mm X 40mm X 40mm. For voxel equalization, isotropic re-sampling is imposed on cropped VOI because voxel may contain anisotropic contents. The rest of the process of segmentation of the nodules according to the method shown in the block diagram.

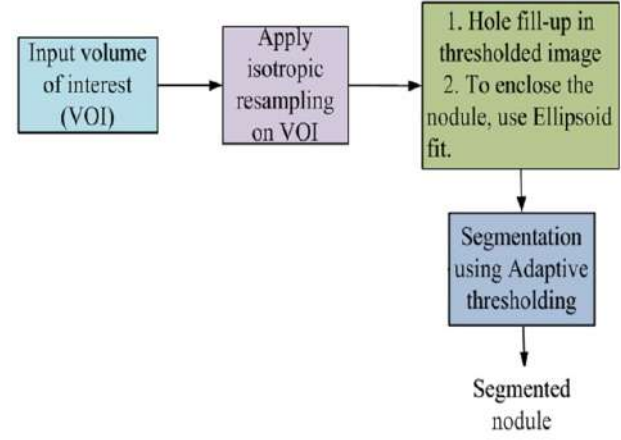


Fig. 2: Proposed segmentation process

C. VOI Preprocessing

After thresholding, connected component analysis is employed followed by the morphological closing operation to fill up the holes being in the nodule as suggested by Dhara *et al.* [12]. To enclose the nodules, the ellipsoid is fitted as described above. In this proposed work, there is no checking, as well as any removal of pleural attachment or blood vessels are required, which makes it novel.

ADAPTIVE THRESHOLDING

When different thresholding values are applied in different regions of an image depending on the intensity value of neighboring pixel, that is termed as adaptive thresholding. To segment the input image, the following steps are used to segment [17], where, *i_img* is the input image, *o_img* is the output image, *wid* is the image width and *hei* is the image height.

Pseudo Code: Adaptive Threshold (i img,o img,wid,hei)

```
for p = 0 to wid do
2..
          total \leftarrow 0
3.
           for q = 0 to hei do
              total \leftarrow total + in_img[p, q]
4.
5.
               if p = 0 then
6.
                  Img[p,\,q] \leftarrow total
8.
                  Img[p, q] \leftarrow Img[p-1, q] + total
9.
               end if
10
          end for
      end for
11.
12.
      for p = 0 to wid do
          for q = 0 to hei do
13.
14.
              x_1 \leftarrow p - u/2
15.
               x_2 \leftarrow p + u/2
16.
              y_1 \leftarrow q -\!u/2
17.
              y_2 \leftarrow q + u/2
               cnt \leftarrow (x_2 - x_1) \times (y_2 - y_1)
18.
19.
              total \leftarrow Img[x_2,y_2] - Img[x_2,y_1-1] - Img[x_1-1,y_2]
       +Img[x_1-1,y_1-1]
20.
               if (in\_img[p, q] \times cnt) \le (total \times (100-t)/100) then
21.
                  out_img[p, q] \leftarrow 0
22.
23.
                  out_img [p, q] \leftarrow 255
24.
               end if
25.
           end for
     end for
```

RESULTS EVALUATION USING PERFORMANCE METRIC

For evaluating the segmentation result, here three region-based metrics (accuracy, sensitivity and specificity) are calculated using the formulation by Byrd *et. al* [18]. For comparing the result, two binary images are required. Here, the segmented mask of the nodules using the robust proposed method is being examined with the provided ground truth, made by four radiologists.

$$Accuracy = \frac{XTP + XTN}{XTP + XTN + XFP + XFN}$$

$$Sensitivity = \frac{XTP}{XTP + XFN}$$

$$Specificity = \frac{XTN}{XTN + XFP}$$

XTP - True positive voxels number

XTN - True negative voxels number

XFP - False positive voxels number

XFN - False negative voxels number

The limit of those metric values lies between [0 to 1], where 1 implies 100% match whereas 0 signifies full mismatch between two objects.

RESULT AND DISCUSSION

A. System Configuration

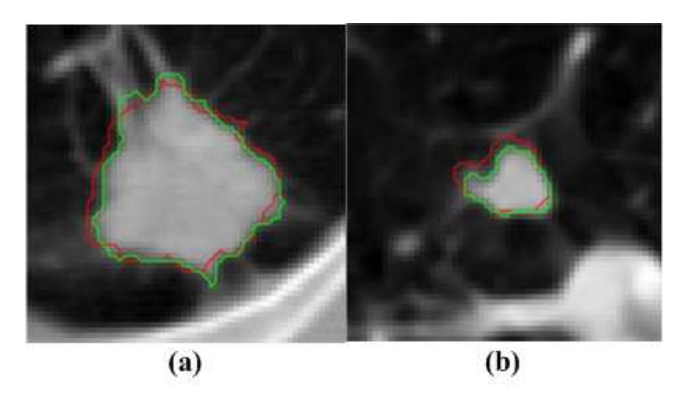
This proposed work is accomplished on MATLAB (version R2013a), using 8 GB RAM, Core i3. However, this job is also done in lower configurations. The time for execution includes image read and metrics calculation. The time varies from 3 seconds to 8 seconds depending upon the size of the image.

TABLE II
PROPOSED SEGMENTATION RESULTS ARE BEING COMPARED WITH
KUBOTA ET AL., KUHNIGK ET AL., AND MOLTZ ET AL.

Comparative	Sensit	ivity	Speci	ficity	Accu	racy
analysis	Solid, part- solid	Non- solid	Solid, part- solid	Non- solid	Solid, part- solid	Non- solid
Kuhnigk et al.	0.39	0.01	1	1	0.99	0.98
Moltz et al.	0.48	0.03	1	1	0.99	0.98
Kubota et al.	0.56	0.4	0.97	0.95	0.97	0.94
Proposed method	0.5	9	0.9	96	0.9	96

B. Result analysis

Figure 3 represents the qualitative result as pictorial form of the segmentation algorithm. Red mark represents the ground truth and green portion represents the segmented output. Figure 3 shows the segmented output using the proposed method.



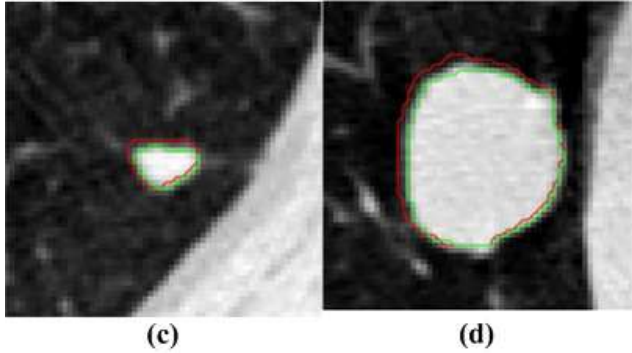


Fig. 3 Segmentation results using proposed scheme for nodule numbers LIDC/IDRI 1, 21, 766 and 791. The segmentation outcome is marked by (—) and ground truth by (—)

C. Discussion

To make the experiment complex and rapid, superficial attachments are not checked and hence not removed. This makes the framework less time consuming. The major challenge is the ground truth (GT), because the marking of nodules by four radiologists are not the same at all. And the final reference mask is created by the union operation of these four distinct results [12]. As can be seen from the Table 2 the proposed method shows improvement regarding the metrics. These results could be even better if the accurate ground truth is available.

LIMITATION

Despite that, the method fails only for few nodules from the database having 891 nodules. The segmentation result could have been better if it is possible to segregate the nodules into small, medium and comparatively large for non-solid and solid/ part solid types. As the internal structure for all the nodules is not same, that's why the selection of metrics to determine the performance is very challenging work.

CONCLUSION

Here, a robust method is proposed to segment all types of pulmonary lung nodules, where the external attachments are not eliminated which is performed in the commonly used ways; that makes it faster. Proper segmentation is done by retaining the accurate boundary information and limiting the boundary leakage issue of the subject duly by using the level set algorithm that depicts in the result. This novel experiment is being applied on 891 CT images and shows that, this framework is highly effective. This method is tested on three types of lung nodules; in each case the result is very appreciable. The segmented outcomes have been appraised in terms of metrics (Accuracy, Sensitivity and Specificity) and these achieve a score of approximately 0.96, 0.58 and 0.96 respectively. The engrossing achievement of the model emerges that the framework is fully efficient of propagating excellent developments even in large variation among the four radiologists for creating the ground truth as stated by Dhara et al. [12]. But in case of mean distance metric calculation, there still a scope of further upliftment. However, this result could be good enough, if the image database contains more images and precise ground truth.

REFERENCE

- [1] American Cancer Society: Cancer facts & figures. The Society 2008.
- [2] R. Siegel, D. Naishadham, A. Jemal, "Cancer statistics 2013". CA: A Cancer Journal for Clinicians, vol. 63, no. 1, pp. 11–30, 2013.
- [3] J. M. Kuhnigk, V. Dicken, L. Bornemann, A. Bakai, D. Wormanns, S. Krass, H. O. Peitgen, "Morphological segmentation and partial volume analysis for volumetry of solid pulmonary lesions in thoracic CT scans", *IEEE Transactions on Medical Imaging*, vol. 25, no. 4, pp. 417–434, 2006.
- [4] W. J. Kostis, A. P. Reeves, D. F. Yankelevitz, C. I. Henschke, "Three-dimensional segmentation and growth-rate estimation of small pulmonary nodules in helical CT images", *IEEE Transactions* on *Medical Imaging*, vol. 22, no. 10, pp. 1259–1274, 2003.
- [5] A. P. Reeves, A.B. Chan, D. F. Yankelevitz, C. I. Henschke, B. Kressler, W. J. Kostis, "On measuring the change in size of pulmonary nodules", *IEEE Transactions on Medical Imaging*, vol. 25, no. 4, pp. 435–450, 2006.
- [6] J. H. Moltz, J. M. Kuhnigk, L. Bornemann, H. Peitgen, "Segmentation of juxtapleural lung nodules in CT scan based on ellipsoid approximation" First International Workshop on Pulmonary Image Processing, 2008.
- [7] J. Dehmeshki, H. Amin, M. Valdivieso, X. Ye, "Segmentation of pulmonary nodules in thoracic CT scans: A region growing approach", *IEEE Transactions on Medical Imaging*, vol. 27, no. 4, pp. 467–480, 2008.
- [8] S. Diciotti, S. Lombardo, M. Falchini, G. Picozzi, M. Mascalchi, "Automated segmentation refinement of small lung nodules in CT scans by local shape analysis", *IEEE Transactions on Biomedical Engineering*, vol. 58, no. 12, pp. 3418–3428, 2011.
- [9] J. Zhou, S. Chang, D. N. Metaxas, B. Zhao, M. S. Ginsberg, L. H. Schwartz, "An automatic method for ground glass opacity nodule detection and segmentation from CT studies", *Engineering in Medicine and Biology Society*, EMBS'06, pp. 3062–3065, 2006.
- [10] Y. Tao, L. Lu, M. Dewan, A. Y. Chen, J. Corso, J. Xuan, M. Salganicoff, A. Krishnan, "Multi-level ground glass nodule detection and segmentation in CT lung images", *Medical Image Computing and Computer-Assisted Intervention*—MICCAI 2009, pp. 715–723. Springer, 2009.
- [11] H. Liu, F. Geng, Q. Guo, C. Zhang, C. Zhang, "A fast weak-supervised pulmonary nodule segmentation method based on modified self-adaptive FCM algorithm", Soft Computing, pp. 1–13, 2017
- [12] A. K. Dhara, S. Mukhopadhyay, R. Das Gupta, M. Garg, N. Khandelwal, "A Segmentation Framework of Pulmonary Nodules in Lung CT Images", *Journal of Digital Imaging*, vol. 29, no. 1, pp. 148–148, 2015.
- [13] A. Mehdi, N. Beig, M. Orooji, P. R. V. Velcheti, S. Rakshit, N. Reddy, "An integrated segmentation and shape-based classification

- scheme for distinguishing adenocarcinomas from granulomas on lung CT", *Medical physics*, vol. 44, no. 7, pp. 3556-3569, 2017.
- [14] T. Kubota, A. K. Jerebko, M. Dewan, M. Salganicoff, A. Krishnan, "Segmentation of pulmonary nodules of various densities with morphological approaches and convexity models", *Medical Image Analysis*, vol. 15, no. 1, pp. 133–154, 2011.
- [15] S. G. Armato III, G. McLennan, L. Bidaut, M. F. McNitt-Gray, C. R. Meyer, A. P. Reeves, B. Zhao, D. R. Aberle, C. I. Henschke, E. A. Hoffman, E. A. Kazerooni, H. MacMahon, E. J. R. Beek, D. Yankelevitz, A. M. Biancardi, P. H. Bland, M. S. Brown, R. M. Engelmann, G. E. Laderach, D. Max, R. C. Pais, D. P. Y. Qing, R. Y. Roberts, A. R. Smith, A. Starkey, P. Batra, P. Caligiuri, A. Farooqi, G. W. Gladish, C. M. Jude, R. F. Munden, I. Petkovska, L. E. Quint, L. H. Schwartz, B. Sundaram, L. E. Dodd, C. Fenimore, D. Gur, N. Petrick, J. Freymann, J. Kirby, B. Hughes, A. V. Casteele, S. Gupte, M. Sallam, M. D. Heath, M. H. Kuhn, E. Dharaiya, R. Burns, D. S. Fryd, M. Salganicoff, V. Anand, U. Shreter, S. Vastagh, B. Y. Croft, L. P. Clarke, "The lung image database consortium (LIDC) and image database resource initiative (IDRI): a completed reference database of lung nodules on CT scans", Medical physics, vol. 38, no. 2, pp. 915–931, 2011.
- [16] M. Biswas, D. Maji, A. K. Dhara, G. Sarkar, "Segmentation of Pulmonary Nodules Based on Modified Framework Using Hybrid Level-Set", *IEEE 16th International Symposium on Biomedical Imaging* (ISBI 2019), April 8-11, 2019, Venice, Italy, 2019.
- [17] D. Bradley, G. Roth, "Adaptive thresholding using the integral image", *Journal of graphics tools*, vol. 12, no. 2, pp. 13-21, 2007.
- [18] A. K. Byrd, Z. Jianchao, C. Mohamed, "A validation model for segmentation algorithms of digital mammography images", *Journal* of Applied Science & Engineering Technology, vol. 1, 2007.

Automatic Patch Based Tortuous Retinal Vessel Classification using VGG-16 Network

Debasis Maji¹, Souvik Maiti², Mainak Biswas³, Goutam Kumar Ghorai⁴, Sandip Sadhukhan⁵, Debprasad Sinha⁶, Ashis Kumar Dhara⁷, Gautam Sarkar⁸

¹Department of Electrical Engineering, Haldia Institute of Technology, Haldia-721657

²Department of Electronics and Instrumentation Engineering, Bundelkhand University, Jhansi-284128

³Department of Electrical Engineering, Techno International New Town, Kolkata-700156

⁴Department of Electrical Engineering, Ghani Khan ChoudhuryInstitute of Engineering & Technology,Maliha, West Bengal 732102,

^{5, 6, 8}Department of Electrical Engineering, Jadavpur University, Kolkata-700032

⁷National Institute of Technology, Durgapur-713209

Corresponding author's email: debasis.maji39@gmail.com

Abstract - A large proportion of children and neonates throughout the world are suffering from Retinopathy, an optical disease that affects much adversely to people who have diabetes for long time. If undiagnosed and not treated in early stage, it can lead to blindness. Early and fast detection using automated system will be of great help in this domain. The proposed work is aimed to develop an automatic computer-aided diagnosis system to solve the above stated difficulty with less computational complexity and with high precision. In this work an automatic grading method using patch based VGG16 model is presented. The novelty of this technique lies in term of oppressive amends of neural networks to 16 weight layers, which is deeper than previous works on gradation of vessel tortuosity. To minimize the parameters in deep networks, filters of size 3x3 are considered in each convolution. The outcome of this proposed model parades its prosperity in respect of accurate gradation of tortuous retinal blood vessels with an accuracy of 78% and a precision score of 0.73.

Keywords - Blood vessels, Diabetic retinopathy, Deep learning.

Introduction

The major cause of damage of blood vessels in the retina is prolonged diabetes. Early diagnosis is the only the way to prevent retinopathic diseases. This is a dangerous malady, which not only affect the human eyes but also damages other organs silently. In the developed country the main cause of blindness is Diabetic Retinopathy (DR) [7]. The initial sign of this include the increase in the thickness of the vessels and twisting of the vessels termed as tortuosity [8]. As the vessels are so gaunt by nature, the chance of internal bleeding may occur [15]. So it is very essential to measure the curvature of the vessels. Lotmar [14] proposed a method based on Chord and Arc Length. This method is widely used in [3], [10]. However due to the disadvantage of the measurement of proper curvature [5], [8] rectified some parameters that is having same convexity; the vessels

are grouped together with a weighted summation. Curvature based approach was introduced by Hart et al.[9]. To measure tortuosity, the integration is opted over squared curvature derivative in [17].



Fig. 1: Sample images of tortuosity vessel patch.

The classification divides an eye in several zones [10] and the severity of the disease is analyzed based on three parameters: (i) the position of the zone where new vessels are located, (ii) how much area of the vessel patches is involved and (iii) how many small vessels are associated with the blood vessels. There also exist another fourth parameter that is the presence of 'plus disease' which is associated with ROP and is characterized by an increase in width and tortuosity of the retinal vessels. An overview of the methods used in retinal vessel tortuosity calculation is analyzed in [11]. Chain Coding technique has been used for analyzing the tortuosity in [4]. To quantify ROP, change in width and tortuosity of blood vessel is analyzed in [10]. In another work quadratic polynomial decomposition method has been used for tortuosity analysis [6]. Machine learning technique, has been adapted for measuring tortuosity exploring thickness dependent and curvature based improved chain code in [2], [16], [19]. Morphological approaches have been considered where vessel partition has been carried out, followed by method for measuring tortuosity [12]. A possibility of providing some automatic assistance in this screening process lies in accurate computation of vessel width and tortuosity near the optic disc, which is present in the retina patches. These vessels can be easily visualized and hence analyzing this region can be done efficiently during the screening test. A sample image of tortuosity vessel patch has shown in fig.1.

A. Proposed Method

The fundus images are resized and enhanced by gamma correction. The resizing step is necessary because of the variety of sizes of the images in the EIARG1 database. All the images are resized to 244x244 pixels. The trained VGG-16 network is then fine-tuned with the images from EIARG1 dataset [1]. To introduce the robustness of this process, geometry based augmentation is performed on 70 percent of EIARG1 dataset Patch images and then fed those images into the network. We have trained our network using the images from EIARG1 dataset and then tested on 30 percent of same database patch images. VGG-16 model has been used to fine tune the pre-trained network with 120 images using different epoch values. The proposed patch based retinal blood vessel grading algorithm using VGG-16 model shown in fig.2 outperforms both for low contrast as well as high contrast images.

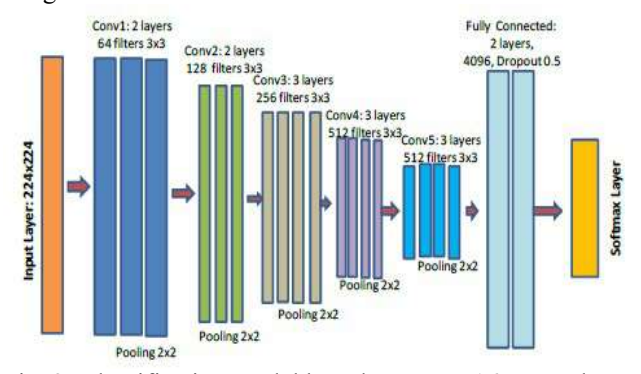


Fig. 2: Classification model based on VGG-16 network.

The model is a reformed version of VGG network. The VGG-16 net is used as a base network because the 32x32 input would not die out through the VGG's architecture and the VGG architecture is very straight forward for analyzing the results easily. Moreover, VGG net is one of the most dominant deep convolutional neural networks.

This VGG-16 based deep model is much more robust than a 4-layer CNN even in the task of classifying patch based fundus image. The model involves of five groups of convolution layers and one group of fully-connected layer, along with thirteen convolution layers and two fully-connected layers. Every convolution filter has a kernel size

of 3x3 with stride of 1 and pooling region of 2x2 without overlap [13].

The objective behind designing the proposed model is to have a network that will automatically learn valuable features essential for grading blood vessel. In the initial stage, pre-processing is employed to facilitate the learning procedure while preserving the original image information. The patched images in the training set have a height to width ratio of 3:4. Colour images are fed as an input to the VGG-16 model and each channel is then rescaled.

B. Results and Discussions

The proposed blood vessel grading framework is evaluated on 120 images from EIARG1 database [1]. Fig.3 focuses on some of diabetic affected blood vessels which are difficult to classify. Sample images of vessel patches which are used to train the neural network for learning the features of the wide and tortuous vessels that correlate with plus-disease are shown in fig.4.

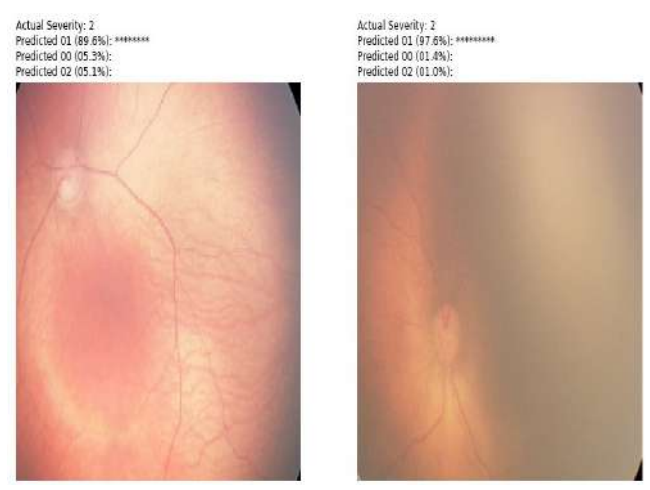


Fig. 3: Focus on diabetic affected vessels

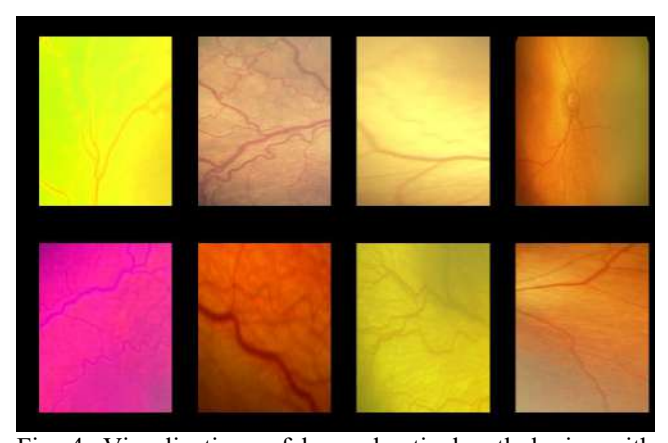


Fig. 4: Visualizations of learned retinal pathologies with the projected pre-GAP activation layer superimposed.

Table 1: Observation Table

Test	Precision	Recall	F1-	Accuracy	Time
Image			Score		(sec)
Count					
30	0.73	0.72	0.77	78%	12
42	0.65	0.67	0.66	67%	25
48	0.48	0.42	0.40	42%	37
78	0.65	0.57	0.54	57%	83

The prediction efficiency of the proposed algorithm in grading tortuous vessels is visualised from the confusion matrix shown in Fig. 5. The proposed method has achieved 78% accuracy and a precision score of 0.73 in grading the retinal blood vessel on EIARG1 database [1] in 12 seconds as shown in Table 1.

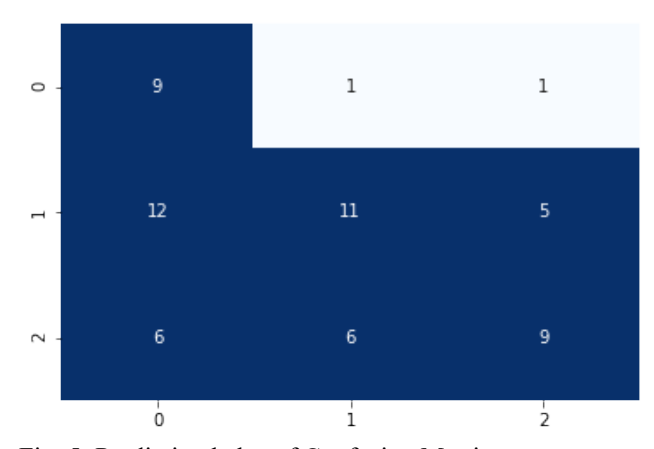


Fig. 5: Prediction helps of Confusion Matrix.

The observed accuracies in the figure-6 where higher then the accuracies observed in the data, because most of the fundus images where of tested images without any changes related to traning data. However, doing so did not raise accuracy but only reduce over fitting. The VGG-16 net is trained for 35 epochs with batch size of 1. Weighted spatial cross entropy is being used to minimise the training and testing loss. The losses while training and testing at various values of epoch are shown in fig. 6. Adam optimization [13] and softmax are used for the classification. The F1 score was changes for all test image count. To increase the precision and recall value, a trained ophthalmologist can identify classified images. Table 2 displays that the Spearman's rank correlation coefficient (SRCC) score of the proposed work outperforms that of the existing works.

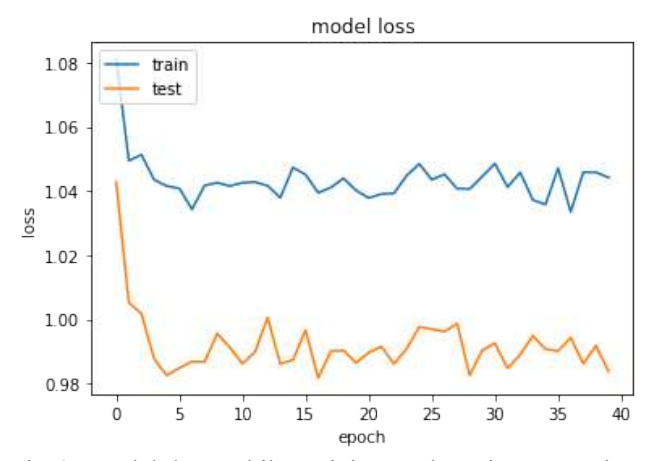


Fig.6: Model loss while training and testing at various epoch values.

Table 2: Comparative study of correlation score with existing works

Publication	SRCC Score
Aghamohamadian-Sharbaf	0.71
et al., 2016	
Narasimhan and	0.66
Vijayarekha, 2015	
Proposed work	0.72

C. Working Dataset

The EIARG1 database [1] has been provided by the Eye Images Analysis Research Group for image based studies on retinal blood vessel tortuosity in diabetic retinopathy. The database is publicly available in www.eiarg.um.ac.ir for tortuosity of ROP images.

D. Conclusion

In the proposed fully automatic based VGG-16 network for patch based retinal blood vessel grading on fundus images several effective training strategies are implemented to tackle the challenges that the network may face when limited training data is available. This model can be refined further to yield more classification accuracy by accepting certain correction technique for the few misclassified images shown by the confusion matrix in Fig. 5. The approach outperforms the state-of-the art methods while evaluating on open challenge database for fundus image classification.

REFERENCES

- [1] M. A. -Sharbaf, H.R.Pourreza, and T. Banaee, "A novel curvature-based algorithm for automatic grading of retinal blood vessel tortuosity," *IEEE journal of biomedical and health informatics*, vol. 20, no. 2, pp. 586-595, 2016.
- [2] H.Azegrouz, E.Trucco, B.Dhillon, T.MacGillivray, and I. J. MacCormick, "Thickness dependent tortuosity estimation for retinal blood vessels," In Engineering in Medicine and Biology Society, 28th Annual International Conference of the IEEE, pp. 4675-4678, 2006.

- [3] P. B. -Aguirre, M. E. Craig, M.B.Sasongko, A. J. Jenkins, T. Y. Wong, J. J. Wang, N. Cheung, and K. C.Donaghue, "Retinal vascular geometry predicts incident retinopathy in young people with type 1 diabetes: a prospective cohort study from adolescence," *Diabetes Care*, p. 102419, 2011.
- [4] E.Bribiesca, "A measure of tortuosity based on chain coding," *Pattern recognition*, vol. 46, no. 3, pp. 716-724,2013.
- [5] E. Bullitt, G.Gerig, S.M.Pizer, W. Lin, and S. R.Aylward, "Measuring tortuosity of the intracerebral vasculature from mraimages," *IEEE transactions on medical imaging*, vol. 22, no. 9, pp. 1163-1171, 2003.
- [6] A.Chakravarty and J.Sivaswamy, "A novel approach for quantification of retinal vessel tortuosity using quadratic polynomial decomposition," Medical Informatics and Telemedicine, [Indian Conference IEEE], pp. 7-12, 2013.
- [7] D. S. Fong, L. Aiello, T. W. Gardner, G. L. King, G. Blankenship, J.D.Cavallerano, F. L. Ferris, and R.Klein, "Retinopathy in diabetes," *Diabetes care*, vol. 27(1) pp. s84-s87, 2004.
- [8] E.Grisan, M.Foracchia, A. Ruggeri, et al, "A novel method for the automatic grading of retinal vessel tortuosity," *IEEE Transactions on Medical Imaging*, vol. 27, no. 3, pp. 310-19, 2008.
- [9] W. E. Hart, M.Goldbaum, B. Cote, P.Kube, and M. R. Nelson, "Measurement and classification of retinal vascular tortuosity," *International journal of medical informatics*, vol. 53(2-3), pp. 239-252, 1999.
- [10] C.Heneghan, J. Flynn, M. O. Keefe, and M.Cahill, "Characterization of changes in blood vessel width and tortuosity in retinopathy of prematurity using image analysis", Medical image analysis, vol. 6, no. 4, pp. 407-429, 2002.
- [11] A.A.Kalitzeos, G. Y. H. Lip, and R.Heitmar. "Retinal vessel tortuosity measures and their applications." *Experimental eye research*, vol. 106, pp. 40-46, 2013.
- [12] Sk. Latib, M. Mukherjee, D.K. Kole, and C. Giri, "Automatic tortuosity detection and measurement of retinal blood vessel network," *Advanced Computing, Networking and Informatics, Springer*, vol. 1, pp. 483-492, 2014.
- [13] S. Liu and W.Deng, "Very deep convolutional neural network based image classification using small training sample size", 3rd IAPR Asian conference on pattern recognition, IEEE, pp. 730-734, 2015.
- [14] W. Lotmar, A. Freiburghaus, and D. Bracher, "Measurement of vessel tortuosity on fundus photographs," Albrecht von Graefes Archiv fur klinische and experimental Ophthalmology, vol. 211, no. 1, pp. 49-57, 1979
- [15] M.Mizutani, T. S. Kern, and M.Lorenzi, "Accelerated death of retinal microvascular cells in human and experimental diabetic retinopathy," *The Journal of clinical investigation*, vol. 97, no. 12, pp. 2883-2890, 1996.
- [16] D.Onkaew, R.Turior, B.Uyyanonvara, N.Akinori, and C.Sinthanayothin, "Automatic retinal vessel tortuosity measurement using curvature of improved chain code," In Electrical, Control and Computer Engineering (INECCE), [International ConferenceIEEE], pp. 183-186, 2011.
- [17] M. Patasius, V. Marozas, A. Lukosevicius, and D. Jegelevicius, "Evaluation of tortuosity of eye blood vessels using the integral of square of derivative of curvature," *EMBEC*, vol. 5, pp. 20-25, 2005.
- [18]M. B.Sasongko, T. Y. Wong, T. T. Nguyen, C. Y. Cheung, J. E. Shaw, and J. J. Wang, "Retinal vascular tortuosity in persons with diabetes and diabetic retinopathy," *Diabetologia*, vol. 54, no. 9, pp. 2409-2416,2011.
- [19] R. Turior, P. Chutinantvarodom, and B. Uyyanonvara, "Automatic tortuosity classification using machine learning approach," Applied Mechanics and Materials, vol. 241, pp. 3143-3147, 2013.

Optimum Energy Mix Planning for Power Generation considering Cost and Environmental Impact

Maneesha Naresh, Shashwati Ray, and Anirban Guha
Department of Electrical Engineering
MATS University
Raipur (C.G.)India
Email:maneeshanaresh@gmail.com

Abstract - Towards its commitment to climate change Government of India (GOI), being a part of Nationally Determined Contributions (NDC) has taken up an ambitious program of renewable energy sources to increase its capacity to 40% by the year 2030 without considering its implications on the overall power system. The installed capacity for base load intends to serve primarily the demand based on the minimum load requirements. This paper focuses mainly on computing the optimum installed capacity of based load power plants considering the average hourly demand over the months of the year and the cost of generation of each of the sources of base load power plants. To compute the optimum installed capacity of base load power plants, based on the past trends, lowest out of average of the average hourly demand has been considered . The approximate costs of generation of each of sources used for base load, i.e. coal, gas and hydro are calculated based on data taken from the Central Electricity Regulatory Commission regulations. The proposed methodology for installed capacity has been implemented on the average demand chart of state of Maharashtra, India for the year 2018. The energy mix for base load is suggested based on the installed capacity and the cost factor. This mitigates the environmental impact to a reasonable extent and simultaneously makes these plants operate at their optimal levels with increased plant load factor and reduced energy losses thus reducing the overall cost of generation.

Keywords: Base load, Optimization, Environmental impact, Emissions, Minimum and Average demand.

I. INTRODUCTION

India is the third largest producer of coal, therefore, coal will remain the preferred fuel for power generationin future. India is taking signicant step towards adopting clean energy. Government of India (GOI) hastaken various policy initiatives to give exibility to thermal generating companies to reduce the overall cost of generation and emissions [1].

Government of India has also taken up an ambitious programme of renewable energy sources without considering its implications on the overall system [2]. For example, solar power station covers most of the day load as a must run power station. The solar generation would be maximum during day time when the system demand is quite low and almost nil when system demand is maximum. As a result, the plant load factors of coal red power stations reduce signicantly and they run with enhanced station heat rate and auxiliary oil consumptions. In this way, the whole power system runs very inefficiently affecting the environment and hence, the overall cost of generation. This necessitates the

thermal power stations to run at its optimal capacity with maximum efficiency as base load stations resulting in less pollution and hence cost effective. The base load power is mainly contributed by three sources, viz., coal, gas and hydro. Of these coal has the largest share followed by hydro and gas respectively.

Coal is the most pollutant fuel out of all sources of generation but each source has its own characteristics. The advancement in new technologies has made coal fired power plants increase the overall cost of the power generation which in turn neutralise the effect of the advantages, therefore, the choice has to be made among other technologies like hydro and gas power stations for meeting the base load demand. Generation cost, the cost of emission, social cost and their characteristics should be the criteria for the optimization of these kind of energy mix for base load.

Hydropower has the inherent ability for instantaneous starting, stopping and managing load variability Hydro power critical role in sustainable development and energy security for the country is based on the elements of sustainability, availability and affordability. Typically, hydro projects have high capital costs, long gestation projects and highly vulnerable to many uncertainties for example, land acquisition issues, environment and forest, rehabilitation and resettlement issues, law and order, technical challenges, natural calamities.

Natural gas has emerged as the most preferred fuel due to its inherent environmentally benign nature, easy transportability, ease of use, greater efficiency and cost effectiveness. It is one of the cleanest fuels with less carbon emissions and pollutants. Gas based power plants require significantly less land and water as compared to coal based power plants of same capacity, have advantage of quick ramping up and can support the renewable balancing power requirements. Due to acute shortage of domestic gas and higher price of imported natural gas, gas based plantsare not in a position to run their plants efficiently. Very low PLF (23%) and are lying idle due to non-availability of domestic natural gas [3]. Therefore, the aim is to calculate the optimum installed capacity of the base load plants depending upon the average minimum demand based on past trends keeping in view the variation of demand with the changing seasons and the cost of generation of each sources using Central Electricity Regulatory Commission (CERC) regulations [4] and Maharashtra Electricity Regulatory Commission (MERC) Regulations [5]. For this, hourly demand load data for that particular year is required to be taken from load dispatch centre (LDC) of the state.

The idea to nd the optimum base load installed capacity is relatively new; and not many studies have been carried out so far. Studies are mainly on the combined energy mix optimization of base load and non-base load. For instance, Gruenwald and Oprea in [6] proposed an energy mix to minimize the cost of electricity generation and GHG emissions. They developed the methodology to determine the optimalenergy mix. According to [7], clean coal technology reduces the emissions and the environmental impact of coal based power plants, where the author has stated that coal will still remain the major source of electricity generation in the coming years The generation costs vary depending upon factors like location type and source of fuel. With hydro having capacity constraints due to long lead time of construction and gas limited in its domestic supply, coal therefore by far has the largest share. While coal is abundant in its supply but has wide variation in terms of calorific value depending upon the source of supply. Similarly, hydro is not available when needed most i.e. during the time of lean months. Gas forms a very small portion and India depends on imports.

Since the objective is to minimize the cost of generation keeping environment in view, the base load capacity therefore has to be optimized first to arrive at the minimum base load installed capacity. This would ensure that the most environmentally harmful of fuels i.e. coal will be used only to the minimum extent to support the just minimum base load capacity that too in mix with other sources like hydro and gas depending on their availability. In addition, it has also to be ensured that the coal based generation is achieved at a PLF which keeps generation at its efficient best.

In this paper with the help of the average hourly demand chart for a year, we have designed an algorithm for base load power stations to optimally meet the base load demand of that year. Having found the installed capacity of base load station, we calculate the generation cost of each of coal [8], gas and hydro power [9] plants. The paper is organised as: in section 2 we give the necessary background to understand the problem, in section 3 we give the complete formulation and the algorithm of our proposed method. In section 5 we implement our methodology on the data of Maharashtra state for the year 2018 followed by the conclusions.

II. BACKGROUND

Base load power sources are the plants that operate all day continuously to meet the minimum level of power demand 24x7. The base load power plants typically are mainly thermal i.e.coal base and gas base plants due to their low-cost fuels and steady state power generations. Hydropower and geothermal power can also be used for base load electricity generation if these resources are regionally available. But problem lies in the fact that this minimum demand of a day varies widely depending on the seasons.

Thus, if the lowest of the daily minimum demand is targeted as to be the installed capacity meant for base load operation, i.e., thermal/coal fired power station, but prediction of accurate demand however is not possible on account of huge uncertainties due to continuous change in climate pattern and also uncertainty in economy. While planning is being done for future years, the demand will increase with time, because in real time over the years this is the normal trend on annual basis computation, while exception being some isolated events when it may decrease.

The cost of each of the generating sources of base load plants will serve the purpose of proper energy mix for base load along with their characteristics.

III. PROPOSED METHODOLOGY FOR CALCULATING BASE LOAD CAPACITY

With the above background, while targeting to meet the base load demand through thermal power stations, we have to keep in mind the following uncertainties:

- The increase in lowest demand of a year from previous year may not follow the normal prediction and may change either way due to variation in climate/weather/season or economic recession/ acceleration or combination of both factors.
- The projected capacity addition in supply side may slip.
- Unforeseen shut-down of generators.

In view of the above fact while planning/designing the installed capacities, it would not be prudent to target precisely the lowest demand. Using the load variation capacity of coal fired power station within a band of reasonable heat rate (boiler), the targeted base load demand will also cover band of demand that represents in general the lean-demand period. Thus, while planning for the targeted demand, we would consider the lowest out of average of the average hourly demands over the months of the year to cover different statistically arrived data on the lower demand side as given below:

A. Formulation

Let the average hourly demands over the months of a year be represented by a $n \times m$ matrix P_a where, the number of hours, n=24 and the number of months, m=12. Then the elements of the matrix are $P_a(i,j)$, with i=1,...,n and j=1,...,m. Let the highest and average of the average hourly demand over the every hour respectively be $P_{max}(i)$ and $P_{avg}(i)$ with i=1,...,n. Then

$$P_{max}(i) = \max\{P_a(i, 1:m)\}, i = 1, ..., n$$
 (1)

$$P_{avg}(i) = \frac{1}{m} \sum P_a(i, 1:m), i = 1, ..., n$$
 (2)

Let the lowest out of average of the average hourly demands over the months of the year be P_{Lavg} and maximum out of highest of average hourly demand over the months of the year (P_{max}) be P_{Hmax} . Then,

$$P_{Lavg} = \min\{P_{avg}(1:n)\} \tag{3}$$

$$P_{Hmax} = \max\{P_{max}(1:n)\} \tag{4}$$

Hence, we can state that base load (BL) demand is mathematically represented by (3). Against the targeted demand data, required installed capacity is computed considering 85% availability factor. Moreover, the range of demand variations without oil support to have a reasonable heat rate is also considered. Therefore, the installed capacities for the BL is

$$P_{inst-BL} = P_{Lavg}/0.85 \tag{5}$$

To find out the capacity of peaking power station, the installed capacities is

$$P_{peak} = (P_{Hmax} - P_{Lavg})/0.85 \tag{6}$$

If 5% additional demand is considered as the spinning reserve P_{res} , then

$$P_{res} = .05 P_{Hmax}$$

and the installed capacity of spinning reserve $P_{inst-res}$ is

$$P_{inst-res} = P_{res}/0.85 \tag{7}$$

Therefore, the total installed capacity P_{total} required for meeting the total demand is

$$P_{total} = (P_{Hmax} + P_{res})/0.85 \tag{8}$$

IV. PROPOSED METHODOLOGY FOR ESTIMATION OF APPROXIMATE COST OF COAL, GAS AND HYDRO POWER PLANTS

The computation of tariff of electricity from thermal and gas power generating stations comprise of:

- 1) Annual fixed charge,
- 2) Energy charge, which is a variable cost.

The annual fixed charge comprises of the following components:

- (a) Operation and maintenance expenses
- (b) Depreciation
- (c) Interest on loan capital
- (d) Interest on working capital
- (e) Return on equity capital

The computation of tariff of electricity from hydro power generating stations comprises of:

- 1) Capacity charge which is a fixed cost
- 2) Energy charge which is a variable cost

A. Calculation of annual Fixed cost for coal, gas based and hydro power generating stations

Let, CP be the capacity of plant in MW and CC be the capital cost. Then, as per annexure 11.1 of Central Electricity Authority, National Electricity Plan [3]

 $CP = 7.03 \times CC$ coal based power generating station

 $=4.56 \times CC$ gas based power generating stati(h1)

 $= 10.8 \times CC$ hydro power generating station (11)

As per MERC Regulations 27, debt equity ratio is 70:30 of CC. Taking equity as EQ and debt as DB, then as per

MERC Regulations 29 and 30 respectively return on equity RE and interest on loan IL are,

$$RE = 15.5\% \times EQ \tag{12}$$

$$IL = 9.45\% \times DB \tag{13}$$

Taking IWC as the interest on working capital, then as per MERC Regulations 32

$$IWC = 9.83\% \times 10\% \times CC \tag{14}$$

With DR as depreciation rate, as per MERC Regulations 28

$$DR = 5.28\% \times CC \tag{15}$$

According to MERC Regulations 47.2, the operation and maintenance cost OMC are fixed at 14.99 lac/MW/Year, 15.63 lac/MW/Year and 18.9 lac/MW/Year, respectively for coal based, gas based and hydro power generating stations, i.e., $14.99 \times CP$, $15.63 \times CP$ and $8.9 \times CP$. As per MERC Regulations 46, the plant load factor PLF and plant availability factor PAF, are respectively fixed at 80% and 85% for coal and gas based power generating stations. For hydro power generating stations PAF is fixed at 90%. Total fixed cost TFC is given by

$$TFC = RE + IL + IWC + DR + OMC \tag{16}$$

Total power generation TPG is

$$TPG = CP \times 365 \times 24 \times PAF \times \frac{1000}{10^6} \tag{17}$$

and fixed cost per unit FCU is

$$FCU = \frac{TFC}{TPG} \tag{18}$$

B. Calculation of variable cost for coal and gas based power generating stations

To calculate the energy charges, let SHR be the station heat rate which is fixed as 2390 and 1544 respectively for coal based power generating station and gas based power generating station according to the MERC Regulations 46.4, and PAC be the % auxiliary consumption which is fixed as 7.5% as per MERC Regulations 46. Specific oil consumption SOC is 0.50 to 1 ml/KWh, station heat rate SHR respectively for coal and gas based power generating stations are 2390 and 1544 (MERC Regulations 46.4), and gross calorific value of oil GCVO is 10000 Cal. Let cost of oil per litre be COIL, then cost of specific oil consumption per unit CSOC is

$$CSOC = SOC \times COIL$$
 (19)

Heat contribution of oil HCO is

$$HCO = GCVO \times SOC$$
 (20)

Heat contribution of fuel (coal/gas) HCOF is

$$HCOF = SHR - HCO$$
 (21)

Specific coal consumption SCC is

$$SCC = HCOF/GCVO$$
 (22)

With cost of fuel (coal/gas) as COF, cost of specific fuel consumption per unit CSFC

$$CSFC = SCC \times COF \tag{23}$$

Therefore, total variable cost of fuel (coal/gas) per unit TVC is the sum of cost of specific oil consumption and cost of specific fuel consumption which is given as

$$TVC = CSOC + CSFC \tag{24}$$

7.5% of this power is consumed by the auxiliaries so for the power ex-bus we must subtract this power from the total ex-bus power. Therefore, cost of variable ex-bus power CVEBP is

$$CVEBP = TVC/(1 - PAC) \tag{25}$$

Thus total generation cost of coal/gas based power generating station TGC is the sum of fixed cost per unit and cost of variable power which is given as

$$TGC = FCU + CVEBP \tag{26}$$

V. RESULTS

We have implemented our proposed algorithm on average demand chart of Maharashtra state for the year 2018. With the daily hourly load data taken from [10], we first prepare a hourly monthly data by calculating the average hourly demand of the state considering the data of the working days only of that month. The average demand data chart of 2018 is finally prepared by compiling these hourly monthly data for all the twelve months which is shown in Table I, where the row and column entries show the hours (0-24) and months (January - December) of the year respectively. The pictorial representation of the same is given in Figure 1.

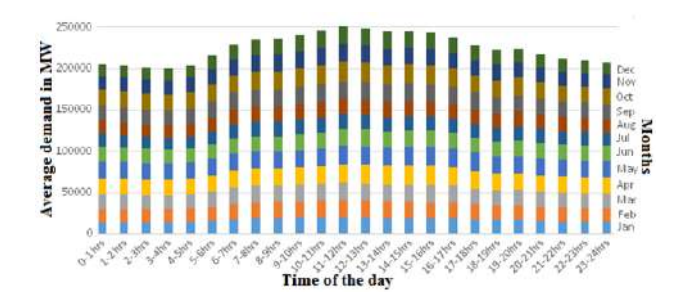


Fig. 1. Average Demand Chart of Maharashtra State for the Year 2018

Following the methodology given in Section III-A, the derived results are shown in Table II

The total demand can be met by optimising various base load and non-base load generation options. In line with the discussions of uncertainties mentioned in the preceding section, installed capacity for total demand of 29332 MW, the base load installed capacity is 19618 MW. Therefore, the capacity of 19618 MW will give the optimum installed capacity to meet the minimum load requirements for the state of Maharashtra considering availability of 85% for uninterrupted service and quality power. We can conclude here that with this base load capacity thermal power stations

to be used as base load stations will operate economically at their optimum level with increased plant load factor and hence with minimum environmental impact.

To calculate the approximate annual generation cost of coal, gas and hydro power plants which comprises of fixed as well as variable costs, we implement our proposed methodology as given in Section IV-A and Section IV-B respectively. In order to calculate the fixed generation costs of coal, gas and hydro power plant, we considered the coal power plant of capacity 660MW, gas and hydro power plants of capacities 500MW each. Following the formulations given in Section IV-A, the results obtained are shown in Table III.

For variable cost calculations we have taken the cost of coal and gas to be 1400 Rs/MT and 23.84 Rs/SCM respectively. Specific oil consumption of oil for coal and gas is assumed to be 1 ml/KWh. Variable cost of hydro is considered nil as the total cost consists mainly of capital cost only. We calculate the values of variable costs from the proposed methodology given in Section IV-B and the results are tabulated in Table IV.

Therefore, the total cost of generations of coal, gas and hydro power generation is shown in Table V.

The costs calculated above are the cost of generation only and it does not include the real cost, i.e., the social and environment costs. Keeping in view the obtained value of installed capacity of base load, the obvious query is with installed capacity base demand determined the natural corollary is how to meet it? The sources available are three fold viz coal, hydro and gas generation to meet the base load demand. While purely cost factor will lead us to using hydro, gas and coal in order of preference. However, characteristics mentioned above of each of the sources would constrain driving purely on cost basis. It would therefore be pragmatic to use coal to the point where it can be used at maximum PLF to ensure that not only the plant is optimally run but at the same time would take care of both cost (cost would go up if not used at maximum PLF) as well as environmental fall outs in terms of emissions. Hydro would come to fill up the next level of core demand as well as to even out the first level of demand changes. Gas would be the third option keeping in view the cost and flexibility of operation to meet immediate demand gaps.

VI. CONCLUSION

This paper presents a methodology to compute the optimum value of installed capacity of power plants for base load and peak load demand using the data for the past year. The same can be done for last 5 years to see the demand pattern to be predicted for future years. A methodology is also developed for the tentative generation cost of each of coal, gas and hydro plants so that a proper energy mix is done for base load station. We have tried to target such demand data representing minimum of average hourly demand or leaning towards the minimum hourly demand to nd the installed capacity of based load power plants. The capacity of coal based plants will serve to operate all the time at their full capacity along with gas and hydro power plants.

	Jan-18	Feb-18	Mar-18	Apr-18	May-18	Jun-18	Jul-18	Aug-18	Sep-18	Oct-18	Nov-18	Dec-18
0-1 hrs	13851	15582	17975	19612	20678	17826	15284	15792	17956	19176	16512	14322
1-2 hrs	13682	15278	17654	19523	20519	17321	15018	15540	17685	19250	16646	14538
2-3hrs	13599	15092	17283	19100	20195	16980	14791	15360	17524	19390	16755	14828
3-4hrs	13652	15098	17175	18900	19884	16774	14738	15327	17419	19441	16810	14885
4-5hrs	14151	15512	17428	19041	19828	16795	15160	15671	17707	19786	17246	15448
5-6hrs	15283	16645	18382	19700	20333	17450	16113	16767	18785	20627	18134	16574
6-7hrs	16970	18371	19755	20585	20790	18066	17376	18153	20102	21454	18947	17785
7-8hrs	18231	19572	19744	20619	20666	18290	17836	18791	20534	21529	19527	19023
8-9hrs	18466	19720	19493	20440	20646	18482	17996	18856	20663	21594	20062	19625
9-10hrs	18832	19821	20026	20893	21201	18949	18121	19010	20811	22170	20709	20172
10-11hrs	19082	20384	20525	21299	21617	19166	17953	18909	21047	23055	21620	20734
11-12hrs	19513	20624	21546	22286	22466	19489	17911	18894	21555	23664	21762	20600
12-13hrs	19155	20198	21369	22447	22644	19468	17560	18704	21334	23389	21291	20034
13-14hrs	18688	19761	21006	22275	22546	19334	17280	18304	21042	23077	20907	19572
14-15hrs	18630	19789	21103	22395	22939	19558	17174	18252	21045	23244	20694	19404
15-16hrs	18321	19600	21158	22577	23096	19580	17122	18325	21014	22933	19964	18920
16-17hhrs	17887	19087	20746	22310	22960	19163	16953	18144	20442	22011	19347	18314
17-18hrs	16828	17910	19461	21305	21943	18392	16863	17749	19635	20924	18752	17991
18-19hrs	16689	17259	18539	19871	20445	18027	17035	17891	19164	20730	19083	18076
19-20hrs	16352	17724	18844	20094	20521	18529	17496	18274	19642	20672	18597	17495
20-21hrs	15449	16919	18247	19756	20433	18481	17207	17703	18857	19882	17732	16432
21-22hrs	14794	16335	18117	19433	20258	18266	16677	17137	18496	19378	17167	15548
22-23hrs	14351	16050	18208	19668	20511	18221	16251	16676	18227	19116	16849	14867
23-24hrs	14024	15820	18069	19679	20698	17997	15628	16128	18111	19245	16735	14453

TABLE II

PATTERN DETERMINATION OF INSTALLED CAPACITIES IN MW

Base Load	Peak Load	Spinning Reserve	Total Demand
19618	8222	1392	29232

TABLE III
FIXED COST CALCULATIONS

Generation	Fixed	Power	Total Fixed)
	Cost (Rs)	Generation (MU)	Cost (Rs/MWh)
Coal	933.98	4914.36	1.90×10^{3}
Gas	477.78	3723	1.283×10^{3}
Hydro	1041.01	3942	2.668×10^{3}

Therefore, the base load power plants will operate at their maximum capacity with maximum efficiency resulting in less pollution and minimum overall cost of generation. The demand above the load can be met by the renewable energy sources. Therefore, proper energy mix planning considering the optimal installed capacity of coal based power plants will result into an economic and pollution free energy sector.

It should be emphasized here that this paper presents the very rst approach of developing the data table and then computing the optimum installed capacity of based power plant along with their costs keeping in view the economic and environmental aspects. It may be noted that the installed capacity in the advanced country is being kept well above the demand. In fact, the concept of considering 85% availability factor is a very tight target from the concept of meeting the demand uninterruptedly. The demand above the base load, i.e., the peak load is to be met by various other renewable sources and non-renewable sources of generation by estimating and comparing their true cost of generation and their associated externalities. The next stage of this work is

TABLE IV
VARIABLE COST CALCULATIONS

Type of	Cost of specific	Total variable
Generation	oil consumption Rs/Unit	cost Rs/MWh
Coal	8.44	9.16×10^{3}
Gas	3.812	3.956×10^{3}
Hydro	-	i

TABLE V
TOTAL GENERATION COSTS

Generation	Fixed	Variable	Total
Generation	cost	Cost	cost (Rs/MWh)
Coal	1.9×10^{3}	9.16×10^{3}	11.06×10^{3}
Gas	1.283×10^{3}	3.956×10^{3}	5.239×10^{3}
Hydro	2.668×10^{3}	-	2.668×10^{3}

the optimization of different renewable sources of energy to meet the peak load based on the true cost that includes social and environmental costs of all types of generating sources.

Traditionally costs of the fuel have been arrived at only taking into account the commercial factors based on which tariffs are determined. But as the environmental awareness has increased other social and economic costs are also coming into reckoning. There is realization that every fuel as well as type of generation has some deleterious impact on surroundings which exceeds commercial costs. These costs need to be taken into account to arrive at the real costs accruing to the society and environment. This can be based on the studies done on normative basis or can be arrived at based on certain accepted parameters which can be built into calculation of real tariff. To elaborate coal contributes to land, air and water pollution, hydro in addition to affecting surrounding area during construction also affects

the up-stream and down-stream environment. Gas also has emissions and other factors which need to be considered while arriving the real costs.

REFERENCES

- G. of India, "Flexibility in generation and scheduling of thermal power stations to reduce emissions," Government of India, Technical Report, April 2018.
- [2] _____, "Flexibility in generation and scheduling of thermal power stations to reduce the cost of power to the consumer," Government of India, Technical Report, August 2018.
- [3] National Electricity Plan, Volume 1, "Generation," https://powermin.nic.in, Ministry of Power, GOI, 2018, central Electricity Authority.
- [4] Central Electricity Regulatory Comission., "Tariff regulations," www.cercind.gov.in, New Delhi, 2019.
- [5] Maharashtra Electricity Regulatory Comission., "Tariff regulations," Maharashtra, mYT Regulations 2019.
- [6] O. Gruenwald and D. Oprea, "Optimization model of energy mix taking into account the environmental impact," in 11th International Conference ENERGY ECOLOGY ECONOMY, High Tatras, Slovak Republic, May 2012.
- [7] M. K. Upadhyay, "Analyzing the impact of clean coal technology on the overall energy scenario," NITI Aayog, Government of India, New Delhi, India, Joint Report between NITI Aayog and Institute of Energy Economics Japan IEEJ, June 2017.
- [8] P. M. Vivek Khare, Ashish Bhargava, "Estimation of generation cost of electricity at 500 mw thermal power plant," *International Journal* of Scientific Research Engineering and Technology (IJSRET), vol. 7, pp. 1–4, 2018.
- [9] K. R. V. M.E, "Tariff determination for hydro power plant."
- [10] Maharashtra State Electricity Transmission Co. Ltd., "Maharashtra state load despatch centre," https://mahasldc.in/home.php/daily-reports/, Maharashtra, 2018, state load despatch center, Airoli (MSETCL) hourly load data.

Prediction of unknown fault of Induction Motor using SVM following Decision Directed Acylic Graph

¹Arunava Kabiraj Thakur, ²Palash Kumar Kundu, ³Arabinda Das

¹Department of Electrical Engineering (Techno Main Salt Lake, Kolkata, India) ^{2,3}Department of Electrical Engineering (Jadavpur University, Kolkata, India)

{Corresponding author's email: arunava.kabiraj007@ gmail.com}

Abstract - Fault prediction in induction machines is now an essential task to reduce downtime cost due to unscheduled shut down of motor. This technique not only prevents the motor from breakdown but also to increase component lifetime. In this work, an unknown fault has been classified using Support Vector Machine(SVM) following Decision Directed Acylic Graph(DDAG). Support Vector Machine is a machine learning techniquewas built on the basis of statistical learning theory is a pattern recognition technique which is generally utilized in classification problem. Classification is done by finding the hyperplane which separates two classes or linearly multiclasses or non linearly. samples(amplitude vs time) of three phase stator currents are collected from different faulty motors(known type) and one unknown faulty motor which is running as prime mover of a dc generator. PCA based feature extraction processes are used to extract the information from each fault condition and two eigen values which are called principal components (i.e. PC-1 and PC-2) of stator currents are effective features of faults are captured by PCA transformation. RBF type kernel trick is used to separate the classes non linearly and DDAG is used to solve multiclass problem and to classify the unknown fault accurately.

Keywords - Induction motor, PCA, Multiclass SVM, DDAG

I. INTRODUCTION

Induction motors has become essential component in modern industries. The unscheduled shutdown due to failure of motors cause enormous downtime costs and it reduces component lifetime. Fault prediction of induction motor has become very necessary to reduce the costs and to increase the component lifetime. According to the different component parts of the machines the faults are categorized such as -a) Stator faults, b) Bearing faults c) Rotor faults, and d) Other faults[1]. There are different fault detection techniques which are used to detect the faults in the machine [2,3]. The main techniques are generally used for fault analysis are (a) Vibration analysis[4,5] (b) Motor current signature analysis (MCSA)[6,7] (c) Thermal monitoring [8,9] (d) Partial discharge [10] etc. Using those techniques faults can be predicted but among them MCSA is a useful technique which is capable to localize the abnormal conditions in the motor and using this technique the cost can be reduced because electrical signals are very easier to measure than the other signals. This technique does not need the multiple costly sensors so using this technique cost can be reduced.

Feature extraction processes are used to extract the information from each fault condition goal of feature selection is to select features which allow for an accurate description of the defective condition, and subsequently, reliable defect classification, diagnosis, and prognosis [11-13]. These processes enable to define machine's health status. It was developed to reduce the dimensionality of the input features for both supervised and unsupervised classification purposes which can be used for feature selection for machine fault classification[14]. The proposed method uses Support Vector Machine for fault classification using PCA based feature extraction technique[15-17]. A Support Vector Machine (SVM) is gaining increasing attention from researchers for its outstanding performance in real world applications[18]. SVM has been used for different fault classification of machines based on vibration signals[19,20]. Conventional SVM can be used for fault classification separating two classes by optimized linear hyperplane. To solve multiclass problems is still an open research areaextending the SVMs, which are binary classifiers. In this work multiclass SVM technique has been used to classify unknown faults from four known type fault classes using current signals as input parameters. Two PC scores (i.e. PC-1 and PC-2) of stator currents are effective features of faults are captured by PCA transformation. The PCs are computed for three phases individually. The three phase known and unknown PC scores are plotted for fault classification. RBF type kernel function is used to separate the classes non linearly because for all types of problems the classes can not be separated linearly. A new learning architecture has been proposed named Decesion Direct Acylic Graph (DDAG) which reduces training and evaluation time maintaining accuracy[21]. Applying DDAG the unknown data point has been classified accurately among the other four classes and the fault has been predicted from unknown current data sample.

II. METHODS

In most of the research area Support vector machine, (SVM) has now become more important choices as one of the classification methods due to it's class separation process, and the facilities of kernel space makes SVM is a robust and powerful tool to solve the most classification problems. It has the advantages in nonlinear and high-dimensional pattern recognition problems and good generalisation capability. Modifying the original SVM algorithm or combining several binary SVMs a multi-class classifier can be designed. A multiclass SVM technique is very important to predict unknown fault among few many types of fault. Principal Component Analysis is also applied here for feature extraction and it has the capability of dimension reduction. PCA based technique need less computational cost.

A. Principal Component Analysis(PCA)

Principal Component analysis is a statistical method used for feature selection and dimensionality reduction. In the case of feature selection process the data space is transformed into a feature space and the both spaces have the same dimensionality. It can reduce the dimensionality of a data set, such that one might start with thirty original variables, but might end with only two or three meaningful axes. The formal name for this approach of rotating data such that each successive axis displays a decreasing among of variance is known as Principal Components Analysis, or PCA. In PCA the linear combinations of the original variables happen to generate the axes which are also known as principal components, or PCs.

The data Y can be represented as the combination of a set

of m orthonormal vectors v_i as given by : $Y = \sum_{i=1}^m A_i v_i$ -----

(1), where the coefficients A_i can be written from the following equation $A_i = u_i^T x$ ------

-(2) Only a subset (k < m) of the basic vectors is preserved to reduce the dimensions of the data set. The remaining coefficients are replaced by constants B_i and each vector x is then approximately written as

$$\tilde{x} = \sum_{i=1}^{M} A_i v_i + \sum_{i=1}^{d} B_i v_i$$
 -----(3)

The vectors v_i which are equal to the eigenvectors of the covariance matrix of the data set is called principal components. The coefficients B_i and the principal components should be chosen such that the best approximation of the original vector x on average is obtained. The sum of squares of the errors is minimized over the whole data set if user selects the vectors v_i corresponds to the largest eigen values of the covariance matrix.

B. Support Vector Machine(SVM)

A machine learning approach was proposed by Vapnik and others named Support Vector Machine(SVM)[24] was built on the basis of statistical learning theory is a pattern recognition technique which is generally utilized in classification problem. SVM improves the capacity of generalization through structural risk minimization principle. Many problems have been solved by means of SVM, such as small sample, non-linear, high-dimension, the local minimum, and other practical problems. SVM is a regression prediction and classification tool which uses machine learning theory for maximization of predictive accuracy while automatically avoiding over-fit to the data. This algorithm is utilized to solve the optimization problem. Classification is done by finding the hyperplane that separates the functions: linear function, nonlinear function. SVM finds an isolation hyperplane in the feature space and classifies points in the space. SVM technique can be used for fault detection in Induction Motor which has been presented.

1) Linear Function: Support vector machine (SVM) is a supervised learning method which generates mapping of input-output functions from a set of labeled training data. The features are extracted from input and the main goal of SVM algorithms is to separate the set of training data (x_1, y_1) , (x_2, y_2) (x_n, y_n) into two classes(+1,-1) by a function and to produce a classifier that will generalises well[23]. Where x_i is called the feature vector and $y_i \in \{+1, -1\}$ is the class vector. It separate the classes by a hyperplane as given by $(w^T.x) - b$ ------ (4) .wherex denotes a vector with components x_i are called patterns or examples and w_i , b are called the weight vector and bias respectively. The hyperplane $[(\mathbf{w}^T.\mathbf{X}) + b]$ separates the data if and only if $(\mathbf{w}^T.\mathbf{X}) + b > 0$ when $y_i = -1$ ----(5).

In order to be qualified as a better classifier the distance between the hyperplanes or margin (2/||w||) should be as large as possible. The optimal separinghyperplane is that hyperplane which maximises the distance between it and the nearest data point of each class. These data points are called support vectors.

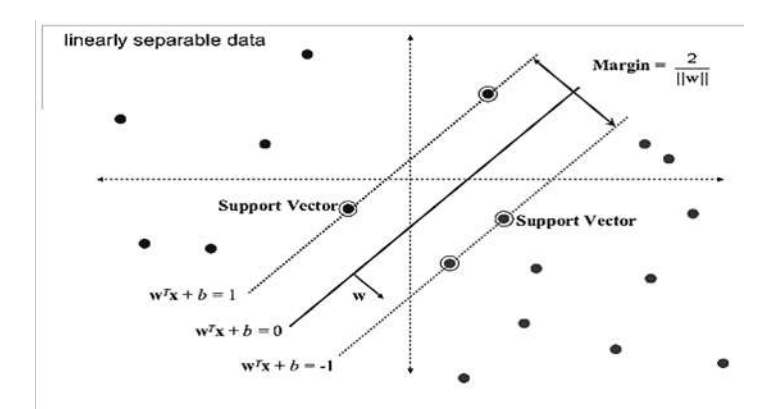


Fig 1 Linear Classification.

2) Non linear function: Linear classifiers can not be extended to generate non-linear decision boundaries, a non-linear classifier provides better accuracy in many applications. There is a way of making a non-linear classifier out of a linear classifier is to map our data from the input space X to a feature space F using a non-linear function $\Phi: X \to F$. F the discriminant function is: $f(X) = W^T\Phi(X) + b$ ------(6) in the space. Suppose support vectors are designated by αi , where $\alpha i > 0$ and weight vector are obtained by $W = \sum_{i=1}^n \alpha_i x_i^i - \cdots - (7)$. Then $f(X) = \sum_{i=1}^n \alpha_i^i x_i^i - \cdots - (8)$.

The feature space F may be high dimensional, making this trick impractical unless the kernel function k(x, x') defined as $k(x, x') = \Phi(X)^T \Phi(X')$ can be computed efficiently[25]. The discriminant function in terms of the kernel function is: $f(X) = \sum_{i=1}^n \operatorname{cd} k(x, x') + b$ -----(9).

For linear SVM the hyperplane separates the feature vectors in two set of classes but if the classes are not linearly separable then kernel trick is used to separate the classes using a hypersurface by increasing the no of dimensions.

Three kernels are commonly used:

- (i) The polynomial kernel: $k(x, x') = (X^TX' + 1)^d$ -----(10)
- (ii) The linear kernel: $k(x, x') = (X^TX' + 1) [d=1]$ -----(11)
- (iii) The RBF kernel: $k(x, x') = \exp(|x-x'|^2/2\sigma^2)$ -----(12)

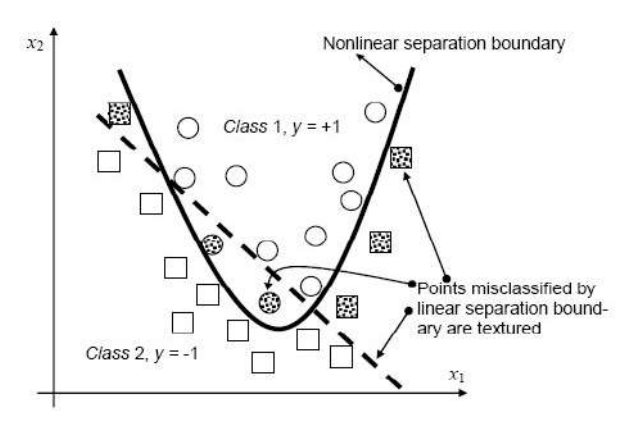


Fig 2 Non Linear classification

3) Pairwise SVM: The SVM principle is described for a binary classification, but so many problems are there which have more than two-class and three class problem. There exists different algorithms to multiclass problem as "One Against All" (OAA) and "One Against One" (OAO). If we consider a problem with 'n' class, OAA algorithm consists in the construction of n hyperplanes that separate respectively one class and the (n-1) other classes. OAO

algorithm consists in the construction of n(n-1)/2 hyperplanes which separate each pair of classes. In the two cases the final label is that mainly chosen.

A pictorial example is needed to illustrate the OAO approach. The issue of a 4-class classification problem in two-dimensional space, as shown in Fig 3. In this figure, '1', '2', '3' and '4' are the class labels. As shown in the Figure 1, data points in the shaded area are classified differently depending on the sequence of nodes in the DDAG (or the sequence of elements in theimplementation list). Consider a unknown data point 'x' located in the solid region. To classify the unknown value from the fourclasses the hyperplane 1vs4 eliminates class '4' because the data point 'x' is not in the side of class '4'. The list then becomes 1-2-3. Next, 1vs3 removes class '3' from the list. Finally, with the list 1-2 the hyperplane 1vs2 gets rid of class '1'. As a result, the data point 'x' is classified as class '2'.

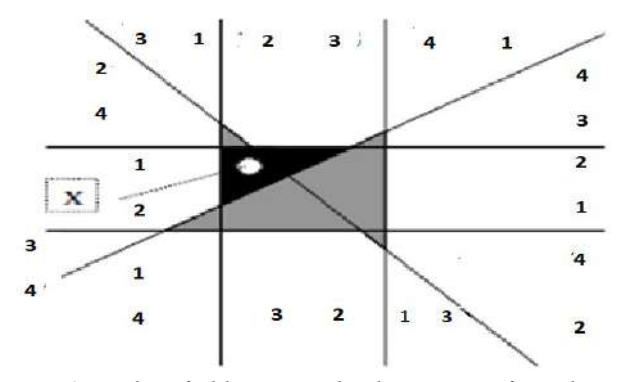


Fig -3 Unclassifiable regions by the pairwise formulation.

4) Decesion Direct Acylic Graph: Decision Directed Acyclic Graph (DDAG) developed by Platt[22] is the variant of One vs One SVM approach similar to pairwise SVM classification method. In the training phase similar to OvO method n(n-1)/2binary SVMs are required to be solved and in the testing phase, it uses a rooted binary decision directed acyclic graph. The graph contains n(n-1)/2internal nodes and nleaves. For an nclass classification problem and the number of binary classifiers is equal to n(n-1)/2and each classifier is trained which can classify two classes and it is treated as a node in the graph structure. Each node of binary tree is a binary SVM of class C_i and class C_j . A data point x is given for test whichisstarting at the root node and the binary decision function is evaluated. The data point xmoves to left or right branches on such decision tree depending on the output value. At each level of the tree one class is eliminated until only one class remains. This leads a path to a leaf node, It predicts the class label for data point x. The decision directed acyclic graph(DDAG) for these three class problem with class label set $\{1, 2, 3\}$ is shownin Fig 4.

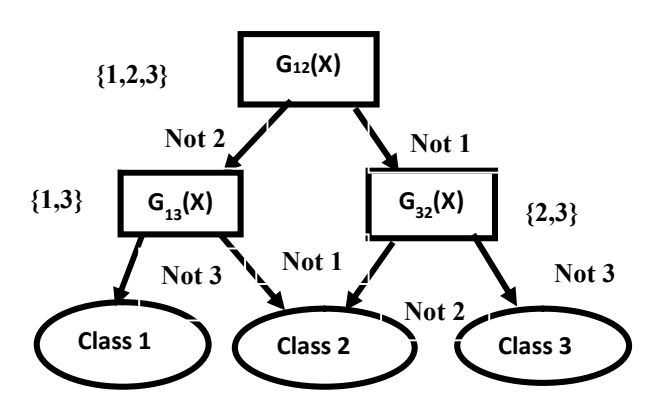


Fig 4.The DDAG Finding the Best Class out of three classes.

III. EXPERIMENTATION

A experimental set up[Fig-5] is made in the laboratory for the analysis with three phase induction motor which is used as a prime mover of a dc generator and electrical loads are connected in the load of the generator. One three phase digital power analyzer(Yokogawa WT 500) is used for data collection and it is used as a data acquisition system also which captures three phase stator currents with the help of current sensors from different faulty induction motors and it interfaces with PC through USB cable .The four different faulty induction motors [(1/3 hp, 50 HZ), RPM - 2850] are used for the analysis which act as a prime mover of a dc generator (0.75 KW, 230 V) and the three phase current waves are captured by the power analyzer when the system is running. The sampling time for data acquisition task has been set to 5ms. Numerical conversion of current waves[amplitude vs time] are necessary to carry out this research work. Therefore the WT Viewer software is used in the pc to converted the current waveforms to numerical value and the sampled data are recorded and stored into CSV file. The wave from data is converted to numerical data (amplitudevs time) and 1002 sampled data were recorded and stored into .CSV file by the help of WT viewer software.



Figure -5 A laboratory experimental set up

IV. RESULT AND ANALYSIS

A data set was prepared considering 6 known type faulty motor's current samples[Broken rotor bar(BR), Faulted bearing(FB), Rotor Misalignment (RM) and Rotor unbalance(RU) each containing three sets of data] captured by the power analyzer in the laboratory. The data samples (amplitude vs time) of one unknown faulty motor has also been collected. The classifier designed here is unlike the unsupervised PCA and similarity/dissimilarity-based PCAs.

Two eigen values which are called PCs (Principal Component) are computed from the data samples of four fault types and one unknown samples by the help of PCA algorithm and using MATLAB software. Only 2 PC scores (i.e. PC-1 and PC-2) of stator currents are effective features of faults are captured by PCA transformation and the three phase known and unknown PC scores are plotted for each fault and three phase PC plots are treated as one class. The RBF type kernel trick is used to separate the classes non lineraly using a hypersurface by increasing the no of dimensions [Fig 6 (a,b,c,d,f)]. The DDAG method has been here for multiclass classification of the above mentioned faulty motors using the decisions generated by the binary classifiers. For classification among four faulty motors 6(6-1)/2=15 classifiers has been designed, out of them 6 plots have been shown in Fig 7.

To describe the maximum membership count to detect unknown class a example of 4 class problem has been taken. The DDAG method has been used here for multiclass classification of the above mentioned 4 classes using the decisions generated by the binary classifiers. The decision tree has been drawn to classify the unknown class among four classes 6(6-1)/2=15 classifiers has been designed. The multiclass classification was executed by evaluating decisions of all 15 binary classifiers and assigning the instance to the class which got the highest number of resulting outputs (decision class). The membership values of each class have been determined based on the evaluation paths[Fig 6]. The outputs in terms of membership values for each class has been shown in the table 1 in accordance with the evaluation paths of the designed DDAGs. The unknown class has been authenticated counting the maximum membership number. The six classes for six faulty motors are numbered by 1(Broken Rotor Bar),2(Faulted Bearing),3(Rotor Misalignment),4(Rotor Unbalance), 5(Stator Winding Fault), 6(Single phase Voltage Unbalance) respectively. Applying DDAG algorithm one confusion matrix has been found[Table-1]. After classifying pairwise SVM the result can be interpreted as:

TABLE-1: Membership for fault type of the DDAG in Figure 6

Membership	Number of detected classes
(Class) number	

Class 6	1:(6-1)
Class 5	4: (5-1),(5-3), (5-4), (5-6)
Class 4	2: (4-1), (4-3)
Class 3	2: (3-1), (3,6)
Class 2	5: (2-1), (2-3), (2-4), (2,5), (2-
	6)
Class 1	0

From the decision tree[Fig 6] and table 1 classifying by pairwise SVM it has been seen that unknown class does not resembles to class 6,5,4,3 and 1 because the number of detected classes for 6,5,4,3 and 1 are 1,4,2,2 and 0 respectively. According to maximum voting count, the decision is that the unknown class resembles to class 2 because the number of detection for class 2 is 5. From this analysis it can be concluded that unknown data sample is 'Faulted bearing'.

Fig 6 The decesion tree.

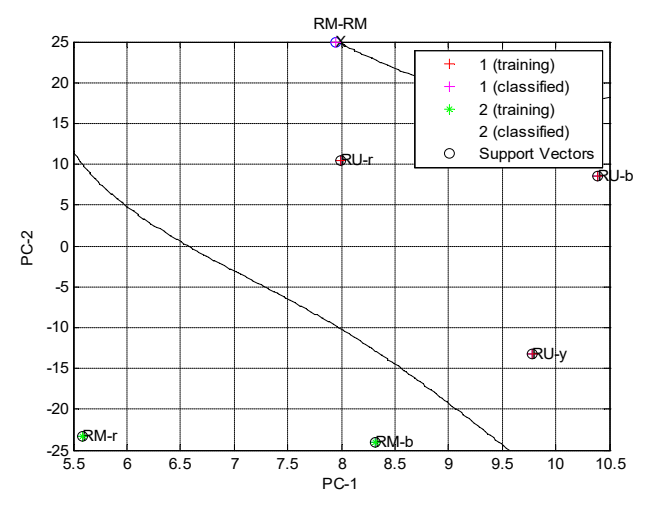
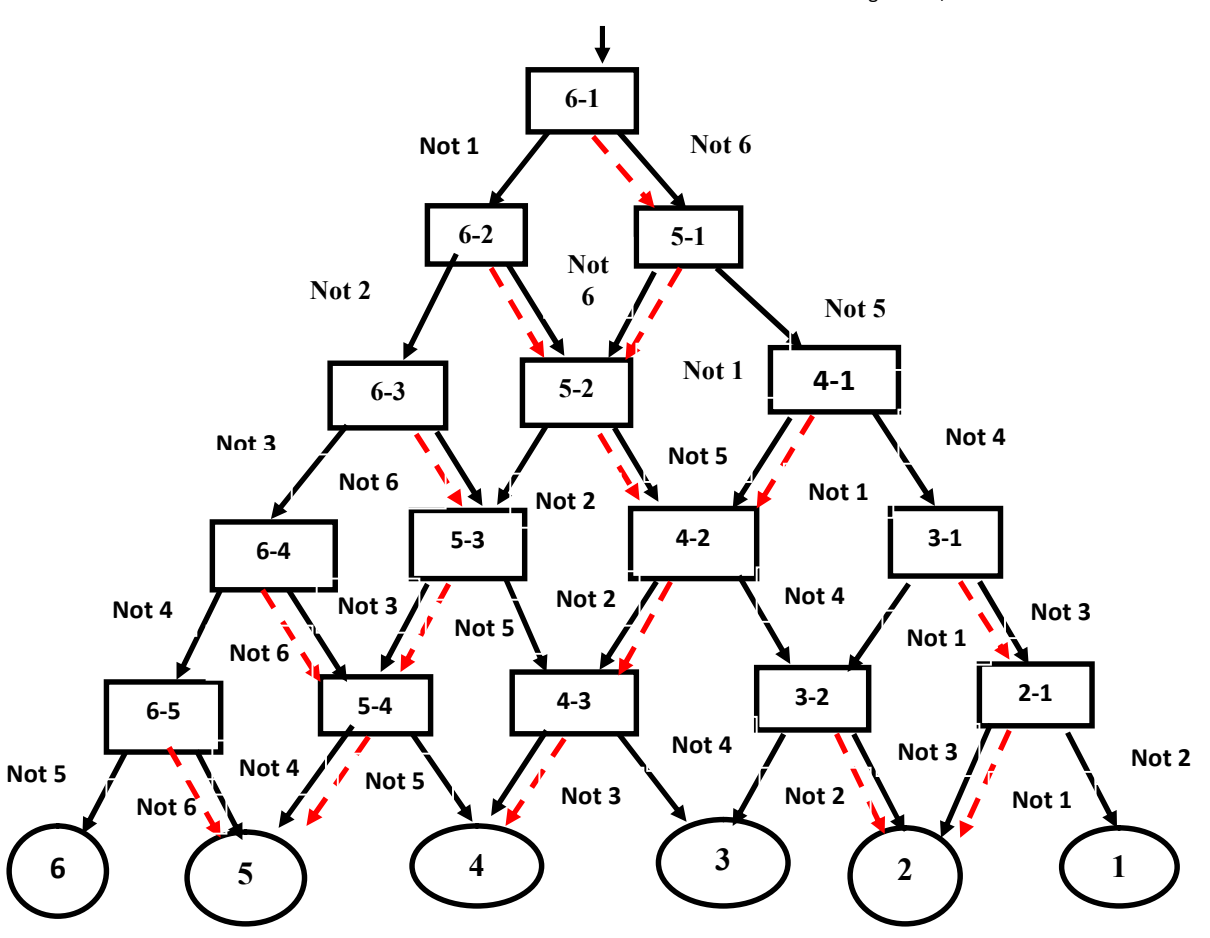


Fig 7 (a) One output out of 15 binary classifiers where unknown current data samples the test sample(X=unknown test sample)

*Note: RM=Rotor misalignment , RU=Rotor unbalance



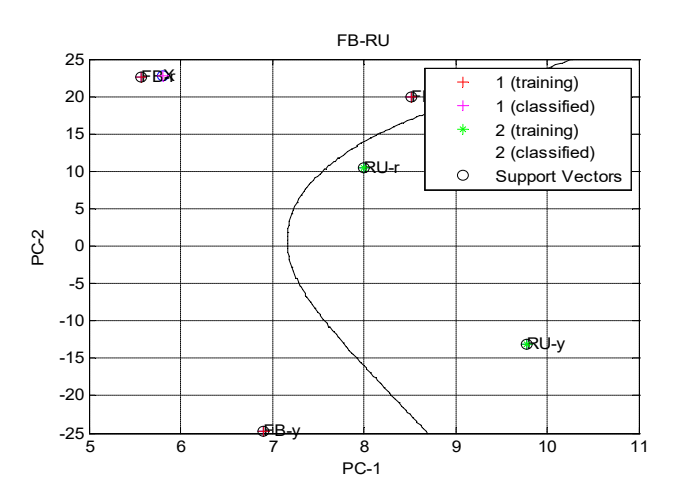


Fig 7 (b) One output out of 15 binary classifiers where unknown current data samples the test sample(X=unknown test sample)

*Note: FB= Faultedbearing, RU=Rotor unbalance.

IV Discussion and Conclusion

The fault classification using linear separating hyperplanes has some limitations so RBF based kernel function is used for separating the classes. One of the obstacles in the classification process is the dispersion of data tending diversely, so it will be difficult to be separated linearly. In original feature space the data is not linearly separable. The fault classification using linear separating hyperplanes has some limitations. Kernel function methods can be used for an SVM because of the scalar product in the dual form, but can also be used elsewhere - they are not tied to the SVM formalism. Classifiers can be learnt for high dimensional features spaces, without actually having to map the points into the high dimensional space. Data may be linearly separable in the high dimensional space, but not linearly separable in the original feature space. In the present case, the RBF kernel function, K(x, x'), which transforms the original data space into a new space with a higher dimension; this process includes the transformation function with dot product as given by f(x) = k(x, x') = $\Phi(X)^T\Phi(X')$. So RBF based kernel function separates the multi classes data more efficiently compared to other types of kernel function such that overlapping among the classes can be eliminated which results hard classification for unknown sample to be classified with higher classification rate.

REFERENCES

- G.K Singh, Sa'ad Ahmed Saleh Al Kazzaz, "Induction machine drive condition monitoring and diagnostic research—a survey", Electrical Power Systems Research, Volume 64, Issue 2, February 2003, pp: 145–158.
- [2] P.J. Tavner, "Review of condition monitoring of rotating electrical machines", IET Electric Power Applications, Volume:2, Issue: 4,2008, pp: 215-247.
- [3] R. C. Bhavsar, R. A. Patel, "Various Techniques for Condition Monitoring of Three Phase Induction Motor- A Review", International Journal of Engineering Inventions, (November 2013), Volume 3, Issue 4, pp. 22-26.
- [4] W. Zhaoxia, L. Fen, Y. Shujuan, W. Bin, "Motor Fault Diagnosis Based on the Vibration Signal Testing and Analysis", Third International Symposium on Intelligent Information Technology Application(IITA)(Volume 2), 21-22 Nov. 2009, pp:433-436.
- [5] C. Costa, M.H. Mathias, P. Ramos, P. S. Girão, "A new approach for real time fault diagnosis in induction motor is based on vibration measurement", Instrumentation and Measurement Technology Conference (I2MTC), IEEE, 3-6 May, 2010, pp: 1164-1168.
- [6] M. E. H. Benbouzid, M. Vieira, C. Theys "Induction motors' fault detection and localization using stator current advanced signal processing techniques", IEEE Transactions on Power Electronics (Volume:14, Issue: 1) Jan 1999, pp: 14-22.
- [7] M. E. H. Benbouzid, "A Review of Induction Motors Signature Analysis as a Medium for Faults Detection", IEEE Transactions on Industrial Electronics, October 2000, VOL. 47, NO. 5, pp. 983-993.
- [8] J.F. Moreno, F.P. Hidalgo, M.D. Martinez, "Realisation of tests to determine the parameters of the thermal model of an induction machine", IEEE Proc. Electrical Power Applications(Volume:148,Issue: 5), September 2011, pp. 393-397.
- [9] Z. Gao, T.B. Habetler, R.G. Harley, "An online adaptive stator winding temperature estimator based on a hybrid thermal model for induction machines", in Conf. Rec. IEEE IEMDC' 05, San Antonio, Texas, USA, May 2005, PP. 754-761.
- [10] G. Paoletti , A. Golubev, "Partial Discharge Theory and Applications to Electrical Systems", IEEE IAS Pulp and Paper Industry Conference in Seattle, 1999, 21-25 June, pp: 124 – 138.
- [11] I. T. Jolliffe, Principal Component Analysis, New York, Springer-Verlag, 1986.
- [12] J. F. Martins, V. F. Pires, A. J. Pires, "PCA Based On Line Diagnosis of Induction Motor Stator Fault Feed by PWM Inverter", IEEE International Symposium on Industrial Electronics (Volume: 3), 9-13 July 2006, pp: 2401-2405.
- [13] V. FernaoPires, J. F. Martins and A. J. Pires, "On-Line Diagnosis of Three-Phase Induction Motor Using an Eigenvalue αβ-Vector Approach" Proc. Of IEEE ISIE 2005, Dubrovnik, Croatia, 2005.
- [14] A. Malhi, R. X. Gao, "PCA Based Feature Selection Scheme for Machine Defect Classfication", IEEE Transactions on Instrumenation and Measurement, VOL. 53, NO. 6, DECEMBER 2004, pp : 1517-1525.
- [15] Y.K.Gu, X.Q.Zohu, D.P.YU, Y.J.Shen, "Fault diagnosis method of rolling bearing using principal component analysis and support vector machine", Journal of Mechanical Science and Technology 32 (11) (2018). pp: 5079~5088.
- [16] L. Shuang, Y. Fujin, "Fault Pattern Recognition of Bearing Based on Principal Components Analysis and Support Vector Machine", Second International Conference on Intelligent Computation Technology and Automation, 10-11 Oct. 2009, pp: 533-536.
- [17] C. Jing, J. Hou, "SVM and PCA based fault classification approaches for complicated industrial process", Volume: 167, November 2015, pp: 636-642.

- [18] N. Deng, Y. Tian, The new method of data mining, in: Support Vector Machine, Science Press, 2004.
- [19] A. K. Panda, J. S. Rapur, R. Tiwari, "Prediction of flow blockages and impending cavitation in centrifugal pumps using Support Vector Machine(SVM) based on vibration measurements", Volume 130, December 2018, pp. 44-56.
- [20] Z. Liu, H. Cao, X. Chen, Z. He, Z. Shen, "Multi-fault classification based on wavelet SVM with PSO algorithm to analyze vibration signals from rolling element bearings", Volume 99, January 2013, Pages 399-410.
- [21] B. Kijsirikul, N. Ussivakul, "Multiclass support vector machines using adaptive directed acyclic graph", Proceedings of the 2002 International Joint Conference on Neural Networks. IJCNN'02 (Cat. No.02CH37290), 12-17 May 2002.
- [22] J.C. Platt, N. Cristianini, John Shawe-Taylor, "Large margin DAGS for multiclass classification", Advances in Neural Information Processing Systems 12, pp. 547-553, The MIT press, 2000.
- [23] A. Agasthian, R. Pamula, L. A. Kumaraswamidhas, "Fault classification and detection in wind turbine using Cuckoooptimized support vector machine", Neural Computing and Applications, May 2019, Volume 31, Issue 5, pp:1503-1511.
- [24] V. Vapnik. The Nature of Statistical Learning Theory. NY: Springer-Verlag. 1995.
- [25] A. Hur, J.Weston, "A User's Guide to Support Vector Machines", Data Mining Techniques for the Life Sciences, pp: 223-239, 2009.

The Institution of Engineers (India), WBSC

23rd & 24th Nov. 2019

Title: Accommodation of Solar Power and its impact on the tariff Amit Kumar Sil, Dy. Chief (Engineer), Damodar Valley Corporation

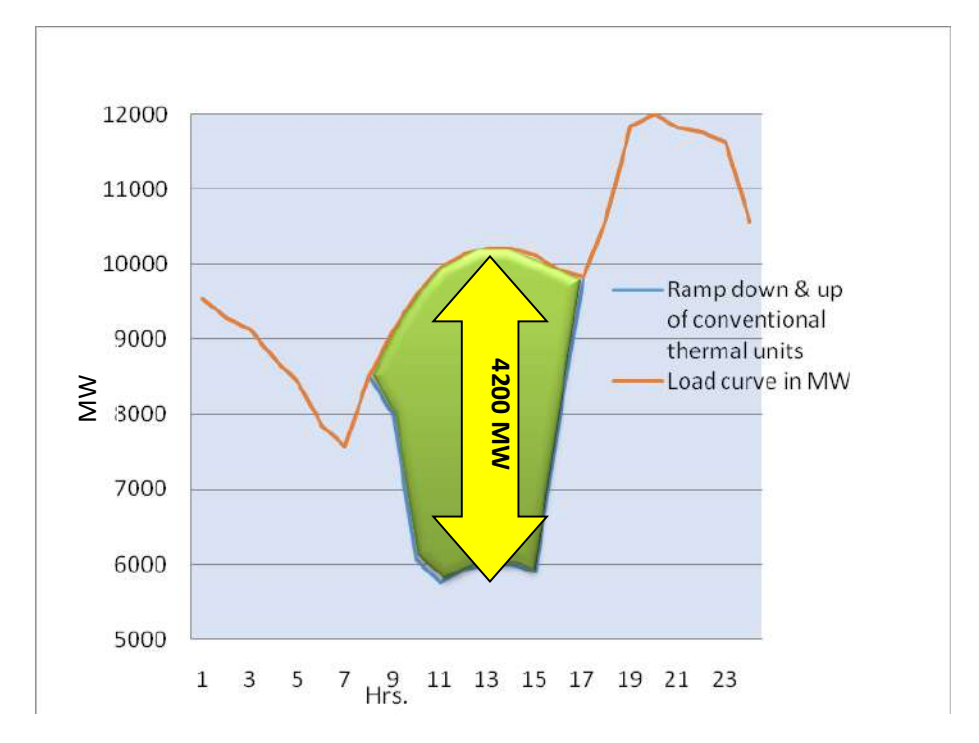
Key Words: renewable energy, conventional coal based units, modulation, operating norms, accommodation

Introduction: The government of India has set a target of 175 GW of renewable energy capacity by 2022, out of which solar capacity will be 100 GW. The generation of conventional thermal generating units is to be modulated to accommodate a huge amount of generation from renewable generators specifically during day time when plenty of solar power generation will be available in the grid. Modulation of conventional thermal generating stations has to be done judiciously considering the age of units and type of technology used in these units. The modulation of the conventional thermal generating units will invite additional operating cost. The same has to be borne by the consumers. One case study has been done for the West Bengal Distribution Company Limited considering its latest tariff order for the period 2017-18.

Accommodation of Solar Power: Out of 100000 MW solar generating capacity target in India, the target for the State of West Bengal is 4223 MW. This solar generation will have to be accommodated during the day hours. The expected load curve for the year 2022 during summer season will look as below:

The Institution of Engineers (India), WBSC

23rd & 24th Nov. 2019



While the solar generation will start increasing the conventional coal based units are to be backed down upto its technical minimum operating limit. Again these coal based units are to be ramped up in the afternoon. The output of conventional thermal generating units is to be modulated during day time considering the solar generating units are as must run accordingly conventional coal based generating units are to be flexible.

Modulation of coal based generating units and increase in generation tariff: To accommodate solar generation during day time, the coal based generating units should be flexible to ramp up & down with required rate and maintain minimum and maximum output while these are in operation. Additional operational flexibility is also required to address the error in forecast in solar generation.

This flexibilisation of coal based generating units will invite additional cost which has to be considered in generation tariff, ultimately in retail tariff which will be passed on to the consumers. The following cost will increase:

- a) Additional capital expenditure cost to be incurred to bring down the minimum technical limit of the generating units to operate without oil support.
- b) Cost of operation and maintenance cost and capital overhauling cost.

The Institution of Engineers (India), WBSC

23rd & 24th Nov. 2019

- c) Cost of energy charges due to higher heat rate and auxiliary power consumption for low load operation during daytime.
- d) Capacity cost due to reduce in life for variable load operation.

Issues need to be addressed to accommodate solar power during daytime: The following steps can be adopted for accommodating solar generation during day time.

- Exploration of Technical and Commercial solution for modulation of coal based units from 40% to 105% without oil support
- Quick start and stop with around 3% ramping up / down rate.
- Till this is achieved in the majority of conventional coal based units have to be backed down to its technical minimum limit.

Central Electricity Regulatory Commission / State Electricity Regulatory Commissions need to fix up compensation norms with respect to the normative parameters of heat rate and auxiliary power consumption to run the coal based units at 40% to 55% of its capacity regularly.

A case study on increase on retail tariff to accommodate solar generation: A case study is being carried out taking inputs from the last tariff order of West Bengal Distribution Company Limited (WBSEDCL) issued by Hon'ble West Bengal Electricity Regulatory Commission (WBERC) and the Central Electricity Regulatory Commission (Indian Electricity Grid Code) (Fourth Amendment) Regulations, 2016. WBSEDCL is mainly purchasing power from West Bengal Power Development Company Limited (WBPDCL). The output of the coal based units of WBPDCL has to be modulated to accommodate solar generation during daytime. The coal based units are to be backed down upto its technical minimum limit during solar peak generation as per requirement of the system while accommodating the solar generation throughout the day. In the said tariff order, the sale to the own consumer of WBSEDCL is shown as 25327 MU. If the solar power purchase obligation (SPPO) is taken as 8% of this consumption in the year of 2021-22 then SPPO will be 2026 MU. This amount of solar generation has to be accommodated in the system of WBSEDCL during daytime. Although this figure of sale i.e 25327 MU to its own consumer will change in the year 2021-22 accordingly SPPO figure will also change. But for the sake of calculation of current impact considering SPPO as 8% of the sale figure to its own consumer on retail tariff the

The Institution of Engineers (India), WBSC

23rd & 24th Nov. 2019

present figures of the tariff order are being considered in respect of sale figure, power purchase units and costs etc.

During modulation of coal based units, the distribution licensee will have to pay full fixed, if the unit is available as per its share and also the increase in energy cost as per compensation clause incorporated by the Hon'ble Central Electricity Regulatory Commission(CERC) in CERC (Indian Electricity Grid Code) (Fourth Amendment) Regulations, 2016. The Hon'ble CERC has incorporated the following mechanism for compensation for degradation of station heat rate (SHR) and aux energy consumption (AEC) compensation clause in CERC (Indian Electricity Grid Code) (Fourth Amendment) Regulations, 2016.

The following station heat rate degradation or actual heat rate, whichever is lower, shall be

S1.	Unit loading as a % of installed	Increase in SHR (for	Increase in SHR (for		
No.	capacity of the unit	supercritical units) (%)	sub critical units) (%)		
1	85-100	Nil	Nil		
2	75-84.99	1.25	2.25		
3	65-74.99	2	4		
4	55-64.99	3	6		

considered for the purpose of compensation:

The following auxiliary energy consumption degradation or actual, whichever is lower, shall be considered for the purpose of compensation:

S1.	Unit loading (% of maximum	% degradation in AEC
No.	continuous rating)	admissible
1	85-100	Nil
2	75-84.99	0.35
3	65-74.99	0.65
4	55-64.99	1.00

The energy charges of the coal based units will increase as per the above compensation clause incorporated in CERC (Indian Electricity Grid Code) (Fourth Amendment) Regulations, 2016. Accordingly the energy charges of the coal based units of WBPDCL will increase while

The Institution of Engineers (India), WBSC

23rd & 24th Nov. 2019

accommodating solar generation, moreover the fixed cost during this period as per the availability of the units will have to bear by the distribution licensee and finally the retail consumers.

Here, we will calculate the increase in energy charges for different coal based units of WBPDCL considering backing down to 60% of its Maximum Continuous Rating (MCR). Here two sample calculations are shown one for Kolaghat Thermal Power Station and other for Sagardighi Thermal Power Station:

Change in Energy charge of Kolaghat Thermal Power Station due to 40% B/D

	Change in Energy charge of Kolagnat Thermal Power Station due to 40% B/D							
	Description	Units	Kolaghat at normative	increase by	Backed down to 60% of MCR			
(1	(2)	(3)	(4)	(5)	(6)			
1	Generation	MU	8278.2		7795.31			
2	AUC rate	%	9.60%	up by 0.29%	9.89%			
3	AUC in Units	MU	794.71		770.96			
4	Ex bus generation (4=1-3)	MU	7483.49		7024.35			
5	Station heat rate normative	Kcal/kWh	2700.00	up by 1.75%	2747.25			
6	Total heat rate required (6=1X5)	M.kcal	22351140.00		21415651.66			
7	Heat value of oil	Kcal/lt	9689.65		9689.65			
8	Specific Oil consumption	ml/kWh	2.00		2.00			
9	Oil consumption (9=1X8)	KL	16556.40		15590.61			
10	Heat from oil [10=(7X9)/1000]	M.kcal	160425.72		151067.55			
11	Heat from coal (11=6-10)	M.kcal	22190714.28		21264584.11			
12	Heat value of coal	kcal/kg	3549.79		3549.79			
13	Coal consumption [13=(11/12)X1000]	MT	6251275.22		5990378.05			
14	Coal requirement with permissible transit loss	MT	6301688.73		6038687.55			
15	Average cost of oil	Rs/kL	61291.50		61291.50			
16	Average price of coal	Rs/MT	2754.05		2754.05			
17	Cost of oil [17=(9X15)/100000]	Rs.lakh	10147.67		9555.72			
18	Cost of coal [18=(14X16)/100000]	Rs.lakh	173551.66		166308.47			
19	Cost of fuel (19=17+18)	Rs.lakh	183699.32		175864.19			
20	Average Fuel cost /kWh	Paise/kWh	245.47		250.36			

Change in Energy charge of Sagardighi Thermal Power Station U#3&4 due to 40% backing down

	Description	Units	Sagardighi at normative	increase by	backed down to 60% of MCR
1	Generation	MU	7151.00		6480.31
2	AUC rate	%	5.25%	up by 0.29%	5.54%

The Institution of Engineers (India), WBSC

23rd & 24th Nov. 2019

3	AUC in Units	MU	375.43		359.01
4	Ex bus generation (4=1-3)	MU	6775.57		6121.30
5	Station heat rate normative	Kcal/kWh	2322.00	up by 1.75%	2362.64
6	Total heat rate required (6=1X5)	M.kcal	16604622.00		15310613.12
7	Heat value of oil	Kcal/lt	9560.72		9560.72
8	Specific Oil consumption	ml/kWh	1.00		1.00
9	Oil consumption (9=1X8)	KL	7151.00		6480.31
10	Heat from oil [10=(7X9)/1000]	M.kcal	68368.71		61956.45
11	Heat from coal (11=6-10)	M.kcal	16536253.29		15248656.67
12	Heat value of coal	kcal/kg	4199.00		4199.00
13	Coal consumption [13=(11/12)X1000]	MT	3938140.82		3631497.18
14	Coal requirement with permissible transit loss	MT	3969900.02		3660783.45
15	Average cost of oil	Rs/kL	39182.71		39182.71
16	Average price of coal	Rs/MT	3775.27		3775.27
17	Cost of oil [17=(9X15)/100000]	Rs.lakh	2801.96		2539.16
18	Cost of coal [18=(14X16)/100000]	Rs.lakh	149874.44		138204.46
19	Cost of fuel (19=17+18)	Rs.lakh	152676.40		140743.62
20	Average Fuel cost /kWh	Paise/kWh	225.33		229.92

The Institution of Engineers (India), WBSC

23rd & 24th Nov. 2019

After accommodating the solar generation there will be change in the energy balance of the distribution company and the change in power purchase from WBPDCL will be as follows:

Power Station	Capacity (MW)	Availability factor	Exbus gen. (MU)	Share of WBSEDCL (MU)	Share of WBSEDCL after accommodation of solar generation (MU)
Kolaghat	1260	75%	7843.49	5018	4709.06
Bakreswar	1050	85%	7114.65	7164	6461.64
Bandel	450	77%	2740.91	1676	1556.48
Santaldih	500	85%	3387.93	3651	3306.82
Sagardighi 1	600	85%	4065.52	2409	2172.82
Sagardighi 2	1000	85%	6775.52	3250	2931.35

23168 21138.2

Now increase in retail tariff per unit can be calculated as follows:

Purchase of power by WBSEDCL from WBPDCL

		As per t	tarrif order	•	To accommodate RE Power			wer
	Energ y MU	cap ch Rs in lakh	E. Ch p/kWh	Amount Rs in lakh	Energy MU	cap ch Rs in lakh	E. Ch p/kWh	Amount Rs in lakh
(1)	(2)	(3)	(4)	(5)	(6)	(7)	(8)	(9)
Kolaghat	5018	35407.44	245.47	158584.29	4709.06	35407.44	250.36	153305.20
Bakreswar	7164	75485.63	216.33	230464.44	6461.65	75485.63	219.88	217561.83
Bandel	1676	10629.27	270.27	55926.52	1556.48	10629.27	278.77	54018.68
Santaldih	3651	46552.76	217.05	125797.72	3306.83	46552.76	221.17	119691.13
Sagardighi Ph #1	2409	28719.78	217.23	81050.49	2172.82	28719.78	221.36	76816.84
Sagardighi Ph #2	3250	54885.74	225.33	128117.99	2931.36	54885.74	229.92	122284.74
•	251680.6 7799		779941.4					
	23168	2		4	21138	251680.62		743678.42

Cost of sola			
	Rate		
		P/kWh	Rs in lakh
Solar RE Power MU	2030.00	450	91350
		Total	91350
Total nower nurchase cos	835028 42		

Total increase in power purchase cost (Rs. In Lakh)

55087.0

Sale to Consumers (MU)

25327

The Institution of Engineers (India), WBSC

23rd & 24th Nov. 2019

Increase in retail tariff per unit due to accommodation of solar power

21.75 Paise

Conclusion: The increase in per unit cost in retail tariff is only 21.75 paise. But we shall have to go ahead adding more renewable energy generators in spite of the increase in electricity tariff for the betterment of the environment.

Although the consumers will have to pay little higher tariff due to the accommodation of solar energy but in long run, the present consumers or their next generation will be benefited avoiding more number of natural calamities and health hazard.

Further, if we consider the present downward trend of solar generation cost and increasing trend of coal cost and freight, the hike in retail tariff will be lowered down to zero even though it might reduce the retail tariff due to accommodation of solar generation in near future. But there is only one warning regarding disposal of solar cells on completion of its life and we can start thinking of the environment friendly way to dispose of the exhausted solar cells.

Reference: 1. Tariff orders in respect of WBSEDCL & WBPDCL issued by Hon'ble West Bengal Electricity Regulation.

2. Central Electricity Regulatory Commission (Indian Electricity Grid Code) (Fourth Amendment) Regulations, 2016.

The Institution of Engineers (India), WBSC

23rd & 24th Nov. 2019

SCADA integration into Smart Grid for Power Efficiency in Indian Economy

Soumen Sen, Paromita Banerjee

Abstract: Smart grid is a new power distribution system that uses Information Technology .Smart grid technology can make electricity more efficient, safe and easier for one to handle in 21st century. SCADA (Supervisory Control and Data Acquisition) systems can be integrated by electrical, communications and networks, and it allows for distributed and central aggregation of information and control over the entire electrical utility network. SCADA optimizes the grid assets by monitoring and optimizing those assets while minimizing operations and maintenance costs. The Smart Grid, intelligence and control need to exist along the entire power supply chain. This includes the electricity generation and transmission from beginning to delivery end-points at the customer's side and includes both fixed and mobile devices in the SG architecture.

The trend today is **digital India** with **one nation-one grid** concept and introduction of **smart grid in PSU's** in **power sector** is a must to sustain the privatization with competition. After 72 years of independence, there is an ongoing process

of replacement of old thermal units into solar power and National Smart Grid mission is also on the move.

In this paper, we will focus on the benefits of Smart grid technology merged with Advanced SCADA which will be beneficial for Indian power sector. Smart grids allow for automatic rerouting and have self diagnostic, self healing technology with facility of Real Time Dynamic pricing.Smart grids are built on advanced infrastructure and include renewable energy sources. There electronic power conditioning and controlled production and distribution of electricity.

Keywords: SCADA,SG, power conditioning, Real time dynamic pricing.

The Institution of Engineers (India), WBSC

23rd & 24th Nov. 2019

POWER SECTOR RESOURCES SECURITY IN VIEW OF CLIMATE CHANGE

Subhendu Podder Amar Nath Bhadra

Abstract: Green House Gases (GHGs) are not "Poison" unless it is in "Excess". It, was, is and will be present in the planet Earth, being balanced by the Nature making the Environment habitable for all kinds of Livingbeings. Excess of everything is uncontrolled, unmanageable and hence "Bad". It is being observed that from the beginning of 20th Century, for making our lives more and more comfortable, use of Natural Resources have become rampant leading to exponential increase in concentration GHG. Currently, GHG level has reached alarmingly high level, 415 PPM, causing major effect on leading ecological balance sustainability, due to increased negative radiative flux. It needs to be mentioned that while introduction of large scale renewable plaving a significant minimising the level of the GHG emissions, Nuclear Energy is poised to play an effective role also, as it does not emit CO2 and other GHGs into the atmosphere. Current proportion of Nuclear Energy is only 1.9% out of total basket size of 360 GW. Thanks to the Government for taking various policy and regulatory measures, under recommendations of NITI AAYOG, towards ensuring proper energy mix and sustainability of the environment. Authors believes that we have enough reserve of Thorium which can be bring a big boost on Nuclear generation capacity as matured technologies are available to ensure safety within regulatory ambit.

This paper is aimed at initiating debate/discussions on the right energy-mix

and enabling policy initiatives to ensure Energy Security and Sustainable Environment together thereby supporting the dream target of becoming a USD of 5 trillion dollars economy by the year 2025.

Keywords: Energy mix, Nuclear Energy, Energy Security, GHG.

Investigations on causes of blackout and possible recommendations for maintaining reliability and security in smart power grid

Mehebub Alam

Executive Engineer (E), Damodar Valley Corporation(DVC)
Raghunathpur Thermal Power Station(RTPS), DVC, Purulia-723133, West Bengal, India

{mehebubjgec1990@gmail.com}

Abstract - In the past few years, several blackout events have occurred across the whole world. This has seriously affected the whole power sector causing direct and indirect impact on economy as well as society. Furthermore, significant increase of renewable energy penetration into the power grid has made the power system more and more complex.. Moreover, incorporation of various Flexible AC Transmission System (FACTS) devices impose additional challenges to the power system due operation of the power system near to the critical limit. Hence, slight variation from operating point without proper monitoring and control may lead to collapse of the entire power system network. Further, the researchers and planners are striving to convert the conventional into Smart Grid which is supposed to have excellent features like reliability, flexibility, self-healing capability wide are monitoring and control capability etc. In view of this, it has become an urgent need to develop suitable schemes to ensure wide area situational awareness and wide area monitoring protection and control (WAMPAC) of the entire systems so that any contingency situations can be properly handled and corrective actions can be taken easily. In light of this, researchers, power system planners and professional engineers are looking for developing appropriate strategies to cope with such catastrophic events in upcoming days. This paper highlights a comprehensive review of the various blackout events happened in various countries i.e., North America (2003), Southern Sweden and Eastern Denmark (2003), Italy(2003) India (2012).These and

blackouts are among worst power system failures in the last few decades. In introduction background section. of power svstem monitoring, protection and control issues are outlined. In section 2, brief discussion on some major blackout events are highlighted. In section 3, root causes of the blackout events are investigated through exhaustive literature survey. In section 4, impact of blackout events are discussed on different domains. In section 5, suitable recommendations are proposed to mitigate such issues and to ensure the quality and reliable power supply like smart grid environment. Finally, the conclusions are drawn at last section. In a nutshell, this paper will be helpful to provide clear guidelines to the power system operators and decision makers so that the blackout events can be mitigated in near future and the reliability as well as resiliency can be ensured.

Keywords – Blackout; situational awareness; Smart Grid; reliability

1. Introduction

Nowadays it has become an critical issue and challenge to ensure continuous and quality electrical supply to the customers. The power system is widely spread over large geographical area and thus it is quite natural that several faults and disturbances may occurred on the power system network. In this context, unpredictable faults and cascading tripping of

equipment may lead to serious consequences which affect the entire society directly or indirectly. With the ever increasing demand of energy, the modern power system is bound to operate at the vicinity of the steady state stability limit which can easily lead to a critical situation. suitable control and protection Therefore, schemes must be available to cope with these disturbances. Hence, steady state and transient stability is one of the hot topic of research since last few decades. It is to ne noted that the frequency, voltage and rotor angle of generators are the critical parameters which must be properly controlled to maintain the power system stability. The imbalance between generation and demand directly affects the frequency stability, while the system voltage is affected by reactive power imbalance. On the other hand, rotor angle characteristics also an indicator of stability and synchronism in the whole power system. In power system, any abnormal situation like overloading, line tripping, frequency and voltage instability, malfunctioning of the protective system etc. must be addressed as early as possible. If these abnormal situations are not addressed in timely manner the entire system may experience cascading events which further may lead to blackout [1-10].

2 .MAJOR BLACKOUT EVENTS

A. North America blackout (August 14, 2003) [2]

The most severe blackout occurred in US-Canadian blackout on Aug 14, 2003[].As reported, at least 50 million people were affected. An estimated 63 GW of power was disrupted. It is worthy to mention that this power is approximately 11% of total demand of the America system. More than generating stations at 261 power plants and 400 transmission lines tripped according to the published report. It is to be noted that before the event, the whole system was operating according to the North American Electric Reliability Council (NERC) standards. The key issue was mal-operation of Midwest ISO (MISO) state estimator and real time contingency analysis (RTCA) software. The software related problem together with other led to the unavailability of real time system information of the network.

Initially the outage of East lake unit 5 generator

was recorded. It is worth mentioning that this unit and other units in Northern Ohio were operating under stressed reactive power condition [12]. MISO and RTCA software were malfunctioning from 12.15 to 16.04. This prevented the MISO performing proper early warning assessment of the system, Moreover, at the fast energy (FE) control center a number of computer software failures happened on their energy management system (EMS) software starting at 14.14 hr. As a result, adequate information of events taking place on its system until approximately 15.45 not conveyed were properly.

Firstly, the outage of FE's Eastlake unit 5 generator at 13.31 occurred. Eastlake unit 5 and several other generators in FE's northern Ohio service area were generating high amount of reactive power. It is to be noted that high reactive power loading indicates limited margin to support system against outages. Therefore due to high reactive power output over excitation occurred at voltage regulator of East 5 generator and subsequently it tripped due to changeover in manual mode from auto mode. Later on, the operator made an attempt to restore AVR but the generator tripped. This suggest the need for prioritized replacement of old system with modern digital equipment.

B. Italian blackout (September 28, 2003) [4], [5]

This blackout was initiated when tree flashover caused tripping a major tie line between Italy and Switzerland. This happened due to failure of reclosing operation arising from phase angle difference across the lines. As the redistribution of power was not happened properly, a second 380 KV line also tripped on same border due to tree contact. This cascading phenomenon continued. Later on, the line on the interface between Italy and France tripped due to distance relay operation. Moreover, 220 KV transmission line between Italy and Australia also get tripped. Subsequently, final 380 KV corridor between Italy and Slovania tripped due to overloading.

These outages resulted in shortage of 6400 MW power and frequency of Italian system started to fall. Finally, the generation tripped due to under frequency as the frequency decrease was beyond the control.

C. Indian blackout (July 30 and 31, 2012) [13]

During the summer of 2012, extreme weather conditions led to a high demand in power for cooling systems. In the same season due to limited water supplies, the hydro power plants were generating below their full capacity. On 30 July 2012, around 2:00 a.m. in the morning, a 400 kV Gwalior-Binar circuit breaker tripped, triggering a series of events, which later led to a system collapse [13]. The major power stations in the area were affected leading to a loss of 32 GW in generated power. Because of this power loss, nearly 300 million customers were left without power. Serious consequences were experienced due to this power loss. Railways, airports, passenger trains and traffic signals were all shutdown causing commotion in business areas. Hospitals without reliable power back up supplies had to endure 3 to 5 h of no power. After restorative actions, about 80% of the power was restored after almost 15 h [13]. The following day on 31 July, at around 1:02 p.m., the power system experienced another disturbance [13]. This was due to a relay problem near the Taj Mahal and several power stations were again grounded [13]. More than 600 million individuals lost their power

3. CAUSES OF BLACKOUT

The U.S-Canada Power System Outage Task Force report indicates that the key reasons [12] behind the blackout were as follows:

- Inadequate understanding of the system
- Lack of situational awareness
- Improper vegetation management
- Lack of support from Reliability Coordinator(RC)

Several causes (percentage sharing basis) of blackout occurred all over the world are summarized in Fig. 1.

4. IMPACT OF BLACKOUT

The impact [13] of blackout in different sector are categorized below:

- Social sector
- Economic sector
- Political sector

The graphical illustration regarding impact of blackout is shown in Fig.2.

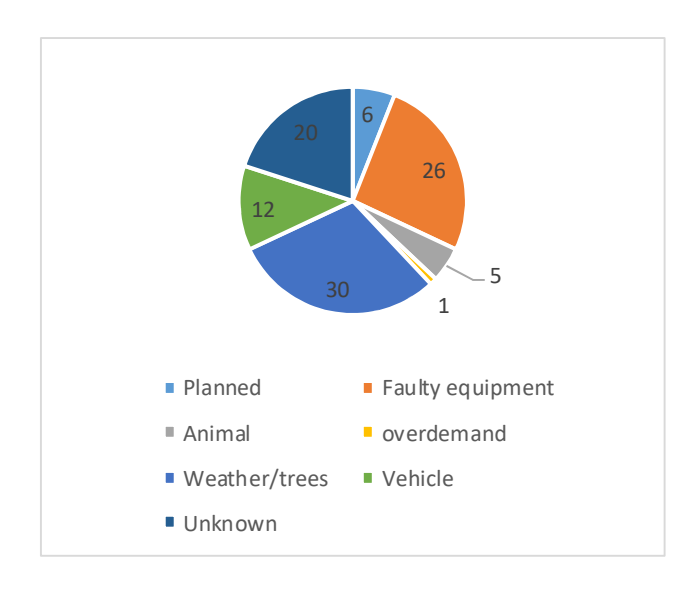


Fig.1: Causes of blackout occurred all over the world

The various causes [13] of major blackouts around the world are shown in Table 1.

Table 1: Causes of major blackouts occurred around the world

Countr y	Date of occurr ence	D ur ati on (h ou rs)	Affec ted peopl e(mill ion)	Causes
Mexico and USA	Sept 8,201 1	12	2.7	Transmission line tripping
Brazil	Feb 4,201 2	16	53	Transmission line fault and fluctuated power flow
Vietna m	May 22,20 13	10	10	Crane operator
Philippi	Aug	12	8	Voltage collapse

nes	6,201			
1100	3			
India	July 30,20 12	15	620	Transmission line overload
Bangla desh	Nov 1,201 4	24	150	HVDC station outage
Pakista n	Jan 26,20 15	2	140	Plant technical fault
Hollan d	Mar 27,20 15	1. 5	1	Bad weather condition
Turkey	Mar 31,20 15	4	70	Power system failure
Ukarai ne	Nov 21,20 15	6	1.2	Power system failure
Ukarai ne	Dec 23,20 15	6	230	Cyber attack
Kenya	Jun 7,201 6	4	10	Animal shorted the transformer
Sri Lanka	Mar 3,201 6	16	10	A severe thunderstorm
South Australi a	Mar 1,201 6	6. 1	1.7	Storm damage transmission network
US(NY)	Sept 8,201 7	11	21	Cascading failure in transmission system
Urugua y	Aug 26,20 17	4	3.4	Bad weather condition lead to cascading failure
US(sou theast)	Sept 10,20 17	5	7.6	Cascading events and transmission

				tripping
Sudan	Jan 10,20 18	24	41.5	Cascading failures
Azerba zzan	Sept 8,201 8	8	8	Unexpectedly high temperature
Barzil	Jul 3,201 8	1	10	Transmission line failure
Canad a	Mart 21,20 18	4	0.6	Wind reached speed of 100 km/hr

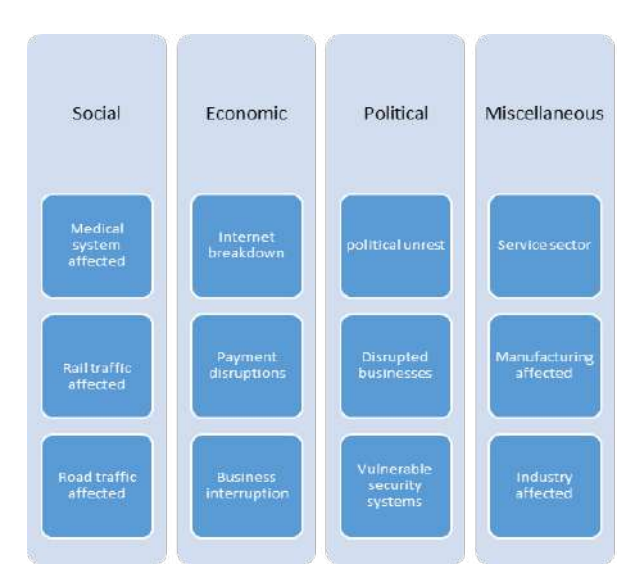


Fig.2: Graphical representation of impact of blackout

A. Social impact

When a blackout occurred, health systems, rail and road traffic systems are heavily disturbed. Loss of power results in disturbance of the water supply system in big cities and towns. Loss of water in big cities poses a big health risk, as impure water may lead to serious diseases. Vaccines and drugs are at risk in the event of

prolonged blackout which also causes loss in monetary value as new vaccines and drugs will be needed for replacement. Several important equipment in hospital like X-rays, ventilators, MRI, CT scan and theatre depend on electricity, thus paralyzing the hospital and causing danger to life.

B. Economic impact

Huge economic losses occur due to internet breakdown, failure of payment systems and downtime of production industries. Ports of entry (sea/air/rail) drive economies and heavily depend on power supply. The delay in loading/unloading of goods at seaports will have cascading effects i.e., critical goods like oil, medicines and foods. Several IT companies heavily rely on the data center and information. These crucial information and data may be lost due to power outage which cause delay in project implementation. Even a short–term outage can have significant impact on the stock market as transaction happens in every second.

C. Political impact

During a blackout, the security systems are disabled which may impose threat to the nation. Power supply is required to operate military bases. Due to power outages valuable equipment and weapons become useless in the event of an attack. The bases may have also important facilities like airports and hospitals that also needs power supply.

5. RECOMMENDATIONS

Some recommendations to mitigate the blackout events are discussed below:

A. Data management [12]

To facilitate a smoother and more expeditious process for data gathering and processing in the aftermath of a blackout, the following recommendations are suggested:

- Improve the calibration of recording instruments, especially in establishing time synchronization.
- Establish pre-defined data reporting requirements and standardized data formats.
- Establish pre-defined commercial logistics, such as confidentiality agreements.

Establish an infrastructure to support a centralized blackout investigation

B. Disturbance monitoring [12]

To facilitate better insights into the cause of blackouts and enable detailed post-mortem analysis, adequate, and appropriate disturbance monitoring is required. This has been achieved to some extent in the development of the wide area measurement systems (WAMS [8]). Some Recommendations are as follows:

- Refine the process for integration, analysis, and reporting of WAMS data. This must also include the development and support of staff and resources.
- Establish a WAMS Website to allow the free exchange of WAMS data, documents, and software and thus promote its development
- Extend the collection of benchmark events and dynamic signatures to determine the range of normal system behavior.
- Perform related studies (including eigenanalysis) to assist proper interpretation of observed system behaviour
- Fully utilize the capabilities often available in modern HVDC and/or FACTS equipment to directly examine system response to test inputs.

C. U.S Canadian Task Force recommendations[12]

The joint U.S. and Canadian Task Force made a list of recommendations following the detailed investigation of the August 14th event. A summary of the key points in [2], [11],[12] are listed below

- Reliability standards should be made mandatory and enforceable, with penalties for noncompliance
- A regulator-approved funding mechanism should be developed for NERC, and the regional reliability councils, to ensure their independence from the utilities that they oversee.
- At a federal policy level, clarification is needed on expenditures and investments

- for bulk system reliability (including investments in new technologies) and how such expenditure will be recoverable through transmission rates.
- Track implementation of recommended actions to improve reliability.
- Improve the near-term and long-term training and certification requirements for operators, reliability coordinators, and operator support staff.
- Evaluate and adopt better real-time tools for operators and reliability coordinators.
- Develop enforceable standards for transmission line ratings
- Employ automatic load shedding.
- Resolving issue related to zone -3 relays

Some other perspectives are suggested below:

- The use and enhancement of special protection systems can be quite effective at times in preventing cascading outages
- The application of automatic controls such as automatic voltage regulators, and where applicable power system stabilizers, should be mandatory for generators.
- It is of vital importance to enforce and constantly encourage training programs for system operators and their supporting staff.
- The lessons learned from past mistakes must be incorporated into new procedures as well as using such lessons learned to help develop new and improved technologies for system control and monitoring.
- Normal planning studies cannot capture all of the possible scenarios that may lead to a blackout condition, due to the vast number of possible uncertainties and operating actions.
- Ensure the redundancy and reliability of remote control and telecommunication devices

- Operators who initiate load shedding pursuant to approved guidelines should be shielded against liability or retaliation
- Rapid system restoration is extremely important in order to minimize the impact of a blackout on society
- Specific attention should be given to voltage stability. Proper reactive power management, having under voltage load shedding schemes to protect against severe disturbances and proper deployment of shunt reactive compensation are key for ensuring system reliability

6. CONCLUSIONS

In this paper, the state of the art on blackout and cascading events in modern power systems is presented. Due to their importance, blackout and cascading events in power systems around the globe are completely reviewed. Different causes and reasons behind the different blackout in power systems are marked out. Furthermore, classical and modern methods for modeling the cascading events are surveyed. The key points [13] that can be derived from this paper are:

- Most power system blackouts start due to bad weather followed by subsequent cascading events; therefore, weather forecasting techniques must be updated and power systems operators must have this information to prepare for such events.
- The other major cause was faulty equipment and human error, power system equipment is rated to operate under specific conditions and for specific durations before periodic checks or planned maintenance. These issues must be emphasized in power systems and standards adhered to.
- An upgrade of the power system monitoring, control and protection schemes is required to enhance system reliability. The wide area measurement

- systems (WAMS) platform is one of the promising platforms.
- Customers must be encouraged to participate in the demand side management programs such as the emergency demand response.
- Reserve management of most power systems must be improved—at any time, a specific share of generation must be allocated as a reserve. Ways to minimize the initial costs of renewable energies to be found and renewables must be used to supplement conventional generation.
- Pre-disturbance systems studies must be done and also include the possible cascading events.

ACKNOWLEDGMENT

Author is thankful to Damodar Valley Corporation (DVC) to carry out the research and providing sponsorship.

REFERENCES

- [1] P. Kundur, "Power grid blackouts," presented at the IEEE PES General Meeting, Denver, CO, 2004.
- [2] N. B. Bhatt, "August 14, 2003 U.S.-Canada blackout," presented at the IEEE PES General Meeting, Denver, CO, 2004.
- [3] S. Larsson and E. Ek, "The blackout in Southern Sweden and Eastern Denmark, September 23, 2003," in Proc. IEEE PES General Meeting, Denver, CO, 2004.
- [4] S. Corsi and C. Sabelli, "General blackout in Italy Sunday September 28th, 2003, h 03:28:00," in Proc. IEEE PES General Meeting, Denver, CO, 2004.
- [5] A. Berizzi, "The Italian 2003 blackout," in Proc. IEEE PES General Meeting, Denver, CO, 2004. [6] C. Taylor, "Preventing blackouts," presented at the IEEE PES General Meeting, Denver, CO, 2004.
- [7] J. E. Dagle, "Data management issues associated with the August 14th, 2003 blackout

- investigation," in Proc. IEEE PES General Meeting, Denver, CO, 2004.
- [8] J. F. Hauer, N. B. Bhatt, K. Shah, and S. Kolluri, "Performance of WAMS East in providing dynamic information for the North East blackout of August 14, 2003," in Proc. IEEE PES General Meeting, Denver, CO, 2004.
- [9] P. Gomes, "New strategies to improve bulk power systems security: Lessons learned from large blackouts," in Proc. IEEE PES General Meeting, Denver, CO, 2004.
- [10] S. Imai, "TEPCO observations on August 14 blackout and recommendations to prevent future blackouts based on TEPCO's experience," presented at the IEEE PES General Meeting, Denver, CO, 2004.
- [11] U.S.-Canada Power System Outage Task Force. (2004) Final Report on the August 14, 2003 Blackout in the United States and Canada: Causes and Recommendations. [Online]. Available: http://www.nerc.co
- [12] G. Andersson *et al.*, "Causes of the 2003 major grid blackouts in North America and Europe, and recommended means to improve system dynamic performance," in *IEEE Transactions on Power Systems*, vol. 20, no. 4, pp. 1922-1928, Nov. 2005.
- [13] Alhelou *et al.*, "A survey on Power System blackout and Cascading Events: Research Motivations and Challenges" in *Energies*, vol. 2, no. 4, 2018. https://doi.org/10.3390/en12040682

Study and Analysis of Resistive Superconducting Fault Current Limiters (SFCL) In Grid Connected Power System

Bhagyashri Belle, Uday B Sarode and Mangesh S Thakare
Department of Electrical Engineering
PVG's COET Pune
India 411009
bhagyashrikbelle@gmail.com

Abstract - Superconducting Fault Current limiters (SFCLs) are playing important role in power system protection. SFCL is used to reduce the effect of unforeseen disturbances within transmission and distribution system. The occurrence of faults in the grid are very common which leads to be breakdown of the system. Therefore, it is important to study and analyze SFCL characteristics and behavior in the grid connected system to limit the fault current in minimum time. In this paper study of SFCL characteristics is carried out and its effectiveness for three phase and line to ground fault by using the MATLAB Simulink model. For the purpose of study, Simulink model of 10 MVA wind farm connected to grid system is considered. Three different location of three phase fault and four different locations of SFCL are considered for the analysis of fault current. Analysis of SFCL can be useful to system designers to understand behavior of systems during faults. It can be also useful to decide different positions of multiple SFCLs in grid connected systems.

Keywords -Resistive superconducting fault current limiter; power system protection; fault current limitation; renewable system; grid connected systems.

INTRODUCTION

Now-a-days power system network increased widely due to increase in consumption of electrical energy. Due to increase in capacity of generating stations and size of interconnected grid system which results in increase of fault current level and other abnormal conditions. It also demands the use of advanced protective devices. Protective equipment in power systems like circuit breakers are expensive and affected

by fault currents. Fault current controllers and shunt reactors were used to limit the fault current but due to their fixed impedances generally not preferred for higher fault current. Superconducting fault current limiter (SFCL) is the most promising device to limit the fault current used in transmission and distribution system [1]. SFCL in normal conducting mode work as normal conductor whenever fault occurs SFCL reduces peak of fault current within short period of time and normal current flows in the system after fault is removed [1].

There are two basic concept of SFCL namely resistive and inductive. In the resistive type SFCL superconductor is connected in series to the transmission line to be protected; and in the inductive SFCL concept, superconductor is magnetically coupled to the line. Resistive SFCL is simple in construction and design. As the losses in the resistive SFCL are low as compared to inductive, Resistive SFCL is preferred [2]. Demand of SFCL is increased but few are commercialized hence study of High Temperature Superconductor material done by researchers due to low refrigeration cost [10]. Thus the work is carried out in Matlab Simulink environment to analyse the SFCL modelling in different conditions.

This paper mainly focuses on SFCL at different locations of grid system for the three phase to ground fault (LLL-G) and line-to-ground fault (L-G) at distribution grid. Different transient conditions of resistive SFCL model and its Current Time characteristics are studied. For simulation purpose, a wind farm with a capacity of 10 MVA is considered.

A. SFCL and its Characteristics

Resistive type SFCL is merely a length of superconductor material. For the analysis it is important to understand resistance characteristics of **SFCL** The model. characteristics is based on three possible states for a superconductor. It includes superconducting region, flux flow region and normal conducting (resistive) region. Fig.1 shows the typical relationship between electric field E and Current density J i.e. E(j) characteristics. After entering the flux-flow state, the superconductor heats up rapidly so E increases. The two parameters, electric field and temperature are important factors in the performance determination of a superconductor [3]. The changing impedance of superconductor depends on these parameters. When these are coupled with the current density it shows the characteristics of the nonlinearity of superconductor. Comparing the E1, E2and E3 the lower absolute value is considered as operation current density.

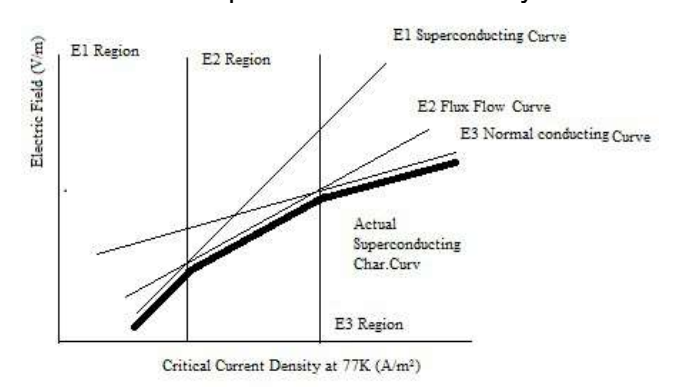


Fig.1 SFCL E (j) characteristics [3]

The thermal sub-system has been modelled [2] as follows:

$$T(t) = Ta + \frac{1}{csc} \int_0^1 [Qsc(t) - Qremoved(t)]$$
 dt (1)

Here the assumption is that the resistivity varies linearly with temperature, when $T(t) \ge Tc$. This assumption is justified and supported by the experimental results in [6]. The variation of critical current density (Jc) with temperature is also assumed to be linear. The parameter values are taken from [7]. The SFCL model equations are studied to approximate the current-time grading i.e. the time taken to quench for a given fault current. The temperature of the superconductor is calculated using (1) where E (t, T) is calculated according to [8], in flux-flow region $E(t, T) \ge E_0$ and $T(t) < T_c$. When $T(t) > T_c$, it is

assumed that the superconductor quenches. To simplify the analysis current is assumed as a constant dc fault current I. Equation (1) can be differentiated and manipulated [2] as follows:

$$\frac{dT}{dc} = \frac{1}{Gsc} \left[i(t) E(t, T) lsc - \frac{T(t) - Ta}{\theta sc} \right]$$
 (2)

Therefore, E can be simplified as a function of temperature as below and E (T) is formulated as [17]

$$E(T) = E0 \left(\frac{g_0}{g_0}\right)^{\frac{\beta}{\alpha(7/K)}} \left(\frac{J_0(77K)}{J_0(T)}\right) \left(\frac{J_1(t)}{J_0(77K)}\right)^{\beta}$$
(3)

Substituting (2) into (3) gives,

$$E(T) = E0 \left(\frac{E\sigma}{E\theta}\right)^{\frac{\beta}{\mu(T/K)}} \left(\frac{T\sigma - 77}{T\sigma - T}\right) \left(\frac{J(E)}{J\sigma(T/K)\cos\sigma}\right)^{\beta} \tag{4}$$

Above equations is simple and can be solved easily. In common case using liquid nitrogen as the cryogen where Ta =77 K, Tc = 95 K and T = 95 K; it gives an expression for t, the time for the superconducting fault current limiter to reach a particular temperature T as,

$$t = 6Csc \theta sc \frac{\tan^{-1}\left[\frac{3}{\sqrt{2\theta sck-9}}\right]}{\sqrt{2\theta sck-9}}$$
(5)

Where Csc is superconductor heat capacity, so is thermal resistance from superconductor to cooling reservoir, k is the coefficient for heat transfer to cooling reservoir. For example, for Ta = 77 K, a fault current of at least 1.9 kA is observed [2]. The Table 1 shows the current-time characteristics of SFCL for different values of ambient temperature of the superconductor and cooling reservoir.

Table 1. Current –Time characteristics of SFCL [2].

[-]	•			
Sr.	Та	Тс	I (Amp.)	Time
No	(K)	(K)		(msec.)
1	77	95	1.9 KA	1.062858m
				sec
2	80	95	1.6 KA	2.370msec
3	85	95	1.4 KA	3.689336m
				sec

B. Power System Model

Power system model considered was designed with distribution network and integrating a wind farm with capacity 10 MVA [1]. Considering standard block diagram of SFCL containing grid system. Fig.2 shows power system model in Matlab Simulink SimPowerSystem. This model is composed of a 100MVA conventional plant with 154 kV through a step-up transformer TR1. This model contain industrial and domestic load with separate distribution network. The wind farm is integrated with branch network through TR3 and provides power to domestic loads. Locations of SFCL and artificial fault shown in fig 2. At the same Fault location on distribution grid most severe symmetrical three phase-to-ground and mostly occurring single line-to-ground faults are created. Four identified locations of SFCL marked as Location 1 (at Substation), Location 2 (at Branch network), Location 3 (at integration point with wind farm and distribution grid) and Location 4 (at wind farm). Change in fault current of wind farm of TR3 for different locations of SFCL have been measured and analysed in D section for finding best location of SFCL in grid system.

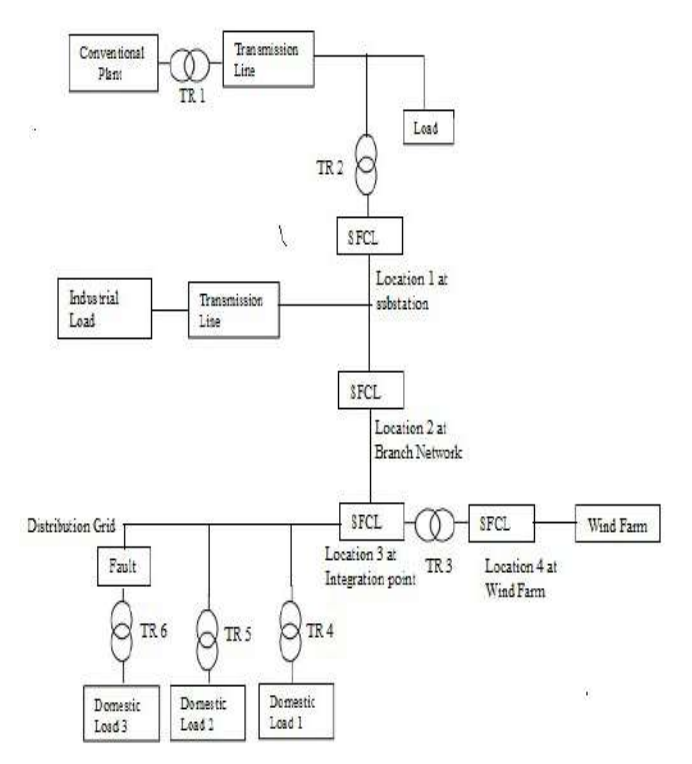


Fig.2 Three phase power system Simulink model with SFCL locations and Fault [1].

1. Resistive model

Resistive type SFCL was modeled in Simulink SimPowerSystem shown in fia. 3. parameters and their selected values are given as: 1) minimum impedance = 0.01 ohms 2) maximum impedance = 20 ohms, 3) triggering current 550 A, 4) recovery time = 10msec, transition time = 2msec, its working voltage is 22.9 KV. Two different case studies of two different faults are taken for analysis . Considering one SFCL at a time fault current was analysed. Optimum location of SFCL which reduces fault current of wind farm was considered.

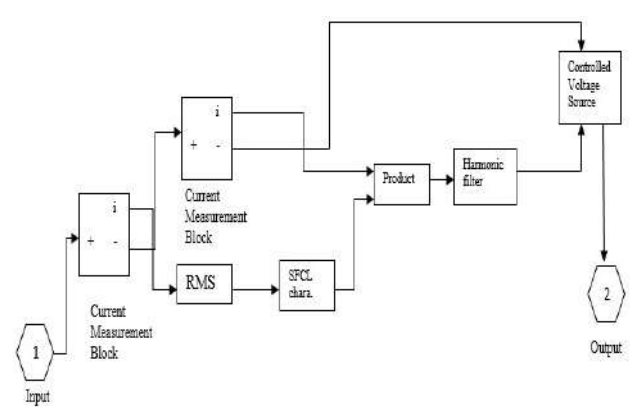


Fig. 3 Resistive SFCL model [1].

C.Case study and Results Analysis

Four possible scenarios of SFCL's locations were analysed for different faults occurring in Distribution grid system. This is the analysis of fault current at interconnection point of wind farm when we put SFCL at different locations and three phase fault at distribution grid. This study shows that best suitable location for SFCL is at interconnection point to reduce wind farm fault current.

Case Study 1: Three phase to Ground fault at Distribution Grid

Fig.4 shows comparison of waveforms of fault current of wind farm for the different SFCL locations. It is easy to decide the feasible location of SFCL from the waveforms of fault current. The SFCL can be location where maximum fault current reduction can be found. In Fig. 4, Graph A shows the large fault current when SFCL is not used in this system for a LLL-G fault occurred at distribution grid. Graph B and C indicate the same fault current occurred at the SFCL at substation (locations 1) and at branch network (Location 2) respectively and slightly greater than graph A. Graph D shows less fault

current when SFCL is at integration point (location 3) than SFCL at location 1 and 2. Graph E shows SFCL at combined location 1 and 4 (at wind farm) where the fault current is higher than SFCL at location 3. So over all SFCL at integration point (location 3) is feasible for wind farm fault current reduction.

Case Study 2 : Single Line to Ground fault at Distribution Grid

The analysis of variation in fault current when single line to ground fault occurred at distribution grid system for the different SFCL locations is shown in Fig. 5. Graph F shows that without SFCL less current flows than SFCL is placed at substation (location 1) graph G. Graph H and I shows the fault current when SFCL at branch (location 2) and at integration point(location 3) respectively. It observed that fault current is minimum at location 3. In this case, when SFCL at combined location 1 and 4 (at wind farm), graph J shows the maximum fault current reduction than graph H and I. So feasible location of SFCL is at 1 and 4 combined that the fault current of wind farm is reduced.

Case Studies of Three phase LLL-G and L-G fault at distribution grid gives brief information as

For the symmetrical three phase-to-ground fault SFCL is located either at location 1 or location 2. It is found that fault current of wind farm is

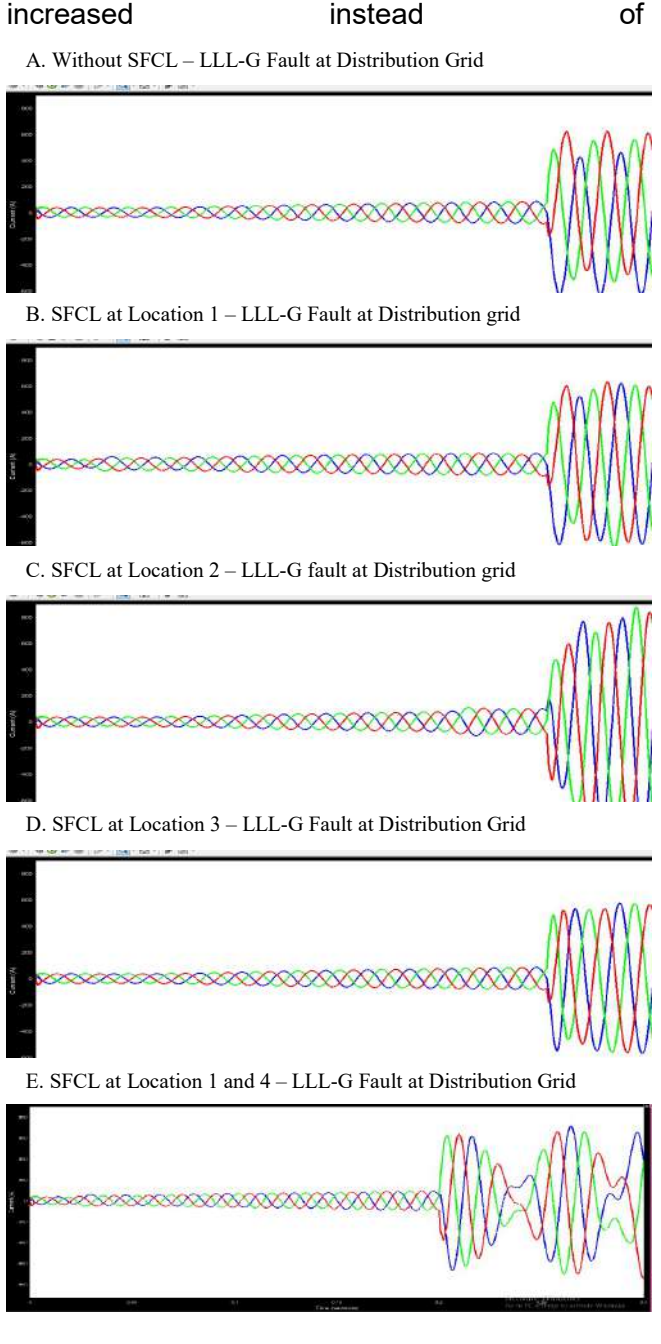
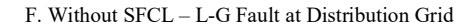
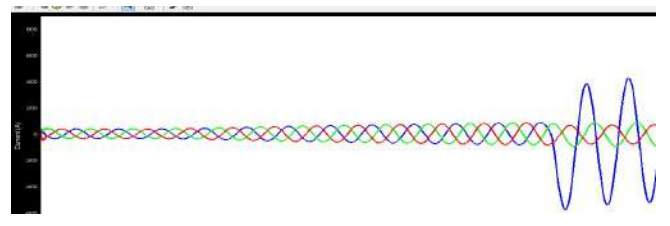
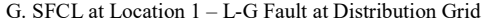
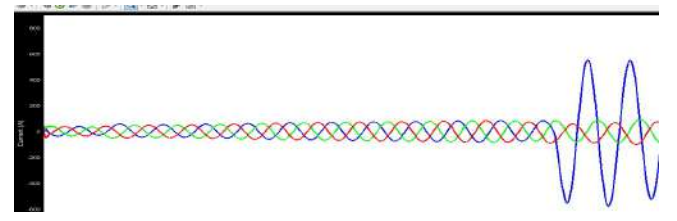


Fig. 4 Comparison of the wind farm fault current for four SFCL locations and Without SFCL for LLL-G fault at Distribution Grid

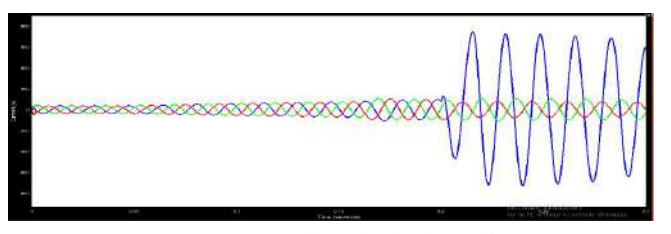




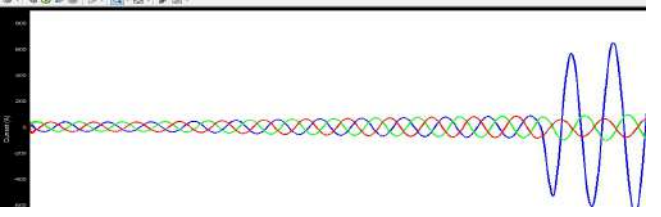




H. SFCL at Location 2 - L-G Fault at Distribution Grid



I. SFCL at Location 3 – L-G Fault at Distribution Grid



J. SFCL at Location 1 and 4 - L-G Fault at Distribution Grid

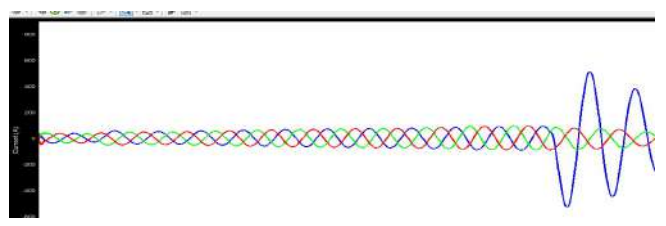


Fig. 5 Comparison of the wind farm fault current for four SFCL locations and Without SFCL for L-G fault at Distribution Grid

decreasing so these locations of SFCL is not preferred. For the location of SFCL at integration point of wind farm, it is found that grid fault current magnitude is reduced than the combination of locations of SFCL at 1 and 4. When SFCL is not placed in the grid connected power system fault current occurred is large that affects the whole grid. So it is more advantageous to place SFCL at location 3 i.e. at integration point effect of fault current is minimum. Table 2 shows variation in fault

currents of wind farm integration point for different locations of SFCL. For the single line-to-ground fault at distribution grid shown in block diagram i.e. Fig. 2. Triggering fault current is taken as 150A. For SFCL at location 1, 2 and 3 L-G fault current

Table 2. Change in Wind Farm Fault current for the different locations of SFCL

the different lo	oduono oi	0, 0		
Fault	Distribu	tion	Distribut	tion
loc.	Grid		Grid	
	`LLL-G	Fault	L-G	fault
SFCL loc.	current		current	
	(A)		(A)	
Location 1 at	640		440	
substation				
Location 2 at	800		460	
branch				
network				
Location 3 at	570		510	
integration				
point				
Location 1	600		410	
and 4				
combined				
No SFCL	760		550	

is more than at combined location of 1 and 4. Effectiveness of fault current reduction is found at combined location of 1 and 4 of SFCL. This scheme analyses effective locations of SFCLs to limit the fault current of wind farm.

D. Conclusions

The resistive superconducting fault current limiters has an inverse current-time characteristics. The study carried out for the resistive type SFCL with symmetrical faults in a three phase system and unsymmetrical fault of a single line-to-ground fault. The paper shows analysis of the Current-Time characteristics of resistive type SFCL for LLL-G and L-G fault conditions and fault current at different locations. The paper presented convenient positioning of SFCL in different locations in grid connected power system for the analysis of change in fault current of wind farm. It observed that use of SFCL can reduce large fault currents to a lower level so that the lower rating of circuit breakers can be used in the system. The optimal position of SFCL identified is at integration point of wind farm and distribution grid system which limit the fault currents effectively. The study confirms the

importance of SFCL in power system for selection of lower rating circuit breakers.

REFERENCES

- [1] U. A. Khan, J. K. Seong, and B. W. Lee, "Feasibility analysis of the Positioning of superconducting fault current limiters for the smart grid application using simulink and Simpowersystem," IEEE Trans. Appl. Supercond., vol. 21, no. 3.pp.2165-2169,Jun. 2011.
- [2] S. M. Blair, C. D. Booth, and G. M. Burt, 'Current -Time Characteristics of Resistive Superconducting Fault Current Limiters', IEEE Trans. Appl. Supercond., vol. 22, no. 2, pp. 5600205–5600205, Apr. 2012.
- [3] S. Nemdili and S. Belkhiat, 'Modeling and Simulation of Resistive Superconducting Fault-Current Limiters', J. Supercond. Nov. Magn., vol. 25, no. 7, pp. 2351–2356, Jun. 2012.
- [4] L. Dessaint, K. Al-Haddad, H. Le-Huy, G. Sybille, and P. Brunelle, "A power system tool based on simulink," IEEE Trans. Industrial Electron., vol. 46, no. 6, pp. 1252–1254, Dec. 1999
- [5] A. Etxegarai, A. Iturregi, M. Larruskain, I. Zamora, and P. Eguia, "Modelling and Parameterization of Resistive Superconducting Fault Current Limiters," presented at the International Conference on Renewable Energies and Power Quality (ICREPQ'17) Malaga(Spain), ISSN 2172-038 X, No.13, April 2017.
- [6] S. L. Liu, G. Longyan, B. Gang, W. Haiyun, and L. Yongtao, "The temperature dependence of the resistivity in Ba1-xKxFe2As2 superconductors," Supercond. Sci. Technol., vol. 24, no. 7, p. 075005, Jul. 2011.
- [7] J. Langston, M. Steurer, S. Woodruff, T. Baldwin, and J. Tang, "A generic real-time computer simulation model for superconducting fault current limiters and its application in system protection studies," *IEEE Trans. Appl. Supercond.*, vol. 15, no. 2, pp. 2090–2093, Jun. 2005.
- [8] W. Paul, M. Chen, M. Lakner, J. Rhyner, D. Braun, W. Lanz, and M. Kleimaier, "Superconducting fault current limiter: applications, technical and economical benefits, simulations and test results," CIGRE, Paris, France, Tech. Rep. CIGRE SC 13, 2000.

- [9] K. Maki, S. Repo, and P. Jarventausta, "Effect of wind power based distributed generation on protection of distribution network," in *IEEE Developments in Power System Protection*, Dec. 2004, vol. 1, pp. 327–330.
- [10] L. Salasoo, A.F. Imece, R.W. Delmerico, R.D. Wyatt, "Comparison of superconducting fault limiter concepts in electric utility applications", IEEE Transactions on *Applied Superconductivity*, vol. 5, pp. 1079-1082, 1995.

Effects of Load Dynamics on a Solar Photovoltaic Panel Fed Power Electronic System

Aranya Bandyopadhyay and Sukanya Parui

Department of Electrical Engineering

Indian Institute of Engineering Science and Technology, Shibpur

P.O. Botanic Garden, Howrah-711103, India

Corresponding author's email: aranya.rs2016@ee.iiests.ac.in

Abstract - One fundamental impact of change in energy mix is the increasing penetration of power electronic systems in the microgrid and main grid. In cascaded power electronic converters tightly regulated downstream converters behave as constant power load (CPL) to the upstream converters and cause negative impedance instability. A practical load in power electronic system consists of different combinations of constant power, impedance, voltage and current sources. This paper explores the dynamical behavior of a solar photovoltaic panel fed boost converter connected to a mixture of linear resistive and nonlinear constant power load under perturb and observe maximum power point tracking control mechanism. The switched nonlinear modeling incorporates the nonlinearity of source, load, power electronic converter and controller. One striking observation is the absence of the commonly observed fast-scale period-doubling bifurcation reported previously in similar systems. Bifurcation diagrams have been plotted in terms of load parameters to indicate a panoramic view of system's behavior. Chaotic, DCM, slow-scale and negative impedance instability have been observed.

Keywords – Constant power load; stability analysis; slow-scale instability; negative impedance instability; dc microgrid; boost converter.

INTRODUCTION

The primary impacts of change in energy mix are caused by the increasing penetration of renewable energy sources and various types of nonlinear and power-electronic loads in the main grid and microgrid. Installed capacity of renewable energy has seen a growth 36.5 GW in March 2014 to 74.8 GW in November 2019 contributing to 20% of India's total capacity [1]. However, due to low capacity utilization factor, share of generation mix has increased from 5.6% to 7.8% in the same period. Installed solar power capacity has seen an average annual growth of over 70% and has increased from 2.6 GW in March 2014 to 26 GW in December 2018. With this increase, power electronic converter dynamics is becoming more and more pronounced in the distributed power

system and microgrid dynamics, as they are required extensively for facilitating operations such as processing the obtained power and extracting maximum power from the renewable energy sources as well as for grid connection and supplying variety of loads. Cascaded power electronic converters help in maintaining desired point-of-load regulation [2].

Unfortunately tightly regulated downstream converters with one-to-one voltage-current characteristic as well as electric motor drive loads with one-to-one torque-speed characteristic behave as a constant power load (CPL) which exhibits negative impedance instability and tend to destabilize upstream converters.

Usually each converter is analysed, modeled, designed and controlled in an individual manner for a stand-alone operation while being supplied from a well regulated source and feeding a resistive or constant impedance load only [3]. However the dynamics of inter-connected and cascaded converters can be drastically different from the individual converters. Due to the complexity in modelling and simulating multi-converter power electronic systems, linearized averaged and reduced order model are employed instead of the switched nonlinear models. In a multi-converter power electronic system, two main types of loads can be seen which are constant voltage load and constant power load. Stability of such a system can be assured without implementing a stabilizing controller only when the power of the constant voltage load is greater than that of the constant power load [4].

Ref. [5] reported transient stability analysis in AC distribution system for various relative combinations of CPL and induction motor and concluded that CPL has the most destabilizing effects among all the load types.

Ref. [6] was first to report fast-scale period-doubling bifurcation where the same state repeats after two clock cycles in a solar photovoltaic (PV)

panel fed boost converter with resistive load by considering the nonlinearity of the nonlinear current source as well as the nonlinearity arising due to feedback controlled switches in boost converter. Stability of the period-1orbit was lost with variation in solar photocurrent, load resistance and current reference values. Later, Ref. [7] reported period-doubling bifurcation with border increasing collision with values of photocurrent and battery voltage in a solar PV panel fed current mode controlled boost converter acting as a battery charger system. Both smooth and non-smooth period-doubling bifurcation with variation in proportional gain parameter values for different bus voltage levels were observed [8]. Unlike the previous two works, input capacitance of the boost converter was taken into consideration.

Period-doubling bifurcation in a solar PV panel fed Ćuk converter with fractional open-circuit voltage maximum power-point tracking (MPPT) control and connected to constant impedance, voltage and current loads was observed [9]. As the solar irradiance and the load parameters often changes uncontrollably and abruptly delimiting the parameter space for stable sub-harmonics free operation and identifying the critical parameter values of onset of instability is of importance from practical and design perspective which has been facilitated in this study. Both fast-scale and slow-scale bifurcations in a similar system with resistive load, with increase in controller parameters, K_p and K_i respectively were reported also [10].

Regulated dc source fed boost converter is not globally stable under constant power loads [11]. Based on a large signal analysis with state feedback control, the authors observed two equilibrium points. The region of convergence did not include the origin and hence for such a system having a pure constant power load, the "start-up process" i.e., initial conditions play a vital role. A boost converter connected to a combination of resistive and CPL was stabilized by a feedback linearization method [12]. It would be pertinent to mention in this regard that a boost converter with a CPL is inherently an unstable system due to the existence of a RHS pole and zero. A plethora of passive and active methods exist in literature for stabilizing the negative impedance instability problem which reduces system damping, equivalent system resistance, stability margins and may results in high inrush current, limit cycle oscillation, voltage collapse in microgrid [13][14].

In a realistic multi-converter system, the load is not a pure load of any kind, be it constant power load, constant impedance load, constant voltage or constant current load. The load exists as a combination of the four basic types which varies from time to time. There remains a lacuna in present literature to ensure stability of power electronic converters and systems when they are feeding a mixture of linear and nonlinear loads instead of pure resistive load or pure CPL. Here stability is defined as the subharmonic and negative-impedance instability free behavior where same state repeats exactly after one switching clock cycle.

In this study, CPL stabilization scheme has not been implemented to focus and explore the basic CPL dynamics.

This paper is organised as follows: First, the power electronic system under investigation is described and the selection of this particular system is justified. Then, the dynamical behaviors exhibited by the system are explored. After discussing some crucial points based on the witnessed behavior concluding remarks are presented.

SYSTEM DESCRIPTION

A. Modeling of Solar PV Panel:

The solar PV panel has been implemented by the single diode model whose *v-i* characteristic is described by the following transcendental equation:

$$I_{ph} - I_o \{ e^{\frac{q}{\gamma kT}(v_{pv} + i_{pv}R_s)} - 1 \} - \frac{v_{pv} + i_{pv}R_s}{R_{sh}} = i_{pv}$$
(1)

By using Newton-Raphson method and by employing algorithms like Trust-region, Trust-region Dogleg, Levenberg-Marquardt etc. the above equation can be solved. Here $q=1.6\times10^{-19}$ coulomb which is the charge of an electron, $k=1.38\times10^{-23}$ J/K being the Boltzmann's constant, T is the absolute temperature, γ is diode ideality factor and I_0 is saturation current of the diode.

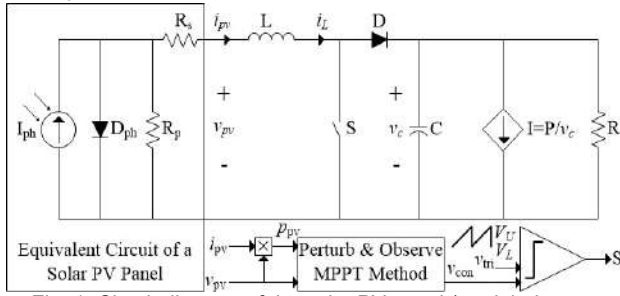


Fig. 1. Circuit diagram of the solar PV panel (modeled as a single diode model) fed boost converter supplying constant power and constant impedance load with P&O MPPT control method

B. Power Circuit:

For processing and extracting maximum power from solar photovoltaic (PV) panels dc-dc

converters are mostly employed whose selection depends on various factors [15]. The widely used boost converter has been considered here which satisfies conditions such as continuous input current characteristics facilitating accurate tracking of the MPP, low cost and complexity, low passive component count, low input current ripple, ability to provide continuous input-output energy flow, same output voltage polarity, simple low-side and low-cost driver circuit requirement etc. However inability to track MPP efficiently under all irradiance, temperature, load conditions and all over the VI curve along with limited inclination angle constitutes some disadvantages of boost converter for this purpose.

Boost converter toggles between two LTI statespace subsystems based on the switching signal. The state-space equations representing the dynamics of the boost converter are mentioned below:

$$\frac{di_{pv}}{dt} = \frac{v_{pv}}{L} - \frac{v_c}{L}(1-d)$$

$$\frac{dv_c}{dt} = \frac{i_{pv}}{C}(1-d) - \frac{v_c}{RC} - \frac{P}{v_cC}$$

which are solved numerically by the Runge-Kutta method. Here *d* is the duty cycle.

C. Control Circuit:

Extraction of maximum power from the solar photovoltaic panels is facilitated by various MPPT methods whose selection depends upon factors like ease of implementation, no, of sensors, ability to track true maxima in the presence of multiple local maxima caused by partial shading, cost, reliability, application requirement, convergence speed etc. [16]. The widely used perturb and observe (P&O) MPPT has been considered in this study. This control method is characterized by several advantages like low implementation complexity, possibility of both analog and digital implementation, no dependency upon the solar panel parameters and characteristics and a true MPPT mechanism. However, the requirements of voltage as well as the costly and bulky current sensor, inability to track the MPP in a rapidly varying environmental condition are some notable disadvantages of this method.

Here, frequency of the sawtooth carrier signal sets the clock frequency of this non-autonomous system.

TABLE I (TITLE: POWER AND CONTROL CIRCUIT PARAMETERS' NOMINAL VALUES)

SI. No.	Power Circuit Parameters	Control Circuit Parameters
1.	Solar Photocurrent (I _{ph})=	$V_L = 0V$

	1A	
2.	Inductor (L) = 3 mH	$V_U = 1V$
3.	Capacitor (C) = 20 μF	Clock Frequency (f) = 10 kHz

DYNAMICAL BEHAVIOR OF THE SYSTEM:

Now the nonlinear switched model will be simulated to give a glimpse of the possible dynamical behaviors and in the exact simulation model all the nonlinearities will be considered and modeled which arises due to:

- a) Nonlinear current source
- b) Nonlinear feedback controlled boost converter
- c) Nonlinear constant power load
- d) Nonlinear P&O MPPT controller.

Since, the objective of this work is to explore the effect of load dynamics on the overall system, the case of constant power load and constant impedance (resistive) load will be dealt with individually while the solar photocurrent is assumed to be constant. After that the combined effect of both constant power and impedance load will be considered.

At first, the system with only resistive load is investigated. For lower values of resistance, stable period-1 behavior with low THD can be seen as shown in Fig. 2. (a) and (b) for R= 15Ω . However with increase of resistance, slow scale oscillations set in. The wideband frequency spectrum with slightly higher THD can be termed as a type of chaotic behavior for R= 50Ω .

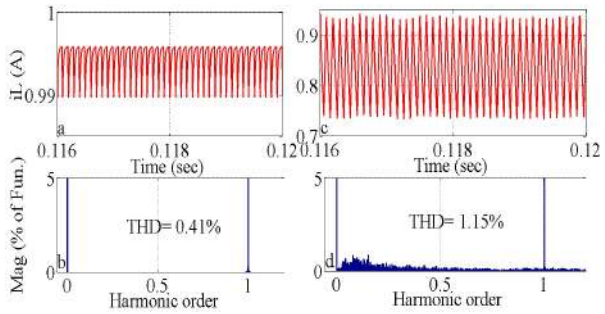


Fig. 2. (a) & (b). Inductor current (i_L) waveform and FFT plot for R= 15 Ω ; (c) & (d). i_L waveform and frequency spectrum for R= 50 Ω .

Then the dynamics of the system with only constant power load is investigated. The system exhibits chaotic behavior for low values of P. In this system, the maximum power that can be extracted from the solar PV panels is 12.9 W. From 11 W to 12.8 W, stable period-1 behavior can be witnessed with low THD. Hence a critical condition arises if the load demand exceeds the supply demand and the system collapses with load current $\rightarrow \infty$ and load voltage $\rightarrow 0$ in an exponential fashion.

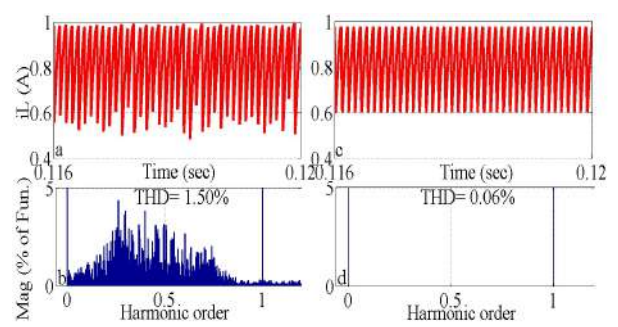


Fig. 3. (a) & (b). Inductor current (iL) waveform and FFT plot for P= 4W; (c) & (d). iL waveform and frequency spectrum for P= 11W.

Now the bifurcation diagrams are plotted to give a panoramic view of the system's dynamical behavior over a wide parameter space as shown in Fig. 4. It is plotted by sampling the value of inductor current at the beginning of every clock cycle when the system has reached steady state condition. Stable period-1 behavior can be observed with resistive load which gives way to slow-scale oscillation of very small amplitude with increasing load resistance. For low values of CPL, chaotic behavior with relatively higher THD, DCM behavior and behavior with long transient condition have been observed.

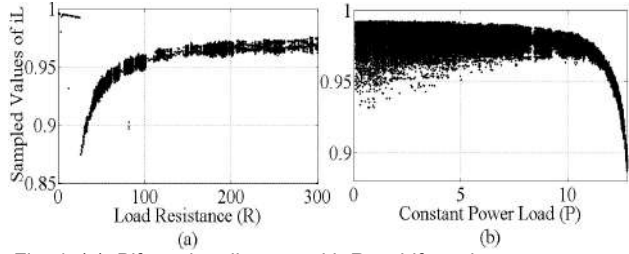


Fig. 4. (a). Bifurcation diagram with R as bifurcation parameter. (b) Bifurcation Diagram with P as bifurcation parameter.

Fig. 5. Shows the complete dynamical behavior where the solar PV panel is supplying a mixed load of CPL and parallel resistive load (R). CPL has been given a parametric swing while R is kept constant. THD decreases with increasing P and a slow-scale oscillation cycle with minor amplitude has been detected. Beyond P=12.1W the system collapses with exponential load current rise.

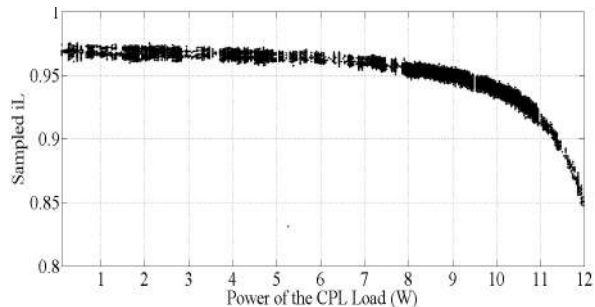


Fig. 5. Bifurcation diagram with constant power (P) as the bifurcation parameter for R=300 Ω

DISCUSSION

Period-doubling bifurcation has been reported so far as the predominant phenomenon in solar panel fed boost converter. Ref. [6], [7] took into consideration the nonlinearity of the solar PV panel along with the nonlinearity of the boost converter while linear controllers were implemented. The authors stated that stable zone of operation extended due to the interaction between these two types of nonlinearities. Ref. [8] contradicted with the previous authors and stated that nonlinearity of the solar PV panel and the MPPT have no or little impact upon the period-doubling bifurcation. The authors' logic behind this argument was that the dynamics of MPPT controller is slower than the fast switching dynamics of the converter. In case of a solar PV panel fed Ćuk converter with the linear fractional open-circuit voltage MPPT controller and feeding linear loads, period-doubling bifurcation was once again observed predominantly [9][10].

In the present system under investigation, in addition to the source and switching converter nonlinearity, the nonlinearity of the load and MPPT controller have been considered. The argument made by the authors of reference [8] contradicts with the observations in this work. The behavior has been devoid of fast-scale instabilities which had been witnessed in similar systems till date and that may be attributed to the nonlinear P&O MPPT controller which is a dynamic and true MPPT controller. Slow-scale, chaotic behavior along with DCM behavior were witnessed. Hence, the incorporation of the additional nonlinearities of the switched nonlinear modeling of this practical and widely used system has thrown some insights into its dynamics.

CONCLUSION

Dynamics of a solar PV panel fed boost converter has been investigated by constructing an exact switched nonlinear model and by considering all the source, load, switching converter and controller nonlinearities. The absence of fast-scale period-

doubling bifurcation in this widely used practical system is notable. Chaotic, DCM, slow-scale and negative-impedance instability have been witnessed. Future scope of work involves extensive analysis, corroboration of simulation results with analytical and hardware results where the combination all the four basic linear and nonlinear load types as well as other practical nonlinear loads will be considered.

REFERENCES

- [1]P. Bhati et al., The State of Renewable Energy in India 2019 A Citizen's Report, Centre for Science and Development, 2019.
- [2]S. Singh, A. R. Gautam and D. Fulwani, "Constant Power Loadsand Their Effects in DC Distributed Power Systems: A Review", in *Renewable and Sustainable Energy Reviews*, vol. 72, pp. 407-421, May 2017.
- [3]A. Emadi and M. Ehsani, "Multi-converter Power Electronic Systems: Definion and Applications", 2001 IEEE 32nd Annual Power Electronics Specialists Conference, Vancouver, Canada, June 2001, pp. 1230-1236.
- [4]J. Yang and Y. Wang, "A Review of the Effects of Distributed Energy Resources and Power-electronic Controlled Loading on Distribution Network Stability", 2014 IEEE 9th Conference on Indistrial Electronics and Applications (ICIEA), Hangzhou, China, June 2014, pp. 2029-2034.
- [5]M. Molinas, D. Moltoni, G. Facsendini, J. A. Suul and T. Undeland, "Constant Power Loads in AC Distribution Systems: an Investigation of Stability", 2008 IEEE International Symposium on Industrial Electronics, Cambridge, United Kingdom, June-July 2008, pp. 1531-1536
- [6]A. Abusorrah et al., "Stability of a Boost Converter Fed From Photovoltaic Source", in *Solar Energy*, vol. 98, pp. 458– 471, December 2013.
- [7] M. M. Al-Hindawi et al., "Nonlinear Dynamics and Bifurcation Analysis of a Boost Converter for Battery Charging in Photovoltaic Applications", in *International Journal of Bifurcation and Chaos*, vol. 24, no. 11, pp. 1450142 1- 1450142 12, November 2014.
- [8] M. Zhioua et al., "Modelling, Dynamics, Bifurcation Behavior and Stability Analysis of a Dc-dc Boost Converter in Photovoltaic Systems", in *International Journal of Bifurcation and Chaos*, vol. 26, no. 10, pp. 1650166 1-1650166 16, September 2016.
- [9] A. Bandyopadhyay and S. Parui, "Bifurcation Behavior of Photovoltaic Panel Fed Ćuk Converter Connected to Different Types of Loads", in 2018 International Symposium on Devices, Circuits and Systems (ISDCS), Howrah, India, March 2018, pp. 1-5.
- [10] A. Bandyopadhyay and S. Parui, "Dynamical Behavior of Cuk Converter Fed from a Photovoltaic Source", in *IEEE Calcutta Conference*, Kolkata, India, December 2017, pp. 397-402.
- [11] C. Rivetta and G. A. Williamson, "Global Behaviour Analysis of a Dc-dc Boost Power Converter Operating with Constant Power Load", 2004 IEEE International Symposium on Circuits and Systems (ISCAS), Vancouver, Canada, May 2004, pp. V956-V959.
- [12] S. Arora, P. Balsara and D. Bhatia, "Input-output Linearization of a Boost Converter with Mixed Load (Constant Voltage Load and Constant Power Load)", in

- IEEE Transactions on Power Electronics, vol. 34, no. 1, pp. 815-825, January 2019.
- [13] M. Cespedes, L. Xing and J. Sun, "Constant-Power Load System Stabilization by Passive Damping," in *IEEE Transactions on Power Electronics*, vol. 26, no. 7, pp. 1832-1836, July 2011.
- [14] E. Hossain, R. Perez, A. Nasiri and S. Padmanaban, "A Comprehensive Review on Constant Power Loads Compensation Techniques," in *IEEE Access*, vol. 6, pp. 33285-33305, 2018.
- [15] G. Dileep, and S.N. Singh, "Selection of Non-isolated Dc-dc Converters for Solar Photovoltaic System," in Renewable and Sustainable Energy Reviews, vol. 76, pp. 1230-1247, September 2017.
- [16] T. Esram and P.L. Chapman, "Comparison of Photovoltaic Array Maximum Power Point Tracking Techniques", in IEEE Transactions on Energy Conversion, Vol. 22, No. 2, June 2007.

A review of recent trend in electroless duplex Nano Composite coatings on Advance Materials

Rajsekhar Chakrabarti¹, Pradipta Basu Mandal²

ABSTRACT

Various surface modification methods such as electro/electroless plating, thermal spray coating and physical and chemical vapor depositions, are existing to-date to advance surface behavior of mechanical components in oil and gas, automobile, aerospace and chemical industries. During the electroless process of salt containing metal ions in solution, are catalytically reduced and deposited onto metallic substrates. The plating strongly depends on process parameters i.e. concentrations of complexant (e.g. mono-carboxylic acid), accelerators (e.g. HCl, PdCl₂, AgCl), reducing agent (e.g. NaPO₂H₂), stabilizer (e.g. Pb, Sn, etc.), buffer (e.g. Sodium salt of complexants), pH and temperature of electroless bath. Recently, the development of electroless coating of metalion, alloy, and composite coatings on various metal/non-metal surfaces has witnessed enormous interest among researchers due to corrosion and abrasive wear resistance and excellent physical, mechanical, electrical properties. Various studies have been carried out by depositing duplex composite coatings using micro/nano reinforcement have shown promising properties to enhance the corrosion resistance.

Keywords: Electroless duplex coatings, Co-deposition, SEM, Vickers Hardness test Corrosion.

1. INTRODUCTION

Electroless (EL) Ni-P coatings have been used increasingly in various industries since the early 1980's. Some of the characteristics of the coatings exhibit excellent corrosion and wear resistance, uniformity of thickness as well as enhance mechanical and physical properties. Ni-P coatings are widely used as protective or decorative coatings in many industries including petroleum, chemical, plastic, optics, aerospace, nuclear, printing, mining, automotive, electronics, computer, textile, and food processing. Further paper, improvement of properties of Ni-P coating has been observed by using the addition of second phase hard particles i.e. diamond, SiC[6], B₄C [29], Si₃N₄ [2,28], CeO₂ [28], TiO₂ [5], Al₂O₃,[9] etc. At low temperature, during codeposition technique of suspended hard particle or non-metallic particles embedded physically on Ni-P matrix. Adherence of the particles on the metal matrix improved by thermal treatment increases corrosion and mechanical properties of the deposited layers. Codeposition of the particles relies upon size, shape, concentration, and density in the electroless bath. The composite coating method relies on the electric charges of the particles [7-9]. Fig.1. shows the schematic diagram of the apparatus used for EL coating.

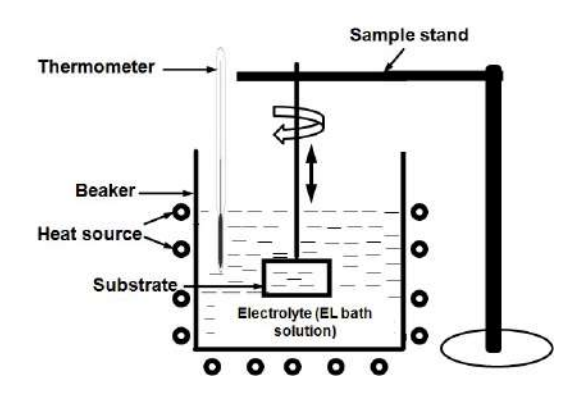


Fig.1. Schematic diagram of the apparatus used for EL coating.

2. BACKGROUND

J.N. Pang et al worked with Ni coating on surface of nanosized Al₂O₃ particles. The size of nickel particles adhering to the surface of the Al₂O₃ particles were about 50-80 nm. It is found that the SnCl₂ sensitization process and the subsequent PdCl₂ activation technique

¹ Assistant Professor, Department of Mechanical Engineering, Techno India University, Kolkata, Pin -700091, West Bengal, India

²Assistant Professor, Department of Mechanical Engineering, Techno India University, Kolkata, Pin -700091, West Bengal, India

monitored the formation of Ni layer on alumina particles[1]. Electroless coating of Ni-P-Cg-SiC on steel piston ring has been performed. The micro hardness has been improved drastically due to the existence of SiC particles. Crystallization of hard Ni₃P phase after heat treatment increased the hardness. As graphite particle intruded in Ni-P coating, it reduced frictional co-efficient due to a loose coating of Cg particles on the surface[6]. Serin et al. (2015)[7] reported that for electroless Ni-B-Mo Coatings the corrosion resistance and thermal stability have improved at the higher temperature due presence of molybdenum which retains its ductility. The morphology of the as-plated coating presented small localized corrosion regions (black spots). The hardness and wear resistance increased with high temperature due to complete crystalline structure [7]. Ni-W-P was deposited on the mild steel substrate using electroless plating by varying sodium tungsten concentration. Better micro hardness and anti fouling property indicated due to tungsten content. Cheng et al. presented that higher tungsten content increases the crystallization temperature [8]. Mild steel has been coated with Ni-P-Al₂O₃ composite coatings[9]. Effect of concentration of nickel source, the concentration of reducing agent, the concentration of Al₂O₃ particles, and annealing temperature have been studied on the hardness of Ni-P- Al₂O₃ composite coatings. The hardness of the composite coating increases significantly after 300°C due to precipitation of Ni₃Pparticles[15].Higher temperatures increase the growth of nickel grains and Ni₃P particles, which has resulted in softening of the Ni-P coating. The increase in hardness of surface coating after the heat treatment at 400 °C and above was due to 1) dispersion strengthening of hard particles and 2)precipitation strengthening of Ni-P alloy[9]. The mixture state of amorphous and crystalline will transform into pure crystalline phase provided after heat treatment. Aluminum 7075 substrate was used for the preparation of electroless Ni-P/Ni-B duplex coatings. The surface morphology of the duplex coatings was revealed the formation of well-developed crystallites[10]. The roughness and hardness increased with Al₂O₃ particles content[9]. A comparative study has been performed for Micro hardness of duplex coating for different substrates. The Vickers hardness for stainless steel, Al alloy, and Mg alloy has been

compared in Fig.2. Subramanian C et al.found some pores in the coatings at the initial deposition stage which may be resulted from the evolution of the hydrogen during the electroless Ni-P coating[10]. The smaller grain of the coating and the Cu in the Ni-Cu-P coating was helpful for the adsorption of the polar groups of the organics in bio-oil on the worn surfaces which led to excellent frictionreducing effect. Yufu Xu et al. found the sliding speed was increased from 0.5 m/s to 1.0m/s, and a reduced frictional coefficient at stable stages [11]. Many researchers investigated the electroless micro and nano coating with Al₂O₃ particles with different substrate. Co-deposition of Al₂O₃ particles in electroless nickel has been attempted by many researchers and the co-deposition continues to be at the experimental stage. Adhesion is an interfacial property and vital in figuring out the durability of thin coatings. Within the subject of surface chemistry, adhesion is a fundamental parameter and in detail associated with wear [15]. The alumina is broadly used for the excessive elasticity modulus, the high potential of maintaining at high temperatures, and the superb wear resistance. Table 2, illustrates different types of baths and operating condition of Various Duplex coatings

3. Electroless nickel duplex coatings on different substrate

3.1 Plating onto Magnesium

Selvi et al.[23] proposed a process involving Autocatalytic duplex Ni-P/Ni-W-P coatings AZ31B magnesium alloy. Coatings characterization was performed for surface morphology, corrosion resistance composition. The phosphorous content was investigated by EDX testing and found that it was decreased from 6 % to 3% due to the codeposition of tungsten in the coating. FESEM test for the coated samples was performed and found that the morphology of the surfaces was nodular in nature. Potentiodynamic polarization test was performed in 0.15 M NaCl solution for corrosion resistance behaviour of the coatings.

3.2 Plating on Aluminium alloy substrate

Protective nickel—phosphorous coating is required on aluminium substrate before nickel-boron plating. The purpose of Ni-P coating is due to the fact that sodium borohydride is highly unstable in acidic media, so the plating

bath usually should have alkaline (pH higher than 9) in nature. Due to this, electroless nickel-boron coatings can only be deposited on aluminium as duplex electroless NiP/NiB coatings, with Ni-P as the inner layer. Specific treatments were thus developed to increase properties of electroless nickel-boron coatings without detrimental effects on the resistance of aluminium substrate [2,12,13]. properties of electroless nickel-boron coatings on aluminium alloys have been studied before [2,12,13] but there are few works focusing on the corrosion resistance of those systems [14]. The properties and corrosion resistance of duplex NiP/NiB coatings have been studied before on steel substrates [10]. On aluminium alloys, the mechanical properties of this duplex coating are similar to what is obtained on steel with NiB. However, their corrosion behaviour is still unknown on aluminium.

3.3 Plating on mild steel substrate

Low carbon steel discs are coated with Ni-P-WS₂ which results in change in the surface morpholology of the coating[30]. The surface morphology of Ni-P coating is nodular with a cauliflower-like structure but smoother than Ni-PWS2 coating that is rough with some porosity. Heat treatment of this composite coating converted the background to a crystalline structure. For some electroless composite coatings, it has been reported that heat treatment produced new peaks due to the reaction between composite particles and based elements (such as Ni and P). Such incidence was not observed in Ni-P-WS2 composite coatings, because tungsten disulfide possesses a rather high thermal stability, and heat treatment at 400°C caused no decomposition reaction[30]. The reduction in coating hardness due to the presence of WS2 solid lubricant particles was estimated at about 60% which is similar to other soft composite particles as reported, for example, in Ni-PPTFE coating. From Table 1, coating thickness of different Duplex coatings on different metal alloy substrate has been illustrated.

Table 1: Coating thickness of different Duplex coatings

Specimen	Substrate	Thickness, t
		(μm)
Duplex (Ti,	AISI H13 Steel	2.6–2.7

Duplex NiP/NiB(27)	2024 aluminum alloys	25
Duplex Ni-P- ZrO2/Ni-P(25)	Stainless steel	22
Duplex Ni– P/Ni–W–P (23)	AZ31B magnesium alloy	25-30
Duplex Cr–N (24)	AISI H13 Steel	2.0–2.1
Al)N (24)		

Table 2: Different types of baths and operating condition of Various Duplex coatings

condition of V	condition of Various Duplex coatings					
Ni-P	NiSO4,6H2O (10g/L)	pH 7.1				
plating[23]/ All	$Na_2H_2PO_2,H_2O$ (9 g/L)	80–82 °C				
	$NaC_2H_3O_2$ (5 g/L)	45 min				
	HF (40%, v/v) (10 g/L)	Mild magnetic				
	NH ₄ HF ₂ (20 g/L)	Stirring				
	Thiourea (1 g/L)					
Duplex Ni–P /Ni–P–ZrO2	NiSO ₄ ,6H ₂ O (15 g/L)	PH: 6.0–6.4				
[25]/ AZ31	NaH ₂ PO ₂ ,H ₂ O (14	Agitation: 200 rpm				
magnesium alloy	g/L)	Temperatur e: 80 ± 2 °C				
	CH ₃ COO Na (10-15 g/L)	Time: 60 min				
	Thiourea (1 g/L)					
	ZrO ₂ sol (variable)					
Duplex Ni-P	NiCO ₃ (10 g/L)	pH 7				
/Ni–W–P [25]	HF(48%) (9 g/L)	82 ± 2 °C				
/ AZ31B	Citric acid (5 g/L)	1.15 h				
magnesium	NH ₄ HF ₂ (10 g/L)	Mild magnetic				
alloy	Na ₂ H ₂ PO ₂ ·H ₂ O (25 g/L)	stirring				
	Na ₂ WO (12 g/L)					
	NH ₃ ·H ₂ O (30 g/L)					
Duplex Ni- P/Ni-	NiCl ₂ ,6H ₂ O (0.127mol/L)	pH >13				
B[21][22]/20 24 aluminum	C ₂ H ₈ N ₂ (1.5 mol/L)	Temperatur e 85 ±2°C				

alloys NaBH₄ (0.021 mol/L Time 4 h
)
Thiourea (2.25 mol/L
)
NaOH (1.32E-mol/L)

4.1Microhardness

Many researchers have been observed that Ni-P/Ni-B duplex coating improved the hardness of 2024 Al alloy to 854Hv and further improved to 1014Hv after heat treatment (for 4 h under Ar avoiding oxidation, at 180 °C) [22]. Heat treatment improves the hardness by refining grain structures and makes pure crystalline structure of the coating. Researchers made experiments on Mg alloys by developing a duplex coating. Microhardness of various duplex coating is shown in fig.2. for different metal alloy substrate. The base Mg alloy had a hardness value of 100Hv.Hardness behavior of Mg alloy has been widely investigated for duplex coating of Ni-P/Ni-W-P which shows considerable change in hardness of 740Hv which is further improved to 857Hv after heat treatment [23]. When AZ31 magnesium alloy is coated with Ni-P/Ni-P-ZrO2, the hardness is increased from 640 HV to 820 HV due to the enhanced nano ZrO2 co-deposittion in the outer layer [25]. This can be explained by the larger agglomerated ZrO2 particles present in the coating which is decreasing the dispersion strengthening effect [25].

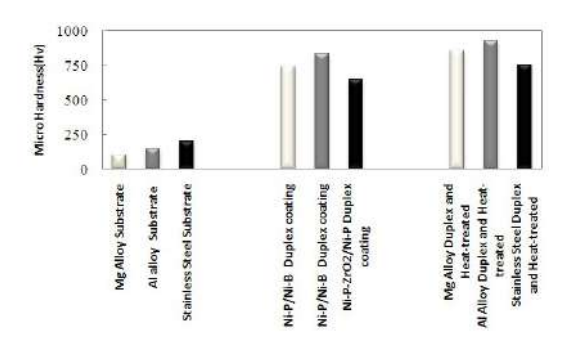


Fig. 2. Vickers hardness of duplex coating [22-25].

4.2 Wear Resistance

Various laboratory tests are conducted to estimate the wear resistance of the EL duplex coating. Wear rate is nothing but the volume of material loss per unit applied force per unit revolution. Taber wear test, pin-on-disk methods are very popular as they readily derive the material loss with their handy tool setup.In duplex coating it raises a very good chance of protecting inner coating layer of Ni-P as much wear will be encountered on the outer layer. As depicected in the following figure in fig.3. the outer Ni-W-P layer will have less erosion or material loss than inner layer of Ni-P[23]. Mild steel coated with Ni-P/Ni-W-P [23] shows poor wear resistance in Ni-P layers it shows 57×10^{-15} m³N⁻¹m⁻¹ in terms of wear rate, while the outer layer shows very less amount of wear nearly just $30 \times 10^{-15} \text{m}^3 \text{N}^{-1} \text{m}^{-1}$ in terms of wear rate. Whereas ductile iron shows much lower wear rate than mild steel and aluminum alloy defining the fact it has excellent wear resistance property [21, 22, and 23]. It can be explained due to the fact that duplex Ni-P/Ni-W-P coating exhibited less nodular, dense and smooth which improve the wear resistance compared to Ni-P coating which exhibited nodular morphologywith porosity.

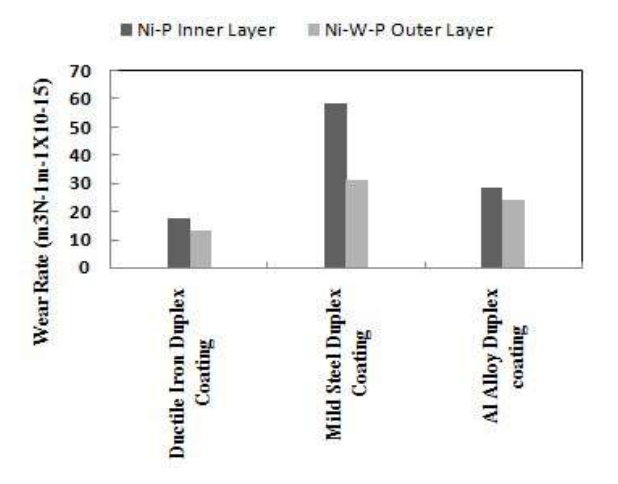


Fig. 3. Wear Rate of Duplex Coating [21, 22, 23].

4.3 Corrosion Resistant

Corrosion resistance can be measured by various available methods like salt spray test, immersion test, potentiodynamic polarization test etc. The Potentiodynamic test yields good results in the form of determining corrosion potential (E_{corr}) and corrosion current (I_{corr}) . Both of them can be correlated to form a

graphical representation (Tafel curve). The below figure fig.4. describes polarization potential of three different alloys i.e. Mg alloy, Al alloy and mild steel .The value of corrosion voltage becomes less negative and just coming near to zero shows less chance of getting corrode as they are less susceptible to chemical reaction and reaching towards a stable value. Mg alloy [21] shows less corrosion resistance than Aluminum alloy [22] and mild steel shows least protective to corrosion when they are coated with Duplex coating. Duplex coating develops inner layer and outer layer in which outer layer shows the greatest resistance to environment. corrosion Mainly potentiodynamic polarization test is carried out in an immersed bath containing 3.5% of NaCl (Brine solution).

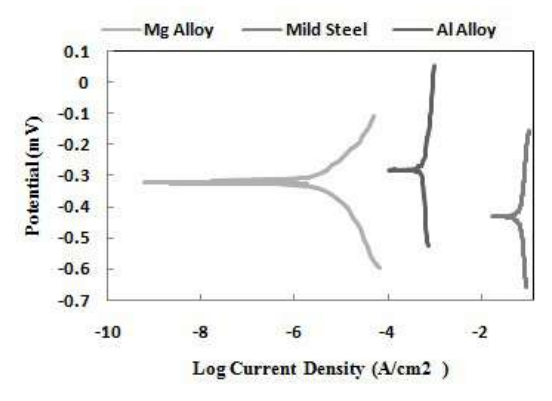


Fig. 4. Comparative polarization curves of Duplex Coating [20, 21, 22].

5. CONCLUSIONS

This review reveals that electroless Ni–P/Ni–B duplex coatings could be prepared using dual bath. SEM of the cross-sectional view of the electroless nickel duplex coatings reveals that the coatings are uniform and the compatibility between the layers is good. The microhardness of electroless nickel duplex coatings is higher than Ni–P and Ni–B coatings and between the two types of duplex coatings the coating that has Ni–B as the outer layer exhibit a higher microhardness, both in as-plated and heat-treated conditions. The specific wear rate is less for duplex coatings compared to Ni–P and Ni–B coatings of similar thickness, both in as-plated and heat-treated conditions. Among the

coatings studied, the specific wear rate is less for electroless nickel duplex coatings that has Ni–B coating as the outer layer. The wear process of duplex coatings is governed by adhesive wear mechanism, which is confirmed by the presence of torn patches and detachment of coatings.

If higher hardness and wear resistance are desired, then the duplex coating having Ni–B as the outer layer will be the ideal choice whereas the duplex coating having Ni–P as the outer layer is the preferred option where higher corrosion resistance is sought.

6. REFERENCES

- [1] Pang J.N. ,Jiang S.W. , Lin H. , Wang Z.Q., "Significance of sensitization process in electroless deposition of Ni on nanosizedAl₂O₃ powders", Ceramics International, 2016. Vol-42(3), pp. 1-7
- [2] Ulaş Matik, "Structural and wear properties of heattreated electroless Ni-P alloy and Ni-P-Si3N4 composite coatings on iron based PM compacts", Surface & Coatings Technology,2016 (302)
- [3] Popoola A.P.I. et al., "Corrosion and wear properties of Ni-Sn-P ternary deposits on mild steel via electroless method", Alexandria Engineering Journal, 2016, Volume 55(3)
- [4] Qianzhi Wang et al., "Evolution of structural, mechanical and tribological properties of Ni-P/MWCNT coatings as a function of annealing temperature", Surface & Coatings Technology 2016, Vol 6(11)
- [5] Shibli S.M.A. et al., "Development and electrochemical characterization of Ni-P coated tungsten incorporated electroless nickel coatings" , Materials Chemistry and Physics, 2016, Vol1(10)
- [6] Bahaaideen Farhad B et al. By 2010, "Electroless Ni-P-Cg(graphite)-SiC composite coating and it's application onto piston rings of a small two stroke utility engine", Journal Of Scientific and Industrial Research,2010, Vol 69, pp.830-834
- [7] Ihsan Go" khan Serin, Ali Go" ksenli, Behiye Yu" ksel, and Rasid Ahmed Yildiz By 2015, "Effect of Annealing Temperature on the Corrosion Resistance of Electroless Ni-B-Mo Coatings", Journal of Materials Engineering and Performance August 2015
- [8] Cheng Yanhai, Cao Shuai, Hou Qingqiang, Han Dongtai, Han Zhengtong, "Effect of Tungsten Addition on the Anti-fouling Property of the Electroless Ni-W-P Deposits", Rare Metal Materials and Engineering, 2016, 45(8),pp. 1931-1937
- [9] Prasanna Gadhari, Prasanta Sahoo, "Effect of process parameters on microhardness of Ni–P–Al2O3composite coatings", Procedia Materials Science 6 (2014), pp.623 632
- [10] Subramanian C., Palaniradja K., "Effect of Surfactant on the Electroless Ni-P/Ni-B Duplex Coatings on Aluminium 7075", International Journal of Metallurgical Engineering 2015, 4(2),pp. 25-32

- [11]Yufu Xu , Xiaojing Zheng , Xianguo Hu , Yanguo Yin, Tanming Lei, "Preparation of the electroless Ni–P and Ni–Cu–P coatings on engine cylinder and their tribological behaviors under bio-oil lubricated conditions", Surface & Coatings Technology 258 (2014),pp. 790–796
- [12] Naiming Lin ,Peng Zhou,Jiaojuan Zou,Faqin Xie,Bin Tang , "Wear and corrosion resistance of electroless plating Ni-P coating on P110 steel" , Journal ofMaheshkumar AR Wuhan University of Technology-Mater. Sci. Ed. June 2015
- [13]. , Manimaran C., Sudhakar G. , Suriyaprakash K. ," To Improve Wear Resistance of Magnesium Alloy by Electroless Coating in IC Engine", International Journal of Emerging Technology and Advanced Engineering, Volume 5, Issue 3, March 2015,pp.629-632
- [14] Jie Jin., Dacai Zheng., Haojie Liu.,"The corrosion behavior and mechanical properties of CrN/NieP multilayer coated mild steel",international journal of hydrogen energy,2017
- [15] H. Ashassi-Sorkhabi, H. Aminikia, and R. Bagheri, "Electroless Deposition of Ni-Cu-P Coatings Containing Nano-Al2O3 Particles and Study of Its Corrosion Protective Behaviour", International Journal of Corrosion, Volume 2014, Article ID 391502, 9 pages
- [16] Ramesh Chandra Agarwala, Vijaya Agarwala ,Rahul Sharma,"Electroless Ni-P Based Nanocoating Technology—A Review", Synthesis and Reactivity in Inorganic, Metal-Organic,and Nano-Metal Chemistry,2007
- [17] K. Krishnavenia, T.S.N. Sankara Narayanana,*, S.K. Seshadrib,"Corrosion resistance of electrodeposited Ni–B and Ni–B–Si3N4 composite coatings",Journal of Alloys and Compounds,2009
- [18] Shusheng Zhang, Kejiang Han, Lin Cheng,"The effect of SiC particles added in electroless Ni–P plating solution on the properties of composite coatings",Surface & Coatings Technology,2008
- [19] E. Matijević, A.M. Poskanzer and P. Zuman, "The Characterization of the Stannous Chloride/ Palladium Chloride Catalysts for Electroless Plating", Plating and Surface Finishing
- [20] D. Dong, X.H. Chen, W.T. Xiao, G.B. Yang, P.Y. Zhang, "Preparation and properties of electroless Ni–P–SiO2 composite coatings", Applied Surface Science, 2009
- [21]Elsa Georgiza , Jelica Novakovic, Panayota Vassiliou,"Characterization and corrosion resistance of duplex electroless Ni-P composite coatings on magnesium alloy",Surface & Coatings Technology, 2013,Page 432–439
- [22] V. Vitry, A. Sens, A.-F. Kanta, F. Delaunois,"Wear and corrosion resistance of heat treated and as-plated Duplex NiP/NiB coatings"on 2024 aluminum alloys",Surface & Coatings Technology,vol 206,2012
- [23] V. Ezhil Selvi,, Purba Chatterji, S. Subramanianb, J.N. Balaraju"Autocatalytic duplex Ni–P/Ni–W–P coatings on AZ31B magnesium alloy", Surface & Coatings Technology vol 240, 2014,page 103–109
- [24] J.C.A. Batista, C. Godoy, V.T.L. Buono, A. Matthews,"Characterisation of duplex and non-duplex (Ti, Al)N and Cr–N PVD coatings",Materials Science and Engineering,2002,page 39–51
- [25] Xin Shu, YuxinWang, Chuming Liu, Abdullah Aljaafari, Wei Gaob"Double-layered Ni-P/Ni-P-ZrO2 electroless coatings on AZ31 magnesium alloy with improved corrosion resistance", Surface & Coatings Technology, vol 261, 2015, page 161–166

- [26] T.S.N. Sankara Narayanan, K. Krishnaveni, S.K. Seshadri,"Electroless Ni–P/Ni–B duplex coatings: preparation and evaluation of microhardness, wear and corrosion resistance", Materials Chemistry and Physics,vol 82,2003,page 771–779
- [27] Cheng-Hsun Hsu, Chun-Ying Lee, Kai-Lin Chen, Jia-Hong Lu, "Effects of CrN/EN and Cr2O3/EN duplex coatings on corrosion resistance of ADI", Thin Solid Films, vol 517,2009
- [28] J.N. Balaraju, T.S.N. Sankara Narayanan, S.K. Seshadri,"Mater.Res.Bulletin 41",2006, page 847-860
- [29] Feldstein N., "Electroless Plating: Fundamentals and Application", 1990, chapter 11, William Andrew Publishing
- [30] I. Sivandipoor, F. Ashrafizadeh, "Synthesis and tribological behaviour of electroless Ni–P-WS2 composite coatings", Applied Surface Science 263 (2012) 314–319

Design and fabrication of bladeless wind power Generator using wind energy

Anish Deb¹, Sumanta Karmakar², Subhrajit Ghosh³, Sujoy Garain³, Sanjay Saha³, Prantha Kumar Das³, Santu Sar³, Bikash Bhagat⁴, Sandip Haldar⁵

Department of: (¹Mechanical Engineering, ²Electronics and Communication Engineering, ³Final year Mechanical Engineering, ⁴Third year Mechanical Engineering, ⁵Basic Science)

(Asansol Engineering College)

(Asansol-713305, India)

{Email of first author:anishdebjgec@gmail.com} {Email of corresponding author:sand-ju@yahoo.com} {Email of corresponding author: sumanta.karmakar"gmail.com}

Abstract-The design of bladeless wind power generation system is completely different from a traditional wind turbine and is a new approach to capture the wind energy with relatively very low cost of investment. The device has a fixed mast, a power generator and a hollow, light weight and semi rigid fibre glass cylinder on top which makes its construction and assembly very simple. The mast will start to oscillate due to vortex induced vibration (VIV) when wind strikes or passes through it. The vibrational energy of the mast will create kinetic energy and this energy will be transformed into electrical energy with the help of electromagnetic induction. This technology proves to be very budget friendly, requires low maintenance and easy installation and all these things makes it highly competitive not only against generations of alternative or renewable energy, but even compared to conventional technologies.

Keywords-Mast, Vortex, Spring, VIV, Electromagnetic induction.

I. INTRODUCTION

PRESENT day scenario requires high demand of electricity without more and more consumption of fossil fuels and coals. Wind energy is available abundantly in the earth. Traditional wind turbines are the devices which extract energy from wind, however this proven set up has got some drawbacks. Firstly, it is not economical in view of installation, running and maintenance, secondly, substantial wind is required to rotate the blades, thirdly, heavy noise produced by rotor blades, which reduces the efficiency of the system, and also becomes vulnerable for the birds

The nature of the circulation regions around a bluff body in a cross flow can vary considerably from the normal von Karman vortex-shedding mode when subjected to external excitations.

Different authors in their work on the vortex induced vibration on a bluff body as well as lateral vibration of cylinder mounted on spring:

Krishnan et al.[1] correlated the spectral content and characteristics of the force coefficients for asquare prism externally excited by inline sinusoidal pulsation, to near body vortical events. Sareen A et al. [3] in their paper discussed that the effect of transverse rotation on the vortex induced vibration response of sphere. The axis of rotation was perpendicular to the flow direction. Unlike cylinder, the VIV response of the sphere reduced gradually and steadily with increase in the rotation ratio. Bourget R. et al. [4] observed that free oscillations of the rotating cylinder may also develop in the absence of vortex shedding. The symmetry breaking due to the rotation is shown to directly impact the selection of the higher harmonicsappearing in the fluid force spectra. The rotation also influences the mechanism of phasing between the force and the structural response.Behara S. and Sotiropoulos F. [5] observedIn the wake of a stationary sphere, vortex shedding begins at Re~270 and a steady separation bubble appears with two trails stretching downstream for Re = 180-270 and for $Re \ge 270$, hairpin mode of vortices is shed periodically. Objective of the present study is to design and fabricate a model that is able to generate electricity from wind energy as well as from different modes of vibration.

II. WORKING METHODOLOGY

A. WORKING PRINCIPLE

The proposed model is having a very simple construction and made up of easily available materials. The model is based on fundamental principle of Von Karman vortex-shedding effect which states that when an oscillatingflow takes place whenafluid such as, air or water flow past a bluff body at certain velocities, depending on the size and shape of the body. In this flow, vortices are created at the back of the body and detached periodically from either side of the body. Due to this effect, if any object placed in the direction of wind it oscillates. Due to relative motion between the upper and lower part of the model, any vibration from base also can be utilized to generate electricity through the alternator. Also, the proposed model can be designed in such a wayso that not only the flow of fluid but also other types of vibrations (on shores, railway tracks, etc.) can be used to vibrate the mast.

B.WORKING GUIDELINES

Vortex Shedding Effect: Vortex shedding is an oscillating flow that takes placewhen a fluid such as air or water flows past a bluff(as opposed to streamlined) body at certain velocities, depending on the size and shape of the body. In this flow, vortices are created at the back of the body and detach periodically from either side of the body.

Vortex Induced Vibration: The fluid flow past the object creates alternating low pressure vortices on the downstream side of the object. The object will tend to move towards the low pressure zone if the bluff structure is not mounted rigidly and the frequency of vortex shedding matches the resonance frequency of the structure, then the structure can being to resonate vibrating with harmonic oscillations driven by the energy of the flow. This phenomenon is known as Vortex Induced Vibration.

Von Karman Vortex Street: In fluid dynamics, a Von Karman vortex street is a repeating pattern of swirling vortices, caused by a process known as vortex shedding which is responsible for the unsteady separation of flow of a fluid around blunt bodies.

Boundary layer separation:Boundary layer separation is the detachment of aboundary layer from the surface into a broader wake.Boundary layer separation occurs when the portion of the boundary layer closest to the wall or leading edge reverses in flow direction. The separation point is defined as the point between the forward and backward flow, where the shear stress is zero. The overall boundary layer initially thickens suddenly at the separation point and is then forced off the surface by the reversed flow at its bottom.

Faraday's law of electromagnetic Induction:

First law- First Law of Faraday's Electromagnetic Induction state that whenever a conductor is placed in a varying magnetic field emf are induced which is called induced current.

Second law-Second law of Faraday's law of electromagnetic induction state that the induced emf is equal to the rate of change of flux linkages.

Mathematically

$$\varepsilon = -n \frac{d\phi}{dt}$$

$$\varepsilon = -n \frac{d(\beta A \cos \theta)}{dt}$$

$$\varepsilon = nBA\sin \theta \frac{d\theta}{dt}$$

$$\varepsilon = nBA\sin \theta \omega \quad \text{Where,}$$

= Instantaneous induced

voltages in volts

n = Number of turns in the coil = 160

B = Magnetic field strength.

 θ (avg)= 4 degree

$$B = \frac{B_r}{2} \left[\frac{D+z}{\sqrt{R_a^2 + (D+z)^2}} - \frac{z}{\sqrt{R_a^2 + z^2}} - \left(\frac{D+z}{\sqrt{R_i^2 + (D+z)^2}} - \frac{z}{\sqrt{R_i^2 + z^2}} \right) \right]$$

 $A = Enclosed area of coil = 0.00384m^2$

 $\omega = \text{Angular velocity}(\text{avg}) = 5.98$

B_r: Remanence field, independent of the magnet's geometry (physical magnet data for ferrire magnet, 0.41 T)

z: Distance from a pole face on the symmetry axis = 50 mm.

D: Thickness (or height) of the ring = 17 mm

Ra: Outside radius of the ring = 44 mm

Ri: Inside radius of the ring = 22.5 mm

B = 0.003973T

So, $\ge 0.00407 \text{V}$ (approx theoretical value)

C.EXPERIMENTAL SETUP

Basic components of the model:

- 1- Selection of mast The mast should have the following criteria.
 - *Light weight* –The weight will play a significant role in the balancing of the wholedevice.
 - High heat transfer- The device would be in open and so it will experience a wide range of temperature. If the material is having high heat transfer capability, it would easily conduct heat to the surrounding.
 - The perfect choice of material for the mast can be carbon fiber or any polymer
- 2- Helical springs- Helical springs have been used to get lateral vibrations. The springshave been chosen in accordance with the mass of the mast. The stiffness of the spring is an important factor and the mass of the mast will be adjusted according to the stiffness of the spring.

Oscillation of Mast:

In the proposed model, the mast considered as solid body, if placed in wind flow, the wind would strike on the surface of mast. The vortex, usually present in the wind at higher altitudes will act on the peripheryof surface and the wake vortex will detach periodically. As the wind strikes or passes the mast of the bladeless turbine it will create vortex also known as the spinning motion of air. The vibration of the mast will create kinetic energy and this energy will be transformed into electrical energy with the help of alternator.

As the frequency of vortex shedding is proportional to wind speed which is not constant, we need a tuning system for a sustained and continuous vibration over a period of time. It will consist of two round magnets having same poles facing each other. This pair of magnets has one fixed to the oscillating mast and the other fixed to the base.

The magnetic force that appears between two permanent magnets is inversely proportional to the square of theaverage distance between their poles,in a way that they behave like a compression spring with inconsistent elasticity depending on the displacement.

During design and development of the system the following two things have to be maintained-

- 1- At equilibrium the center of gravity of the system should lie on the axis of the system.
- 2- The set-up should start oscillating with a minimal amount of air flow hitting the mast.

Proposed model will be like half portion of elastic rod will be fixed to ground and the other half portion of the same rod will support the mast on its periphery. Both the rods will be joined with spring, which will help oscillating the mast as well as provide support for the rod to be straight. When wind passes one of the cylindrical object, it shears off the downward side of the cylinder in a spinning whirlpool or vortex. That vortex then exerts force on the cylinder, causing it to vibrate/oscillate.

This kinetic energy of oscillating cylinder can be converted to electricity through a linear generator similar to those used to harnesswave energy. This wind generator generates electricity through systems of coil and magnet.

Faraday's Law of electromagnetism has been used for generation of induced emf and the circuit is made closed for flow of current. Insulated copper coils are used during experiment. Up to 11 mA current was generated with 4 coils of diameter 70 mm (approx.) with 160 turns.

Below is the list of components used in model:-

- 1- Base: To provide strong foundation to mast.
- 2-Spring: To support the load acting on it and for oscillation of mast.
- 3- Mast: made up of glass fiber or polymer sheet due to its low weight.
- 4- Carbon fiber rod To support the mass on its periphery. (optional)

- 5-Permanent round magnets and Copper coil: For generating electricity.
- *Load In our case it is a resistance wire of 0.6Ω .

The design completely eliminates mechanical elements that can suffer wear and tear due to friction leading to a reduction in maintenance cost compared to the conventional wind turbine with blades. There is a huge scope of scaling up the model geometrically, kinematicallyand kinetically with the help of dimensional and model analysis. The dimensional scale up will depend upon the height of installation of turbine.

This project has three main advantages-

- 1- Utilizing less area
- 2- Generation of green electricity
- 3- Economical

The frequency of vortex shedding is proportional to the wind speed which is not constant. On the other hand, the range of wind velocities within the structure resonates is narrow due to the fact that the normal oscillation frequency of a structure is single one. To increase the number of equivalent working hours per year, we have to increase this range of useful wind velocities. Two pairs of permanent magnets have been added to the damped harmonic oscillator. The same poles are facing each other. These pair of magnets has one fixed to the oscillating mass and the other fixed to the ground. The magnetic force that appears between two permanent magnets is inversely proportional to the square of the average distance between their poles, in a way that they behave like a compression spring withinonconstant elasticity dependent on he displacement. As they get closer, the growth of the repulsive force between them grows higher than a linear order.

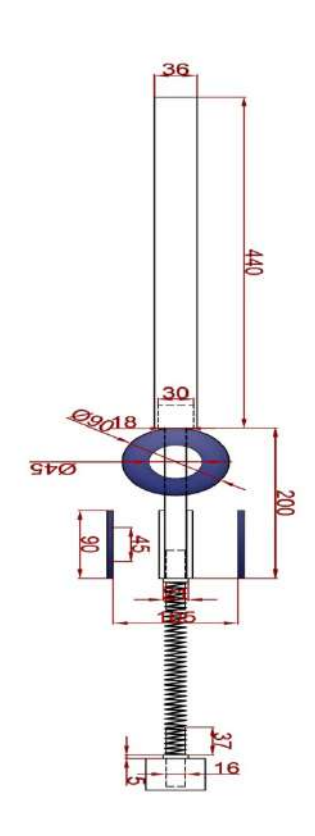


FIG 1

FIG 1: DIAGRAM OF PROPOSED MODEL SHOWING ORIENTATION OF MAST, MAGNETS, HELICAL SPRINGS, COIL AND CARBON FIBER ROD.

III. OBSERVATION TABLE

TABLE 1 TITLE (Table of Load voltage, Wind Velocity Current and $\,$ induced emf) Resistance = 0.6 Ω

S.L.	Load	Wind	Current	INDUCED EMF
No.	voltage	velocity	(mA)	(mV)
	(mV)	(m/s)		
1	5	0.62	8.33	0.981
2	7.5	1.014	12.5	2.933
3	5.3	1.35	8.33	3.527
4	15.2	1.58	25.3	3.525
5	1.3	1.94	2.16	3.0125
6	16.8	2.56	28	3.566
7	1.9	2.925	3.16	3.462
8	1.8	4.54	3.0	37.4
9	5.5	5.0	9.28	32
10	5.7	5.5	9.5	25

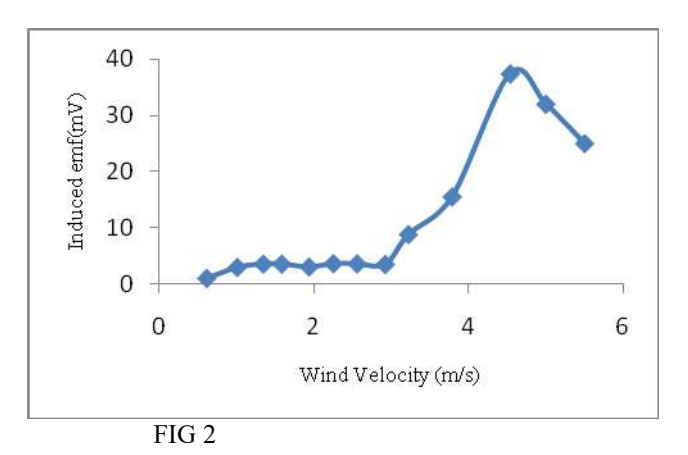


FIG 2: VARIATION OF INDUCED EMF WITH WIND VELOCITY FOR A PARTICULAR SPRING.

 TABLE 2

 TITLE (Table of induced emf and oscillating frequency)

S.L. NO.	INDUCED EMF	OSCILLATING
	(mV)	FREQUENCY (Hz)
1	0.0	3.272
2	0.4	9.778
3	2	11.758
4	3.9	11.889
5	6.7	12.008
6	9.45	29.311
7	14.7	51.670
8	22.8	124.675
9	28.4	125.756
10	39.1	119.388

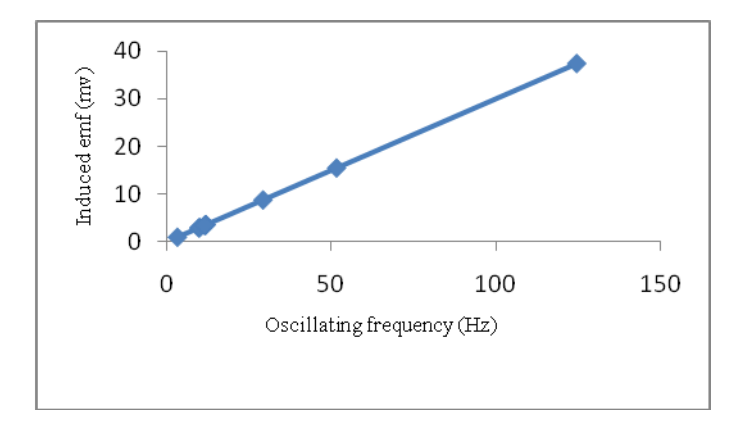


FIG 3: VARIATION OF INDUCED EMF WITH OSCILLATING FREQUENCY FOR A PARTICULAR SPRING.

 TABLE 3

 TITLE (Table of oscillating frequency and wind velocity)

S.L. NO.	OSCIILATING FREQUENCY(Hz)	WIND VELOCITY(m/s)
1	3.27	0.62
2	9.77	1.01

Balancing the forces;

3	11.75	1.35
4	11.7508	1.58
5	10.04	1.94
6	12.00	2.25
7	11.54	2.92
8	29.31	3.22
9	51.67	3.79
10	124.67	4.54

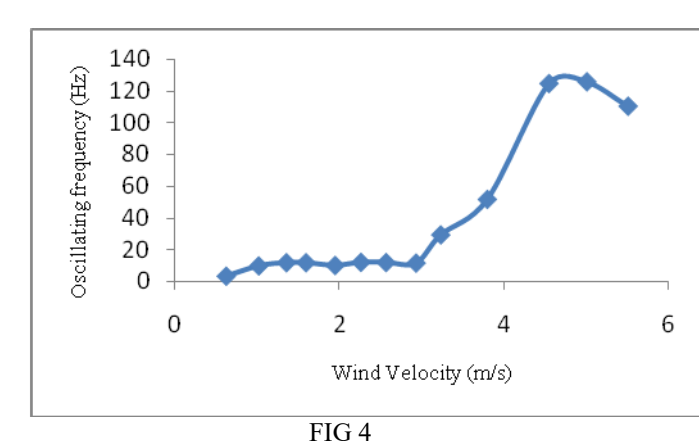


FIG 4: VARIATION OF OSCILLATING FREQUENCY WITH WIND VELOCITY FOR A PARTICULAR SPRING

POWER GENERATED IN ONE OSCILLATION

Average Velocity, Vavg = 2.90 m/s Average current, I = 14.63 mA = 0.010956 A Resistance of one coil= 0.6Ω Total no. of coils = 4Total resistance = 2.4Ω Power generated = $I^2R = 0.02629$ W

IV. MATHEMATICAL CALCULATIONS

Kinematic equation of motion of mast

Let,
x=displacement of mast in horizontal direction
t=time period of oscillation
g=acceleration due to gravity
l=length of mast
k=spring constant
m=mass of mast

weight)-Restoring force (spring force) = 0 $d^2x/dt^2+gx/1-kx^2/ml=0$ $d^2x/dt^2 + ax - bx^2 = 0$ Here, a = g/l and b = k/mlLet, v=dx/dtThen, $d^2x/dt^2=vdv/dx$ vdv/dx+ ax-bx²=0 $V.dv = (bx^2-ax).dx$ $v^2/2 = bx^3/3 - ax^2/2 + c$ At, t=0, x=0Therefore v=0, c=0 $v^2/2 = bx^3/3 - ax^2/2$ Putting, v=dx/dt $dx/dt = (\sqrt{2b/3}) x^{3/2} - (\sqrt{a})x$ $dx/\{(\sqrt{2b/3})^{3/2}-(\sqrt{a})x\}=dt$ $\int dx / \{(\sqrt{2b/3}) x^{3/2} - (\sqrt{a}) x\} = \int dt$ $\int dx / \{ (\sqrt{2}b^3) x^{3/2} - (\sqrt{a})x \}$ * $(\sqrt{2b/3})x^{3/2}+(\sqrt{a})x(\sqrt{2b/3})x^{3/2}+(\sqrt{a})x=\int dt$] $\int (\sqrt{2b/3}) x^{3/2} + (\sqrt{a})x \cdot dx/2bx^3/3 - ax^2 = \int dt$ $\int (\sqrt{2b/3}) x^{1/2} + (\sqrt{a}) \cdot dx / (2bx^2/3 - ax) = \int dt$ $[(\sqrt{2b/3})\sqrt{x}.dx/2bx^2/3-ax]+\int(3/\sqrt{2b})dx/(x^2-3ax/2b)=\int dt$ Solving 1st part of equation $\int [(\sqrt{2b/3})\sqrt{x}.dx]/[2bx^2/3-ax]$ $\int [(\sqrt{3}/2b).dx]/[x^{3/2}-3a\sqrt{x}/2b]$ $\int (\sqrt{3}/2b).dx/\left[\sqrt{x(x-3a/2b)}\right]$ Let, $x=t^2$ Then, dx=2t.dt $\int [(3/2b)^{1/2}.2t.dt]/t(t^2-3a/2b)$ $\sqrt{6/b^*} \left[\int dt / (t^2 - 3a/2b) \right]$ $\sqrt{(6/b)*(2b/6a)} \ln [(t-3a/2b)/(t+3a/2b)] + C1$ $\sqrt{(6/b)*(b/3a)} \ln \left[(\sqrt{x-3a/2b}) / (\sqrt{x+3a/2b}) \right] + C1$ Solving 2nd part of the equation $\int (3\sqrt{2b})x / (x^2 - (3ax/2b))$ $\int (3\sqrt{2b})x/x (x-(3a/2b))$ $3/(\sqrt{2b})/(x-(3a/2b))=A/x+B/\{x-(3a/2b)\}$ Solving above equation $A=-\sqrt{2/ba}$ And, $B = \sqrt{2b/a}$ $\int (3/\sqrt{2b})x/\left[x(x-3a/2b)\right]$ $= \int -(\sqrt{2b/a})x/x + \int (\sqrt{2b/a})/dx/[x - (3a/2b)]$ $\int (3/\sqrt{2b})x/[x(x-(3a/2b))]$ $=(-\sqrt{2b/a})\ln x + (\sqrt{2b/a})\ln (x - (3a/2b)) + C2$ Therefore, $\int dt = \int dx / [(\sqrt{2}b/3) x^{3/2} - (\sqrt{a})x]$ $t=(\sqrt{6/b})*(b/3a)\ln{\sqrt{x}-(3a/2b)/\sqrt{x}+(3a/2b)}-{(\sqrt{2}b)}$ $(a)^* \ln x$ + $[(\sqrt{2b/a}) \ln(x - (3a/2b))]$ + C3

When force applied on the mast, then it deflects in other side due to weight of the mast but due to spring it deflects in another side and thus oscillating motion takes place.

Bending force (force due to wind + force due to mast

Where C3 is constant of integration

V. APPLICATIONS

- 1. It can be installed beside railway tracks.
- 2. It can also be used to some extent in very small scale industries for some work
- 3. It can be used in remote areas with high air flow and vibration, where a lesser amount of electricity is available.
- 4. It can be installed at on-shore and off-shore where there is significant vibration from any source.

VI. ADVANTAGES

- 1. The impact on the bird population is expected to be much smaller
- 2. Reduction in maintenance costs compared to traditional wind turbine and easy installation
- 3. It does not have moving parts in contact, which eliminates the need for lubrication and reduces the wear and tear.

VII. CONCLUSIONS

The major contribution of our model is that it can give us significant power generation with less occupying area, less number of components and can even work under low average wind speed. As of now we are not aiming to increase the power output, rather focus on auxiliary demands and for household purposes. The allure of the model is its wide range of installation points. It can be installed on the sides of highways, besides railway tracks and can also be installed on the off-shore. This developed model can become challenging in the power sector of India if proper scaling up was done in a study by D.J. Milborrow[2], he assessed that there is a loss in power output (about 25% of the total output) if the rotors diameter is less than 10 m and they are placed together. On basis of this study, we are concluding that since our model doesn't have any rotors like in traditional wind turbine, there won't be any loss in power output. Instead the net output may increase in array as in the below figure it can been seen that the path line of the breeze is such that the shedding which is formed at the first device will go on increasing and in the last row, the vortex shedding will be maximum.

ACKNOWLEDGEMENT

This research work was supported by Institution of Engineers (India), Grant-in-Aid Scheme. Project grant ref. no. UG2020001 dated 17th May 2019. Support for all characterizations of the fabrication and experiments conducted at Student Innovation Centre, Asansol Engineering College, Asansol, West Bengal, India.

REFERENCES

- [1] Krishnan H, Agrawal A, Sharma A, Thompson M, Sheridan J, Characteristics of force coefficients and energy transfer for vortex shedding modes of a square cylinder subjected to inline excitation. Journal of Fluids and Structures 2018; 81:270-288.
- [2] D. J. Milborrow, Performance of arrays in wind turbines J. wind engineering and industrial aerodynamics 1980, Vol 5.
- [3] Sareen A, Zhao J, Jacono D. L., Sheridan J, Hourigan K, Thompson M. C., Vortex-induced vibration of a rotating sphere, J. Fluid Mech. 2018, 837: 258–292.
- [4] Bourguet R., Jacono D. L., Flow induced vibrations of a rotating cylinder, J. Fliud. Mech., 2014, 740: 342-380
- [5] Behara S. and Sotiropoulo F. Department of Civil Engineering, College of Engineering and Applied Sciences, 100 Engineering Building, Stony Brook University, Stony Brook, NY 11794-2200, USA.

Cost Optimal Design of A 3-Phase Power Inductor by Evolutionary Optimization

Sampurna Mukherjee*, Pratosh Kumar Jha, Anshuman Pradhan, Amardyuti Basu, Prasanta saha, Raju Basak

Students in Electrical Engineering Department, Techno India University - EM-4, Salt Lake City, Sector V, Kolkata, West Bengal 700091

ABSTRACT

The presents paper the design methodology of a 3-phase high voltage VARcompensating inductor. These are used with EHV-lines, mostly long terminal equipment, to compensate capacitive VARgeneration of the line and to avoid VAR-IN under-excited operation of and the alternators. The inductor resembles a 3-phase core type transformer with the exception that it has only one coil per phase and an appropriate airin each limb. optimization has been made by using the technique of evolutionary optimization. The method is simple and straight-forward and could be easily applied to the design of power inductors. The key variables were identified and initialized consulting design data-books. A suitable step length and convergence constant were chosen. The optimal solution could be reached within a few cycles of iterations. The annual cost towards depreciation, interest etc. plus the annual cost of energy was chosen as the cost function. The cost function was computed by a specially constructed sub-routine. Application of this method saves much computer run-time compared to the method of exhaustive search.

Keywords:Power inductor, optimal design, design variables, design constraints, evolutionary optimization.

Introduction

Power inductors find application in systems [1], [2] illumination engineering^[3] and in power electronics^[4]. In power system, they are used as grounding reactors, fault current limiters and as compensators of capacitive VAR. In illumination engineering they are used as chokes or ballasts. In power electronics they are used as electrical inertia in CSI and choppers, elements of filter etc. The inductors may be iron-cored or air-cored, 3phase or single phase. Air-cored inductors are bulkier and costlier. Hence they are used only where the inductance required is small and saturation is to be avoided^[5]. Most of the inductors used in electrical industry are of iron-core types. Both shelltype and core type constructions are used. A calculated amount of air-gap is kept in the magnetic circuit to realize the required amount of inductance^[6].

Single phase power inductors have been in use since a long time back as currentlimiting reactors in the bus-bars, as faultcurrent limiters and as grounding reactors to compensate for the capacitive currents^[7]. The use of inductors as VAR-compensators is rather new. In the earlier days only capacitive compensation had to be made, shunt compensation to improve the power factor and series compensation to increase the limits of power flow. But now-a-days due to advent of long EHV lines, which are highly capacitive rather than inductive, a new situation has cropped up. The leading VAR generated by EHV lines partially compensates for the lagging VAR drawn by the loads and lost in the lines to improve the over-all power factor during the peak hours. But during lean hours of operation, the inductive VAR requirement is much smaller. The capacitive VAR generated by the long lines forces the system to leading power factor operation. It reduces the stability margin, creates Ferranti effect and worsens the cross-country voltage profile and makes the system prone to both power

angle and voltage instability^[8]. Therefore, the recent practice is to use inductive compensators with long transmission lines, either at the ends or at a no. of points over the span of the line to imitate distributed compensation.

While used at the terminals, the general practice is to partly compensate for the capacitive VAR generation by fixed 3-phase high voltage inductors. These are like 3-phase 3-limbed core-type transformers with only one coil per phase and a calculated amount of air-gap in the limb. The design is somewhat similar to that of high voltage 3-phase transformers with several exceptions^{[6],[9]}.

1. The optimizing techniques

There are several classical and nonclassical optimizing techniques. Many of them have found application in electrical equipment design. For single variable search, the following techniques are used^[10], [11]:

- 1) Bracketing technique- exhaustive search, bounding phase method. These are not computationally very efficient.
- 2) Region elimination methods- interval halving, Fibonacci search, golden section search. These processes are rather slow.
- Point estimation method- successive quadratic approximation. This method is good.
- 4) Gradient search- Newton-Raphson method, Secant method, cubic search method. These methods are computationally efficient. But the initial estimate must be judiciously made.
- 5) Most of the design problems are multivariable constrained optimization problems. The methods commonly used are as follows:
- 6) Successive unidirectional search along the direction of each variable. This is applicable to concave or convex functions.

- 7) Direct search methods- evolutionary optimization, simplex search, Hook and Jeeves pattern search, Powell's conjugate direction method. These methods are quite efficient, provided the initial point can be chosen judiciously.
- 8) Gradient-based methods- Cauchy's steepest decent, Newton's method, Conjugate gradient method etc. These methods are faster than the direct search methods as they possess derivative information. However it is difficult to find derivatives of a function which is not amenable to a single mathematical expression. So these methods are avoided, if possible.

Out of all these methods mentioned above, we have made use of evolutionary optimization in this paper as it is simple to implement and has been successfully employed for solving a large no of industrial optimization problems.

2. Method of evolutionary optimization

Evolutionary optimization method is a direct search technique. It was developed by G.E.P. Box in 1957. It is a simple method and has been applied to many optimization problems since formulation. The first task is to identify the key variables, initialize them and choose suitable step-lengths for each of these variables. Then the coordinates of the corner points are found out by adding to and subtracting from the initial value, half of the step-length for each. If there be N no of variables, there will be 2^N of corner points around the initialized center point which forms a hyper-cube. The cost function is computed for all these $(2^{N} + 1)$ points and the set giving minimum cost function is retained as new initial values. In the next cycle another hypercube is formed with the new values. The process is continued until convergence. convergence constant is chosen (in this case a few rupees which is insignificantly small

in comparison to the cost of production). If the reduction in cost functions is less than the convergence constant the process is terminated^[10].

3. Constructional features

The 3-phase power inductors resemble 3-phase core type transformers. The design is also similar to that of a 3-phase core-type transformer^[12]. However the KVA-rating is halved before application of the formula for emf/turn as there is only one coil. A 3limbed construction is used. The core is made up of high grade cold-rolled grainoriented steel (CRGOS) stampings. A multi-step core construction is used to make effective utilization of the space inside the coil. I-type laminations have been used and the joints between limbs and yokes have been interleaved to reduce the reluctance of the magnetic path. Cores are kept in position by clamping between side plates at intervals^[13], ^[14].

Best grade insulation has been used for the coil and for wrapping the core as the voltage is very high. Concentric disc type winding has been used for their greater mechanical strength. The coils are made of rectangular strips of pure annealed copper and are assembled as double coils. A no. of coils are in series but they are not jointed. They are made from a single conductor to avoid jointing losses. The windings are regularly transposed.

The core-coil structure is placed in an oil-filled tank fitted with radiators. Airblast has been used to improve the cooling. Breather, conservator and other auxiliaries like Buchholtz relay have been added^[6]. The optimal solution has been found out by making recourse to fast-acting digital computer ^[15]. The software for evolutionary optimization has been indigenously developed.

4. Design variables and constraints

There are several design variables for the design of power inductors. Some of them affect the objective function to a large extent. These are called key variables.

Other variables have rather less influence on the objective function. The optimal solution is sought by varying the key variables only. Other variables are kept constant at their usual values^[16].

The variables may be continuous or integer. For example, the no of turns/coil of the concentric disc or the no of tubes in a radiator must be an integer. However, as the number is large in this case, they have been treated as continuous variables. The following key variables have been identified:

The following key variables have been chosen^[6], ^[12]:

K = emf constant (in $E_t = K\sqrt{S}$, where $E_t = \text{emf/turn}$, S = rating in KVA)

 $R_w = H_w / W_w$ = Height: Width ratio of the transformer:

 δ = current density in the conductor in A/mm²; B_m = Maximum flux-density, Tesla

It has been found that the cost function continuously reduces with increasing B_m . Hence its maximum value for which the constraint on iron loss is not violated has been retained. The other three key variables have been chosen as candidates for evolutionary optimization.

In addition, there are decision-variables [6],[12]e.g.

- a. Core or shell construction: Core construction has been used for greater economy
- b. Conductor material- copper or aluminium: Copper is to be used for such large rating for compact design^[17].
- c. Core material- CRNOS or CRGOS: CRGOS has been used to reduce the iron loss to minimum
- d. Cooling- ON or ONAF: Oil natural airforced type cooling has been used to keep the temperature rise within statutory limits. The speed of air-blast has been judiciously chosen.

Constraints have been imposed on:

Maximum %copper $loss \le 0.35$ %;Maximum % iron $loss \le 0.1$ %, with a view to limit the size of theradiators.

5. Algorithm

The algorithm for evolutionary optimization as applied to 3-phase power inductor design is given below^[10]:

- Read ratings of the power inductor: S,V,f (MVA-rating, Line-to-line voltage, nominal frequency), connection (Y or D)
- 2. Find out the phase quantities of voltage, current and the equivalent MVA $\leftarrow S/2$
- 3. Read constants $\leftarrow K_s, K_w, N_{st}$ (stacking factor, window space factor, no of core steps), Resistivity of copper at operating temperature $\leftarrow \rho$, Specific costs of core and conductor materials, oil and tank wall, cost of a BOT unit, % overhead, no. of radiators, no of turns in a coil of continuous disc etc.
- 4. Assign fixed values to variables which are not to be altered e.g. 1.7 Tesla $\leftarrow B_m$. Compute iron loss per Kg for the core material using: $p_i \leftarrow 0.5(B_m^{2.91})$ (obtained from design data book by least square fitting.)
- 5. Read step lengths for the variables $VK, VR_w, V\delta$ and the convergence constant, ε
- 6. Set: Count = 1; Initialize key variables: K_o, R_{wo}, δ_o
- Find coordinates of the corners of the hypercube
 ← K_a ±VK/2; R_{wa} ± VR_w/2; δ_a ±Vδ/2
- 8. Form an array with the coordinates of the central point and the corners of the hypercube.
- 9. Goto power inductor subroutine for all the corners of the hypercube and the central point (dimension=2³+1=9), one by one, compute the objective function (of) in each case and put the values in the array.

- 10. Find the minimum value of the objective function and the corresponding values of the variables from the array as: of (count) etc.
- 11. Change initial values of the variables by the values obtained in step 9.
- 12. $count \leftarrow count + 1$
- *13. If count* = 1 *gotostep* 6
- 14. If $abs[of(count) of(count 1) > \varepsilon$ then gotostep 6

The problem has converged.

- 15. Run through the steps of the modified program to account for integer variables.
- 16. Print out the results.
- 17. Stop
- 18. End

The design data has been obtained from the design data book. [18]

6. Example EHV lines- Vulnerability to VAR-IN

Some examples of EHV long lines in West Bengal with their π – circuit parameters (in p.u. on 100 MVA base) are given in table-1 [19].

The Farakka400-Jeerut400 line has a VAR-generation of 65.13 MVA at the terminals. It is advantageous to keep the power factor high at peak hours but is detrimental at lean hours while the line flow is small. So, compensation has been made for this line by installing 50 MVAR inductor units. We take up the next one in the table: the case of Farakka400-Durgapur400. For this line, the VARgeneration is 44.16 MVAR at the terminals. As the load in the lean hours is gradually compensation increasing, by inductors of 30 MVAR rating at the terminals will be sufficient. We proceed to make its optimal design using evolutionary optimization technique.

7. The design problem

Dual optimization has been made looking after the interest of the manufacturer and the utility. The objective function is the sum of annual cost against depreciation, interest, repair and

maintenance and the cost of lost energy units per annum.

The problem has converged to minimal solution in only 9 cycles. The results obtained in each cycle are given below in table-2.

There was no improvement in the 10th. Iteration.The cost function minimizes for:

K = 0.405 ; $R_{\rm o} = 3.45$; $\delta = 2.65$

The design procedure has been repeated to take care of integer variables e.g. no of turns/coil in the disk winding, no. of radiators and no of tubes in each radiator etc. The details of the optimal machine are given below:

Rating:

MVA-rating of the inductor= 30; Rated line voltage = 400Kv; Nominal frequency= 50 Hz.

Connection: STAR; Conductor material: COPPER; Phase Current = 43.301 A

Dimensions:

The EMF- constant= 0.405;

Number of turns of the winding= 4640 Chosen current density = 2.65 A/mm²;

Cross section of the conductor = 16.038 mm²

Net area of core iron= 0.13305m²;

Stacking factor= 0.92;

Gross area of core iron=0.14462 m²

3-stepped core has been used.

Diameter of the core circle= 0.46811 m;

Length of the core sides in mm: 424 / 331/

Area of the window= 1.4752E-03m²;

Window height/width in m:

7.1854E-02/2.0530E-02

Distance between core centers= 0.44417 m Width/height of yoke in m: 0.42364 /0.34138

Total length/height of core in m: 1.4009/0.75462

Losses, impedance and air-gap:

Iron loss = 11071 W /% Iron loss = 0.0738

Mean length of turn= 1.4964 m;

Resistance of winding= 9.0116Ω

Copper loss = 50690W

% Copper loss = 0.33794;

Total % loss = 0.41174

The impedance of the coil= 9.0116 +j5333.3 Ω ; The inductance of the coil= 16.976 Henry

AT required for iron path is negligible.

AT required for gap/m at this flux-density = 956857

Length of air-gap required per limb= 210 mm

Tank and radiators:

The tank length, width, height in m: 0.604 / 1.581 / 0.955

Radiators with air-blast have been used for better cooling. Air velocity = 20m/s

Dissipation by radiation from polished surface= 8 W/m²/°C

Dissipation by convection raised to: 38.476W/m²/°C

Cooling area of the tank is insufficient to keep the temperature rise within limit.

Artificial cooling is provided by the air-cooled radiators.

The no. of radiators= 8;

Area of each radiator = 3.7015 m^2

Radiators are provided with elliptical tubes each of 75x25 mm

Distance between tubes=125 mm.

There are two rows of tubes in each radiator.

No of tubes in a row/ width of the radiator: 13 / 0.8125m

Cost analysis:

The weight/ cost of tank with radiator: 515.88; Rs. 38691/-

The volume/ cost of oil: 0.23563 liters; Rs. 14138/-

Volume of iron= 0.40148 m³; Weight of iron= 3151.6 Kg; Cost of iron = Rs. 504255/-Volume of copper= 0.33112 m3; Weight of copper= 2946.9 Kg ; Cost of copper = Rs. 1679749/-Direct cost allowing 25 % labour charge=

Rs. 2796040/-

Selling cost allowing 35 % overhead = Rs. 3774655/-

Annual cost of lost energy at Rs. 4/- per BOT unit = Rs. 1307118/-

The annual cost has been taken as the objective function. It includes:

Interest, depreciation, repair and maintenance, taken as 30% of selling cost, and the capitalized annual energy loss.

The objective function= Rs. 2439515/-

The cost function has increased by an amount of Rs. 464/- for replacing real variables by integer variables.

8. Conclusion

The paper has dealt with the design optimization of a high voltage 3-phase used for inductive inductor compensation of long EHV transmission lines. As the length of the line and its power rating increase, it becomes economic to use Extra High voltage for transmission. For this reason, a 400 Kv power network has already evolved in the country and a 765/800 Kv network is in the offing. The EHV lines are highly capacitive and generate VAR. During peak hours this generation of VAR is benevolent as it improves the system power factor but is malevolent during lean hours of night as it creates cross-country overvoltage Ferranti action and reduces the stability margins of the alternator by forcing them to leading power factor operation. Hence, long transmission lines are inductively compensated. Though distributed compensation is good, the general practice in our country is to use power inductors of appropriate rating at the terminals.

3-phase power inductors resemble 3-phase power transformers in construction. The 3limbed construction is used with a calculated amount of air-gap in the limb to realize the required inductance. There is only one high voltage coil in each limb, which is normally of concentric disc type. Copper conductors with best grade of insulation are used. The core is made of interleaved high grade CRGOS stampings with proper clamping. The core-coil structure is placed in an oil-filled tank fitted with radiators, expansion tank and other accessories. Improved cooling is obtained by air-blast- the velocity of blast is a design variable.

The design of electrical equipment is in general multi-variable constrained optimization problem. objective The function chosen in this paper is the annual cost towards interest, depreciation, repair and maintenance and the annual cost of lost energy so that dual optimization from the point of view of the manufacturer and the user is realized. A no of key variables have been chosen and the optimization has been made by the evolutionary method.

There are several methods for optimizing the design of electrical equipment. The gradient search methods are fast-acting, but they are to be provided with information on derivatives at the points of interest. As the objective function of a transformer or inductor can hardly be expressed as a single mathematical expression, it is difficult (but not impossible) to evaluate the derivatives at each point of iteration. Therefore, direct search methods are preferred to gradient methods. The evolutionary optimization is a direct search method which is straightforward and is easy for implementation. So recourse has been made to this method for searching out the optimal solution. The convergence is fast and comparable to

gradient methods provided the initial point is not far away from the point of optimality.

References:

- [1] J.J. Grainger, W.D. Stevenson (Jr), "Power system analysis", Tata-McGraw-Hill, 2003; ISBN 0-07-058515-6
- [2] R.K. Rajput, "A text-book of power system engineering", Laksmi Publications Pvt. Ltd., 2012
- [3] H. Partab, "Art and science of utilization of electrical energy", DhanpatRai and Co., 2010
- [4] M.D. Singh and K.B. Kanchandani, "Power Electronics", McGraw-Hill Education (India) Pvt. Ltd., ISBN: 978-0-07-058389-4
- [5] Nagaoka, Hantaro, "The inductance coefficients of solenoids", Journal of the College of Science, Imperial University, Tokyo, Japan. p. 18.
- [6] A.K. Shawney, "A course in electrical machine design", DhanpatRai& Sons, 2003
- [7] A. Chakraborty, S. Halder, "Power system analysis, operation and control", PHI, ISBN-978-81-203-4015-2
- [8] P. Kundur, "Power system stability and control", McGraw-Hill Inc.
- [9] M.V. Deshpande, "Electrical power system design", TMG, ISBN-13: 978-0-07-451575-4 and ISBN-10: 0-07-451575-6.
- [10] K. Deb, "Optimization for engineering design", PHI, 2010. ISBN 978-81-203-0943-2
- [11] S.S. Rao, "Engineering optimizationtheory and practice", New Age Int.; ISBN 978-81-224-2723-3
- [12] IndrajitDasgupta, "Design of transformers", TMH, New Delhi, 2002.
- [13] Alfred Still, "Principles of transformer design", John Wiley and Sons Inc, 2007.
- [14] Martin J. Heathcote, "The J & P transformer book", 12th. Edition- a

- practical technology of the power transformer.
- [15] M. Ramamoorty, "Computer-aided design of electrical equipment", Affiliated East-West press, 1987, ISBN: 81-85095-57-4
- [16] A. Maity, K. Bhattacharya, A.N. Sanyal, "Cost optimal design of a 3-phase 400 Kv power inductor for compensating an EHV line", International Journal of Emerging Technology and Advanced Engineering (ISSN 2250–2459(online), an ISO 9001:2008 certified journal)
- [17] J.C. Olivares-Galván, "Selection of copper against aluminium windings for distribution transformers, IET Electrical Power Application, 2010, Vol. 4, Iss. 6, pp. 474-485.
- [18] Shanmugasundaram, G. Gangadharan, R. Palani, "Electrical machine design data book", Wiley eastern Ltd. ISBN 0 85226 813 0
- [19] Transmission line data, NHPC (collected from WBSETCL)

								0				0				8
					0	3	2	2	0	3	2	2	0	3	2	2
								4				4				4
From	То	R	X_L	Y/2	4Ra	ting	5	4	4	1	6	4	4	1	5	4
Farakka400	Jeerut400	0.0043	0.0489	0.6513	4	75	5	6	4			3	3	5	5	3
Farakka400	Durgapur400	0.0029	0.0332	0.4416	5	7		4				9	5			2
KTPS400	NewHowrah400	0.0006	0.0052	0.2759		7		1				4				2
T (400	N 11 1 100	0.0000	0.0107					9				8				6
Jeerut400	NewHowrah400	0.0009	0.0107	0.1435	0	′3	2	2	0	3	2	2	0	3	2	2
Durgapur400	NewHowrah400	0.0027	0.0306	0.4164		7.		4				4				4
	1		l		4	0	6	4	4	1	7	4	4	1	6	4
					4	5	5	5	4			4	3	5	5	2

Table-1. π – Circuit Parameters for some EHV Lines

Ite no	rat . 1	ion		Iteration no. 2				Ite no	rat . 3	ion	
K	$R_{_{\scriptscriptstyle{I\! I}}}$	δ	С	K	R_{ω}	δ	С	K	$R_{_{\scriptscriptstyle{N}}}$	δ	С
			os				os				os
			t				t				t
0	3	2	2	0	3	2	2	0	3	2	2
			4				4				4
4		6	4	4	0	6	4	4	1	6	4
5			7	4	5	5	5	4			3
			6	5			5 5				3 9
			0				4				4
			3				8				8
0	2	2	2	0	3	2	2	0	3	2	2
			4				4				4
4	9	5	4	4		6	4	4	0	5 5	4
4 5	5	5	6	4			4	3 5	5	5	3
5			5				0	5			
			0				2				0
			2				6				1
0	2	2	2	0	3	2	2	0	3	2	2 4
			4				4				
4	9	6	4	4		7	4	4	0	6	4
4 5	5	5	5	4			4	3 5	5	5	
5			6				7	5			2 4 3
			3				7 5				3

0	⁷ 3	2	9 2 4 4	0 . 4	3 . 1	2	3 9 4 8 2 4 4	0	3	2	3 2 2 6 2 4 4
4 4 5	0 5	6 5	5 5 4 8	4 4		7	4 4 6 7 3 2 4 4	4 3 5	1 5	6 5	4 2 3 6 3 2 4 4
0 4 5 5	2 9 5	2 5 5	2 4 5 0 5 2 8	0 . 4 5	3	2 . 6	2 4 7 6 0 3	0 4 4 5	3 . 0 5	2 . 5 5	6 4 1 9
0 4 5 5	2 9 5	2 6 5	2 4 9 6 4 9	0 . 4 5	3	2 . 7	2 4 8 3 0 9	0 4 4 5	3 0 5	2 6 5	2 4 5 5 4 8
0 4 5 5	3 0 5	2 5 5	2 4 5 0 4 6 7	0 . 4 5	3 . 1	2 . 6	2 4 7 5 4 6	0 4 4 5	3 1 5	2 5 5	2 4 6 3 6 5
0 4 5 5 5	3 . 0 5	2 6 5	2 4 4 9 5 8 8	0 4 5	3 . 1	2 . 7	2 4 7 9 1 9	0 4 4 5	3 1 5	2 6 5	6 5 2 4 4 5 4 9 5

no	. 4			no	. 5			no	. 6		
0	3	2	2	0	3	2	2	0	3	2	2
			2 4 4				2 4 4 1 2 2 8 2 4 4 1 0 5 9				2 4 4
4	1	6	4	4	2	6	4	4	2	6	4
3	1 5	6 5	2	3			1	2	2 5	5	0
3 5			3				2	4 2 5			4
			2 3 6 3				2				0 4 6 2
			3				8				2
0	3	2	2	0	3	2	2	0	3	2	2
			2 4 4 1 2 9				4				4
4	1	6	4	4	1	5 5	4	4	2	6	3
3	•		1	2	5	5	1	2	_		9
			2	5			0	_			5
			9				5				5
			9				9				3
0	3	2		0	3	2		0	3	2	2 4 3 9 5 5 3 2 4 4
		_	2 4 4 2 0 4				2 4 4				1
4	1	7	 	4	1 5	6	1 1	4	2	7	1
3	1	/	2		1 5	5		2		′	4
3			2	2 5	3)	0 5 3 0	2			0 3 1 8
			0	3			3				3
							3				
	_	_	4		2	_	0	_	2	_	8
0	3	2	2 4 4 1 2 2 8	0	3	2	2 4 4	0	3	2	2 4 3 9 4 8 6
4	2		4	4		٠ <u>.</u>	4	4	3		4
4	2	6	4	4	2 5	5 5	4	4	3	6	3
3			1	5	5	5	0	2			9
			2	5			9				4
			2				9 9 0				8
			8								
0	3	2	2 4 4	0	3	2	2 4 4	0	3	2	2 4 4
			4				4				4
4	2	7	l .	4	2	6		4	3	7	
3			1	5	5	5	0	2			0
			9	5			4				2
			7				6				5
			3				2	L			2
0	3	2	2	0	3	2	2	0	3	2	2
			4				4				4
4 4	1	6	4	4	1 5	5 5	4	4 3	2	6	4
4			3	4 2 5	5	5	3	3			1
			9	5			2				2
			4				2				2
			1 9 7 3 2 4 4 3 9 4 8				0 4 6 2 2 4 4 3 2 2 6				0 2 5 2 2 4 4 1 2 2 8
0	3	2	2	0	3	2	2	0	3	2	2

								,			
4 4	1	7	4 4 4 6 7 3	4 2 5	1 5	6 5	4 4 2 3 6 3	3	2	7	4 4 1 9 7 3
0 4 4	3 . 2	2 . 6	2 4 4 3 8 9 8	0 4 2 5	3 . 2 5	2 5 5	2 4 4 3 1 7 8	0 . 4 3	3 . 3	2 . 6	3 2 4 4 1 1 8 2
0 . 4 4	3 . 2	2 . 7	2 4 4 4 6 2 4	0 . 4 2 5	3 . 2 5	2 6 5	2 4 4 2 3 1 6	0 . 4 3	3 . 3	2 . 7	2 4 4 1 9 2 8
Ite	erat	ion		Ite	rat	ion		Iteration			
1					. 8			no	. 9		
0 4 2		2 . 6	2 4 3 9 4 8 6	0 4 1 5	. 8 3 . 3 5	2 6 5	2 4 3 9 2 3 2	0 4 1	3 . 4	2 . 6	2 4 3 9 0 9
0 4	3	2	3 9 4 8	0 4 1	3 . 3	6	3 9	0 . 4	3		3 9 0 9
0 4 2 0 4	3 . 3	2 . 6	3 9 4 8 6 2 4	0 4 1 5	3 5	2	3 9 2 3 2 2 4	0 4 1	3 . 4	2	3 9 0 9 3 2 4

			1				1				
4 1 5	3 5	5 5	4 3 9 7 5 4	4 1	. 4	6	4 3 9 0 9 3	4 0 5	4 5	5 5	4 3 9 5 6 8
0 4 1 5	3 . 3 5	2 6 5	2 4 3 9 2 3 2	0 . 4 1	3 . 4	2 . 7	2 4 3 9 5 5 5	0 4 0 5	3 . 4 5	2 6 5	2 4 3 9 0 5 1
0 4 2 5	3 . 2 5	2 . 5 5	2 4 4 0 9 9	0 4 2	3 . 3	2 . 6	2 4 3 9 4 8 6	0 4 1 5	3 . 3 5	2 . 5 5	2 4 3 9 7 5 4 2 4 3 9 2 3 2
0 4 2 5	3 . 2 5	2 6 5	2 4 4 0 4 6 2	0 . 4 2	3 . 3	2 . 7	2 4 4 0 2 5 2	0 4 1 5	3 . 3 5	2 6 5	2 4 3 9 2 3 2
0 4 2 5	3 . 3 5	2 5 5	2 4 4 0 9 4 5	0 4 2	3 . 4	2 . 6	2 4 3 9 4 4 4	0 4 1 5	3 4 5	2 5 5	2 4 3 9 7 1 1
0 4 2 5	3 . 3 5	2 6 5	2 4 4 0 4 1 9	0 4 2	3 . 4	2 . 7	2 4 4 0 2 1 0	0 4 1 5	3 4 5	2 6 5	2 4 3 9 1 9

Table-2. Iteration table for minimizing the cost

